UC Berkeley
UC Berkeley Electronic Theses and Dissertations

Title

Harnessing Biology's Leviathan: Ribosomal Catalysis of Unnatural Bonds and Chemo-Ribosomal Methods for the Synthesis of Atropisomeric and Macrocyclic Peptides

Permalink

https://escholarship.org/uc/item/91h7c6bn

Author

Knudson, Isaac

Publication Date

2024

Peer reviewed|Thesis/dissertation

eScholarship.org Powered by the California Digital Library
University of California

Harnessing Biology's Leviathan: Ribosomal Catalysis of Unnatural Bonds and Chemo-Ribosomal Methods for the Synthesis of Atropisomeric and Macrocyclic Peptides

By

Isaac Jacob Knudson

A dissertation submitted in partial satisfaction of the

requirements for the degree of

Doctor of Philosophy

in

Chemistry

in the

Graduate Division

of the

University of California, Berkeley

Committee in charge:

Professor Alanna Schepartz, Chair
Professor Jamie Douda-Cate
Professor Nickolas Ingolia

Summer 2024

Abstract

Harnessing Biology's Leviathan: Ribosomal Catalysis of Unnatural Bonds and Chemo-Ribosomal Methods for the Synthesis of Atropisomeric and Macrocyclic Peptides

By

Isaac J. Knudson

Doctor of Philosophy in Chemistry

University of California, Berkeley

Professor Alanna Schepartz, Chair

The ribosome is the most complex molecular machine known to man. It is an ancient behemoth, a twisted megadalton mass of RNA and protein, whose molecular motions underly the translation of the genetic code into language of proteins. Like a leviathan, that great mythological sea monster**,** the ribosome looms large as the central figure in the imagination of the cellular stew. Huge expenditures of energy are dedicated to its critical task: sequence-defined polymerization of proteins with remarkable speed and fidelity via amide-bond formation. Proteins, composed of combinations of a mere twenty-two α-amino acids, give rise to the myriad biological functions we ascribe to life. What if those polymers were instead composed of other monomers? What if the ribosome and its adjacent machinery could be convinced to catalyze other types of bonds, such as carbon-carbon (C-C) bonds? What functions and materials could follow from an expanded molecular repertoire?

The **first chapter** of this dissertation surveys a body of work surrounding the translation of noncanonical backbone monomers and formation of non-amide bonds by the ribosome. I explain the key technologies that enable a sequence-defined polymerization of unusual monomers and novel bond formation in the ribosome, while also exploring current challenges, such as C-C bond formation, and important applications of the field, such as peptide drug discovery.

In **Chapter 2,** I describe efforts towards C-C bond formation which include monomer synthesis, tRNA-acylation, and *in vitro* translation. In order to explore the fundamental features of acyl-transfers onto carbon nucleophiles, a chemical model system was developed an a series of monomers screened.

In **Chapter 3,** I provide an extended account of a chemical and ribosomal strategy for the synthesis of peptides bearing embedded heterocycles that support atropisomerism and macrocyclization. This includes the discovery of new carbonyl-containing monomers for

translation and chemistry for their transformation into diversified, atropisomeric, and macrocyclic peptides with embedded quinolines.

Table of Contents

Table of Contents ..... *i*

Acknowledgements ..... *iii*

Chapter 1: Ribosomal Catalysis of Unnatural Bonds *1*

Introduction **1**

Genetic Code Expansion *in vivo* **2**

Genetic Code Expansion *in vitro* **3**

tRNA acylation **4**

Middlemen: EF-Tu, EF-P, tRNA and other translation factors **5**

Ribosome **6**

Applications in peptide drug discovery **8**

References **9**

Chapter 2: Efforts Towards the Ribosomal Catalysis of Carbon-Carbon Bonds *21*

Introduction **21**

S-to-C acyl rearrangements **23**

Dicarbonyls **27**

Nitro-aldol aka Henry Reaction **28**

Cryo-EM of benzyl malonates in the ribosome **33**

Cryo-EM of β-nitro phenylalanine in the ribosome **35**

Systematic reappraisal of possible carbon nucleophiles **37**

Carbon acidities of potential ribosomal monomers **38**

Intramolecular model systems to test O-to-C acyl transfer reactions **38**

Intermolecular model systems to test X-to-C acyl transfer reactions **40**

Cyclic enamines for C-C bond formation **44**

In ribosome Friedlander reaction **44**

Conclusions **44**

References **45**

Supplemental Figures: calculated C-H acidities **48**

Materials and Methods **52**

Chapter 3: Chemo-ribosomal synthesis of atropisomeric and macrocyclic peptides with embedded quinolines *82*

Abstract **82**

Introduction **83**

Results **84**

Introduction of a reactive 1,3-dicarbonyl motif at the *N*-terminus via in vitro translation 84

Friedländer reactions of β-keto amides proceed readily under mild aqueous conditions 87

Post-translational Friedländer reactions of IVT products proceed under mild conditions 88

Friedländer reactions of β-keto amides generate stable atropisomers 89

Lewis acid catalysis of post-translational Friedländer reactions generates atropisomeric products 91

Friedländer macrocyclizations 92

Discussion **95**

References cited **97**

Supplemental Figures **105**

Supplemental References Cited **140**

Materials and methods **141**

Acknowledgements

Graduate school has been a truly formative and enjoyable experience and I have many people to thank for this. First and foremost, I must thank Alanna for her years of scientific guidance and steadfast support. These qualities were most appreciated in the early years of my scientific training, with the coincidences of the lab's recent move to Berkeley, the COVID lockdowns, and my personal journey with back problems. It is under Alanna's tutelage that I learned how to truly think scientifically, see the larger picture of a project, and interrogate every claim we make down to its minute foundations. Inevitably, I learned how to properly control my experiments and figured out how to present data in an intelligible fashion. Perhaps most importantly, I learned how to fail and how to fly on my own. I have an immense appreciation for the independence that students to pursue new projects or follow their interests. I treasure the countless subgroups, group meetings, and impromptu discussions we have shared and your never ending enthusiasm for our work. The Schepartz lab is a rigorous and generous environment to receive ones scientific training and I am lucky to have experienced it. I am also fortunate to have been a part of CGEM and to have benefited from excellent collaborations from the Cate lab (Jamie, Chandrima, Alexandra) and the Miller lab (Scott, Taylor, Diondra, Jacob).

I must also thank my first mentors in the lab, Tent, who taught me the delicacies of RNA work, and Josh, who was my first point of contact for general questions, big picture ideas, or new project ideas over the first few years in graduate school. Josh is also very funny, which I appreciated and miss. In the later years of graduate school, I have valued Carly for fielding countless questions on peptide synthesis miscellanea and mass spectrometry. I also want to extend my appreciation to all my mentees: Hannah, Cameron, Alex, and Thomas. Each of them did tremendous work and each taught me much about how to be a successful mentor in different ways. I trust Alex and Thomas will carry forth on CC bond, sulfonamide, and peptide macrocycle projects fearlessly and with much success.

Of course, I must also express my gratitude for all of my other cherished colleagues. Neville, Maddie, and Cameron, my fellow cohort-mates, I am proud of all our achievements and will miss you all greatly. To my additional close friends in lab (Noah, Leah, Dan, Izzi), I will miss everyone who I've spent countless hours with inside and outside of lab, getting coffee, having lunch in the concrete box that is the chem plaza, getting coffee, and going climbing. Graduate School in Berkeley has been full of excellent friendships outside of lab – Jake, Nate, Jack, Emma, Kerry, Alvaro, and Ethan. Our Wednesday night dinner party and our championship-winning frisbee team are some of my most cherished memories. I would also like to thank my close friend Sam for keeping me sane during COVID and understood across time.

Andrea, I thank for her tireless support and keeping life zesty, as well as her tributes to the gods that oversaw my experiments. Though none of the sacraments ever seemed to entail success, I still always appreciated the thought. I look forward to our future adventures.

Finally, I must express gratitude to my family for their endless support in my life and career regardless of where it heads. I'd like to thank my brother for encouraging in me a rich cultural and scientific mind, and my parents for providing models of compassion and comportment. I would also like to thank Mango, for his purrs.

Chapter 1: Ribosomal Catalysis of Unnatural Bonds

Introduction

Sequence-defined polymers are macromolecules of uniform length and precisely defined monomeric sequence. This class of molecules is scarcely accessible to modern synthetic polymer chemistry, yet the existence of living systems is contingent upon them. Sequence-definition endows molecules with massive structural and functional diversity through well-defined interactions of sidechains and backbones in 3D space. These interactions enable critical processes like oligonucleotide replication, protein folding, and enzymatic function. The most chemically competent species in modern biology, the protein, is a biopolymer composed of only twenty-two amino acids, and often with some post-translational modifications. Yet from only this small set of building blocks, all linked together through amide bonds, emerges a great capacity for biological activity.

The ribosome is the central figure in protein synthesis. During translation, it is able to perform sequence-defined polymerization of proteins or peptides with remarkable fidelity and speed in a template-directed fashion from an oligonucleotide code (mRNA). Genetic code expansion (GCE), the practice of recoding the cellular translation machinery to incorporate non-natural substrates into ribosomal polypeptides, has become a paradigmatic method for modulating protein function and manufacturing new therapeutics. To date, more than 300 unnatural monomers have been incorporated in polypeptide ribosomal products, evidencing the tolerance of the ribosome for exogenous monomers.

This expanded suite of monomers for ribosomal translation are composed of a few major categories: α-L amino acids with alternate side chains, D-amino acids, N-Methyl or N-substituted amino acids, alternative backbone lengths (α-, β-, γ-amino acids), or alternative nucleophile identities (non-amino nucleophiles such as hydroxy acids or thioacids). Alternative side chain monomers constitute the largest pool of successful monomers for GCE because the backbone architecture and chemistry catalyzed by the ribosome is synonymous with natural substrates. Every other category of monomer has posed significant challenges to GCE researchers, often requiring optimization at many points along in the translation machinery: monomer synthesis/stability, acylation onto tRNA, delivery to the ribosome, and ribosomal catalysis. Moreover, the ability to perform GCE on an expanded repertoire of monomers has been vastly emboldened by technological advances for *in vivo* GCE as well as a system to perform GCE *in vitro* (purified components of translation in a test tube).

I will briefly orient the reader on a few aspects of modern GCE with respect to the style (*in vivo* or *in vitro*), the critical components (tRNAs, EF-Tu and other translation factors, and the ribosome), before discussing the scope and purposes of monomers previously employed for unusual bond formation. It should be noted that GCE is a large area of research, and this introduction aims primarily to situate the reader with respect to unusual bond formation and less as a synopsis of the history and purview of the field as a whole.

Genetic Code Expansion *in vivo*

The application of GCE into living cells is work widely credited to the labs of Peter Schultz, who introduced orthogonal synthetases for stop codon recoding for site-specific recoding, and David Tirrel, who applied residue-specific replacement with auxotrophic organisms[1]. Significant work to develop GCE *in vivo*, in bacteria, yeast, and mammals has been reviewed elsewhere, with applications for expanded enzyme catalysis or therapeutic proteins. The vast majority of monomers for *in vivo* incorporation have utilized L-amino acids with modified sidechains.

Attempts to advance backbone modified monomers *in vivo* has generally been limited by the multi-parameter optimization required. In order to be incorporated into a protein, a given monomer must enter the organism, survive metabolism, be acylated by tRNA, survive tRNA proofreading, be a reasonable substrate for EF-Tu ternary complex formation, and be accepted by the ribosome at multiple positions(A-site, P-site, exit tunnel) through the series of mechanistic steps. For many non-α-amino monomers, each one of these steps can pose a significant challenge[2]. It has been widely understood that decoupling each of these requirements of translation *in vivo* would be highly desirable and enable more straightforward evolution of individual components of the system for new monomers.

Recently, two important contributions from the Chin[3] and the Chatterjee[4] labs have discovered ways to evolve tRNA synthetases on a monomer of interest using tRNA acylation as a readout. These methods provide a strategy to isolate a single step on the translational machinery for optimization. Amazingly, the Chin lab was able to show both an α-disubstituted and a β-amino acid were able to be incorporated with high efficiency after evolving their synthetases for acylation. The β amino acid was shown to be incorporated not only by mass spectrometry, but convincingly with a crystal structure. This strategy represents an important step, and provides a guiding principle, for the *in vivo* evolution of the translational apparatus for unusual monomers.

Other examples of the *in vivo* incorporation of non-α-amino monomers exist in the literature. Our lab was able to show that β-Phenylalanine could be incorporated into a protein *in vivo* utilizing a mutant ribosome dubbed P7A7 and residue-specific replacement[5]. The Schultz[6] and Yokoyama[7] labs were able to show that α-hydroxy tyrosine (*Mj*TyrRS-tRNA^{Tyr}) and α-hydroxy boc-lysine (PylRS–tRNA^{Pyl}) was capable of ester bond formation *in vivo*, respectively. Additional work to expand the substrate scope to include α-hydroxy-*m*-CF_3-Phenylalanine in proteins was performed in our lab[8], while the Chin lab showed that multiple hydroxy acids could be incorporated into macrocyclic peptides[9]. In a remarkable display of flexibility in the translational apparatus, our lab recently showed that β-hydroxy-acids could be incorporated into proteins[10]. This is a hallmark example of the substrate promiscuity of the translational machinery to accept extended backbone architectures and altered nucleophile identities.

Nonetheless, challenges of *in vivo* work substantially limit the substrate scope of monomers compared to *in vitro* translation systems. Many monomers and alternative chemistry shown to work *in vitro* cannot yet be recapitulated *in vivo*. Fascinating efforts to expand the scope of *in vivo* translation, or to improve the optimization are underway. Limiting metabolism, opening up space in the codon table, the discovery of new orthogonal tRNA/synthetase pairs,

the use of quadruplet codons, or the development of orthogonal ribosomes are examples of this work. The preeminent strategy to explore new chemistry for ribosomal translation has always been, and continues to be, with *in vitro* translation.

Genetic Code Expansion *in vitro*

In vitro translation (IVT) entails the use of purified translational components outside a cellular context. A few features of IVT make it a more tractable system to explore new chemistry in the ribosome. Most importantly, a fantastic variety of monomers can be acylated onto tRNAs outside of cells using chemical ligation, ribozymes, or synthetases, and then employed *in vitro*. Since the process of translating monomers begins with monomer acylation onto tRNAs, this first step is arguably the most crucial for monomer exploration. The diversity of monomers accessible for stable acylation *in vitro* vastly exceeds those accessible *in vivo*, and as a result, *in vitro* experiments can challenge the translational machinery to accept more monomers and catalyze different reaction much more effectively. For instance, *in vivo* translation has only yielded robust evidence for two examples of β-amino acids, a handful of examples of α-hydroxy acids, and one example of a β-hydroxy acid. Meanwhile, *in vitro* translation has been definitively evidenced for an impressive variety of monomers at internal positions, meaning these monomers can all act as nucleophiles and electrophiles. These include D-amino acids[11], N-methyl or N-substituted amino acids[12–14], alternative backbone lengths (β[15–19] or γ[18,20–22] amino acids), aminobenzoic acids[23,24], or alternative nucleophile identities (hydroxy acids[25,26], thioacids[27], hydrazine[28], and hydroxyamine[28]). The scope of altered electrophiles in translation (ie non-esters at the P-site) is significantly smaller, but the ribosomal synthesis of thioamides stands out as an example[29]. N-terminal incorporation of unusual monomers by reprogramming translation initiation has an even more expansive scope. Monomers for initiation need not be capable of nucleophilic attack and surprisingly large monomers can be accommodated, presumably because the ribosome assembles around them and their need only to fit into the exit tunnel.

The ability to acylate monomers of interest is compounded with the ability to isolate individual components of translation. This provides robust control over the conditions of translation. Issues of metabolism, nuclease- or protease-digestion, transport, product purification, and variable expression levels in the cell can all be circumvented. The complexity of the mixture can be reduced and the contribution of individual components can be more easily assessed in comparison to *in vivo* translation. For new and challenging monomers, it is possible to simultaneously reduce the competition from endogenous amino acids through exclusion and to employ forcing conditions to push certain monomers through translation with altered stoichiometry of important components. This had simultaneously lead to advances in the understanding of which components can be reengineered to improve the translation of various recalcitrant monomers. This includes the tRNA body, EF-Tu, and EF-P among others. In the following sections, I will describe important methods and findings related to tRNA acylation, translation factors, and ribosomal catalysis of unusual monomers.

tRNA acylation

For the acylation of unusual monomers onto tRNAs, there are four essential categories: synthetase acylation, ribozyme acylation with flexizyme, dinucleotide chemical acylation followed by RNA ligation, and full tRNA chemical acylation.

In nature, tRNAs are acylated with amino acids by aminoacyl tRNA synthetases. A great variety of unnatural monomers can also be installed using endogenous synthetases, or evolved variants thereof, including a number of β-amino acids and N-methyl amino acids[30,3132]. The use of orthogonal synthetases from other organisms or from rare amino acids (pyrrolysine or selenocysteine) are of particular note because they avoid crosstalk with the endogenous acylation machinery in a cell, or in the test tube with purified components. Orthogonal synthetases have been shown to accept a limited set of β-amino, α-hydroxy, α-thio, and N-formyl-α-amino, and α,α-disubstituted amino acids, as well as α-carboxy acid monomers[3,6–8]. Most examples listed above were found to be substrates for unevolved variants of synthetases, which has limited discovery to a few sidechain motifs. Synthetase evolution for new monomers has generally been challenging to achieve, because translation is used as a readout for screening, and non-α-amino substrates tend to be poor substrates for the rest of the translational apparatus. Yet the two strategies of translation-independent synthetase evolution mentioned above are sure to make the evolution of orthogonal synthetases a significantly more productive strategy for monomers with unusual architectures.

Arguably the most flexible and most widely employed strategy for genetic code expansion with unusual monomers *in vitro* is with flexizyme[33]. Flexizyme is a semi-catalytic ribozyme that was evolved to acylate tRNAs with a wide variety of activated esters. A number of different flexizymes with corresponding activating esters with different leaving groups exist. These include cyanomethyl esters (CME) for monomers that contain aromatic groups, dinitrobenzyl esters (DBE or DNB) for monomers which do not contain aromatics, chlorobenzyl thioesters (CBT) for modulating of the reactivity of nonaromatic monomers, and aminobenzyl thioester (ABT) for improving the aqueous solubility of nonaromatic monomers[34,35]. Importantly, the various flexizymes only recognize the CCA tail of the tRNA, which is highly conserved and therefor can acylate any given tRNA, or mini-tRNA mimic. They can even acylate GCCA oligos more efficiently than full tRNAs[36]. This overcomes one limitation of synthetases, that they are evolved for specific tRNA bodies. The flexibility of the tRNA substrate is matched by the flexibility of the monomer substrate for acylation. Flexizyme can generally provide reasonable acylation yields for all amino acid monomers, and are largely agnostic to sidechain identity. Unusual backbone monomers are also often substrates for flexizyme, although the rules for recognition and acylation are much less apparent. Work from our lab and the Jewett lab have explored some of the design principles for efficient flexizyme translation[37,38]. A few of the important features are similarity to Phenylalanine, upon which flexizyme was originally evolved, sufficient activation of the ester carbonyl with electron withdrawing groups, and a lack of steric bulk near the ester carbonyl. H-bonding interactions in the monomer also likely play a role in flexizyme recognition. Utilizing this technology, a huge number of exciting monomers have been acylated onto tRNAs and tested in translation. Internal incorporation has been evidenced for β- and γ-amino acids, various hydroxyl and thioacids, hydrazine, aminoxy, and aminobenzoic

acids[16,17,20,39–42]. Interestingly, thioamides have also been demonstrated in this fashion[29]. Translation initiation is known to be significantly more tolerant a wide variety of monomers, even some that are extremely large. Flexizyme has been used to initiation translation with the monomers for elongation but also large peptides, fluorophores, foldamers[24,43], and a huge diversity of other chemically reactive or conformationally fascinating groups. Flexizyme is extremely useful for acylating monomers *in vitro*, but its dramatic flexibility comes at a cost. It requires nonphysiological magnesium concentrations, utilizes a massive excess of monomer, and is generally employed stoichiometrically with tRNA. It can be used in up to only 20% DMSO concentration, which requires that monomers of interest be reasonable soluble in aqueous environments, thus limiting the monomer scope. Each acylation reaction must be independently performed and desalted before use in IVT, making the process somewhat arduous to employ compared to one-pot enzymatic acylation and IVT reactions. Flexizyme remains the gold standard for diverse unusual monomers, but the advances in synthetase discovery may soon challenge the dominance of flexizyme.

Chemical acylation involves the use of chemical reagents to install monomers of interest onto functional tRNA bodies. The first example of unnatural bond formation utilized a phenylalanine-acylated tRNA, which was ingeniously deaminated to yield the α-hydroxy phenylalanine-acylated tRNA which was polymerized by the ribosome[44]. Another popular and highly modular strategy for synthesizing tRNAs acylated from unnatural monomers was introduced by the Hecht lab. A small dinucleotide fragment could be chemically acylated at its 3'end using activated carboxylic acids, then the acylated fragment could be ligated with T4 RNA ligase to generate a full sized tRNA[45]. This method proved instrumental for a variety of early investigations on the limits of ribosomal catalysis, and amazingly, is still used today in mRNA display drug discovery efforts[46]. Because this method is more labor intensive than all other strategies for acylation, it should generally be taken up as the strategy of last resort.

A final strategy of acylation involves the direct acylation of tRNAs with an activated acyl group. The Schepartz lab used isatoic anhydride derivatives to acylate tRNAs with aminobenzoic acids[37], taking inspiration from reagents used to acylate 2'hydroxyl groups on RNA for structural characterization in Selective 2′ Hydroxyl Acylation analyzed by Primer Extension (SHAPE) assays. Because this strategy involves potentially polymerizing or acylating multiple 2'hydroxyls on the tRNA, conditions for acylation need to be somewhat optimized to avoid deleterious over-modification across the tRNA body. Chemical acylation on full tRNAs still has the potential for further progress, especially by taking inspiration from known acylation reagents for SHAPE. There may be further improvements for selectivity possible for chemical acylation at only the 2',3'-diol, potentially through the use of chemical catalysts or transition metals[47], though this method tends to still require the synthesis of activated amino acids and has gained less traction than other strategies.

Middlemen: EF-Tu, EF-P, tRNA and other translation factors

Other translation factors play critical roles in the efficiency of monomer incorporation in the ribosome. A few of these factors have received significant attention in recent years. EF-Tu is required for binding acylated tRNAs and shuttling them into the A-site. Binding of tRNAs to EF-

Tu must be sufficiently strong to enable EF-Tu to shuttle the acyl-tRNA into the ribosome, yet sufficiently weak to allow release of the tRNA into the A-site. EF-Tu and acyl-tRNA binding must achieve a thermodynamic Goldilocks zone, but this is complicated by the need to select for acylated-tRNAs over unacylated-tRNAs. EF-Tu selects for acylated tRNAs over unacylated tRNAs to avoid brining monomer-less tRNAs to the ribosome, and resultantly it engages in molecular recognition of the acylated amino acid itself, with key interactions on the α-amine but also with contributions from the sidechain. Each acylated amino acid has a different binding affinity to EF-Tu. In order to compensate for this, EF-Tu also engages in tRNA binding on the T-stem, and tRNAs that carry strong EF-Tu binders have T-stem sequences with weaker binding affinities for EF-Tu and vice versa. This principle of thermodynamic compensation between a given tRNA and amino acid was outlined in seminal work from the Uhlenbeck lab[48].

The requirement of achieving the Golidlocks zone with unusual monomers, where the amine is replaced by other substituents or the backbone architecture modified, presents a significant challenge to researchers. Work by our collaborators indicates that the ternary complex stability is dramatically reduced with β amino acids[49]. The Suga lab has also noted that the translation efficiency of tRNAs acylated with N-methyl amino acids is quite poor. To improve the translation efficiency of these monomers, they designed a series of chimeric tRNA bodies with T-stems of variable binding strength to EF-Tu and show that this can rescue translation yield[12]. Another route to achieve thermodynamic compensation is by redesigning or evolving EF-Tu, rather than editing the tRNA. The Suga lab has also engineered EF-Tu, termed EF-Sep to improve incorporation of negatively charged d-amino acids and N-methyl amino acids[13].

Another translation factor that has seen significant attention for unnatural amino acid incorporation is EF-P. EF-P plays an active role in translation initiation and in polyproline stretches. It enters the ribosome via E-site and binds to tRNA D-arm[50]. It is thought to aid in positioning the electrophile in the P-site for nucleophilic attack, while preventing mistranslocation and skipping by blocking the E-site exit channel for the P-site tRNA. Reengineering tRNAs to improve D-arm binding affinities for EF-P, by borrowing sequences from proline tRNAs, while increasing the concentration of EF-P in IVT reactions has been widely employed for a number of challenging to translate monomers for initiation and for elongation[24,51,52]. Other tRNA engineering efforts have been sought to improve translation[53], including anticodon arm mutations for β-amino acids[15].

Ribosome

The ribosome itself is the central character in translation. Its machinery matches tRNA anticodons with their respective mRNA codons on one end, while in its catalytic center, the peptidyl transferase center (PTC), it brings together monomers and stiches them together in a sequence defined fashion. While the exact energetic contributions of catalysis are still debated, at least a few general features can be established with respect to α-amino acids. (1) The ribosome functions as an “entropy trap”[54]. It excludes water, physically entraps monomers, and orients them for bond formation and elongation. This is the most powerful feature of ribosomal catalysis for unusual bond formation, because it is largely monomer-agnostic. The ribosome can

potentially bring many types of monomers into close proximity. In the parlance of chemistry, this is known as effective molarity, and is known to dramatically increase the rate of chemical reactions. (2) Ribosomal catalysis is enabled via an extended proton wire mechanism, which performs proton abstraction from the nucleophilic amine, activates the ester electrophile, stabilizes the tetrahedral intermediate, and hastens the withdraw of the 3'-oxygen leaving group by donating a proton[55]. Through the wire, it is thought that the proton abstracted from the amine, is ultimately donated back to the 3'-hydroxyl on the tRNA. (3) A key feature of ribosomal catalysis is that it is substrate-assisted catalysis, in that the tRNA themselves play a crucial role in the catalytic mechanism[56]. tRNAs fit into the ribosome to induces an active conformation through a series of base-pairing interactions, but even more crucially, the 2'-hydroxyl is an important member of the proton wire mechanism. The catalytic rate of translation is vastly diminished in the absence of this group. As a whole, the ribosome should be seen as remarkably flexible catalytic engine, as evidenced by the hundreds of monomers it can translate, yet one that is so delicately tuned to its role, that it resists most changes near its catalytic center.

Generally, the ribosome has been left untouched in experiments to expand the altered backbone monomer scope in translation. Nonetheless a few exceptions exist, including one purported ribosome evolved for D-amino acid incorporation[57], one purported ribosome for dipeptide incorporation[58], and ribosomes for β-amino acids[5,59]. These evolved ribosomes have shown significant defects in overall fitness or in assembly[60], and have not seen widespread adoption as a result. The high complexity of ribosomal function and universal sequence conservation of the ribosome PTC have proved challenging for evolutionary campaigns on new monomers. As the PTC is composed entirely of oligonucleotides, the mutability of this critical region is even more limited because of constraints in chemical space accessible to the four base pairs, as compared to the twenty amino acids of proteins. Nonetheless, borrowing ribosomal sequences from thermophilic archaea in regions adjacent to the PTC has proven effective to increasing the thermal stability of bacterial ribosomes[61]. Improved stability or long-range interactions to modulate the PTC the may impart important benefits for the translation of unusual monomers.

A wide literature exists around some of the other challenges of evolving ribosomes, namely the need to maintain cell viability by minimizing disruption to the remarkable fidelity of ribosomes. One prevailing aim is to design orthogonal ribosomes that can be evolved independently of the ribosomes required for cellular viability. These efforts are ongoing, and a number of reviews provide accounts on the status of the field[62–66].

While the PTC is highly resistant to mutation, the fact that ribosomal catalysis is substrate-assisted presents an opportunity to modulate catalysis by providing altered tRNAs. The replacement of the hydroxyl groups with other atoms, such as thiols, is an active area of research, for instance. Perhaps other more ambitious features, such as radical initiators, redox groups, transition metals, or photocatalysts could be introduced into tRNAs, if not the ribosome itself, to expand the toolbox of ribosomal translation.

Applications in peptide drug discovery

While long-term applications of ribosomal-mediated biopolymerization of sequence-defined polymers may reach into such wide applications as textiles, electronics, materials, and elsewhere in the fabric of modern society, the near-term applications of genetic code expansion are definitively in biotechnology and drug discovery[67,68]. The incorporation of non-proteinogenic monomers into proteins provide opportunities for new conformational arrangements[69], secondary structures[70], and novel functions, such as improved proteolytic stability[71], embedded drug-like features[72], or novel chemical reactivity[1,73]. These features have been widely explored with sidechain modified α amino acids to improve the stability of antibody-drug conjugates[74–76], to provide handles for biorthogonal modification of proteins[77–79], and to generate enzymes with improved or novel function through the introduction of noncanonical active site residues[67,80–83].

Yet undoubtably the most immediate and impactful application of genetic code expansion, especially for backbone-modified peptides, has been in the development of peptide drug development[84–89]. Peptides have proven to be a remarkable class of therapeutics, from the initial application of insulin, to hormone therapies, to the recent interest in GLP-1 agonists. Critically, peptides can be synthesized by the ribosome, which means that various platforms of biological display can be used for their discovery. This includes phage-display[90–92], ribosome-display[93], and mRNA-display[94–96]. These methods provide access to billion to multi-trillion member libraries for screening with a direct phenotype-genotype link. Methods for biological display in drug discovery have skyrocketed over the past twenty years and many major pharmaceutical companies now engage in some level of peptide drug discovery from biological display for lead discovery. A number of emergent clinical examples are a testament to this fact[97–100].

A key feature of many of these peptide therapeutics is macrocyclization. Peptides are an outstanding platform for generating macrocycles, which can then target traditionally undruggable protein surfaces with antibody like affinity and specificity, because of a reduced entropic penalty to binding[101–104]. Cyclization confers significant conformational restriction and reduces the molecular motion. If the macrocycle is well organized for binding a target it can exhibit truly exceptional affinity. Cyclic peptides from biological display regularly produce low nanomolar to picomolar binders for therapeutic targets.

Yet, historically, the application of peptides has been limited by low oral bioavailability, rapid clearance, proteolysis, and a lack of intracellular penetration[105–107]. A renaissance in interest in this category of drugs has opened new doors to thinking about means of improving the various physiochemical properties in which peptides are deficient[108].

The incorporation of unusual monomers presents opportunities for introducing chemical features that provide novel motifs for molecular recognition, reduce biodegradation/extend half-life, and improve deliverability. Improving biodegradation is often achieved by altering the backbone chemistry to include extended backbones or cyclic backbones to reduce proteolytic vulnerability. Molecular recognition capabilities are of course highly context dependent, but can be augmented by introducing new conformations or peptide folds, by introducing macrocyclization to limit entropic penalties to binding, and by introducing aromatic groups capable of strong molecular interactions with targets. Lipidation can be used to improve half-life by albumin binding[109,110]. To improve deliverability, monomers that improve lipophilicity such as

N-methyl amino acids, or monomers that encourage conformations with intramolecular H-bonds, in analogy to cyclosporin, can be used[12,46,111–119]. Improving molecular recognition can be achieved through the use of non-proteogenic motifs, these include various heterocycles or fluorination[99,120–122]. Many of these physiochemical properties can be simultaneously augmented with the introduction of unusual monomers. For instance, heterocycles, such as pyridine, provide lipophilicity for delivery, new molecular recognition capability through unique electrostatic interactions, and are likely to disrupt metabolism. Heterocycles for this reason are extremely common motifs in natural products (include peptide natural products) and pharmaceuticals[122,123].

By introducing more of these drug-like elements into the biological display, it is hoped that lead compounds can be generated with better physiochemical properties. Unusual monomers also have the capacity to improve these features directly during ribosomal synthesis, or to generate them post-translationally through chemical transformation[124–127]. This is an exciting prospect that I will explore further in Chapter 3.

References

1. Link, A. J., Mock, M. L. & Tirrell, D. A. Non-canonical amino acids in protein engineering. *Curr. Opin. Biotechnol.* **14**, 603–609 (2003).
2. Yamane, T., Miller, D. L. & Hopfield, J. J. Discrimination between D- and L-tyrosyl transfer ribonucleic acids in peptide chain elongation. *Biochemistry* **20**, 7059–7064 (1981).
3. Dunkelmann, D. L. *et al.* Adding α,α-disubstituted and β-linked monomers to the genetic code of an organism. *Nature* **625**, 603–610 (2024).
4. Soni, C. *et al.* A Translation-Independent Directed Evolution Strategy to Engineer Aminoacyl-tRNA Synthetases. *ACS Cent. Sci.* **10**, 1211–1220 (2024).
5. Melo Czekster, C., Robertson, W. E., Walker, A. S., Söll, D. & Schepartz, A. In Vivo Biosynthesis of a β-Amino Acid-Containing Protein. *J. Am. Chem. Soc.* **138**, 5194–5197 (2016).
6. Guo, J., Wang, J., Anderson, J. C. & Schultz, P. G. Addition of an α-hydroxy acid to the genetic code of bacteria. *Angew. Chem. - Int. Ed.* **47**, 722–725 (2008).
7. Kobayashi, T., Yanagisawa, T., Sakamoto, K. & Yokoyama, S. Recognition of Non-α-amino Substrates by Pyrrolysyl-tRNA Synthetase. *J. Mol. Biol.* **385**, 1352–1360 (2009).

8. Fricke, R. *et al.* Expanding the substrate scope of pyrrolysyl-transfer RNA synthetase enzymes to include non-α-amino acids in vitro and in vivo. *Nat. Chem.* **15**, 960–971 (2023).
9. Spinck, M. *et al.* Genetically programmed cell-based synthesis of non-natural peptide and depsipeptide macrocycles. *Nat. Chem.* **15**, 61–69 (2023).
10. Hamlish, N. X., Abramyan, A. M., Shah, B., Zhang, Z. & Schepartz, A. Incorporation of Multiple β2-Hydroxy Acids into a Protein In Vivo Using an Orthogonal Aminoacyl-tRNA Synthetase. *ACS Cent. Sci.* **10**, 1044–1053 (2024).
11. Achenbach, J. *et al.* Outwitting EF-Tu and the ribosome: translation with d-amino acids. *Nucleic Acids Res.* **43**, 5687–5698 (2015).
12. Iwane, Y., Kimura, H., Katoh, T. & Suga, H. Uniform affinity-tuning of N-methyl-aminoacyl-tRNAs to EF-Tu enhances their multiple incorporation. *Nucleic Acids Res.* (2021) doi:10.1093/nar/gkab288.
13. Katoh, T. & Suga, H. Ribosomal incorporation of negatively charged d-α- and N-methyl-l-α-amino acids enhanced by EF-Sep. *Philos. Trans. R. Soc. B Biol. Sci.* **378**, 20220038 (2023).
14. Kawakami, T., Murakami, H. & Suga, H. Ribosomal Synthesis of Polypeptoids and Peptoid−Peptide Hybrids. *J. Am. Chem. Soc.* **130**, 16861–16863 (2008).
15. Katoh, T. & Suga, H. Fine-tuning the tRNA anticodon arm for multiple/consecutive incorporations of β-amino acids and analogs. *Nucleic Acids Res.* **52**, 6586–6595 (2024).
16. Fujino, T., Goto, Y., Suga, H. & Murakami, H. Ribosomal Synthesis of Peptides with Multiple β-Amino Acids. *J. Am. Chem. Soc.* **138**, 1962–1969 (2016).
17. Adaligil, E., Song, A., Hallenbeck, K. K., Cunningham, C. N. & Fairbrother, W. J. Ribosomal Synthesis of Macrocyclic Peptides with β2- and β2,3-Homo-Amino Acids for the Development of Natural Product-Like Combinatorial Libraries. *ACS Chem. Biol.* **16**, 1011–1018 (2021).
18. Katoh, T. & Suga, H. Ribosomal Elongation of Cyclic γ-Amino Acids using a Reprogrammed Genetic Code. *J. Am. Chem. Soc.* **142**, 4965–4969 (2020).

19. Katoh, T., Sengoku, T., Hirata, K., Ogata, K. & Suga, H. Ribosomal synthesis and de novo discovery of bioactive foldamer peptides containing cyclic β-amino acids. *Nat. Chem.* 1–8 (2020) doi:10.1038/s41557-020-0525-1.
20. Adaligil, E., Song, A., Cunningham, C. N. & Fairbrother, W. J. Ribosomal Synthesis of Macrocyclic Peptides with Linear γ ^{4} - and β-Hydroxy-γ ^{4} -amino Acids. *ACS Chem. Biol.* acschembio.1c00292 (2021) doi:10.1021/acschembio.1c00292.
21. Ohshiro, Y. *et al.* Ribosomal Synthesis of Backbone-Macrocyclic Peptides Containing γ-Amino Acids. *ChemBioChem* **12**, 1183–1187 (2011).
22. Lee, J., Schwarz, K. J., Kim, D. S., Moore, J. S. & Jewett, M. C. Ribosome-mediated polymerization of long chain carbon and cyclic amino acids into peptides in vitro. *Nat. Commun.* **11**, 4304 (2020).
23. Katoh, T. & Suga, H. Ribosomal Elongation of Aminobenzoic Acid Derivatives. *J. Am. Chem. Soc.* jacs.0c05765 (2020) doi:10.1021/jacs.0c05765.
24. Katoh, T. & Suga, H. In Vitro Selection of Foldamer-Like Macrocyclic Peptides Containing 2-Aminobenzoic Acid and 3-Aminothiophene-2-Carboxylic Acid. *J. Am. Chem. Soc.* **144**, 2069–2072 (2022).
25. Kuroda, T., Huang, Y., Nishio, S., Goto, Y. & Suga, H. Post-translational backbone-acyl shift yields natural product-like peptides bearing hydroxyhydrocarbon units. *Nat. Chem.* **14**, 1413–1420 (2022).
26. Ohta, A., Murakami, H. & Suga, H. Polymerization of α-hydroxy acids by ribosomes. *Chembiochem Eur. J. Chem. Biol.* **9**, 2773–2778 (2008).
27. Takatsuji, R. *et al.* Ribosomal Synthesis of Backbone-Cyclic Peptides Compatible with In Vitro Display. *J. Am. Chem. Soc.* **141**, 2279–2287 (2019).
28. Katoh, T. & Suga, H. Consecutive Ribosomal Incorporation of α-Aminoxy/α-Hydrazino Acids with l/d-Configurations into Nascent Peptide Chains. *J. Am. Chem. Soc.* **143**, 18844–18848 (2021).

29. Maini, R. *et al.* Ribosomal Formation of Thioamide Bonds in Polypeptide Synthesis. *J. Am. Chem. Soc.* **141**, 20004–20008 (2019).
30. Hartman, M. C. T. Non-canonical Amino Acid Substrates of E. coli Aminoacyl-tRNA Synthetases. *ChemBioChem* **23**, e202100299 (2022).
31. Hartman, M. C. T., Josephson, K. & Szostak, J. W. Enzymatic aminoacylation of tRNA with unnatural amino acids. *Proc. Natl. Acad. Sci.* **103**, 4356–4361 (2006).
32. Crnković, A., Vargas-Rodriguez, O. & Söll, D. Plasticity and Constraints of tRNA Aminoacylation Define Directed Evolution of Aminoacyl-tRNA Synthetases. *Int. J. Mol. Sci.* **20**, 2294 (2019).
33. Goto, Y., Katoh, T. & Suga, H. Flexizymes for genetic code reprogramming. *Nat. Protoc.* **6**, 779–790 (2011).
34. Katoh, T., Goto, Y., Passioura, T. & Suga, H. Development of Flexizyme Aminoacylation Ribozymes and Their Applications. in *Ribozymes* 519–543 (John Wiley & Sons, Ltd, 2021). doi:10.1002/9783527814527.ch20.
35. Morimoto, J., Hayashi, Y., Iwasaki, K. & Suga, H. Flexizymes: Their Evolutionary History and the Origin of Catalytic Function. *Acc. Chem. Res.* **44**, 1359–1368 (2011).
36. Fujino, T., Kondo, T., Suga, H. & Murakami, H. Exploring the Minimal RNA Substrate of Flexizymes. *ChemBioChem* **20**, 1959–1965 (2019).
37. Ad, O. *et al.* Translation of Diverse Aramid- and 1,3-Dicarbonyl-peptides by Wild Type Ribosomes *in Vitro*. *ACS Cent. Sci.* **5**, 1289–1294 (2019).
38. Lee, J. *et al.* Expanding the limits of the second genetic code with ribozymes. *Nat. Commun.* **10**, 5097 (2019).
39. Iskandar, S. E., Haberman, V. A. & Bowers, A. A. Expanding the Chemical Diversity of Genetically Encoded Libraries. *ACS Comb. Sci.* **22**, 712–733 (2020).
40. Dengler, S. *et al.* Display Selection of a Hybrid Foldamer–Peptide Macrocycle. *Angew. Chem. Int. Ed.* **62**, e202308408 (2023).

41. Hirose, H., Tsiamantas, C., Katoh, T. & Suga, H. In vitro expression of genetically encoded non-standard peptides consisting of exotic amino acid building blocks. *Curr. Opin. Biotechnol.* **58**, 28–36 (2019).
42. Katoh, T. & Suga, H. In Vitro Genetic Code Reprogramming for the Expansion of Usable Noncanonical Amino Acids. *Annu. Rev. Biochem.* **91**, 221–243 (2022).
43. Goto, Y. *et al.* Reprogramming the Translation Initiation for the Synthesis of Physiologically Stable Cyclic Peptides. *ACS Chem. Biol.* **3**, 120–129 (2008).
44. Fahnestock, S. & Rich, A. Ribosome-Catalyzed Polyester Formation. *Science* **173**, 340–343 (1971).
45. Heckler, T. G. *et al.* T4 RNA ligase mediated preparation of novel 'chemically misacylated' tRNAPhes. *Biochemistry* **23**, 1468–1473 (1984).
46. Ohta, A. *et al.* Validation of a New Methodology to Create Oral Drugs beyond the Rule of 5 for Intracellular Tough Targets. *J. Am. Chem. Soc.* (2023) doi:10.1021/jacs.3c07145.
47. Duffy, N. H. & Dougherty, D. A. Preparation of Translationally Competent tRNA by Direct Chemical Acylation. *Org. Lett.* **12**, 3776–3779 (2010).
48. LaRiviere, F. J., Wolfson, A. D. & Uhlenbeck, O. C. Uniform Binding of Aminoacyl-tRNAs to Elongation Factor Tu by Thermodynamic Compensation. *Science* **294**, 165–168 (2001).
49. β-Amino Acids Reduce Ternary Complex Stability and Alter the Translation Elongation Mechanism | ACS Central Science. https://pubs.acs.org/doi/10.1021/acscentsci.4c00314.
50. Katoh, T., Wohlgemuth, I., Nagano, M., Rodnina, M. V. & Suga, H. Essential structural elements in tRNAPro for EF-P-mediated alleviation of translation stalling. *Nat. Commun.* **7**, 11657 (2016).
51. Katoh, T. & Suga, H. Translation initiation with exotic amino acids using EF-P-responsive artificial initiator tRNA. *Nucleic Acids Res.* gkad496 (2023) doi:10.1093/nar/gkad496.
52. Tajima, K., Katoh, T. & Suga, H. Drop-off-reinitiation triggered by EF-G-driven mistranslocation and its alleviation by EF-P. *Nucleic Acids Res.* **50**, 2736–2753 (2022).

53. Albers, S. *et al.* Repurposing tRNAs for nonsense suppression. *Nat. Commun.* **12**, 3850 (2021).
54. Sievers, A., Beringer, M., Rodnina, M. V. & Wolfenden, R. The ribosome as an entropy trap. *Proc. Natl. Acad. Sci. U. S. A.* **101**, 7897–7901 (2004).
55. Polikanov, Y. S., Steitz, T. A. & Innis, C. A. A proton wire to couple aminoacyl-tRNA accommodation and peptide-bond formation on the ribosome. *Nat. Struct. Mol. Biol.* **21**, 787–793 (2014).
56. Weinger, J. S., Parnell, K. M., Dorner, S., Green, R. & Strobel, S. A. Substrate-assisted catalysis of peptide bond formation by the ribosome. *Nat. Struct. Mol. Biol.* **11**, 1101–1106 (2004).
57. Dedkova, L. M., Fahmi, N. E., Golovine, S. Y. & Hecht, S. M. Construction of Modified Ribosomes for Incorporation of d-Amino Acids into Proteins. *Biochemistry* **45**, 15541–15551 (2006).
58. Maini, R. *et al.* Ribosome-Mediated Incorporation of Dipeptides and Dipeptide Analogues into Proteins in Vitro. *J. Am. Chem. Soc.* **137**, 11206–11209 (2015).
59. Maini, R. *et al.* Protein Synthesis with Ribosomes Selected for the Incorporation of β-Amino Acids. *Biochemistry* **54**, 3694–3706 (2015).
60. Ward, F. R., Watson, Z. L., Ad, O., Schepartz, A. & Cate, J. H. D. Defects in the Assembly of Ribosomes Selected for β-Amino Acid Incorporation. *Biochemistry* **58**, 4494–4504 (2019).
61. Nissley, A. J., Penev, P. I., Watson, Z. L., Banfield, J. F. & Cate, J. H. D. Rare ribosomal RNA sequences from archaea stabilize the bacterial ribosome. *Nucleic Acids Res.* gkac1273 (2023) doi:10.1093/nar/gkac1273.
62. Chin, J. W. Expanding and reprogramming the genetic code. *Nature* **550**, 53–60 (2017).
63. de la Torre, D. & Chin, J. W. Reprogramming the genetic code. *Nat. Rev. Genet.* 1–16 (2020) doi:10.1038/s41576-020-00307-7.

64. Arranz-Gibert, P., Patel, J. R. & Isaacs, F. J. The Role of Orthogonality in Genetic Code Expansion. *Life* **9**, 58 (2019).
65. Aleksashin, N. A. *et al.* A fully orthogonal system for protein synthesis in bacterial cells. *Nat. Commun.* **11**, 1858 (2020).
66. Liu, Y., Kim, D. S. & Jewett, M. C. Repurposing ribosomes for synthetic biology. *Curr. Opin. Chem. Biol.* **40**, 87–94 (2017).
67. Huang, Y. & Liu, T. Therapeutic applications of genetic code expansion. *Synth. Syst. Biotechnol.* **3**, 150–158 (2018).
68. Wang, T. *et al.* Engineering the Translational Machinery for Biotechnology Applications. *Mol. Biotechnol.* **62**, 219–227 (2020).
69. Mortenson, D. E. *et al.* Evaluation of β-Amino Acid Replacements in Protein Loops: Effects on Conformational Stability and Structure. *ChemBioChem* **19**, 604–612 (2018).
70. Daniels, D. S., Petersson, E. J., Qiu, J. X. & Schepartz, A. High-Resolution Structure of a β-Peptide Bundle. *J. Am. Chem. Soc.* **129**, 1532–1533 (2007).
71. Goettig, P., Koch, N. G. & Budisa, N. Non-Canonical Amino Acids in Analyses of Protease Structure and Function. *Int. J. Mol. Sci.* **24**, 14035 (2023).
72. Hickey, J. L., Sindhikara, D., Zultanski, S. L. & Schultz, D. M. Beyond 20 in the 21st Century: Prospects and Challenges of Non-canonical Amino Acids in Peptide Drug Discovery. *ACS Med. Chem. Lett.* (2023) doi:10.1021/acsmedchemlett.3c00037.
73. Birch-Price, Z., Hardy, F. J., Lister, T. M., Kohn, A. R. & Green, A. P. Noncanonical Amino Acids in Biocatalysis. *Chem. Rev.* **124**, 8740–8786 (2024).
74. Oller-Salvia, B., Kym, G. & Chin, J. W. Rapid and Efficient Generation of Stable Antibody–Drug Conjugates via an Encoded Cyclopropene and an Inverse-Electron-Demand Diels–Alder Reaction. *Angew. Chem. Int. Ed.* **57**, 2831–2834 (2018).
75. Axup, J. Y. *et al.* Synthesis of site-specific antibody-drug conjugates using unnatural amino acids. *Proc. Natl. Acad. Sci.* **109**, 16101–16106 (2012).

76. Agarwal, P. & Bertozzi, C. R. Site-Specific Antibody–Drug Conjugates: The Nexus of Bioorthogonal Chemistry, Protein Engineering, and Drug Development. *Bioconjug. Chem.* **26**, 176–192 (2015).
77. Lang, K. *et al.* Genetically encoded norbornene directs site-specific cellular protein labelling via a rapid bioorthogonal reaction. *Nat. Chem.* **4**, 298–304 (2012).
78. Tamshen, K., Wang, Y., Jamieson, S. M. F., Perry, J. K. & Maynard, H. D. Genetic Code Expansion Enables Site-Specific PEGylation of a Human Growth Hormone Receptor Antagonist through Click Chemistry. *Bioconjug. Chem.* **31**, 2179–2190 (2020).
79. Wang, Y. *et al.* Noncanonical amino acids as doubly bio-orthogonal handles for one-pot preparation of protein multiconjugates. *Nat. Commun.* **14**, 974 (2023).
80. Davis, L. & Chin, J. W. Designer proteins: applications of genetic code expansion in cell biology. *Nat. Rev. Mol. Cell Biol.* **13**, 168–182 (2012).
81. Manandhar, M., Chun, E. & Romesberg, F. E. Genetic Code Expansion: Inception, Development, Commercialization. *J. Am. Chem. Soc.* jacs.0c11938 (2021) doi:10.1021/jacs.0c11938.
82. Shandell, M. A., Tan, Z. & Cornish, V. W. Genetic Code Expansion: A Brief History and Perspective. *Biochemistry* **60**, 3455–3469 (2021).
83. White, M. F. M. & Wallace, S. A New PETase from the Human Saliva Metagenome and Its Functional Modification via Genetic Code Expansion in Bacteria. *Angew. Chem. Int. Ed.* **62**, e202216963 (2023).
84. Cabrele, C., Martinek, T. A., Reiser, O. & Berlicki, Ł. Peptides Containing β-Amino Acid Patterns: Challenges and Successes in Medicinal Chemistry. *J. Med. Chem.* **57**, 9718–9739 (2014).
85. Chan, A. I. *et al.* Evaluating Translational Efficiency of Noncanonical Amino Acids to Inform the Design of Druglike Peptide Libraries. *ACS Chem. Biol.* **18**, 81–90 (2023).

86. Craik, D. J., Fairlie, D. P., Liras, S. & Price, D. The Future of Peptide-based Drugs. *Chem. Biol. Drug Des.* **81**, 136–147 (2013).

87. Drucker, D. J. Advances in oral peptide therapeutics. *Nat. Rev. Drug Discov.* **19**, 277–289 (2020).

88. Fosgerau, K. & Hoffmann, T. Peptide therapeutics: current status and future directions. *Drug Discov. Today* **20**, 122–128 (2015).

89. Wang, L. *et al.* Therapeutic peptides: current applications and future directions. *Signal Transduct. Target. Ther.* **7**, 1–27 (2022).

90. Oppewal, T. R., Jansen, I. D., Hekelaar, J. & Mayer, C. A Strategy to Select Macrocyclic Peptides Featuring Asymmetric Molecular Scaffolds as Cyclization Units by Phage Display. *J. Am. Chem. Soc.* (2022) doi:10.1021/jacs.1c12822.

91. Ekanayake, A. I. *et al.* Genetically Encoded Fragment-Based Discovery from Phage-Displayed Macrocyclic Libraries with Genetically Encoded Unnatural Pharmacophores. *J. Am. Chem. Soc.* **143**, 5497–5507 (2021).

92. Oller-Salvia, B. & Chin, J. W. Efficient Phage Display with Multiple Distinct Non-Canonical Amino Acids Using Orthogonal Ribosome-Mediated Genetic Code Expansion. *Angew. Chem. Int. Ed.* **58**, 10844–10848 (2019).

93. Zahnd, C., Amstutz, P. & Plückthun, A. Ribosome display: selecting and evolving proteins in vitro that specifically bind to a target. *Nat. Methods* **4**, 269–279 (2007).

94. Iskandar, S. E. *et al.* Identification of Covalent Cyclic Peptide Inhibitors in mRNA Display. *J. Am. Chem. Soc.* **145**, 15065–15070 (2023).

95. Fleming, M. C., Bowler, M. M., Park, R., Popov, K. I. & Bowers, A. A. Tyrosinase-Catalyzed Peptide Macrocyclization for mRNA Display. *J. Am. Chem. Soc.* **145**, 10445–10450 (2023).

96. Melsen, P. R. A., Yoshisada, R. & Jongkees, S. A. K. Opportunities for Expanding Encoded Chemical Diversification and Improving Hit Enrichment in mRNA-Displayed Peptide Libraries. *ChemBioChem* **23**, e202100685 (2022).

97. Mudd, G. E. *et al.* Discovery of BT8009: A Nectin-4 Targeting Bicycle Toxin Conjugate for the Treatment of Cancer. *J. Med. Chem.* **65**, 14337–14347 (2022).

98. Alleyne, C. *et al.* Series of Novel and Highly Potent Cyclic Peptide PCSK9 Inhibitors Derived from an mRNA Display Screen and Optimized via Structure-Based Design. *J. Med. Chem.* **63**, 13796–13824 (2020).

99. Tucker, T. J. *et al.* A Series of Novel, Highly Potent, and Orally Bioavailable Next-Generation Tricyclic Peptide PCSK9 Inhibitors. *J. Med. Chem.* **64**, 16770–16800 (2021).

100. Ballantyne, C. M. *et al.* Phase 2b Randomized Trial of the Oral PCSK9 Inhibitor MK-0616. *J. Am. Coll. Cardiol.* **81**, 1553–1564 (2023).

101. Bechtler, C. & Lamers, C. Macrocyclization strategies for cyclic peptides and peptidomimetics. *RSC Med. Chem.* **12**, 1325–1351 (2021).

102. He, J., Ghosh, P. & Nitsche, C. Biocompatible strategies for peptide macrocyclisation. *Chem. Sci.* **15**, 2300–2322 (2024).

103. Costa, L., Sousa, E. & Fernandes, C. Cyclic Peptides in Pipeline: What Future for These Great Molecules? *Pharmaceuticals* **16**, 996 (2023).

104. Damjanovic, J., Miao, J., Huang, H. & Lin, Y.-S. Elucidating Solution Structures of Cyclic Peptides Using Molecular Dynamics Simulations. *Chem. Rev.* **121**, 2292–2324 (2021).

105. Lamers, C. Overcoming the Shortcomings of Peptide-Based Therapeutics. *Future Drug Discov.* **4**, FDD75 (2022).

106. Tran, H. & ElSayed, M. E. H. Progress and limitations of oral peptide delivery as a potentially transformative therapy. *Expert Opin. Drug Deliv.* **19**, 163–178 (2022).

107. Kaspar, A. A. & Reichert, J. M. Future directions for peptide therapeutics development. *Drug Discov. Today* **18**, 807–817 (2013).

108. Sawyer, T. K. CHAPTER 1. Renaissance in Peptide Drug Discovery: The Third Wave. in *Drug Discovery* (ed. Srivastava, V.) 1–34 (Royal Society of Chemistry, Cambridge, 2017). doi:10.1039/9781788011532-00001.

109. Kowalczyk, R., Harris, P. W. R., Williams, G. M., Yang, S.-H. & Brimble, M. A. Peptide Lipidation – A Synthetic Strategy to Afford Peptide Based Therapeutics. *Pept. Pept.-Based Biomater. Their Biomed. Appl.* **1030**, 185–227 (2017).

110. Protein Lipidation: Occurrence, Mechanisms, Biological Functions, and Enabling Technologies | Chemical Reviews. https://pubs.acs.org/doi/10.1021/acs.chemrev.6b00750.

111. Bockus, A. T. *et al.* Probing the Physicochemical Boundaries of Cell Permeability and Oral Bioavailability in Lipophilic Macrocycles Inspired by Natural Products. *J. Med. Chem.* **58**, 4581–4589 (2015).

112. Rezai, T. *et al.* Conformational Flexibility, Internal Hydrogen Bonding, and Passive Membrane Permeability: Successful in Silico Prediction of the Relative Permeabilities of Cyclic Peptides. *J. Am. Chem. Soc.* **128**, 14073–14080 (2006).

113. Tamura, T. *et al.* Chemical Synthesis and Cell-Free Expression of Thiazoline Ring-Bridged Cyclic Peptides and Their Properties on Biomembrane Permeability. *Bull. Chem. Soc. Jpn.* (2022) doi:10.1246/bcsj.20210409.

114. Rossi Sebastiano, M. *et al.* Impact of Dynamically Exposed Polarity on Permeability and Solubility of Chameleonic Drugs Beyond the Rule of 5. *J. Med. Chem.* **61**, 4189–4202 (2018).

115. Chen, H., Katoh, T. & Suga, H. Macrocyclic Peptides Closed by a Thioether–Bipyridyl Unit That Grants Cell Membrane Permeability. *ACS Bio Med Chem Au* (2023) doi:10.1021/acsbiomedchemau.3c00027.

116. Schwochert, J. *et al.* Peptide to Peptoid Substitutions Increase Cell Permeability in Cyclic Hexapeptides. *Org. Lett.* **17**, 2928–2931 (2015).

117. Zhang, C., Chen, S., Fu, X., Dedkova, L. M. & Hecht, S. M. Enhancement of N-Methyl Amino Acid Incorporation into Proteins and Peptides Using Modified Bacterial Ribosomes and Elongation Factor P. *ACS Chem. Biol.* **19**, 1330–1338 (2024).

118. van Neer, R. H. P. *et al.* Serum-Stable and Selective Backbone-N-Methylated Cyclic Peptides That Inhibit Prokaryotic Glycolytic Mutases. *ACS Chem. Biol.* (2022) doi:10.1021/acschembio.2c00403.

119. Merz, M. L. *et al.* De novo development of small cyclic peptides that are orally bioavailable. *Nat. Chem. Biol.* 1–10 (2023) doi:10.1038/s41589-023-01496-y.

120. Saunders, G. J. & Yudin, A. K. Property-Driven Development of Passively Permeable Macrocyclic Scaffolds Using Heterocycles**. *Angew. Chem. Int. Ed.* **61**, e202206866 (2022).

121. Walsh, C. T. & Nolan, E. M. Morphing peptide backbones into heterocycles. *Proc. Natl. Acad. Sci.* **105**, 5655–5656 (2008).

122. Marshall, C. M., Federice, J. G., Bell, C. N., Cox, P. B. & Njardarson, J. T. An Update on the Nitrogen Heterocycle Compositions and Properties of U.S. FDA-Approved Pharmaceuticals (2013–2023). *J. Med. Chem.* **67**, 11622–11655 (2024).

123. Gomtsyan, A. Heterocycles in drugs and drug discovery. *Chem. Heterocycl. Compd.* **48**, 7–10 (2012).

124. Iskandar, S. E. *et al.* Enabling Genetic Code Expansion and Peptide Macrocyclization in mRNA Display via a Promiscuous Orthogonal Aminoacyl-tRNA Synthetase. *J. Am. Chem. Soc.* **145**, 1512–1517 (2023).

125. Liu, M. *et al.* Selective thiazoline peptide cyclisation compatible with mRNA display and efficient synthesis. *Chem. Sci.* (2023) doi:10.1039/D3SC03117A.

126. Huang, Y., Wiedmann, M. M. & Suga, H. RNA Display Methods for the Discovery of Bioactive Macrocycles. *Chem. Rev.* **119**, 10360–10391 (2019).

127. Vinogradov, A. A. *et al.* De Novo Discovery of Thiopeptide Pseudo-natural Products Acting as Potent and Selective TNIK Kinase Inhibitors. *J. Am. Chem. Soc.* **144**, 20332–20341 (2022).

Chapter 2: Efforts Towards the Ribosomal Catalysis of Carbon-Carbon Bonds

Introduction

Efforts in genetic code expansion have shown that the ribosome is capable of catalyzing acyl-transfer reactions for a variety of nucleophiles. These result in the formation of N-C (amide), O-C(ester), and S-C (thioester) bonds, where the C is the carbon on the carbonyl. Missing from this repertoire are C-C bonds. One of the holy grails in genetic code expansion is to expand the capacity of the ribosome to generate C-C bonds. In the following chapter I will outline my efforts to find carbon nucleophiles that might be amenable for ribosomal C-C bond formation. First, I will explore some of the precedent and considerations related to C-C bond formation.

C-C bonds are one of the fundamental atomic arrangements in organic chemistry, yet C-C bond chemistry is notoriously challenging from the synthetic chemist's perspective. Generation of active carbon nucleophiles in the form of carbanions or carbenes often requires transition metal catalysis, radical initiators, or the use of powerful bases to abstract protons from extremely basic carbon protons. Additionally reactive carbons tend to be short-lived and unstable. The generation of requisite carbon nucleophiles for ester or ester-type electrophiles used by the ribosome under biomimetic conditions has proved quite challenging, yet a few examples do exist[1,2].

In nature, a huge number of strategies are employed to build this fundamental framework[3]. The most common class of C-C bond forming enzymes are aldolases, which function via two separate mechanisms. They either employ enamine (Class 1) or Zn^{2+} (Class 2) catalysis to couple together two activated carbonyl species, mainly aldehydes[4]. Thiamine-dependent enzymes catalyze another major class of C-C bond reactions through umpolung chemistry via the famous Breslow intermediate. Extensive reviews of C-C bond enzymes, including other classes such as SAM-dependent methyltransferases, can be found elsewhere[5]. It should be noted that the vast majority of C-C bond biocatalysis is performed on aldehydes as the electrophile, and in some cases on activated ketones. Amazingly, a ribozyme has even been evolved to catalyze aldol reactions using Zn^{2+}, showing that oligonucleotides are capable of catalyzing these types of reactions[6]. Few if any C-C bond reactions are performed on esters as the electrophile. Yet, thioesters, do feature prominently as C-C bond electrophiles in the case of polyketide synthesis. The order of carbonyl activation for these species is: aldehyde > ketone > thioester > ester. Perhaps reactions that utilize thioester electrophiles are a better inspiration for ribosomal C-C bonds.

Polyketide synthesis has been a major inspiration for our efforts towards C-C bond synthesis in the ribosome. Polyketide and fatty acid synthesis employ decarboxylative Claisen reactions from half-malonic thioesters. In this case, decarboxylation yields a reactive thioester

enolate which reacts with an adjacent thioester carbonyl electrophile, kicking off the thiol to yield a ketone-methylene (ketide) linkage[7].

Polyketide synthesis has a number of parallels with ribosomal synthesis, in that it builds sequence defined polymers from monomers linked via ester-like bonds. The requirement for monomers to be shuttled via other biomolecules during polymerization, either by tRNA for the ribosomal synthesis via ester bonds or acyl carrier proteins/CoA for polyketide synthesis via thioester bonds, imparts a unique constraint on the consideration of electrophiles for C-C bond formation in the ribosome. The reaction to generate C-C bonds must simultaneously cleave the bond which links the monomer to the tRNA. For this reason, the chemical space that can be explored for electrophiles is quite limited. Indeed, our efforts have only ever considered esters or more recently, thioesters. There may be opportunities for considering other alternative polymerization chemistries in the ribosome that simultaneously release the tRNA.

In the world of organic chemistry, aldol additions are likely the most common and simplest method of C-C bond formation. A variant of aldol additions, known as the Claisen condensation, is an aldol reaction utilizing esters as the nucleophile and the electrophile. Use of esters as electrophiles draws a direct comparison to ribosomal chemistry, and inspired many of our attempts that follow in this chapter. Yet the requisite activation of ester as a nucleophile, via an enolate intermediate, requires strong basic conditions. In our case, with a limited ability to modulate the active site of the ribosome, we sought other methods of lowering the barrier to enolate formation. Predominantly, this involved the substitution of monomers with strong electron withdrawing moieties to lower the pKa of the carbon acid to generate a nucleophilic carbanion. We also increased the scope of anion formation beyond enolates to include other stabilized carbanions, such as nitronates. In essence, we aimed to synthesize simple carbanion nucleophiles that could exist in biological conditions, without the need of transition metal catalysts or cofactors. **It was hypothesized that the ribosome could continue to provide significant catalytic benefit by entropically trapping the nucleophile and electrophile in the PTC, desolvating them, and activating the electrophilic carbonyl ester, while we could synthesize nucleophilic monomers that would encourage carbanion generation at biological pH and induce a productive fit within the PTC to preorganize an S_N2 type reaction.**

In the following chapter, I will outline efforts towards C-C bond formation in the ribosome using IVT. Our initial attempts included a sidechain-to backbone S-to-C acyl transfer mimicing the chemistry of polyketides. This is followed by more direct ribosomally catalyzed C-C bond formation. Requisite carbon nucleophilicity was provided by malonate, dicarbonyl, nitro-alkyl, and nitrile monomers. The position of the nucleophilic carbon and the impact of sidechain substituents were also tested. Cryo-EM provided structural data to guide design efforts, while computational simulations were explored to provide added dynamic understanding of monomer fit. pKa calculations were also employed to determine the deprotonation ability of monomers of interest. A small molecule model system was generated in order to test the reactivity of many carbon nucleophile monomers against carbonyl electrophiles of varied strength, given the surprising realization that the literature was lacking much information of the relevant chemistry. In the process, we also gleaned many lessons about monomer acylation, peptide design and purification for analysis, and other considerations in IVT. While, at the end of my tenure as a graduate student, we have yet to achieve ribosomal C-C bond formation, we do have some interesting leads and avenues for further exploration.

S-to-C acyl rearrangements

Our lab previously showed that protected malonic acids were substrates for tRNA acylation by flexizyme and ribosomal initiation[8]. The effort to incorporate malonates into the ribosome was in service to the possibility of bridging the chemistry of polyketides with that of peptides and proteins. If activated malonates could enter the ribosome and undergo a well-timed decarboxylation to form reactive enolates, they might be able to perform Claisen condensations to elongate the polymer and simultaneously form 1,3-dicarbonyls (Fig 2.1). Unfortunately, free carboxylate malonic acids were not substrates for flexizyme, following a general understanding that negatively charged sidechains perform quite poorly. Without a means of acylating deprotected malonates, we sought other means to introduce polyketide-like chemistry into the ribosome. The first of these attempts, tested in close collaboration with the Miller lab at Yale, sought to introduce an α-thiol monomer with a protected malonate on the sidechain (Figure 2.2). A-thio monomers have recently been shown to be substrates for the ribosome to generate thioester backbones in peptides[9]. If this monomer could be acylated, it could be incorporated by the ribosome as a thioester backbone. Upon unmasking of the malonate sidechain, we presumed it could undergo an intramolecular decarboxylative Claisen reaction, with the enolate attacking the backbone thioester, to yield an S-to-C acyl transfer and effectively installing a 1,3-dicarbonyl in the backbone of via C-C bond formation. This strategy can be seen as a synthesis of the mechanisms involved in native chemical ligation and of polyketide synthesis (Figure 2.3).

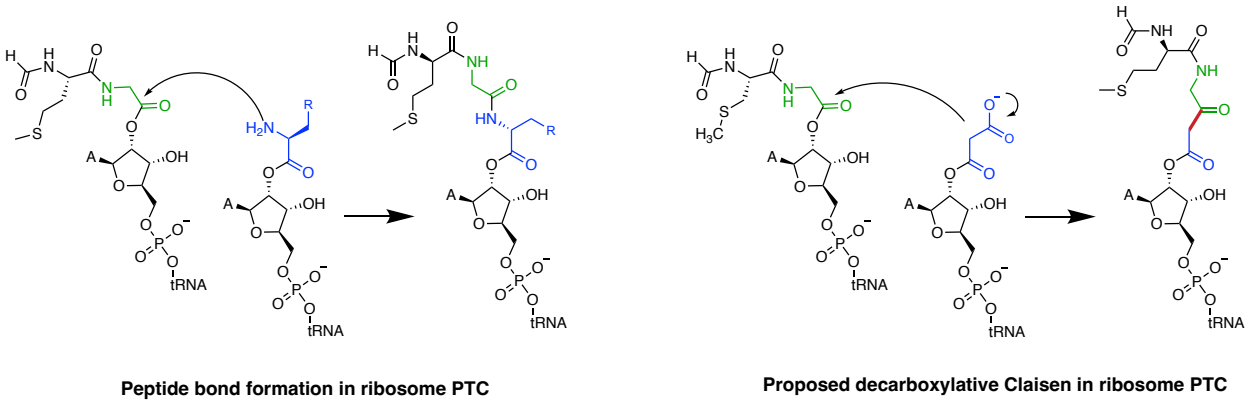


Figure 2.1. Comparing peptide bond formation with the proposed decarboxylative Claisen pathway.

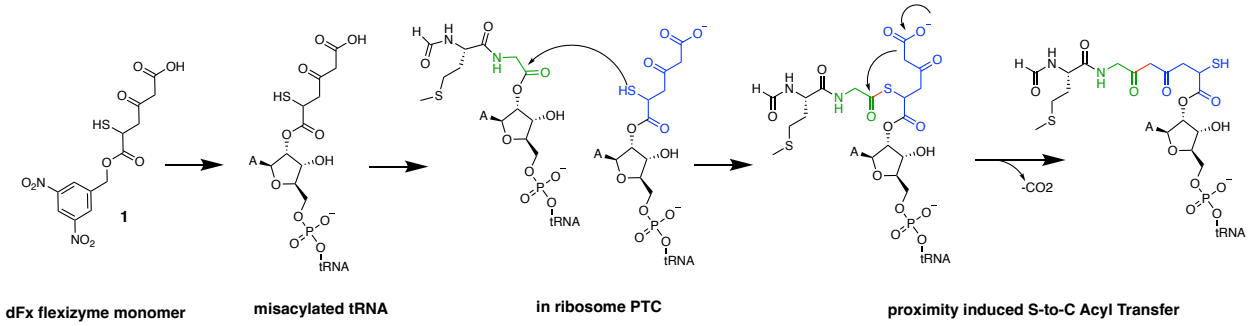


Figure 2.2. Workflow for S-to-C acyl transfer and backbone rearrangement.

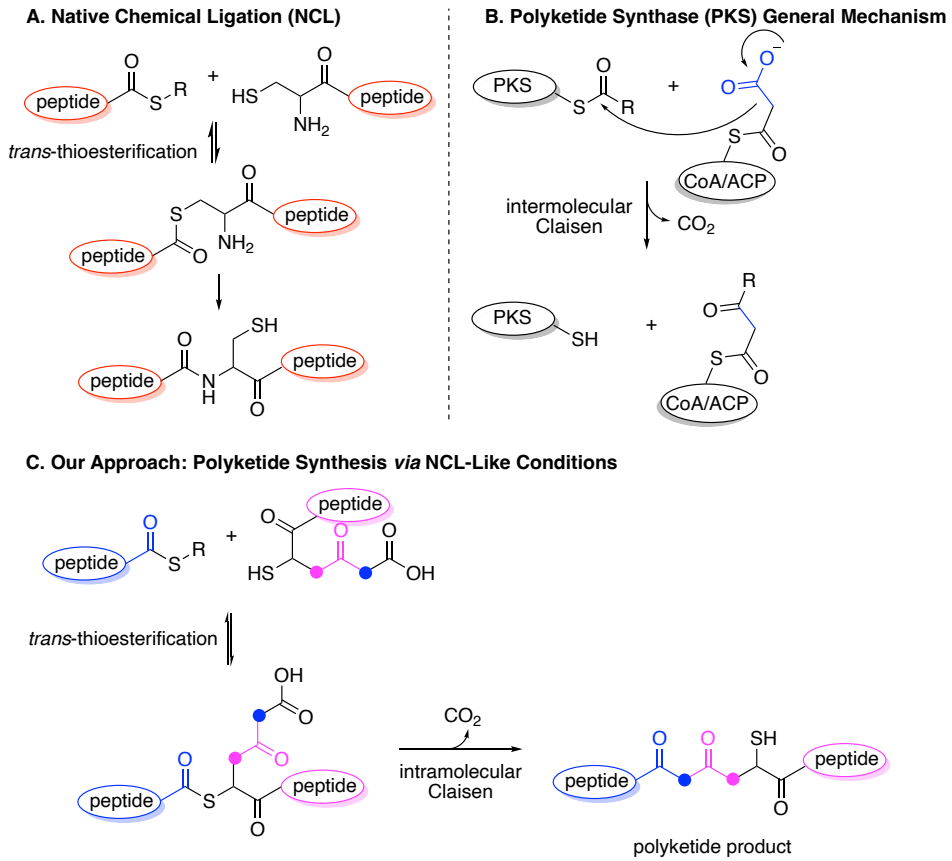


Figure 2.3. Analogies between native chemical ligation, polyketide synthesis, and our proposed S-to-C acyl shift and backbone rearrangement.

The Miller lab synthesized the monomer 1a and 1b, but unfortunately 1b was discovered to rapidly degrade (for stuctures see Figure 2.4). Efforts to purify 1b were unsuccessful and 1a was not acylatable by flexizyme, likely due to extremely poor solubility and poor steric accessibility from the trityl protecting group, in addition to the weakly activated ester. In the process we discovered that α-thio nucleophiles were challenging to work with due to the reduced electrophilicity of their activated ester form. Moreover their propensity to form disulfides was another challenge. In control experiments, α-thio glycine was effectively acylated onto mini tRNA, as evidenced by RNAse-A assays, but we were never able to detect these acylated tRNAs by intact tRNA mass spectrometry or acidic polyacrylamide gel electrophoresis (Figure 2.4-2.7). Simultaneously, the Miller lab established a small peptidic model system to test for the capacity of decarboxylative Claisen chemistry to perform intramolecular S-to-C acyl transfers under

biomimetic conditions (Figure 2.8). Unfortunately, the results of numerous efforts toward this goal were largely ambiguous and indicated very poor yield and high instability of the suspected product. Potential rearrangement products were proposed, but in negligible yields. The combined challenges of acylation and the poor results in the model system convinced us to change tactics. Despite our challenges at the time, these kinds of sidechain-to-backbone NCL-style rearrangements were later shown to work well in IVT peptides and proteins for O-to-N acyl shifts[10,11]. Ongoing work in our lab suggests the O-to-X acyl shift strategy may be broadly generalizable to other nucleophiles, including carbon.

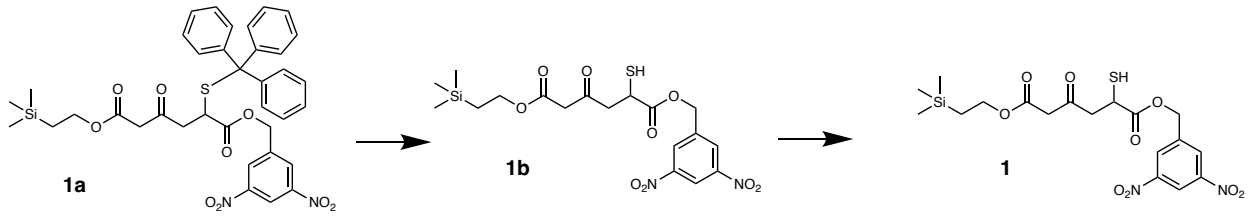


Figure 2.4 Deprotection strategy towards monomer 1. Unfortunately, monomer 1b proved to be highly unstable and monomer 1a was showed no appreciable yield in flexizyme acylations.

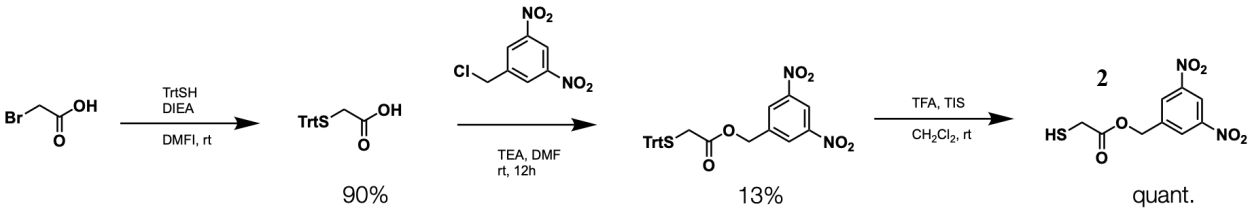
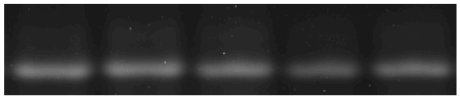


Figure 2.5. Synthesis of α-thio-glycine dinitrobenzyl ester **2**.



	8	9	10	11	12
Time (h):	2	24	24	24	24
pH:	9	7.5	9	9	10
TCEP:	x	x	x		x

Figure 2.6. Gel-based assesment of tRNA acylation by α-thio-glycine dinitrobenzyl ester **2**.

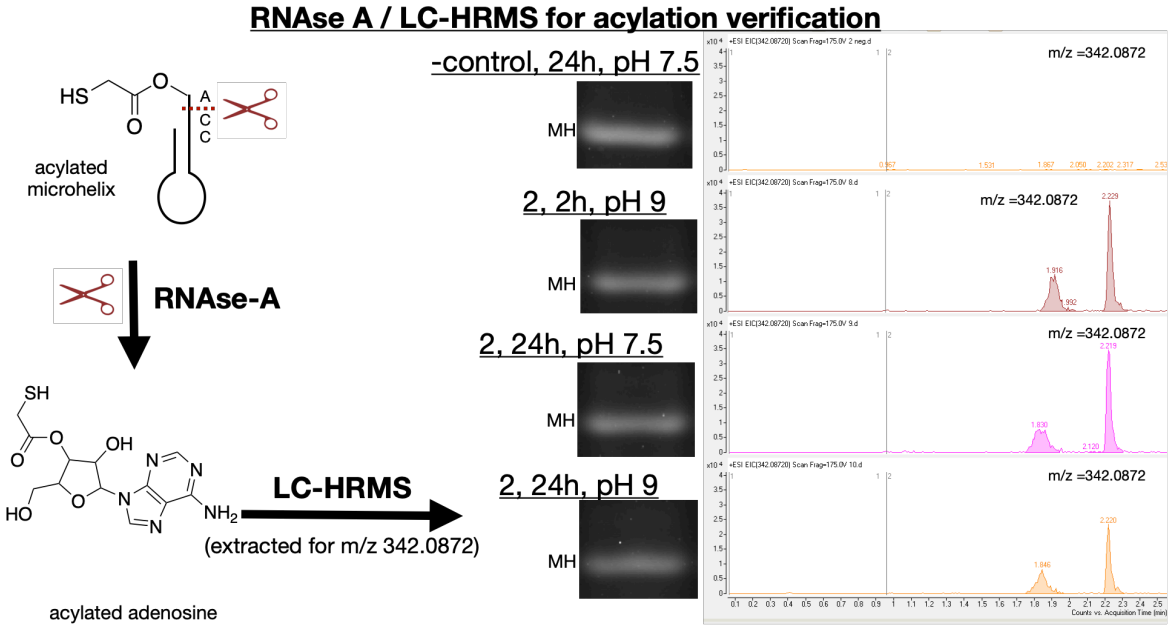


Figure 2.7. RNAse-A and LC-MS based assessment of tRNA acylation by α-thio-glycine dinitrobenzyl ester **2**. Acylation is evidenced at the terminal adenosine. Qualitative estimates, by comparing the signal intensity to a tRNA acylated with fMet indicate that the acylation yield was around 10% or less (not shown).

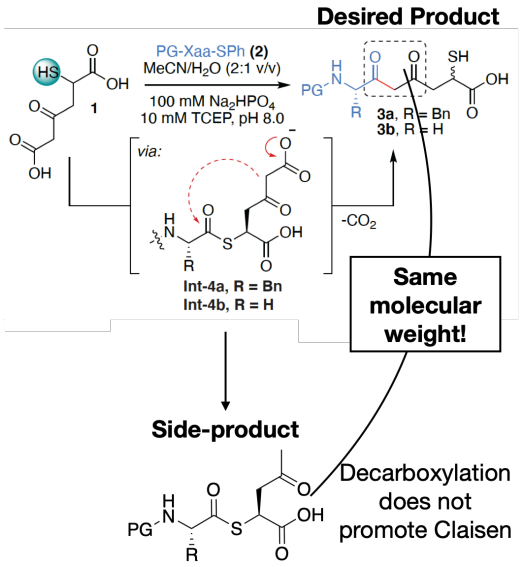


Figure 2.8. Model peptide to test for productive S-to-C acyl transfer via decarboxylative Claisen reactions with intramoleclar thioesters on a peptidic scaffold. The identical mass of the side product and the desired product, coupled with challenges in stability and purification made this system ultimately untenable to work with. Work done by Diondra Dilworth in the Miller lab.

Dicarbonyls

Following from the work to install protected malonates, we sought to ribosomally incorporate simple dicarbonyl monomers into ribosomal translation. We expected that by replacing the carboxylic acid of the malonate with a ketone, we could generate β-keto esters or other polycarbonyl species that would have an activated carbon, with a relatively low pka (~11), that may be able to function as nucleophiles directly in the PTC (Figure 2.9). Instead of requiring a well-timed decarboxylation to generate an enolate, simple deprotonation could generate an enolate. In the case of 1,3-dicarbonyl species, it is also known that divalent cations, such as magnesium, which is present in the ribosome and in IVT systems, stabilize the enolate and might lower the activation energy required for their generation. Thus, these polycarbonyl monomers were synthetically more accessible, mechanistically simpler, and we suspected, more likely to acylate tRNAs.

Towards this end, four dicarbonyl monomers were synthesized as substrates for flexizyme (Figure 2.10) then tested acylation under a variety of conditions with a miniturized tRNA acceptor stem known as microhelix. Only the β-keto ester and γ-keto ester were capable of microhelix acylation in meaningful yields. Both monomers containing an α-keto ester moiety (pyruvate-like) were unable to acylate microhelix effectively. Using intact tRNA LC-MS, and extracting for the expected m/z range for the acylated tRNAs, we were able to detect extremely low acylation yield of the α, γ-diketoester monomer maxing out around 1% yield. We suppose that the α-ketone adjacent to the activated ester may preclude effective acylation for a variety of reasons. One possibility is an electronic or steric effect of the carbonyl, while another is the possibility that the α-ketone is hydrated in water and the hydrate both electronically deactivates the ester while also sterically crowding the ester electrophile from attack. NMR experiments confirm that the hydration analogue is present in reasonable proportion. Ion extractions were performed on all monomers of interest, including their hydrated analogues, for comparison with 260 nm absorbance based detection. We generally find good agreement between the absorbance acylation yields and the ion extraction. We also find good correlation between microhelix action yields and tRNA acylation yields, although tRNA acylation yields are always lower. Data regarding the acylation of these molecules onto tRNAs can be found in Chapter 3.

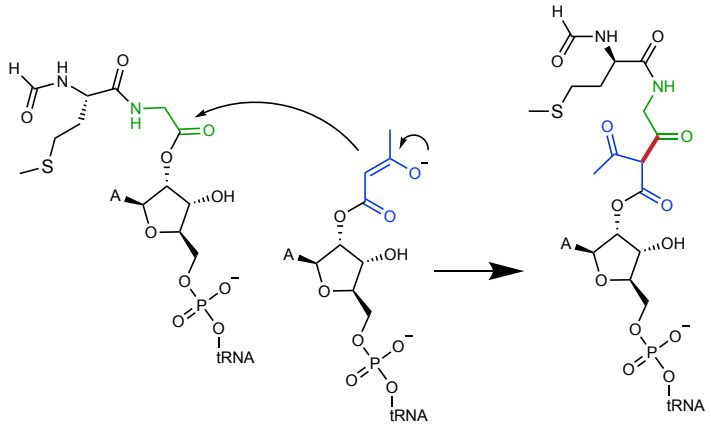


Figure 2.9 B-keto ester monomer undergoing proposed in ribosomal aldol-style C-C bond forming reaction.

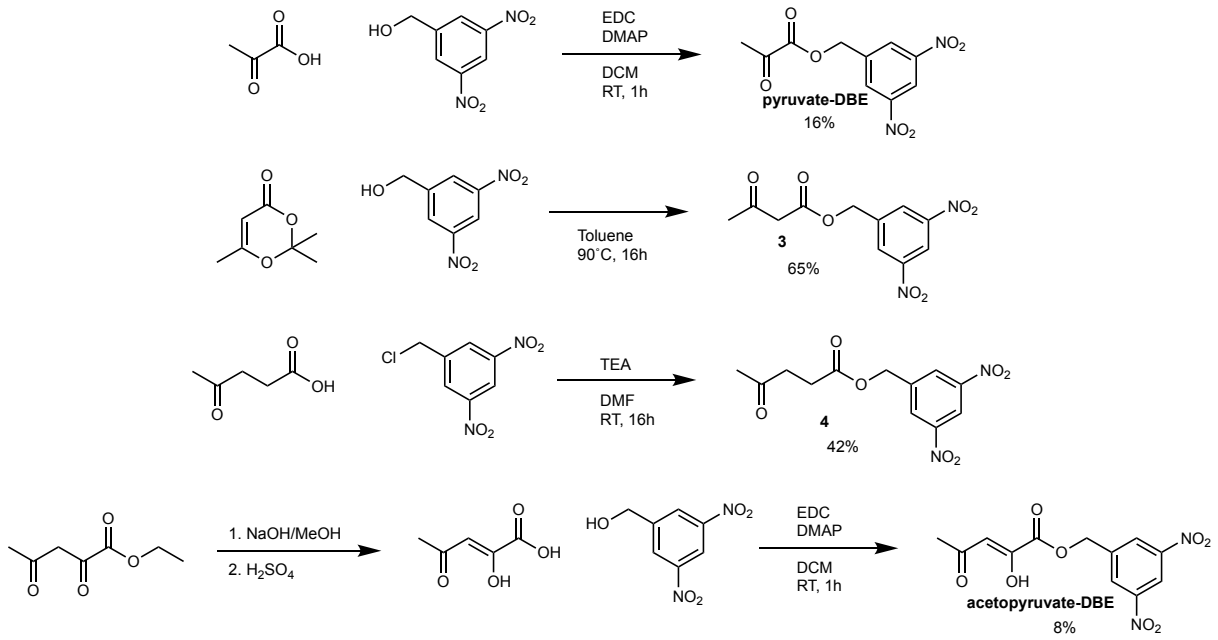


Figure 2.10 Synthesis of Dinitrobenzyl esters of carbonyl containing monomers for C-C bond formation.

Disappointingly, when tRNAs acylated with the β-keto ester and the γ-keto ester were added into an IVT reaction to test their capacity to form C-C bonds, no evidence of the desired product was detected. Nonetheless, these monomers were effectively incorporated at the N-terminus of a peptide when acylated on $tRNA^{fMet}$, and thus functioned effectively as translation initiators. These monomers became the impetus for later studying post-translational chemistry to convert these simple keto-amides into a variety of heterocycles. (See Chapter 3)

Nitro-aldol aka Henry Reaction

Our next inspiration for C-C bond nucleophiles came from considering alternative activating groups, namely nitro-alkyl compounds (Figure 2.11). The Henry reaction, also known as a nitro-aldol, is an aldol type reaction that can proceed from a carbon acid adjacent to a strong electron-withdrawing nitro substituent. Nitro-alkyl compounds have a remarkably low pKa of around 9, making nitronate equivelents potentially accessible withing biological pH ranges. Diondra Dilworth and the Miller lab first proposed this reaction as a possible route forward and as the reader will see, this reaction has featured heavily in our thinking. Intriguingly, this reaction can be performed in aqueous media at neutral pH with phosphate buffers[12,13], albeit only with aldehyde electrophiles. The use of ester electrophiles has been evidenced, but required double deprotonation of the nitro-alkyl component using a strong base under non-aqueous conditions[14].

Three nitro-containing flexizyme monomers **5, 6, and 8** (see Fig 2.12) were synthesized with the aim of testing them for tRNA acylation and IVT. These monomers feature the nitro-group substituted onto an alkyl chain of variable lengths from the ester, either from the β- or γ-position, to variablize the position of the potential carbon nucleophile. Monomer **5** positions the carbon nucleophile isosteric to the α-amine of endogenous substrates. Monomer **6** positions the

carbon nucleophile one atom further down the chain but potentially provides more flexibility to the monomer within the PTC. Monomer **8** appends a phenylalanine sidechain onto the monomer **5**, with the aim of improving tRNA acylation and ribosomal fit. It was hypothesized that the phenylalanine style sidechain would improve tRNA acylation for flexizyme, as it is widely known that monomers resembling phenylalanine are the best substrates for the flexizyme eFx. We also suspected that the phenylalanine sidechain would provide a handle for orthogonal synthetase recognition. Finally, the ribosome can undergo an induced fit, wherein the sidechain of A-site monomers aids in a conformational switch that properly positions monomers for bond formation, and phenylalanine is known to induce this mechanism effectively by Cryo-EM[15]. In systems that study ribosomal bond formation using the fragment reaction, a minimal system for measuring ribosomal catalysis, phenylalanine has been shown to have one of the highest rates of peptide bond formation, perhaps owing it its exceptional fit within the A-site[16,17].

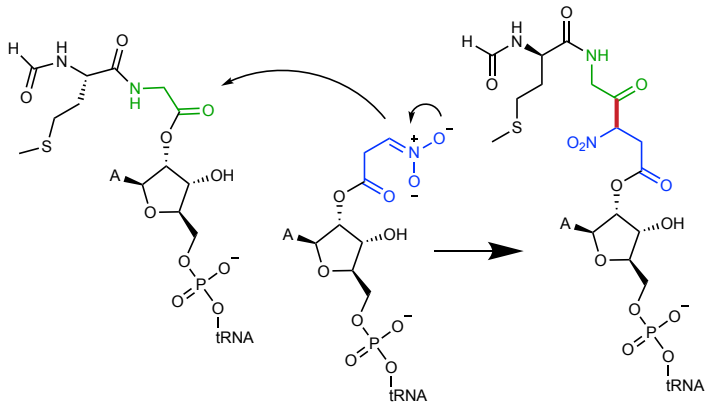


Figure 2.11 Proposed Henry reaction in ribosome PTC.

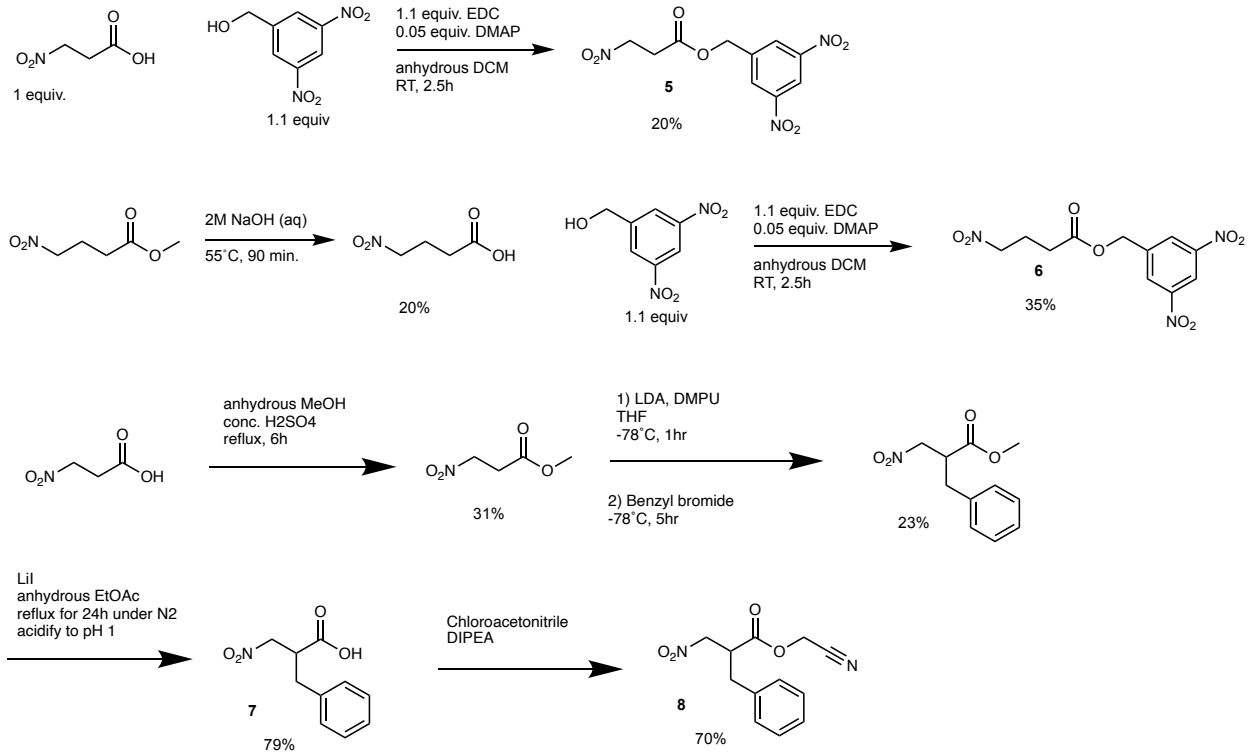


Figure 2.12 Synthesis of flexizyme-compatible activated esters of Nitro-containing monomers for C-C bond formation.

To our delight, all three of these monomers could be acylated onto tRNAs with appreciable yields with flexizyme, with the yield of monomer **8** being the highest (Table 2.1). Furthermore, we found that monomer **7** was a substrate for PylRS enzymes (data not shown – collected by Cameron Swenson). These monomers were tested for C-C bond formation by recoding valine codons in a variety of mRNA templates, but unfortunately we never saw any evidence of C-C bond formation. mRNA templates included a variety of flag-encoding peptides with variable sequences, but all with valine recoding. Templates included variants where the valine codon was placed at an internal position, thus requiring monomers to be capable as nucleophiles and electrophiles during translation elongation, or in scenarios where the valine codon was positioned at the C-terminus of the peptide, thus challenging the monomers only in nucleophilicity and hydrolysis for chain termination. As has been reported elsewhere, generally yields for peptide recoding is best when the peptide template is a small and simple as possible[18]. Ion extractions were performed on numerous possible derivatives following the proposed C-C bond forming Henry reaction in the ribosome, including the Nef reaction, reductions, eliminations, and oxidations (Figure 2.13).

In an effort to overcome any deficits in EF-Tu binding by tRNAs acylated with these monomers, I synthesized a series of tRNAs with different EF-Tu binding T-stems that previously showed improved incorporation for N-methyl amino acids, which have deficient EF-Tu binding[19]. Additionally, the pH tolerance of the IVT system, PURExpress, was evaluated (Figure 2.14). We hypothesized that by pushing the pH of the IVT system higher, we could generate more activated carbanions for C-C bond formation as we approached the pKa of our nitro-alkyl

monomers. Despite both of these efforts, we were unable to ever detect evidence of bond formation by LC-MS ion extraction.

monomer	flexizyme	pH (buffer)	hours	EIC yield	UV yield	Gel yield
5	dFx	7.5 (HEPES)	24.0	n/a	15.7	n/a
5	dFx	7.5 (HEPES)	48.0	32.0	32.8	n/a
5	dFx	7.5 (HEPES)	120.0	29.8	35.1	n/a
5	**dFx**	**9.0 (Bicine)**	**24.0**	**37.5**	**40.4**	**n/a**
5	dFx	9.0 (Bicine)	48.0	11.4	29.2	n/a
6	dFx	7.5 (HEPES)	24.0	n/a	3.3	n/a
6	dFx	7.5 (HEPES)	48.0	4.1	7.0	n/a
6	dFx	7.5 (HEPES)	120.0	8.8	16.6	n/a
6	dFx	9.0 (Bicine)	24.0	7.7	13.7	n/a
6	**dFx**	**9.0 (Bicine)**	**48.0**	**10.7**	**17.7**	**n/a**
8	eFx	7 (HEPES)	2.0	19.5	17.7	27.3
8	eFx	8 (HEPES)	2.0	53.0	51.5	58.4
8	eFx	7 (HEPES)	4.0	30.3	27.8	n/a
8	eFx	8 (HEPES)	4.0	59.7	61.1	62.6
8	eFx	7 (HEPES)	6.0	35.8	35.0	n/a
8	eFx	8 (HEPES)	6.0	60.7	63.3	66.4
8	eFx	7 (HEPES)	24.0	56.2	60.9	58.1
8	**eFx**	**8 (HEPES)**	**24.0**	**76.9**	**78.3**	**73.7**

Table 2.1. Acylation yields for monomers **5, 6,** and **8** with flexizyme onto microhelix mini-tRNAs. Acylation was determined by either LC-MS extracted ion integration of the -4 charge state envelope for acylated and unacylated microhelix, $Absorbance_{260nm}$ integrations of acylated and unacylated peaks on the LC-MS chromatogram, and using UV desiometry of acid polyacrylamide gel electrophoresis.

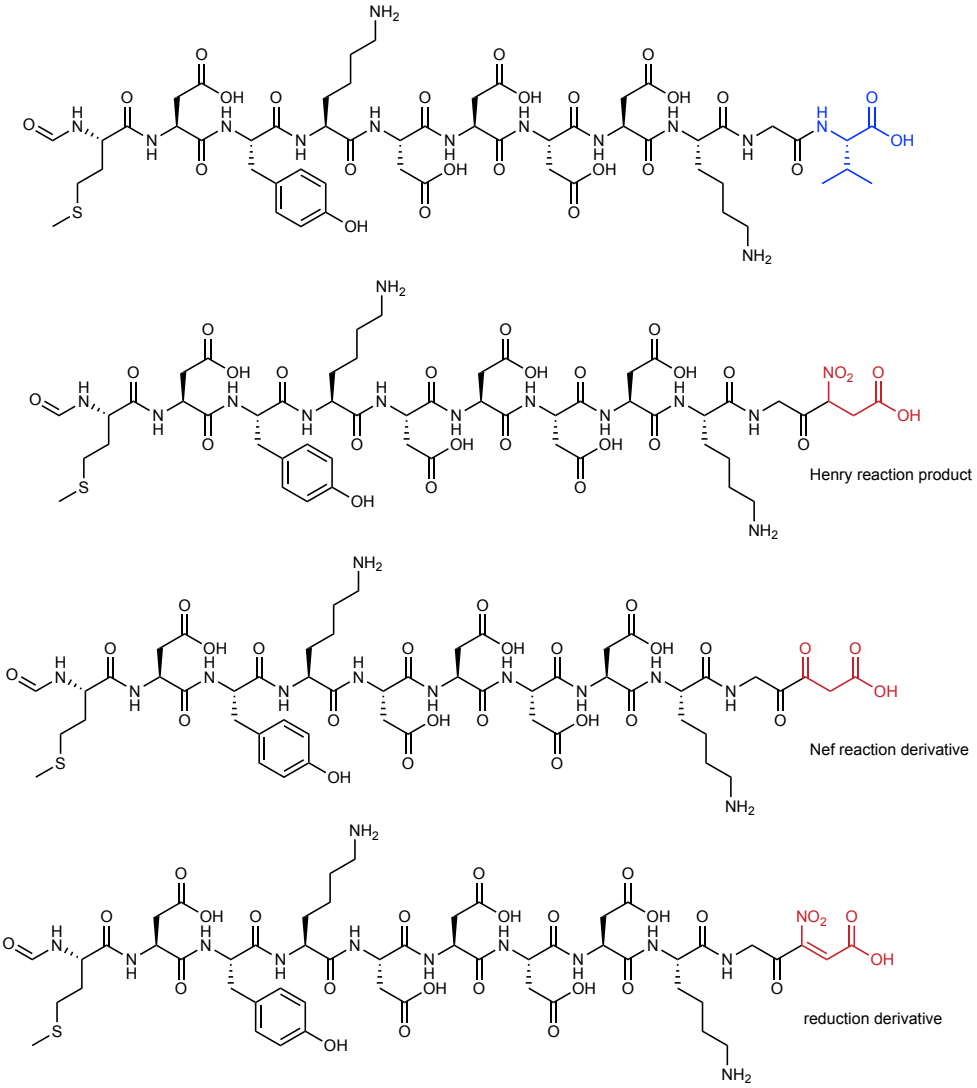
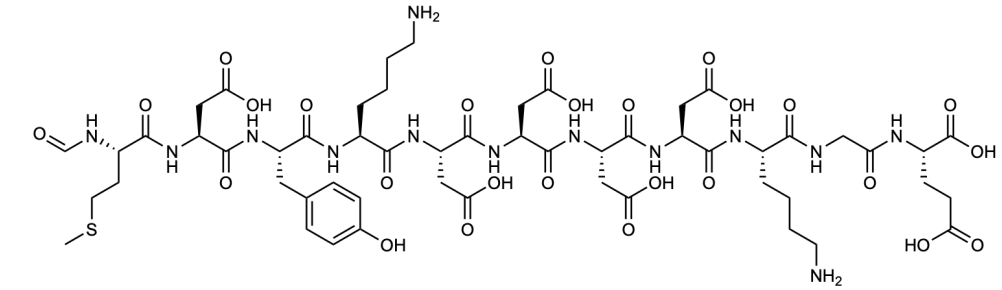


Figure 2.13. Peptide MDYKDDDDKGV used for valine recoding with nitro-alkyl monomers at the C-terminus. A series of possible products are shown. Each of these, in addition to the usual possibilities of methionine oxidation were searched for in +1,2, and 3 charge states. No evidence of C-C bond formation was ever seen.



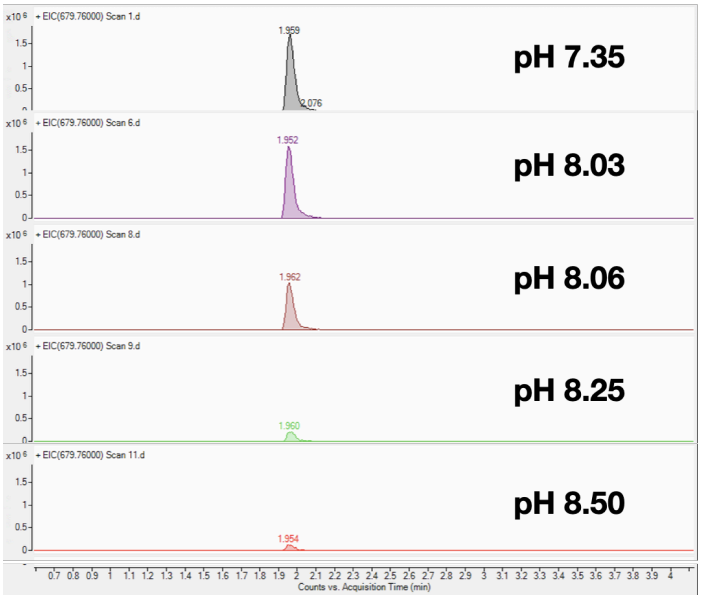


Figure 2.14. Effect of pH and buffer on IVT synthesis of MDYKDDDDKGE peptide. pH of the IVT solution was measured using a micro-pH meter. Yield drops precipitously between pH 8.06 and 8.25.

Cryo-EM of benzyl malonates in the ribosome

While work proceeded on carbonyl and nitro-alkyl monomers by flexizyme acylation, a fortuitous discovery was made in our lab by Riley Fricke that benzyl-malonates were substrates for a promiscuous class of pyrrolysine synthetases[20]. Using an initiation codon skipping procedure, we were also able to directly incorporate the benzyl malonate into the N-terminus of IVT peptides. Unfortunately, attempts to incorporate this motif via internal incorporation into the peptide, via a potential decarboxylative Claisen reaction, were unsuccessful.

In an effort to gain more structural information about the fit of C-C bond monomers in the ribosome, we attempted to gather Cryo-EM data with benzyl-malonate monomers acylated onto an A-site (nucleophilic) tRNA. tRNAs for Cryo-EM are synthesized utilizing 3'-deoxy-3'-amino-adenosine at the 3' end. When acylated, this allows for a non-labile amide bond to link the monomer and the tRNA, which can effectively trap translation in the ribosome just before the key bond formation step. It was found that the FRS1 synthetase was also able to acylate this

amino-tRNA effectively. Achieving a structure of the benzyl-malonate monomer in the ribosome sought to answer a few important questions that would guide future C-C bond efforts. First, we wanted to know how the monomer was positioning inside the ribosome, and if it was inducing the proper fit and base-pairing interactions known to be important to bond formation. Next, we wanted to know about the exact orientation of the monomer, and importantly, if the carboxylate was still intact or if it had undergone decarboxylation.

The Cate lab was able to obtain a 1.9 Å high-resolution Cryo-EM structure of the monomer situated in the ribosome PTC (Figure 2.15). This level of resolution allowed us to see that a single stereoisomer of the monomer was being accommodated, and that the benzyl-malonate monomer was engaged properly in the A-site cleft. It was able to induce the fit of the ribosome, thus opening a passageway for P-site carbonyl attack from the A-site via U2585 repositioning. It was also apparent that the proton-wire was intact and therefor the ribosome looked catalytically competent. We also observed that the carboxylate was still intact, and moreover, it was positioned directly in-between the nucleophilic carbon and the P-site carbonyl electrophile, thus blocking the path of the reaction. In addition to the carboxylate being intact and in the way, the nucleophilic carbon was also positioned too far away from the electrophile for bond formation.

It is worth pausing a moment to consider the dramatic chemical difference between an α-amino acid, such as phenylalanine, and benzylmalonate. Where phenylalanine is expected to bear a largely protonated and positively charged amine (ammonium), the benzylmalonate is expected to be mostly deprotonated and negatively charged. The malonate is also dramatically larger than the amine. Finally the position of the nucleophile for these two monomers is quite different, on the β-position for α-amino acids, while at the α-position for benzylmalonate. Notably, there is no evidence for any α-position nucleophile ever performing bond formation in the ribosome, so it is completely unknown if this change in chain length and nucleophile positioning will be possible.

The Cate lab and Schrodinger, in collaboration with our lab, have computationally tested the nucleophile positioning for extended and aminobenzoic monomers in the ribosome, which provide evidence for two important features in metadynamics simulations: the A-site nucleophile being <4 Å from the P-site carbonyl electrophile and a Bürgi–Dunitz angle of 76–115°[21]. In addition to being blocked by the carboxylate, the carbon nucleophile is positioned 4.7 Å away from the electrophile, and thus not predicted to be reactive.

Despite our disappointment in the lack of reactivity of this monomer, and its failure to decarboxylate under physiological conditions, it is amazing that the ribosome accommodated this monomer with significant differences in size and charge into the active site while preserving key interactions required for catalysis. This should encourage future efforts at C-C bond formation, and hints at the benefits of a phenylalanine-like scaffold, utilizing the sidechain phenyl sidechain to aid in inducing the fit of the ribosome and opening up a pathway to the P-site electrophile for attack.

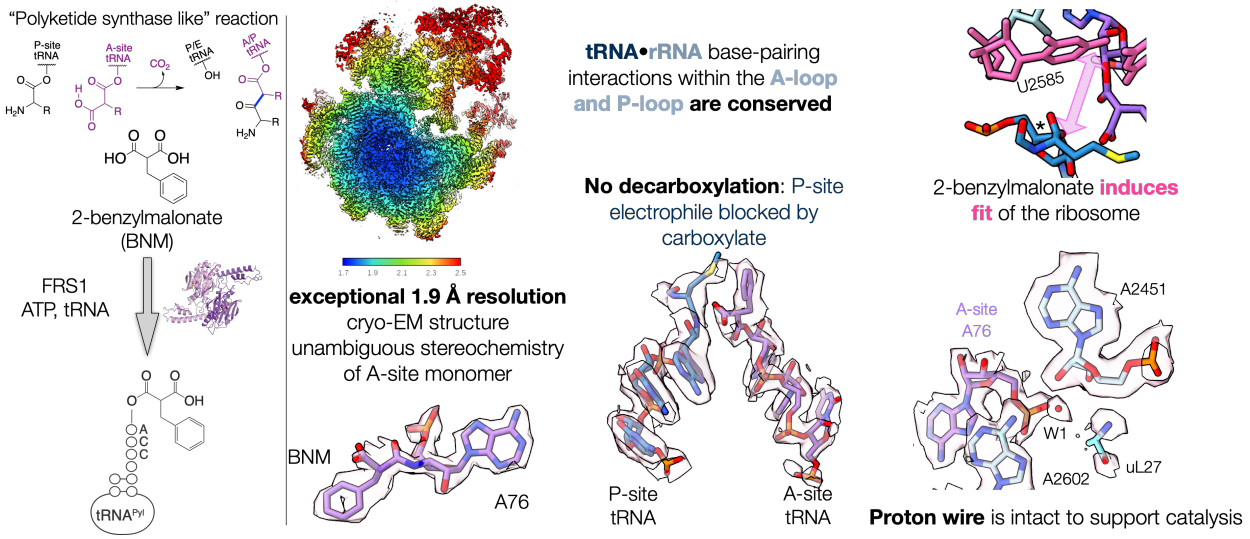


Figure 2.15. Benzylmalonate acylation and Cryo-EM structure of benzylmalonate in the ribosome A-site. High-resolution structure reveals a well-ordered ribosome, with conservation of tRNA-rRNA interaction at both the A- and P-loops, an induced fit organization with U2585 positioned in the open conformation for bond-formation, and the proton wire intact. The benzylmalonate monomer maintains density in the carboxylate, and is therefore not decarboxylated into an active enolate, and the carboxylate is positioned between the carbon nucleophile and the carbonyl electrophile, thus blocking C-C bond formation. Figure made by and reproduced with permission from Chandrima Majumdar.

Cryo-EM of β-nitro phenylalanine in the ribosome

Buoyed by the successful ribosomal accomdation of benzyl malonate, and encouraged by the physiochemical features of monomer **7** — Phe sidechain, Carbon acid pKa of ~9, nucleophilic carbon isosteric to natural amino acids — we attempted to gather Cryo-EM data with nitro-alkyl monomer **7** acylated onto an A-site tRNA. Cryo-EM studies were led by Chandrima Majumdar, with my assistance in chemical synthesis and tRNA acylation. To selectively acylate the 3'-amine of tRNAs for Cryo-EM, we first attempted to synthesize NHS-esters of the relevant nitro-alkyl monomers presented above. We attempted to optimize these acylation reactions on a small microhelix modified with a PEG linker which terminated in a free amine, but ultimately found that these optimizations did not correspond well with the conditions required for acylation of the 3'-amino-tRNAs. NHS chemistry on precious samples of 3'-amino tRNAs, followed by arduous ion-pairing reverse phase chromatography to purify the acyl-tRNA, proved both challenging and time consuming. We were happy to discover that monomer **7** could be acylated by Pyl-RS FRS2 enzymes at reasonable yields, and enzymatic acylation was then used to supply materials for Cryo-EM.

Upon analysis of the structure, a few interesting features were apparent. The A-site tRNA was well positioned in the ribosome with the rRNA-tRNA interactions at the A-loop intact and the ribosome in the induced fit. Monomer density in the A-site was well-defined, except for the Nitro group, which may be a feature of the electron microscopy itself. The density for the

nucleophilic carbon adjacent to the nitro is well positioned for bond formation, and it superimposes with the α-amine of natural amino acids. Interestingly the P-site tRNA is disordered, with disrupted P-loop interactions and unclear density at the monomer and in the tRNA body. As a result a distance between the nucleophile and electrophile cannot be determined. The lack of density for the nitro group may alternatively indicate a highly dynamic molecular motion of the nitro group. In either event it is challenging to determine what the steric impact of this moietie is, and whether it is blocking the path of nucleophilic attack or if it is even pushing the P-site monomer and tRNA out of position. Ongoing efforts continue to investigate this monomer from a structural perspective. This includes efforts to utilize modified ribosomes with more room for the P-site monomer, or attempting to solve structures with longer peptides occupying the exit tunnel, and therefore stabilizing the P-site peptide-tRNA within the ribosome.

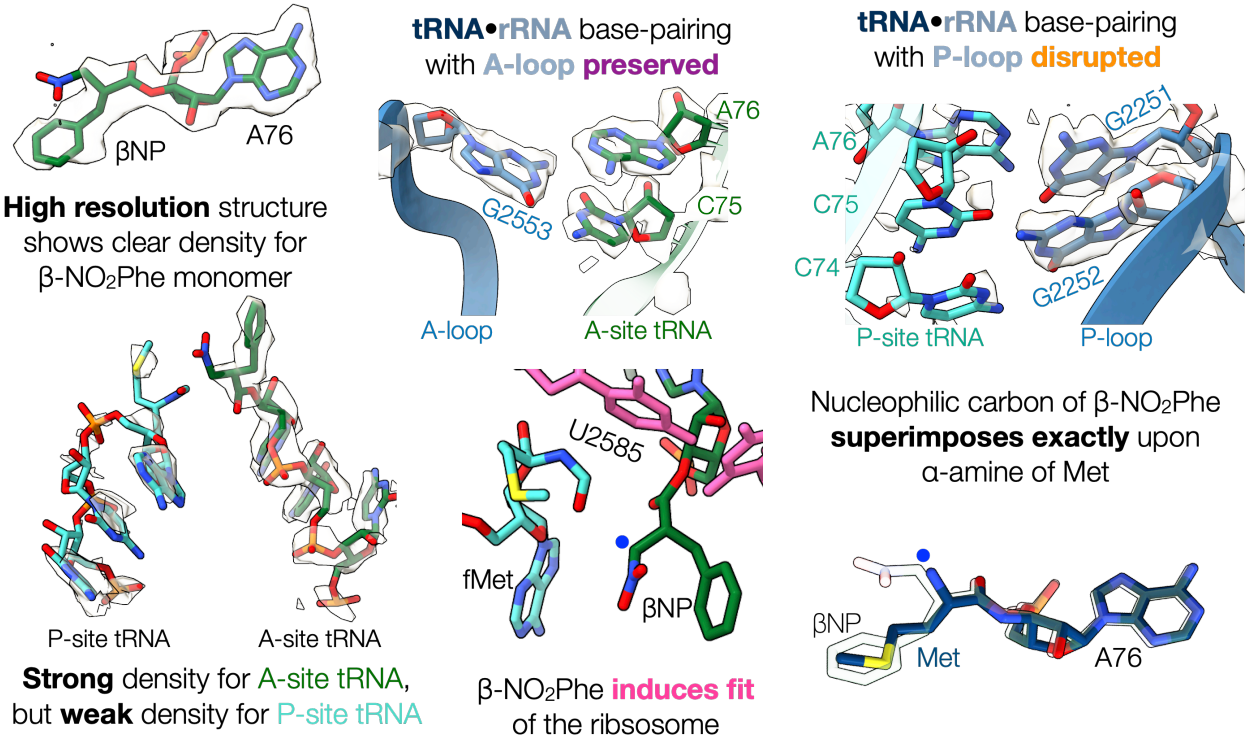


Figure 2.16. Cryo-EM structure of B-NitroPhe in the ribosome A-site. High-resolution structure reveals a ribosome well organized around the A-site tRNA, with conservation of tRNA-rRNA interaction at the A-loop and an induced fit with U2585 positioned in the open conformation for bond-formation, but with weak density at the P-site. The B-NitroPhe monomer appears to be excellently positioned, with the nucleophilic carbon in an identical location to an α amino acid. Unfortunately, the nitro group itself is lacking density, but this may be a feature of the electron microscopy. Figure made by and reproduced with permission from Chandrima Majumdar.

Systematic reappraisal of possible carbon nucleophiles

In lieu of our previous somewhat scattered attempts to test C-C bond formation, a more systematic reappraisal was undertaken. We identified two key variables in monomer design that were likely to have dramatic effects on C-C bond capacity in the ribosome. The first was the position of the carbon nucleophile relative to the ester that links it to a tRNA. Nucleophiles closer to the ester, ie. at the α-position, may not be capable of reaching far enough towards the P-site electrophile to form a bond. Meanwhile if the carbon nucleophile were positioned too far away, it may benefit from increased flexibility and reach, but perhaps it would struggle to fit into the ribosomes A-site, especially with the added requirement for an adjacent electron withdrawing group to provide activation. We hypothesized that carbon nucleophiles isosteric to endogenous nucleophiles (ie the nucleophile at the β-position) would be preferred for ribosomal compatibility. In tandem to this consideration, was also a consideration for sidechain identity and placement. In general we were interested in monomers either without sidechain interference, or those that would aid in activation, in inducing the ribosomal induced fit, or could modulate the position of the nucleophile. In general, this meant exploring phenyl sidechains at varying distances from the backbone.

The other primary variable we considered was the exact type of C-C bond reaction we aimed to employ. More specifically, we considered the various methods for generating carbon nucleophiles, including malonates, dicarbonyls, nitro-alkyls or nitro-esters, and nitrile or dinitrile monomers. We also considered designs for monomers that could access transient cyclic enamines. Enamines are highly prone to hydrolysis, but perhaps by imagining a reversible cyclic enamine would allow us to generate the cyclic enamine with a nucleophilic enamine carbon well-positioned for bond formation. All of these ideas are schematized in Figure 2.17.

As opposed to synthesizing the many combinations of these molecular variables for tRNA acylation and ribosomal synthesis, an expensive and extremely time consuming process, we decided instead to computationally determine the pKa values of a wide range of carbon acids of interest and develop small molecule model systems to assess the C-C bond capability of many of these monomers in the context of acyl transfer reactions. This was necessary because of the surprising lack of literature on these reactions.

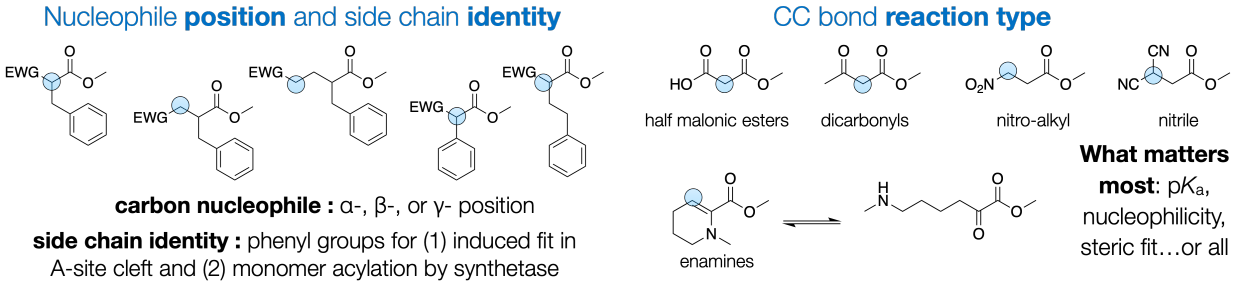


Figure 2.17. Important variables under consideration for C-C bond formation and ideas for types of monomers and reactions for ribosomal C-C bonds.

Carbon acidities of potential ribosomal monomers

In order to quickly survey the carbon aciditiy of potential ribosomal monomers, we utilized DFT pKa calculations on a wide array of monomers. The full list of monomers evaluated can be found in the supplemental figure section of this chaper, while a few of the most promising monomers are shown below in Figure 2.18. A few interesting features include the remarkably low pKa of α-cyano-α-phenyl methyl ester, the low pKa of the malonitirle species, and the exceptionally low pKa of the α-nitro methyl ester. Indeed, positioning the nucleophilic carbon at the α position provides a tremendous benefit because of the adjacent electron withdrawing capacity of the ester. Fluorination may also be a worthwhile strategy to modulate the pKa of carbon acids with a minimal impact on sterics. Interestingly, many of the dicarbonyl and malonate species tested deviated substantially from literature values. Notably, the β-nitrophenylalanine monomer we previously tested and took Cryo-EM of had a reasonably low pKa of 8.5. Information from this screen allowed us to prioritize monomers for testing in model systems in the next section.

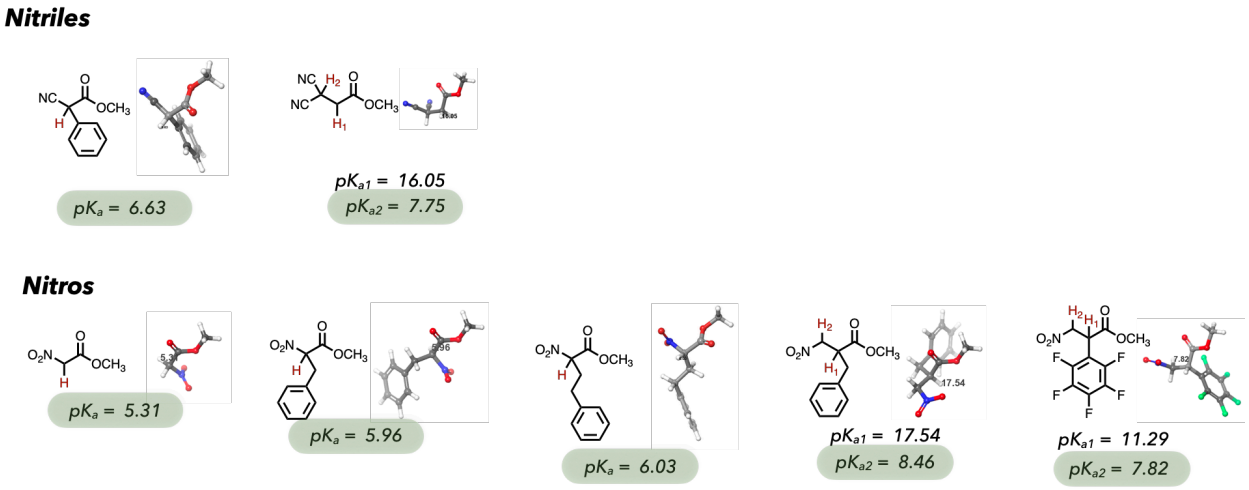


Figure 2.18. A select set of monomers tested with Jaguar DFT "thourough" pka calculations, courtesy of Prof. Matt Francis.

Intramolecular model systems to test O-to-C acyl transfer reactions

Our first attempts to develop a model system to test O-to-C acyl transfer reactions are shown in Figure 2.19. The esterification of a dimethylaniline-containing species produced **9**. The dimethyl aniline provides a handle for both UV detection and ionization for LC-MS analysis, while limiting the nucleophilicity of the amine. It was supposed that the intramolecular nature of this reaction would help to simulate the pseudo-intramolecular nature of ribosomal catalysis in the PTC. Following from our interest in nitro-alkyl carbon acids, we synthesized **9**, where a nitro-alkyl alcohol was esterified to provide a nucleophilic carbon adjacent to the nitro group. We imagined alcohols with other carbon acids could also be synthesized in a similar fashion. Next we tested a variety of reaction conditions to assess intramolecular rearrangement via O-to-C acyl transfer (Figure 2.20). A variety of semi-aqueous buffer conditions were tested at room

temperature or heated. Organic solvent conditions (THF or DCM) were also tested with the presence of a nonnucleophilic base (TEA) for carbon deprotonation at either 0, 25, or 50˚C. Additionally, two Lewis acid catalysts ($Zn(OTf)_2$ and $Yb(Otf)_2$) were evaluated as additives for increasing the activation of the electrophilic ester. These have previously been employed for Henry (nitro-aldol) reactions on aldehydes and activated ketones[22,23].

Unfortunately, we never detected a clear and obvious formation of **10**, the product of a Henry reaction for O-to-C acyl transfer, by LC-MS. Because **9** and **10** have identical masses, we were dependent on a change in retention time to detect the formation of species **10**. It is possible that **9** and **10** have identical retention times, although somewhat unlikely. In an effort to derivatize free alcohols that would be present in **10**, TMS-Cl was added to the reactions, but no derivatized product was detected.

Instead of continuing in the intramolecular model system, which requires a fair amount of synthesis to generate the molecule for intramolecular rearrangement for each of the desired nucleophiles, and which could produce equally ambiguous results, we decided instead to pursue and intermolecular model system that would provide more clear evidence of product formation, more modularity, and an easier synthetic route.

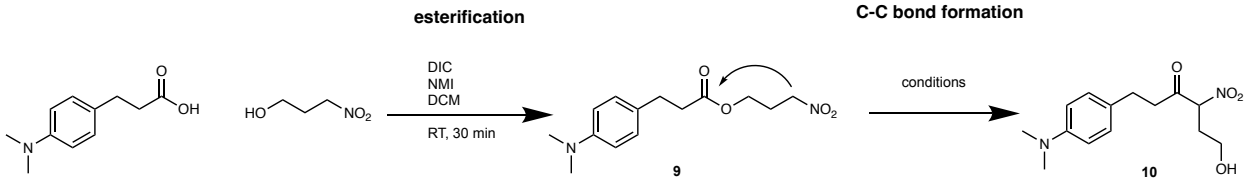


Figure 2.19 Synthesis of **9** and reaction screening for the intramolecular O-to-C acyl transfer to **10.** The model system was designed with a dimethyl aniline component to provide a UV and ionization handle, without much nucleophilic risk. It was expected that **9** and **10** would have distinct chromatographic peaks given the significant change in molecular structure. Reaction conditions explored for C-C bond formation can be found in Figure 2.20

Solvent	Base / Buffer	Additive?	Temp
2:1 MeCN:H2O	2uL of 500mM HEPES 7.0		RT
2:1 MeCN:H2O	2uL of 500mM HEPES 8.0		RT
2:1 MeCN:H2O	2uL of 500mM Bicine 9.0		RT
2:1 MeCN:H2O	2uL of 500mM CHES 10		RT
2:1 MeCN:H2O	2uL of 500mM PBS 7.0		RT
2:1 MeCN:H2O	2uL of 500mM Bicine 9.0		50
THF	13mM TEA		0
THF	13mM TEA	13 mM Zn(OTf)2	0
THF	13mM TEA	13 mM Yb(OTf)3	0
THF	13mM TEA		RT
THF	13mM TEA	13 mM Zn(OTf)2	RT
THF	13mM TEA	13 mM Yb(OTf)3	RT
DCM	13mM TEA		RT
DCM	13mM TEA	13 mM Zn(OTf)2	RT
DCM	13mM TEA	13 mM Yb(OTf)3	RT
THF	13mM TEA		50
THF	13mM TEA	13 mM Zn(OTf)2	50
THF	13mM TEA	13 mM Yb(OTf)3	50
DCM	13mM TEA		50
DCM	13mM TEA	13 mM Zn(OTf)2	50
DCM	13mM TEA	13 mM Yb(OTf)3	50
THF	6.5mM TEA		RT
THF	6.5mM TEA	6.5 mM Zn(OTf)2	RT
THF	6.5mM TEA	6.5 mM Yb(OTf)3	RT
THF	none	13 mM Zn(OTf)2	RT
THF	none	13 mM Yb(OTf)3	RT

Table 2.2. Reaction conditions screened for the intramolecular O-to-C acyl transfer reaction to transform **9** into **10**. All reactions were run at 6.4 mM and monitored at 2 and 16 hours. No evidence of a distinct peak with the correct m/z were developing other than the starting material **9**. This does not rule out the possibility of a reaction occurring, and **10** having the same retention at **9** on the column.

Intermolecular model systems to test X-to-C acyl transfer reactions

Developing an intermolecular system to test acyl transfer reactions onto carbon provided us a significantly more modular platform to explore C-C bond chemistry. We could use synthetically accessible, often commercial, carbon acids with adjacent esters (**12-23**) as

nucleophiles (Figure 2.20), while building an electrophilic carbonyl with a variety of activating groups (Figure 2.21). For the electrophilic component of the reaction, we again used the dimethyl-aniline motif as a UV and ionization handle for LC-MS, but this time the carbonyl was activated with a variety of leaving groups ranging in electrophilicity from the least activated cyanomethylester (**11-O**), to the medium activated thioester (**11-S**), to the most activated benzotriazole (**11-TriN**). The activation of these carbonyls varies in inverse proportion to the pKa of the leaving group. Benzotriazole was chosen because its known compatibility with nitroaldol reactions for acyl transfers[24]. This platform allowed us to evaluate a wider dynamic range in the reactivity of carbon nucleophiles (**12-23)** under a variety of conditions.

An example of the LC-MS data collected is provided in Figure 2.22, for the reaction of monomer **12** (0.3 M) with **11-TriN, 11-S,** or **11-O** (0.3 M) in DMF with 1 equiv. of TEA for deprotonation at RT for 24 hours. Absorbance chromatograms measured at 254 nm are shown, with the peak corresponding to the m/z of the expected product **24** highlighted with an arrow and in red. The area of extracted ion chromatogram for the product m/z was then compared to the area of the extracted ion chromatogram of the starting material m/z(**11-LG)** to provide a yield. This allowed us to exclusively detect compounds of the correct mass, while excluding any coeluting compounds. Moreover, it enabled us higher sensitivity to detect less reactive pairs.

As expected the reactivity of **12** with **11-TriN** was the highest, with 60% conversion, followed by **11-S** with 20% conversion, and **11-O** with a modest 1% conversion by EIC yields (Figure 2.23). This correlated well with the Absorbance chromatogram. Tyrosine also performed well in this reaction, with near 100% conversion with **11-TriN,** but similar 7% conversions for **11-S** and **11-O.** This confirms computational findings that thioesters are significantly better electrophiles for carbon nucleophiles, when compared against esters[25]. Yet when amines are used as nucleophiles, this difference in electrophilicity between esters and thioesters are erased. This finding reenforces our appreciation for the biosynthetic logic of polyketide and polyamide synthesis. Polyketide natural products are produced via thioester electrophiles with carbanion enolate nucleophiles, while polypeptide synthesis proceeds via ester electrophiles with amine nucleophiles.

LC-MS yields for each of the combinations of nucleophiles with electrophiles is shown in Figure 2.23 for organic conditions. Generally, all of these monomers showed reactivity with the most activated electrophile, with the exception of the tertiary nucleophiles **13** and **14** (data for **14** not shown, only collected in single replicate). This leads us to hesitantly conclude that tertiary carbanions may encounter too much steric encumbrance for acyl transfer, especially as the adjacent electron withdrawing groups planarize to promote resonance of the carbanion. The two fluorinated β-ketoesters **20** and **21** performed surprisingly poorly, especially compared to the unfluorinated β-ketoester **19**. We had expected that the increased acidity of these monomers would more readily generate carbanion nucleophiles for attack, but it is possible that instead these features over-stabilized the carbanion and lessened its reactivity. Alternatively, these reactants may have undergone other reaction pathways, though we did not immediately identify this. The remaining α-cyanoester **12**, nitro-alkyl esters **15-17**, and dicarbonyls **18, 19, 22** and **23** all reacted reasonably well with **11-TriN** to yields of 30% or greater. When **11-S** was employed, reactivity was much more limited. α-cyanoester **12** stood out dramatically with a yield of 20%. A yield of 1% was evidenced for **15**, while **16** and **17** were slightly above background. All other compounds failed to show reactivity with **11-S**. When **11-O** was used as the acyl donor, product formation was only seen with **Try** and **12.**

Next, we employed semi-aqueous (1:1 H_2O/DMF) conditions buffered to pH 7.5 with HEPES to test the effect of a biological pH and the presence of water on the reaction. We expected lower reactivity in general due to the more limited deprotonation capable in aqueous pH 7.5 compared to the previously tested TEA in organic solvent. In general this expectation was validated across the board, with a few notable exceptions. **Tyr**, **12,** and **15** maintained high reactivity with **11-TriN**, each with 50% or greater acyl-transfer conversion. B-ketoesters **18** and **19** were both attenuated down to around 5% conversion. The parity of these two species was surprising given the pKa difference of 5.2 and 10.7. Perhaps the increase in acidity for **18** is balanced by a reduced nucleophilicity because of conformational rigidity or over-stabilization of the carbanion in water. **22** was the most reactive of the dicarbonyls with a 10% yield. Fluorinated derivatives **20** and **21** had negligible yields. In the nitro class of nucleophiles, **15** was much more reactive at 50% yield compared to near zero yield for the extended alkyl chains of **16** and **17.** In tandem with the impressive reactivity of **12**, there is a strong case to be made for α-position nucleophiles relative to esters. Compound **12** was also the only candidate, other than **Tyr**, to show any reactivity with either **11-S** or **11-O**.

Efforts to confirm the identity of the products by NMR and evaluate the stability of these compounds are currently underway. In addition to providing more confidence in the chemistry reported here, this also allows us to understand possible degradation or derivitization that might occur to the product of C-C bond formation in the ribosome. It would not be surprising for some of these products to undergo further reactivity. This will be important when searching for products of ribosomal C-C bond formation in the future.

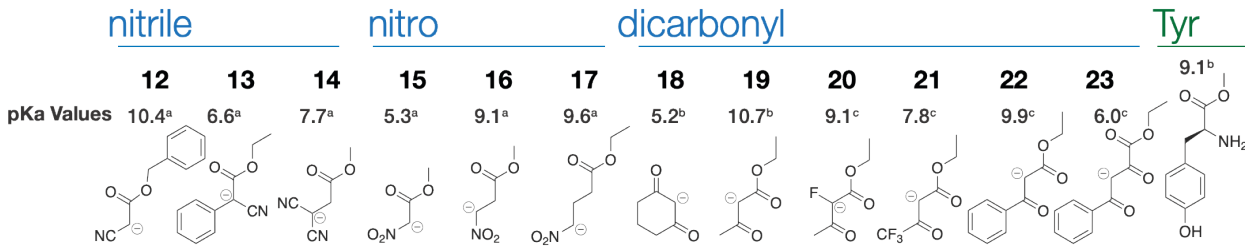


Figure 2.20. Carbon nucleophiles evaluated in the intermolecular model system. These monomers come from three distinct classes of activating groups: nitriles, nitro, and dicarbonyl. Tyrosine (Tyr) was also included as an amino acid control. The experimental or calculated pKas are provided: a – Maestro Jaguar DFT calculations, b – experimental values[26], and c – predicted values from ACD acid dissociation calculator[27].

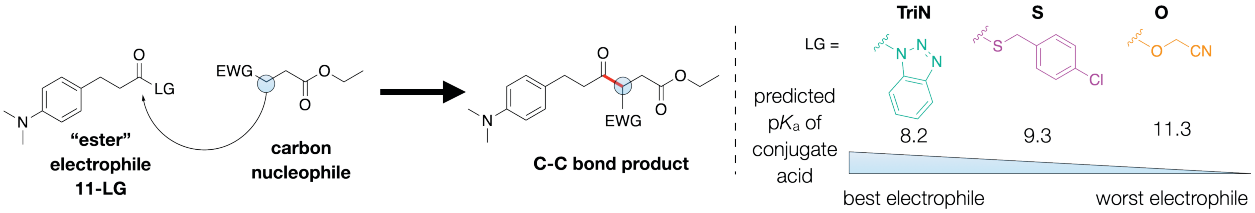


Figure 2.21. General model for intermolecular X-to-C acyl transfer reactions with a variety of activated electrophiles (**11-TriN, 11-S**, and **11-O**).

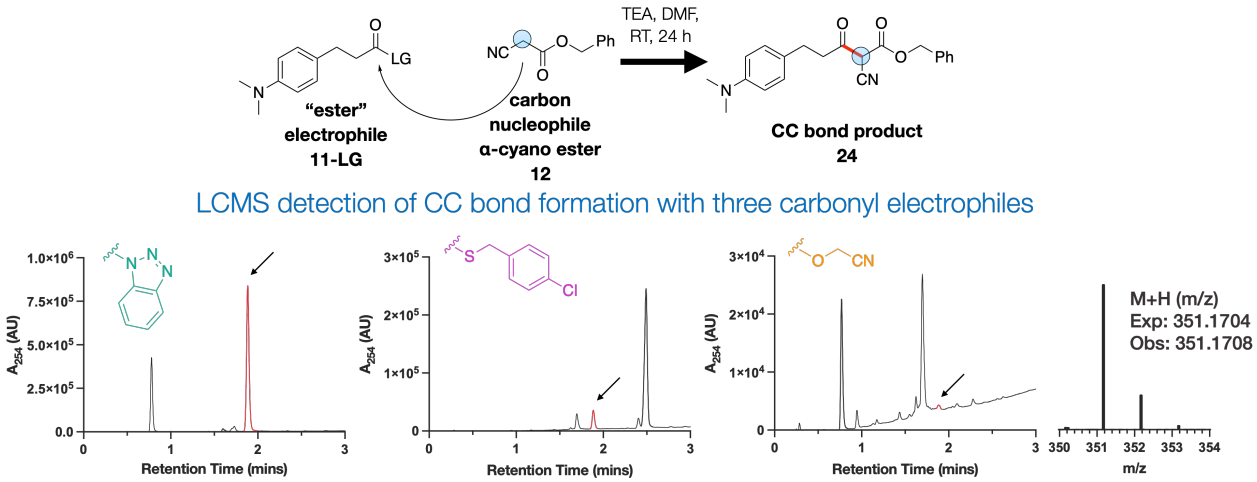


Figure 2.22. Example of LC-MS monitoring of intermolecular X-to-C acyl transfer reactions between α-cyanoester **12** with a range activated electrophiles (**11-TriN, 11-S, and 11-O**). Top of the figure shows the reaction under organic conditions, with the product **24** drawn with a highlighted red bond to indicate the new C-C bond. The bottom of the figure shows the formation of product **24** (red peak with arrow delineating it) with the three different electrophiles by LC-MS analysis. Shown are the Absorbance (254 nm) traces, followed by a high-resolution MS.

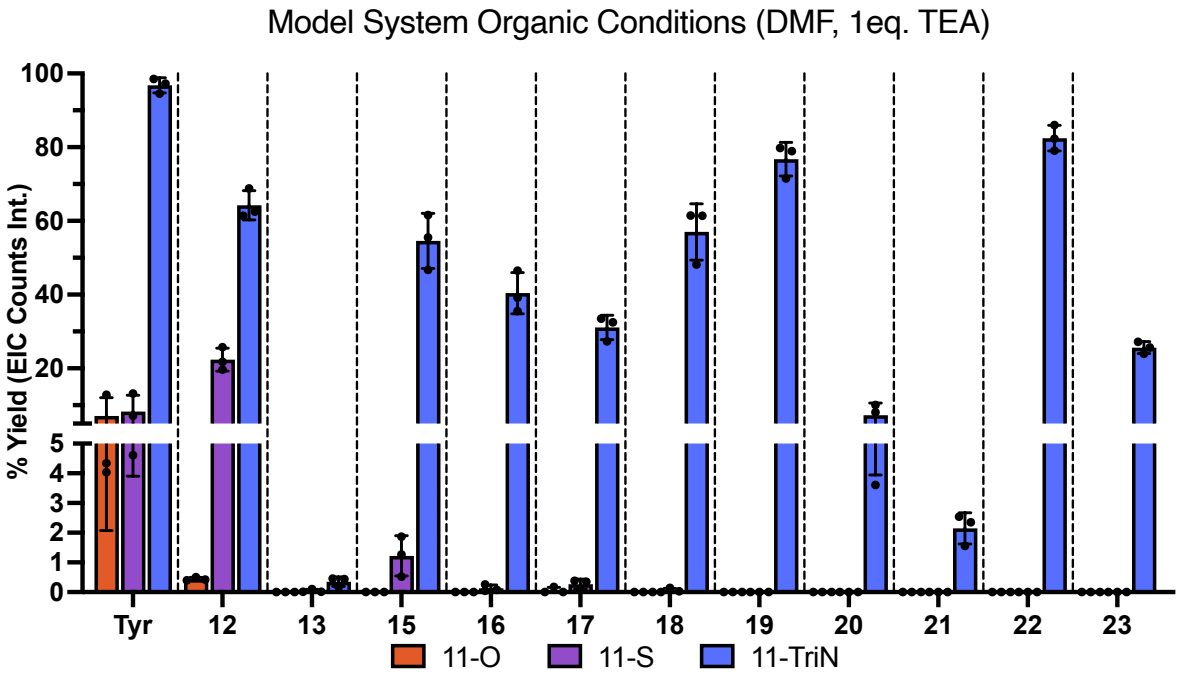


Figure 2.23. Yield of X-to-C acyl transfer reactions under organic conditions with TEA as base. Red bars show reactivity of each monomer with **11-O**, purple bars with **11-S**, and blue bars with **11-TriN**. Yields were calculated by comparing the integrated areas of extraction ion chromatogram peaks for the expected m/z of the remaining starting material and the product of each reaction.

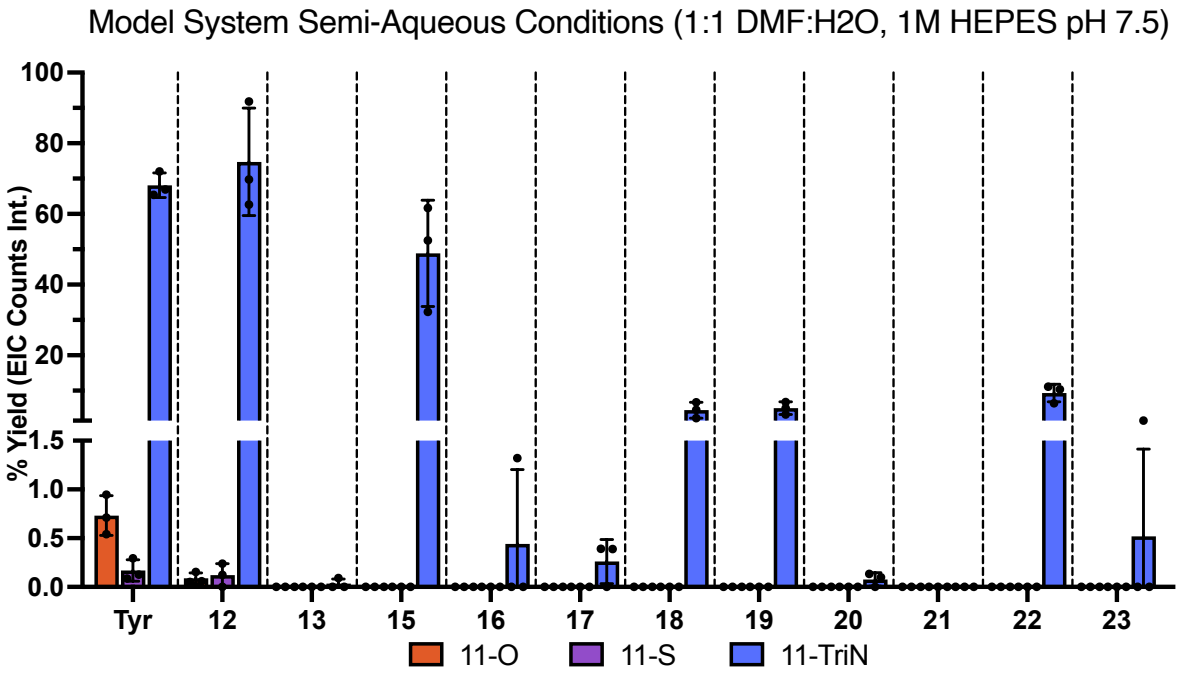


Figure 2.24. Yield of X-to-C acyl transfer reactions under semi-aqueous conditions with HEPES buffer pH 7.5. Red bars show reactivity of each monomer with **11-O**, purple bars with **11-S**, and blue bars with **11-TriN**. Yields were calculated by comparing the integrated areas of extraction ion chromatogram peaks for the expected m/z of the remaining starting material and the product of each reaction.

Conclusions

Initial attempts at C-C bond formation in the ribosome have as of yet been unsuccessful. Many attempts at this holy grail of genetic code expansion have been attempted in our lab, as well as others. The findings outlined above, bring us one step closer to understanding the requirements of C-C bond formation primarily through structural insights and chemical model systems of reactivity. Information gleaned from these experiments allows us to prioritize monomers for synthesis, tRNA acylation, and ribosomal polymerization. Our favored monomers include the α-position nucleophiles such as α-cyanoester **12** and α-nitroester **15**, followed by β-ketoesters **18, 19,** and **22.** We are currently attempting to synthesize these monomers for tRNA acylation in formats compatible with flexizyme or synthetases.

Future work will hopefully provide an iterative design of monomers, structural information, and computational prediction. Building in phenyl sidechains to induce fit or modulate monomer position may prove as important as a well-positioned nucleophile or a high carbon acidity. Alternatively, ribosome engineering may prove crucial to these efforts.

One strategy we are particularly keen on exploring is the modulation of the electrophile in the ribosome PTC to compliment carbon nucleophiles. The obvious example is to replace the ester linking monomers to tRNAs with thioesters. This is currently being explored in CGEM. Other options include the addition of more electro withdrawing groups onto the A-site monomer itself, such as fluorinated phenylalanine. In analogy to our chemical model system, altered electrophilicity of the carbonyl plays a dramatic role in these acyl transfer reactions. Admittedly, increasing the lability of the monomer-tRNA bond comes with huge risks in hydrolytic stability.

Other reaction types, such as enamines or thiamine-style umpolung may open the door to novel carbon nucleophiles. Otherwise, perhaps more dramatic engineering efforts of tRNAs or ribosomes may need to be employed before ribosomal C-C bonds come to fruition.

References

1. Sakai, N., Sordé, N. & Matile, S. Mg2+-Imidazole-Catalyzed Self-Condensation of Malonyl Thioesters: Getting Tuned for Biomimetic Polyketide Synthesis? *Molecules* **6**, 845–851 (2001).
2. Pan, Y. & Tan, C.-H. Catalytic Decarboxylative Reactions: Biomimetic Approaches Inspired by Polyketide Biosynthesis. *Synthesis* **2011**, 2044–2053 (2011).
3. Zetzsche, L. E. & Narayan, A. R. H. Broadening the scope of biocatalytic C–C bond formation. *Nat Rev Chem* **4**, 334–346 (2020).
4. Bolt, A., Berry, A. & Nelson, A. Directed evolution of aldolases for exploitation in synthetic organic chemistry. *Archives of Biochemistry and Biophysics* **474**, 318–330 (2008).
5. Schmidt, N. G., Eger, E. & Kroutil, W. Building Bridges: Biocatalytic C–C-Bond Formation toward Multifunctional Products. *ACS Catal.* **6**, 4286–4311 (2016).
6. Fusz, S., Eisenführ, A., Srivatsan, S. G., Heckel, A. & Famulok, M. A Ribozyme for the Aldol Reaction. *Chemistry & Biology* **12**, 941–950 (2005).
7. Fischbach, M. A. & Walsh, C. T. Assembly-Line Enzymology for Polyketide and Nonribosomal Peptide Antibiotics: Logic, Machinery, and Mechanisms. *Chem. Rev.* **106**, 3468–3496 (2006).
8. Ad, O. *et al.* Translation of Diverse Aramid- and 1,3-Dicarbonyl-peptides by Wild Type Ribosomes *in Vitro*. *ACS Cent. Sci.* **5**, 1289–1294 (2019).

9. Takatsuji, R. *et al.* Ribosomal Synthesis of Backbone-Cyclic Peptides Compatible with In Vitro Display. *J. Am. Chem. Soc.* **141**, 2279–2287 (2019).
10. Roe, L. T. *et al.* Backbone extension acyl rearrangements enable cellular synthesis of proteins with internal β2-peptide linkages. 2023.10.03.560714 Preprint at https://doi.org/10.1101/2023.10.03.560714 (2023).
11. Kuroda, T., Huang, Y., Nishio, S., Goto, Y. & Suga, H. Post-translational backbone-acyl shift yields natural product-like peptides bearing hydroxyhydrocarbon units. *Nat. Chem.* **14**, 1413–1420 (2022).
12. Ballini, R. & Bosica, G. Nitroaldol Reaction in Aqueous Media: An Important Improvement of the Henry Reaction. *J. Org. Chem.* **62**, 425–427 (1997).
13. Bora, P. P. & Bez, G. Henry Reaction in Aqueous Media at Neutral pH. *European Journal of Organic Chemistry* **2013**, 2922–2929 (2013).
14. Seebach, D., Henning, R. & Mukhopadhyay, T. Doubly Deprotonated Methyl 3-Mitropropanoate, an Acrylic Ester d2-reagent. *Chemische Berichte* **115**, 1705–1720 (1982).
15. Martin Schmeing, T., Huang, K. S., Strobel, S. A. & Steitz, T. A. An induced-fit mechanism to promote peptide bond formation and exclude hydrolysis of peptidyl-tRNA. *Nature* **438**, 520–524 (2005).
16. Rychlík, I., Černá, J., Chládek, S., Žemlička, J. & Haladová, Z. Substrate specificity of ribosomal peptidyl transferase: 2′(3′)-*O*-aminoacyl nucleosides as acceptors of the peptide chain on the amino acid site. *Journal of Molecular Biology* **43**, 13–24 (1969).
17. Lehmann, J. Induced fit of the peptidyl-transferase center of the ribosome and conformational freedom of the esterified amino acids. *RNA* **23**, 229–239 (2017).
18. Chan, A. I. *et al.* Evaluating Translational Efficiency of Noncanonical Amino Acids to Inform the Design of Druglike Peptide Libraries. *ACS Chem. Biol.* **18**, 81–90 (2023).

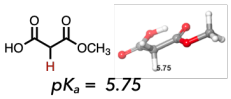
19. Iwane, Y., Kimura, H., Katoh, T. & Suga, H. Uniform affinity-tuning of N-methyl-aminoacyl-tRNAs to EF-Tu enhances their multiple incorporation. *Nucleic Acids Research* (2021) doi:10.1093/nar/gkab288.
20. Fricke, R. *et al.* Expanding the substrate scope of pyrrolysyl-transfer RNA synthetase enzymes to include non-α-amino acids in vitro and in vivo. *Nat. Chem.* **15**, 960–971 (2023).
21. Watson, Z. L. *et al.* Atomistic simulations of the Escherichia coli ribosome provide selection criteria for translationally active substrates. *Nat. Chem.* 1–9 (2023) doi:10.1038/s41557-023-01226-w.
22. Palomo, C., Oiarbide, M. & Laso, A. Enantioselective Henry Reactions under Dual Lewis Acid/Amine Catalysis Using Chiral Amino Alcohol Ligands. *Angewandte Chemie International Edition* **44**, 3881–3884 (2005).
23. Hongming Li, Baomin Wang, and & Deng*, L. Enantioselective Nitroaldol Reaction of α-Ketoesters Catalyzed by Cinchona Alkaloids. *ACS Publications* https://pubs.acs.org/doi/pdf/10.1021/ja057237l (2005) doi:10.1021/ja057237l.
24. Katritzky, A. R., Abdel-Fattah, A. A. A., Gromova, A. V., Witek, R. & Steel, P. J. α-Nitro Ketone Synthesis Using N-Acylbenzotriazoles. *J. Org. Chem.* **70**, 9211–9214 (2005).
25. Yang, W. & Drueckhammer, D. G. Understanding the Relative Acyl-Transfer Reactivity of Oxoesters and Thioesters: Computational Analysis of Transition State Delocalization Effects. *J. Am. Chem. Soc.* **123**, 11004–11009 (2001).
26. Bell, R. P. *The Proton in Chemistry*. (Springer US, Boston, MA, 1973). doi:10.1007/978-1-4757-1592-7.
27. Acid Dissociation Constant Calculator | pKa Prediction Software. *ACD/Labs* https://www.acdlabs.com/products/percepta-platform/physchem-suite/pka/.
28. Albert, A. & Serjeant, E. P. *The Determination of Ionization Constants*. (Springer Netherlands, Dordrecht, 1984). doi:10.1007/978-94-009-5548-6.

29. Blay, G., Hernández-Olmos, V. & Pedro, J. R. Enantioselective Henry Addition of Methyl 4-Nitrobutyrate to Aldehydes. Chiral Building Blocks for 2-Pyrrolidinones and Other Derivatives. *Org. Lett.* **12**, 3058–3061 (2010).
30. Silva, P. C., Costa, J. S. & Pereira, V. L. P. AN EXPEDITIOUS SYNTHESIS OF 3-NITROPROPIONIC ACID AND ITS ETHYL AND METHYL ESTERS. *Synthetic Communications* **31**, 595–600 (2001).
31. Pelletier, S. M.-C., Ray, P. C. & Dixon, D. J. Diastereoselective Synthesis of 1,3,5-Trisubstituted 4-Nitropyrrolidin-2-ones via a Nitro-Mannich/Lactamization Cascade. *Org. Lett.* **13**, 6406–6409 (2011).
32. Wang, S.-H. *et al.* Nitro as a novel zinc-binding group in the inhibition of carboxypeptidase A. *Bioorganic & Medicinal Chemistry* **16**, 3596–3601 (2008).
33. Fricke, R., Knudson, I. & Schepartz, A. Direct, quantitative, and comprehensive analysis of tRNA acylation using intact tRNA liquid-chromatography mass-spectrometry. 2023.07.14.549096 Preprint at https://doi.org/10.1101/2023.07.14.549096 (2023).
34. Majumdar, C., Walker, J. A., Francis, M. B., Schepartz, A. & Cate, J. H. D. Aminobenzoic Acid Derivatives Obstruct Induced Fit in the Catalytic Center of the Ribosome. *ACS Cent. Sci.* (2023) doi:10.1021/acscentsci.3c00153.

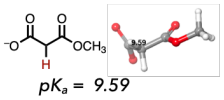
Supplemental Figures: calculated C-H acidities

The following figures were made by Prof. Matthew Francis. Jaguar "Thorough" DFT method in aqueous solution was used to calculate these values. The 5 lowest energy conformers evaluated for all species. We note that there are a few discrepancies between literature experimental values for dicarbonyl and malonate species, with the calculated values being substantially lower than the experimental. For instance, the monomer in the top right of the malonyl monomer figure is calculated to have a pKa of 6.89, yet the published experimental value for the diethyl ester is 12.9[28].

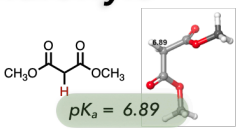
C-H Bond Acidities for C-GEM Monomers: Malonyls



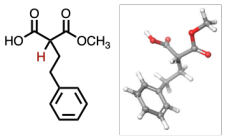
pK_a = 5.75



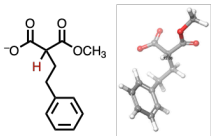
pK_a = 9.59



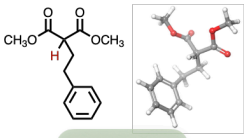
pK_a = 6.89



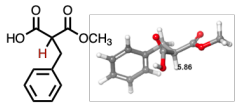
pK_a = 5.80



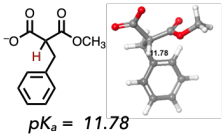
pK_a = 12.08



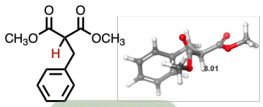
pK_a = 7.94



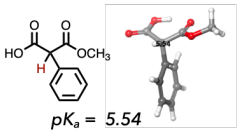
pK_a = 5.86



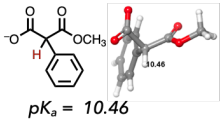
pK_a = 11.78



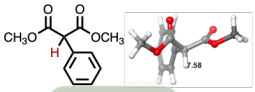
pK_a = 8.01



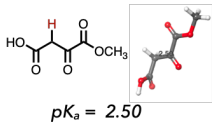
pK_a = 5.54



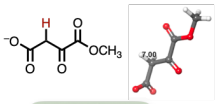
pK_a = 10.46



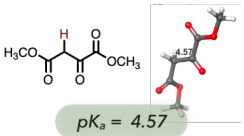
pK_a = 7.58



pK_a = 2.50

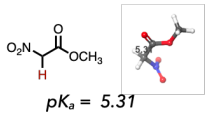


pK_a = 7.00

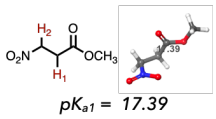


pK_a = 4.57

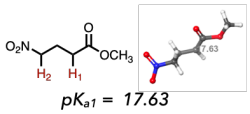
C-H Bond Acidities for C-GEM Monomers: Nitro Compounds



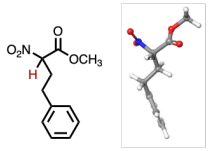
pK_a = 5.31



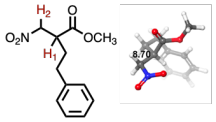
pK_{a1} = 17.39
pK_{a2} = 9.13



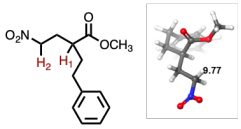
pK_{a1} = 17.63
pK_{a2} = 9.56



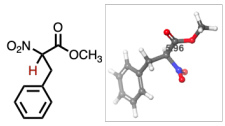
pK_a = 6.03



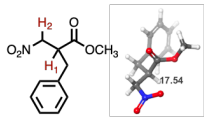
pK_{a1} = 17.75
pK_{a2} = 8.70



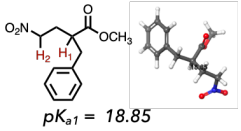
pK_{a1} = 19.07
pK_{a2} = 9.77



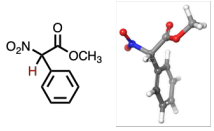
pK_a = 5.96



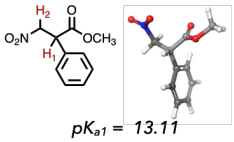
pK_{a1} = 17.54
pK_{a2} = 8.46



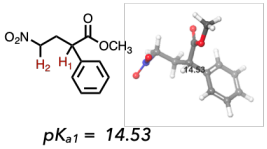
pK_{a1} = 18.85
pK_{a2} = 9.30



pK_a = 6.02

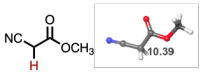


pK_{a1} = 13.11
pK_{a2} = 8.51

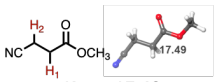


pK_{a1} = 14.53
pK_{a2} = 9.57

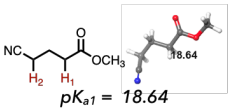
C-H Bond Acidities for C-GEM Monomers: Nitriles



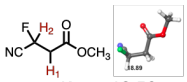
pK_a = 10.39



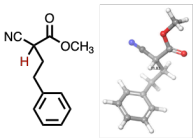
pK_{a1} = 17.49
pK_{a2} = 19.96



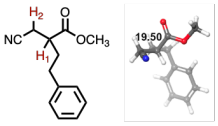
pK_{a1} = 18.64
pK_{a2} = 21.01



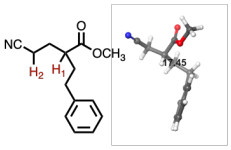
pK_{a1} = 12.58
pK_{a2} = 18.89



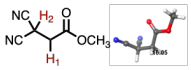
pK_a = 11.83



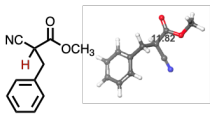
pK_{a1} = 17.45
pK_{a2} = 19.50



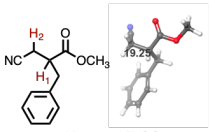
pK_{a1} = 17.45
pK_{a2} = 19.35



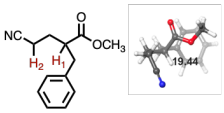
pK_{a1} = 16.05
pK_{a2} = 7.75



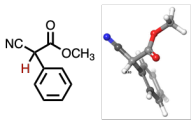
pK_a = 11.82



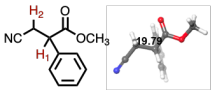
pK_{a1} = 17.22
pK_{a2} = 19.25



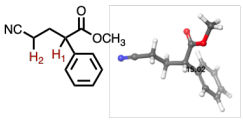
pK_{a1} = 19.44
pK_{a2} = 20.94



pK_a = 6.63

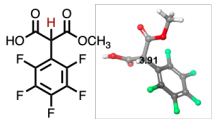


pK_{a1} = 13.73
pK_{a2} = 19.79

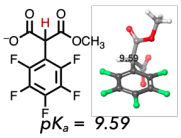


pK_{a1} = 15.02
pK_{a2} = 21.53

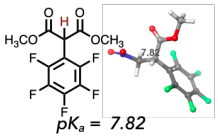
C-H Bond Acidities for C-GEM Monomers: Fluoro Compounds



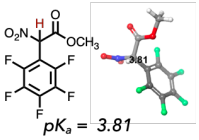
pK_a = 3.91



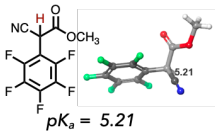
pK_a = 9.59



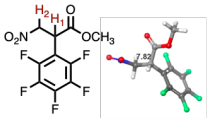
pK_a = 7.82



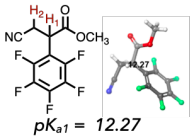
pK_a = 3.81



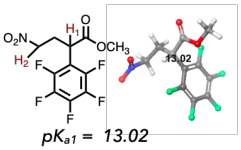
pK_a = 5.21



pK_{a1} = 11.29
pK_{a2} = 7.82



pK_{a1} = 12.27
pK_{a2} = 18.37



pK_{a1} = 13.02
pK_{a2} = 8.92

Materials and Methods

General Details

DNase-free water, 3 M $MgCl_2$ solution, sodium acetate solution (pH 5.2), and 20,000x ethidium bromide were purchased from AmericanBio (Canton, MA). Flexizyme RNA (eFx and dFx) along with microhelix (MH) RNA were purchased from Integrated DNA Technologies (IDT) (Coralville, IA). DNA oligonucleotides were purchased from IDT. HiScribe® T7 Quick High Yield RNA Synthesis Kit and PURExpress® Δ (aa, tRNA) Kit were purchased from New England Biolabs (Ipswich, MA). Dimethylsulfoxide (DMSO), HEPES, phenol, chloroform, methanol, ethyl acetate, dichloromethane (DCM), toluene, triethylamine (TEA), magnesium acetate, and sodium chloride were purchased from Sigma-Aldrich (St. Louis, MO) or Fisher Scientific (Hampton, NH). L-tyrosine methyl ester, benzyl 2-cyanoacetate, methyl 4-nitrobutanoate, ethyl 4,4,4-trifluoroacetoacetate, ethyl benzoylacetate, and ethyl 2,4-dioxo-4-phenylbutanoate were purchased from Sigma-Aldrich (St. Louis, MO). ethyl 2-cyano-2-phenylacetate was purchased from Thermo Scientific (Waltham, MA). methyl 2-nitroacetate and 1,3-cyclohexanedione were purchased from Tokyo Chemical Industry (Tokyo, JPN). ethyl 2-fluoroacetoacetate was purchased from Matrix Scientific (Columbia, SC).

Ytterbium(III) trifluoromethanesulfonate ($Yb(OTf)_3$, 99.99%) was purchased from Sigma-Aldrich (St. Louis, MO). Absolute ethanol was purchased from Decon Labs (King of Prussia, PA) or from AmericanBio (Canton, MA). Glacial acetic acid was purchased from J.T. Baker [Avantor] (Radnor, PA). Unless otherwise noted, all water used in biochemical work or achiral HPLC was dispensed from a MilliporeSigma™ Milli-Q™ system at 18.2 megohm ionic purity. Stock solutions of flexizyme, microhelix, tRNA, amino acids, acyl-tRNA, primers, and DNA templates were assembled using unbuffered Milli-Q water. All other chemical reagents were purchased from commercial sources and used without further purification unless otherwise noted.

All reactions were carried out under ambient atmosphere unless otherwise noted. Room temperature (RT) is defined as 21–23 °C. *N,N*-diisopropylethylamine (DIPEA) was distilled over CaH under a nitrogen atmosphere prior to use or dispensed from a Sigma-Aldrich Sure/Seal™ container (99.5%, purified via redistillation) under a nitrogen atmosphere. Dry dichloromethane (DCM) and dry *N*,*N*-dimethylformamide (DMF), when indicated, were dried over alumina and dispensed under argon from a GlassContour® Seca Solvent Purification System or from a Sigma-Aldrich Sure/Seal™ container under a nitrogen atmosphere. Deionized water was used for reactions, extraction solutions, and automated reverse phase column chromatography. Acetonitrile (MeCN) and ethyl acetate (EtOAc) used for chromatography were High-Performance Liquid Chromatography (HPLC) grade, while hexanes used for chromatography was either certified ACS grade or HPLC grade. Methanol used for chromatography was either certified ACS grade or electronic grade.

High-resolution mass spectrometry (HRMS) was performed using: (i) a Shimadzu Scientific Instruments Quadrupole Time-of-Flight (Q-TOF) 9030 high resolution mass spectrometer using

electrospray ionization (ESI); (ii) an LTQ FT-ICR mass spectrometer equipped with an electrospray ionization source (Finnigan LTQ FT, Thermo Fisher Scientific, Waltham, MA) operated in either positive or negative ion mode; or (iii) an Agilent 6530 Accurate-Mass Q-TOF LC-MS using electrospray ionization in positive mode. For crude data analysis, ultra-performance liquid chromatography-mass spectrometry (UPLC-MS) was performed with a Waters Acquity LC-MS instrument equipped with a reverse phase BEH C18 column (1.7 mm particle size, 2.1 x 50 mm), a dual atmospheric pressure chemical ionization (APCI)/electrospray ionization (ESI) mass spectrometry detector, and a photodiode array detector.

Fourier-Transform (FT) infrared (IR) spectroscopy measurements were recorded on a Shimadzu IRTracer-100 spectrometer equipped with a diamond ATR unit, and select ν_{max} are reported in cm^{-1}, rounded to the ones digit. Data was recorded in the range from 400 to 4000 cm^{-1} with a resolution of 2 cm^{-1}. For each reported spectrum, 64 scans were averaged, and air was subtracted as background. Data acquisition and post-processing were performed with LabSolutions IR Version 2.23.

Analytical thin-layer chromatography (TLC) was performed using 60 Å Silica Gel F254 pre-coated plates (0.25 mm thickness). TLC plates were visualized by irradiation with a UV lamp. Flash chromatography was performed using either a Biotage® Isolera One purification system equipped with a 10, 25, 50, 100 or 340 g SNAP Ultra (HP Sphere, 25 μm silica) or Sfär Duo (60 μm silica) cartridge for normal phase column chromatography, and 12, 30, 60, or 120 g SNAP C18 or SNAP Ultra C18 columns for reverse phase column chromatography; or a Teledyne ISCO Combiflash NextGen 300+ equipped with a 4, 12, or 24 g RediSep columns for normal phase column chromatography. Reverse phase preparative HPLC purification was performed on an Waters LC Prep 150 system equipped with a Waters 2998 UV photodiode array detector, a Waters 2707 autosampler, and an Waters Fraction Collector III using a preparative reverse phase C18 column (CSH C18 19 x 150 mm OBD Column 5 μm). The mobile phase for reverse phase preparative HPLC was water with 0.1% (v/v) trifluoroacetic acid (solvent A) and acetonitrile with 0.1% (v/v) trifluoroacetic acid (solvent B), at a flow rate of 20 mL/min. Analytes were collected based on their absorbance at 280 nm or 214 nm. Chiral normal phase semi-preparative HPLC purification was performed on a Shimadzu 20A series HPLC equipped with a Shimadzu SPD-20AV UV/visible detector, a DGU-20A 5R degassing unit, two LC-20AR solvent delivery units, a CBM-20A HPLC system controller, and an LH-40 liquid handler.

Routine ^1H nuclear magnetic resonance (NMR) spectra were recorded on Agilent or Bruker 400, 500, 600, or 700 MHz spectrometers at ambient temperature unless otherwise stated. Chloroform-*d* ($CDCl_3$, with or without 1% v/v tetramethylsilane [TMS]) and dimethylsulfoxide-d_6 (DMSO-d_6) were purchased from Cambridge Isotope Laboratories and used without further purification. $CDCl_3$ (with or without 1% v/v TMS) was stored at ambient temperature over 5Å molecular sieves or anhydrous K_2CO_3. DMSO-d_6 in 1 g ampoules was used immediately upon opening. Larger volumes of DMSO-d_6 were dried, at minimum, overnight and stored over freshly-activated 3 Å molecular sieve beads. Methanol-d_4 (CD_3OD) was purchased from Cambridge Isotope Laboratories or from Sigma Aldrich in ampoules that were used immediately upon opening. Deuterium Oxide (D_2O) was purchased from Sigma Aldrich and used as received.

Spectra were processed using MestReNova 14.3.3 using the manual or automatic phasing and baseline correction capabilities, as well as zero-filling and COSY-like symmetrization, as appropriate. Splitting was determined using the automatic multiplet analysis function with intervention as necessary. Spectral data are reported as follows: chemical shift (multiplicity [singlet (s), broad singlet (br s), doublet (d), triplet (t), quartet (q), pentet (p), multiplet (m), doublet of doublets (dd), doublet of doublet of doublets (ddd), doublet of triplet of doublets (dtd), doublet of doublet of doublet of doublets (dddd), doublet of triplets (dt), triplet of doublets (td), etc.], coupling constant (Hz), integration). The abbreviation "app" denotes an apparent multiplicity (e.g., "app t" denotes an apparent triplet). Chemical shifts are reported in parts per million (ppm, δ), and coupling constants are reported in Hz. ^{1}H resonances are referenced to solvent residual peaks for $CDCl_3$ (7.26 ppm), DMSO-*d*$_6$ (2.50 ppm), TMS (0.00 ppm), methanol-*d*$_4$ (CD_3OD, 3.31 ppm) or D_2O (4.79 ppm). Routine ^{13}C NMR spectra were recorded on Agilent or Bruker 400 (101), 500 (126), 600 (151), or 700 (176) MHz spectrometers with protons fully decoupled. ^{13}C Resonances are reported in ppm relative to solvent residual peaks for $CDCl_3$ (77.16 ppm), DMSO-*d*$_6$ (39.52 ppm), or methanol-*d*$_4$ (CD_3OD, 49.00 ppm).

Abbreviations

Ac – acetyl
AcOH – acetic acid
ACS – American Chemical Society
AJS – Agilent Jet Stream
APCI – Atmospheric Pressure Chemical Ionization
aq. – aqueous
ATR – Attenuated Total Reflectance
Bn – benzyl
Boc – *tert*-butoxycarbonyl
βk – β-keto [amide]
ca. – *circa* ("approximately")
CaH – calcium hydride
Calcd, calcd., or calc. – calculated
CAN – ceric ammonium nitrate
CCD – charge-coupled device
CCDC – Cambridge Crystallographic Data Center
$CDCl_3$ – chloroform-*d*
CD_3OD – methanol-*d*$_4$
$CeCl_3$•$7H_2O$ – cerium(III) chloride heptahydrate
$CHCl_3$ – chloroform
CH_2Cl_2 – (see DCM)
CIF – Crystallographic Information File
CME – cyanomethyl ester
conc. – concentrated
COSY – Correlated Spectroscopy
CV – column volume(s)
D_2O – deuterium oxide
DAA – diketene acetone adduct (2,2,6-Trimethyl-4*H*-1,3-dioxin-4-one)
DCM – dichloromethane (methylene chloride)

dFx – dinitro-flexizyme
DI – deionized
DIPEA – *N,N*-diisopropylethylamine (Hünig's base)
DMAP – 4-dimethylaminopyridine
DMF – *N,N*-dimethylformamide
DMSO – dimethyl sulfoxide
DMSO-d_6 – dimethyl sulfoxide-d_6
DNB – 3,5-dinitrobenzyl [ester]
d.r. – diastereomeric ratio
EDC – 1-ethyl-3-(3-dimethylaminopropyl)carbodiimide hydrochloride
EDTA – ethylenediaminetetraacetic acid
eFx – enhanced flexizyme
EIC – Extracted Ion Chromatogram
equiv – equivalent(s)
ESI – Electrospray Ionization
Et_2O – diethyl ether
EtOAc – ethyl acetate
EtOH – ethanol (ethyl alcohol)
FAIR – Findable, Accessible, Interoperable, and Reusable
$FeCl_3 \cdot H_2O$ – iron(III) chloride monohydrate
fM – *N*-formyl-L-methionine or *N*-formyl-L-methionyl
Fmoc – fluorenylmethyloxycarbonyl
FT – Fourier-Transform
h – hour(s); min – minute(s)
H_2O – water
H_2SO_4 – sulfuric acid
HATU – hexafluorophosphate azabenzotriazole tetramethyl uronium
HBTU – hexafluorophosphate benzotriazole tetramethyl uronium
HCCA – α-cyano-4-hydroxycinnamic acid
HCl – hydrochloric acid
HEPES – 4-(2-hydroxyethyl)-1-piperazineethanesulfonic acid
Hex – hexanes
HFIP – hexafluoroisopropanol
HMBC – Heteronuclear Multiple Bond Correlation
HOBt – 1-hydroxybenzotriazole
HOTf – trifluoromethanesulfonic acid
HPLC – High-Performance Liquid Chromatography
HRMS – High-Resolution Mass Spectrometry
HSQC – Heteronuclear Single Quantum Coherence
ICR – ion cyclotron resonance
IR – Infrared
IVT – in vitro transcription/translation
K_2CO_3 – potassium carbonate
KOH – potassium hydroxide
Kyn – kynurenine
LC-(HR)MS – Liquid Chromatography-(High-Resolution)Mass Spectrometry

LiCl – lithium chloride
LTQ – linear trap quadrupole
M – molar (i.e., mol/L); N – normal
MALDI – Matrix-Assisted Laser Desorption/Ionization
MBHA – (4-methyl)benzhydrylamine
MeCN – acetonitrile
MeOH – methanol (methyl alcohol)
2-MeTHF – 2-methyltetrahydrofuran
$MgCl_2$ – magnesium chloride
$MgSO_4$ – magnesium sulfate
MH – microhelix
MS-MS – tandem mass spectrometry
MsOH – methanesulfonic acid
Na_2CO_3 – sodium carbonate
Na_2SO_4 – sodium sulfate
$NaHCO_3$ – sodium bicarbonate (sodium hydrogen carbonate)
NaOAc – sodium acetate
NaOH – sodium hydroxide
NMR – Nuclear Magnetic Resonance
PAGE – polyacrylamide gel electrophoresis
PCR – polymerase chain reaction
$Pd(TFA)_2$ – palladium(II) trifluoroacetate
PTFE – polytetrafluoroethylene
PyBOP – benzotriazole-1-yl-oxy-tris-pyrrolidino-phosphonium hexafluorophosphate
Q-TOF – Quadrupole Time-of-Flight
RP-HPLC – Reverse Phase High-Performance Liquid Chromatography
rt or RT – room temperature (21–23 °C)
SiO_2 – silicon dioxide (silica)
SPPS – solid-phase peptide synthesis
t-Bu – *tert*-butyl
TBE – Tris/Borate/EDTA
TBS – Tris-Buffered Saline
TCEP-HCl – tris(2-carboxyethyl)phosphine hydrochloride
TEA – triethylamine (also represented as Et_3N or NEt_3)
TEMED – tetramethylethylenediamine
TFA – trifluoroacetic acid
THF – tetrahydrofuran
TIPS – triisopropylsilane
TLC – Thin-Layer Chromatography
TMS – tetramethylsilane
TOCSY – Total Correlation Spectroscopy
Trt – triphenylmethyl (trityl)
U(H)PLC-MS – Ultra-(High) Performance Liquid Chromatography-Mass Spectrometry
UV – ultraviolet
v/v – volume/volume (i.e., mL/100 mL)
vide infra – “see below”

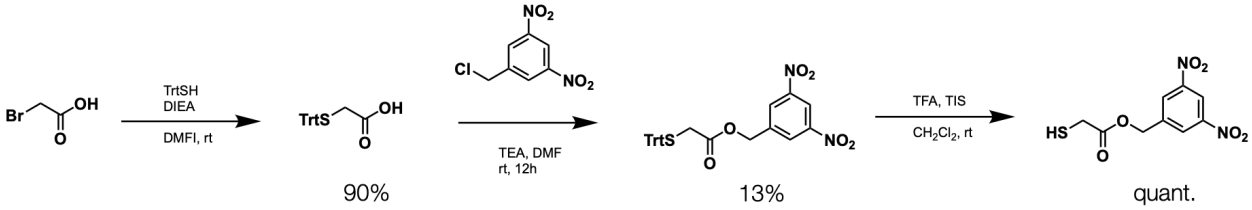
w/w – weight/weight (i.e., g/100 g)
$Yb(OTf)_3$ – ytterbium(III) trifluoromethanesulfonate
$Zn(OTf)_2$ – zinc(II) trifluoromethanesulfonate

Synthetic details

Synthesis of 1

The synthesis of monomer **1a**, **1b**, and **1** was performed in the Miller lab at Yale. Detailed methods for the preparation can be found in the dissertation of Diondra Dilworth entitled "Chemical Platforms for Non-Extant Ribosomal Chemistry: Synthetic Efforts Towards Ribosome-Assisted Polyketide-Polypeptide Products", which at the time of writing is embargoed.

Synthesis of 2

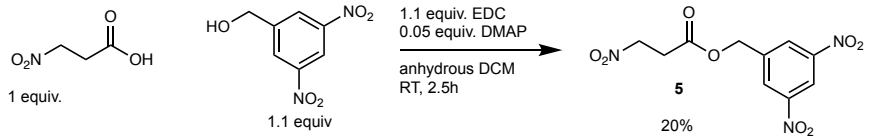


(S)-3,5-dinitrobenzyl 2-mercaptoacetate **2** was synthesized in accordance with literature precedent[9]. **^{1}H NMR** (500 MHz, $CDCl_3$) δ 9.04 – 9.00 (m, 2H), 8.59 (dd, *J* = 10.3, 1.7 Hz, 4H), 5.38 (d, *J* = 12.7 Hz, 4H), 3.67 (s, 2H), 3.38 (d, *J* = 8.5 Hz, 2H), 2.06 (t, *J* = 8.5 Hz, 1H), 1.25 (s, 1H).

*Synthesis of dicarbonyl monomers **3, 4, pyruvate-DBE**, and **acetopyruvate-DBE***

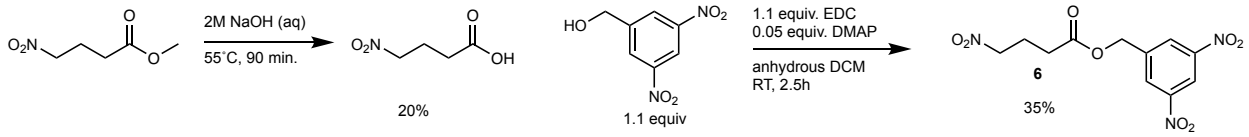
Synthetic information for these monomers can be found in Chapter 3 of this thesis. Compounds are renumbered as **1-4 DBEs**.

*Synthesis of Nitro-alkyl monomers **5, 6, 7,** and **8***



3,5-dinitrobenzyl 3-nitropropanoate (5): 3-Nitropropanoic acid (50 mg, 0.42 mmol, 1 equiv), 3,4-Dinitrobenzyl alcohol (83 mg, 1.1 equiv), 1-Ethyl-3-(3-dimethylaminopropyl)carbodiimide (89 mg, 1.1 equiv) and 4-Dimethylaminopyridine (2.6 mg, 0.05 equiv) were added into a microwave vial, which was then pump-purged 3x with nitrogen. 1 mL of dry DCM was then added to the reaction vessel and stirred for 2.5 hours. The reaction mixture was diluted with DCM then transferred to a separatory funnel. The solution was then washed with dilute aqueous HCl (0.01M). The aqueous layer was reextracted twice with DCM. Combined organics were then

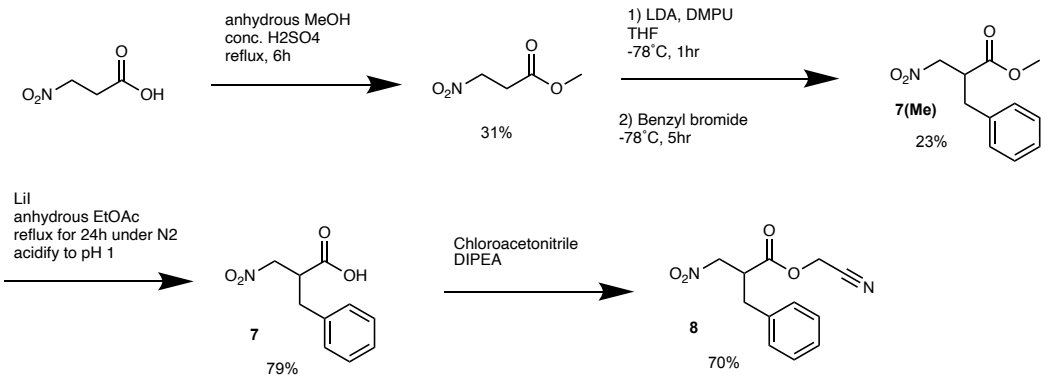
washed with brine, dried over Na_2SO_4, then filtered and rotovaped. The sample was then dry loaded onto silica and purified over 45 col volumes with a gradient of 0-50% EtOAc in Hexanes to yield the title compound in 20% yield (26 mg). **^{1}H NMR** (500 MHz, $CDCl_3$) δ 9.05 (t, *J* = 2.0 Hz, 1H), 8.59 (d, *J* = 2.0 Hz, 2H), 5.41 (s, 2H), 4.76 – 4.70 (m, 2H), 3.16 – 3.10 (m, 2H). **^{13}C NMR** (126 MHz, $CDCl_3$) δ 169.25, 148.85, 139.77, 128.06, 118.91, 77.41, 77.16, 76.91, 69.48, 64.81, 31.01, 14.33.



3,5-dinitrobenzyl 4-nitrobutanoate (6):

4-nitrobutanoic acid was first synthesized in accordance with literature precedent[29]. In short, Methyl 4-nitrobutanoate (2, 1.02 mL, 8 mmol) was added to a solution of NaOH (400 mg, 10 mmol) in 5 mL of water and the resulting solution was heated at 55 °C for 90 min. The mixture was extracted with CH2Cl2 (3 x1 5 mL) to remove unreacted compound 2. The aqueous layer was then acidified until pH ≈ 1 by addition of 2 M HCl and extracted with CH2Cl2 (3 x 15 mL). The combined organic layers were dried over anhydrous MgSO4 and evaporated under reduced pressure. Deviating from literature, I then purified the acid on with normal phase chromatography using a gradient of 0-5% MeOH in DCM. This yielded 260 mg (26%) of 4-nitrobutanoic acid. **^{1}H NMR** (500 MHz, $CDCl_3$) δ 4.51 (t, *J* = 6.7 Hz, 2H), 2.58 (t, *J* = 7.0 Hz, 2H), 2.35 (p, *J* = 6.9 Hz, 2H).

4-nitrobutanoic acid (72mg, 0.54 mmol, 1 equiv), 3,4-Dinitrobenzyl alcohol (118 mg, 1.1 equiv), 1-Ethyl-3-(3-dimethylaminopropyl)carbodiimide (114 mg, 1.1 equiv), and 4-Dimethylaminopyridine (3.3 mg, 0.05 equiv) were added into a microwave vial, which was then pump-purged 3x with nitrogen. 1.3 mL of dry DCM was then added to the reaction vessel and stirred for 2.5 hours. The reaction mixture was diluted with DCM then transferred to a separatory funnel. The solution was then washed with dilute aqueous HCl (0.01M). The aqueous layer was reextracted twice with DCM. Combined organics were then washed with brine, dried over Na_2SO_4, then filtered and rotovaped. The sample was then dry loaded onto silica and purified over 45 col volumes with a gradient of 0-50% EtOAc in Hexanes. The title compound was afforded in 35% yield (60 mg). **^{1}H NMR** (500 MHz, $CDCl_3$) δ 9.05 (t, *J* = 2.1 Hz, 1H), 8.58 (d, *J* = 2.1 Hz, 2H), 5.35 (s, 2H), 4.56 – 4.50 (m, 2H), 2.65 (t, *J* = 7.1 Hz, 2H), 2.39 (p, *J* = 6.9 Hz, 2H). **^{13}C NMR** (126 MHz, $CDCl_3$) δ 171.46, 148.86, 140.14, 128.08, 118.83, 77.41, 77.16, 76.91, 74.24, 64.34, 30.42, 22.29.



2-benzyl-3-nitropropanoic acid (7) – mixture of enantiomers:

Methyl 3-nitropropanoate was first synthesized in analogy to literature precedent[30]. 3-Nitropropanoic acid (400 mg, 2.26 mmol, 1 equiv.) and 67µL of concentrated H_2SO_4 were boiled in 5 mL of methanol for 5 hours under reflux. The reaction mixture was then concentrated down to one third the original volume, dissolved in diethyl ether and washed with brine. After drying over $MgSO_4$, rotary evaporation and high vacuo overnight yielded 138 mg of Methyl 3-nitropropanoate (31%). **^{1}H NMR** (500 MHz, $CDCl_3$) δ 7.26, 4.67, 4.65, 4.65, 4.64, 3.75, 3.00, 2.99, 2.98. **^{13}C NMR** (126 MHz, $CDCl_3$) δ 170.00, 77.41, 77.16, 76.91, 69.79, 52.57, 30.99.

methyl 2-benzyl-3-nitropropanoate (**7(Me))** was then synthesized in accordance with the literature[31]. A microwave vial equipped with a magnetic stirrer and a nitrogen line, was charged with dry tetrahydrofuran (3 mL) and diisopropylamine (2.13 mmol, 2.2 eq.). The mixture was cooled to -78˚C, and n-butyllithium (2.5 M in hexanes, 857 µL, 2.0 eq.) was added dropwise. The mixture was stirred at 0˚C for 30 min, then cooled to -78˚C and a solution of methyl 3-nitropropanoate (124 mg, 0.93 mmol, 1.0 eq.) and 1,3-dimethyl-3,4,5,6-tetrahydro-2(1H)-pyrimidinone (DMPU) (1.1 mL, 10.0 eq.) in dry tetrahydrofuran (1 mL) was added dropwise. The reaction was stirred for 30 min at -78˚C, then benzyl bromide (110 µL, 0.93 mmol, 1.0 eq.) was added dropwise. After 2 hours, TLC showed full conversion. The reaction was quenched with 1M HCl and extracted three times with EtOAc. The organic layer was washed once with water then once with a saturated aqueous solution of sodium bicarbonate. It was dried over anhydrous Na2SO4, filtered and the filtrate was concentrated under vacuum. The purification was achieved by flash column chromatography 5-90% EtOAc in Hexanes to give 47 mg (23 % yield) of methyl 2-benzyl-3-nitropropanoate as a light yellow oil. **^{1}H NMR** (500 MHz, $CDCl_3$) δ 7.38 – 7.17 (m, 4H), 7.15 (d, J = 7.0 Hz, 2H), 4.66 (dd, J = 14.6, 9.0 Hz, 1H), 4.35 (dd, J = 14.6, 4.5 Hz, 1H), 3.73 (s, 3H), 3.51 – 3.42 (m, 1H), 3.14 (dd, J = 14.0, 5.9 Hz, 1H), 2.82 (dd, J = 14.0, 9.0 Hz, 1H). **^{13}C NMR** (126 MHz, $CDCl_3$) δ 172.15, 136.53, 129.12, 128.98, 128.56, 127.53, 77.41, 77.16, 76.91, 74.20, 52.66, 44.64, 35.25.

2-benzyl-3-nitropropanoic acid (7) was then synthesized as previously reported[32]. methyl 2-benzyl-3-nitropropanoate **7(Me)** (40 mg, 0.18 mmol, 1 equiv.) and Lithium iodide (215 mg, 1.61 mmol, 9 equiv.) was added to a solution of anhydrous ethyl acetate (500 µL) in a microwave vial. The mixture was headed to reflux for 24 h under nitrogen. The solution was then cooled to RT, treated with water, acidified to pH 1.0 with 10% citric acid. The solution was then extracted with EtOAc three times, dried over sodium sulfate, filtered, and purified by flash column chromatography (20-50% EtOAc in Hexanes). The desired compound was afforded in in 79%

yield (29.7 mg). **^{1}H NMR** (500 MHz, $CDCl_3$) δ 7.46 – 7.06 (m, 6H), 4.65 (dd, *J* = 14.9, 8.9 Hz, 1H), 4.37 (dd, *J* = 14.9, 4.2 Hz, 1H), 3.52 (tdd, *J* = 9.4, 5.5, 4.3 Hz, 1H), 3.24 (dd, *J* = 14.1, 5.5 Hz, 1H), 2.86 (dd, *J* = 14.1, 9.3 Hz, 1H). **^{13}C NMR** (126 MHz, $CDCl_3$) δ 176.74, 136.08, 129.12, 128.87, 127.58, 77.28, 77.23, 77.03, 76.78, 73.57, 44.19, 34.83.

cyanomethyl 2-benzyl-3-nitropropanoate (8): 2-benzyl-3-nitropropanoic acid **(7) (3.7** mg, 0.018 mmol, 1 equiv) was dissolved in chloroacetonitrile (112 µL) under nitrogen in a microwave vial. DIPEA (3 µL, 0.018 mmol, 1 equiv) was added and the reaction was stirred at RT for 16 h. The solution was diluted in EtOAc, washed with 10% citric acid, followed by water, and brine. The organic was dried under sodium sulfate and filtered. It was then dried by rotary evaporation and on high vacuum overnight to afford the title compound without further purification (3 mg, 69% yield). **^{1}H NMR** (500 MHz, $CDCl_3$) δ 7.38 – 7.28 (m, 3H), 7.16 (dd, *J* = 7.0, 1.7 Hz, 2H), 4.80 (d, *J* = 15.6 Hz, 1H), 4.75 – 4.64 (m, 2H), 4.44 (dd, *J* = 15.0, 4.1 Hz, 1H), 3.53 (tdd, *J* = 9.0, 6.3, 4.2 Hz, 1H), 3.15 (dd, *J* = 14.0, 6.3 Hz, 1H), 2.87 (dd, *J* = 14.0, 8.8 Hz, 1H). Note: some vacuum grease is present in the NMR sample.

tRNA acylation and IVT

Transcription and purification of tRNAs.

DNA templates. DNA templates used for transcribing $tRNA^{fMet}$ and $tRNA^{AsnE2\#2}$ were prepared by annealing and extending the appropriate forward (Fwd) and reverse (Rev) ssDNA oligonucleotides (final concentration of 2 µM for each ssDNA) using Q5® High-Fidelity 2X Master Mix (NEB). Annealing and extension reactions followed the following protocol on a BioRad C1000 Touch™ thermocycler: 98 °C for 30 s, 10 cycles of [98 °C for 10 s, 55 °C for 30 s, 72 °C for 45 s], 10 cycles of [98 °C for 10 s, 67 °C for 30 s, 72 °C for 45 s], and 72 °C for 300 s. Following extension, the reaction mixture was supplemented with 3 M sodium acetate solution (pH 5.2) to a final concentration of 300 mM. It was then washed once with 1:1 (v/v) basic phenol (pH 8.0):chloroform and twice with chloroform. Ethanol was then added to 70% (v/v), the suspension of dsDNA was cooled at -80 °C for at least 1 h, and then centrifuged at 4 °C, 21,300 x G for 30 min. The supernatant was removed and the DNA pellet was washed with cold 70% (v/v) ethanol in water and centrifuged again at 4 °C, 21,300 x G for 10 min. The 70% ethanol wash was repeated and the pellet was air dried for 5 min before being resuspended in RNAse-free water. Excess nucleotides were removed from the product using a Micro Bio-Spin™ P-30 Gel Column (BioRad), pre-equilibrated with water, following the manufacturer's protocol. The concentration of dsDNA was determined using a NanoDrop ND-1000 (Thermo Scientific). Each one encodes a GG initiation sequence to increase T7 fidelity. Reverse primers for each tRNA carries a 2'-methoxy modification at the penultimate position, which reduces non-templated nucleotide addition by T7 RNA polymerase during in vitro transcription.

Transcription. HiScribe® T7 Quick High Yield RNA Synthesis Kit (New England Biolabs (NEB)) was used to generate each tRNA in 300 µL reactions containing 10 µg of DNA template,

20 µL of HiScribe® T7 RNA polymerase, and 100 µL of NTP buffer mix (final concentration of 6.7 mM each NTP). Transcription reactions were incubated at 37 °C for 2 h in a thermocycler with a heated lid, and then treated with 200 µL of nuclease-free water and 20 µL of RNAse-free DNAse I before an additional 1 h on the thermocycler to digest template DNA. 3M sodium acetate, pH 5.2 was added to a final concentration of 300 mM and the tRNA product was extracted once with 1:1 (v/v) acidic phenol (saturated with 0.1 M citrate buffer, pH 4.3):chloroform, twice with chloroform, and the tRNA product was precipitated upon addition of ethanol to 70% (v/v). Suspensions were incubated at -80 °C for at least 1 h before being centrifuged at 4 °C, 21,300 x G for 30 min and the supernatant removed. RNA pellets were washed with 70% (v/v) ethanol and centrifuged at 4 °C, 21,300 x G for 10 min. The ethanol wash was repeated once more and the pellet was air dried for 5 min before being resuspended in RNAse-free water. Excess nucleotides were removed from the product using a Micro Bio-Spin™ P-30 Gel Columns (BioRad), pre-equilibrated with water, following the manufacturer's protocol. The concentration of RNA was determined using a NanoDrop ND-1000 (Thermo Scientific). tRNA stock solutions (250 µM in water) were stored at -80 °C. If the concentration was too low after the spin column, the tRNA was ethanol precipitated once more, resuspended in water, quantified using a NanoDrop ND-1000, aliquoted, and stored at -20 °C at 250 µM.

Acylation of microhelix (MH) and tRNA using Flexizymes

tRNA and microhelix (MH) acylation protocols were modified from previously reported methods[6,7]. 1 µL of 250 µM Flexizyme (dFx or eFx) was added to 1 µL of 500 mM HEPES-KOH (pH 7.5) or 500 mM Bicine-KOH (pH 9.0) and 1 µL of 250 µM microhelix or tRNA. The samples were incubated at 95 °C for 2 min and cooled to RT over 5 min on a linear gradient using a thermocycler (BioRad C1000 Touch™). 2 µL of 3 M $MgCl_2$ was then added, followed by 1 µL of a DMSO solution of each flexizyme monomer (50 mM). Water was then added to 10 µL in all cases. The reaction was incubated at 4 °C for 2 to 48 h.

The extent of MH acylation was analyzed by gel-shift as described in previous work[8]. Specifically, 2 µL of acid-PAGE buffer (150 mM sodium acetate (pH 5.2), 10 mM EDTA, 95% (v/v) formamide, 0.02% (w/v) bromophenol blue) was added to 2 µL of the flexizyme reaction. The resulting samples subject to electrophoresis using an acid-urea PAGE-gel (20% acrylamide, 36% (w/v) urea, 50 mM sodium acetate (pH 5.2), 0.1% (w/v) ammonium persulfate, 0.08% (v/v) TEMED). The gel was run at RT at 120 V over the course of 3.5-4 h with 50 mM sodium acetate (pH 5.2) as the running buffer. The gel was imaged with ethidium bromide (1.0 µg/mL) in 50 mL TBE (10.8 g/L Tris, 5.5 g/L boric acid, 10 mM EDTA) for 1-2 min. The gel was destained in 50 mL TBE for 1 min and imaged on a Bio-Rad ChemiDoc™ Imager. UV densitometry was carried out using ImageJ (NIH, Bethesda, MD).

Analysis of MH and tRNA acylation products using intact tRNA LC-HRMS

Intact tRNA LC-MS was performed as previously reported[33]. Samples were ethanol precipitated and resuspended in water before analysis using intact tRNA LC-MS. In general, 20 pmol of tRNA was injected to ensure adequate signal in the UV and ion chromatograms. Samples were resolved on a ACQUITY UPLC BEH C18 column (130 Å, 1.7 µm, 2.1 mm X 50 mm, Waters

part # 186002350, 60 °C) using an ACQUITY UPLC I-Class PLUS (Waters part # 186015082). The mobile phases used were (A) 8 mM TEA, 80 mM HFIP, 5 µM EDTA (free acid) in 100% MilliQ water; and (B) 4 mM TEA, 40 mM HFIP, 5 µM EDTA (free acid) in 50% MilliQ water/50% methanol. Samples were eluted using a flow rate of 0.3 mL/min. The elution method began with Mobile Phase B at 22%; the fraction of Mobile Phase B increased linearly to 40% B over 10 min and from 40 to 60% B over 1 min and was then held at 60% B for 1 min. The fraction of Mobile Phase B was then decreased linearly from 60 to 22% B over 0.1 min and held at 22% B for 2.9 min to equilibrate the column. For more difficult separations, the method was extended as needed. For tRNA acylation, the linear gradient of Mobile Phase B from 22% to 40% was extended to 20 min. The mass of the RNA was analyzed using LC-MS with a Waters Xevo G2-XS Tof (Waters part #186010532) in negative ion mode with the following parameters: capillary voltage: 2000 V, sampling cone: 40, source offset: 40, source temperature: 140 °C, desolvation temperature: 20 °C, cone gas flow: 10 L/h, desolvation gas flow: 800 L/h, 1 spectrum/s. Expected masses of oligonucleotide products were calculated using https://www.cusabio.com/m-299.html#a02 or OligoCalc (for OligoCalc, the mass of H_2O must be added to accurately account for the full molecular weight of the triphosphate). Deconvoluted mass spectra were obtained using the MaxEnt software (Waters Corporation).

Acylation yields were estimated in two ways: In most cases, the relative absorbance of the chromatographically resolved peaks representing acyl- and non-acylated tRNA at 260 nm was adequate to estimate acylation yield. In some cases, low acylation obscured clear A_{260} signals or multiple UV-active species eluted simultaneously. In these cases, extraction of the expected major ion for acylated-MH, over the range of a single ionization envelope, was compared to an equivalent extracted ion chromatogram for the unacylated-MH. A detailed description of these methods is found in previous reports from our lab.

Preparative acylation of tRNA using Flexizymes in preparation for *in vitro* translation

For tRNA acylation reactions performed in preparation for IVT experiments, 3 µL of 250 µM Flexizyme (dFx or eFx) was added to 3 µL of 500 mM HEPES-KOH (pH 7.5) or 500 mM Bicine-KOH (pH 9.0) and 3 µL of 250 µM tRNA. The samples were incubated at 95 °C for 2 min and cooled to RT over 5 min on a linear gradient using a thermocycler (BioRad C1000 Touch™). To this solution was added 6 µL of 3 M $MgCl_2$ followed by 3 µL of a DMSO solution of the appropriate esterified monomer (DNB or CME) to a final concentration 50 mM. Water was then added to a final volume of 30 µL and the reaction was incubated at 4 °C for the optimal time determined in the microhelix acylation optimization experiment. A small sample of the reaction mixture was analyzed using intact tRNA LC-MS of acylated tRNA as described above.

Transcription of DNA templates encoding peptide for *in vitro* translation

Templates for the expression of flag-tagged peptide were prepared by annealing and extending the forward (Fwd) and reverse (Rev) ssDNA oligonucleotides (final concentration of 2 µM for each ssDNA) using Q5® High-Fidelity 2X Master Mix (NEB) and a BioRad C1000 Touch™ thermocycler. The preparation of these DNA templates is identical to the preparation of DNA templates for tRNA found above. The concentration of dsDNA was determined using a

NanoDrop ND-1000 (Thermo Scientific). The dsDNA was diluted to a concentration of 500 ng/µL and stored at -20 °C until use in translation.

In vitro translation (IVT) with tRNAs acylated with C-C bond monomers

In vitro transcription/translation of peptide encoding DNA templates was performed using the PURExpress® Δ (aa, tRNA) Kit (New England Biolabs, E6840S) according to a previous protocol with minor modifications[1]. IVT reactions (12.5 µL) were set up by mixing the following components sequentially in a 200 µL microcentrifuge tube: Solution A (ΔtRNA, Δaa; 2.5 µL), an amino acid stock mix (1.25 µL; 3.3 mM L-glycine, 3.3 mM L-valine, 3.3 mM L-aspartic acid, 3.3 mM L-tyrosine, 3.3 mM L-lysine), tRNA solution (1.25 µL), Solution B (3.75 µL), 250 ng dsDNA MGVDYKDDDDK template (0.5 µL), and 750 pmol $tRNA^{fMet}$ acylated with **monomers of interest** (3.25 µL). IVT reactions were incubated in a thermocycler (BioRad C1000 Touch™) at 37 °C for 2 h and quenched on ice prior to purification and analysis by mass spectrometry.

Anti-FLAG magnetic bead purification

Translated peptides were purified from in vitro translation reactions by enrichment using Anti-FLAG® M2 Magnetic Beads (Millipore Sigma) according to the manufacturer's protocol with slight modifications. First, 12.5 µL of a 50% (v/v) magnetic bead suspension was dispensed in a 200 µL microcentrifuge tube. [Note that to preserve the integrity of the beads and reduce the shear forces they experience, the end of a 20 µL pipette tip was removed with scissors and used to dispense the bead slurry. The beads should not be vortexed, and should be gently mixed by rotation or flicking to resuspend the slurry.] The beads were washed by adding 100 µL of TBS (150 mM NaCl, 50 mM Tris-HCl, pH 7.6), the tube was flicked by hand to mix, placed on a magnetic manifold, and the supernatant was removed. The beads were washed twice more with 100 µL of TBS, incubating for 10 min at RT in TBS, each time removing the supernatant using the magnetic manifold. The entire IVT reaction mixture described above (12.5 µL) was added to the washed beads and incubated at RT for 30 min with periodic agitation by flicking. The beads were washed three times with 100 µL of TBS as described above and the bound products eluted using 20 µL of 0.1 M glycine-HCl (pH 2.8) for 10 min. The supernatant was transferred to LC-MS vials for analysis.

Peptide analysis by LC-HRMS

The peptide products generated using IVT were analyzed using a previously reported protocol[1]. Briefly, 17 µL of the eluent obtained after anti-FLAG magnetic bead purification was injected on an ZORBAX Eclipse XDB-C18 column (1.8 µm, 2.1 Å, ~ 50 mm, RT, Agilent) using an 1290 Infinity II UHPLC (G7120AR, Agilent). The products of most IVT reactions were resolved using the following method: an initial 0.5 min at 95% Solvent A (0.1% formic acid in water) and 5% Solvent B (0.1% formic acid in acetonitrile) followed by a linear gradient from 5 to 50% Solvent B over 4.5 min at flow rate of 0.7 mL/min. Peptides were identified using LC-HRMS with an Agilent 6530 Q-TOF AJS-ESI (G6230BAR). The following parameters were used: a fragmentor voltage of 175 V, gas temperature of 300 °C, gas flow rate of 12 L/min, sheath gas

temperature of 350 °C, sheath gas flow rate of 11 L/min, nebulizer pressure of 35 psi, skimmer voltage of 75 V, Vcap of 3500 V, and collection rate of 3 spectra/s. Expected exact masses of the major charge state for each peptide were calculated using ChemDraw 19.0 and extracted from the total ion chromatograms ± 100 ppm.

Cryo-EM Studies

3'-amino tRNAs and Cryo-EM preparation were performed as previously described[34]. Enzymatic acylations were performed as previously described[20].

Intramolecular Model System



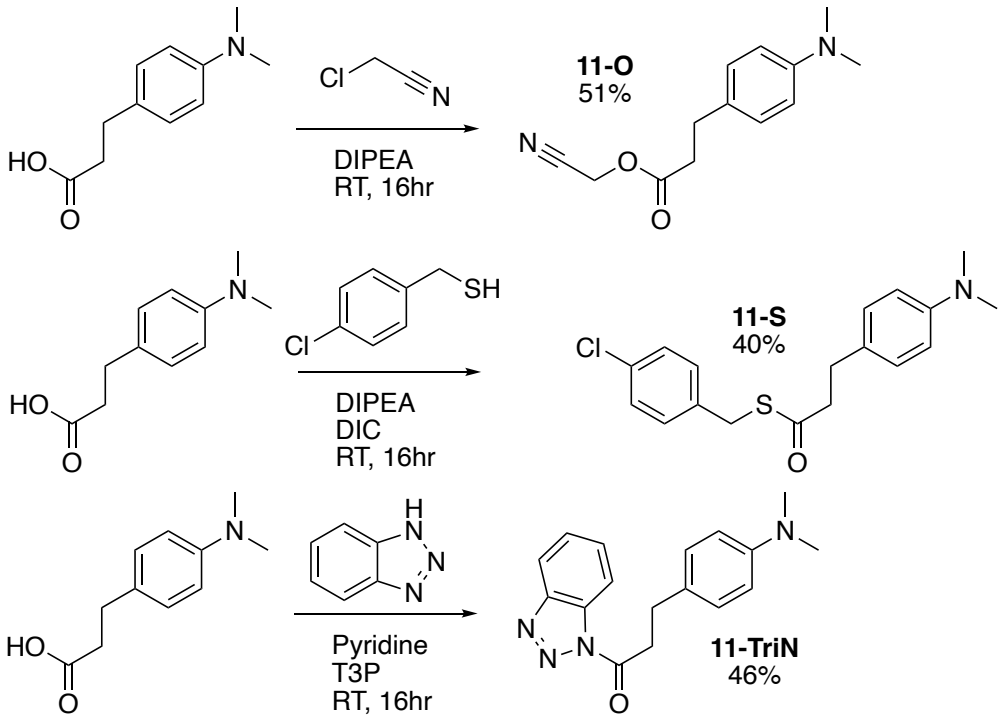
9

Synthesis of 3-nitropropyl 3-(4-(dimethylamino)phenyl)propanoate (9). To a 1.5 mL centrifuge tube was added 3-nitropropan-1-ol (0.024 mmol, 1 equiv., 2.1 µL), 3-(4-(dimethylamino)phenyl)propanoic acid (1.5 equiv. 4.5 mg), N,N′-Diisopropylcarbodiimide (1.5 equiv, 5.5 µL), and N-methylimidazole (1.5 equiv., 2.8 µL) in 40 µL of DCM. The reaction was flicked to mix and left at RT for 30 minutes. Upon completion by LCMS, 200 µL of water was added. A small hole was punched in the top of the tube and the tube was put into inside of a scintillation vial, which was then used as a vessel to contain the centrifuge tube for rotary evaporation. The DCM was evaporated off. The remaining aqueous solution was then injected onto reverse phase HPLC using a gradient that ramped up from 5-95% MeCN with 0.1% TFA in H2O with 0.1% TFA over 15 minutes. The product containing fractions were frozen at -80˚C and then lyophilized to yield the title compound as a white solid. (4.1 mg, 61% yield). **^{1}H NMR** (600 MHz, DMSO) δ 7.11 (d, *J* = 7.6 Hz, 2H), 6.86 (s, 2H), 4.54 (t, *J* = 6.8 Hz, 2H), 4.08 (t, *J* = 6.2 Hz, 3H), 2.76 (t, *J* = 7.5 Hz, 2H), 2.56 (t, *J* = 7.6 Hz, 2H), 2.18 (p, *J* = 6.5 Hz, 2H).

Test reactions on 9. 4.1 mg of material was taken up in H2O/MeCN and divided into 41 microcentrifuge tubes, which were then lyophilized. The dry material in microcentrifuge tubes was then used to test the reactivity of intramolecular O-to-C acyl shifts. Conditions tested are outlined Table 2.2. in all cases monomers were present at 6.4 mM and monitored at 2 and 16 hours by LC-MS. For LC-MS monitoring 1 µL of sample was taken up into 49 µL of H2O/MeCN and then 4 µL were injected onto a Waters Acquity ultra-performance liquid chromatography-mass spectrometry (UPLC-MS) instrument equipped with a reverse phase Acquity UPLC HSS T3 C18 column (1.8 mm particle size, 2.1 x 30 mm), a dual atmospheric pressure chemical ionization (APCI)/electrospray ionization (ESI) mass spectrometry detector (SQD2), and a photodiode array detector. The following method was used for separation: an initial condition of 90% Solvent A (0.1% formic acid in water) and 10% Solvent B (0.1% formic acid in acetonitrile) followed by a linear gradient from 10 to 95% Solvent B over 3.5 min at flow

rate of 0.5 mL/min. A linear gradient from 95% to 10% B over 0.1 min was used to reset the initial condition on the column, and the column was re-equilibrated at 10% B for 1.4 min before the next injection.

Intermolecular Model System



Synthesis of cyanomethyl 3-(4-(dimethylamino)phenyl)propanoate (11-O)

3-[4-(Dimethylamino)phenyl]propanoic acid (0.100mg, 0.517mmol, 1.0 equiv) was added to a flame-dried microwave vial that was cooled, sealed, and kept under N_2. Chloroacetonitrile (327uL, 5.17mmol, 10.0 equiv) and DIPEA (108uL, 0.621mmol, 1.2 equiv) were added to the vial. The reaction was stirred at RT for 16hr. EtOAc and water were used to transfer the reaction to a separatory funnel. The aqueous phase was extracted with EtOAc thrice, collecting and pooling the organic phase after each extraction. The organic layer was washed once with brine, dried over Na_2SO_4, and concentrated with rotary evaporation. The resulting oil was resuspended in EtOAc, absorbed onto SiO_2, and purified by automated flash column chromatography (0-40% EtOAc in hexanes) to afford the title compound (62 mg, 52%).
^{1}**H NMR** (500 MHz, CDCl3) δ 7.07 (d, J = 8.2 Hz, 2H), 6.71 – 6.67 (m, 2H), 4.70 (s, 2H), 2.92 (s, 6H), 2.89 (t, J = 7.8 Hz, 2H), 2.68 (dd, J = 8.3, 7.1 Hz, 2H).
^{13}**C NMR** (126 MHz, CDCl3) δ 171.62, 149.60, 129.02, 127.62, 114.53, 113.09, 48.32, 40.88, 35.74, 29.82.

Synthesis of S-(4-chlorobenzyl) 3-(4-(dimethylamino)phenyl)propanethioate (11-S)

3-[4-(Dimethylamino)phenyl]propanoic acid (0.100mg, 0.517mmol, 1.0 equiv) was suspended in 5mL DCM in a flame-dried microwave vial that was cooled, sealed, and kept under N_2. The vial was placed in an ice bath and allowed to stir for 10 minutes. DIPEA (90uL, 0.517mmol, 1.0 equiv) and DIC (81uL, 0.517mmol, 1.0 equiv) were added to the vial, and the solution was allowed to stir for 10 minutes. 4-Chlorobenzyl mercaptan (68uL, 0.517mmol, 1.0 equiv) was then added to the vial. The reaction was stirred at RT for 16hr. EtOAc and water were used to transfer the reaction to a separatory funnel. The aqueous phase was extracted with EtOAc thrice, collecting and pooling the organic phase after each extraction. The organic phase was washed once with brine, dried over Na_2SO_4, and concentrated with rotary evaporation. The resulting oil was resuspended in EtOAc, absorbed onto SiO_2, and purified by automated flash column chromatography (0-10% EtOAc in hexanes) to afford the title compound (70 mg, 40%).
^{1}**H NMR** (500 MHz, CDCl3) δ 7.25 (d, J = 8.6 Hz, 2H), 7.19 (d, J = 8.5 Hz, 2H), 7.03 (d, J = 8.6 Hz, 2H), 6.66 (d, J = 8.6 Hz, 2H), 4.06 (s, 2H), 2.91 (s, 6H), 2.89 (dd, J = 8.6, 1.7 Hz, 2H), 2.83 (ddd, J = 8.8, 6.4, 1.9 Hz, 2H).
^{13}**C NMR** (126 MHz, CDCl3) δ 198.13, 149.49, 136.54, 133.15, 130.33, 129.08, 128.85, 127.88, 113.05, 45.89, 40.91, 32.59, 30.70.

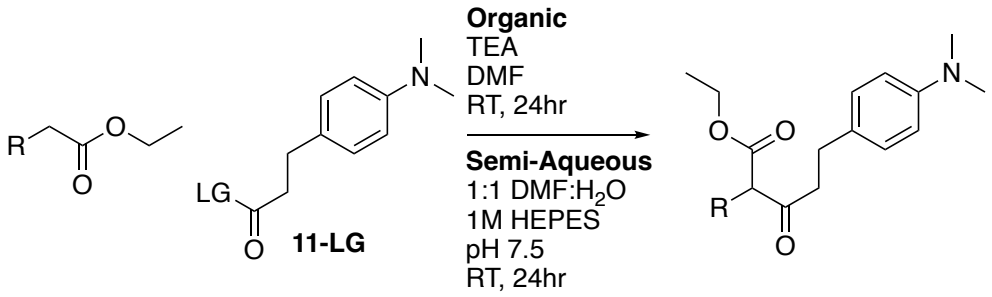
Synthesis of S-(4-chlorobenzyl) 3-(4-(dimethylamino)phenyl)propanethioate (11-TriN)

3-[4-(Dimethylamino)phenyl]propanoic acid (0.100mg, 0.517mmol, 1.0 equiv) was suspended in 1mL DMF, followed by the addition of pyridine (125uL, 1.552mmol, 3.0 equiv). 50% T3P in DMF (462uL, 0.776mmol, 1.5 equiv) was added dropwise to the reaction vessel while stirring, followed by the addition of benzotriazole (74mg, 0.621mmol, 1.2 equiv). The reaction was stirred at RT for 16hr. EtOAc and water were used to transfer the reaction to a separatory funnel. The organic phase was washed five times with water to remove DMF. The organic phase was washed once with brine, dried over Na_2SO_4, and concentrated with rotary evaporation. The resulting oil was resuspended in EtOAc, absorbed onto SiO_2, and purified by automated flash column chromatography (0-20% EtOAc in hexanes) to afford the title compound (71 mg, 46%).
^{1}**H NMR** (500 MHz, CDCl3) δ 8.30 (d, J = 8.3 Hz, 1H), 8.12 (d, J = 8.3 Hz, 1H), 7.65 (ddd, J = 8.2, 7.1, 1.0 Hz, 1H), 7.50 (ddd, J = 8.1, 7.1, 1.0 Hz, 1H), 7.19 (d, J = 8.6 Hz, 2H), 6.71 (d, J = 8.7 Hz, 2H), 3.72 (dd, J = 8.1, 7.2 Hz, 2H), 3.15 (t, J = 7.6 Hz, 2H), 2.92 (s, 6H).
^{13}**C NMR** (126 MHz, CDCl3) δ 172.13, 149.60, 146.33, 131.28, 130.48, 129.25, 127.89, 126.23, 120.28, 114.63, 113.15, 40.93, 37.72, 29.51.

Procedure for Intermolecular X-to-C acyl transfer model system

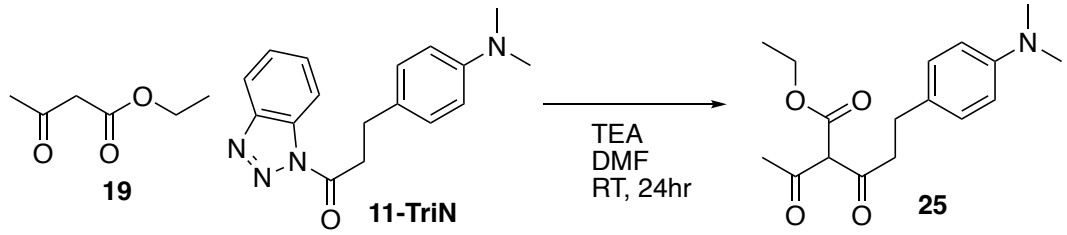
11-LG Preparation. Pure samples of **11-O, 11-S**, and **11-TriN** were dissolved in water:acetonitrile to a concentration of 30 mM (11-O; 30% ACN in H_2O. 11-S; 70% ACN in H_2O. 11-TriN; 50% ACN in H_2O). Solutions were allotted into 0.2 mL 8-well PCR tube strips at

0.1 mL (3 umol 11-LG) per well. Tube strips were closed with punctured caps and flash frozen. Aliquots were allowed to lyophilize overnight. Powdered **11-LG** aliquots were centrifuged and had their punctured caps removed and replaced with new caps. Aliquots were stored at -20˚C.



X-to-C acyl transfer **11-LG** aliquots were allowed to come up to room temperature. Stock solutions of nucleophile molecules (**12** - **23**) were prepared. For **Organic** conditions, nucleophile molecules were dissolved to a concentration of 0.3 M in a solution of TEA (1 eq.) in DMF. For **Semi-Aqueous** conditions, nucleophile molecules were dissolved to a concentration of 0.3 M in a solution of 1M HEPES in 1:1 DMF:H_2O that was brought to pH 7.5 with NaOH and HCl. 10uL of the stock solution was added to the 11-LG aliquots and the reaction mixture was thoroughly mixed. Reactions were sealed and placed on a 60 rpm shaker at room temperature for 24 hr. 2 uL of each reaction was taken and put into an empty 2 mL HPLC vial. 798 uL 70% ACN in water was added to each vial and gently mixed to evenly distribute the reaction mixture. For data analysis, ultra-performance liquid chromatography-mass spectrometry (UPLC-MS) was performed with a Waters Acquity LC-MS instrument equipped with a reverse phase BEH C18 column (1.7 mm particle size, 2.1 x 50 mm), a dual atmospheric pressure chemical ionization (APCI)/electrospray ionization (ESI) mass spectrometry detector, and a photodiode array detector. The major ion signal of the expected products were extracted and resultant extracted ion chromatograms were integrated. This integral value was compared against the integral value for the remaining 11-LG in the same total ion chromatogram to estimate the % yield of each reaction.

NMR Verification of Elongation Model System Products

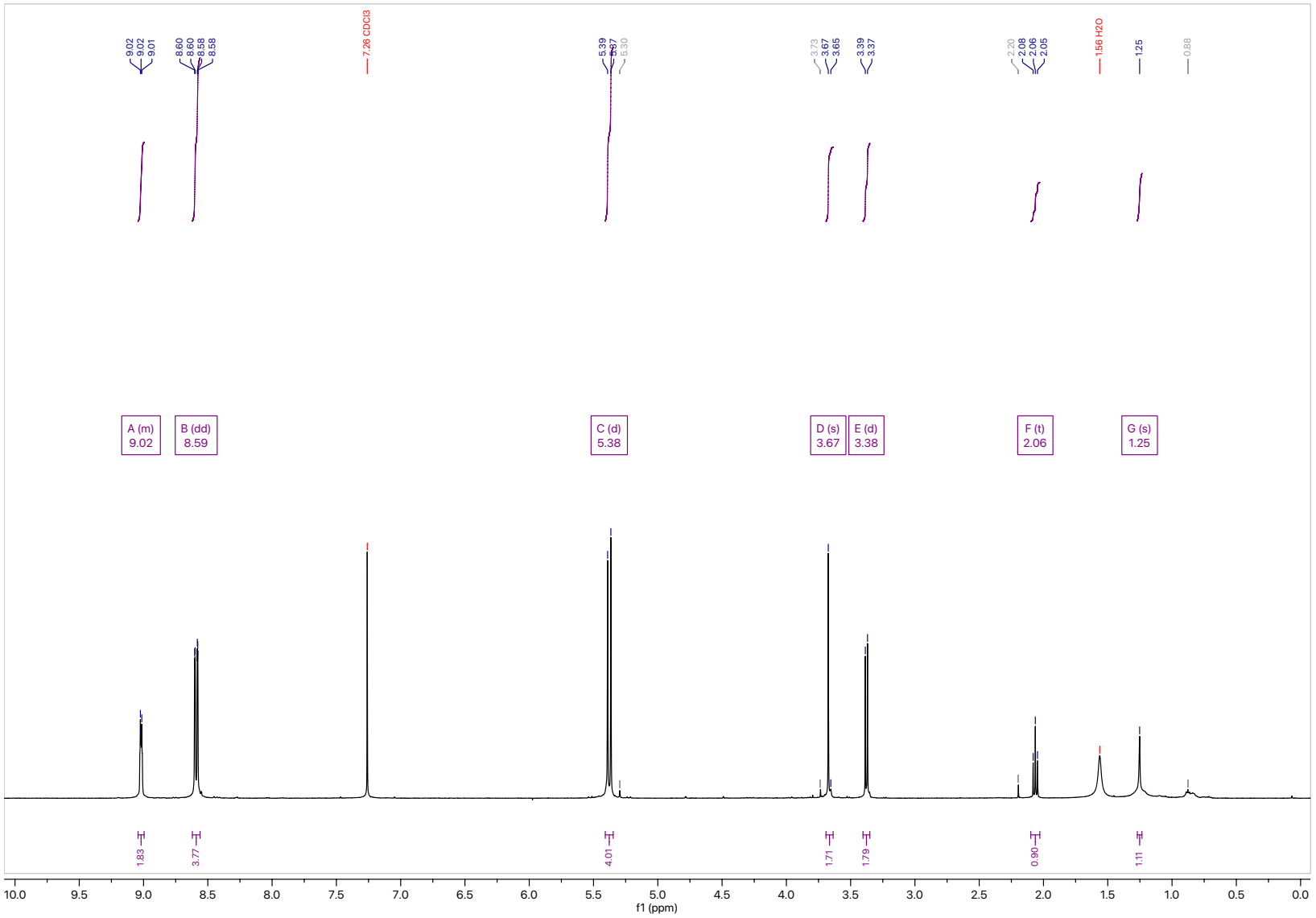


An Elongation Model System reaction was performed with **19** and **11-TriN** at a 24x scale (71 umol). EtOAc and water were used to transfer the reaction to a separatory funnel. The organic phase was washed five times with water to remove DMF. The organic phase was washed once with brine, dried over Na_2SO_4, and concentrated with rotary evaporation. The resulting oil was used to obtain ^{1}H and ^{13}C NMRs to observe the **25** product.

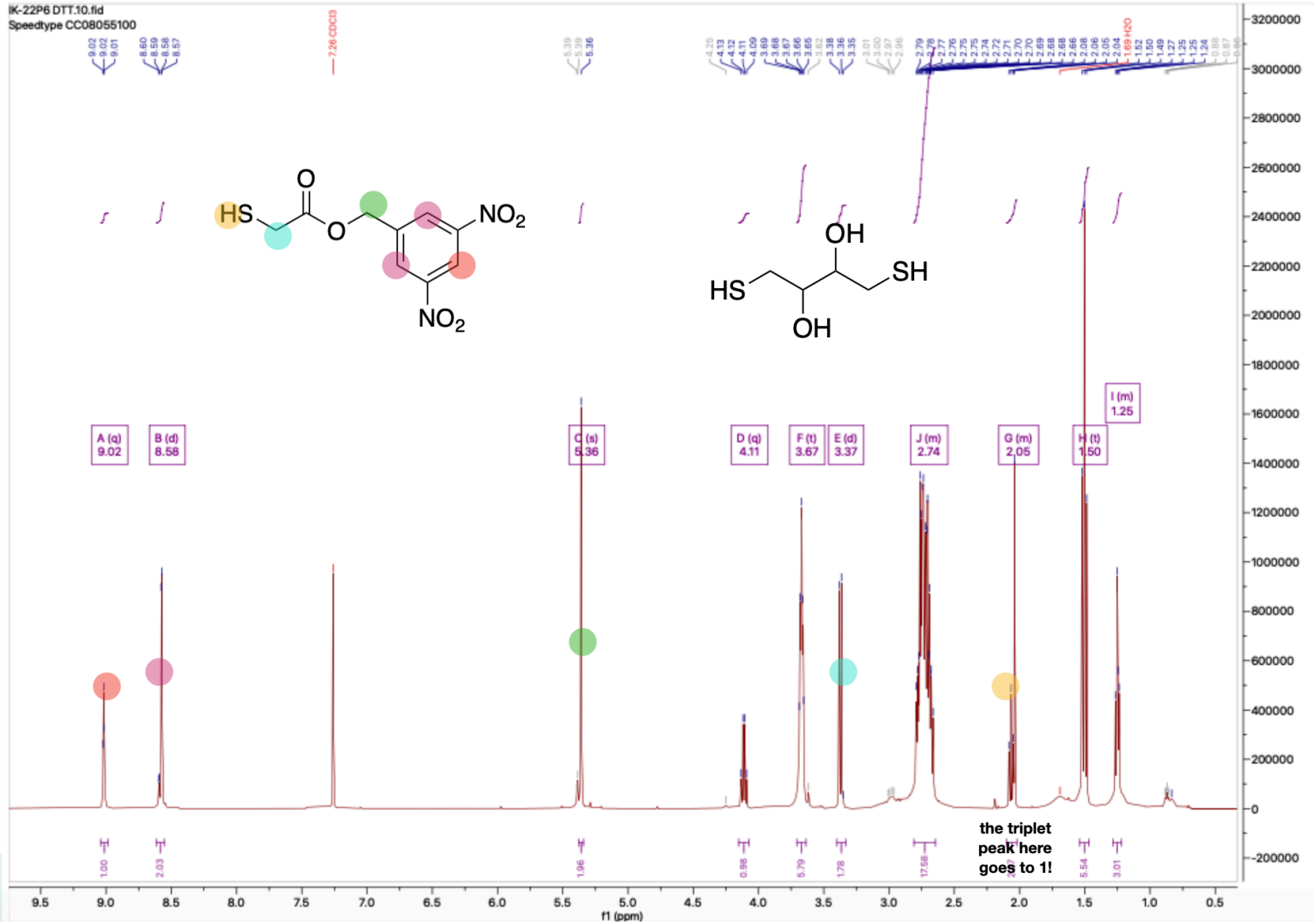
Note: *Due to 11-TriN and 11-8 having similar polarities, we were unable to obtain a pure sample 11-8. The spectra provided here has a notable amount of 11-TriN that was unable to be removed by purification. Using the* ^{1}*H NMR, it can be estimated that the molar ratio between 11-8 and 11-TriN is 10:3, which is consistent with the reactivity of* ***8*** *seen in 1x scale reactions within the same condition set. For the* ^{13}*C NMR, 2 peaks that should have appeared around 166.0 ppm and 148.3 ppm could not be found, likely due to the signal blending into the baseline noise.*
^{1}**H NMR** (500 MHz, CDCl3) δ 8.30 (d, J = 8.2 Hz, 1H), 8.12 (d, J = 8.3 Hz, 1H), 7.65 (ddd, J = 8.2, 7.1, 1.0 Hz, 1H), 7.53 – 7.48 (m, 1H), 7.19 (d, J = 8.7 Hz, 3H), 7.08 (d, J = 8.7 Hz, 2H), 6.70 (t, J = 8.9 Hz, 5H), 4.26 (q, J = 7.2 Hz, 2H), 3.72 (dd, J = 8.2, 7.2 Hz, 3H), 3.15 (t, J = 7.7 Hz, 3H), 2.91 (s, 6H), 1.32 (t, J = 7.1 Hz, 4H).
^{13}**C NMR** (126 MHz, CDCl3) δ 198.34, 195.74, 129.07, 128.88, 113.13, 60.95, 40.98, 40.17, 30.86, 29.86, 25.75, 14.39.

NMRs

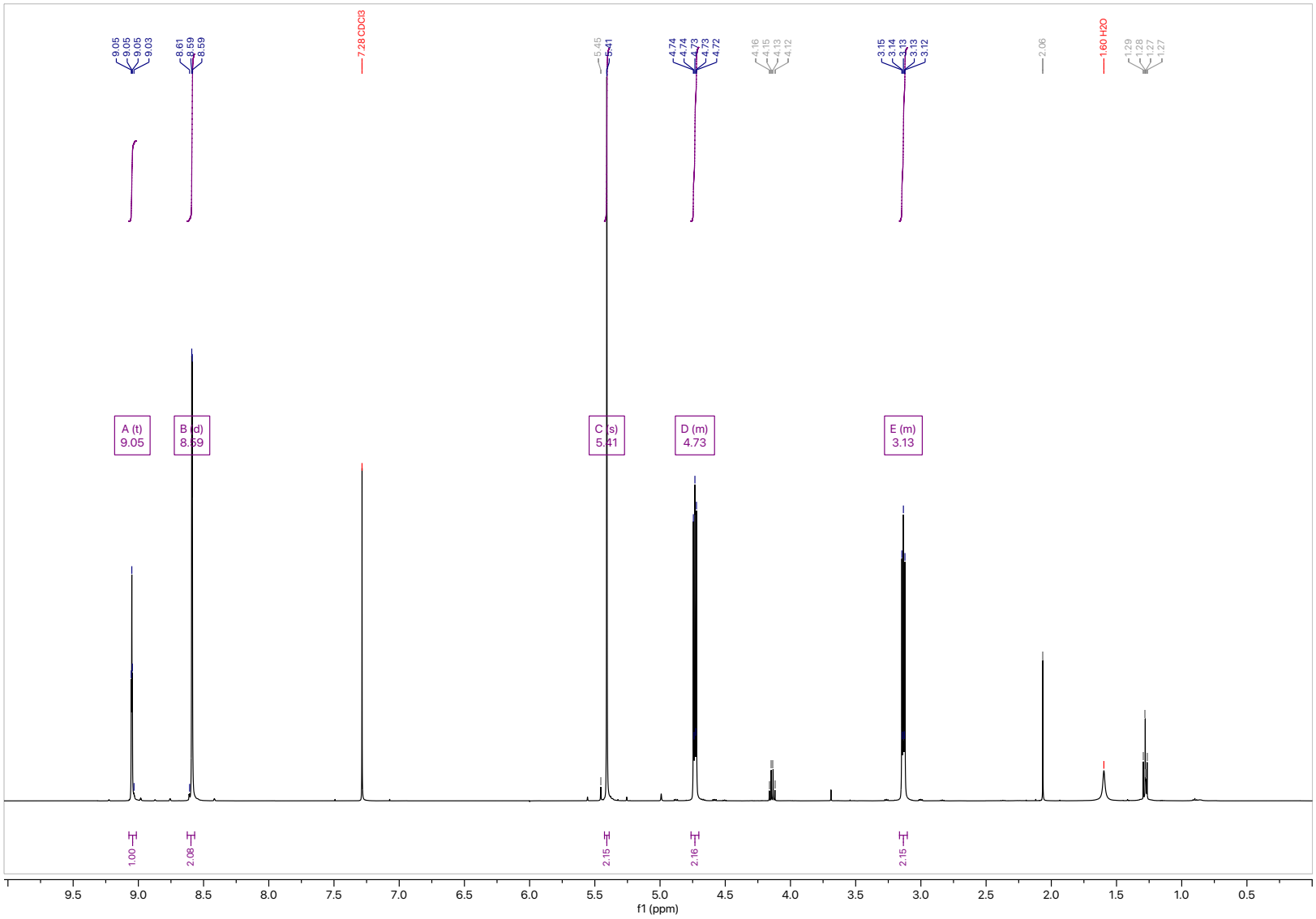
^{1}H NMR (500 MHz, $CDCl_3$) – standard view **(2)**



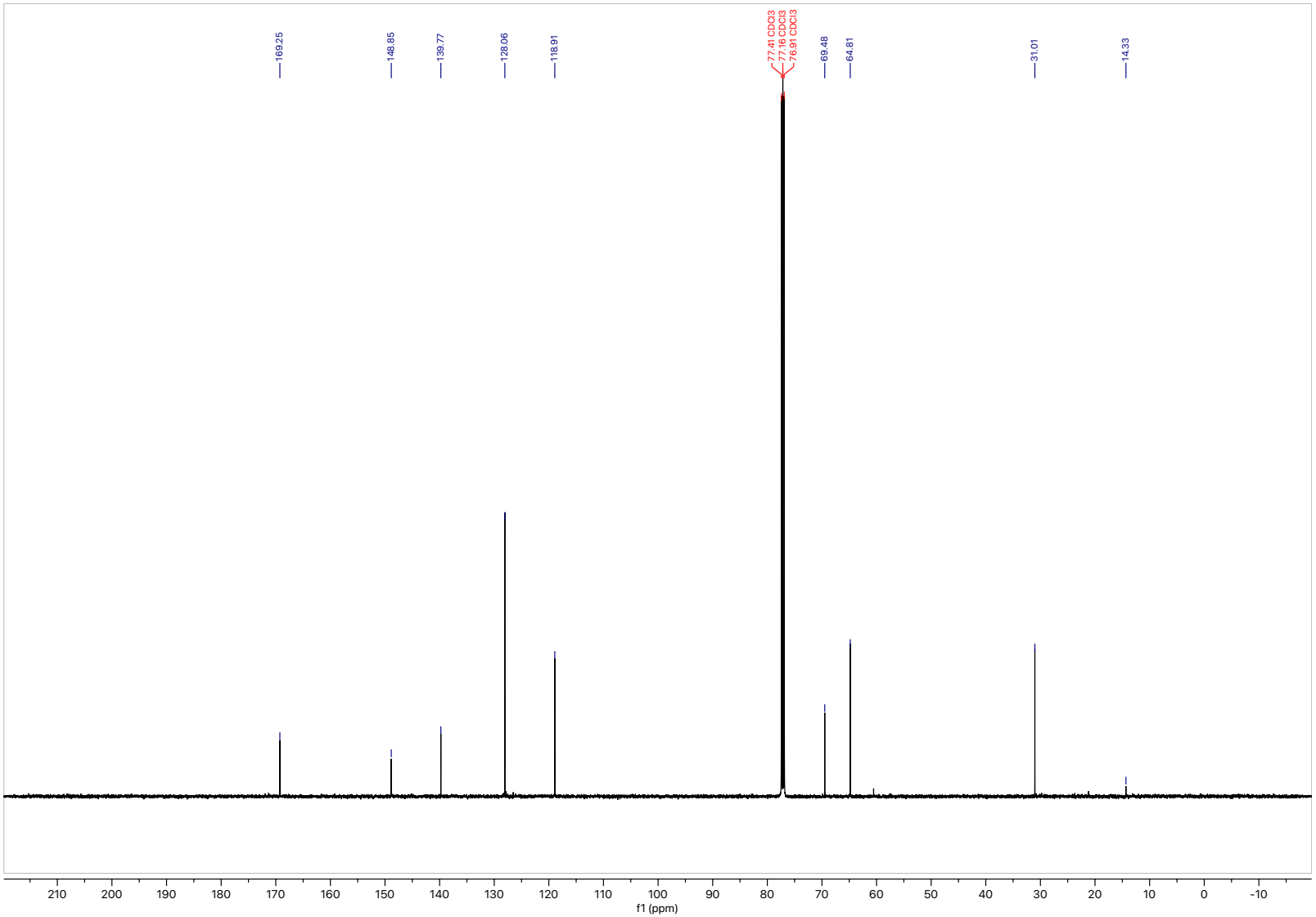
^{1}H NMR (500 MHz, $CDCl_3$) – standard view **(2** with **DTT)**



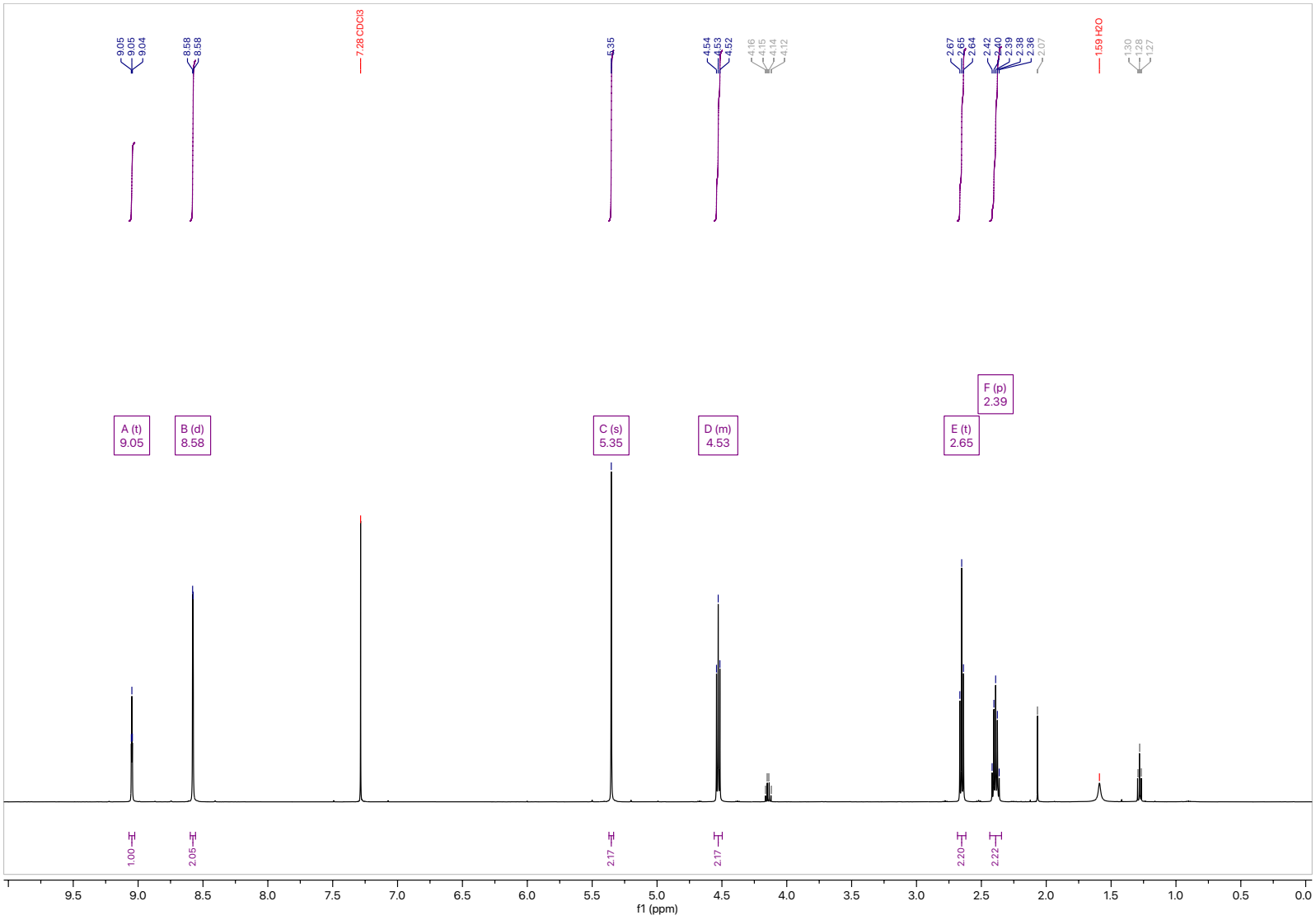
^{1}H NMR (500 MHz, $CDCl_3$) – standard view **(5)**



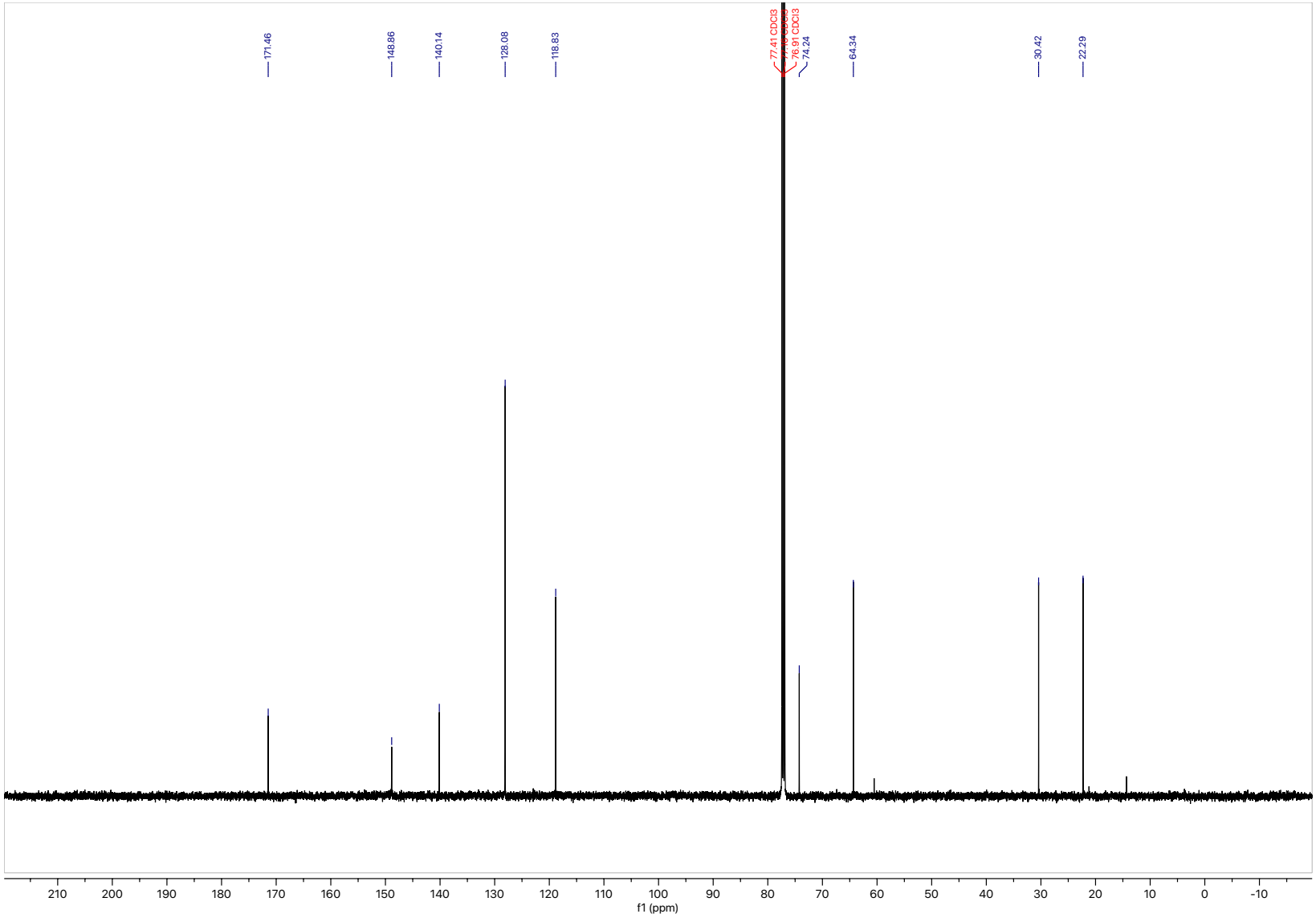
$^{13}C\{^{1}H\}$ NMR (126 MHz, $CDCl_3$) – standard view **(5)**



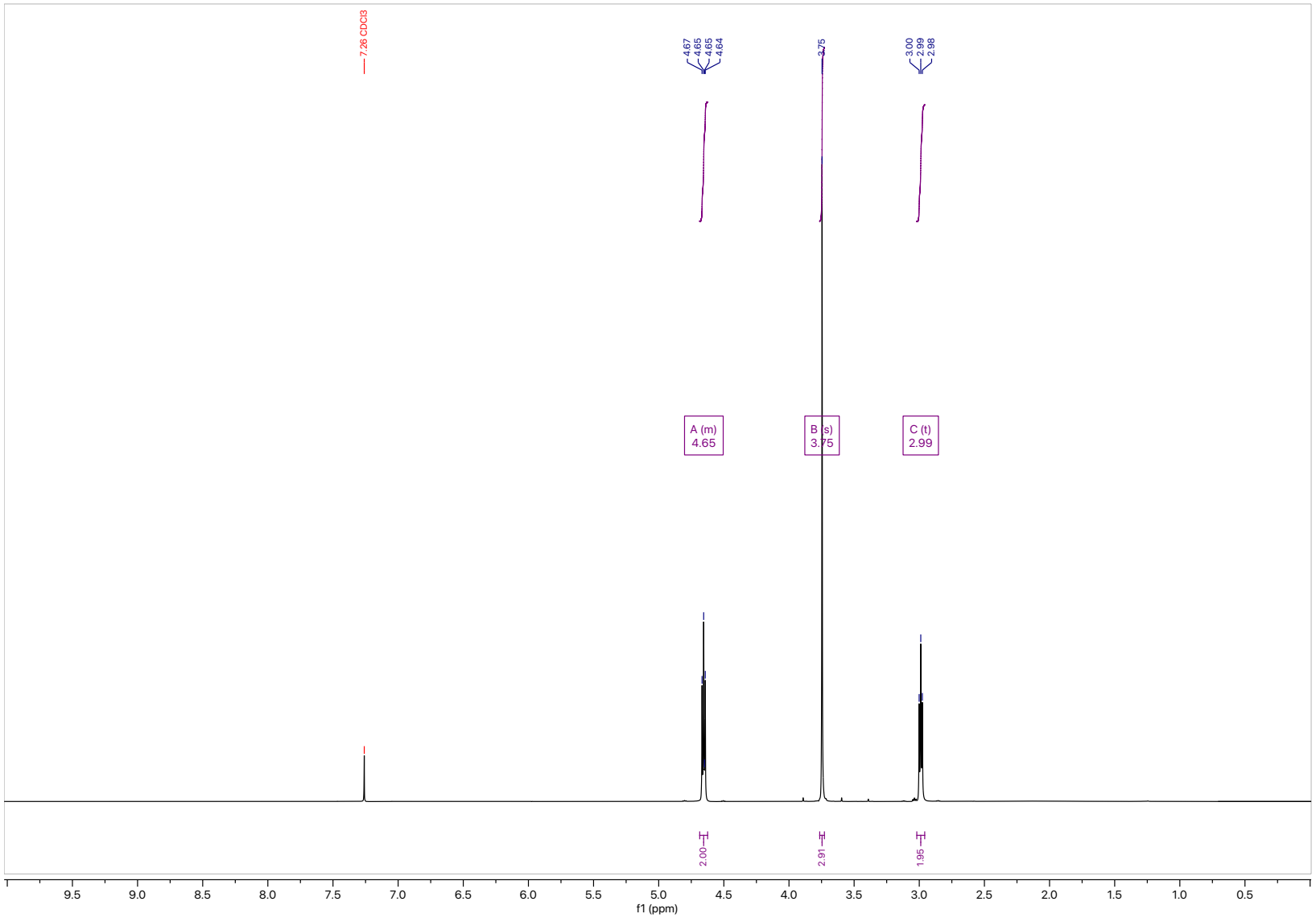
^{1}H NMR (500 MHz, $CDCl_3$) – standard view **(6)**



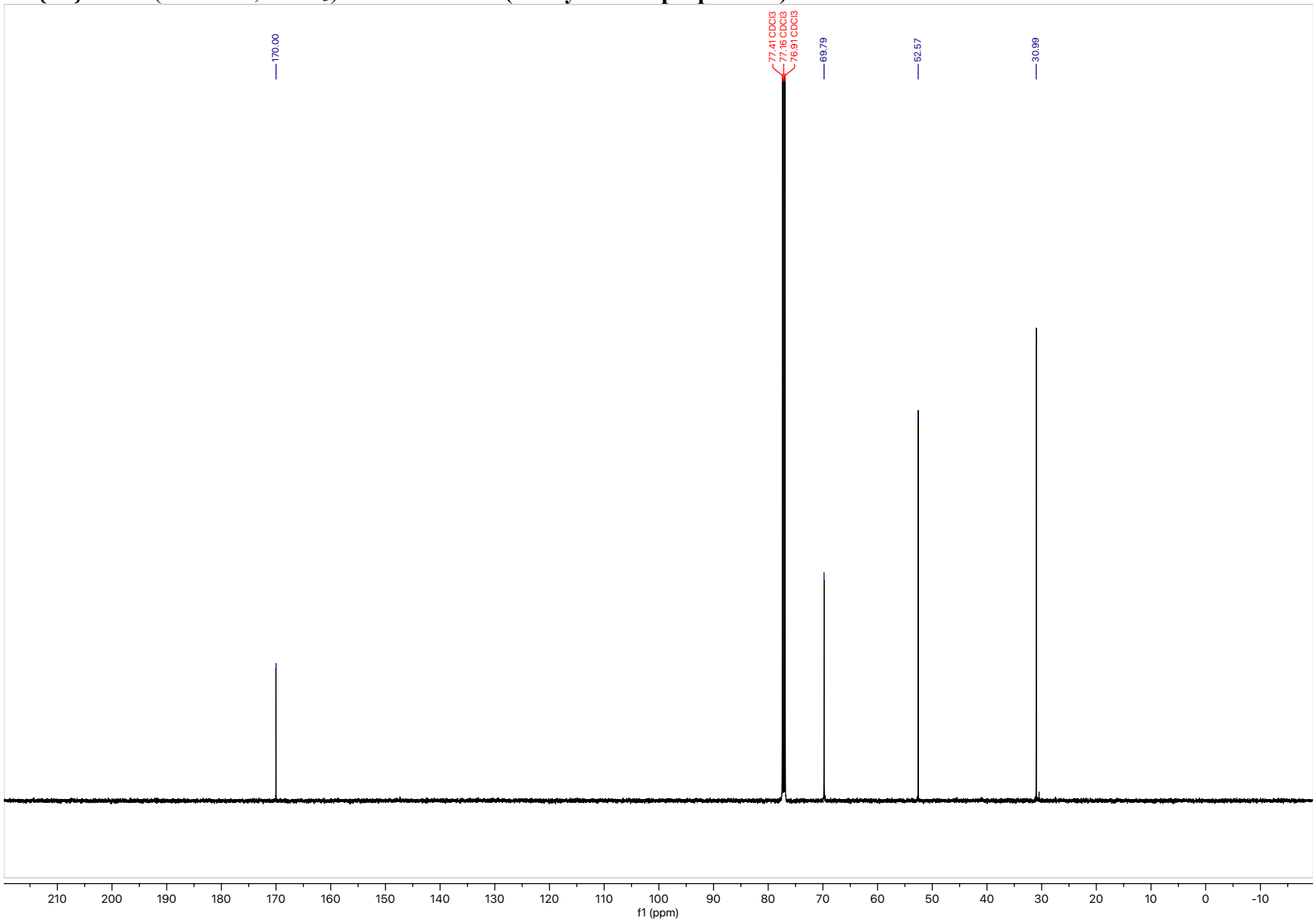
$^{13}C\{^{1}H\}$ NMR (126 MHz, $CDCl_3$) – standard view **(6)**



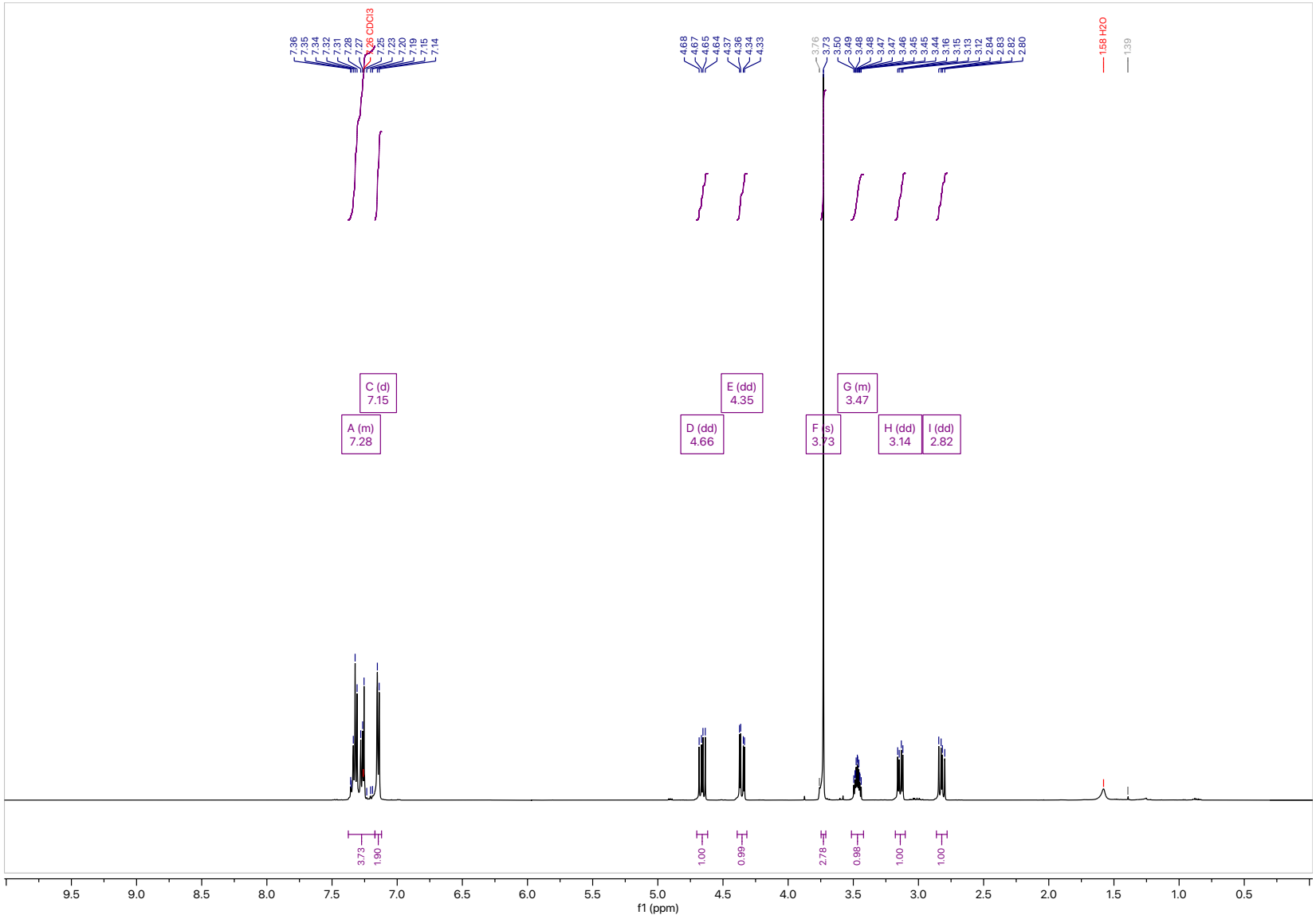
^{1}H NMR (500 MHz, $CDCl_3$) – standard view **(methyl 3-nitropropanoate)**



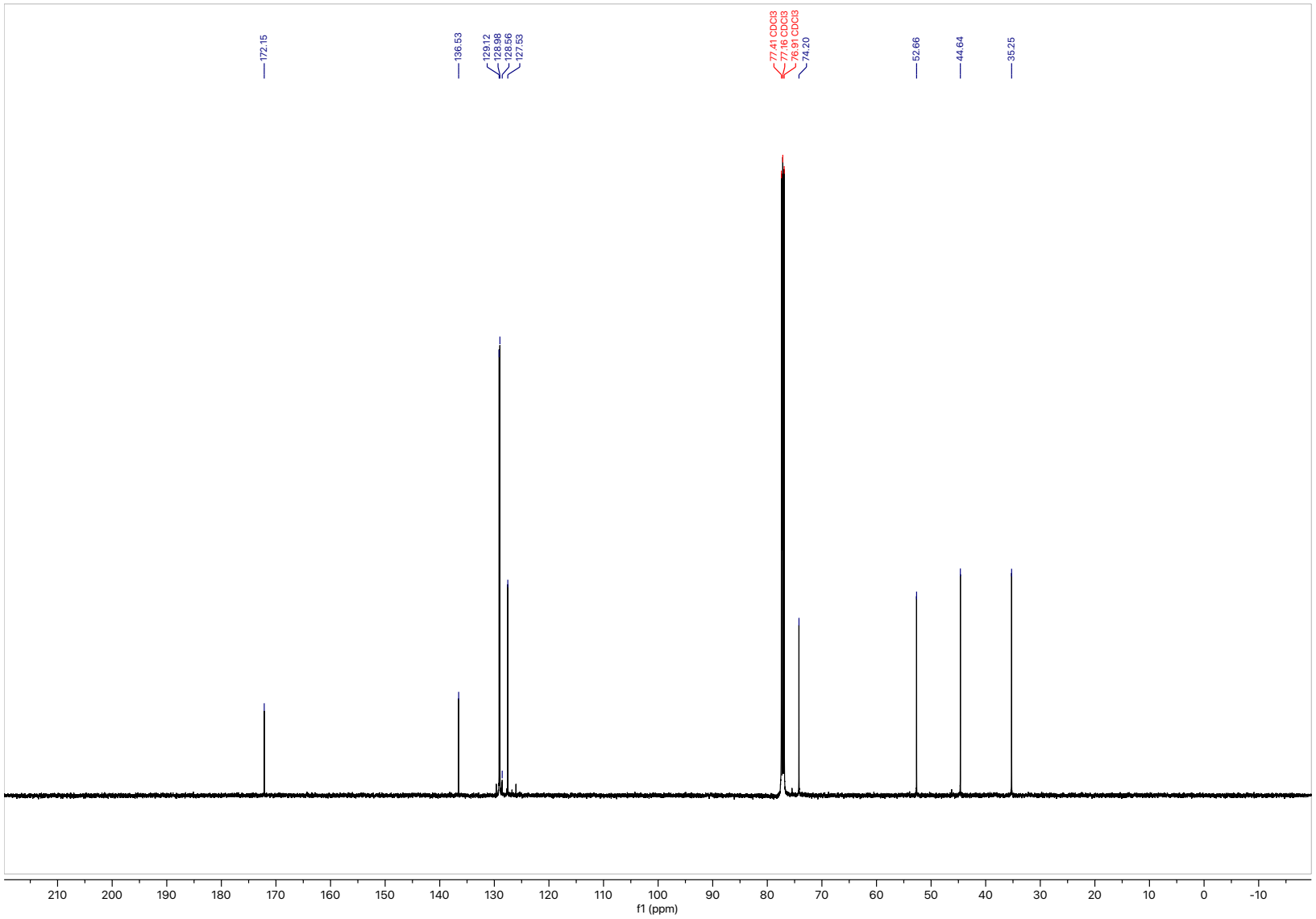
$^{13}C\{^{1}H\}$ NMR (126 MHz, $CDCl_3$) – standard view **(methyl 3-nitropropanoate)**



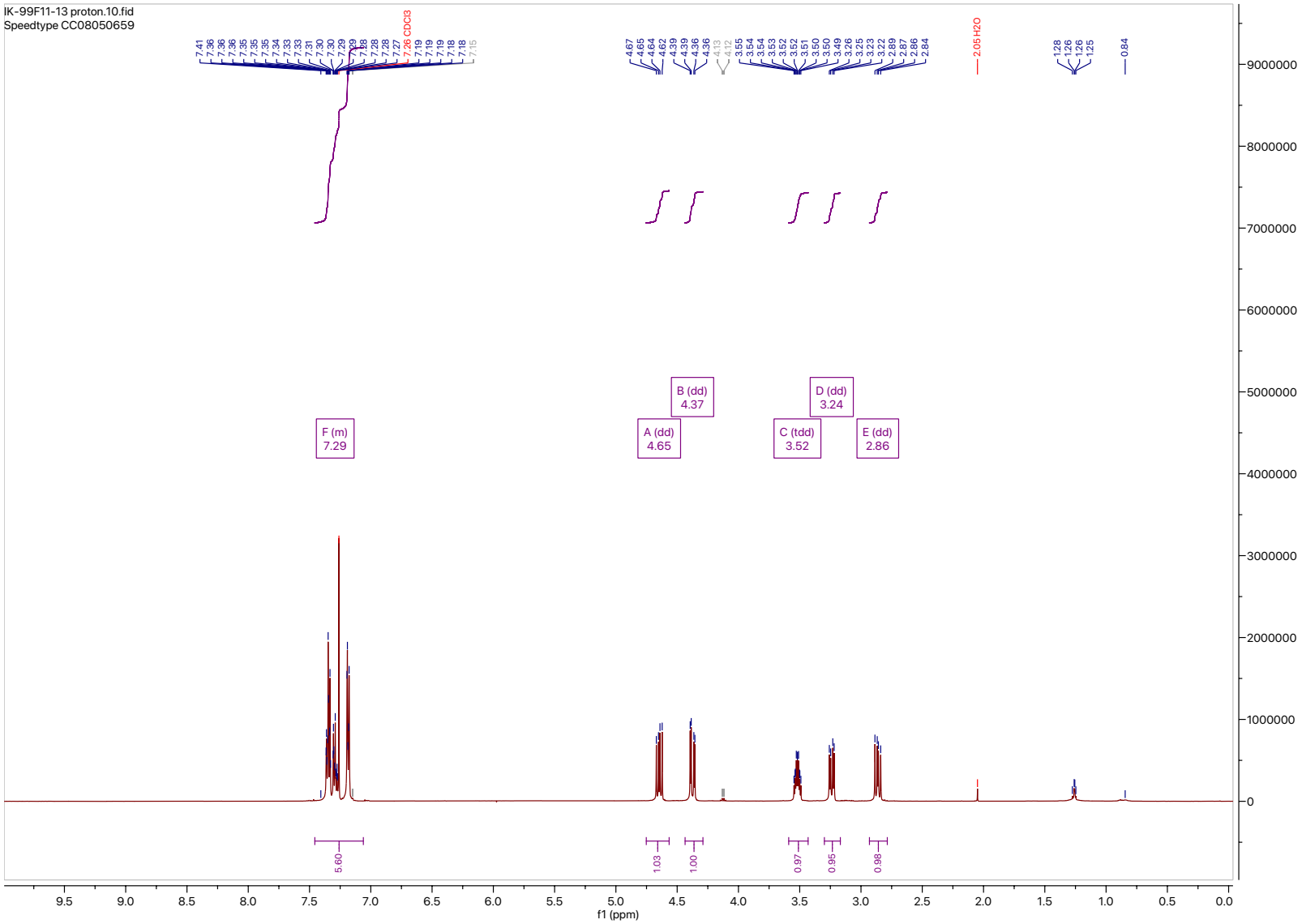
^{1}H NMR (500 MHz, $CDCl_3$) – standard view **(7(Me))**



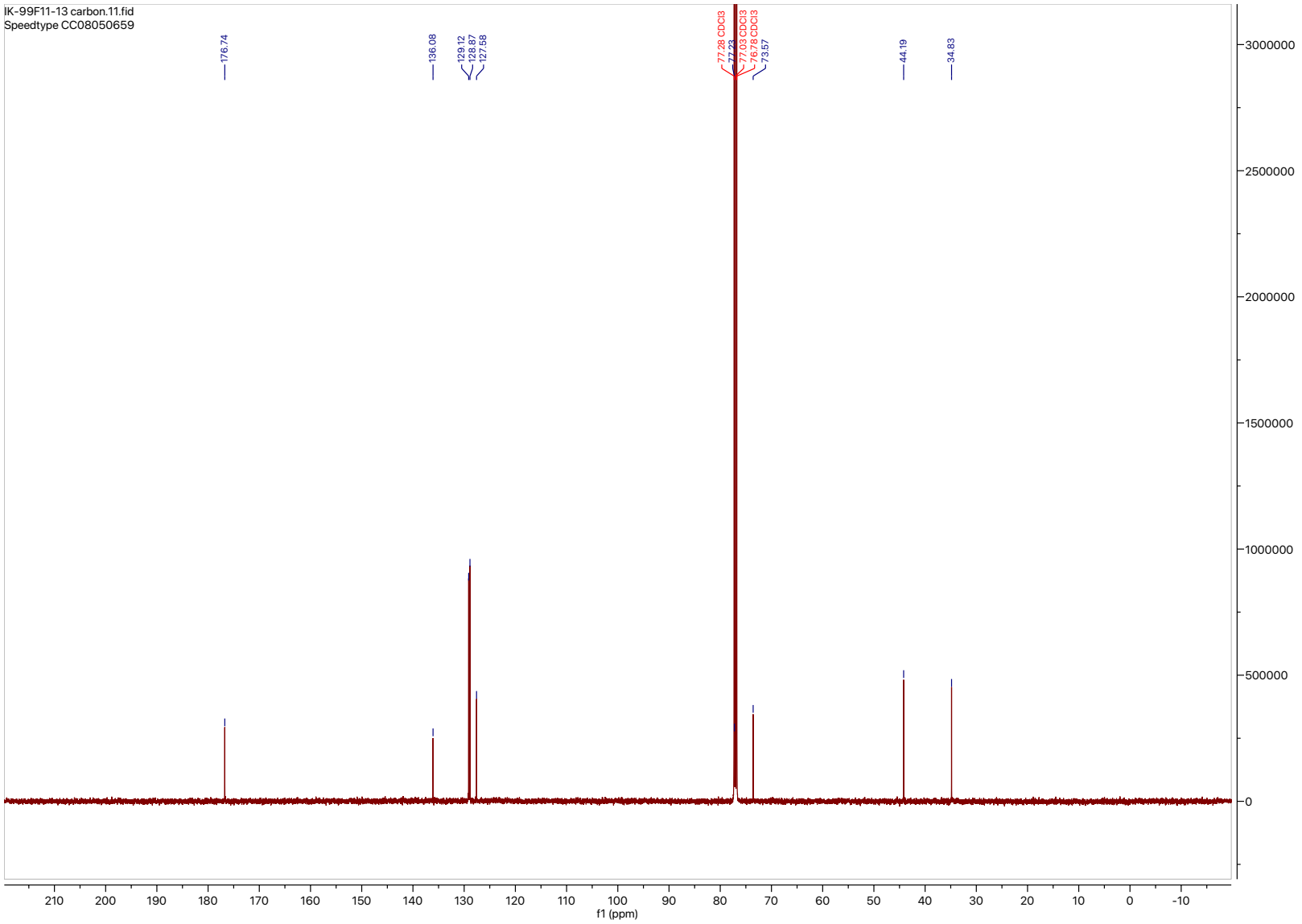
$^{13}C\{^{1}H\}$ NMR (126 MHz, $CDCl_3$) – standard view **(7(Me))**



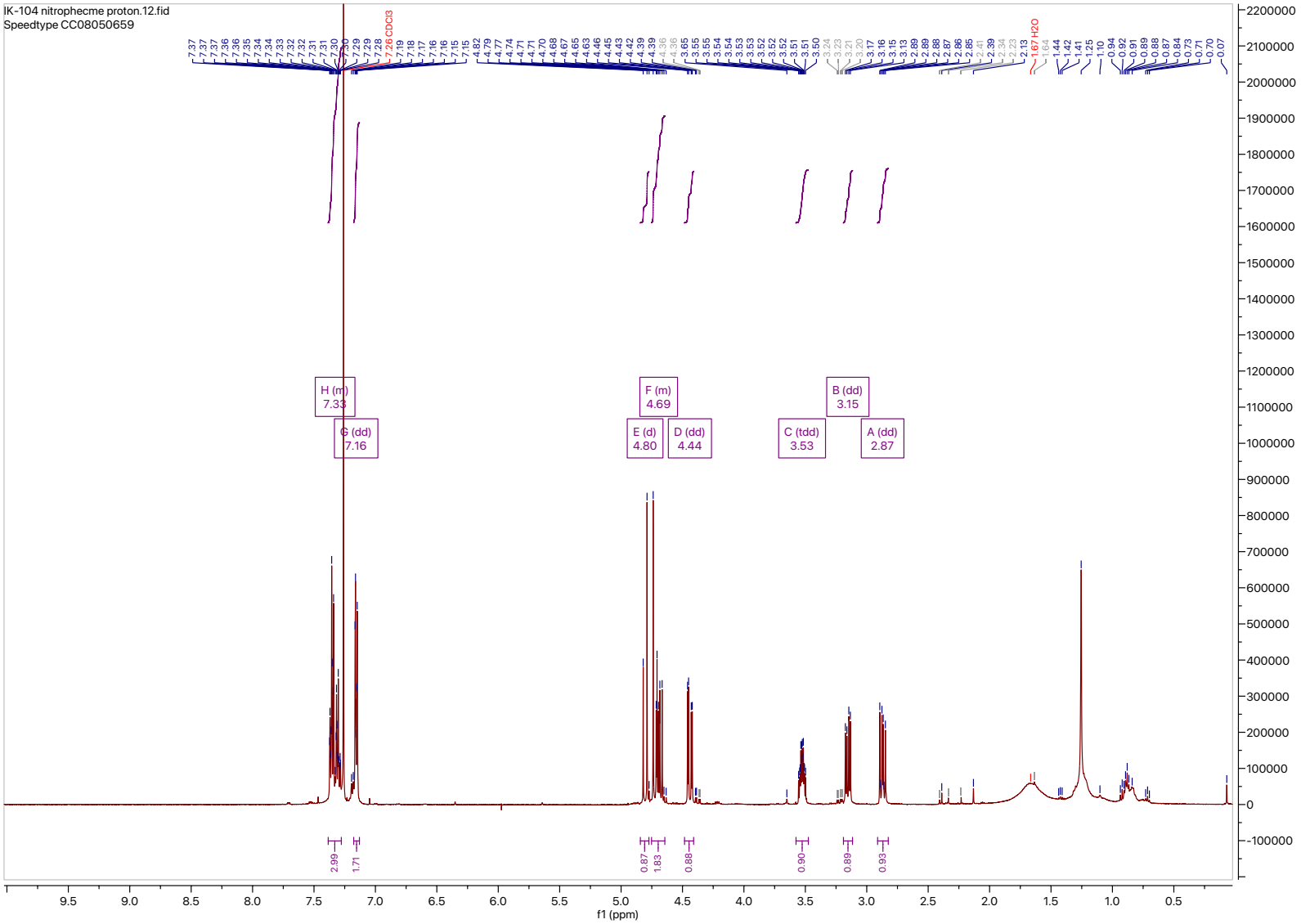
^{1}H NMR (500 MHz, $CDCl_3$) – standard view **(7)**



$^{13}C\{^{1}H\}$ NMR (126 MHz, $CDCl_3$) – standard view **(7)**



^{1}H NMR (500 MHz, $CDCl_3$) – standard view **(8)**



Chapter 3: Chemo-ribosomal synthesis of atropisomeric and macrocyclic peptides with embedded quinolines

This chapter is based on a preprint:

Knudson, I. J.; Dover, T. L.; Dilworth, D. A.; Paloutzian, C.; Cho, H.; Schepartz, A.; Miller, S. J. Chemo-Ribosomal Synthesis of Atropisomeric and Macrocyclic Peptides with Embedded Quinolines. ChemRxiv June 10, 2024. https://doi.org/10.26434/chemrxiv-2024-kvdpq.

It has been reproduced with permission from all coauthors.

Abstract

Expanding the chemical and structural complexity of genetically encoded peptides remains a challenge in peptide therapeutics discovery. Here we report that linear peptides with a reactive β- or γ-keto amide at their *N*-termini can be synthesized ribosomally using in vitro translation methods. We show that peptides carrying an *N*-terminal β-keto amide can be converted into diverse heterocyclic quinoline-peptide hybrids via Friedländer reactions with a variety of 2-aminoarylcarbonyl co-substrates. Reactions with appropriately substituted 2-aminobenzophenones generated quinoline-peptide hybrids with stable biaryl atropisomeric axes. In vitro-translated peptides carrying both an *N*-terminal β-keto amide and an internal 2-aminoacetophenone motif undergo intramolecular Friedländer macrocyclization reactions that embed a quinoline pharmacophore directly within the macrocyclic backbone. The introduction of *N*-terminal ketide building blocks into genetically encoded materials and their post-translational derivatization with carbonyl chemistry simultaneously expands the chemical diversity and structural complexity of genetically encoded materials and provides a paradigm for the programmed synthesis of peptide-derived materials that more closely resemble complex natural products.

Introduction

From the first clinical application of insulin in 1921[1,2] to the recent triumph of GLP-1 agonists[3,4], peptides have proven a valuable therapeutic modality. Advances in genetic code reprogramming, biological display, and computational design have set the stage for the next generation of peptide-derived therapeutics[5]. The first wave of these compounds represent some of the most exciting therapeutic candidates of the past decade because of their antibody-like affinity for traditionally "undruggable" targets such as protein-protein interfaces, while also showing promise for oral or intracellular delivery. Several therapeutic candidates derived from *de novo* peptide leads have progressed into clinical trials or onto the market[6–13]. In each of these cases, the initial lead identified by mRNA or phage display required extensive modification to improve its physicochemical properties[10]. Modifications introduced during lead optimization often include the installation of one or more macrocyclic rings and other backbone alterations that enhance protease resistance, target affinity, bioavailability, and/or cell permeability[14,15]. Chemical strategies to install these modifications earlier in the drug discovery process–ideally, prior to biological display–would offer distinct advantages.

Many strategies exist to install macrocyclic rings within peptides before or after biological display. Common methods include disulfide formation between Cys side chains, thioether formation between a Cys side chain and a terminal chloroacetamide or benzyl halide, copper-catalyzed azide-alkyne cycloaddition, amide bond-forming reactions[16–18], and a variety of metal-catalyzed macrocyclizations[19–21]. Although widely employed, each of these methods suffers from at least one liability with respect to downstream applications and none provide added value: Disulfide bonds are reversible, while thioethers are flexible and, like click reaction products, prone to oxidation. Alternative macrocyclization strategies that generate stable and drug-like linkers are widely recognized as an unmet need[9,22–27]. Chemistry that exploits the macrocyclization event to establish a known pharmacophore within the peptide backbone prior to biological display is a promising strategy towards this end[28].

Quinolines are an established class of aromatic pharmacophores replete in natural products, FDA-approved drugs, and high-affinity ligands for both protein and RNA. Quinoline-containing small molecules that engage proteins include FDA-approved therapeutics such as chloroquine, moxifloxacin, topotecan, lenvatinib, and saquinavir, which is itself a peptidomimetic with an *N*-terminal quinoline[29,30]. Quinolines are especially privileged with respect to RNA[31–34]: Quinoline-peptide conjugates function as helix-threading intercalators[35,36], and substituted quinolines are found within small molecules that target pre-mRNA to modulate splicing[37]. Perhaps the most unique aspect of the quinoline pharmacophore is its ability to support axial chirality and exist, in certain cases, as stable atropisomers. This stereochemical complexity would add a new level of topological diversity to genetically encoded linear or cyclic peptides.

Recently, we reported that linear peptides with a β-dicarbonyl functionality at the *N*-terminus could be synthesized ribosomally using in vitro translation to generate novel β-dicarbonyl-peptide hybrid molecules[38]. Other β-dicarbonyl functionality could be introduced into

polypeptides using orthogonal aminoacyl-tRNA synthetases[39]. In both cases, the β-dicarbonyl species reported were derivatives of malonic acid, which are among the least reactive of all 1,3-dicarbonyl species, especially under mild conditions. We hypothesized that if we could ribosomally incorporate a more reactive β-dicarbonyl species at the *N*-terminus, then the resulting peptide or protein could be modified post-translationally into a heterocyclic pharmacophore using any one of a number of classic or modern chemical transformations. If the post-translational modification made use of a side chain as a co-substrate, then the resulting macrocycle would contain an embedded heterocycle. Such a macrocyclization strategy embodies the post-translational modification logic of RiPP natural products while appropriating chemical intermediates produced by polyketide synthase modules.

Here, we report that linear peptides with a reactive *N*-terminal β-keto amide functionality can be synthesized ribosomally using in vitro translation (IVT), and that peptides carrying an *N*-terminal β-keto amide are substrates for Friedländer reactions capable of generating a diverse set of quinoline-peptide hybrid products. Reaction of the *N*-terminal β-keto amide with an appropriately substituted 2-aminobenzophenone provides a Friedländer product possessing a stable atropisomeric axis whose structure could be characterized by NMR and X-ray crystallography. Finally, synthetic or IVT peptides carrying both an *N*-terminal β-keto amide and an internal kynurenine residue are substrates for intramolecular Friedländer macrocyclization reactions that embed a quinoline pharmacophore into the peptide backbone. The introduction of simple ketide building blocks into ribosomal synthesis and their post-translational derivatization with carbonyl chemistry expands the structural and stereochemical diversity available to genetically encoded peptides and provides a paradigm for the programmed synthesis of peptide-derived materials that more closely resemble complex natural products.

Results

Introduction of a reactive 1,3-dicarbonyl motif at the *N*-terminus via in vitro translation

We began by exploring the extent to which tRNAs could be acylated with monomers carrying a reactive dicarbonyl motif, and the extent to which these acylated tRNAs could initiate the in vitro translation of short peptides (**Fig. 1a**). *N*-formyl methionine (**fM**) and monomers **1-4** (**Fig. 1b)** were converted into activated 3,5-dinitrobenzyl (DNB) esters (**Supplementary Fig. 1a**) and their ability to acylate a model tRNA microhelix (MH, **Supplementary Fig. 2a and Supplementary Table 1**) in the presence of flexizyme dFx[40] was evaluated as a function of time and pH. The extent of MH acylation was monitored using both acidic polyacrylamide gel electrophoresis (aPAGE) (**Supplementary Fig. 2b)** and intact tRNA LC-MS[39,41] (**Supplementary Fig. 2c-g).** Although gel electrophoresis failed to resolve any acylated MH product from the non-acylated MH substrate, presumably due to similarity in mass and charge, intact tRNA LC-MS revealed that both **2-DNB** and **3-DNB** were substrates for dFx in MH-acylation reactions, especially at

higher pH and longer incubation times (**Supplementary Table 1**). It is likely that the activity of **3-DNB** as a substrate for dFx was previously missed because of the low resolving power of gel electrophoresis[42]. Although we were unable to identify conditions that led to detectable MH acylation by the 3,5-dinitrobenzyl ester of monomer **1** (**Fig. 1b**), in the case of monomer **4**, intact tRNA LC-MS detected formation of acylated MH in 0.6% yield **(Supplementary Fig. 2g and Supplementary Table 1).** In vitro-transcribed *E. coli* initiator tRNA ($tRNA^{fMet}$) was subsequently acylated on a preparative scale with the 3,5-dinitrobenzyl esters of monomers **2** and **3**; in each case, product identity was confirmed using intact tRNA LC-MS (**Fig. 1c-e**).

With acylated $tRNA^{fMet}$ in hand, we next evaluated the extent to which monomers **2** and **3** could be introduced at the *N*-termini of short peptides prepared using in vitro translation (IVT). We made use of a commercial IVT kit (PURExpress® Δ (aa, tRNA) Kit), supplemented with the requisite amino acids and tRNAs, $tRNA^{fMet}$ pre-acylated with **fM** or monomers **2** or **3**, and a duplex DNA template encoding the FLAG-containing polypeptide MGVDYKDDDDK (MGV-flag). Peptides initiated with monomers **2** or **3** were translated at levels comparable to those initiated with $tRNA^{fMet}$ that had been pre-acylated with *N*-formyl methionine (**fM**) (**Fig. 1f-h** and **Supplementary Fig. 3)**.

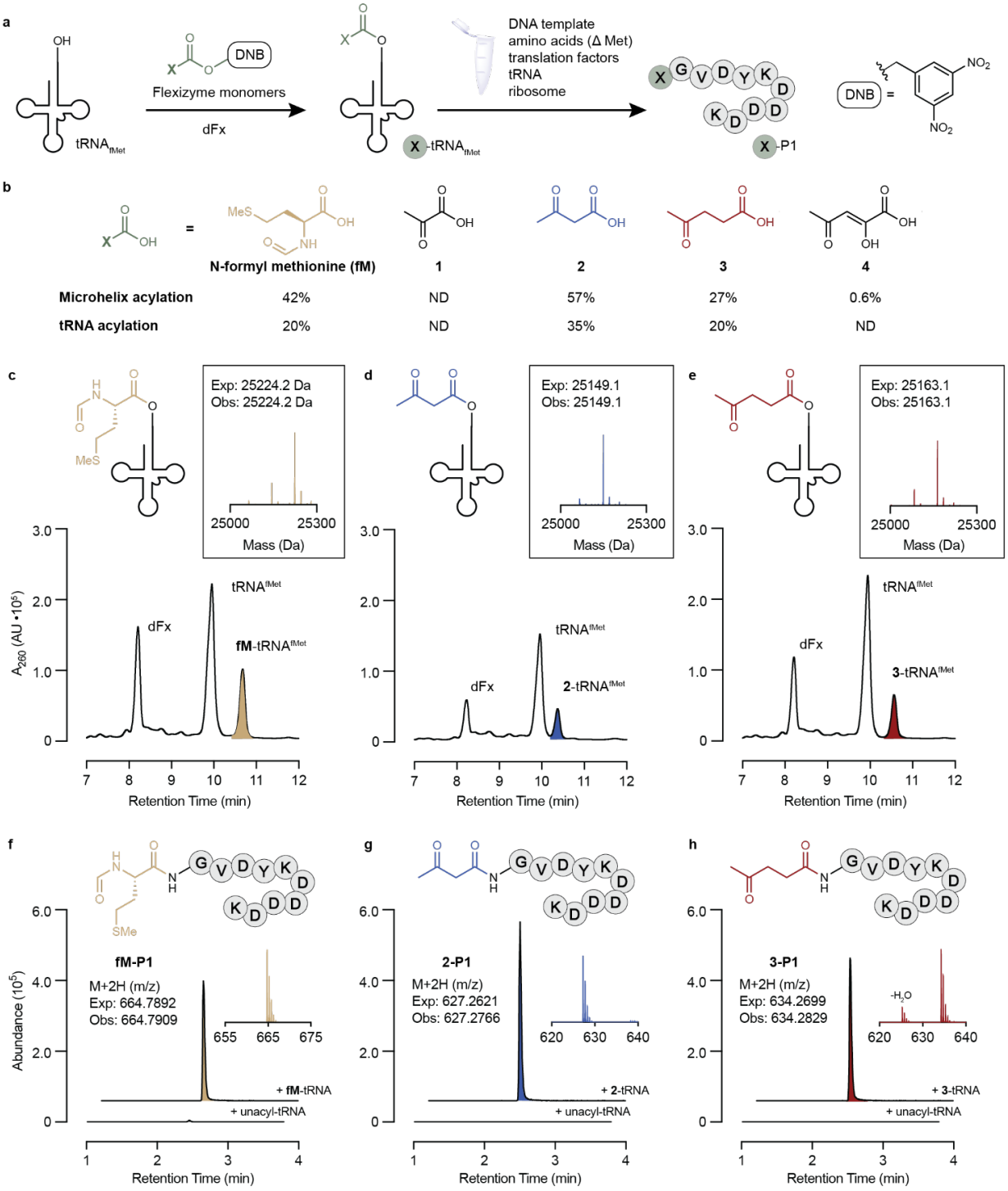


Figure 1. Introduction of a reactive 1,3-dicarbonyl motif at the *N*-terminus via in vitro translation. a, Scheme illustrating dFx-promoted acylation of tRNA^{fMet} with 3,5-dinitrobenzyl (DNB) esters and use of these tRNAs to initiate the in vitro translation of peptide **P1**, **X**GVDYKDDDDK, where **X** represents *N*-formyl methionine (**fM**) or monomers **1-4**. DYKDDDDK is a FLAG-tag that enables peptide isolation and enrichment prior to LC-HRMS analysis. **b,** Yields for flexizyme-promoted acylation of MH and tRNA^{fMet} by the DNB esters of **fM** and

monomers **1-4.** Yields were determined using intact tRNA LC-MS[39,41]. ND indicates that an acylated product was not detected. A_{260} chromatograms and deconvoluted mass spectra (inset box) of $tRNA^{fMet}$ acylated with the DNB esters of **c,** fM (**fM-DNB**), **d,** monomer **2 (2-DNB)**, and **e,** monomer **3 (3-DNB)**. Extracted ion chromatograms of peptide **P1** containing the *N*-terminal residue **f, fM**, **g, 2**, or **h, 3** in the presence of acylated or non-acylated $tRNA^{fMet}$. The inset shows the mass spectrum of each peptide. All acylations were performed in triplicate. Data shown is representative.

Friedländer reactions of β-keto amides proceed readily under mild aqueous conditions

β- and γ-keto carbonyl groups participate in an array of chemical transformations that generate carbocyclic and heterocyclic frameworks, often with elements of stereocontrol[43–45]. One classic transformation is the Friedländer reaction[46], a double condensation of a 2-aminoarylcarbonyl and an aldehyde or ketone to form a quinoline, a fused [6,6] heterocyclic aromatic ring. Friedländer reactions are typically performed under harsh conditions, requiring a strongly acidic or basic additive and/or reaction temperatures greater than 150 °C (**Fig. 2a**)[47,48]; these conditions would likely degrade sensitive peptides. Although we were encouraged by several reports of high-yielding Friedländer reactions of β-ketoesters performed in acetic acid[49] and acetic acid/water mixtures[50], we could identify only limited literature examples of Friedländer reactions of β-keto amides[51–54], and none that proceeded under mild conditions that would be appropriate for peptides and with a wide substrate scope.

We thus sought to identify mild conditions that would support the Friedländer reaction of model β-keto amide **5 (Fig. 2b, Supplementary Fig. 1b),** and apply these conditions to peptides generated using IVT. We examined the reaction of **5** with 2-aminoacetophenone **6** to generate quinoline **15** in acetic acid and acetic acid/water mixtures at temperatures between RT and 60 °C. Reactions were performed using 330 mM of **5** and **6** and the formation of quinoline **15** was monitored as a function of time using LC-MS (**Fig. 2c**). We found that all conditions tested supported the Friedländer reaction of β-keto amide **5** to generate the expected quinoline product **15**. Conversion was most rapid at 60 °C in AcOH or H_2O/AcOH mixtures or at 40 °C in AcOH (**Fig. 2c**). To evaluate reaction scope under these conditions, we treated β-keto amide **5** with a collection of nine structurally diverse 2-aminoarylcarbonyl substrates **6-14** (**Fig. 2d** and **Supplementary Fig. 4**). Substrates **6** and **9-13** reacted cleanly with β-keto amide **5** with full conversion to the expected quinoline products **15** and **18-22** after 48 h at 60 °C in AcOH. Reactions with 2-aminobenzaldehydes **7** and **8,** which polymerize under acidic conditions[55], and kynurenine **14,** led to lower levels of product formation **(Supplementary Fig. 5)**. Quinolines **15-20** were synthesized on a preparative scale and the products were characterized using LC-HRMS and NMR.

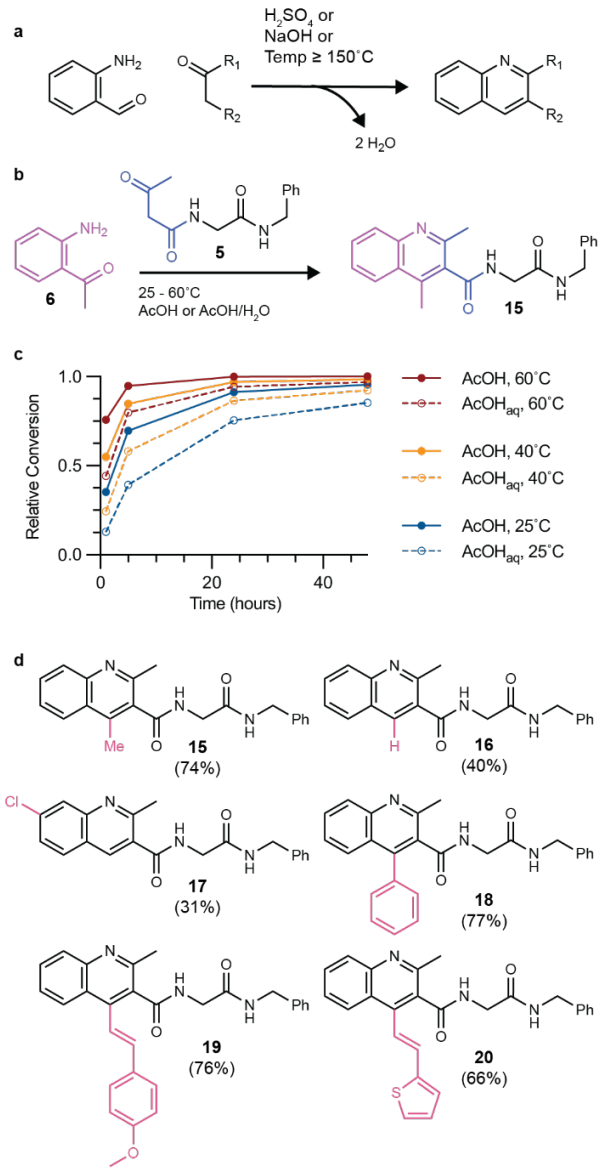


Figure 2. Friedländer reactions of β-keto amides proceed readily in aqueous acetic acid. a, Scheme illustrating a classic Friedländer reaction between 2-aminobenzaldehyde and a substituted ketone. **b,** Model system used to evaluate more mild conditions for the Friedländer reaction of β-keto amide dipeptide **5** and 2-aminoacetophenone **6** (0.33 M each). **c,** Plot illustrating the conversion of **5** and **6** into quinoline **15** under the conditions shown. Relative conversion (RC) values were calculated according to the equation RC = $[A_{15}/(A_5+A_{15})]$ where A_x represents the integrated area of the peaks corresponding to substrate **5** (A_5) or product **15** (A_{15}) on the absorbance chromatogram (214 nm). Each point represents the average of two replicates. **d,** Representative substituted quinoline products generated from Friedländer reactions performed in AcOH at 60 °C for 48 h. Isolated yields are shown in parentheses; corresponding LC-MS traces are shown in **Supplementary Fig. 5**.

Post-translational Friedländer reactions of IVT products proceed under mild conditions

We next asked whether Friedländer reactions would also proceed efficiently when performed on IVT peptides initiated with $tRNA^{fMet}$ acylated with monomer **2**. Performing reactions on in vitro translation products is challenging because the reaction must proceed cleanly at low peptide concentration (< 1 μM) and in the presence of high concentrations of biomolecules and salts. β-keto amide peptide **2-P1** was generated using IVT, isolated using anti-FLAG magnetic beads, lyophilized, and treated with 2-aminoarylcarbonyl substrates **6, 8, 9,** or **12** in acetic acid at 40 °C for 24 h. The formation of Friedländer products **Q6-P1, Q8-P1, Q9-P1,** and **Q12-P1** were monitored using LC-HRMS (**Supplementary Fig. 6a-d**). In each case, the post-translational Friedländer reaction of **2-P1** proceeded to generate peptides with quinoline derivatives at their

N-termini (**Fig. 3b-e**). In theory, identical quinoline-peptide hybrids could be prepared ribosomally using $tRNA^{fMet}$ acylated with a pre-assembled quinoline. Yet treatment of $tRNA^{fMet}$ with eFx and dimethyl quinoline cyanomethyl ester **25-CME (Supplementary Fig. 7a)** led to no detectable acyl-tRNA product under any condition tested (**Fig. 3f** and **Supplementary Table 2**). We conclude that post-translational Friedländer reactions represent a simple path to ribosomally synthesized peptides with diverse quinoline functionality at the *N*-terminus.

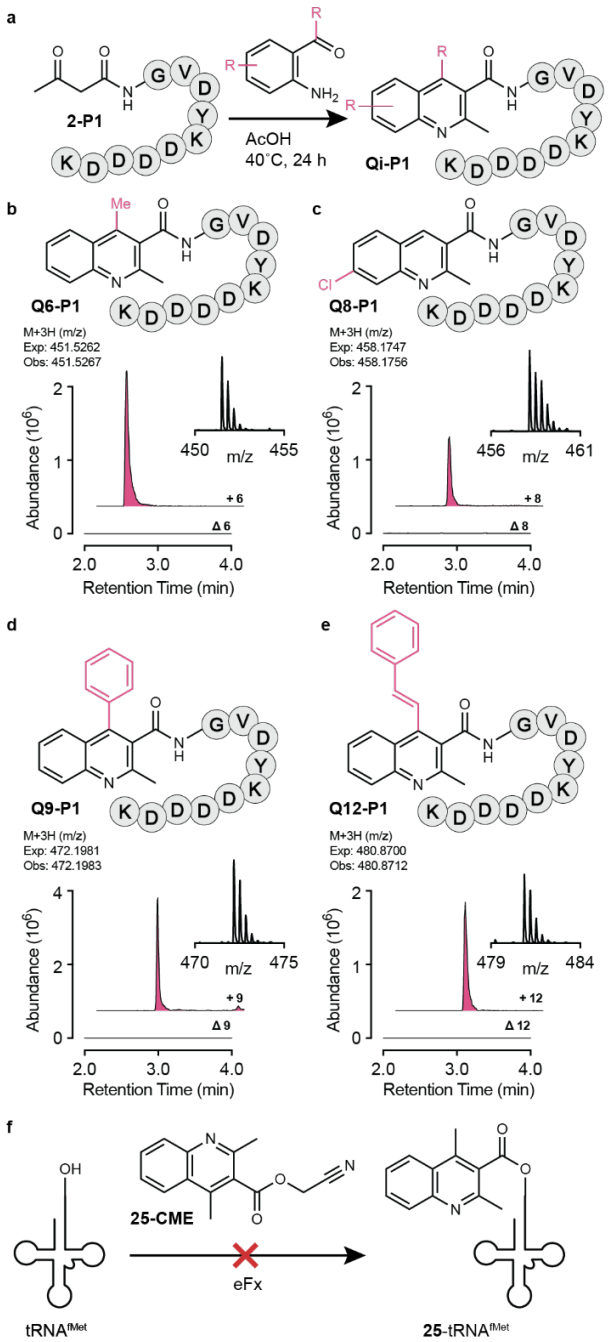


Figure 3. Post-translational Friedländer reactions on IVT products proceed under mild conditions. **a,** Post-translational Friedländer reactions of IVT peptide **2-P1** generate diverse quinoline-peptide hybrid molecules **Qi-P1**, where **i** identifies the 2-aminocarbonyl substrate. **b-e,** Reaction scope. Shown is the extracted ion chromatogram (EIC) for the expected major ion produced when **2-P1** is treated under the conditions shown in the presence and absence of substrates **6, 8, 9,** or **12** to generate **Q6-P1**, **Q8-P1**, **Q9-P1**, and **Q12-P1**, respectively. The mass spectrum of each major ion is inset. **f,** eFx-promoted acylation of $tRNA^{fMet}$ with quinoline cyanomethyl ester **25-CME** led to no detectable acylated tRNA product under any condition tested.

Friedländer reactions of β-keto amides generate stable atropisomers

Appropriately substituted quinolines can exist as atropisomers. Canonical atropisomers are stereoisomers that arise from hindered rotation around a σ-bond[56]. Like stereoisomers with point chirality, atropisomers can bind macromolecular targets with distinct kinetics as well as different affinities[57]. Atropisomeric quinolines and quinoline-like heterocycles are well known. They are found in pharmaceuticals[58–60] such as Sotorasib, a first-in-class mutant KRAS G12C inhibitor[58,59], as well as novel HIV-I integrase inhibitors[63]. Atropisomeric quinolines

also serve as the molecular framework for catalysts with widespread use in organic synthesis and process research, such as QUINAP[58]. Although many macrocyclic peptide natural products contain unusual structural isomers, sometimes called atropisomers[64], non-canonical atropisomers[65], or ansamers[66], that result from threaded-loop or knot-like structures[65,67,68], true canonical atropisomers are also important constituents of this class of compounds, such as the famous case of the cyclic glycopeptide vancomycin[69]. Peptides or cyclic peptides containing atropoisomeric quinolines would add a sophisticated layer of stereochemical complexity to macrocyclic peptide libraries.

To assess whether atropisomeric quinolines could be introduced within ribosomal peptides, we first confirmed that Friedländer reaction of peptide **28** with (2-aminophenyl)(*o*-tolyl)methanone (**26**) in AcOH at 60 °C for 48 h produced the expected product **29** as a roughly 41:59 mixture of atropisomeric products, as determined by ^{1}H NMR (**Fig. 4a**)**.** However, when we attempted to reproduce a post-translational Friedländer reaction between (2-aminophenyl)(*o*-tolyl)methanone (**26**) and IVT-generated peptide **2-P1** in acetic acid, the expected product **Q26-P1** was detected, but in low abundance (**Fig. 4c)**.

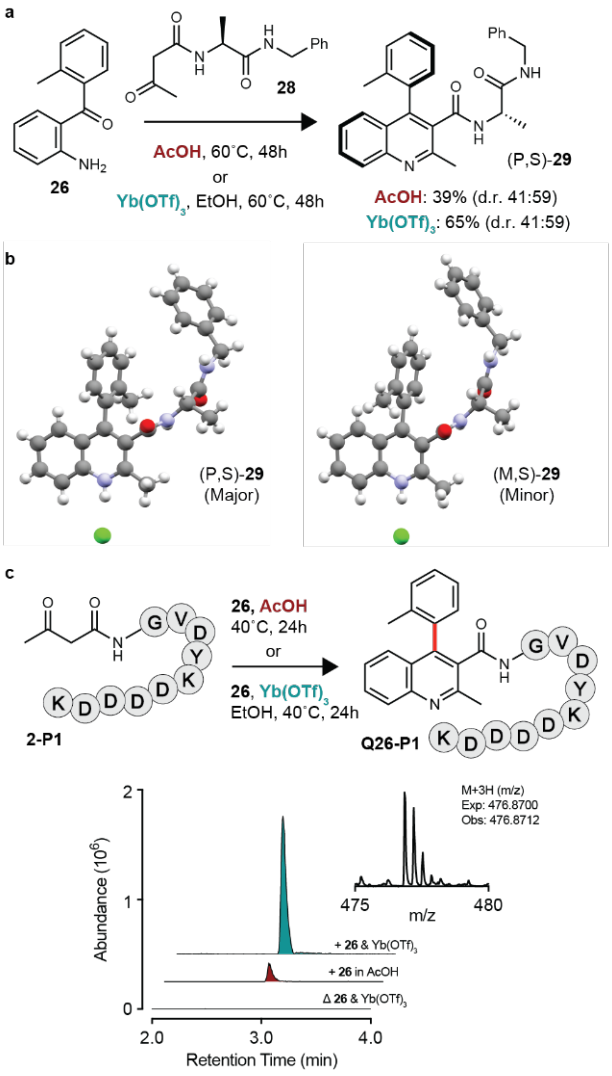


Figure 4. Friedländer reactions of β-keto amides generate stable atropisomers. a, Friedländer reaction of substrate **26** and dipeptide **28** in the presence of either Brønsted or Lewis acids generates quinoline-dipeptide **29**, which exists as a pair of stable atropisomers with a diastereomeric ratio (d.r.) of ~41:59 regardless of the conditions used for its preparation. **b,** X-ray crystal structure of (*P*, *S*)-**29** (left, CCDC: 2341553) and (*M*, *S*)-**29** (right, CCDC: 2341552) as their respective hydrochloride salts. **c,** Friedländer reaction of **2-P1**, prepared using IVT, with aminocarbonyl **26** in the presence of 100 mM $Yb(OTf)_3$ in EtOH generates quinoline-peptide **Q26-P1**. Extracted ion chromatograms for product formation in the presence of $Yb(OTf)_3$ in EtOH with **26** (teal), acetic acid with **26** (red), or $Yb(OTf)_3$ in EtOH without **26** (black) for 24 h at 40 °C. Significantly less product is observed when the reaction is performed using AcOH in place of $Yb(OTf)_3$ in EtOH.

Lewis acid catalysis of post-translational Friedländer reactions generates atropisomeric products

We hypothesized that Friedländer reactions of β-keto amide-containing peptides could be optimized using mild Lewis acid-catalyzed conditions, thus allowing for good reactivity with ribosomal peptides generated by IVT. Indeed, Lewis acids such as the chloride salts of Ce(III)[70] and Fe(III)[71] as well as the triflate salts of Yb(III)[72], Y(III)[73], and Zn(II)[74], can promote Friedländer reactions of β-ketoesters[48]. To evaluate if they could improve atropisomer-forming reactions of β-keto amide **2-P1,** we screened their effect (at 20 mol%) on the Friedländer reaction of dipeptide **5** and (2-aminophenyl)(*o*-tolyl)methanone (**26**) to generate the quinoline **27** (**Supplementary Fig. 9** and **Supplementary Table 3**). Of all Lewis acids tested, the highest yields were obtained with $Yb(OTf)_3$ in ethanol. $Yb(OTf)_3$ was versatile, performing well in DCM, MeCN, THF, and AcOH. Although strong Brønsted acids such as triflic acid, sulfuric acid, phosphoric acid, and trifluoroacetic acid also out-performed acetic acid, these conditions are far less mild. When the Friedländer reaction of **28** and **26** was repeated, this time in the presence of 20 mol% $Yb(OTf)_3$ in EtOH at 60 °C for 48 h, we isolated the product **29** in 65% yield with a similar diastereomeric ratio (**Fig. 4a**). The diastereomers could be separated and subsequently

characterized by ^{1}H NMR (**Supplementary Fig. 8**) and X-ray structure determination (**Fig. 4b, Supplementary Fig. 10 & 11,** and **Supplementary Tables 4 & 5**), revealing that the (*P*, *S*) diastereomer is the major product. The stability of the atropisomeric axis was assessed by heating a pure sample of the minor diastereomer (i.e., (*M*, *S*)-**29**) in DMSO-d_6 at 100 °C for 18 h[75]. Subsequent ^{1}H NMR analysis revealed minimal epimerization (< 1%, **Supplementary Fig. 12**). With optimized conditions in hand, we again attempted modification of a ribosomal peptide generated by IVT. Indeed, when treated with **26** in EtOH containing Yb(OTf)$_3$, the IVT synthesized β-keto amide peptide **2-P1** was transformed cleanly into the quinoline-peptide hybrid **Q26-P1** after 24 h at 40 °C (**Fig. 4c and Supplementary Fig. 6e**). **Q26-P1** is presumed to exist as a mixture of atropisomers in analogy to **29**, but chromatographic separation of distinct isomers by reverse phase UPLC-MS was not observed on this larger IVT peptide.

Friedländer macrocyclizations

We envisioned that Lewis acids might also aid post-translational Friedländer macrocyclization reactions to generate products with a quinoline pharmacophore embedded within the peptide backbone. To test this idea, we prepared four linear peptides containing both an *N*-terminal β-keto amide and an internal 2-aminoarylcarbonyl side chain provided by the non-canonical amino acid kynurenine (**Fig. 5a** and **Supplementary Fig. 13-15**). The linear peptide **LP1** is a heptapeptide related to the FDA-approved drug octreotide[5,76], while **LP2** is a hexapeptide containing a turn-inducing L-proline, **LP3** is a decapeptide bearing diverse functional groups, and **LP4** is a longer diverse tridecapeptide related to the hormone somatostatin[77]. All four linear peptides **LP1-4** (1 mM) underwent intramolecular Friedländer reactions to generate macrocycles **CP1-4** (**Supplementary Fig. 16**) in the presence of 1-2 mM Yb(OTf)$_3$ in EtOH or MeCN at 60 °C, as supported by LC-HRMS (**Fig. 5b-e** and **Supplementary Fig. 17-20**) and NMR experiments (**Supplementary Fig. 21 and 23 and Supplementary Data).** The smaller peptides **LP1** and **LP2** cyclized cleanly and the macrocyclic products **CP1** and **CP2** could be isolated with efficiencies that tracked well with LC-MS and HPLC chromatograms of reaction progress. **CP1** and **CP2** were isolated as salts in complex with TFA employed in the isolation procedure (see **Supplementary Material**). Cyclization of the larger peptides **LP3** and **LP4** proceeded under analogous conditions to deliver their corresponding macrocycles with reduced, but still notable efficiency. For comparison, macrocyclization reactions of **LP1-4** were also performed under aqueous conditions (80 mM glycine pH 2.8 at 60 °C); in all cases, cyclization proceeded faster using the Lewis acid Yb(OTf)$_3$ (**Supplementary Fig. 24**). The isolated macrocycles **CP1-CP4** were also characterized by MALDI-TOF MS to confirm the monomeric mass and the absence of significant quantities of higher order oligomers (**Supplementary Fig 25 and Supplementary Data**).

Finally we asked whether a Lewis acid-catalyzed Friedländer macrocyclization reaction was compatible with the challenging conditions required for post-translational modifications of in vitro translation (IVT) products. First, the cyanomethyl ester of kynurenine (**Kyn-CME)** and the flexizyme eFx were used to acylate $tRNA^{AsnE2\#2}_{GCU}$, a previously reported engineered tRNA[78]

(**Supplementary Figs. 7b & 26**). The resulting Kyn-tRNA$^{AsnE2\#2}_{GCU}$ was added to the IVT reaction while excluding serine and sequestering native tRNA$^{Ser}_{GCU}$ with an antisense oligonucleotide (M5-1) to suppress near cognate read-through[26,79]. We confirmed that β-ketoacid **2** and kynurenine (**Kyn)** could independently and effectively recode methionine at position 1 and serine at position 6, respectively, of a peptide prepared using IVT (**Supplementary Fig. 27**)**.** Using an identical strategy, we then used IVT to generate tetrakaidecapeptide **ivt.LP5**, which contains both an *N*-terminal β-keto amide as well as an internal kynurenine residue **(Fig. 5f).** Subsequent reaction of **ivt.LP5** with 100 mM Yb(OTf_3) in MeCN at 60 °C for 24 h yielded quinoline-cyclized peptide **ivt.CP5 (Fig. 5f,g)** whose retention time and mass spectrum were identical to that of an authentic standard produced by SPPS **(Supplementary Fig. 27)**. This result confirms that mild, post-translational Lewis acid-catalyzed Friedländer reactions can effectively generate macrocyclic quinoline-peptide hybrids even at very low peptide concentrations and in the presence of the high concentrations of salts and biomolecules that are intrinsic to in vitro translation reactions.

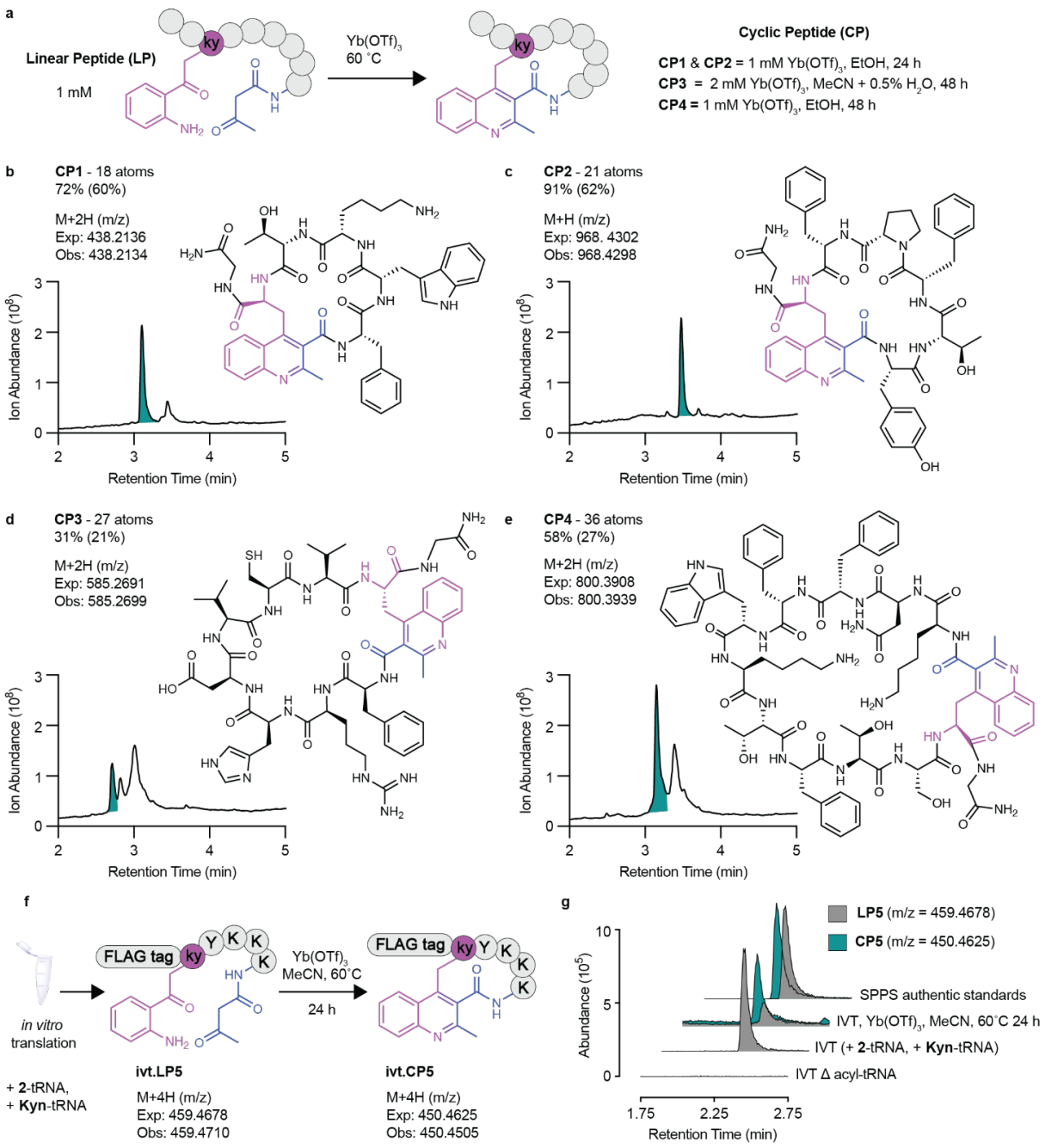


Fig. 5. Intramolecular post-translational Friedländer macrocyclization reactions. a, Preparative scale intramolecular Friedländer reactions to generate peptide macrocycles with an embedded backbone quinoline. Each linear peptide contains monomer **2** at the *N*-terminus and a single internal kynurenine residue. **b-e,** Structures and total ion chromatograms of crude reaction mixtures for synthetic peptides **CP1-4** after Friedländer macrocyclization reactions. The peak containing the cyclic peptide is highlighted in teal. Atom count of the macrocycle backbone, $HPLC_{254nm}$ yield, and isolated yield (in parentheses) are provided. All peptides were prepared using solid phase methods and purified as described in **Supplementary Methods.**

Detailed synthetic information, including LC-HRMS, MS-MS, and NMR of linear and cyclic peptides can be found in **Supplementary Fig. 13-25. f,** Incorporation of both **2** and **Kynurenine** into a single IVT peptide **ivt.LP5** and subsequent Friedländer cyclization into **ivt.CP5**. **g,** Extracted ion chromatograms of **ivt.LP5** and **ivt.CP5** and comparison with an authentic standard prepared using solid phase methods.

Discussion

Peptides and their derivatives are a rapidly expanding class of therapeutic molecules, in part because they condense the expansive recognition properties of a protein into a more compact molecular framework. The extended binding surface of a peptide provides a better complement to the extended and featureless surfaces that comprise many traditionally “undruggable” targets[80]. Perhaps the greatest attribute of peptides, whether linear or cyclic, is that they are genetically encodable, and hence their properties can be optimized using directed evolution methods performed in vitro or in vivo. Many of these methods depend on ribosomal translation and reliably return peptide leads for challenging and clinically relevant targets. For these reasons, *de novo* peptides have attracted significant attention as the next frontier in pharmaceutical development[81].

Yet the difference between the *de novo* peptide lead and the final compound advanced to clinical trials is often profound, and the modifications introduced demand exceptional commitments of labor and state-of-the-art medicinal chemistry[82]. Introducing these modifications earlier in the discovery process would be advantageous. Some important progress has been made, including the introduction of *N*-Me groups[83], D-amino acids[84], β^2- and β^3-amino acids, as well as linkers that introduce rings[7] or even appended pharmacophores[25,28]. Even with these developments, the chemistry available to ribosomally translated-peptides remains limited when compared to the vast array of transformations, functional groups, and architectures that are emblematic of small molecule pharmaceuticals and bioactive natural products. Yudin and others have shown that the introduction of heterocyclic grafts into peptide macrocycles can have profound impacts on passive permeability, bioavailability, and even topological complexity[85,86]. Quinolines, however, are underrepresented among these grafts; thus, the properties imbued by these motifs represent an area ripe for further exploration.

This work was initiated in an attempt to generate ribosomally synthesized peptides with modifications that resemble those found in peptide-derived clinical candidates. We accomplished this goal by installing a reactive β-keto amide functional group at the *N*-terminus and developing mild Friedländer reaction conditions to convert the β-keto amide into quinoline-peptide hybrids, including those that exist in distinct atropisomeric forms. The same mild Friedländer conditions were deployed as a macrocyclization strategy, embedding a quinoline pharmacophore directly into the backbone of a sequence-encoded macrocycle.

Finally we note the *N*-terminal β-keto amide and γ-keto amide peptides generated are suitable substrates for many other macrocyclization or late-stage diversification reactions[44]. Potential

reactions of *N*-terminal β- and γ-keto amides include those that generate pyridines (Hantzsch reaction[87]), pyrazoles (Knorr[88]), pyrroles (Hantzsch, Knorr, Paal-Knorr[89]), dihydropyrimidinones (Biginelli[90]), and carbocycles (Conia-Ene[91]), in addition to Michael additions, alkylations, acylations, and arylations. Some of these reactions also have the potential to install atropisomeric axes into the macrocyclic product. These modifications could be used alone or combined with more traditional backbone diversification strategies to generate biased libraries containing pharmacophores and drug-like motifs. We envision the ribosomal incorporation of β- and γ-keto amides as an important development in the late-stage functionalization and macrocyclization of peptides with validated drug-like features.

References cited

1. Sims, E. K., Carr, A. L. J., Oram, R. A., DiMeglio, L. A. & Evans-Molina, C. 100 years of insulin: celebrating the past, present and future of diabetes therapy. *Nat. Med.* **27**, 1154–1164 (2021).
2. Banting, F. G., Best, C. H., Collip, J. B., Campbell, W. R. & Fletcher, A. A. Pancreatic Extracts in the Treatment of Diabetes Mellitus. *Can. Med. Assoc. J.* **12**, 141–146 (1922).
3. Wilding, J. P. H. *et al.* Once-Weekly Semaglutide in Adults with Overweight or Obesity. *N. Engl. J. Med.* **384**, 989–1002 (2021).
4. Müller, T. D., Blüher, M., Tschöp, M. H. & DiMarchi, R. D. Anti-obesity drug discovery: advances and challenges. *Nat. Rev. Drug Discov.* **21**, 201–223 (2022).
5. Muttenthaler, M., King, G. F., Adams, D. J. & Alewood, P. F. Trends in peptide drug discovery. *Nat. Rev. Drug Discov.* **20**, 309–325 (2021).
6. Costa, L., Sousa, E. & Fernandes, C. Cyclic Peptides in Pipeline: What Future for These Great Molecules? *Pharmaceuticals* **16**, 996 (2023).
7. Zorzi, A., Deyle, K. & Heinis, C. Cyclic peptide therapeutics: past, present and future. *Curr. Opin. Chem. Biol.* **38**, 24–29 (2017).
8. Yang, J. *et al.* Utilization of macrocyclic peptides to target protein-protein interactions in cancer. *Front. Oncol.* **12**, (2022).
9. Ohta, A. *et al.* Validation of a New Methodology to Create Oral Drugs beyond the Rule of 5 for Intracellular Tough Targets. *J. Am. Chem. Soc.* (2023) doi:10.1021/jacs.3c07145.
10. Tucker, T. J. *et al.* A Series of Novel, Highly Potent, and Orally Bioavailable Next-Generation Tricyclic Peptide PCSK9 Inhibitors. *J. Med. Chem.* **64**, 16770–16800 (2021).
11. Li, X., Craven, T. W. & Levine, P. M. Cyclic Peptide Screening Methods for Preclinical Drug Discovery. *J. Med. Chem.* **65**, 11913–11926 (2022).
12. Sawyer, T. Entrepreneurial Drug Hunter: Macrocyclic Peptide Modalities. in

Contemporary Accounts in Drug Discovery and Development (eds. Huang, X., Aslanian, R. G. & Tang, W. H.) 273–292 (Wiley, 2022). doi:10.1002/9781119627784.ch12.

13. Howard, J. F. *et al.* Safety and efficacy of zilucoplan in patients with generalised myasthenia gravis (RAISE): a randomised, double-blind, placebo-controlled, phase 3 study. *Lancet Neurol.* **22**, 395–406 (2023).

14. Rezai, T., Yu, B., Millhauser, G. L., Jacobson, M. P. & Lokey, R. S. Testing the Conformational Hypothesis of Passive Membrane Permeability Using Synthetic Cyclic Peptide Diastereomers. *J. Am. Chem. Soc.* **128**, 2510–2511 (2006).

15. Rossi Sebastiano, M. *et al.* Impact of Dynamically Exposed Polarity on Permeability and Solubility of Chameleonic Drugs Beyond the Rule of 5. *J. Med. Chem.* **61**, 4189–4202 (2018).

16. He, J., Ghosh, P. & Nitsche, C. Biocompatible strategies for peptide macrocyclisation. *Chem. Sci.* **15**, 2300–2322 (2024).

17. White, C. J. & Yudin, A. K. Contemporary strategies for peptide macrocyclization. *Nat. Chem.* **3**, 509–524 (2011).

18. Bechtler, C. & Lamers, C. Macrocyclization strategies for cyclic peptides and peptidomimetics. *RSC Med. Chem.* **12**, 1325–1351 (2021).

19. Miller, S. J., Blackwell, H. E. & Grubbs, R. H. Application of Ring-Closing Metathesis to the Synthesis of Rigidified Amino Acids and Peptides. *J. Am. Chem. Soc.* **118**, 9606–9614 (1996).

20. Walensky, L. D. & Bird, G. H. Hydrocarbon-Stapled Peptides: Principles, Practice, and Progress. *J. Med. Chem.* **57**, 6275–6288 (2014).

21. Rivera, D. G., Ojeda-Carralero, G. M., Reguera, L. & Eycken, E. V. V. der. Peptide macrocyclization by transition metal catalysis. *Chem. Soc. Rev.* **49**, 2039–2059 (2020).

22. Passioura, T. The Road Ahead for the Development of Macrocyclic Peptide Ligands. *Biochemistry* **59**, 139–145 (2020).

23. Melsen, P. R. A., Yoshisada, R. & Jongkees, S. A. K. Opportunities for Expanding

Encoded Chemical Diversification and Improving Hit Enrichment in mRNA-Displayed Peptide Libraries. *ChemBioChem* **23**, e202100685 (2022).

24. Smolyar, I. V., Yudin, A. K. & Nenajdenko, V. G. Heteroaryl Rings in Peptide Macrocycles. *Chem. Rev.* **119**, 10032–10240 (2019).

25. Iskandar, S. E. *et al.* Enabling Genetic Code Expansion and Peptide Macrocyclization in mRNA Display via a Promiscuous Orthogonal Aminoacyl-tRNA Synthetase. *J. Am. Chem. Soc.* **145**, 1512–1517 (2023).

26. Liu, M. *et al.* Selective thiazoline peptide cyclisation compatible with mRNA display and efficient synthesis. *Chem. Sci.* (2023) doi:10.1039/D3SC03117A.

27. Dengler, S. *et al.* Display Selection of a Hybrid Foldamer–Peptide Macrocycle. *Angew. Chem. Int. Ed.* **62**, e202308408 (2023).

28. Ekanayake, A. I. *et al.* Genetically Encoded Fragment-Based Discovery from Phage-Displayed Macrocyclic Libraries with Genetically Encoded Unnatural Pharmacophores. *J. Am. Chem. Soc.* **143**, 5497–5507 (2021).

29. Yadav, P. & Shah, K. Quinolines, a perpetual, multipurpose scaffold in medicinal chemistry. *Bioorganic Chem.* **109**, 104639 (2021).

30. Musiol, R. An overview of quinoline as a privileged scaffold in cancer drug discovery. *Expert Opin. Drug Discov.* **12**, 583–597 (2017).

31. Childs-Disney, J. L. *et al.* Targeting RNA structures with small molecules. *Nat. Rev. Drug Discov.* **21**, 736–762 (2022).

32. Costales, M. G., Childs-Disney, J. L., Haniff, H. S. & Disney, M. D. How We Think about Targeting RNA with Small Molecules. *J. Med. Chem.* **63**, 8880–8900 (2020).

33. Haniff, H. S., Knerr, L., Chen, J. L., Disney, M. D. & Lightfoot, H. L. Target-Directed Approaches for Screening Small Molecules against RNA Targets. *SLAS Discov.* **25**, 869–894 (2020).

34. Donlic, A. *et al.* R-BIND 2.0: An Updated Database of Bioactive RNA-Targeting Small

Molecules and Associated RNA Secondary Structures. *ACS Chem. Biol.* **17**, 1556–1566 (2022).

35. Krishnamurthy, M., Gooch, B. D. & Beal, P. A. Peptide Quinoline Conjugates: A New Class of RNA-Binding Molecules. *Org. Lett.* **6**, 63–66 (2004).

36. Krishnamurthy, M., Simon, K., Orendt, A. M. & Beal, P. A. Macrocyclic Helix-Threading Peptides for Targeting RNA. *Angew. Chem. Int. Ed.* **46**, 7044–7047 (2007).

37. Chen, J. L. *et al.* Design, Optimization, and Study of Small Molecules That Target Tau Pre-mRNA and Affect Splicing. *J. Am. Chem. Soc.* **142**, 8706–8727 (2020).

38. Ad, O. *et al.* Translation of Diverse Aramid- and 1,3-Dicarbonyl-peptides by Wild Type Ribosomes *in Vitro*. *ACS Cent. Sci.* **5**, 1289–1294 (2019).

39. Fricke, R. *et al.* Expanding the substrate scope of pyrrolysyl-transfer RNA synthetase enzymes to include non-α-amino acids in vitro and in vivo. *Nat. Chem.* **15**, 960–971 (2023).

40. Murakami, H., Ohta, A., Ashigai, H. & Suga, H. A highly flexible tRNA acylation method for non-natural polypeptide synthesis. *Nat. Methods* **3**, 357–359 (2006).

41. Fricke, R., Knudson, I. & Schepartz, A. Direct, quantitative, and comprehensive analysis of tRNA acylation using intact tRNA liquid-chromatography mass-spectrometry. 2023.07.14.549096 Preprint at https://doi.org/10.1101/2023.07.14.549096 (2023).

42. Lee, J. *et al.* Ribosome-mediated biosynthesis of pyridazinone oligomers in vitro. *Nat. Commun.* **13**, 6322 (2022).

43. Li, W., Zheng, Y., Qu, E., Bai, J. & Deng, Q. β-Keto Amides: A Jack-of-All-Trades Building Block in Organic Chemistry. *Eur. J. Org. Chem.* **2021**, 5151–5192 (2021).

44. Wu, X. & Li, W. The applications of β-keto amides for heterocycle synthesis. *J. Heterocycl. Chem.* **59**, 1445–1490 (2022).

45. Amarnath, V. & Amarnath, K. Intermediates in the Paal-Knorr Synthesis of Furans. *J. Org. Chem.* **60**, 301–307 (1995).

46. Friedlaender, P. Ueber o-Amidobenzaldehyd. *Berichte Dtsch. Chem. Ges.* **15**, 2572–

2575 (1882).

47. Cheng, C.-C. & Yan, S.-J. The Friedländer Synthesis of Quinolines. in *Organic Reactions* 37–201 (John Wiley & Sons, Ltd, 2005). doi:10.1002/0471264180.or028.02.

48. Marco-Contelles, J., Pérez-Mayoral, E., Samadi, A., Carreiras, M. & Soriano, E. Recent Advances in the Friedl??nder Reaction. *Chem. Rev.* **109**, 2652–71 (2009).

49. Meléndez, A. *et al.* Straightforward Synthesis of Novel 4-Styrylquinolines/4-Styrylquinolin-2-ones and 9-Styryldihydroacridin-1(2H)-ones from Substituted 2′-Aminochalcones. *Synthesis* **52**, 1804–1822 (2020).

50. Shen, Q. *et al.* Synthesis of Quinolines via Friedländer Reaction in Water and under Catalyst-Free Conditions. *Synthesis* **44**, 389–392 (2012).

51. Ţînţaş, M.-L. *et al.* Rational design of carbamate-based dual binding site and central AChE inhibitors by a “biooxidisable” prodrug approach: Synthesis, in vitro evaluation and docking studies. *Eur. J. Med. Chem.* **155**, 171–182 (2018).

52. Atechian, S. *et al.* New vistas in quinoline synthesis. *Tetrahedron* **63**, 2811–2823 (2007).

53. Gopi, P. & Sarveswari, S. Effective water mediated green synthesis of polysubstituted quinolines without energy expenditure. *Monatshefte Für Chem. - Chem. Mon.* **148**, 1043–1049 (2017).

54. Bose, D. S., Idrees, Mohd., Jakka, N. M. & Rao, J. V. Diversity-Oriented Synthesis of Quinolines via Friedländer Annulation Reaction under Mild Catalytic Conditions. *J. Comb. Chem.* **12**, 100–110 (2010).

55. Albert, A. & Yamamoto, H. The structures of the anhydro-polymers of 2-aminobenzaldehyde. *J. Chem. Soc. B Phys. Org.* 956 (1966) doi:10.1039/j29660000956.

56. Christie, G. H. & Kenner, J. LXXI.—The molecular configurations of polynuclear aromatic compounds. Part I. The resolution of γ-6 : 6′-dinitro- and 4 : 6 : 4′ : 6′-tetranitro-diphenic acids into optically active components. *J. Chem. Soc. Trans.* **121**, 614–620 (1922).

57. Perreault, S., Chandrasekhar, J. & Patel, L. Atropisomerism in Drug Discovery: A

Medicinal Chemistry Perspective Inspired by Atropisomeric Class I PI3K Inhibitors. *Acc. Chem. Res.* **55**, 2581–2593 (2022).

58. Basilaia, M., Chen, M. H., Secka, J. & Gustafson, J. L. Atropisomerism in the Pharmaceutically Relevant Realm. *Acc. Chem. Res.* **55**, 2904–2919 (2022).

59. LaPlante, S. R. *et al.* Assessing Atropisomer Axial Chirality in Drug Discovery and Development. *J. Med. Chem.* **54**, 7005–7022 (2011).

60. Toenjes, S. T. & Gustafson, J. L. Atropisomerism in medicinal chemistry: challenges and opportunities. *Future Med. Chem.* **10**, 409–422 (2018).

61. Janes, M. R. *et al.* Targeting KRAS Mutant Cancers with a Covalent G12C-Specific Inhibitor. *Cell* **172**, 578-589.e17 (2018).

62. Lanman, B. A., Parsons, A. T. & Zech, S. G. Addressing Atropisomerism in the Development of Sotorasib, a Covalent Inhibitor of KRAS G12C: Structural, Analytical, and Synthetic Considerations. *Acc. Chem. Res.* **55**, 2892–2903 (2022).

63. Fader, L. D. *et al.* Discovery of BI 224436, a Noncatalytic Site Integrase Inhibitor (NCINI) of HIV-1. *ACS Med. Chem. Lett.* **5**, 422–427 (2014).

64. Nanudorn, P. *et al.* Atropopeptides are a Novel Family of Ribosomally Synthesized and Posttranslationally Modified Peptides with a Complex Molecular Shape. *Angew. Chem.* **n/a**,.

65. Reisberg, S. H. *et al.* Total synthesis reveals atypical atropisomerism in a small-molecule natural product, tryptorubin A. *Science* **367**, 458–463 (2020).

66. Yao, G. *et al.* The occurrence of ansamers in the synthesis of cyclic peptides. *Nat. Commun.* **13**, 6488 (2022).

67. Hegemann, J. D., Zimmermann, M., Xie, X. & Marahiel, M. A. Lasso Peptides: An Intriguing Class of Bacterial Natural Products. *Acc. Chem. Res.* **48**, 1909–1919 (2015).

68. de Veer, S. J., Kan, M.-W. & Craik, D. J. Cyclotides: From Structure to Function. *Chem. Rev.* **119**, 12375–12421 (2019).

69. Moore, M. J. *et al.* Next-Generation Total Synthesis of Vancomycin. *J. Am. Chem. Soc.*

142, 16039–16050 (2020).

70. Bose, D. S. & Kumar, R. K. An efficient, high yielding protocol for the synthesis of functionalized quinolines via the tandem addition/annulation reaction of o-aminoaryl ketones with α-methylene ketones. *Tetrahedron Lett.* **47**, 813–816 (2006).

71. Wu, J., Zhang, L. & Diao, T.-N. An Expeditious Approach to Quinolines via Friedländer Synthesis Catalyzed by $FeCl_3$ or $Mg(ClO_4)_2$. *Synlett* 2653–2657 (2005) doi:10.1055/s-2005-917111.

72. Muchowski, J. M. & Maddox, M. L. Concerning the mechanism of the Friedländer quinoline synthesis. *Can. J. Chem.* **82**, 461–478 (2004).

73. De, S. K. & Gibbs, R. A. A mild and efficient one-step synthesis of quinolines. *Tetrahedron Lett.* **46**, 1647–1649 (2005).

74. Lekhok, K. C., Bhuyan, D., Prajapati, D. & Boruah, R. C. Zinc triflate: a highly efficient reusable catalyst in the synthesis of functionalized quinolines via Friedlander annulation. *Mol. Divers.* **14**, 841–846 (2010).

75. Shao, Y.-D. *et al.* Organocatalytic Atroposelective Friedländer Quinoline Heteroannulation. *Org. Lett.* **21**, 4831–4836 (2019).

76. Pohl, E. *et al.* Structure of octreotide, a somatostatin analogue. *Acta Crystallogr. D Biol. Crystallogr.* **51**, 48–59 (1995).

77. Weckbecker, G. *et al.* Opportunities in somatostatin research: biological, chemical and therapeutic aspects. *Nat. Rev. Drug Discov.* **2**, 999–1017 (2003).

78. Katoh, T., Iwane, Y. & Suga, H. tRNA engineering for manipulating genetic code. *RNA Biol.* **15**, 453–460 (2017).

79. Cui, Z., Wu, Y., Mureev, S. & Alexandrov, K. Oligonucleotide-mediated tRNA sequestration enables one-pot sense codon reassignment in vitro. *Nucleic Acids Res.* **46**, 6387–6400 (2018).

80. Rutledge, S., Volkman, H. & Schepartz, A. Molecular recognition of protein surfaces:

High affinity ligands for the CBPKIX domain. *J. Am. Chem. Soc.* **125**, 14336–14347 (2003).

81. Salveson, P. J. *et al.* Expansive discovery of chemically diverse structured macrocyclic oligoamides. *Science* **384**, 420–428 (2024).

82. Vinogradov, A. A., Yin, Y. & Suga, H. Macrocyclic Peptides as Drug Candidates: Recent Progress and Remaining Challenges. *J. Am. Chem. Soc.* **141**, 4167–4181 (2019).

83. Kawakami, T., Murakami, H. & Suga, H. Messenger RNA-Programmed Incorporation of Multiple N-Methyl-Amino Acids into Linear and Cyclic Peptides. *Chem. Biol.* **15**, 32–42 (2008).

84. Katoh, T., Tajima, K. & Suga, H. Consecutive Elongation of D-Amino Acids in Translation. *Cell Chem. Biol.* **24**, 46–54 (2017).

85. Diaz, D. B. *et al.* Illuminating the dark conformational space of macrocycles using dominant rotors. *Nat. Chem.* **13**, 218–225 (2021).

86. Saunders, G. J. & Yudin, A. K. Property-Driven Development of Passively Permeable Macrocyclic Scaffolds Using Heterocycles**. *Angew. Chem. Int. Ed.* **61**, e202206866 (2022).

87. Hantzsch, A. Condensationsprodukte aus Aldehydammoniak und ketonartigen Verbindungen. *Berichte Dtsch. Chem. Ges.* **14**, 1637–1638 (1881).

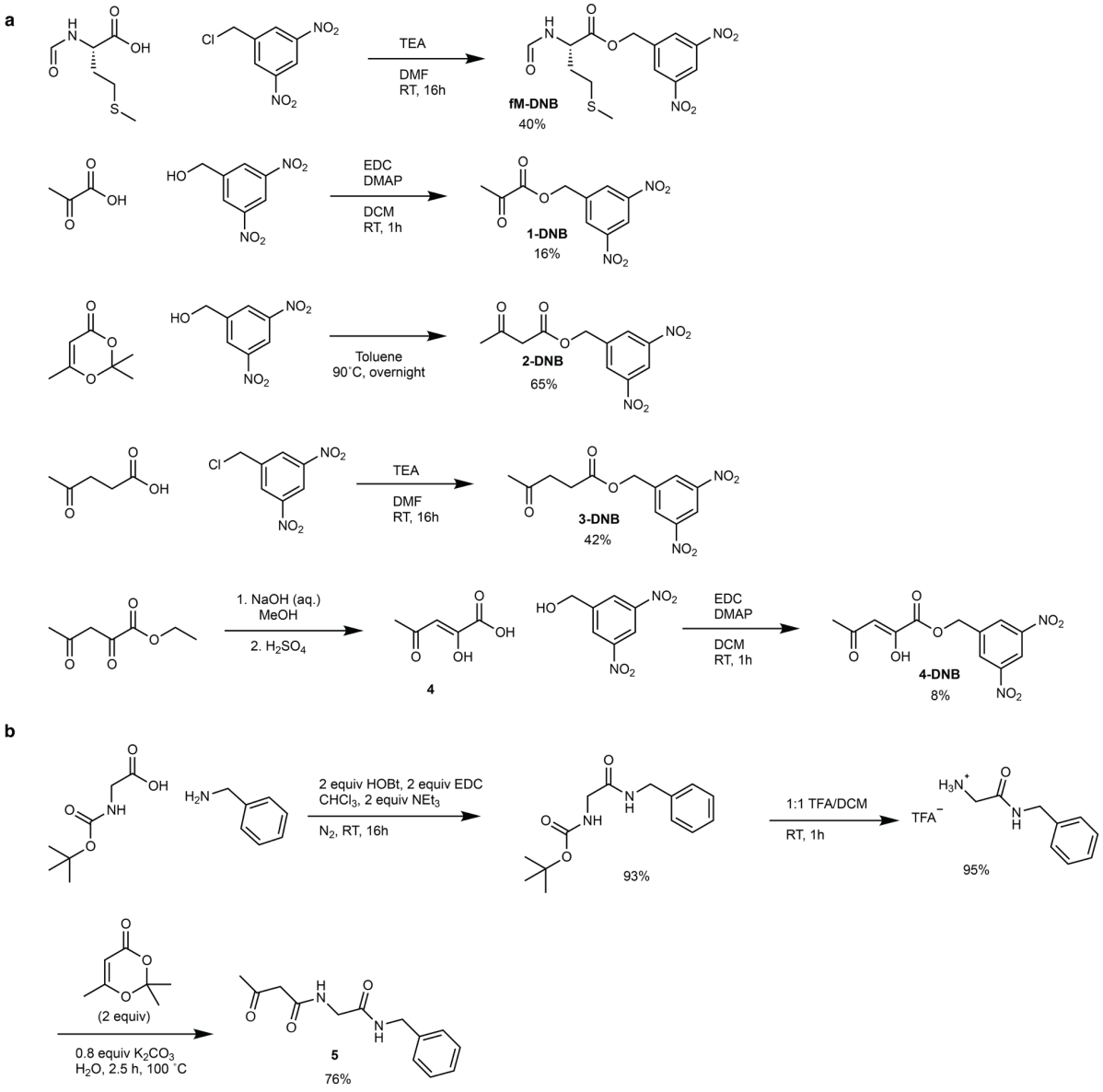
88. Knorr, L. Einwirkung von Acetessigester auf Phenylhydrazin. *Berichte Dtsch. Chem. Ges.* **16**, 2597–2599 (1883).

89. Knorr, L. Synthese von Pyrrolderivaten. *Berichte Dtsch. Chem. Ges.* **17**, 1635–1642 (1884).

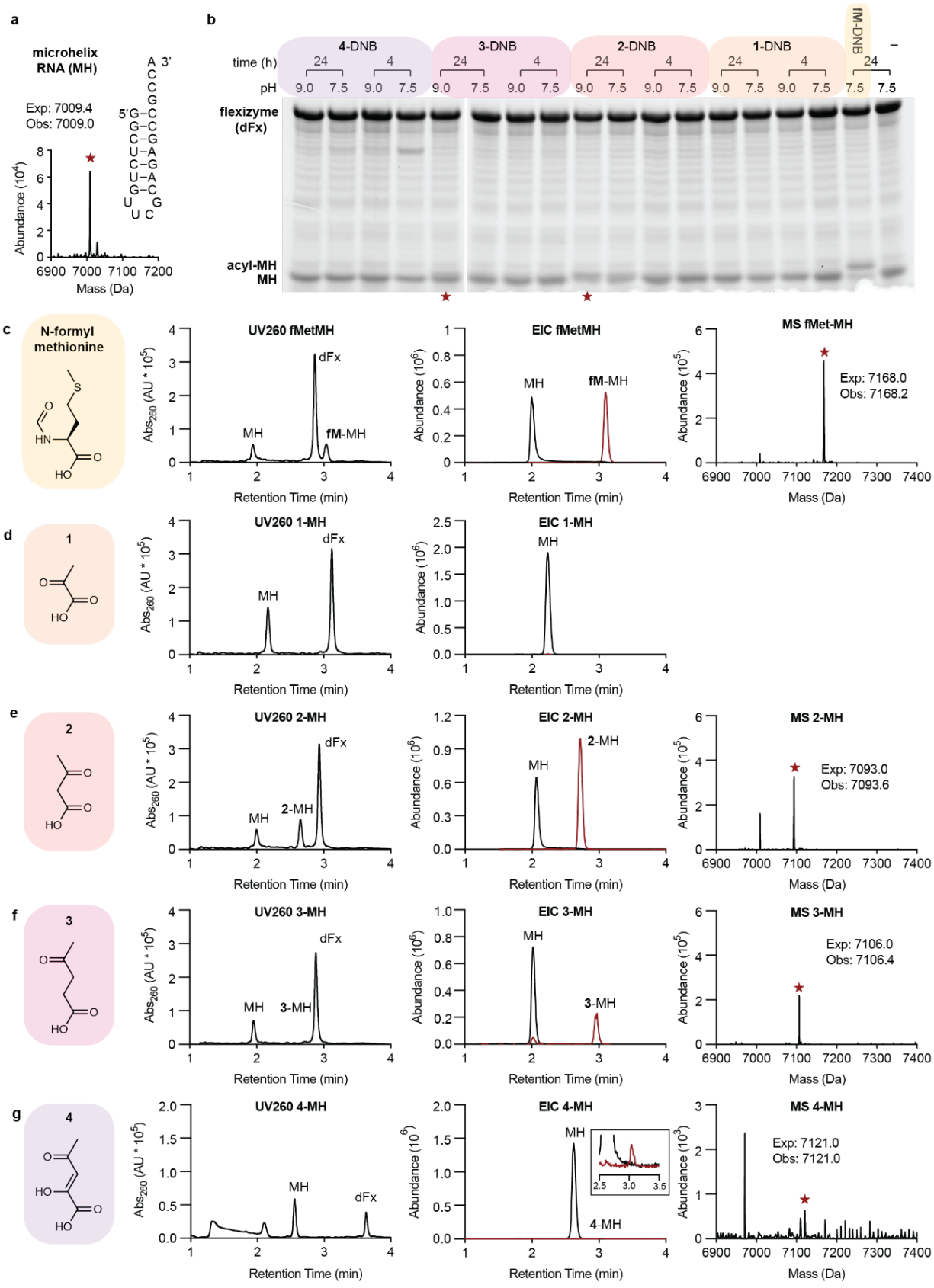
90. Bose, D. S., Fatima, L. & Mereyala, H. B. Green Chemistry Approaches to the Synthesis of 5-Alkoxycarbonyl-4-aryl-3,4- dihydropyrimidin-2(1H)-ones by a Three-Component Coupling of One-Pot Condensation Reaction: Comparison of Ethanol, Water, and Solvent-free Conditions. *J. Org. Chem.* **68**, 587–590 (2003).

91. Kennedy-Smith, J. J., Staben, S. T. & Toste, F. D. Gold(I)-Catalyzed Conia-Ene Reaction of β-Ketoesters with Alkynes. *J. Am. Chem. Soc.* **126**, 4526–4527 (2004).

Supplemental Figures



Supplementary Fig. 1. Synthesis of activated 3,5-dinitrobenzyl (DNB) esters used for microhelix (MH) and tRNA acylation as well as model β-keto amide dipeptide 5 used for Friedländer reaction optimization. a, Schemes illustrating the synthesis of 3,5-dinitrobenzyl (DNB) esters of **fMet (fM)** and monomers **1 - 4** used for Flexizyme-promoted acylation of microhelix (MH) and tRNA substrates. **b**, Scheme showing the synthesis of model β-keto amide dipeptide **5**. For additional experimental details, see **Supplementary Information**.

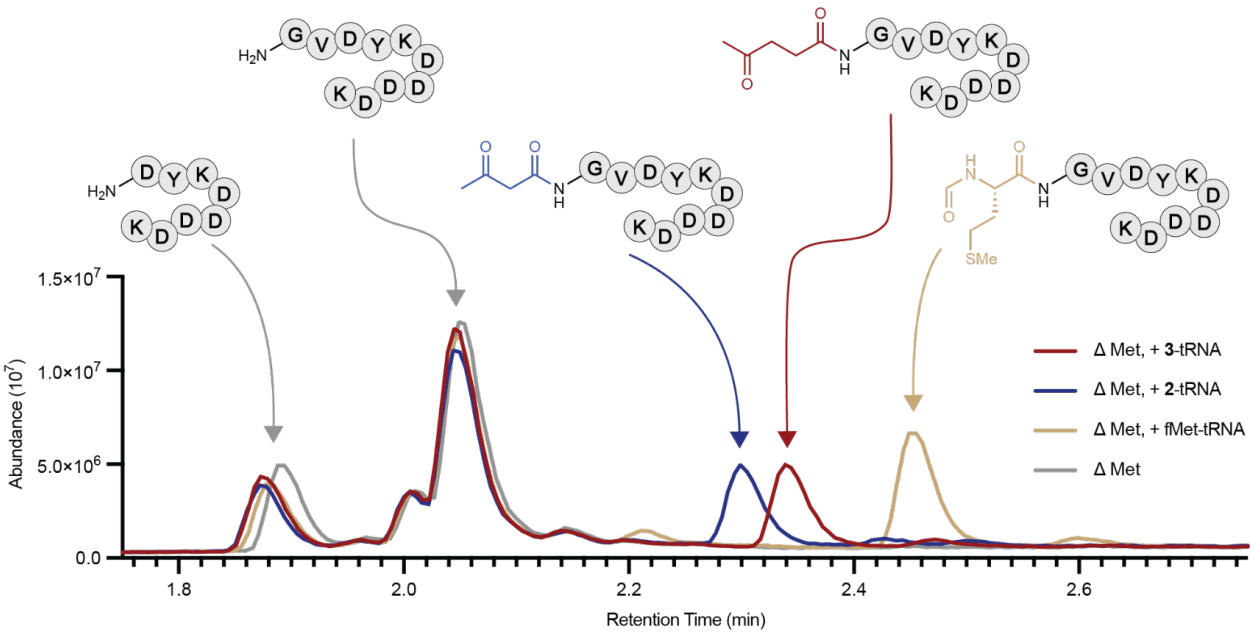

a
microhelix RNA (MH)
Exp: 7009.4
Obs: 7009.0
Abundance (10^4)
Mass (Da)
b
4-DNB
3-DNB
2-DNB
1-DNB
fM-DNB
time (h)
pH
flexizyme (dFx)
acyl-MH
MH
c
N-formyl methionine
UV260 fMetMH
EIC fMetMH
MS fMet-MH
dFx
MH
fM-MH
Exp: 7168.0
Obs: 7168.2
Retention Time (min)
d
1
UV260 1-MH
EIC 1-MH
e
2
UV260 2-MH
EIC 2-MH
MS 2-MH
2-MH
Exp: 7093.0
Obs: 7093.6
f
3
UV260 3-MH
EIC 3-MH
MS 3-MH
3-MH
Exp: 7106.0
Obs: 7106.4
g
4
UV260 4-MH
EIC 4-MH
MS 4-MH
4-MH
Exp: 7121.0
Obs: 7121.0

Supplementary Fig. 2. Flexizyme-promoted acylation of MH with DNB esters of fMet (fM) and monomers 1-4. a, Secondary structure and intact MS of microhelix MH. **b,** Acidic polyacrylamide gel electrophoresis (aPAGE) of dFx-promoted MH acylation reactions of DNB esters. Unreacted MH cannot be resolved from the acyl-MH product in reactions containing the DNB-esters of monomers **1-4**. The red star beneath the gel image denotes the best conditions identified using intact tRNA LC-MS. **c-g,** Abs_{260} chromatograms, extracted ion chromatograms, and deconvoluted mass spectra of the products resulting from flexizyme-promoted acylation of MH by the DNB esters of **fMet (fM)** and **1-4.** In EIC, red traces correspond to the acylated MH, while black traces represent the unacylated MH.The red stars on the mass spectra indicate the acyl-MH peak in the deconvolution.

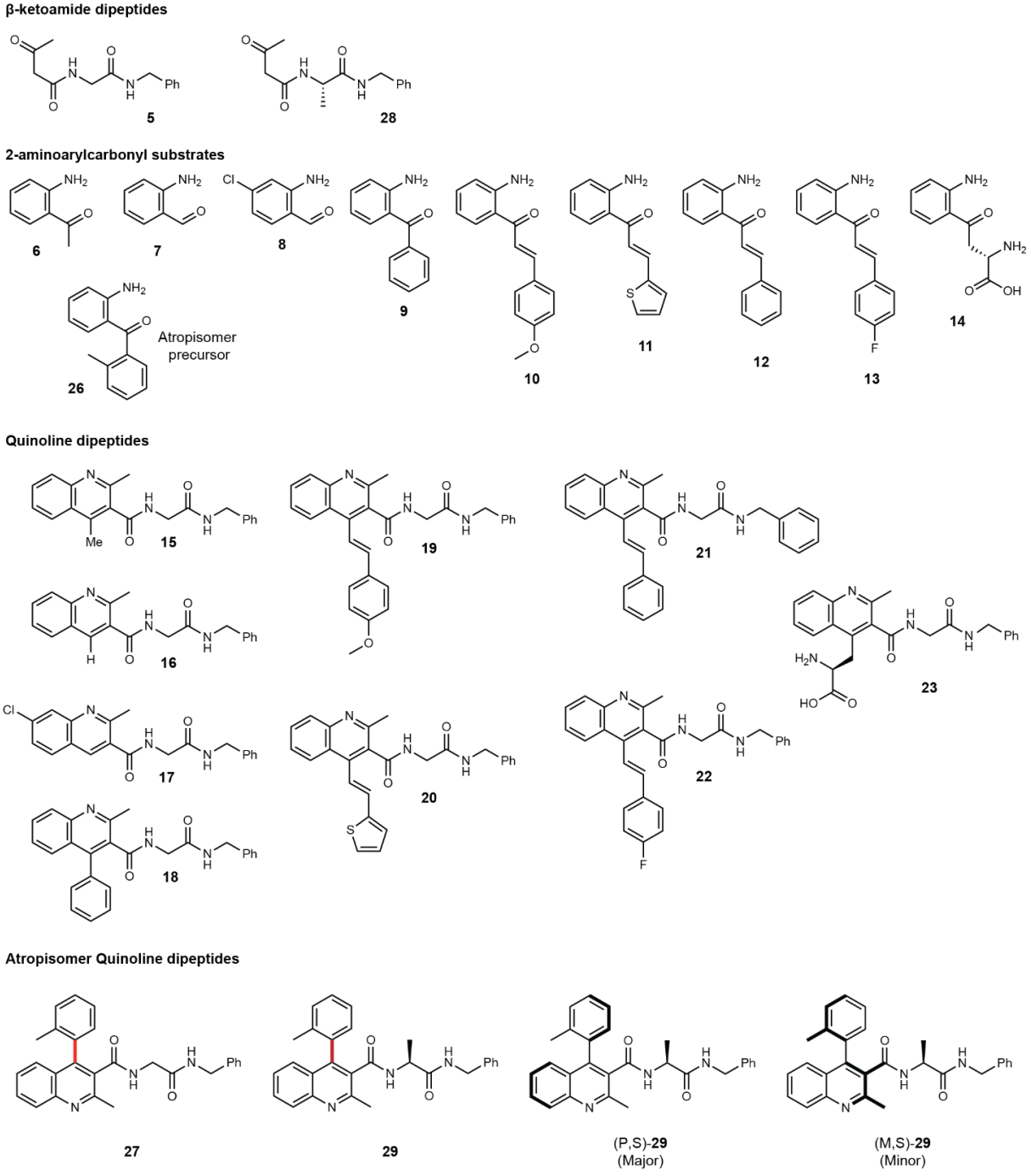
Supplementary Table 1. Yields of acylated MH and $tRNA^{fMet}$ calculated on the basis of A_{260} absorbance and extracted ion chromatograms (EIC). Acylation of microhelix MH or tRNA (25 μM) by the DNB esters of **fM** and monomers **1** - **4** (5 μM) using dFx (25 μM) under the conditions shown. ND = no product detected. Values represent the average of three independent experiments. Conditions resulting in the highest yields of acylated MHs are highlighted. Acylation Yield by A_{260} Absorbance = 100 * [acyl-MH_{A260}/(acyl-MH_{A260} + MH_{A260})]. Note that **3-MH** and dFx coelute, so the A_{260} value could not be used to assess yield. MH acylation yield was also determined by the ratio of the EIC for MH (-4 charge state) and acyl-MH (-4 charge state). The yield calculated on the basis of EIC correlated well with the yield calculated on the basis of A_{260} values.

Monomer	Conditions	MH Acylation % by Absorbance	MH Acylation % by Extracted Ion	$tRNA^{fMet}$ Acylation % by Absorbance	$tRNA^{fMet}$ Acylation % by Extracted Ion
fM-DNB	**pH 7.5, 24h**	**42.4**	**45.6**		
1-DNB	pH 7.5, 24h	ND	ND		
1-DNB	pH 7.5, 48h	ND	ND		
1-DNB	pH 9.0, 24h	ND	ND		
1-DNB	pH 9.0, 48h	ND	ND		
2-DNB	pH 7.5, 24h	40.7	41.0		
2-DNB	pH 7.5, 48h	49.3	51.6		
2-DNB	pH 9.0, 24h	51.2	55.6		
2-DNB	**pH 9.0, 48h**	**56.9**	**55.8**	**35.5**	**31.5**
3-DNB	pH 7.5, 24h	ND	7.3		
3-DNB	pH 7.5, 48h	ND	12.3		
3-DNB	**pH 9.0, 24h**	**ND**	**27.0**	**20.1**	**25.5**
3-DNB	pH 9.0, 48h	ND	18.7		
4-DNB	pH 7.5, 24h	ND	0.3		
4-DNB	pH 7.5, 48h	ND	0.3		
4-DNB	**pH 9.0, 24h**	**ND**	**0.6**		

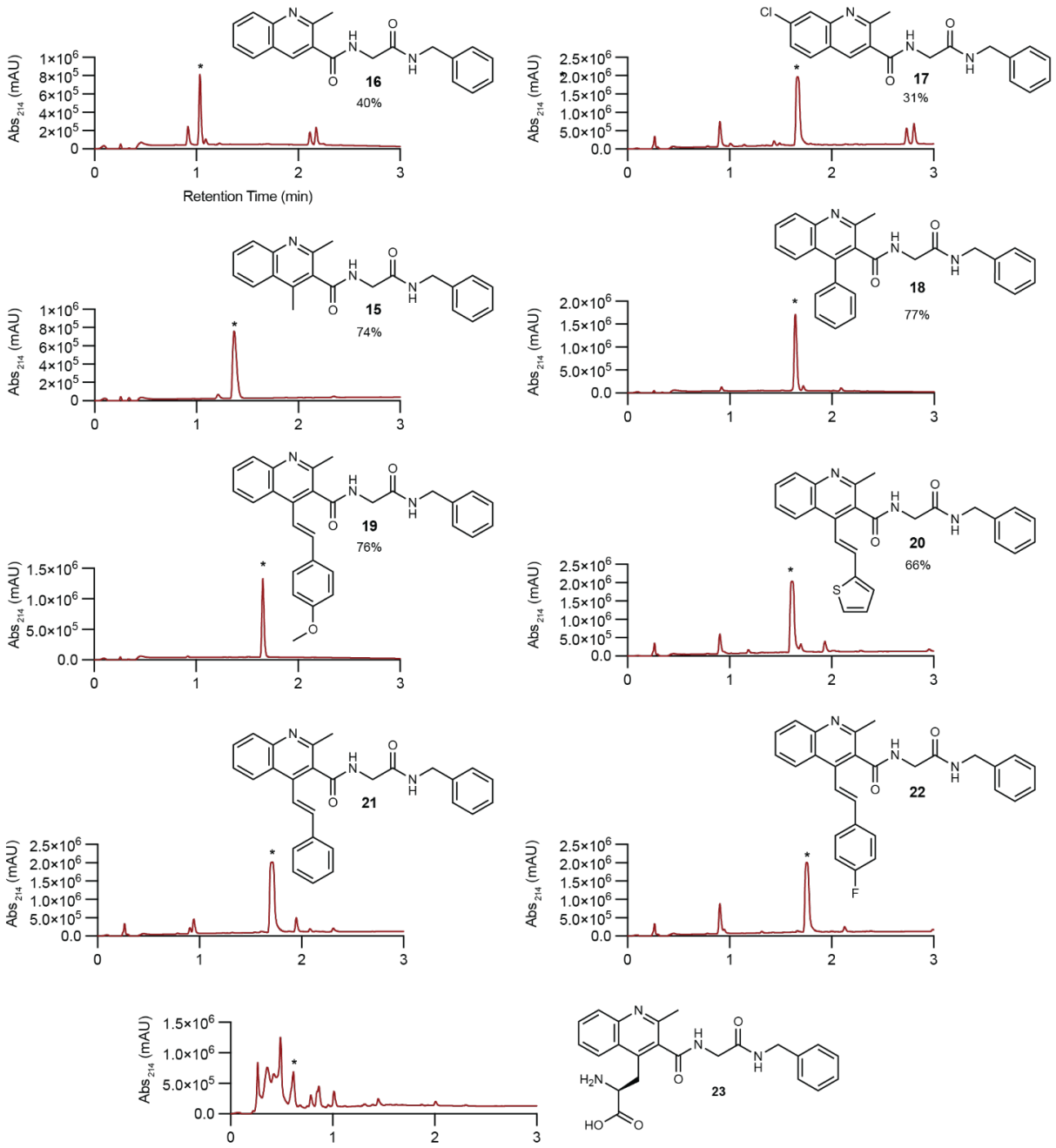
4-DNB	pH 9.0, 48h	ND	0.5		



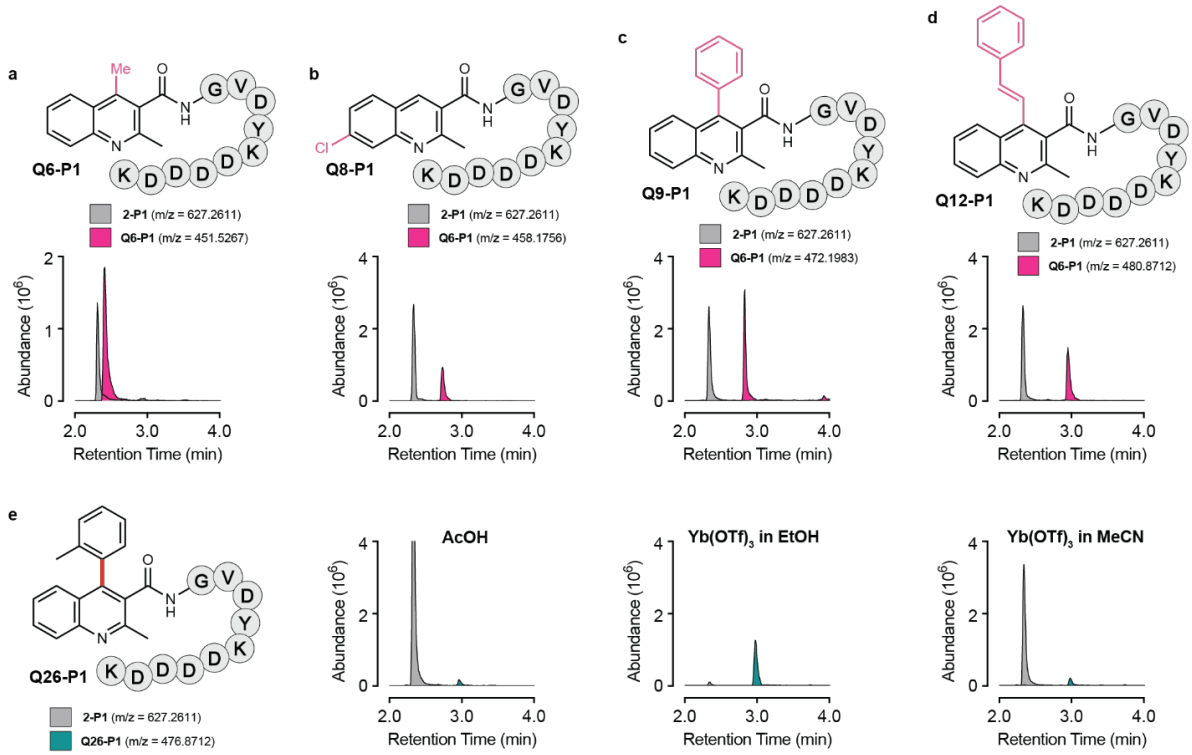
Supplementary Fig. 3. Peptides initiated with 2-tRNA^{fMet} or 3-tRNA^{fMet} were translated at levels comparable to those initiated with fMet-tRNA^{fMet}. a, Total ion chromatogram of IVT reactions programmed with a duplex DNA template encoding the FLAG-containing polypeptide MGVDYKDDDDK (MGV-flag) in the presence or absence of tRNA^{fMet} acylated with the DNB esters of **fMet (fM)** or monomers **2** or **3** following anti-FLAG purification as described in **Supplementary Information**. As previously described by others, we also observe side-products resulting from "drop-off-reinitiation"[1–6].



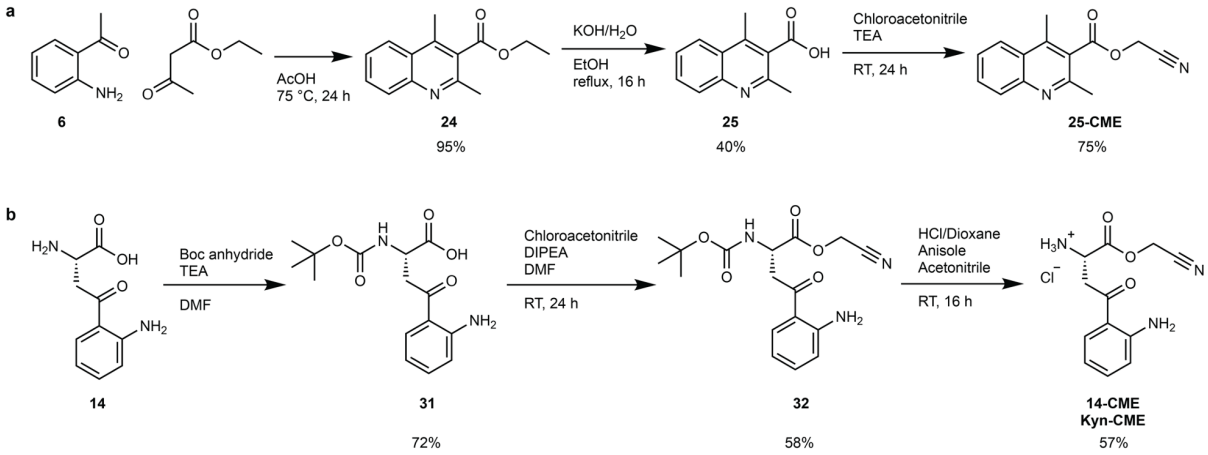
Supplementary Fig. 4. Substrates and products of Friedländer reactions.



Supplementary Fig. 5. Substrate scope of Friedländer reactions on model β-keto amide peptide 5. Shown are A_{214} chromatograms illustrating the products of Friedländer reactions between β-keto amide peptide **5** and 2-aminoarylcarbonyl substrates **6-14** performed in AcOH after 48 h at 60 °C. The Friedländer reaction proceeds smoothly for all substrates tested except kynurenine **14** (product **23**). Aminobenzaldehydes **7** (product **16**) and **8** (product **17**) oligomerize under the reaction conditions (double peaks at 2.1 and 2.9 min, respectively). For experimental details, please refer to **Supplementary Information** (Friedländer reaction (general procedure for **15** to **23**)). Peaks identified with an asterisk represent the desired product as confirmed by mass spectrometry. Isolated yields are presented for representative samples.



Supplementary Fig. 6. Extracted ion chromatograms of Friedländer reactions of peptides synthesized using in vitro translation (IVT) methods. a-d, Extracted mass chromatograms for **2-P1** (grey) and each quinoline peptide (pink) after reaction in AcOH at 40 °C for 24 h. **e,** Extracted mass chromatograms for **2-P1** (grey) and presumed atropisomer quinoline peptide **Q26-P1** (teal) after reaction in AcOH or in the presence of $Yb(OTf)_3$ in EtOH or in MeCN. All reactions were run for 24 h at 40 °C.

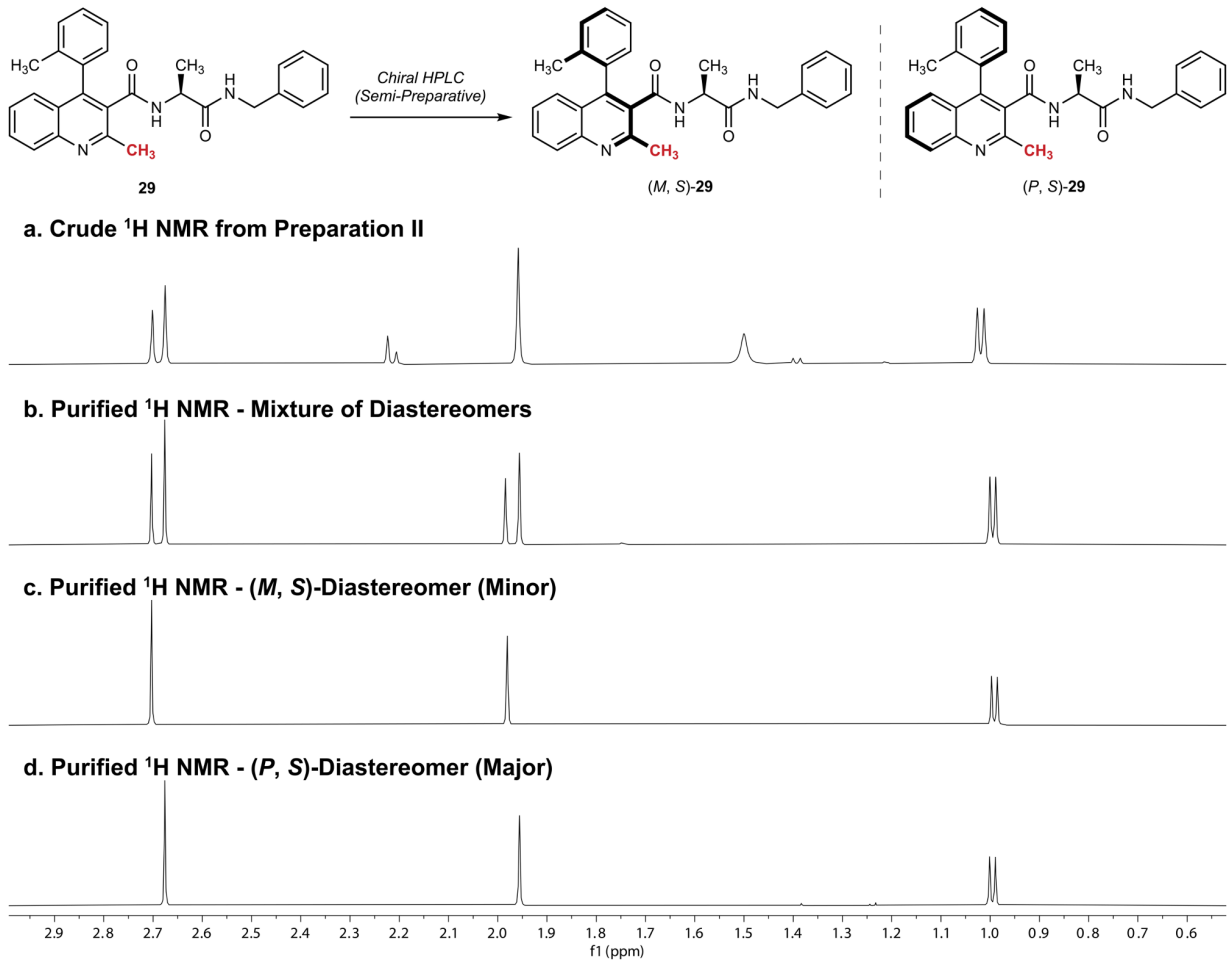


Supplementary Fig. 7. Additional synthetic routes. Synthetic routes used to prepare the cyanomethyl esters of **a,** quinoline **25**, and **b,** kynurenine **14**. For additional experimental details, see **Supplementary Information.**

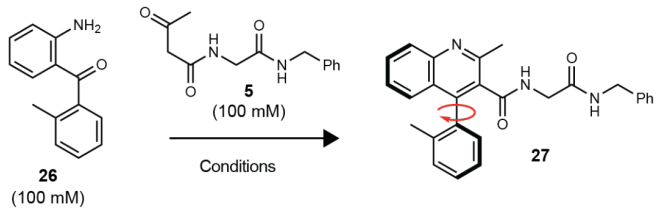
Supplementary Table 2. LC-MS quantification of microhelix (MH) acylation with CME monomers. Acylation of microhelix MH or tRNA (25 μM) with the indicated CME ester (5 μM) using eFx (25 μM) under the conditions shown. ND = no product detected. Values represent the average of three independent experiments. Conditions resulting in the highest yields of acylated MHs are highlighted.

Monomer	Conditions	MH A_{260} (% Acyl)	MH EIC (% Acyl)	tRNA A_{260} (% Acyl)	tRNA EIC (% Acyl)
Kyn-CME	pH 7.5, 2h	18.7	9.9		
Kyn-CME	pH 7.5, 6h	23.8	11.9	20.0	15.4
Kyn-CME	pH 7.5, 24h	17.3	6		
Kyn-CME	pH 7.5, 48h	10.9	3.5		
Kyn-CME	pH 9.0, 2h	16.5	9.2		
Kyn-CME	pH 9.0, 6h	16.4	7.5		
Kyn-CME	pH 9.0, 24h	ND	2		
Kyn-CME	pH 9.0, 48h	ND	1.5		
25-CME	pH 7.5, 2h	ND	ND		
25-CME	pH 7.5, 6h	ND	ND		
25-CME	pH 7.5, 24h	ND	ND		
25-CME	pH 7.5, 48h	ND	ND		
25-CME	pH 9.0, 2h	ND	ND		
25-CME	pH 9.0, 6h	ND	ND		
25-CME	pH 9.0, 24h	ND	ND		

25-CME	pH 9.0, 48h	ND	ND		



Supplementary Fig. 8: The diastereomeric atropisomers of biaryl 29 show distinct chemical shifts and are chromatographically separable. a, The crude ^{1}H NMR spectrum in $CDCl_3$ of biaryl **29** from Preparation II. The signals arising from the red protons in the accompanying structures were used to determine the diastereomeric ratio. **b,** The ^{1}H NMR spectrum of purified biaryl **29** as a mixture of diastereomeric atropisomers in $CDCl_3$. **c,** The ^{1}H NMR spectrum of the minor diastereomeric atropisomer (*M*, *S*)-**29** in $CDCl_3$. **d,** The ^{1}H NMR spectrum of the major diastereomeric atropisomer (*P*, *S*)-**29** in $CDCl_3$. The spectra shown are truncated for clarity. Additionally, the spectra have been manually aligned to the peaks at δ 2.70 and 2.68 ppm in panel (b) to account for minor deviations in chemical shift, presumably arising from differences in concentration and intermolecular interactions. Processed full spectra are provided within the Supplementary Material and raw .fid files are provided in the FAIR data.

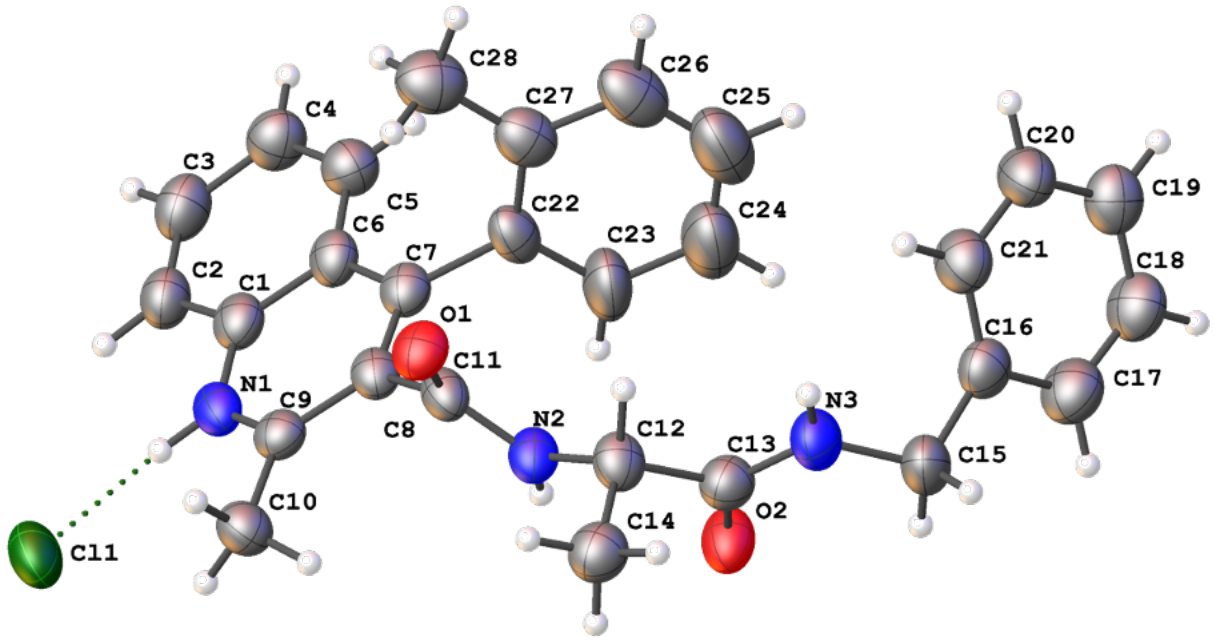


Supplementary Fig. 9. Friedländer reaction of model β-keto amide peptide 5 and 2-amino(*o*-tolyl)phenone (26) to generate 27. Reaction scheme for the generation of atropisomer **27**. Lewis and Brønsted acid conditions explored in **Supplementary Table 3.**

Supplementary Table 3. Lewis and Brønsted acid catalyzed Friedländer reactions to generate atropisomer dipeptides. Various Lewis and Brønsted acids tested for the conversion of β-keto amide dipeptide **5** (100 mM, 5 μmol, 1 equiv) and (2-aminophenyl)(*o*-tolyl)methanone (**26**, 1.1 equiv) into **27**. Reactions were performed at 40 °C for 24 h in PCR tubes. Percentage represents the average of two experiments. Conversion = $\mathbf{27}_{A214}/(\mathbf{5}_{A214}+\mathbf{27}_{A214})$.

	Conditions	Conversion
Brønsted acid conditions	**Glacial AcOH**	**12%**
	AcOH/H_2O	3%
	5% AcOH in EtOH	5%
	0.2 M HCl in H_2O/Dioxane	4%
	HOTf (60 mM) in EtOH	88%
	1% Concentrated sulfuric acid in AcOH	77%
	1.4% (0.2 M) Phosphoric acid in AcOH	44%
	1.4% (0.2 M) Phosphoric acid in MeCN	33%
	10% TFA in DCM	70%
Lewis acid conditions	200 mM $CeCl_3$•$7H_2O$ in EtOH	100%
	200 mM $FeCl_3$•$4H_2O$ in EtOH	63%
	200 mM $ZnCl_2$ in EtOH	15%
	200 mM 4-OH-Pro-COOMe•HCl in EtOH	35%

	20 mM $CeCl_3 \cdot 7H_2O$ in EtOH	50%
	20 mM CAN in EtOH	52%
	20 mM $Zn(OTf)_2$ in EtOH	74%
	20 mM $Y(OTf)_3$ in EtOH	86%
	20 mM $Yb(OTf)_3$ in EtOH	**87%**
	20 mM $Yb(OTf)_3$ in MeCN	61%
	20 mM $Yb(OTf)_3$ in DCM	55%
	20 mM $Yb(OTf)_3$ in DMF	2%
	20 mM $Yb(OTf)_3$ in DMSO	0%
	20 mM $Yb(OTf)_3$ in THF	69%
	20 mM $Yb(OTf)_3$ in AcOH	78%
	20 mM $Yb(OTf)_3$ in 5% AcOH/EtOH	76%

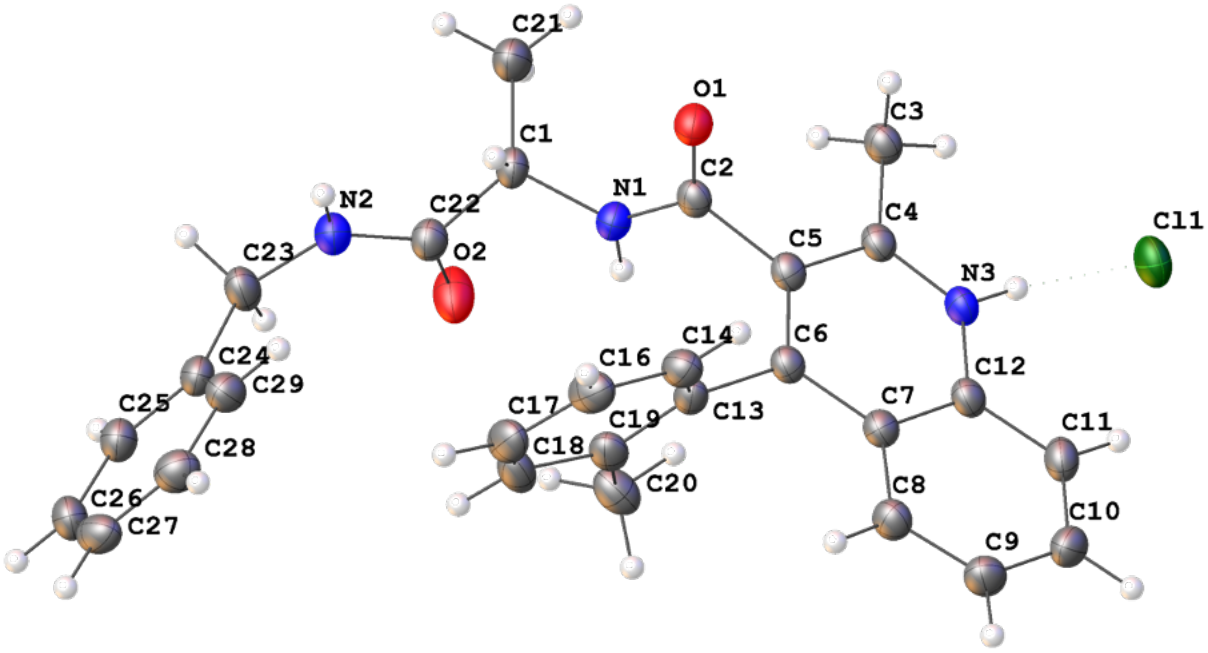


Supplementary Fig. 10: The complete numbering scheme of 007b-24025 ((*M*, *S*)-29·HCl) with 50% thermal ellipsoid probability levels. The hydrogen atoms are shown as circles for clarity. This structure has been deposited in the CCDC with deposition number 2341552.

Supplementary Table 4: Crystal data and structure refinement for 007b-24025 ((*M*, *S*)-29·HCl).

Identification code	007b-24025
Empirical formula	C28 H28 Cl N3 O2
Formula weight	473.98
Temperature	93(2) K
Wavelength	1.54184 Å
Crystal system	Orthorhombic
Space group	$P2_12_12_1$
Unit cell dimensions	a = 9.1054(6) Å, α = 90°.
	b = 15.5707(13) Å, β = 90°.
	c = 17.8113(12) Å, γ = 90°.
Volume	2525.2(3) $Å^3$
Z	4

Density (calculated)	1.247 Mg/m^3
Absorption coefficient	1.569 mm^{-1}
F(000)	1000
Crystal size	0.100 x 0.050 x 0.010 mm^3
Crystal color and habit	Colorless Plate
Diffractometer	Rigaku Saturn 944+ CCD
Theta range for data collection	3.771 to 66.562°.
Index ranges	-10<=h<=10, -18<=k<=18, -21<=l<=21
Reflections collected	50355
Independent reflections	4461 [R(int) = 0.1388]
Observed reflections (I > 2sigma(I))	3166
Completeness to theta = 66.562°	99.9 %
Absorption correction	Semi-empirical from equivalents
Max. and min. transmission	1.00000 and 0.55418
Solution method	SHELXT-2014/5 (Sheldrick, 2014)
Refinement method	SHELXL-2014/7 (Sheldrick, 2014)
Data / restraints / parameters	4461 / 0 / 310
Goodness-of-fit on F^2	1.023
Final R indices [I>2sigma(I)]	R1 = 0.0659, wR2 = 0.1609
R indices (all data)	R1 = 0.1028, wR2 = 0.1809
Absolute structure parameter	-0.007(15)
Extinction coefficient	n/a
Largest diff. peak and hole	0.276 and -0.238 $e.Å^{-3}$

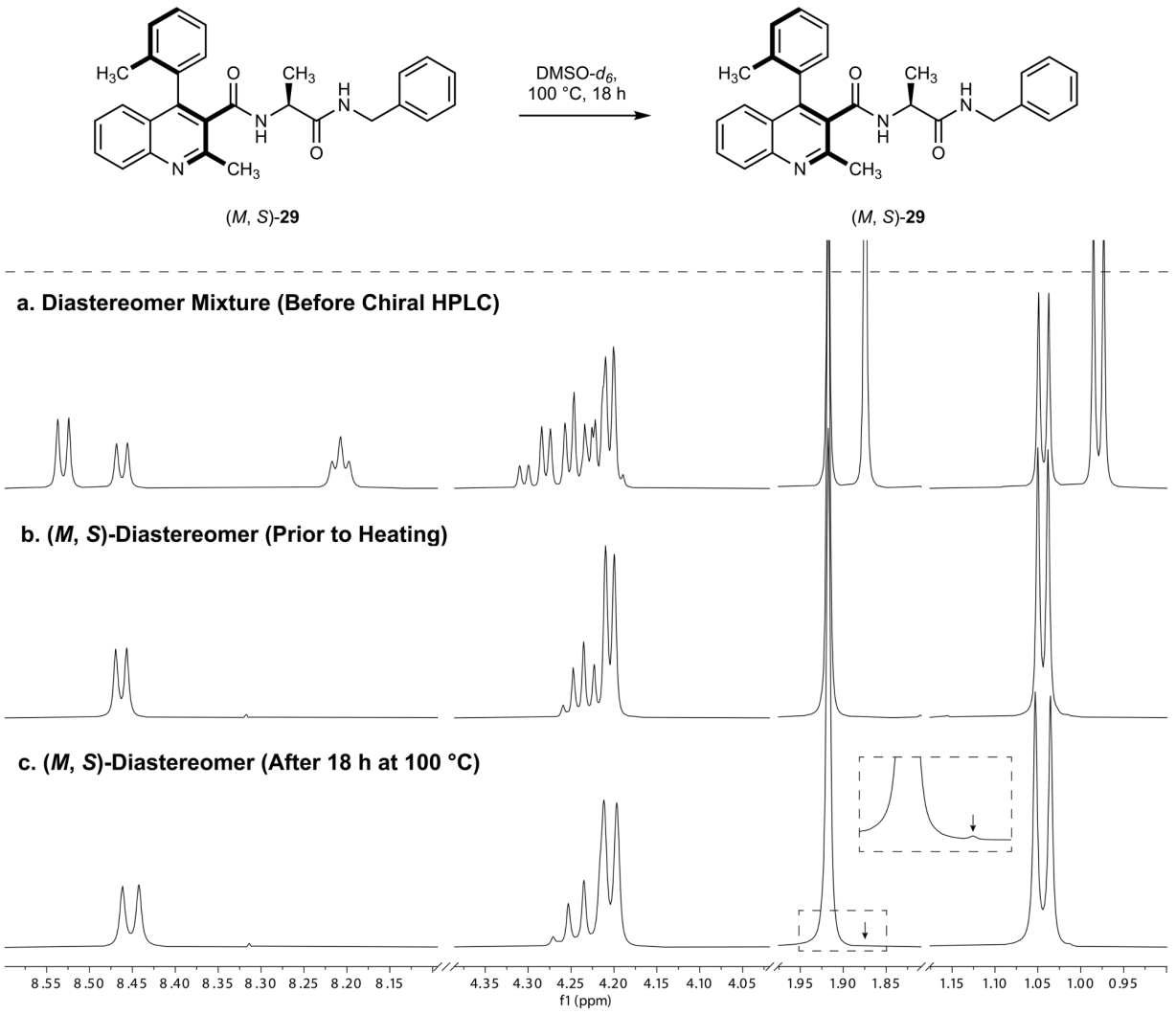


Supplementary Fig. 11: The complete numbering scheme of 007b-24028 ((*P*, *S*)-29·HCl) with 50% thermal ellipsoid probability levels. The hydrogen atoms are shown as circles for clarity. This structure has been deposited in the CCDC with deposition number 2341553.

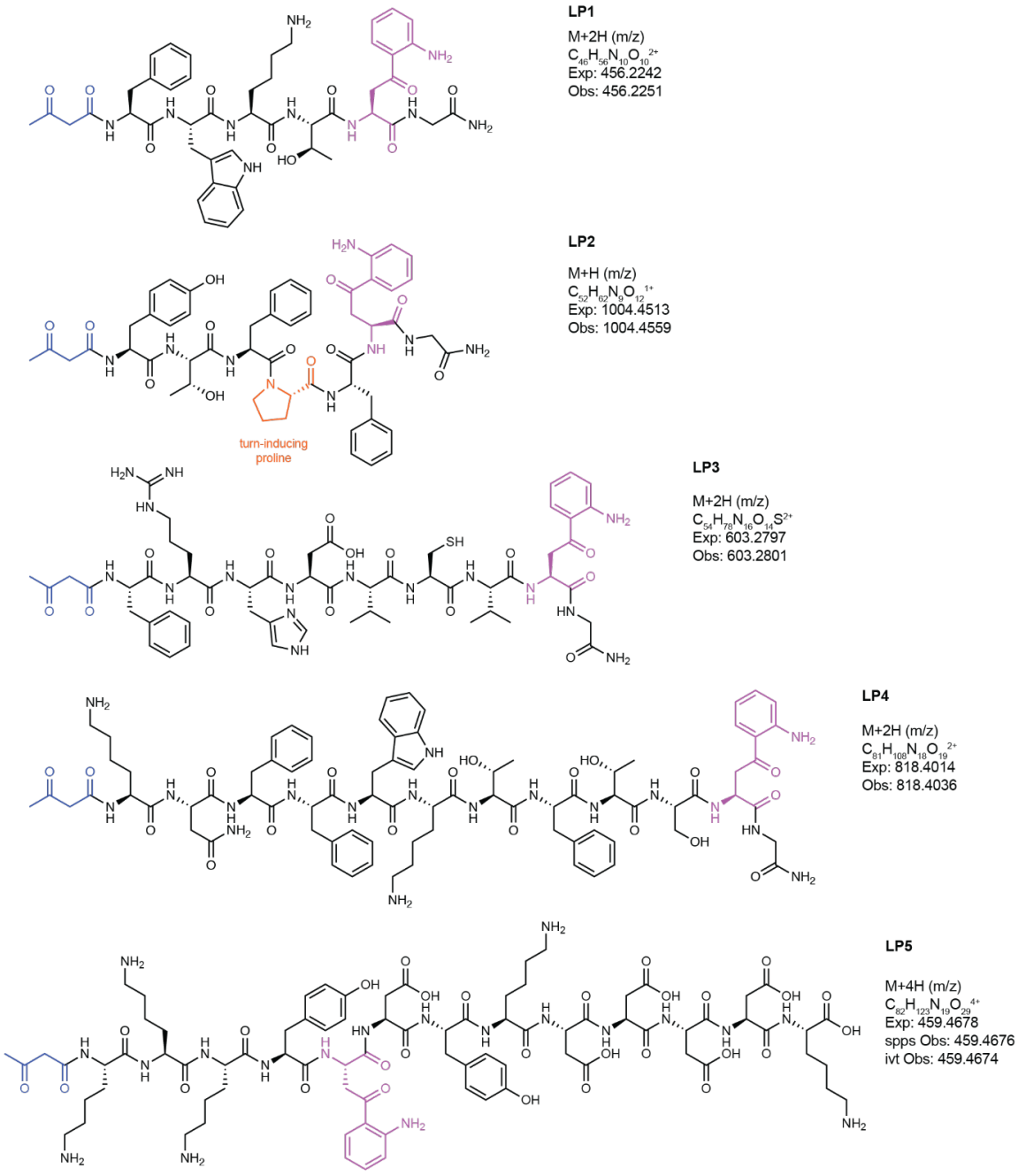
Supplementary Table 5: Crystal data and structure refinement for 007b-24028 ((*P*, *S*)-29·HCl).

Identification code	007b-24028
Empirical formula	C28 H28 Cl N3 O2
Formula weight	473.98
Temperature	93(2) K
Wavelength	1.54184 Å
Crystal system	Orthorhombic
Space group	$P2_12_12_1$
Unit cell dimensions	a = 8.8889(2) Å, α = 90°.
	b = 15.4880(4) Å, β = 90°.
	c = 17.7501(4) Å, γ = 90°.
Volume	2443.68(10) $Å^3$

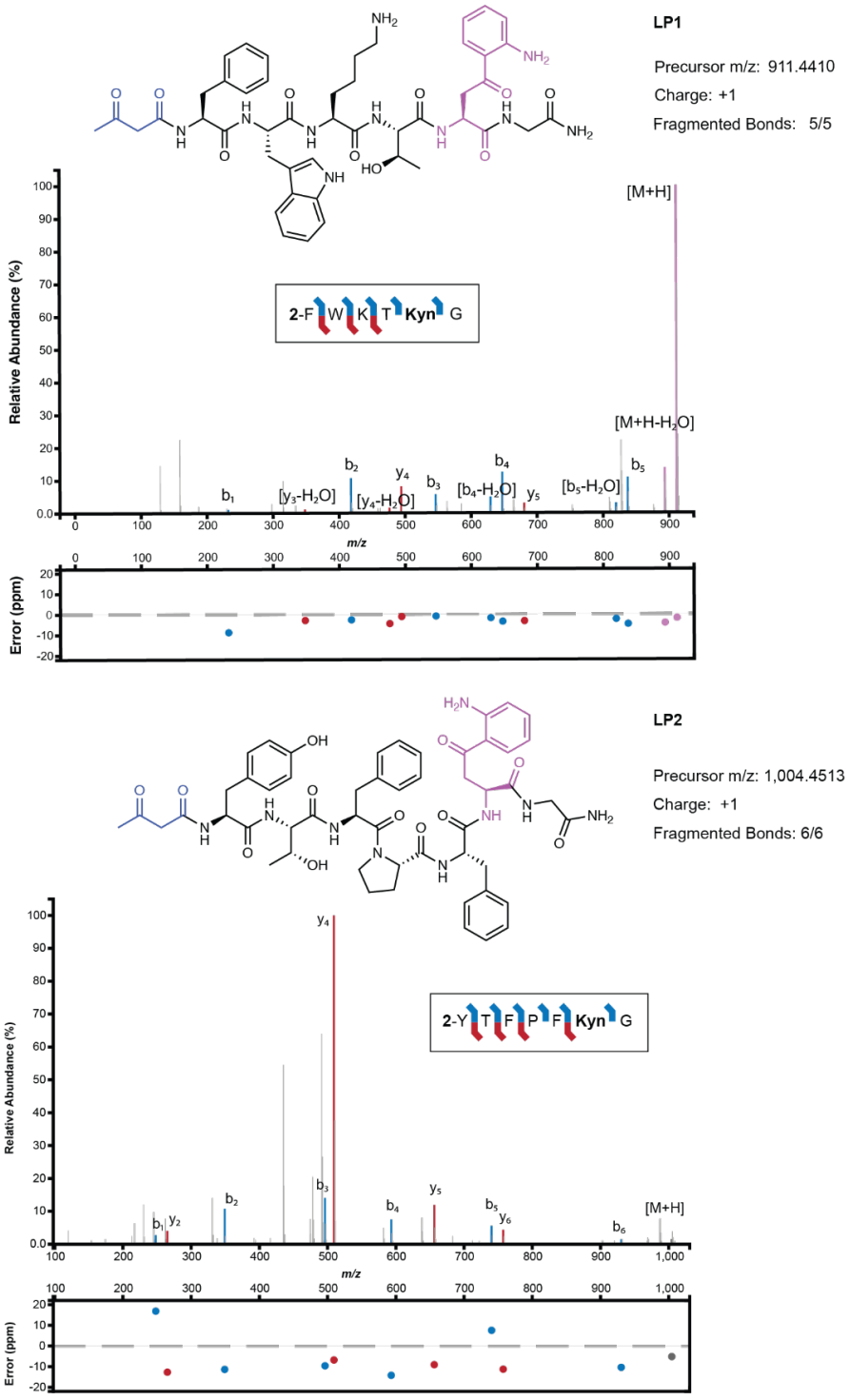
Z	4
Density (calculated)	1.288 Mg/m^3
Absorption coefficient	1.621 mm^{-1}
F(000)	1000
Crystal size	0.200 x 0.100 x 0.020 mm^3
Crystal color and habit	colorless plate
Diffractometer	Rigaku Saturn 944+ CCD
Theta range for data collection	3.788 to 66.596°
Index ranges	-10<=h<=10, -18<=k<=18, -20<=l<=21
Reflections collected	27518
Independent reflections	4320 [R(int) = 0.0844]
Observed reflections (I > 2sigma(I))	3922
Completeness to theta = 66.596°	100.0 %
Absorption correction	Semi-empirical from equivalents
Max. and min. transmission	1.00000 and 0.71354
Solution method	SHELXT-2014/5 (Sheldrick, 2014)
Refinement method	SHELXL-2014/7 (Sheldrick, 2014)
Data / restraints / parameters	4320 / 0 / 310
Goodness-of-fit on F^2	1.023
Final R indices [I>2sigma(I)]	R1 = 0.0360, wR2 = 0.0888
R indices (all data)	R1 = 0.0413, wR2 = 0.0926
Absolute structure parameter	-0.002(11)
Extinction coefficient	n/a
Largest diff. peak and hole	0.193 and -0.212 $e.Å^{-3}$



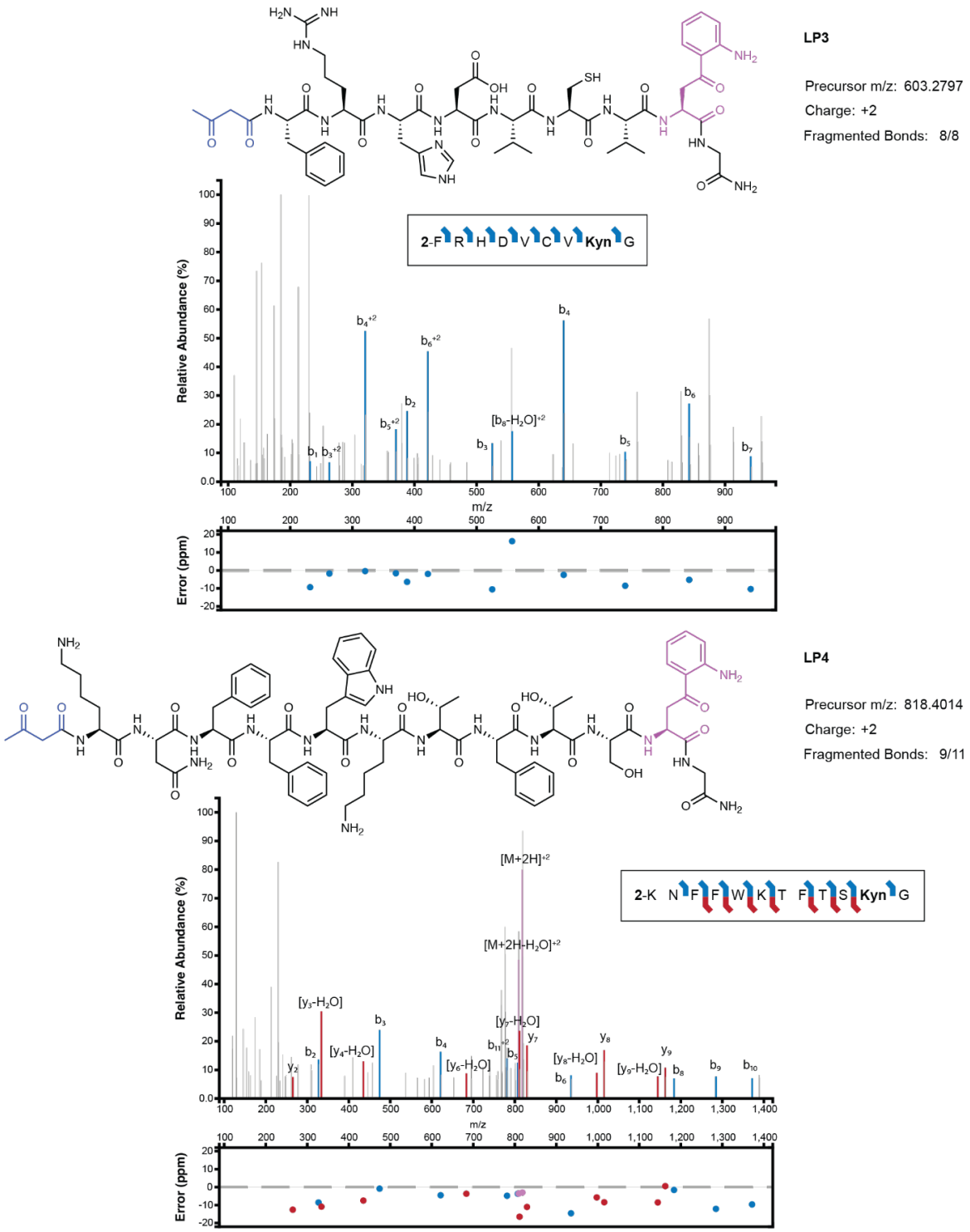
Supplementary Fig. 12: ^{1}H NMR analysis of the isolated diastereomer of biaryl 29 before and after heating for 18 h at 100 °C reveals minimal epimerization (< 1%). a, The ^{1}H NMR spectrum of biaryl **29** as a mixture of diastereomeric atropisomers in DMSO-d_6. **b,** ^{1}H NMR of the isolated minor (*M*, *S*)-diastereomer of biaryl **29** prior to heating. **c**, ^{1}H NMR of the isolated minor (*M*, *S*)-diastereomer of biaryl **29** after heating a total of 18 h (3 h + 15 h) at 100 °C. The spectra shown are truncated to focus on the relevant regions of the x-axis. Processed full spectra are provided within the Supplementary Material and raw .fid files are provided in the FAIR data.



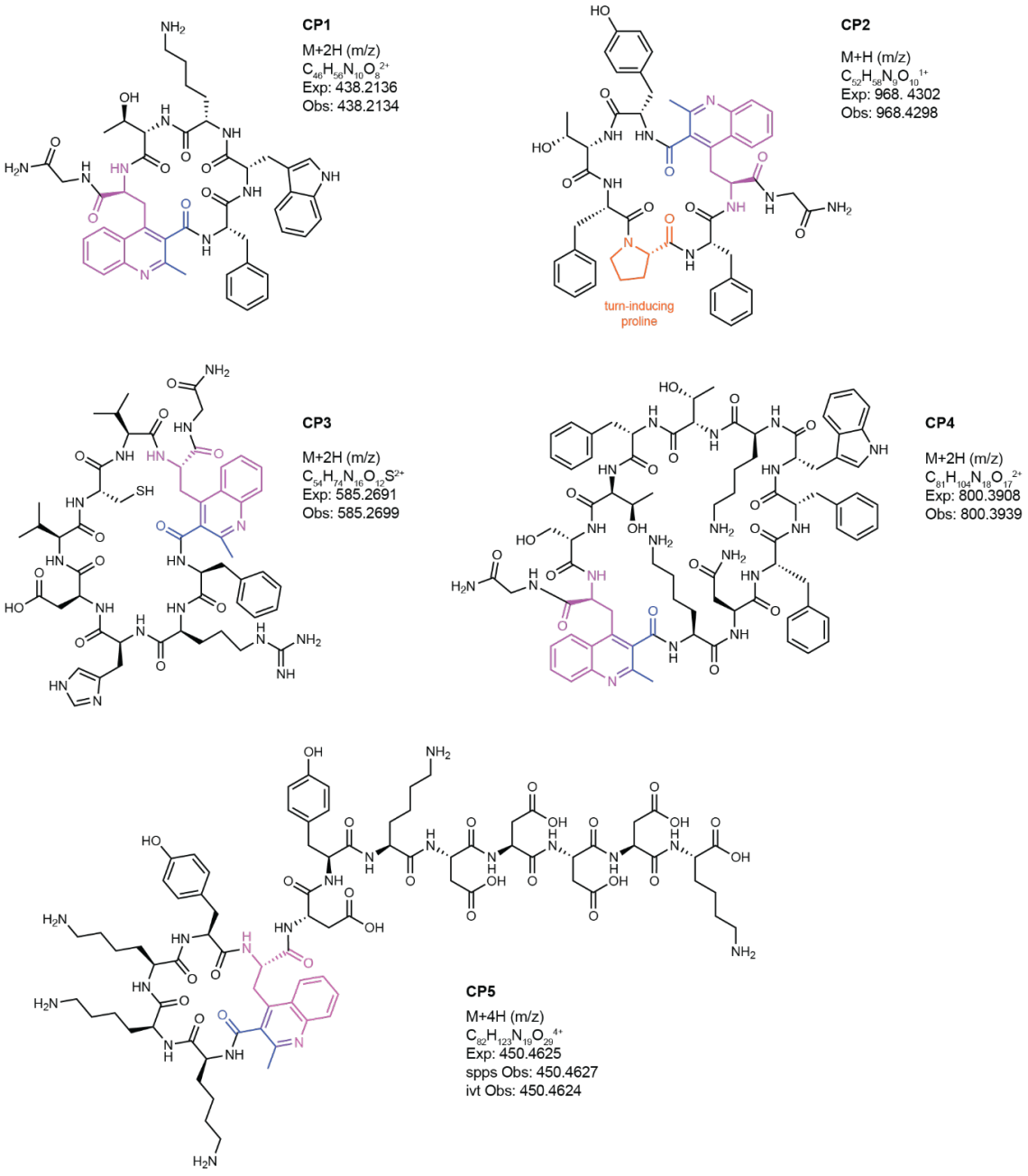
Supplementary Fig. 13. Structures of linear peptides LP1-LP5 containing an *N*-terminal β-keto amide and an internal kynurenine residue. Linear peptides were prepared using solid phase synthesis, purified, and characterized as described in **Supplementary Information.** The expected and observed major ions are shown.



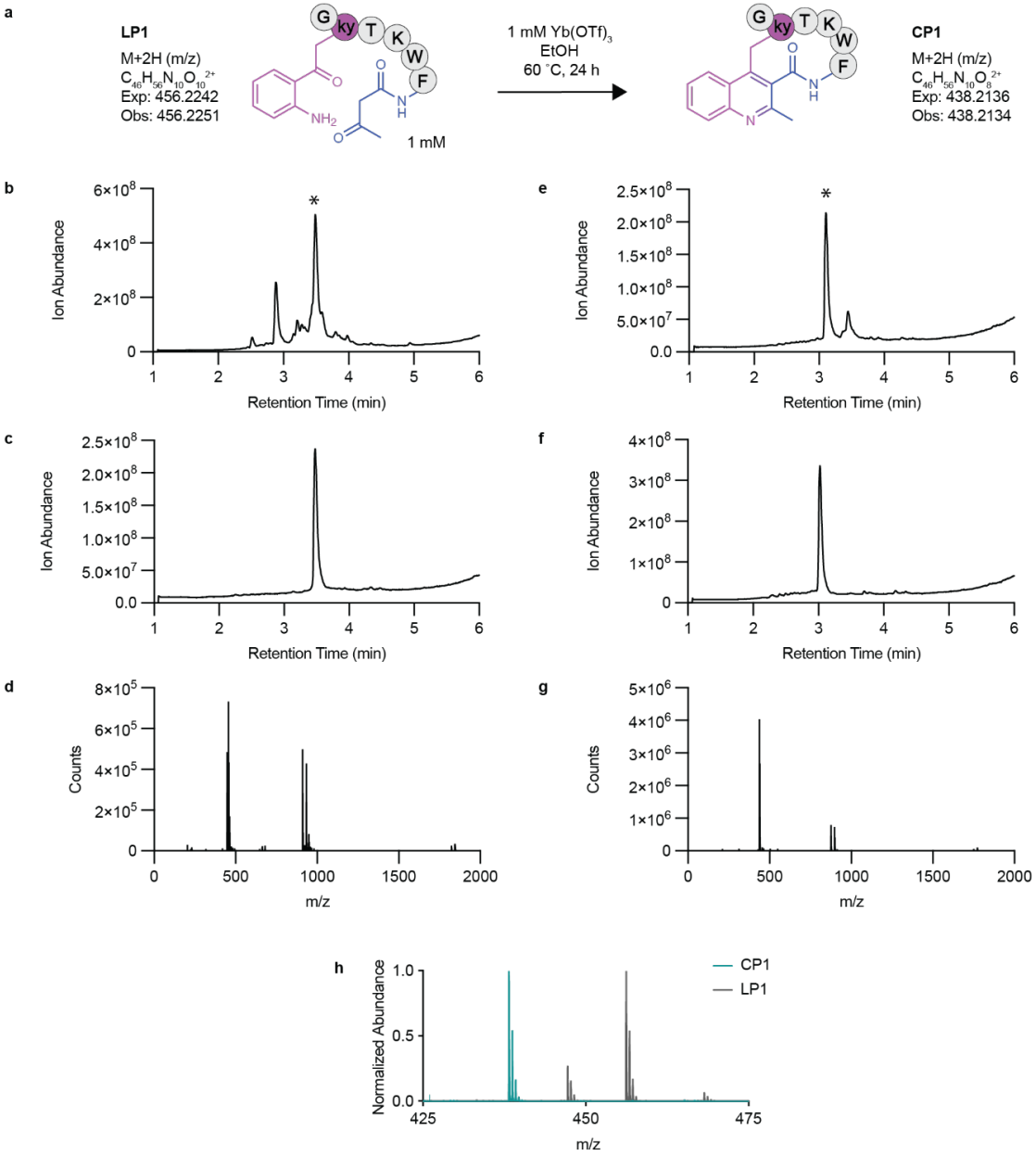
Supplementary Fig. 14. MS-MS spectra of LP1 and LP2.



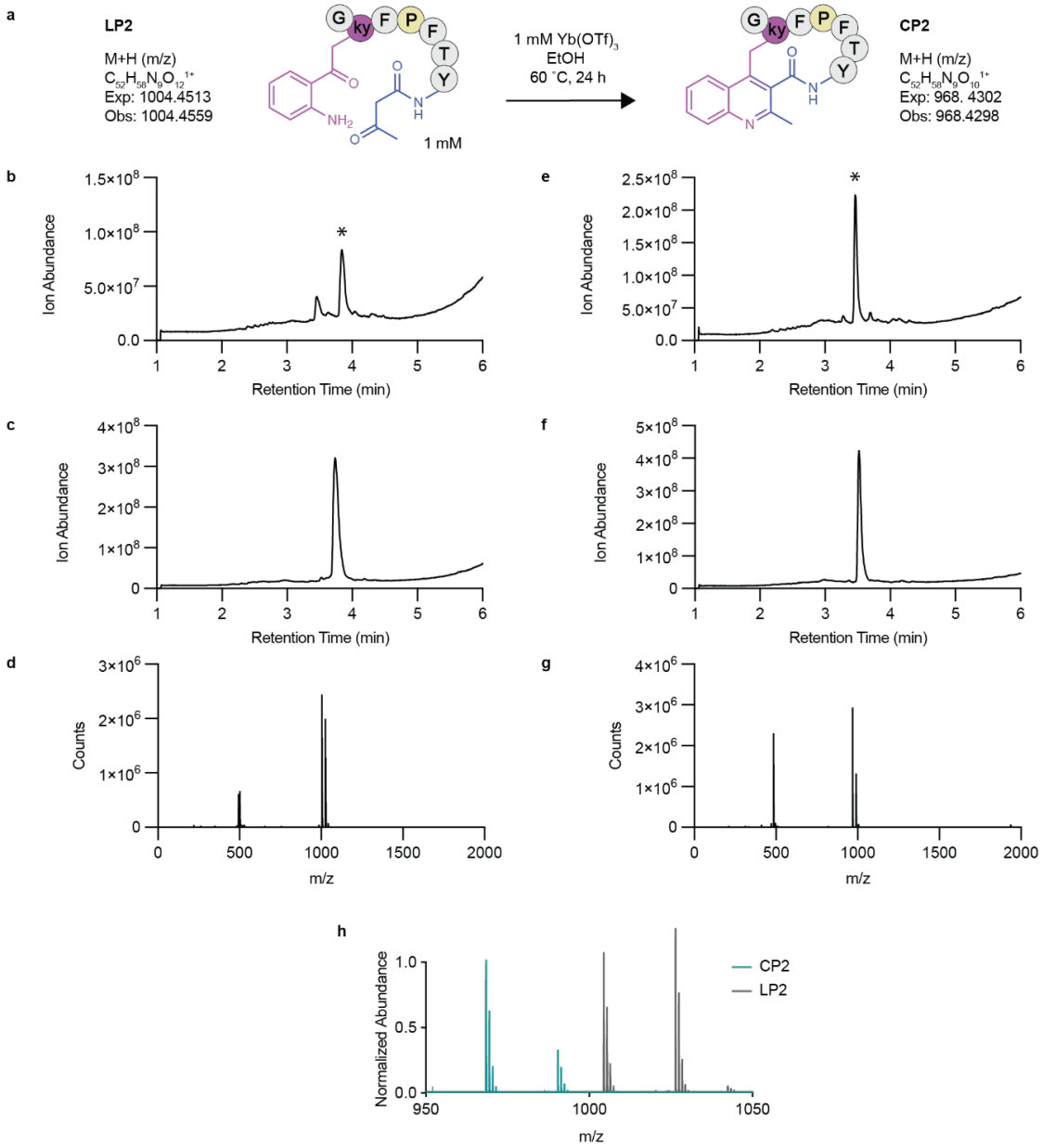
Supplementary Fig. 15. MS-MS spectra of LP3 and LP4.



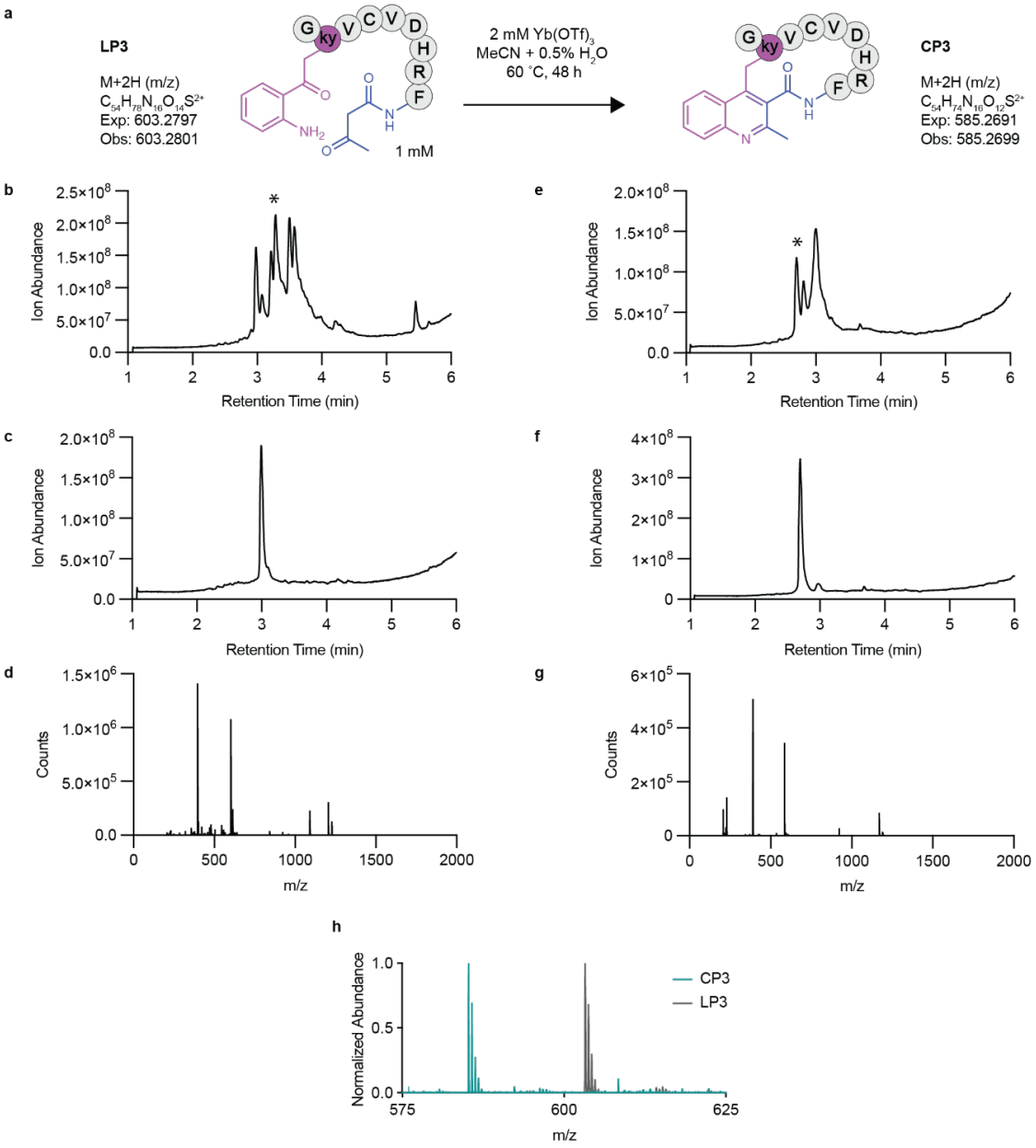
Supplementary Fig. 16. Cyclic products generated via Friedländer macrocyclization of LP1-5. Expected and observed major ions are shown.



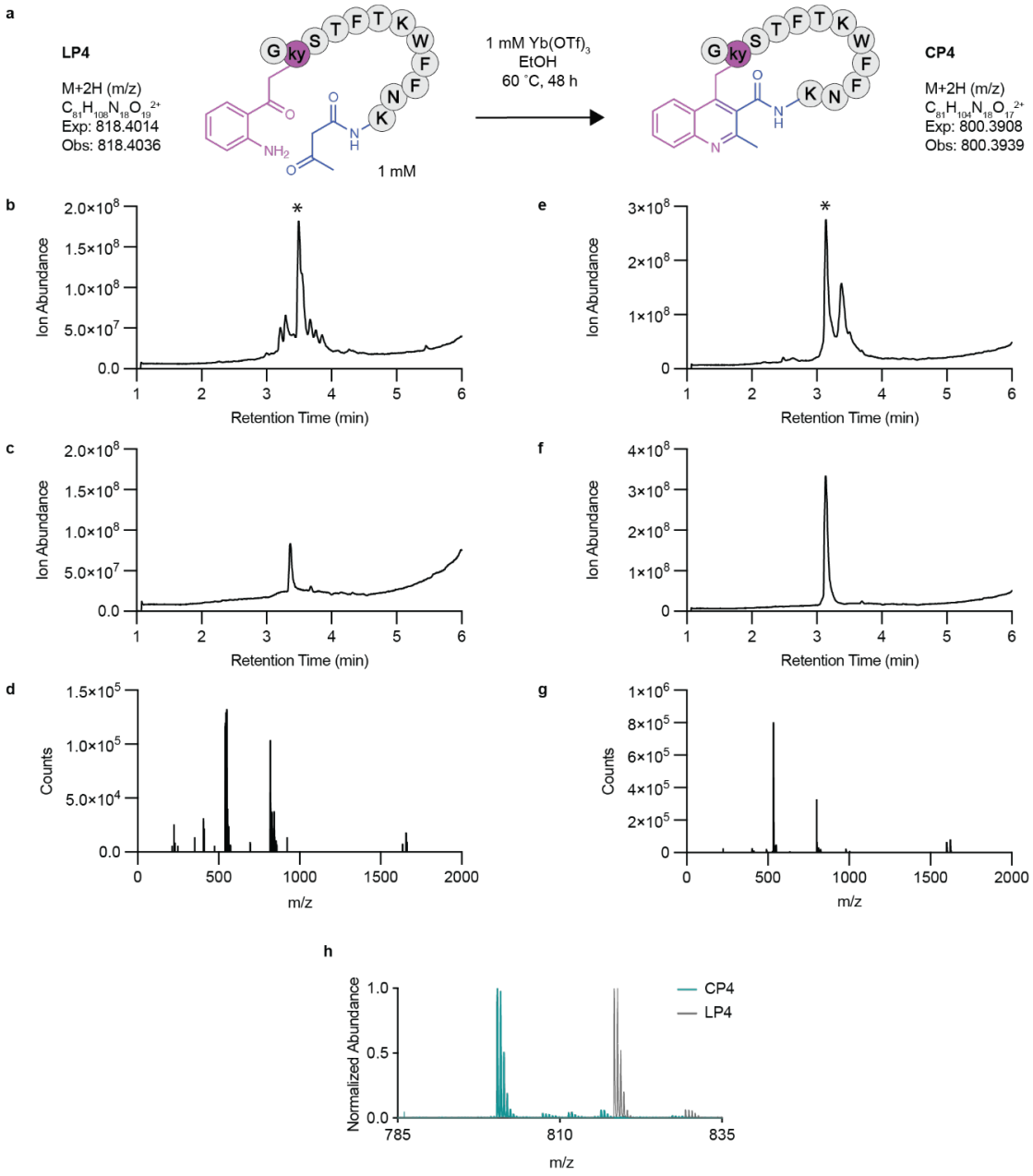
Supplementary Fig. 17. Synthesis and LC-HRMS characterization of CP1. a, Friedländer macrocyclization conditions for **CP1**. **b,** LC-MS chromatogram of the crude linear peptide after SPPS and installation of β-keto amide capping group. **LP1** is denoted with an asterisk. **c,** LC-HRMS chromatogram and **d,** mass spectrum of **LP1** after HPLC purification. **e,** LC-MS chromatogram of the crude Friedländer cyclization. **CP1** is denoted with an asterisk. **f,** LC-HRMS chromatogram and **g,** mass spectrum of **CP1** after HPLC purification. **h,** Overlaid mass spectra of **LP1** (grey) and **CP1** (teal) for the 2+ charge state.



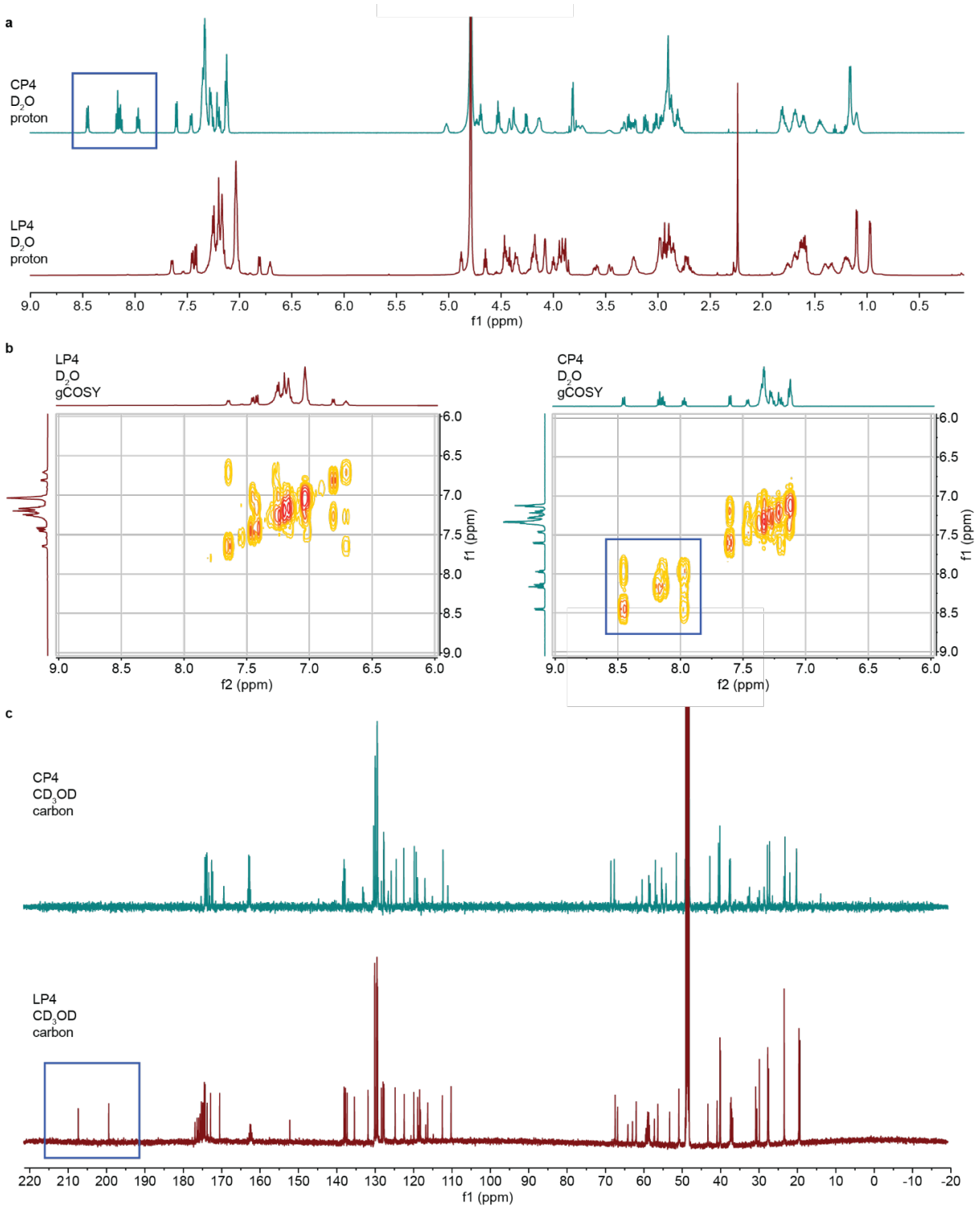
Supplementary Fig. 18. Synthesis and LC-HRMS characterization of CP2. a, Friedländer macrocyclization conditions for **CP2**. **b,** LC-MS chromatogram of the crude linear peptide after SPPS and installation of β-keto amide capping group. **LP2** is denoted with an asterisk. **c,** LC-HRMS chromatogram and **d,** mass spectrum of **LP2** after HPLC purification. **e,** LC-MS chromatogram of the crude Friedländer cyclization. **CP2** is denoted with an asterisk. **f,** LC-HRMS chromatogram and **g,** mass spectrum of **CP2** after HPLC purification. **h,** Overlaid mass spectra of **LP2** (grey) and **CP2** (teal) for the 1+ charge state. Sodium adducts are also present.



Supplementary Fig. 19. Synthesis and LC-HRMS characterization of CP3. a, Friedländer macrocyclization conditions for **CP3**. **b,** LC-MS chromatogram of the crude linear peptide after SPPS and installation of β-keto amide capping group. **LP3** is denoted with an asterisk. **c,** LC-HRMS chromatogram and **d,** mass spectrum of **LP3** after HPLC purification. **e,** LC-MS chromatogram of the crude Friedländer cyclization. **CP3** is denoted with an asterisk. **f,** LC-HRMS chromatogram and **g,** mass spectrum of **CP3** after HPLC purification. **h,** Overlaid mass spectra of **LP3** (grey) and **CP3** (teal) for the 2+ charge state.

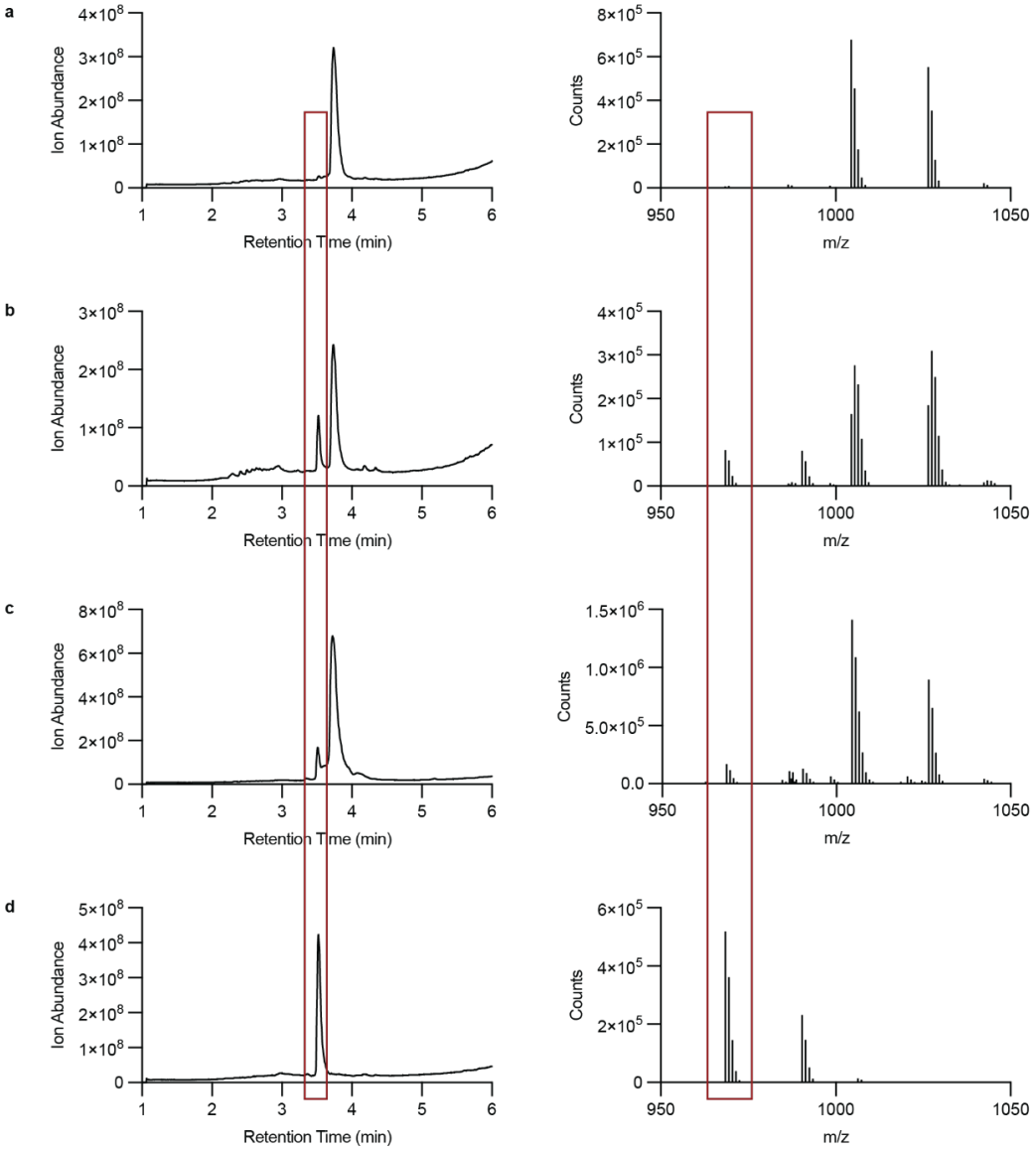


Supplementary Fig. 20. Synthesis and LC-HRMS characterization of CP4. a, Friedländer macrocyclization conditions for **CP4**. **b,** LC-MS chromatogram of the crude linear peptide after SPPS and installation of β-keto amide capping group. **LP4** is denoted with an asterisk. **c,** LC-HRMS chromatogram and **d,** mass spectrum of **LP4** after HPLC purification. **e,** LC-MS chromatogram of the crude Friedländer cyclization. **CP4** is denoted with an asterisk. **f,** LC-HRMS chromatogram and **g,** mass spectrum of **CP4** after HPLC purification. **h,** Overlaid mass spectra of **LP4** (grey) and **CP4** (teal) for the 2+ charge state.

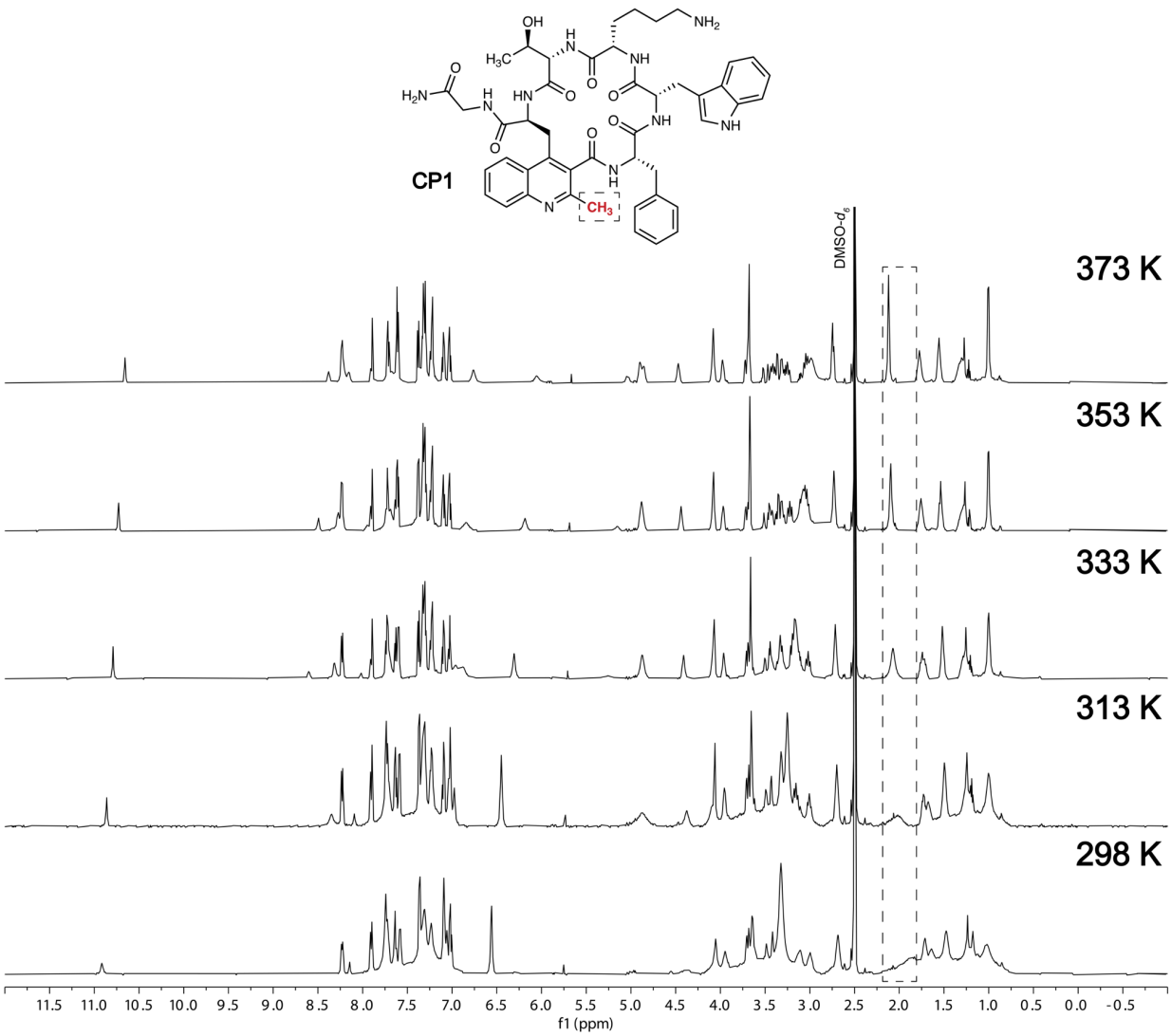


Supplementary Fig. 21. Diagnostic shifts in the NMR spectra upon Friedländer macrocyclization. **a,** Proton NMR of **LP4** (red) and **CP4** (teal) show the emergence of a distinct set of downfield aromatic protons (blue box) corresponding to the quinoline ring protons. **b,** gCOSY NMR spectra of **LP4** (red, left) and **CP4** (teal, right) display the correlated spin-

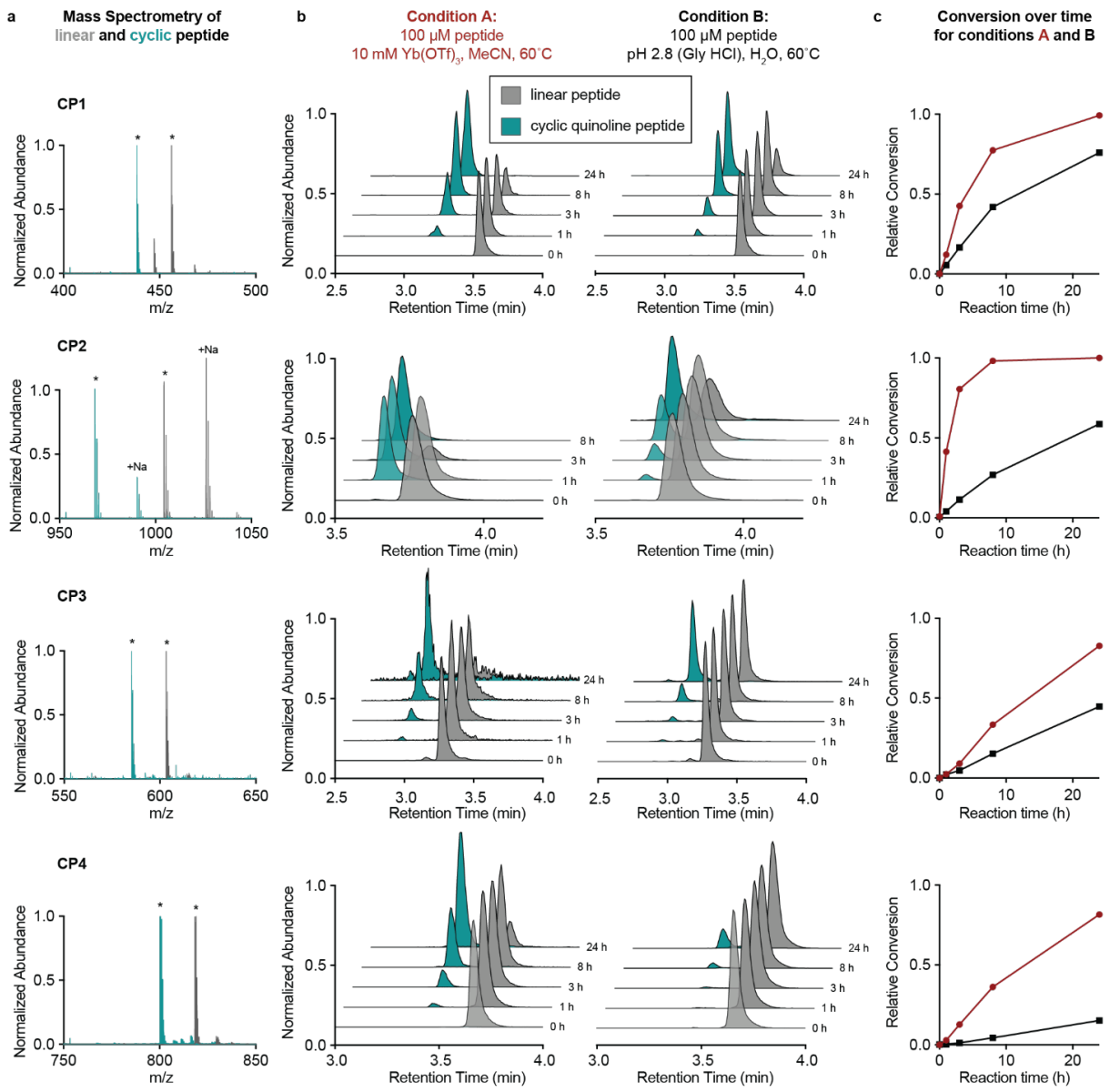
couplings of the quinoline system. **c,** Carbon NMR of **LP4** (red) and **CP4** (teal) show the distinct loss of two ketone carbons around 200-210 ppm.



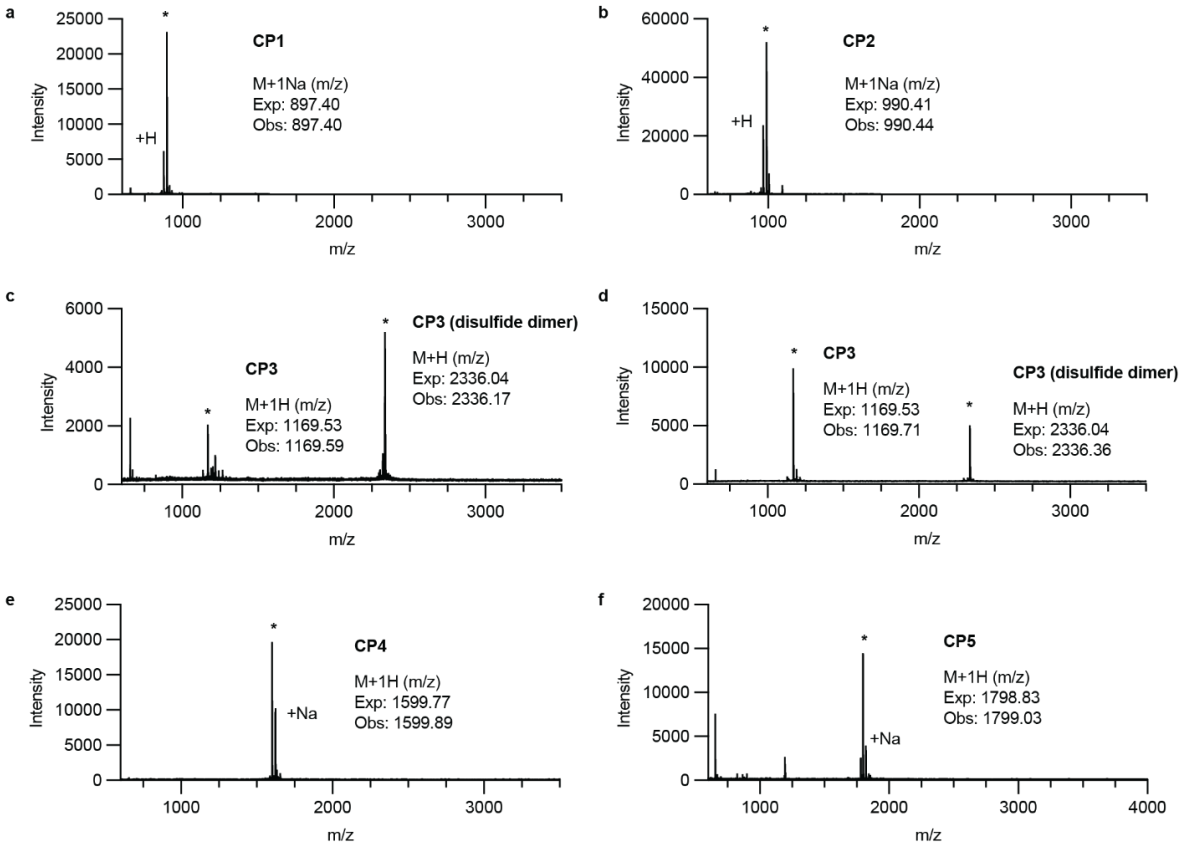
Supplementary Fig. 22. LC-HRMS analysis reveals the spontaneous cyclization of LP2 into apparent CP2 during NMR characterization. Total Ion Chromatogram and Mass Spectra of pure **LP2** (**a**), **LP2** after NMR experiments at RT in CD_3OD (**b**), **LP2** after NMR experiments at RT in DMSO-d_6 (**c**), and pure **CP2** (**d**). Red boxes highlight the peaks corresponding to **CP2**. Mass Spectra were extracted from 3.2 min to 4.2 min in the chromatogram for each sample. Note: Deuteration of amides when exposed to CD_3OD results in a shifted isotope distribution in panel **b.**



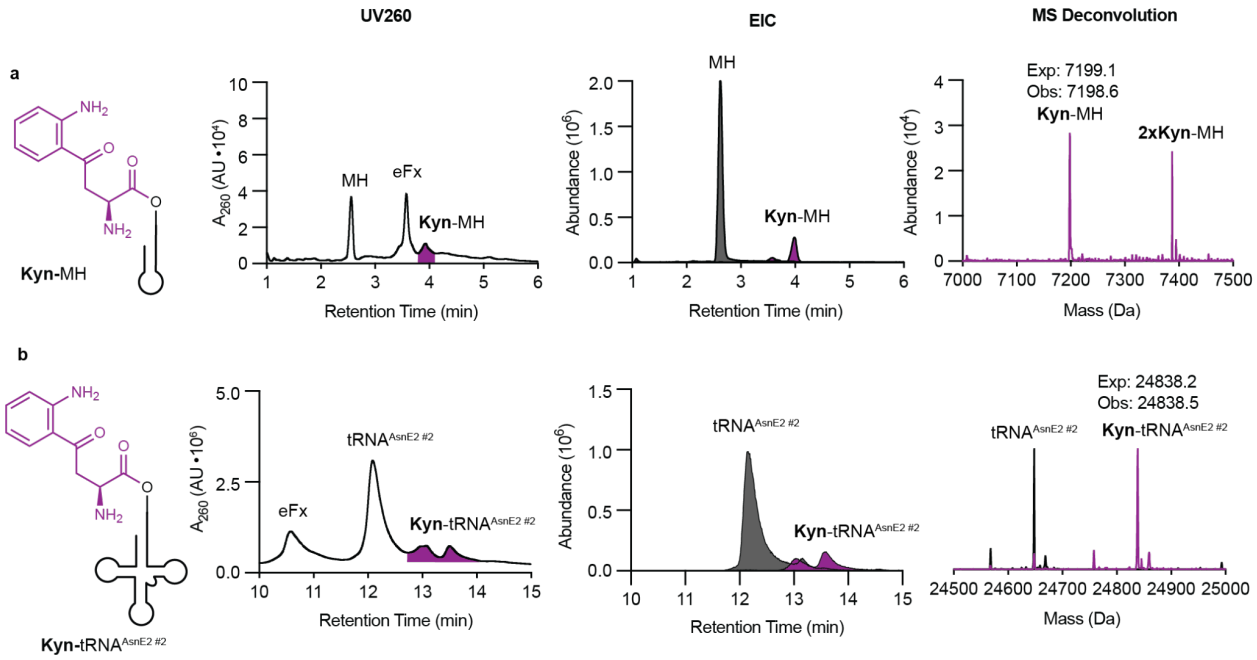
Supplementary Fig. 23: Variable-Temperature NMR (VT-NMR) studies of macrocycle CP1 reveal sharpening of the quinoline methyl signal. The sample was analyzed in DMSO-d_6. As the sample is heated to 373 K, the quinoline methyl signal, indicated by the dashed box, begins to change from a broad, overlapping peak into a well-resolved singlet. Several additional signals also show enhanced resolution at this increased temperature. At the time of these studies, the exchangeable protons were only partially exchanged with deuterons.



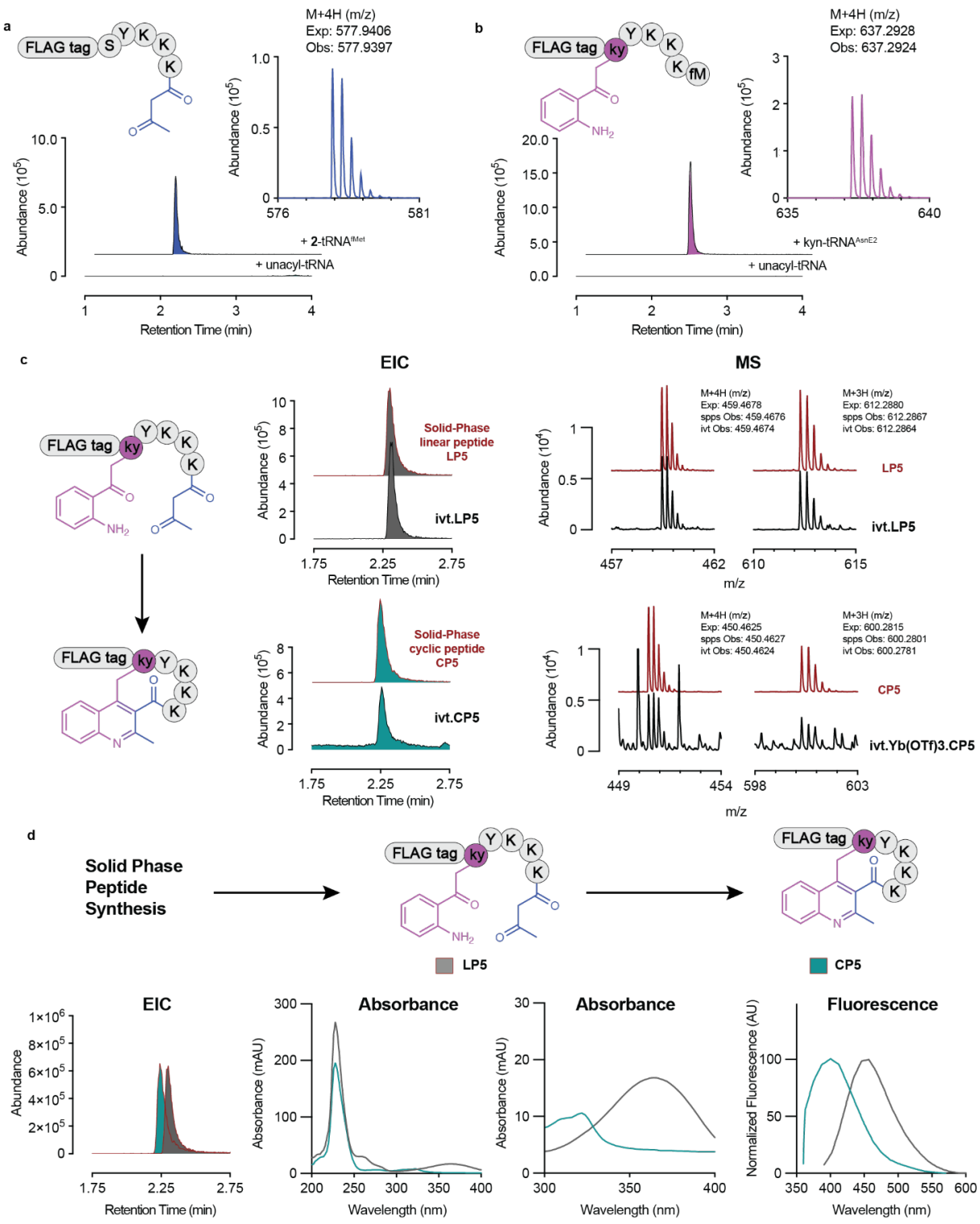
Supplementary Fig. 24. Friedländer cyclization of LP1-4 prepared by solid-phase synthesis. a, HRMS of linear (gray) and cyclic (teal) peptides. An asterisk indicates the major ion detected. Expected and Observed m/z for each species are found in **Supplementary Fig. 10** and **11**. **b,** Extracted ion chromatograms (EIC) over the course of the cyclization reaction under Conditions A and B for **CP1-4**. Lewis acid catalysis with $Yb(OTf)_3$ is significantly faster than the acidic aqueous conditions. **c,** Conversion to cyclic product over time for each peptide when exposed to Condition A (red) and Condition B (black). Relative conversion = $[EIC_{cyclic}]/[EIC_{linear} + EIC_{cyclic}]$, where EIC_x represents the integrated extracted ion counts of the peaks corresponding to the product cyclic peptide (EIC_{cyclic}) or starting material linear peptide (EIC_{linear}).



Supplementary Fig. 25. MALDI-TOF MS of HPLC-purified cyclic peptides. MALDI-TOF MS of **CP1** (**a**), **CP2** (**b**), **CP4** (**e**) and **CP5** (**f**) confirms the monomeric macrocyclization of peptides. **CP3** (**c**) is seen to ionize as a disulfide dimer under these conditions. An overnight incubation of **CP3** with 50mM TCEP (**d**) resulted in conversion to the monomeric macrocycle.



Supplementary Fig. 26. Acylation of MH and tRNA with kynurenine-CME. a, Acylation of **a,** MH (25 µM) or **b,** $tRNA^{AsnE2\#2}_{GCU}$ (25 µM) with **Kyn-CME** (5 mM) using eFx (25 µM) for 6 h at 4°C in 50 mM HEPES pH 7.5. Abs_{260} chromatograms, extracted ion chromatograms (EIC), and deconvoluted mass spectra of the products resulting from flexizyme-promoted acylation. Non-acylated MH and tRNA are shown in gray, **Kyn**-acylated MH and tRNA are shown in purple.



Supplementary Fig. 27. Intramolecular post-translational Friedländer macrocyclization of LP5 prepared using solid phase synthesis or IVT. **a,** Monomer **2** can recode methionine at position 1 to generate **2**-KKKYSDYKDDDDK. Shown is the EIC for the +4 charge state of the product produced by IVT supplemented with either **2**-tRNA^{fMet} or unacylated tRNA^{fMet}. LC-HRMS of the product is inlaid. **b, Kyn** can recode serine at position 5 to generate MKKKY-**Kyn-**

DYKDDDDK. Shown is the EIC for the +4 charge state of the product produced by IVT supplemented with either **Kyn**-tRNA$^{AsnE2\#2}_{GCU}$ or unacylated tRNA$^{AsnE2\#2}_{GCU}$. LC-HRMS of the product is inlaid. **c,** Overlayed extracted ion chromatograms and mass spectra of **LP5 (gray fill)** and **CP5 (teal fill)** generated by either solid-phase peptide synthesis and purified by HPLC (red line) or from in vitro translation and purified by anti-FLAG magnetic beads (black line). **d,** Preparation of authentic standards **LP5** and **CP5** for comparison to IVT peptides. The change in retention time, mass, and absorbance/fluorescence provide additional evidence of cyclization and quinoline ring formation. The extracted ion chromatograms of purified **LP5 (gray fill)** and **CP5 (teal fill)** are overlaid to show the shift in retention time after cyclization. The absorbance of the synthetic LP5 displays an absorbance maximum at 365 nm, while the synthetic quinoline-containing macrocycle **CP5** displays an absorbance maximum at 325 nm. The fluorescence spectra of each peptide excited at their respective Abs max. A characteristic shift in the absorbance spectra from a broad peak at 365, indicative of kynurenine[8], to a narrower peak at 325 nm, assigned to the quinoline, as well as a concurrent change in the fluorescence spectra of each species, provided an additional diagnostic of cyclization for the solid-phase standards.

Supplementary Table 6. Sequence of Flexizymes, microhelix (MH) and tRNA species used in this work.

Name	Sequence
dFx	GGAUCGAAAGAUUUCCGCAUCCCCGAAAGGGUACAUGGCGUUAGGU
eFx	GGAUCGAAAGAUUUCCGCGGCCCCGAAAGGGGAUUAGCGUUAGGU
MH	GGCUCUGUUCGCAGAGCCGCCA
tRNA^{fMet}	GGCGGGGUGGAGCAGCCUGGUAGCUCGUCGGGCUCAUAACCCGAAGG UCGUCGGUUCAAAUCCGGCCCCCGCAACCA
tRNA$^{AsnE2\#2}$	GGCUCUGUAGUUCAGUCGGUAGAACGGCGGAUUGCUAUUCCGUAUG UCACUGGUUCGAGUCCAGUCAGAGCCGCCA
M5-1	mCmUmUmUmUmGmAmCmCmGmCmAmUmAmCmUmCmCmCmUmUmA mGmC

Supplementary Table 7. Sequence of single stranded (ss) DNA primers used to generate DNA templates for tRNA or mRNA.

Name	Sequence

$tRNA^{fMet}$ Fwd	AATTCCTGCAGTAATACGACTCACTATAGGCGGGGTGGAGCAGCCTGGTAGCTCGTCGGG
$tRNA^{fMet}$ Rev	T**mG**GTTGCGGGGGCCGGATTTGAACCGACGACCTTCGGGTTATGAGCCCCGACGAGCTACCAGGCT
$tRNA^{AsnE2\#2}$ Fwd	AATTCCTGCAGTAATACGACTCACTATAGGCTCTGTAGTTCAGTCGGTAGAACGGCGGATTGCTAT
$tRNA^{AsnE2\#2}$ Rev	T**mG**GCGGCTCTGACTGGACTCGAACCAGTGACATACGGAATAGCAATCCGCCGTTCTA
MGV-flag Fwd	GCGAATTAATACGACTCACTATAGGGTTAACTTTAACAAGGAGAAAAACATGGGTGTCGACTACAAGGACGACGA
MGV-flag Rev	AAACCCCTCCGTTTAGAGAGGGGTTATGCTAGTTACTTGTCGTCGTCGTCCTTGTAGTCGACACCCATGTTTTTC
MKKKYS-flag Fwd	GCGAATTAATACGACTCACTATAGGGTTAACTTTAACAAGGAGAAAAACATGAAGAAAAAATACAGCGACTACAAGGACG
MKKKYS-flag Rev	AAACCCCTCCGTTTAGAGAGGGGTTATGCTAGTTACTTGTCGTCGTCGTCCTTGTAGTCGCTGTATTTTTTCTTCATGTT
***mG** represents 2 O-methyl-deoxymethylguanosine	

Supplementary Table 8. Sequence of double stranded (ds) DNA templates used to generate tRNA or mRNA. T7 promoter sequence is highlighted in blue. Ribosome binding site highlighted in red and the coding sequence is bolded.

Name	Sequence
$tRNA^{fMet}$	AATTCCTGCAGTAATACGACTCACTATAGGCGGGGTGGAGCAGCCTGGTAGCTCGTCGGG
$tRNA^{AsnE2\#2}$	AATTCCTGCAGTAATACGACTCACTATAGGCTCTGTAGTTCAGTCGGTAGAACGGCGGATTGCTAT
MGV-flag	GCGAATTAATACGACTCACTATAGGGTTAACTTTAACAAGGAGAAAAAC**ATGGGTGTCGACTACAAGGACGACGACGACAAGTAA**CTAGCATAACCCCTCTCTAAACGGAGGGGTTT
MKKKYS-flag	GCGAATTAATACGACTCACTATAGGGTTAACTTTAACAAGGAGAAAAA

	C**ATGAAGAAAAAATACAGCGACTACAAGGACGACGACGACAAGTA** **A**CTAGCATAACCCCTCTCTAAACGGAGGGGTTT

Supplementary Table 9. RNA molecular weight calculations and observed deconvolutions.

tRNA	Expected (Cusabio RNA Calc)	Observed deconvolution
$tRNA^{fMet}$	25066.4	25065.6
$tRNA^{AsnE2\ \#2}$	24649.2	24648.0
MH	7009.4	7009.0

Supplemental References Cited

1. Katoh, T. & Suga, H. Drop-off-reinitiation at the N-termini of nascent peptides and its regulation by IF3, EF-G, and RRF. *RNA* rna.079447.122 (2023) doi:10.1261/rna.079447.122.
2. Tajima, K., Katoh, T. & Suga, H. Drop-off-reinitiation triggered by EF-G-driven mistranslocation and its alleviation by EF-P. *Nucleic Acids Res.* **50**, 2736–2753 (2022).
3. Katoh, T. & Suga, H. Translation initiation with exotic amino acids using EF-P-responsive artificial initiator tRNA. *Nucleic Acids Res.* gkad496 (2023) doi:10.1093/nar/gkad496.
4. Fricke, R. *et al. Orthogonal Synthetases for Polyketide Precursors*. http://biorxiv.org/lookup/doi/10.1101/2022.02.28.482149 (2022) doi:10.1101/2022.02.28.482149.
5. Liu, M. *et al.* Selective thiazoline peptide cyclisation compatible with mRNA display and efficient synthesis. *Chem. Sci.* (2023) doi:10.1039/D3SC03117A.
6. Lee, J. *et al.* Expanding the limits of the second genetic code with ribozymes. *Nat. Commun.* **10**, 5097 (2019).
7. Thrippleton, M. J. & Keeler, J. Elimination of Zero-Quantum Interference in Two-Dimensional

NMR Spectra. *Angew. Chem. Int. Ed.* **42**, 3938–3941 (2003).

8. Han, Q., Robinson, H. & Li, J. Biochemical identification and crystal structure of kynurenine formamidase from Drosophila melanogaster. *Biochem. J.* **446**, 253–260 (2012).

Materials and methods

General Materials and Methods

General experimental details

DNase-free water, 3 M $MgCl_2$ solution, sodium acetate solution (pH 5.2), and 20,000x ethidium bromide were purchased from AmericanBio (Canton, MA). Flexizyme RNA (eFx and dFx) along with microhelix (MH) RNA were purchased from Integrated DNA Technologies (IDT) (Coralville, IA). DNA oligonucleotides were purchased from IDT. HiScribe® T7 Quick High Yield RNA Synthesis Kit and PURExpress® Δ (aa, tRNA) Kit were purchased from New England Biolabs (Ipswich, MA). Dimethylsulfoxide (DMSO), HEPES, phenol, chloroform, methanol, ethyl acetate, dichloromethane (DCM), toluene, triethylamine (TEA), magnesium acetate, and sodium chloride were purchased from Sigma-Aldrich (St. Louis, MO) or Fisher Scientific (Hampton, NH).

Ytterbium(III) trifluoromethanesulfonate ($Yb(OTf)_3$, 99.99%) was purchased from Sigma-Aldrich (St. Louis, MO). Absolute ethanol was purchased from Decon Labs (King of Prussia, PA) or from AmericanBio (Canton, MA). Glacial acetic acid was purchased from J.T. Baker [Avantor] (Radnor, PA). Unless otherwise noted, all water used in biochemical work or achiral HPLC was dispensed from a MilliporeSigma™ Milli-Q™ system at 18.2 megohm ionic purity. Stock solutions of flexizyme, microhelix, tRNA, amino acids, acyl-tRNA, primers, and DNA templates were assembled using unbuffered Milli-Q water. All other chemical reagents were purchased from commercial sources and used without further purification unless otherwise noted.

All reactions were carried out under ambient atmosphere unless otherwise noted. Room temperature (RT) is defined as 21–23 °C. *N,N*-diisopropylethylamine (DIPEA) was distilled over CaH under a nitrogen atmosphere prior to use or dispensed from a Sigma-Aldrich Sure/Seal™ container (99.5%, purified via redistillation) under a nitrogen atmosphere. Dry dichloromethane (DCM) and dry *N*,*N*-dimethylformamide (DMF), when indicated, were dried over alumina and dispensed under argon from a GlassContour® Seca Solvent Purification System or from a Sigma-Aldrich Sure/Seal™ container under a nitrogen atmosphere. Deionized water was used for reactions, extraction solutions, and automated reverse phase column chromatography. Acetonitrile (MeCN) and ethyl acetate (EtOAc) used for chromatography were High-

Performance Liquid Chromatography (HPLC) grade, while hexanes used for chromatography was either certified ACS grade or HPLC grade. Methanol used for chromatography was either certified ACS grade or electronic grade.

High-resolution mass spectrometry (HRMS) was performed using: (i) a Shimadzu Scientific Instruments Quadrupole Time-of-Flight (Q-TOF) 9030 high resolution mass spectrometer using electrospray ionization (ESI); (ii) an LTQ FT-ICR mass spectrometer equipped with an electrospray ionization source (Finnigan LTQ FT, Thermo Fisher Scientific, Waltham, MA) operated in either positive or negative ion mode; or (iii) an Agilent 6530 Accurate-Mass Q-TOF LC-MS using electrospray ionization in positive mode. For crude data analysis, ultra-performance liquid chromatography-mass spectrometry (UPLC-MS) was performed with a Waters Acquity LC-MS instrument equipped with a reverse phase BEH C18 column (1.7 mm particle size, 2.1 x 50 mm), a dual atmospheric pressure chemical ionization (APCI)/electrospray ionization (ESI) mass spectrometry detector, and a photodiode array detector.

Fourier-Transform (FT) infrared (IR) spectroscopy measurements were recorded on a Shimadzu IRTracer-100 spectrometer equipped with a diamond ATR unit, and select ν_{max} are reported in cm^{-1}, rounded to the ones digit. Data was recorded in the range from 400 to 4000 cm^{-1} with a resolution of 2 cm^{-1}. For each reported spectrum, 64 scans were averaged, and air was subtracted as background. Data acquisition and post-processing were performed with LabSolutions IR Version 2.23.

Analytical thin-layer chromatography (TLC) was performed using 60 Å Silica Gel F254 pre-coated plates (0.25 mm thickness). TLC plates were visualized by irradiation with a UV lamp. Flash chromatography was performed using either a Biotage® Isolera One purification system equipped with a 10, 25, 50, 100 or 340 g SNAP Ultra (HP Sphere, 25 µm silica) or Sfär Duo (60 µm silica) cartridge for normal phase column chromatography, and 12, 30, 60, or 120 g SNAP C18 or SNAP Ultra C18 columns for reverse phase column chromatography; or a Teledyne ISCO Combiflash NextGen 300+ equipped with a 4, 12, or 24 g RediSep columns for normal phase column chromatography. Reverse phase preparative HPLC purification was performed on an Waters LC Prep 150 system equipped with a Waters 2998 UV photodiode array detector, a Waters 2707 autosampler, and an Waters Fraction Collector III using a preparative reverse phase C18 column (CSH C18 19 x 150 mm OBD Column 5 µm). The mobile phase for reverse phase preparative HPLC was water with 0.1% (v/v) trifluoroacetic acid (solvent A) and acetonitrile with 0.1% (v/v) trifluoroacetic acid (solvent B), at a flow rate of 20 mL/min. Analytes were collected based on their absorbance at 280 nm or 214 nm. Chiral normal phase semi-preparative HPLC purification was performed on a Shimadzu 20A series HPLC equipped with a Shimadzu SPD-20AV UV/visible detector, a DGU-20A 5R degassing unit, two LC-20AR solvent delivery units, a CBM-20A HPLC system controller, and an LH-40 liquid handler.

Routine ^1H nuclear magnetic resonance (NMR) spectra were recorded on Agilent or Bruker 400, 500, 600, or 700 MHz spectrometers at ambient temperature unless otherwise stated. Chloroform-*d* ($CDCl_3$, with or without 1% v/v tetramethylsilane [TMS]) and dimethylsulfoxide-d_6

(DMSO-d_6) were purchased from Cambridge Isotope Laboratories and used without further purification. $CDCl_3$ (with or without 1% v/v TMS) was stored at ambient temperature over 5Å molecular sieves or anhydrous K_2CO_3. DMSO-d_6 in 1 g ampoules was used immediately upon opening. Larger volumes of DMSO-d_6 were dried, at minimum, overnight and stored over freshly-activated 3 Å molecular sieve beads. Methanol-d_4 (CD_3OD) was purchased from Cambridge Isotope Laboratories or from Sigma Aldrich in ampoules that were used immediately upon opening. Deuterium Oxide (D_2O) was purchased from Sigma Aldrich and used as received.

Spectra were processed using MestReNova 14.3.3 using the manual or automatic phasing and baseline correction capabilities, as well as zero-filling and COSY-like symmetrization, as appropriate. Splitting was determined using the automatic multiplet analysis function with intervention as necessary. Spectral data are reported as follows: chemical shift (multiplicity [singlet (s), broad singlet (br s), doublet (d), triplet (t), quartet (q), pentet (p), multiplet (m), doublet of doublets (dd), doublet of doublet of doublets (ddd), doublet of triplet of doublets (dtd), doublet of doublet of doublet of doublets (dddd), doublet of triplets (dt), triplet of doublets (td), etc.], coupling constant (Hz), integration). The abbreviation “app” denotes an apparent multiplicity (e.g., “app t” denotes an apparent triplet). Chemical shifts are reported in parts per million (ppm, δ), and coupling constants are reported in Hz. ^1H resonances are referenced to solvent residual peaks for $CDCl_3$ (7.26 ppm), DMSO-d_6 (2.50 ppm), TMS (0.00 ppm), methanol-d_4 (CD_3OD, 3.31 ppm) or D_2O (4.79 ppm). Routine ^{13}C NMR spectra were recorded on Agilent or Bruker 400 (101), 500 (126), 600 (151), or 700 (176) MHz spectrometers with protons fully decoupled. ^{13}C Resonances are reported in ppm relative to solvent residual peaks for $CDCl_3$ (77.16 ppm), DMSO-d_6 (39.52 ppm), or methanol-d_4 (CD_3OD, 49.00 ppm).

Abbreviations

Ac – acetyl
AcOH – acetic acid
ACS – American Chemical Society
AJS – Agilent Jet Stream
APCI – Atmospheric Pressure Chemical Ionization
aq. – aqueous
ATR – Attenuated Total Reflectance
Bn – benzyl
Boc – *tert*-butoxycarbonyl
βk – beta-keto [amide]
ca. – *circa* (“approximately”)
CaH – calcium hydride
Calcd, calcd., or calc. – calculated
CAN – ceric ammonium nitrate
CCD – charge-coupled device
CCDC – Cambridge Crystallographic Data Center
$CDCl_3$ – chloroform-*d*

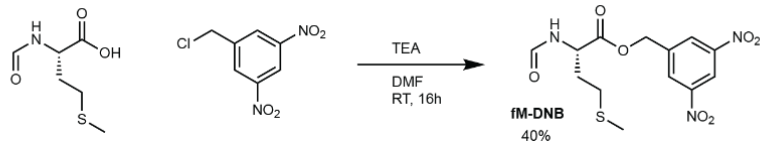
CD_3OD – methanol-d_4
$CeCl_3 \cdot 7H_2O$ – cerium(III) chloride heptahydrate
$CHCl_3$ – chloroform
CH_2Cl_2 – (see DCM)
CIF – Crystallographic Information File
CME – cyanomethyl ester
conc. – concentrated
COSY – Correlated Spectroscopy
CV – column volume(s)
D_2O – deuterium oxide
DAA – diketene acetone adduct (2,2,6-Trimethyl-4*H*-1,3-dioxin-4-one)
DCM – dichloromethane (methylene chloride)
dFx – dinitro-flexizyme
DI – deionized
DIPEA – *N,N*-diisopropylethylamine (Hünig's base)
DMAP – 4-dimethylaminopyridine
DMF – *N,N*-dimethylformamide
DMSO – dimethyl sulfoxide
DMSO-d_6 – dimethyl sulfoxide-d_6
DNB – 3,5-dinitrobenzyl [ester]
d.r. – diastereomeric ratio
EDC – 1-ethyl-3-(3-dimethylaminopropyl)carbodiimide hydrochloride
EDTA – ethylenediaminetetraacetic acid
eFx – enhanced flexizyme
EIC – Extracted Ion Chromatogram
equiv – equivalent(s)
ESI – Electrospray Ionization
Et_2O – diethyl ether
EtOAc – ethyl acetate
EtOH – ethanol (ethyl alcohol)
FAIR – Findable, Accessible, Interoperable, and Reusable
$FeCl_3 \cdot H_2O$ – iron(III) chloride monohydrate
fM – *N*-formyl-L-methionine or *N*-formyl-L-methionyl
Fmoc – fluorenylmethyloxycarbonyl
FT – Fourier-Transform
h – hour(s); min – minute(s)
H_2O – water
H_2SO_4 – sulfuric acid
HATU – hexafluorophosphate azabenzotriazole tetramethyl uronium
HBTU – hexafluorophosphate benzotriazole tetramethyl uronium
HCCA – α-cyano-4-hydroxycinnamic acid
HCl – hydrochloric acid
HEPES – 4-(2-hydroxyethyl)-1-piperazineethanesulfonic acid
Hex – hexanes

HFIP – hexafluoroisopropanol
HMBC – Heteronuclear Multiple Bond Correlation
HOBt – 1-hydroxybenzotriazole
HOTf – trifluoromethanesulfonic acid
HPLC – High-Performance Liquid Chromatography
HRMS – High-Resolution Mass Spectrometry
HSQC – Heteronuclear Single Quantum Coherence
ICR – ion cyclotron resonance
IR – Infrared
IVT – in vitro transcription/translation
K_2CO_3 – potassium carbonate
KOH – potassium hydroxide
Kyn – kynurenine
LC-(HR)MS – Liquid Chromatography-(High-Resolution)Mass Spectrometry
LiCl – lithium chloride
LTQ – linear trap quadrupole
M – molar (i.e., mol/L); N – normal
MALDI – Matrix-Assisted Laser Desorption/Ionization
MBHA – (4-methyl)benzhydrylamine
MeCN – acetonitrile
MeOH – methanol (methyl alcohol)
2-MeTHF – 2-methyltetrahydrofuran
$MgCl_2$ – magnesium chloride
$MgSO_4$ – magnesium sulfate
MH – microhelix
MS-MS – tandem mass spectrometry
MsOH – methanesulfonic acid
Na_2CO_3 – sodium carbonate
Na_2SO_4 – sodium sulfate
$NaHCO_3$ – sodium bicarbonate (sodium hydrogen carbonate)
NaOAc – sodium acetate
NaOH – sodium hydroxide
NMR – Nuclear Magnetic Resonance
4-OH-Pro-COOMe•HCl – L-4-hydroxyproline methyl ester hydrochloride
PAGE – polyacrylamide gel electrophoresis
PCR – polymerase chain reaction
$Pd(TFA)_2$ – palladium(II) trifluoroacetate
*p*TsOH·H_2O – *p*-toluenesulfonic acid monohydrate
PTFE – polytetrafluoroethylene
PyBOP – benzotriazole-1-yl-oxy-tris-pyrrolidino-phosphonium hexafluorophosphate
Q-TOF – Quadrupole Time-of-Flight
RP-HPLC – Reverse Phase High-Performance Liquid Chromatography
rt or RT – room temperature (21–23 °C)
SiO_2 – silicon dioxide (silica)

SPPS – solid-phase peptide synthesis
t-Bu – *tert*-butyl
TBE – Tris/Borate/EDTA
TBS – Tris-Buffered Saline
TCEP-HCl – tris(2-carboxyethyl)phosphine hydrochloride
TEA – triethylamine (also represented as Et_3N or NEt_3)
TEMED – tetramethylethylenediamine
TFA – trifluoroacetic acid
THF – tetrahydrofuran
TIPS – triisopropylsilane
TLC – Thin-Layer Chromatography
TMS – tetramethylsilane
TOCSY – Total Correlation Spectroscopy
Trt – triphenylmethyl (trityl)
U(H)PLC-MS – Ultra-(High) Performance Liquid Chromatography-Mass Spectrometry
UV – ultraviolet
v/v – volume/volume (i.e., mL/100 mL)
vide infra – "see below"
w/w – weight/weight (i.e., g/100 g)
$Yb(OTf)_3$ – ytterbium(III) trifluoromethanesulfonate
$Y(OTf)_3$ – yttrium(III) trifluoromethanesulfonate
$Zn(Cl)_2$ – zinc(II) chloride
$Zn(OTf)_2$ – zinc(II) trifluoromethanesulfonate

Synthesis and characterization of Flexizyme substrates

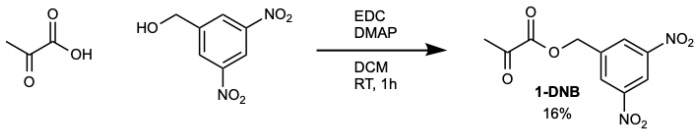
N-Formylmethionyl-3,5-dinitrobenzyl methyl ester (fM-DNB):



(This known compound was prepared following a procedure adapted from Ad et al.[1])
N-formyl-L-methionine (**fM**, 500 mg, 2.82 mmol, 1.0 equiv) and 3,5-dinitrobenzyl chloride (650 mg, 2.82 mmol, 1.0 equiv) were suspended in 3.5 mL of DMF and triethylamine (780 µL, 5.64 mmol, 2.0 equiv) was added. The reaction was stirred at RT for 16 h and then diluted with EtOAc. The mixture was partitioned between EtOAc and 0.1 M aq. HCl. The organic layer was then washed sequentially with 0.2 M aq. $NaHCO_3$, water, and brine, then dried over $MgSO_4$, filtered, and concentrated by rotary evaporation. The resulting oil was re-suspended in 1:5 EtOAc:hexanes, loaded onto SiO_2, and purified by automated flash column chromatography (0–55% EtOAc in hexanes) to give the title compound as a dark orange oil (400 mg, 40%).

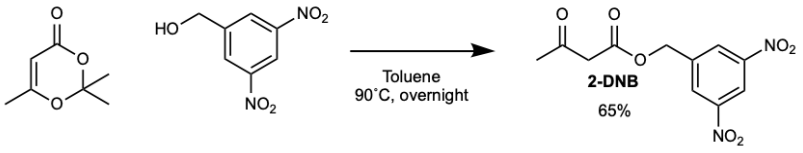
Note: Compound **fM-DNB** could not be fully liberated from close-eluting impurities, providing the compound in up to ~94% purity (via ^{1}H NMR integration). The reported yield is uncorrected.
^{1}H NMR (500 MHz, $CDCl_3$) δ 9.03 (t, *J* = 2.1 Hz, 1H), 8.57 (d, *J* = 2.1 Hz, 2H), 8.26 (d, *J* = 1.5 Hz, 1H), 6.30 (d, *J* = 7.7 Hz, 1H), 5.46 – 5.32 (m, 2H), 4.89 (td, *J* = 7.6, 5.1 Hz, 1H), 2.57 (t, *J* = 7.1 Hz, 2H), 2.26 (dtd, *J* = 14.5, 7.3, 5.2 Hz, 1H), 2.13 – 2.02 (m, 4H).
^{13}C{^{1}H} NMR (126 MHz, $CDCl_3$) δ 171.3, 160.9, 148.9, 139.6, 128.2, 119.0, 65.0, 50.4, 31.2, 30.1, 15.7.
HR-ESI-MS $[M+H]^+$: calculated for $C_{13}H_{16}N_3O_7S^+$ *m/z* 358.0704, found *m/z* 358.0690.
The spectral data is in accord with the literature characterization[1].

3,5-dinitrobenzyl 2-oxopropanoate (1-DNB)



Pyruvic acid (50 µL, 0.71 mmol, 1.25 equiv), 3,5-dinitrobenzyl alcohol (113 mg, 0.57 mmol, 1.00 equiv), DMAP (4.3 mg, 0.036 mmol, 0.06 equiv), and EDC (150 mg, 0.787 mmol, 1.38 equiv) were suspended in 2.0 mL of anhydrous DCM. The reaction was stirred at RT for 1 h. Additional DCM was used to transfer the mixture into a separatory funnel. The organic phase was washed once with water and twice with brine, then dried over Na_2SO_4, filtered, and concentrated by rotary evaporation. The resultant oil was re-suspended in EtOAc, adsorbed onto SiO_2, and purified by automated flash column chromatography (0-20% EtOAc in hexanes) to afford the title compound (24 mg, 16%). Incomplete separation of product and alcohol starting material resulted in a lower purified yield.
^{1}H NMR (500 MHz, $CDCl_3$) δ 9.05 (t, *J* = 2.1 Hz, 1H), 8.61 (d, *J* = 2.1 Hz, 2H), 5.45 (s, 2H), 2.53 (d, *J* = 0.9 Hz, 3H).
^{13}C{^{1}H} NMR (126 MHz, $CDCl_3$) δ 190.4, 160.1, 148.9, 138.9, 128.5, 119.2, 65.4, 26.8. **HR-ESI-MS** $[M+Na]^+$: calculated for $C_{10}H_8N_2NaO_7^+$ *m/z* 291.0225, not found (does not ionize).

3,5-dinitrobenzyl 3-oxobutanoate (2-DNB)



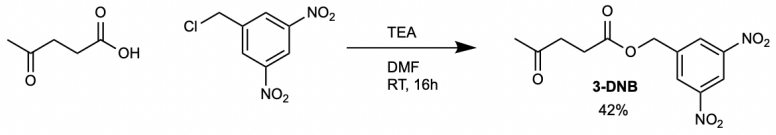
To a round-bottom flask equipped with a magnetic stir bar was added 3,5-dinitrobenzyl alcohol (396 mg, 2.0 mmol, 1 equiv) and toluene (1.5 mL). To the resultant stirring suspension was added 2,2,6-trimethyl-4*H*-1,3-dioxin-1-one (0.27 mL, 2.0 mmol, 1 equiv). The flask was then equipped with a reflux condenser, and the solution was placed under an argon atmosphere and brought to 90 °C (bath temperature) in an oil bath. After stirring overnight, the reaction was concentrated *in vacuo* to afford a red oil. The crude product was purified via normal phase

automated flash column chromatography (0-100% EtOAc/Hexanes) followed by reverse phase automated flash column chromatography (0-100% MeCN/H_2O) to afford the title compound as a yellow oil, which solidified on standing to give a pale yellow solid (367 mg, 1.3 mmol, 65% yield).

Specific Chromatography Details
Normal Phase 1 – Biotage® Sfär Duo 25 g; 0–60% EtOAc/Hex over 15.0 CV, 60-100% over 3.0 CV, 100% for 2.0 CV.
Reverse Phase 1 – Biotage® SNAP C18 30 g; 0–60% MeCN/H_2O over 15.0 CV, 60–100% over 2.0 CV, 100% for 3.0 CV.

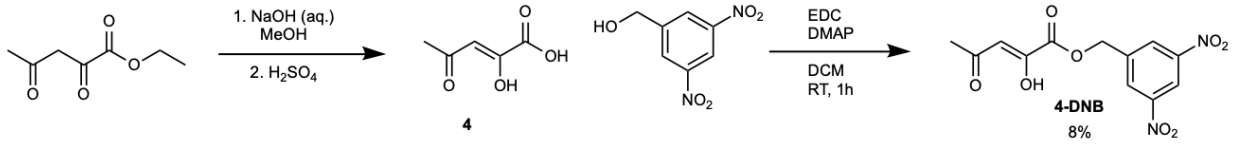
^{1}H NMR (600 MHz, $CDCl_3$, observed as a ca. 6:1 ratio of tautomers [keto:enol] at 25 °C) **keto:** δ 9.00 (t, *J* = 2.1 Hz, 1H), 8.58 (dt, *J* = 2.0, 0.7 Hz, 2H), 5.37 (s, 2H), 3.62 (s, 2H), 2.30 (s, 3H). **enol:** δ 11.73 (s, 1H), 8.99 (t, *J* = 2.2 Hz, 1H), 8.55 (dt, *J* = 2.1, 0.7 Hz, 2H), 5.35 (t, *J* = 0.7 Hz, 2H), 5.13 (q, *J* = 0.7 Hz, 1H), 2.01 (d, *J* = 0.7 Hz, 3H).
^{13}C{^{1}H} NMR (151 MHz, $CDCl_3$) **keto:** δ 199.9, 166.6, 148.8, 140.1, 127.9, 118.7, 64.5, 49.8, 30.5. **enol:** δ 177.7, 171.7, 148.8, 140.9, 127.8, 118.6, 89.0, 63.2, 21.5.
HRMS (ESI) *m/z* $[M-H]^-$ Calcd for $C_{11}H_9N_2O_7^-$ 281.0415; Found 281.0411.
TLC (SiO_2, 60% EtOAc/Hex, UV visualization) R_f = 0.7.
IR (neat, diagnostic peaks) 1745, 1706, 1541 cm^{-1}.
The signals arising from each tautomer were deconvoluted via gCOSY, gHSQCAD, and gHMBCAD analysis. The ^{13}C{^{1}H} peak at ca. 148.8 correlates to both tautomers, suggesting spectral overlap.

3,5-dinitrobenzyl 4-oxopentanoate (3-DNB)



Levulinic acid (80 mg, 0.69 mmol, 1.0 equiv) and 3,5-dinitrobenzyl chloride (190 mg, 0.82 mmol, 1.2 equiv) were suspended in 1.0 mL of DMF and triethylamine (192 µL, 1.37 mmol, 2 equiv) was added. The reaction was stirred at RT for 16 h, and then diluted with 10 mL of EtOAc. The organic layer was then washed three times with brine to remove DMF, then with 0.2 M aq. $NaHCO_3$, before being dried over $MgSO_4$, filtered, and concentrated by rotary evaporation. The resulting oil was re-suspended in EtOAc, adsorbed onto SiO_2, then purified by automated flash column chromatography (0–100% EtOAc in hexanes both with 0.5% acetic acid added) to give the title compound as an oil (87 mg, 43%).
^{1}H NMR (500 MHz, $CDCl_3$) δ 9.00 (t, *J* = 2.1 Hz, 1H), 8.55 (d, *J* = 2.1 Hz, 2H), 5.31 (s, 2H), 2.82 (t, *J* = 6.3 Hz, 2H), 2.69 (dd, *J* = 7.1, 5.5 Hz, 2H), 2.20 (s, 3H).
^{13}C{^{1}H} NMR (126 MHz, $CDCl_3$) δ 206.4, 172.4, 148.8, 140.7, 127.9, 118.6, 64.1, 38.0, 29.9, 27.9.
HR-ESI-MS $[M+Na]^+$: calculated for $C_{12}H_{12}N_2NaO_7^+$ *m/z* 319.0538, found *m/z* 319.0523.
Note: This known compound has been previously characterized in CD_3OD[2].

3,5-dinitrobenzyl (*Z*)-2-hydroxy-4-oxopent-2-enoate (4-DNB)



*(Acetopyruvate (**4**), a known compound, was prepared following a procedure adapted from Narayanan et al.*[3])

Ethyl acetopyruvate (200 mg, 1.26 mmol) was dissolved in methanol (2.5 mL) containing 5 N aq. NaOH (0.5 mL) at 0 °C. The solution was allowed to warm to RT and stirred for 2 h. Filtration yielded a precipitant which was washed with 10 mL methanol, dissolved in 5 mL of 2 N H_2SO_4, and extracted with chloroform. The organic phase was dried over Na_2SO_4 and concentrated by rotary evaporation to afford a mixture of free acid **4** and its corresponding methyl ester (~3.6:1). This mixture was carried forward without further purification.

^{1}H NMR (400 MHz, $CDCl_3$, characterized as a mixture) **free acid:** δ 6.48 (s, 1H), 2.28 (s, 3H), **methyl ester:** δ 6.38 (s, 1H), 3.90 (s, 3H), 2.26 (s, 3H). The characterization of the free acid[4] and methyl ester[5] are in accord with the literature.

Crude acetopyruvate **4** (20 mg, 0.153 mmol, 1 equiv), 3,5-dinitrobenzyl alcohol (33.5 mg, 0.169 mmol, 1.1 equiv), DMAP (0.9 mg, 0.008 mmol, 0.05 equiv), and EDC (32 mg, 0.169 mmol, 1.1 equiv) were suspended in 1.0 mL of anhydrous DCM. The reaction was stirred at RT for 30 min. Additional DCM was used to transfer the mixture into a separatory funnel. The organic phase was washed twice with water, once with brine, and dried over Na_2SO_4, before being concentrated by rotary evaporation. The oil was re-suspended in EtOAc, adsorbed onto SiO_2, then purified by automated flash column chromatography (very slow gradient of 0-20% EtOAc in hexanes over 75 column volumes) to afford the title compound (4.2 mg, 8% [uncorrected for purity of starting material and product]). Compound **4-DNB** could not be fully liberated from minor impurities, resulting in a lower isolated yield.

^{1}H NMR (600 MHz, $CDCl_3$) δ 14.41 (s, 1H), 9.04 (t, *J* = 2.1 Hz, 1H), 8.61 (d, *J* = 2.0 Hz, 2H), 6.41 (s, 1H), 5.48 (s, 2H), 2.29 (s, 3H).

^{13}C{^{1}H} NMR (151 MHz, $CDCl_3$) δ 200.3, 165.7, 161.8, 148.9, 139.2, 128.4, 119.2, 102.9, 65.4, 27.9.

HR-ESI-MS $[M+H]^+$: calculated for $C_{12}H_{11}N_2O_8^+$ *m/z* 311.0510, found *m/z* 311.0524.

tRNA acylation

Transcription and purification of tRNAs.

DNA templates. DNA templates used for transcribing $tRNA^{fMet}$ and $tRNA^{AsnE2\#2}$ were prepared by annealing and extending the appropriate forward (Fwd) and reverse (Rev) ssDNA oligonucleotides (final concentration of 2 µM for each ssDNA) using Q5® High-Fidelity 2X Master Mix (NEB). The ssDNA primer sequences are provided in **Supplementary Table 7**, while the resultant dsDNA template sequences are found in **Supplementary Table 8**. Annealing and extension reactions followed the following protocol on a BioRad C1000 Touch™ thermocycler: 98 °C for 30 s, 10 cycles of [98 °C for 10 s, 55 °C for 30 s, 72 °C for 45 s], 10 cycles of [98 °C for 10 s, 67 °C for 30 s, 72 °C for 45 s], and 72 °C for 300 s. Following extension, the reaction mixture was supplemented with 3 M sodium acetate solution (pH 5.2) to a final concentration of 300 mM. It was then washed once with 1:1 (v/v) basic phenol (pH 8.0):chloroform and twice with chloroform. Ethanol was then added to 70% (v/v), the suspension of dsDNA was cooled at -80 °C for at least 1 h, and then centrifuged at 4 °C, 21,300 x G for 30 min. The supernatant was removed and the DNA pellet was washed with cold 70% (v/v) ethanol in water and centrifuged again at 4 °C, 21,300 x G for 10 min. The 70% ethanol wash was repeated and the pellet was air dried for 5 min before being resuspended in RNAse-free water. Excess nucleotides were removed from the product using a Micro Bio-Spin™ P-30 Gel Column (BioRad), pre-equilibrated with water, following the manufacturer's protocol. The concentration of dsDNA was determined using a NanoDrop ND-1000 (Thermo Scientific). The sequences of all DNA templates used in this study are found in **Supplementary Table 8.** Each one encodes a GG initiation sequence to increase T7 fidelity. Reverse primers for each tRNA carries a 2'-methoxy modification at the penultimate position, which reduces non-templated nucleotide addition by T7 RNA polymerase during in vitro transcription.

Transcription. HiScribe® T7 Quick High Yield RNA Synthesis Kit (New England Biolabs (NEB)) was used to generate each tRNA in 300 µL reactions containing 10 µg of DNA template, 20 µL of HiScribe® T7 RNA polymerase, and 100 µL of NTP buffer mix (final concentration of 6.7 mM each NTP). Transcription reactions were incubated at 37 °C for 2 h in a thermocycler with a heated lid, and then treated with 200 µL of nuclease-free water and 20 µL of RNAse-free DNAse I before an additional 1 h on the thermocycler to digest template DNA. 3M sodium acetate, pH 5.2 was added to a final concentration of 300 mM and the tRNA product was extracted once with 1:1 (v/v) acidic phenol (saturated with 0.1 M citrate buffer, pH 4.3):chloroform, twice with chloroform, and the tRNA product was precipitated upon addition of ethanol to 70% (v/v). Suspensions were incubated at -80 °C for at least 1 h before being centrifuged at 4 °C, 21,300 x G for 30 min and the supernatant removed. RNA pellets were washed with 70% (v/v) ethanol and centrifuged at 4 °C, 21,300 x G for 10 min. The ethanol wash was repeated once more and the pellet was air dried for 5 min before being resuspended in RNAse-free water. Excess nucleotides were removed from the product using a Micro Bio-Spin™ P-30 Gel Columns (BioRad), pre-equilibrated with water, following the manufacturer's protocol. The concentration of RNA was determined using a NanoDrop ND-1000 (Thermo Scientific). tRNA stock solutions (250 µM in water) were stored at -80 °C. If the concentration was too low after the spin column, the tRNA was ethanol precipitated once more, resuspended in water, quantified using a NanoDrop ND-1000, aliquoted, and stored at -20 °C at 250 µM.

Acylation of microhelix (MH) and tRNA using Flexizymes

tRNA and microhelix (MH) acylation protocols were modified from previously reported methods[6,7]. 1 µL of 250 µM Flexizyme (dFx or eFx) was added to 1 µL of 500 mM HEPES-KOH (pH 7.5) or 500 mM Bicine-KOH (pH 9.0) and 1 µL of 250 µM microhelix or tRNA. The samples were incubated at 95 °C for 2 min and cooled to RT over 5 min on a linear gradient using a thermocycler (BioRad C1000 Touch™). 2 µL of 3 M $MgCl_2$ was then added, followed by 1 µL of a DMSO solution of each flexizyme monomer (**fM-DNB, 1-DNB, 2-DNB, 3-DNB, 4-DNB**, **25-CME, or Kyn-CME**) (50 mM). Water was then added to 10 µL in all cases. The reaction was incubated at 4 °C for 2 to 48 h.

The extent of MH acylation was analyzed by gel-shift as described in previous work[6]. Specifically, 2 µL of acid-PAGE buffer (150 mM sodium acetate (pH 5.2), 10 mM EDTA, 95% (v/v) formamide, 0.02% (w/v) bromophenol blue) was added to 2 µL of the flexizyme reaction. The resulting samples subject to electrophoresis using an acid-urea PAGE-gel (20% acrylamide, 36% (w/v) urea, 50 mM sodium acetate (pH 5.2), 0.1% (w/v) ammonium persulfate, 0.08% (v/v) TEMED). The gel was run at RT at 120 V over the course of 3.5-4 h with 50 mM sodium acetate (pH 5.2) as the running buffer. The gel was imaged with ethidium bromide (1.0 µg/mL) in 50 mL TBE (10.8 g/L Tris, 5.5 g/L boric acid, 10 mM EDTA) for 1-2 min. The gel was destained in 50 mL TBE for 1 min and imaged on a Bio-Rad ChemiDoc™ Imager. UV densitometry was carried out using ImageJ (NIH, Bethesda, MD).

Analysis of MH and tRNA acylation products using intact tRNA LC-HRMS

Intact tRNA LC-MS was performed as previously reported[8,9]. Samples were ethanol precipitated and resuspended in water before analysis using intact tRNA LC-MS. In general, 20 pmol of tRNA was injected to ensure adequate signal in the UV and ion chromatograms. Samples were resolved on a ACQUITY UPLC BEH C18 column (130 Å, 1.7 µm, 2.1 mm X 50 mm, Waters part # 186002350, 60 °C) using an ACQUITY UPLC I-Class PLUS (Waters part # 186015082). The mobile phases used were (A) 8 mM TEA, 80 mM HFIP, 5 µM EDTA (free acid) in 100% MilliQ water; and (B) 4 mM TEA, 40 mM HFIP, 5 µM EDTA (free acid) in 50% MilliQ water/50% methanol. Samples were eluted using a flow rate of 0.3 mL/min. The elution method began with Mobile Phase B at 22%; the fraction of Mobile Phase B increased linearly to 40% B over 10 min and from 40 to 60% B over 1 min and was then held at 60% B for 1 min. The fraction of Mobile Phase B was then decreased linearly from 60 to 22% B over 0.1 min and held at 22% B for 2.9 min to equilibrate the column. For more difficult separations, the method was extended as needed. For tRNA acylation, the linear gradient of Mobile Phase B from 22% to 40% was extended to 20 min. The mass of the RNA was analyzed using LC-MS with a Waters Xevo G2-XS Tof (Waters part #186010532) in negative ion mode with the following parameters: capillary voltage: 2000 V, sampling cone: 40, source offset: 40, source temperature: 140 °C, desolvation temperature: 20 °C, cone gas flow: 10 L/h, desolvation gas flow: 800 L/h, 1 spectrum/s. Expected masses of oligonucleotide products were calculated using

https://www.cusabio.com/m-299.html#a02 or OligoCalc (for OligoCalc, the mass of H_2O must be added to accurately account for the full molecular weight of the triphosphate)[10]. Deconvoluted mass spectra were obtained using the MaxEnt software (Waters Corporation).

Acylation yields were estimated in two ways: In most cases, the relative absorbance of the chromatographically resolved peaks representing acyl- and non-acylated tRNA at 260 nm was adequate to estimate acylation yield. In some cases, low acylation obscured clear A_{260} signals or multiple UV-active species eluted simultaneously. In these cases, extraction of the expected major ion for acylated-MH, over the range of a single ionization envelope, was compared to an equivalent extracted ion chromatogram for the unacylated-MH. A detailed description of these methods is found in previous reports.[8,9]

Preparative acylation of tRNA using Flexizymes in preparation for *in vitro* translation

For tRNA acylation reactions performed in preparation for IVT experiments, 3 µL of 250 µM Flexizyme (dFx or eFx) was added to 3 µL of 500 mM HEPES-KOH (pH 7.5) or 500 mM Bicine-KOH (pH 9.0) and 3 µL of 250 µM tRNA. The samples were incubated at 95 °C for 2 min and cooled to RT over 5 min on a linear gradient using a thermocycler (BioRad C1000 Touch™). To this solution was added 6 µL of 3 M $MgCl_2$ followed by 3 µL of a DMSO solution of the appropriate esterified monomer (DNB or CME) to a final concentration 50 mM. Water was then added to a final volume of 30 µL and the reaction was incubated at 4 °C for the optimal time determined in the microhelix acylation optimization experiment (See **Supplementary Table 1** and **2**). A small sample of the reaction mixture was analyzed using intact tRNA LC-MS of acylated tRNA as described above.

in vitro translation reactions

Transcription of DNA templates encoding peptide for *in vitro* translation

Templates for the expression of MGVDYKDDDDK (MGV-flag) or MKKKYSDYKDDDK (MKKKYS-flag) were prepared by annealing and extending the forward (Fwd) and reverse (Rev) ssDNA oligonucleotides (final concentration of 2 µM for each ssDNA) found in **Supplementary Table 7** using Q5® High-Fidelity 2X Master Mix (NEB) and a BioRad C1000 Touch™ thermocycler. The resulting double stranded DNA template sequence can be found in **Supplementary Table 8.** The preparation of these DNA templates is identical to the preparation of DNA templates for tRNA found above (see **section III.A**.). The concentration of dsDNA was determined using a NanoDrop ND-1000 (Thermo Scientific). The dsDNA was diluted to a concentration of 500 ng/µL and stored at -20 °C until use in translation.

In vitro translation (IVT) with tRNAs acylated with fM, 2, or 3

In vitro transcription/translation of DNA templates encoding X-Gly-Val-Asp-Tyr-Lys-Asp-Asp-Asp-Asp-Lys (XGV-flag) where X = **fM, 2, or 3** was performed using the PURExpress® Δ (aa, tRNA) Kit (New England Biolabs, E6840S) according to a previous protocol with minor modifications[1]. IVT reactions (12.5 µL) were set up by mixing the following components sequentially in a 200 µL microcentrifuge tube: Solution A (ΔtRNA, Δaa; 2.5 µL), an amino acid stock mix (1.25 µL; 3.3 mM L-glycine, 3.3 mM L-valine, 3.3 mM L-aspartic acid, 3.3 mM L-tyrosine, 3.3 mM L-lysine), tRNA solution (1.25 µL), Solution B (3.75 µL), 250 ng dsDNA MGVDYKDDDDK template (0.5 µL), and 750 pmol $tRNA^{fMet}$ acylated with **fM, 2,** or **3** (3.25 µL). IVT reactions were incubated in a thermocycler (BioRad C1000 Touch™) at 37 °C for 2 h and quenched on ice prior to purification and analysis by mass spectrometry.

Anti-FLAG magnetic bead purification

Translated peptides were purified from in vitro translation reactions by enrichment using Anti-FLAG® M2 Magnetic Beads (Millipore Sigma) according to the manufacturer's protocol with slight modifications. First, 12.5 µL of a 50% (v/v) magnetic bead suspension was dispensed in a 200 µL microcentrifuge tube. [Note that to preserve the integrity of the beads and reduce the shear forces they experience, the end of a 20 µL pipette tip was removed with scissors and used to dispense the bead slurry. The beads should not be vortexed, and should be gently mixed by rotation or flicking to resuspend the slurry.] The beads were washed by adding 100 µL of TBS (150 mM NaCl, 50 mM Tris-HCl, pH 7.6), the tube was flicked by hand to mix, placed on a magnetic manifold, and the supernatant was removed. The beads were washed twice more with 100 µL of TBS, incubating for 10 min at RT in TBS, each time removing the supernatant using the magnetic manifold. The entire IVT reaction mixture described above (12.5 µL) was added to the washed beads and incubated at RT for 30 min with periodic agitation by flicking. The beads were washed three times with 100 µL of TBS as described above and the bound products eluted using 20 µL of 0.1 M glycine-HCl (pH 2.8) for 10 min. The supernatant was transferred to LC-MS vials for analysis.

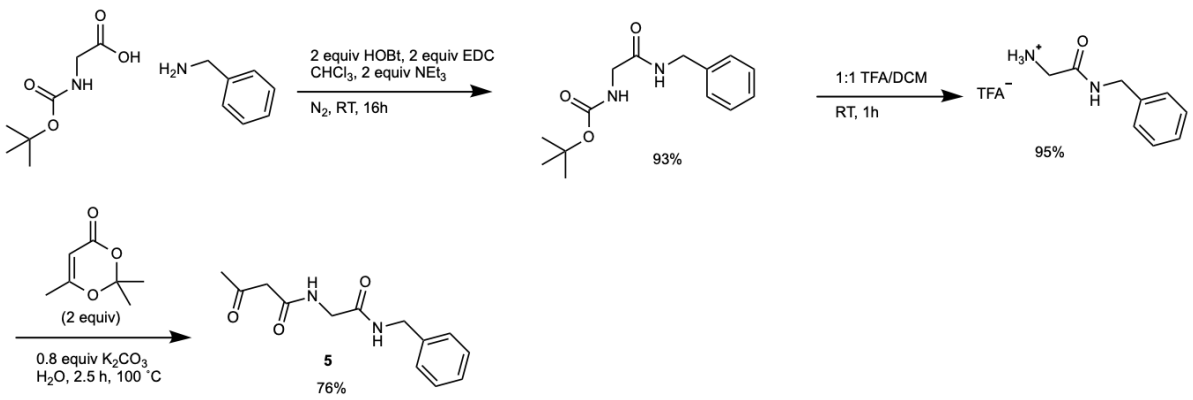
Peptide analysis by LC-HRMS

The peptide products generated using IVT were analyzed using a previously reported protocol[1]. Briefly, 17 µL of the eluent obtained after anti-FLAG magnetic bead purification was injected on an ZORBAX Eclipse XDB-C18 column (1.8 µm, 2.1 Å, ~ 50 mm, RT, Agilent) using an 1290 Infinity II UHPLC (G7120AR, Agilent). The products of most IVT reactions were resolved using the following method: an initial 0.5 min at 95% Solvent A (0.1% formic acid in water) and 5% Solvent B (0.1% formic acid in acetonitrile) followed by a linear gradient from 5 to 50% Solvent B over 4.5 min at flow rate of 0.7 mL/min. Peptides were identified using LC-HRMS with an Agilent 6530 Q-TOF AJS-ESI (G6230BAR). The following parameters were used: a fragmentor

voltage of 175 V, gas temperature of 300 °C, gas flow rate of 12 L/min, sheath gas temperature of 350 °C, sheath gas flow rate of 11 L/min, nebulizer pressure of 35 psi, skimmer voltage of 75 V, Vcap of 3500 V, and collection rate of 3 spectra/s. Expected exact masses of the major charge state for each peptide were calculated using ChemDraw 19.0 and extracted from the total ion chromatograms ± 100 ppm.

Friedländer reactions on model peptide substrates

Synthesis of model dipeptide 5



Boc-Gly-NHBn [tert-butyl (2-(benzylamino)-2-oxoethyl)carbamate]

(This known compound was prepared following a procedure adapted from Vong et al.[11]*)*
N-Boc-glycine (2.00 g, 11.4 mmol, 1 equiv), benzylamine (1.25 mL, 11.4 mmol, 1 equiv), EDC (3.54 g, 22.8 mmol, 2 equiv), and HOBt monohydrate (3.49 g, 22.8 mmol, 2 equiv) were dissolved in 200 mL of $CHCl_3$. TEA (3.18 mL, 22.8 mmol, 2 equiv) was then added and the mixture was stirred for 16 h at RT under N_2. The solvent was evaporated under reduced pressure and the mixture was redissolved in EtOAc. The organic layer was then washed once with water and once with brine. The combined organic extracts were dried over Na_2SO_4, filtered, and evaporated under reduced pressure. The resultant oil was re-suspended in EtOAc, adsorbed onto SiO_2, then purified by automated flash column chromatography (10-50% EtOAc in hexanes) to afford the title compound as a white solid (2.82 g, 93% yield). **^{1}H NMR** (500 MHz, $CDCl_3$) δ 7.35 – 7.22 (m, 5H), 6.59 (s, 1H), 5.24 (s, 1H), 4.44 (d, *J* = 5.7 Hz, 2H), 3.81 (s, 2H), 1.41 (s, 9H). **^{13}C{^{1}H} NMR** (126 MHz, $CDCl_3$) δ 169.5, 156.3, 138.0, 128.8, 127.8, 127.7, 80.5, 44.6, 43.5, 28.4.
The spectral data is in accord with the literature characterization[11]*.*

H-Gly-NHBn•TFA

(This known compound was prepared following a procedure adapted from Vong et al.[11]*)*
Boc-Gly-NHBn (807 mg, 3.05 mmol, 1 equiv) was dissolved in a mixture of TFA (2 mL) and DCM (2 mL) and stirred for 1 h at RT at which point the reaction was complete as judged by TLC. The reaction was subsequently evaporated under reduced pressure to provide a clear oil. The oil was re-suspended in 10% MeOH in $CHCl_3$, adsorbed onto SiO_2, then purified by automated flash column chromatography (0-10% MeOH in $CHCl_3$) to afford the desired compound as a white solid in the form of a TFA salt (806 mg, 95% yield). **^{1}H NMR** (500 MHz, D_2O) δ 7.47 – 7.33 (m, 5H), 4.46 (s, 2H), 3.86 (s, 2H). **^{13}C{^{1}H} NMR** (126 MHz, D_2O) δ 166.9, 137.5, 128.8, 127.6, 127.3, 43.1, 40.4. **HR-ESI-MS** $[M+H]^+$: calculated for $C_9H_{13}N_2O^+$ *m/z* 165.1022, found *m/z* 165.0989.
Note: We posit that this compound exists as a TFA salt on the basis of the following observations: (i) we observe the presence of TFA counterion signals in the $^{13}C\{^1H\}$ spectrum, albeit with limited resolution [MestReNova Detected: δ 162.9, 117.5, 115.2, 112.8]; (ii) the ^{1}H NMR chemical shifts are shifted downfield relative to the reported spectrum of the neutral compound in D_2O[12]; and (iii) the resultant product mass is incompatible with the neutral molecular weight.

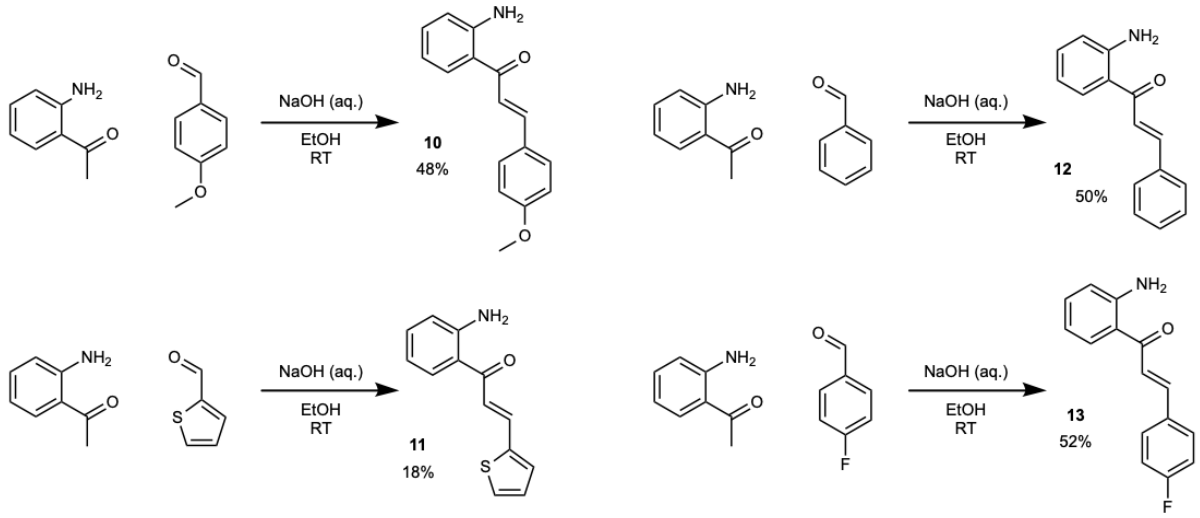
*N-(2-(benzylamino)-2-oxoethyl)-3-oxobutanamide (**5**)*

(This compound was prepared following a procedure adapted from Gama et al.[13]*)*
H-Gly-NHBn•TFA (1.546 g, 5.56 mmol, 1 equiv) and K_2CO_3 (0.614 g, 4.44 mmol, 0.8 equiv) were dissolved in 3 mL of H_2O and the mixture was heated to 100 °C under N_2. 2,2,6-Trimethyl-4*H*-1,3-dioxin-4-one (1.476 mL, 11.1 mmol, 2 equiv) was then added dropwise and the mixture was stirred for 2.5 h, at which point the reaction was complete as judged by TLC analysis. The reaction mixture was immediately filtered through cotton. The reaction flask and cotton plug were rinsed with 1 mL of boiling H_2O, the rinses and filtrate combined, evaporated under reduced pressure, and resuspended in MeOH for adsorption onto SiO_2. Purification by automated flash column chromatography using a gradient of 0-10% MeOH in $CHCl_3$ afforded the title compound as a white solid. (0.917 g, 67% yield). **^{1}H NMR** (500 MHz, $CDCl_3$) δ 7.38 – 7.21 (m, 8H [overlap with solvent residual peak]), 6.63 (s, 1H), 4.46 (d, *J* = 5.8 Hz, 2H), 3.99 (d, *J* = 5.6 Hz, 2H), 3.46 (s, 2H), 2.26 (s, 3H). **^{13}C{^{1}H} NMR** (126 MHz, $CDCl_3$) δ 204.1, 168.5, 166.4, 137.9, 128.9, 127.9, 127.7, 49.8, 43.7, 43.6, 31.1. **HR-ESI-MS** $[M+H]^+$: calculated for $C_{13}H_{17}N_2O_3^+$ *m/z* 249.1234, found *m/z* 249.1232.
Note: Although this compound is known in the literature[14], there are no reports of the corresponding NMR spectra.

General procedure for the synthesis of aminochalcones 10-13

Aminochalcones **10-13** were prepared by adapting established procedures[15]. Briefly, 2-aminoacetophenone (133.7 µL, 1.1 mmol, 1 equiv) and the requisite aldehyde (1.1 mmol, 1 equiv) were dissolved in 830 µL of EtOH. To this solution was added 870 µL of 5.0 M aqueous NaOH and the reaction was stirred at RT for 48 h. The reaction was acidified to pH 2 by

dropwise addition of 6.0 M aqueous HCl. The acidified reaction mixture was extracted three times with EtOAc. The combined organic extracts were washed with water and brine, then dried over $NaSO_4$ and filtered. The solution was adsorbed onto SiO_2, then purified by automated flash column chromatography (0-10% EtOAc in hexanes) to afford the desired compounds.



(E)-1-(2-aminophenyl)-3-(4-methoxyphenyl)prop-2-en-1-one (**10**)

Yield: 133.3 mg, 48%
^{1}H NMR (500 MHz, DMSO-d_6) δ 8.07 (dd, J = 8.3, 1.5 Hz, 1H), 7.89 – 7.77 (m, 3H), 7.61 (d, J = 15.4 Hz, 1H), 7.35 (s, 2H), 7.27 (ddd, J = 8.4, 6.8, 1.5 Hz, 1H), 7.09 – 6.96 (m, 2H), 6.79 (dd, J = 8.4, 1.2 Hz, 1H), 6.59 (ddd, J = 8.1, 6.9, 1.2 Hz, 1H), 3.83 (s, 3H). **^{13}C{^{1}H} NMR** (126 MHz, DMSO-d_6) δ 190.6, 160.9, 151.9, 141.9, 134.1, 131.3, 130.4, 127.7, 120.8, 117.7, 116.8, 114.4, 114.3, 55.3. **HR-ESI-MS** $[M+H]^+$: calculated for $C_{16}H_{16}NO_2^+$ *m/z* 254.1176, found *m/z* 254.1172. *The spectral data is in accord with the literature characterization*[16].

(E)-1-(2-aminophenyl)-3-(thiophen-2-yl)prop-2-en-1-one (**11**)

In this case, the product obtained after flash column chromatography was further purified by reverse phase HPLC.
Yield: 42 mg, 18%
Note: Compound **11** could not be fully liberated from close-eluting impurities, providing the compound in up to ~93% purity (via ^{1}H NMR integration). The reported yield is uncorrected.
HPLC purification: Linear gradient of 5% to 40% (5 min), to 70% (20 min), to 95% (25 min) Solvent B (MeCN with 0.1% TFA) in Solvent A (MilliQ water with 0.1% TFA). Column: CSH C18 19 x 150 mm OBD Column 5 µm.
^{1}H NMR (500 MHz, DMSO-d_6) δ 7.95 (dd, J = 8.3, 1.5 Hz, 1H), 7.79 (d, J = 15.2 Hz, 1H), 7.73 (d, J = 5.0 Hz, 1H), 7.63 (d, J = 3.6 Hz, 1H), 7.59 (d, J = 15.2 Hz, 1H), 7.27 (ddd, J = 8.4, 6.8, 1.5 Hz, 1H), 7.17 (dd, J = 5.0, 3.6 Hz, 1H), 6.79 (dd, J = 8.4, 1.2 Hz, 1H), 6.62 – 6.55 (m, 1H).
^{13}C{^{1}H} NMR (126 MHz, DMSO-d_6) δ 189.8, 151.9, 140.1, 134.7, 134.3, 131.8, 131.1, 129.6,

128.6, 121.7, 117.4, 117.0, 114.6. **HR-ESI-MS** $[M+H]^+$: calculated for $C_{13}H_{12}NOS^+$ *m/z* 230.0634, found *m/z* 230.0638.
Note: This known compound has been previously characterized in $CDCl_3$[17].

(E)-1-(2-aminophenyl)-3-phenylprop-2-en-1-one (**12**)

Yield: 122 mg, 50%
^{1}H NMR (500 MHz, DMSO-*d*$_6$) δ 8.08 (dd, *J* = 8.2, 1.6 Hz, 1H), 7.95 (d, *J* = 15.5 Hz, 1H), 7.88 – 7.81 (m, 2H), 7.63 (d, *J* = 15.5 Hz, 1H), 7.48 – 7.40 (m, 3H), 7.28 (ddd, *J* = 8.4, 6.9, 1.5 Hz, 1H), 6.80 (dd, *J* = 8.4, 1.2 Hz, 1H), 6.60 (ddd, *J* = 8.1, 6.9, 1.2 Hz, 1H). **^{13}C{^{1}H} NMR** (126 MHz, DMSO-*d*$_6$) δ 190.5, 151.9, 141.9, 135.0, 134.3, 131.4, 130.1, 128.9, 128.6, 123.4, 117.5, 116.9, 114.5. **HR-ESI-MS** $[M+H]^+$: calculated for $C_{15}H_{14}NO^+$ *m/z* 224.1070, found *m/z* 223.1066.
The spectral data is in accord with the literature characterization[16].

(E)-1-(2-aminophenyl)-3-(4-fluorophenyl)prop-2-en-1-one (**13**)

Yield: 138 mg, 52%
^{1}H NMR (500 MHz, DMSO-*d*$_6$) δ 8.09 (dd, *J* = 8.2, 1.5 Hz, 1H), 7.99 – 7.88 (m, 3H), 7.63 (d, *J* = 15.5 Hz, 1H), 7.34 – 7.24 (m, 3H), 6.81 (d, *J* = 8.3 Hz, 1H), 6.63 – 6.57 (m, 1H). **^{13}C{^{1}H} NMR** (126 MHz, DMSO-*d*$_6$) δ 190.4, 163.1 (d, J_{CF} = 248.1 Hz), 151.9, 140.7, 134.3, 131.7 (d, J_{CF} = 3.2 Hz), 131.4, 130.9 (d, J_{CF} = 8.4 Hz), 123.3 (d, J_{CF} = 2.6 Hz), 117.5, 116.9, 115.8 (d, J_{CF} = 21.7 Hz), 114.5. **HR-ESI-MS** $[M+H]^+$: calculated for $C_{15}H_{13}FNO^+$ *m/z* 242.0976, found *m/z* 242.0974.
The spectral data is in accord with the literature characterization[18].

Exploration of mild Friedländer reactions in AcOH or $AcOH_{aq}$

These methods describe experiments presented in **Fig. 2b**. Peptide **5** (37 mg, 0.15 mmol) was dissolved in 50% H_2O in MeCN and aliquoted into 30 PCR tubes (0.005 mmol per tube) then flash-frozen and lyophilized. A 0.66 M stock solution of 2-aminoacetophenone (18 µL, 0.15 mmol) in glacial AcOH (209 µL) was prepared. To 18 PCR tubes containing lyophilized peptide **5** was added 7.57 µL of either H_2O or AcOH, followed by 7.57 µL of the 0.66 M stock of 2-aminoacetophenone in AcOH. Thus, each reaction was performed at a 5 µmol scale at 333 mM concentration in either AcOH or 50% AcOH in water ($AcOH_{aq}$). Samples (5 µmol, 333 mM, in either glacial AcOH or 50% AcOH in water) were incubated at RT, 40 °C, or 60 °C. Each of the six reactions (two solvents, three temperatures) was run in duplicate, and timepoints were collected at 1, 5, 24, and 48 h by LC-MS (see section **V.D**)

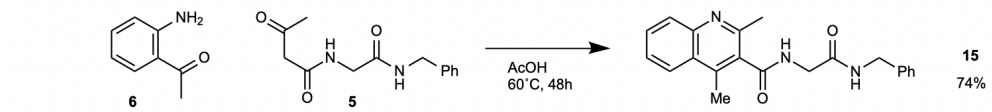
LC-MS analysis of Friedländer reactions on model dipeptide

For LC-MS analysis, 0.5 µL of each reaction was dissolved in 199.5 µL of 1:1 H_2O/MeCN and 1 µL was injected into the LC-MS. Ultra-performance liquid chromatography-mass spectrometry (UPLC-MS) was performed with a Waters Acquity UPLC-MS instrument equipped with a reverse phase Acquity UPLC HSS T3 C18 column (1.8 mm particle size, 2.1 x 30 mm), a dual atmospheric pressure chemical ionization (APCI)/electrospray ionization (ESI) mass spectrometry detector (SQD2), and a photodiode array detector. The following method was used for separation: an initial condition of 90% Solvent A (0.1% formic acid in water) and 10% Solvent B (0.1% formic acid in MeCN) followed by a linear gradient from 10 to 95% Solvent B over 3.5 min at a flow rate of 0.5 mL/min. A linear gradient from 95% to 10% B over 0.1 min was used to reset the initial condition on the column, and the column was re-equilibrated at 10% B for 1.4 min before the next injection.

Friedländer reaction (general procedure for 15 to 23):

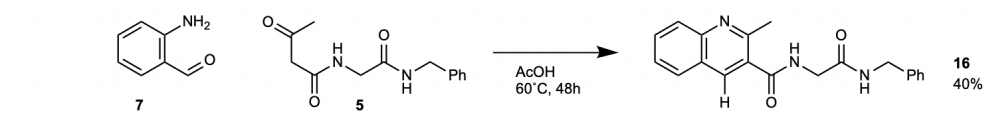
A solution of **5** (39.7 mg, 0.16 mmol, 0.33 M) and requisite 2-aminoaryl ketone (0.16 mmol, 0.33M) in AcOH (480 µL) was stirred for 48h at 60 °C. For LC-MS analysis as presented in **Supplementary Fig. 5**, see section **V.D**. The mixture was neutralized with saturated aq. Na_2CO_3 solution to pH 8.0–9.0, and extracted with EtOAc (3 × 5 mL). The combined organic layers were dried over anhydrous Na_2SO_4, adsorbed onto SiO_2, then purified by automated flash column chromatography (0-100% EtOAc in Hex) to give the desired compounds.

N-(2-(benzylamino)-2-oxoethyl)-2,4-dimethylquinoline-3-carboxamide (**15**)



Yield: 41.0 mg, 74%
^{1}H NMR (500 MHz, DMSO-d_6) δ 8.81 (t, *J* = 6.0 Hz, 1H), 8.51 (t, *J* = 5.9 Hz, 1H), 8.09 (dd, *J* = 8.4, 1.4 Hz, 1H), 7.92 (dd, *J* = 8.5, 1.2 Hz, 1H), 7.73 (ddd, *J* = 8.4, 6.9, 1.4 Hz, 1H), 7.59 (ddd, *J* = 8.3, 6.8, 1.3 Hz, 1H), 7.37 – 7.28 (m, 4H), 7.28 – 7.22 (m, 1H), 4.35 (d, *J* = 5.9 Hz, 2H), 4.00 (d, *J* = 6.0 Hz, 2H), 2.63 (s, 3H), 2.60 (s, 3H). **^{13}C{^{1}H} NMR** (126 MHz, DMSO-d_6) 168.6, 168.5, 154.7, 146.3, 140.0, 139.3, 131.4, 129.5, 128.7, 128.3, 127.3, 126.8, 126.1, 125.7, 124.4, 42.2, 41.9, 23.1, 15.1. **HR-ESI-MS** [M+H]+: calculated for $C_{21}H_{22}N_3O_2^+$ m/z 348.1707, found m/z 348.1719.

N-(2-(benzylamino)-2-oxoethyl)-2-methylquinoline-3-carboxamide (**16**)

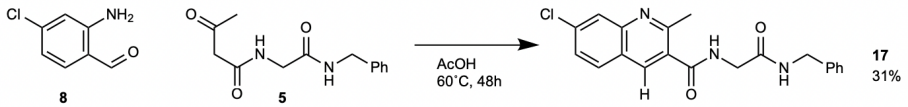


Yield: 21.6 mg, 40%

Note: We observe an apparent impurity in the $^{13}C\{^{1}H\}$ NMR at δ 46.20 ppm; however, the identity of this impurity is not immediately clear from the corresponding ^{1}H NMR spectrum.

^{1}H NMR (500 MHz, DMSO-d_6) δ 8.86 (t, J = 6.0 Hz, 1H), 8.50 (t, J = 6.0 Hz, 1H), 8.40 (s, 1H), 8.02 – 7.92 (m, 2H), 7.78 (ddd, J = 8.4, 6.8, 1.5 Hz, 1H), 7.59 (ddd, J = 8.0, 6.8, 1.2 Hz, 1H), 7.37 – 7.28 (m, 4H), 7.27 – 7.21 (m, 1H), 4.35 (d, J = 6.0 Hz, 2H), 3.97 (d, J = 6.0 Hz, 2H), 2.71 (s, 3H). **$^{13}C\{^{1}H\}$ NMR** (126 MHz, DMSO-d_6) δ 169.2, 168.8, 156.7, 147.5, 139.9, 135.4, 130.9, 130.6, 128.7, 128.6, 128.5, 127.7, 127.2, 126.9, 125.9, 43.0, 42.6, 24.0. **HR-ESI-MS** $[M+H]^+$: calculated for $C_{20}H_{20}N_3O_2^+$ *m/z* 334.1550, found *m/z* 334.1559.

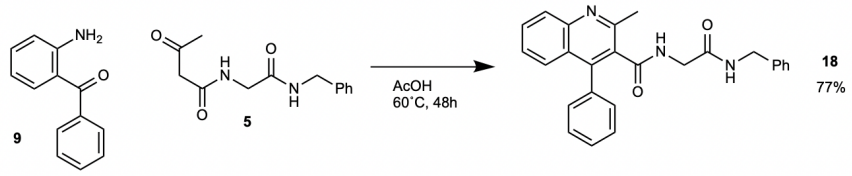
N-(2-(benzylamino)-2-oxoethyl)-7-chloro-2-methylquinoline-3-carboxamide (**17**)



Yield: 18.0 mg, 31%

^{1}H NMR (500 MHz, DMSO-d_6) δ 8.90 (t, J = 6.0 Hz, 1H), 8.51 (t, J = 6.0 Hz, 1H), 8.44 (s, 1H), 8.10 – 7.98 (m, 2H), 7.63 (dd, J = 8.7, 2.1 Hz, 1H), 7.37 – 7.28 (m, 4H), 7.28 – 7.21 (m, 1H), 4.35 (d, J = 5.9 Hz, 2H), 3.97 (d, J = 6.0 Hz, 2H), 2.72 (s, 3H). **$^{13}C\{^{1}H\}$ NMR** (126 MHz, DMSO-d_6) δ 168.6, 168.0, 157.8, 147.4, 139.4, 135.0, 134.9, 130.6, 130.1, 128.2, 127.2, 127.1, 126.82, 126.76, 124.1, 42.5, 42.1, 23.6. **HR-ESI-MS** $[M+H]^+$: calculated for $C_{20}H_{19}ClN_3O_2^+$ *m/z* 368.1160, found *m/z* 368.1134.

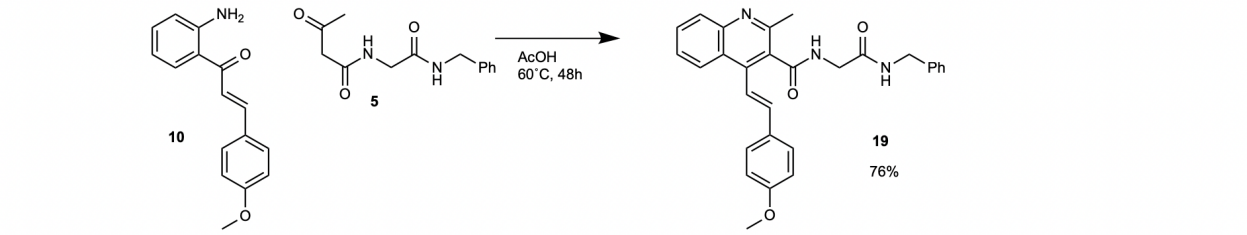
N-(2-(benzylamino)-2-oxoethyl)-2-methyl-4-phenylquinoline-3-carboxamide (**18**)



Yield: 54.9 mg, 77%

^{1}H NMR (500 MHz, DMSO-d_6) δ 8.70 (t, J = 5.9 Hz, 1H), 8.02 (d, J = 8.4 Hz, 1H), 7.96 (t, J = 6.0 Hz, 1H), 7.75 (ddd, J = 8.4, 6.7, 1.4 Hz, 1H), 7.53 – 7.43 (m, 4H), 7.39 (m, 3H), 7.32 (m, 2H), 7.24 (m, 3H), 4.26 (d, J = 5.9 Hz, 2H), 3.66 (d, J = 5.8 Hz, 2H), 2.71 (s, 3H). **$^{13}C\{^{1}H\}$ NMR** (126 MHz, DMSO-d_6) δ 168.3, 167.5, 155.1, 146.8, 143.9, 139.1, 135.1, 130.6, 129.7, 129.5, 128.5, 128.2 (two overlapping peaks), 128.0, 127.1, 126.8, 126.4, 125.8, 124.9, 42.0, 41.9, 23.2. **HR-ESI-MS** $[M+H]^+$: calculated for $C_{26}H_{24}N_3O_2^+$ *m/z* 410.1863, found *m/z* 410.1873.

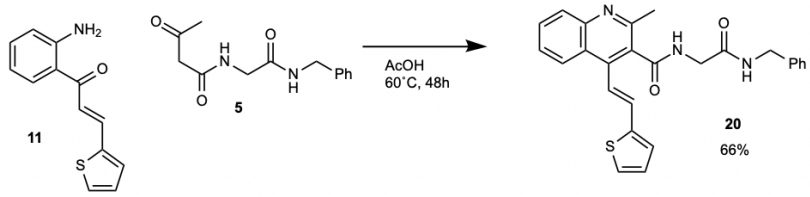
(E)-N-(2-(benzylamino)-2-oxoethyl)-4-(4-methoxystyryl)-2-methylquinoline-3-carboxamide (**19**)



Yield: 56.9 mg, 76%

^{1}H NMR (500 MHz, DMSO-d_6) δ 8.89 (t, *J* = 6.0 Hz, 1H), 8.44 (t, *J* = 6.0 Hz, 1H), 8.27 (dd, *J* = 8.5, 1.4 Hz, 1H), 7.96 (dd, *J* = 8.4, 1.3 Hz, 1H), 7.76 (ddd, *J* = 8.3, 6.8, 1.4 Hz, 1H), 7.66 (m, 2H), 7.59 (m, 2H), 7.30 (m, 4H), 7.24 (m, 1H), 7.13 (d, *J* = 16.6 Hz, 1H), 6.95 (m, 2H), 4.32 (d, *J* = 5.9 Hz, 2H), 3.95 (d, *J* = 6.0 Hz, 2H), 3.79 (s, 3H), 2.64 (s, 3H). **^{13}C{^{1}H} NMR** (126 MHz, DMSO-d_6) δ 168.6, 168.4, 159.7, 155.0, 147.0, 140.1, 139.2, 136.9, 129.6, 129.3, 129.2, 128.7, 128.6, 128.3, 127.3, 126.8, 126.2, 125.3, 124.1, 119.8, 114.1, 55.2, 42.1, 41.9, 23.1. **HR-ESI-MS** $[M+H]^+$: calculated for $C_{29}H_{28}N_3O_3^+$ *m/z* 466.2125 found *m/z* 466.2136.

(E)-N-(2-(benzylamino)-2-oxoethyl)-2-methyl-4-(2-(thiophen-2-yl)vinyl)quinoline-3-carboxamide (**20**)



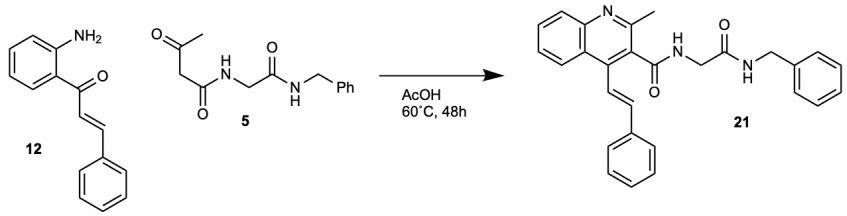
Synthesized at 0.13 mmol scale.

Yield: 38.0 mg, 66%

Note: Compound **20** could not be fully liberated from close-eluting impurities, providing the compound in up to ~91% purity (via ^{1}H NMR integration). The reported yield is uncorrected.

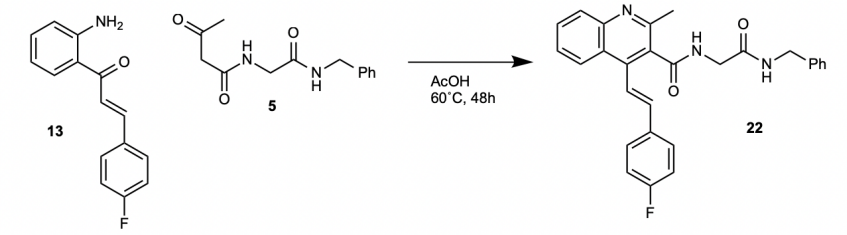
^{1}H NMR (500 MHz, DMSO-d_6) δ 8.93 (t, *J* = 6.0 Hz, 1H), 8.47 (t, *J* = 5.9 Hz, 1H), 8.20 (dd, *J* = 8.6, 1.4 Hz, 1H), 7.97 (dd, *J* = 8.4, 1.3 Hz, 1H), 7.77 (ddd, *J* = 8.3, 6.9, 1.4 Hz, 1H), 7.65 – 7.56 (m, 2H), 7.43 – 7.36 (m, 3H), 7.35 – 7.28 (m, 4H), 7.27 – 7.22 (m, 1H), 7.10 (dd, *J* = 5.1, 3.5 Hz, 1H), 4.33 (d, *J* = 5.9 Hz, 2H), 3.98 (d, *J* = 6.0 Hz, 2H), 2.66 (s, 3H). **^{13}C{^{1}H} NMR** (126 MHz, DMSO-d_6) δ 168.5, 168.2, 155.1, 146.9, 141.4, 139.3, 139.0, 130.4, 129.7, 129.3, 128.8, 128.28, 128.26, 128.1, 127.3, 126.9, 126.8, 126.4, 125.0, 123.9, 120.9, 42.2, 42.0, 23.1. **HR-ESI-MS** $[M+H]^+$: calculated for $C_{26}H_{24}N_3O_2S^+$ *m/z* 442.1584, found *m/z* 442.1552.

(E)-N-(2-(benzylamino)-2-oxoethyl)-2-methyl-4-styrylquinoline-3-carboxamide (**21**)



HR-ESI-MS $[M+H]^+$: calculated for $C_{28}H_{26}N_3O_2^+$ *m/z* 436.2020, found *m/z* 436.1990

(E)-N-(2-(benzylamino)-2-oxoethyl)-4-(4-fluorostyryl)-2-methylquinoline-3-carboxamide (**22**)



HR-ESI-MS $[M+H]^+$: calculated for $C_{28}H_{25}FN_3O_2^+$ *m/z* 454.1925, found *m/z* 454.1892.

2-amino-3-(3-((2-(benzylamino)-2-oxoethyl)carbamoyl)-2-methylquinolin-4-yl)propanoic acid (**23**)



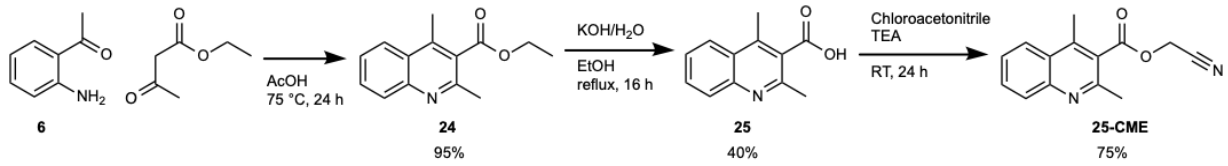
HR-ESI-MS $[M+H]^+$: calculated for $C_{23}H_{25}N_4O_4^+$ *m/z* 421.1870, found *m/z* 421.1862.

Friedländer reactions on IVT peptides

Following IVT of peptide **2-P1** and purification by anti-FLAG magnetic beads, the eluent containing the peptide was flash-frozen and lyophilized into one 200 µL PCR tube per IVT reaction. To the dry peptide, 20 µL of the requisite amino-aryl carbonyl (400 mM) in glacial AcOH was then added, the solution sonicated, and the PCR tube incubated at 40 °C for 24 h. 40 µL of H_2O was then added, and the solution flash-frozen and lyophilized. 20 µL of 0.1 M glycine-HCl (pH 2.8) was then added. Sonication for 2 min was followed by centrifugation on a tabletop centrifuge (1 min at 2000 x G). The supernatant was transferred to a 1.5 mL tube and centrifuged at 21,000 x G for 10 min to remove any excess amino-aryl carbonyl. The

supernatant was then transferred to high-recovery LC-MS vials for analysis (Peptide analysis by LC-HRMS).

Synthesis of cyanomethyl 2,4-dimethylquinoline-3-carboxylate (25-CME)



Ethyl 2,4-dimethylquinoline-3-carboxylate (**24**)

A mixture of 2-aminoacetophenone (**6,** 152 µL, 1.25 mmol, 1.0 equiv) and ethyl acetoacetate (255 µL, 2.0 mmol, 1.6 equiv) in acetic acid (3 mL) was stirred at 75 °C for 24 h in a 5 mL microwave vial. The solvent was evaporated under reduced pressure, the residue was diluted with water, and the pH was adjusted to pH 8 using saturated aqueous $NaHCO_3$. The aqueous solution was extracted three times with EtOAc and the combined organics were dried over Na_2SO_4. The solvent was then removed under reduced pressure in the presence of a small quantity of SiO_2. The adsorbed residue was purified using automated flash column chromatography using a gradient of 0-30% EtOAc in hexanes to provide the title compound (274 mg, 95% yield). **^{1}H NMR** (500 MHz, DMSO-*d*$_6$) δ 8.14 (dd, *J* = 8.5, 1.4 Hz, 1H), 7.99 – 7.91 (m, 1H), 7.79 (ddd, *J* = 8.3, 6.8, 1.4 Hz, 1H), 7.63 (ddd, *J* = 8.2, 6.8, 1.3 Hz, 1H), 4.44 (q, *J* = 7.1 Hz, 2H), 2.62 (s, 3H), 2.59 (s, 3H), 1.36 (t, *J* = 7.1 Hz, 3H). **^{13}C{^{1}H} NMR** (126 MHz, DMSO-*d*$_6$) δ 168.3, 153.6, 146.5, 141.2, 130.3, 128.8, 127.6, 126.6, 125.2, 124.6, 61.5, 23.3, 15.3, 14.0. **HR-ESI-MS** $[M+H]^+$: calculated for $C_{14}H_{16}NO_2^+$ *m/z* 230.1176, found *m/z* 230.1184. *In accord with the literature characterization*[19]*.*

2,4-dimethylquinoline-3-carboxylic acid (**25**)

A mixture of the quinoline ester **24** (274 mg, 1.12 mmol, 1.0 equiv), KOH (112 mg, 2 mmol, 1.8 equiv), ethanol (2 mL) and water (200 µL) was refluxed for 16 h. After cooling and acidification with acetic acid to pH 3, the reaction mixture was concentrated under reduced pressure and the product was precipitated upon addition of water. The precipitate was filtered, rinsed with water, and triturated with EtOH to give the title compound (97 mg, 40% yield). **^{1}H NMR** (500 MHz, DMSO-*d*$_6$) δ 13.75 (s, 1H), 8.12 (dd, *J* = 8.5, 1.4 Hz, 1H), 7.93 (dd, *J* = 8.4, 1.3 Hz, 1H), 7.76 (ddd, *J* = 8.3, 6.8, 1.4 Hz, 1H), 7.62 (ddd, *J* = 8.3, 6.8, 1.3 Hz, 1H), 2.63 (s, 3H), 2.61 (s, 3H).**^{13}C{^{1}H} NMR** (126 MHz, DMSO-*d*$_6$) δ 170.0, 153.5, 146.3, 139.8, 129.9, 129.2, 128.8, 126.4, 125.3, 124.5, 23.4, 15.4. **HR-ESI-MS** $[M+H]^+$: calculated for $C_{12}H_{12}NO_2^+$ *m/z* 202.0863, not found (does not ionize).

Note: This compound has been previously characterized in DMSO-d6 in four independent literature reports[20–23]. We find that our ^{1}H NMR data contrasts with these reports, which are internally consistent with each other. Additionally, we find that our ^{13}C{^{1}H} NMR data contrasts with the two previous reports that provide 13C{1H} NMR data. We believe that these previous

reports are erroneous. This is due, in part, to the presence of $^{13}C\{^{1}H\}$ NMR shifts >200 ppm in two of the reports, which is less consistent with the carboxylic acid motif present in this compound than our signal at 170.0 ppm.

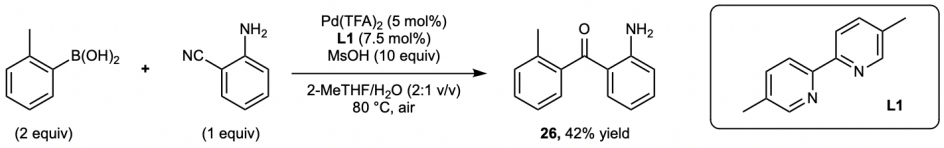
Cyanomethyl 2,4-dimethylquinoline-3-carboxylate (**25-CME**)

2,4-dimethylquinoline-3-carboxylic acid (**25**, 20 mg, 0.10 mmol, 1.0 equiv) was combined with chloroacetonitrile (94 µL, 1.50 mmol, 15.0 equiv), and triethylamine (28 µL, 0.20 mmol, 2.0 equiv) was added. The reaction was stirred 24h at RT, at which point it was judged as complete by TLC analysis. The reaction was partitioned between water/EtOAc, and the aqueous layer was extracted twice more with EtOAc. The combined organic extracts were washed with brine, dried over $MgSO_4$, and the solvent was removed under reduced pressure to afford the title compound (18 mg, 75% yield) **^{1}H NMR** (500 MHz, DMSO-*d_6*) δ 8.17 (dd, *J* = 8.4, 1.4 Hz, 1H), 7.97 (dd, *J* = 8.5, 1.3 Hz, 1H), 7.83 (ddd, *J* = 8.4, 6.8, 1.4 Hz, 1H), 7.66 (ddd, *J* = 8.2, 6.8, 1.4 Hz, 1H), 5.37 (s, 2H), 2.66 (s, 3H), 2.61 (s, 3H). **^{13}C{^{1}H} NMR** (126 MHz, DMSO-*d_6*) δ 167.3, 153.4, 146.8, 142.6, 130.9, 128.8, 126.8, 125.4, 125.0, 124.8, 115.7, 50.3, 23.30, 15.52. **HR-ESI-MS** $[M+H]^+$: calculated for $C_{14}H_{13}N_2O_2^+$ *m/z* 241.0972, found *m/z* 241.0979.

Optimization of Brønsted and Lewis acid-promoted Friedländer reaction to generate atropoisomeric products

These methods provide details related to the experiments described in **Supplementary Figure 9 and Supplementary Table 3**. Glycine model peptide **5** (74 mg, 0.3 mmol, 1.0 equiv) and (2-aminophenyl)(*o*-tolyl)methanone **26** (70 mg, 0.33 mmol, 1.1 equiv) were dissolved in 3 mL of 30% H_2O in MeCN. 50 µL aliquots of this solution were then distributed into 60 PCR tubes. An additional 50 µL of H_2O was added to each aliquot and the 60 tubes were flash-frozen and lyophilized. Each tube contained a dry powder consisting of 5 µmol of **5** and 5.5 µmol of **26**. 50 µL of a solution containing solvent/catalyst was then added and the reactions were incubated for 24 h at 40 °C in duplicate. For analysis, 2 µL of each reaction was dissolved in 198 µL of 1:1 H_2O/MeCN and 1 µL was injected onto a Waters Acquity ultra-performance liquid chromatography-mass spectrometry (UPLC-MS) instrument equipped with a reverse phase Acquity UPLC HSS T3 C18 column (1.8 mm particle size, 2.1 x 30 mm), a dual atmospheric pressure chemical ionization (APCI)/electrospray ionization (ESI) mass spectrometry detector (SQD2), and a photodiode array detector. The following method was used for separation: an initial condition of 90% Solvent A (0.1% formic acid in water) and 10% Solvent B (0.1% formic acid in acetonitrile) followed by a linear gradient from 10 to 95% Solvent B over 3.5 min at flow rate of 0.5 mL/min. A linear gradient from 95% to 10% B over 0.1 min was used to reset the initial condition on the column, and the column was re-equilibrated at 10% B for 1.4 min before the next injection.
Timepoints were collected for selected conditions.

Synthesis of (2-aminophenyl)(*o*-tolyl)methanone (26)

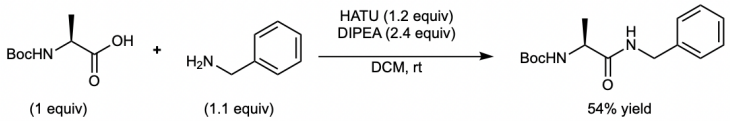


The title compound was prepared according to a literature protocol on a 10 mmol scale to afford arene **26** as a yellow solid (0.88 g, 4.2 mmol, 42% yield)[24].

^{1}H NMR (400 MHz, $CDCl_3$) δ 7.36 (ddd, *J* = 8.2, 5.7, 2.8 Hz, 1H), 7.32 – 7.18 (m, 5H), 6.72 (dd, *J* = 8.3, 1.1 Hz, 1H), 6.53 (ddd, *J* = 8.2, 7.1, 1.2 Hz, 1H), 6.44 (s, 2H), 2.29 (s, 3H). *In accord with the literature characterization*[24]*.*

Synthesis of model peptide 28 (Acetoacetyl-Ala-NHBn)

a. Synthesis of Boc-Ala-NHBn

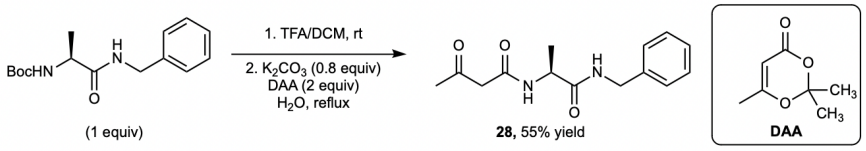


To a round-bottom flask equipped with a magnetic stir bar was added Boc-Ala-OH (1.892 g, 10.0 mmol, 1.0 equiv), HATU (4.563 g, 12.0 mmol, 1.2 equiv), and DCM (33 mL, 0.3 M). The flask was then charged with benzylamine (1.2 mL, 11.0 mmol, 1.1 equiv), followed by slow addition of DIPEA (4.2 mL, 24.0 mmol, 2.4 equiv). After stirring at RT for 3 h, the reaction mixture was diluted with DCM (87 mL), then washed sequentially with saturated aq. sodium bicarbonate (1 x 120 mL), 10% aq. citric acid (2 x 120 mL), saturated aq. sodium bicarbonate (1 x 120 mL), and brine (1 x 120 mL). The organic phase was then dried over Na_2SO_4, filtered, and concentrated *in vacuo* to afford a pink oil. The crude residue was then purified twice via reverse phase automated flash column chromatography (see details below). The desired fractions were blown down under air and co-evaporated with dichloromethane (2x), then diethyl ether (2x) to afford the title compound as a white solid (1.497 g, 5.38 mmol, 54% yield).

Specific Chromatography Details
Reverse Phase 1 – Biotage® SNAP Ultra C18 120 g; 0–50% MeCN/H_2O over 15.0 CV, 50–100% over 2.0 CV, 100% for 2.0 CV. *[5% additive of 2% aq. formic acid throughout]*
Reverse Phase 2 – Biotage® SNAP Ultra C18 120 g; 0–50% MeCN/H_2O over 15.0 CV, 50–100% over 2.0 CV, 100% for 2.0 CV. *[5% additive of 2% aq. formic acid throughout]*

^{1}H NMR (400 MHz, CD_3OD, mixture of rotamers [~5.6:1] at 25 °C) δ 7.38 – 7.14 (m, 5H), 4.43 (d, *J* = 15.1 Hz, 1H), 4.33 (d, *J* = 15.0 Hz, 1H), 4.14 – 3.91 (m, 1H), 1.50 – 1.34 (m, 9H [major rotamer: s]), 1.32 (d, *J* = 7.2 Hz, 3H). *In accord with the literature characterization*[25]*.*

b. Synthesis of Acetoacetyl-Ala-NHBn (**28**)



(This compound was prepared following a procedure adapted from Gama et al.[13])
To a round-bottom flask equipped with a magnetic stir bar was added Boc-Ala-NHBn (1.390 g, 5.0 mmol, 1.0 equiv) and dry DCM (5.0 mL, 1 M). TFA (5.0 mL; 1 mL per mmol of substrate) was slowly added to the flask. The flask was capped with a rubber septum pierced with a vent needle. The solution was then stirred for 1 h. The resultant solution was concentrated *in vacuo* and azeotroped with H_2O to afford crude H-Ala-NHBn•TFA as a brown oil, which was carried forward to the next step without further purification.

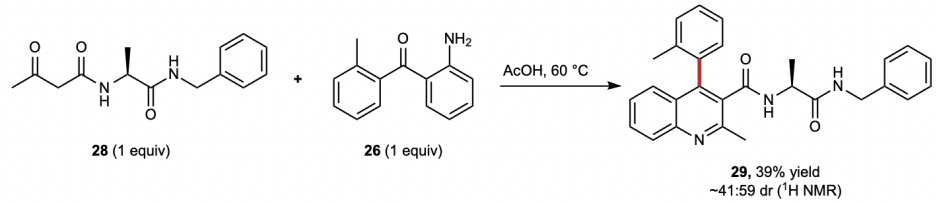
To a round-bottom flask equipped with a magnetic stir bar and crude H-Ala-NHBn•TFA was added K_2CO_3 (0.553 g, 4.0 mmol, 0.8 equiv) and H_2O (10.0 mL, 0.5 M). Once the solution was fully dissolved, a reflux condenser was affixed to the flask. The system was placed under an argon atmosphere and brought to reflux, at which point 2,2,6-trimethyl-4*H*-1,3-dioxin-4-one (**DAA**, 1.33 mL, 10.0 mmol, 2 equiv) was added via syringe. After stirring at reflux for 2.5 h, the solution was allowed to cool to RT and acidified to pH ~1 with 6 N aq. HCl. The aqueous solution was extracted with EtOAc (3 x 30 mL), and the combined organic extracts were washed with brine, dried over Na_2SO_4, filtered, and concentrated *in vacuo* to give a brown oil, which solidified upon standing. The crude product was purified via normal phase automated flash column chromatography (see details below). The desired fractions were concentrated *in vacuo* to afford the title compound **28** as a tan solid (0.723 g, 2.75 mmol, 55% yield).

Specific Chromatography Details
Normal Phase 1 – Biotage® Sfär Duo 50 g; 80–100% EtOAc/Hex over 10.0 CV, 100% for 5.0 CV, 0–10% MeOH/EtOAc over 5.0 CV, 10% for 5.0 CV.

^{1}H NMR (600 MHz, $CDCl_3$, observed as a ca. 16:1 ratio of tautomers [keto:enol] at 25 °C) **keto*:** δ 7.41 (d, *J* = 7.5 Hz, 1H), 7.28 (t, *J* = 7.3 Hz, 2H), 7.25 – 7.19 (m, 3H), 7.11 (t, *J* = 5.9 Hz, 1H), 4.54 (p, *J* = 7.1 Hz, 1H), 4.42 – 4.31 (m, 2H), 3.33 (s, 2H), 2.16 (s, 3H), 1.39 (d, *J* = 7.0 Hz, 3H). **enol*:** δ 13.36 (s, 1H), 6.88 (d, *J* = 6.0 Hz, 1H), 6.29 (d, *J* = 7.5 Hz, 1H), 4.86 (s, 1H), 1.87 (s, 3H).
^{13}C{^{1}H} NMR (151 MHz, $CDCl_3$) **keto:** δ 203.7, 172.1, 166.1, 138.1, 128.7, 127.7, 127.5, 50.2, 49.2, 43.5, 30.8, 18.2. **enol:** δ 173.5, 172.5, 171.6, 138.0, 128.8, 127.62, 127.58, 90.9, 48.3, 43.6, 21.4, 18.5.
HRMS (ESI) *m/z* $[M+H]^+$ Calcd for $C_{14}H_{19}N_2O_3^+$ 263.1390; Found 263.1394.
TLC (SiO_2, 100% EtOAc, UV visualization) R_f = 0.17.
IR (neat, diagnostic peaks) 3283, 1715, 1625, 1538 cm^{-1}.

** The signals arising from each tautomer were partially deconvoluted via gCOSY analysis. Due to spectral overlap, the tautomers could not be fully deconvoluted in the ^{1}H NMR spectrum; Only the resolved enol signals are reported separately; other signals are included under the keto list.*

c. Synthesis of Quinoline-Ala-NHBn (**29**) – Preparation I, AcOH



28 (1 equiv) **26** (1 equiv) **29,** 39% yield ~41:59 dr (^{1}H NMR)

To a 10 mL round-bottom flask equipped with a magnetic stir bar was added Acetoacetyl-Ala-NHBn (**28**, 262 mg, 1.0 mmol, 1.0 equiv) and (2-aminophenyl)(*o*-tolyl)methanone (**26**, 211 mg, 1.0 mmol, 1.0 equiv), followed by AcOH (3.0 mL, 0.33 M). The flask was equipped with a reflux condenser and heated in an oil bath at 60 °C for 48 h. The mixture was cooled to RT and quenched with a small portion of saturated aq. sodium carbonate. The solution was diluted with additional saturated aq. sodium carbonate (30 mL) and extracted with EtOAc (3 x 30 mL). The combined organic phases were dried over Na_2SO_4, filtered, and concentrated *in vacuo* to afford a yellow solid. A crude ^{1}H NMR spectrum was collected to assess the diastereomeric ratio (d.r.) of the product, which was found to be ~41:59 (or ~1.4:1) via integration of the peaks at δ 2.73 ppm (minor) and δ 2.71 ppm (major). The crude yellow solid was then purified via normal phase automated flash column chromatography (0-100% EtOAc/Hex) followed by reverse phase automated flash column chromatography (0-100% MeCN/H_2O) to afford the title compound **29** as a white solid (171 mg, 0.39 mmol, 39% yield) and a mixture of diastereomers. The (*P*, *S*) diastereomer was determined to be the major diastereomer (*vide infra*).

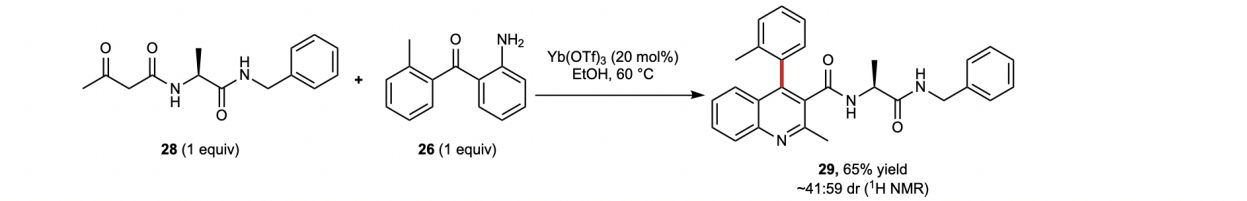
Specific Chromatography Details
Normal Phase 1 – Biotage® Sfär Duo 25 g; 0–100% EtOAc/Hex over 15.0 CV, 100% for 10.0 CV.
Reverse Phase 1 – Biotage® SNAP C18 60 g; 0–50% MeCN/H_2O over 10.0 CV, 50–70% over 10.0 CV, 70–100% over 2.0 CV, 100% for 2.0 CV.

*The following spectral data does not deconvolute the resonances for individual diastereomers. Full characterization of the isolated diastereomers is provided in section **V. K. d.***

^{1}H NMR (600 MHz, $CDCl_3$) δ 8.05 (dt, *J* = 8.7, 1.6 Hz, 1H), 7.70 (ddd, *J* = 8.3, 6.8, 1.4 Hz, 1H), 7.39 (dddd, *J* = 8.2, 6.8, 3.1, 1.2 Hz, 1H), 7.32 (tdd, *J* = 7.6, 2.7, 1.4 Hz, 1H), 7.29 – 7.09 (m, 9H), 6.36 (dt, *J* = 83.1, 5.9 Hz, 1H), 6.22 (dd, *J* = 18.1, 7.6 Hz, 1H), 4.39 – 4.19 (m, 3H), 2.68 (d, *J* = 16.1 Hz, 3H), 1.97 (d, *J* = 19.1 Hz, 3H), 0.99 (dd, *J* = 6.9, 1.1 Hz, 3H).
^{13}C{^{1}H} NMR (151 MHz, $CDCl_3$) δ 171.38, 171.35, 167.9, 155.4, 155.3, 147.7, 147.6, 145.3, 145.2, 137.8, 136.7, 136.5, 135.03, 135.00, 130.5, 130.43, 130.37, 129.6, 129.52, 129.47, 129.1, 129.03, 128.94, 128.88, 128.80, 128.78, 127.71, 127.67, 127.62, 127.60, 126.8, 126.7, 126.32, 126.28, 126.0, 125.8, 125.2, 125.1, 49.2, 49.1, 43.64, 43.58, 23.7, 23.6, 20.1, 19.9, 17.9, 17.8.

HRMS (ESI) *m/z* $[M+H]^+$ Calcd for $C_{28}H_{28}N_3O_2^+$ 438.2176; Found 438.2164.
TLC (SiO_2, 100% EtOAc, UV visualization) R_f = 0.33, 0.40
IR (neat, diagnostic peaks) 3261, 1675, 1622, 1532 cm^{-1}.

d. Synthesis of Quinoline-Ala-NHBn (**29**) – Preparation II, $Yb(OTf)_3$ [20 mol%] in EtOH



To a 10 mL round-bottom flask equipped with a magnetic stir bar was added Acetoacetyl-Ala-NHBn (**28**, 262 mg, 1.0 mmol, 1.0 equiv), (2-aminophenyl)(*o*-tolyl)methanone (**26**, 211 mg, 1.0 mmol, 1.0 equiv), and $Yb(OTf)_3$ (124 mg, 0.2 mmol, 0.2 equiv), followed by EtOH (3.0 mL, 0.33 M). The flask was equipped with a reflux condenser and heated in an oil bath at 60 °C for 48 h. The mixture was cooled to RT, resulting in solidification. A small portion of saturated aq. sodium carbonate was added, and the solid was broken up into small pieces. The suspension was then partitioned between additional saturated aq. sodium carbonate (30 mL) and EtOAc (30 mL), and the aqueous phase was extracted with EtOAc (2 x 30 mL). The combined organic phases were dried over Na_2SO_4, filtered, and concentrated *in vacuo* to afford a yellow solid. A crude ^1H NMR spectrum was collected to assess the diastereomeric ratio (d.r.) of the product, which was found to be ~41:59 (or ~1.4:1) via integration of the peaks at δ 2.74 ppm (minor) and δ 2.72 ppm (major). The crude yellow solid was then purified via normal phase automated flash column chromatography (0-100% EtOAc/Hex) followed by reverse phase automated flash column chromatography (0-100% MeCN/H_2O) to afford the title compound **29** as a white solid (286 mg, 0.65 mmol, 65% yield) and a mixture of diastereomers. The (*P*, *S*) diastereomer was determined to be the major diastereomer (*vide infra*).

Note: the unreacted (2-aminophenyl)(*o*-tolyl)methanone (49.5 mg, 0.23 mmol) could be recovered during the first (normal phase) purification.

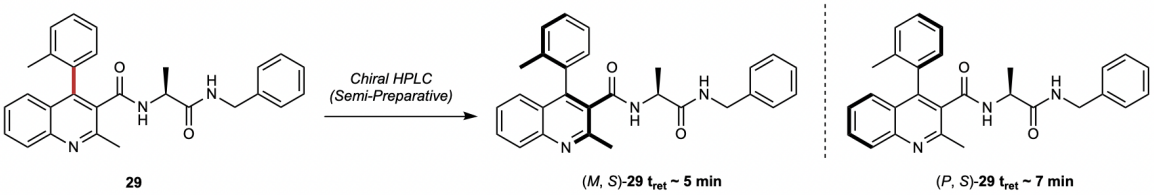
Specific Chromatography Details
Normal Phase 1 – Biotage® Sfär Duo 25 g; 0–100% EtOAc/Hex over 15.0 CV, 100% for 10.1 CV.
Reverse Phase 1 – Biotage® SNAP C18 60 g; 0–50% MeCN/H_2O over 10.0 CV, 50–70% over 10.0 CV, 70–100% over 2.0 CV, 100% for 2.0 CV.

The ^1H and $^{13}C\{^1H\}$ NMR spectra of this compound in $CDCl_3$ were consistent with the spectra provided for Preparation I. Full characterization in DMSO-d_6 is provided below to enable barrier analysis. The following spectral data does not deconvolute the resonances for individual diastereomers. Full characterization of the isolated diastereomers is provided in section ***V. K. d.***

^1H NMR (600 MHz, $CDCl_3$) δ 8.05 (dt, *J* = 8.6, 1.6 Hz, 1H), 7.73 – 7.67 (m, 1H), 7.40 (dddd, *J* = 8.2, 6.8, 2.8, 1.2 Hz, 1H), 7.32 (tdd, *J* = 7.5, 2.7, 1.4 Hz, 1H), 7.30 – 7.10 (m, 9H), 6.31 (dt, *J* =

80.0, 5.9 Hz, 1H), 6.18 (dd, *J* = 16.8, 7.5 Hz, 1H), 4.40 – 4.18 (m, 3H), 2.69 (d, *J* = 16.1 Hz, 3H), 1.97 (d, *J* = 17.0 Hz, 3H), 1.03 – 0.96 (m, 3H).
^{1}H NMR (600 MHz, DMSO-d_6) δ 8.50 (dd, *J* = 41.0, 7.7 Hz, 1H), 8.27 – 7.65 (m, 3H), 7.47 (dddd, *J* = 8.2, 6.8, 2.9, 1.2 Hz, 1H), 7.39 – 7.12 (m, 10H), 4.33 – 4.17 (m, 3H), 2.66 (d, *J* = 7.3 Hz, 3H), 1.90 (d, *J* = 25.9 Hz, 3H), 1.01 (dd, *J* = 38.4, 7.1 Hz, 3H).
^{13}C{^{1}H} NMR (151 MHz, DMSO-d_6) δ 171.7, 171.5, 166.7, 166.5, 155.1, 155.0, 146.7, 146.6, 143.71, 143.68, 139.3, 139.1, 136.1, 136.0, 134.8, 134.6, 130.69, 130.66, 129.8, 129.71, 129.65, 129.61, 129.5, 128.63, 128.59, 128.5, 128.4, 128.3, 128.2, 126.99, 126.95, 126.8, 126.6, 126.5, 125.5, 125.4, 125.3, 125.1, 124.8, 124.7, 48.3, 48.0, 41.96, 41.95, 23.1, 23.0, 19.6, 19.5, 17.8, 17.7.
HRMS (ESI) *m/z* $[M+H]^+$ Calcd for $C_{28}H_{28}N_3O_2^+$ 438.2176; Found 438.2192.
TLC (SiO_2, 100% EtOAc, UV visualization) R_f = 0.33, 0.40 (mixture of diastereomers)
IR (neat, diagnostic peaks) 3257, 1675, 1622, 1533 cm^{-1}.
X-Ray Crystallography: A crystal suitable for structural determination could be obtained by suspending 15.4 mg of the purified compound (as a mixture of diastereomers) in 1 mL of 1 M HCl in Et_2O inside a one-dram vial, followed by evaporation under a gentle stream of air. The resultant salt was dissolved in 0.1 mL MeOH and placed, uncapped, inside a scintillation vial filled with 2.5 mL Et_2O. The scintillation vial was then tightly capped and kept at RT. Vapor diffusion provided the hydrochloride salt of the title compound as white needle-like crystals. The structure obtained from X-ray structural determination revealed only the (*M*, *S*)-diastereomer (**Supplementary Fig. 10**), suggesting preferential crystallization. Full experimental details for X-ray crystallography is provided in section **V. K. f**. Relevant parameters are tabulated in **Supplementary Tables 4 and 10-15.**

e. Protocol for the chromatographic separation of diastereomeric atropisomers (**29**)



Quinoline-Ala-NHBn (**29**) was prepared as a mixture of diastereomers as described in **Preparation II**. The diastereomeric atropisomers were then separated via normal phase chiral semi-preparative HPLC.

A solution of Quinoline-Ala-NHBn (**29,** ~20 mg) in EtOH/Hex (1.5 mL, 30% v/v) was prepared with sonication and gentle heating applied to maximize the solubilized material. The solution was then taken up via syringe and filtered through a syringe filter (Cytiva® Whatman™ Puradisc™ 13, 0.2 µm, PTFE) into an HPLC vial. The material was then chromatographed as described below; three separate runs (each ~20 mg) were combined to isolate the minor (*M*, *S*) diastereomer (t_{ret} ~ 5 min; 17.2 mg) as a white solid and the slightly impure major (*P*, *S*) diastereomer (t_{ret} ~ 7 min; containing ca. 3% of the minor diastereomer as an impurity).

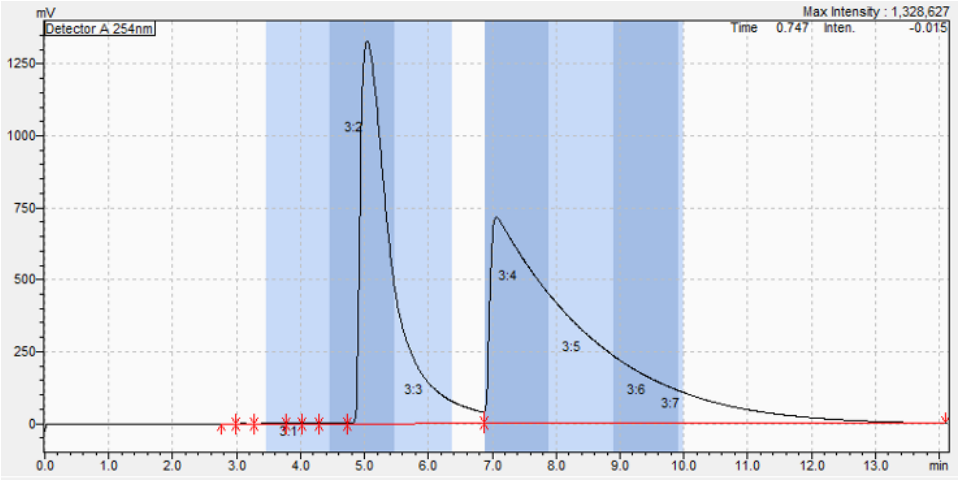
The impure major diastereomer (ca. 25-30 mg) was then taken up in 1.5 mL of 30% EtOH/Hex, treated as described above, and re-subjected to chiral separation to afford the major diastereomer (22.1 mg) as a white amorphous solid.

Note: We detect trace amounts (< 1%) of the undesired diastereomer via NMR.

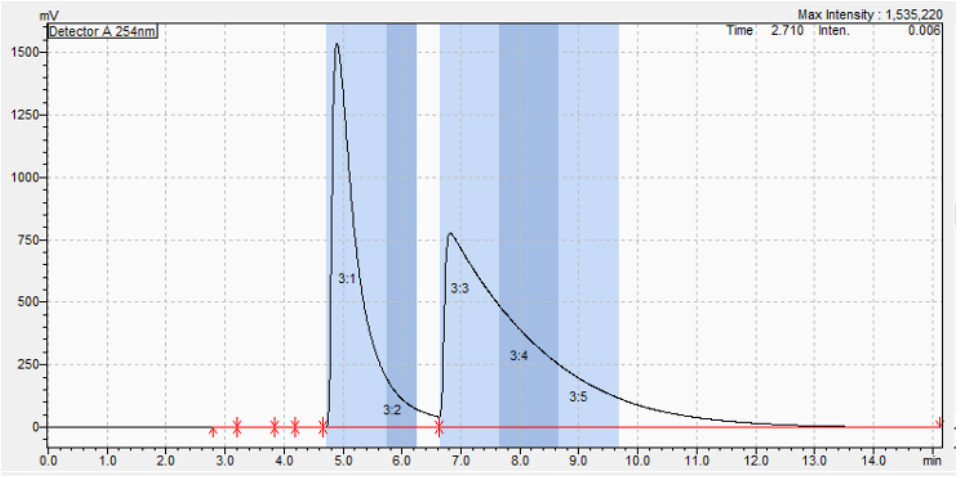
Column: CHIRALPAK® AD-H Semi-Preparative Column; 250 x 10 mm; 5 µm particle size.
Eluent: 30% EtOH/Hex, 5 mL/min.
Injection Volume: 1.5 mL
Fraction Volume: 4.0 mL
Detection Wavelength: 254 nm

Chromatographic Traces (Note: Full HPLC reports are provided as part of the FAIR data.)

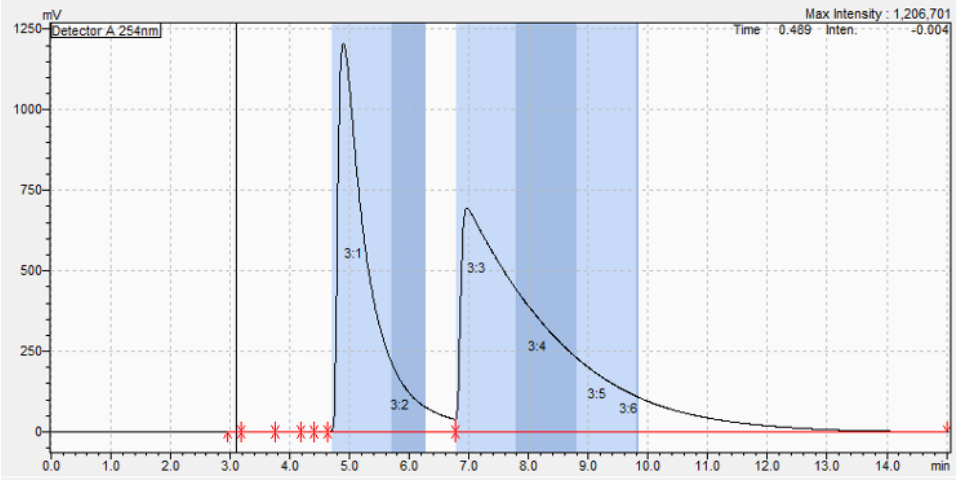
1. Batch I



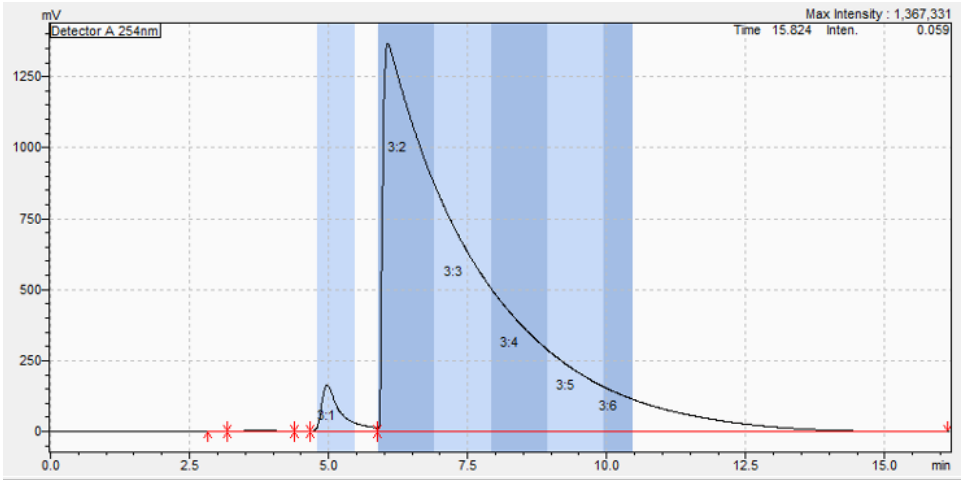
2. Batch II



3. Batch III



4. Re-Purification of Major Diastereomer



f. Characterization of the separated diastereomers

Characterization of (*M*, *S*)-29 – first-eluting; minor diastereomer

^{1}H NMR (600 MHz, $CDCl_3$) δ 8.06 (dt, *J* = 8.4, 0.9 Hz, 1H), 7.70 (ddd, *J* = 8.4, 6.8, 1.4 Hz, 1H), 7.40 (ddd, *J* = 8.2, 6.8, 1.2 Hz, 1H), 7.34 – 7.27 (m, 4H), 7.25 – 7.19 (m, 3H), 7.17 (dd, *J* = 6.9, 1.6 Hz, 2H), 7.12 (dd, *J* = 7.5, 1.4 Hz, 1H), 6.23 (app t, *J* = 5.9 Hz, 1H), 6.16 (d, *J* = 7.4 Hz, 1H), 4.39 – 4.30 (m, 2H), 4.23 (dd, *J* = 14.9, 5.6 Hz, 1H), 2.71 (s, 3H), 1.98 (s, 3H), 0.99 (d, *J* = 6.9 Hz, 3H).

^{13}C{^{1}H} NMR (151 MHz, $CDCl_3$) δ 171.4, 167.9, 155.4, 147.6, 145.3, 137.8, 136.5, 135.0, 130.44, 130.39, 129.6, 129.5, 129.1, 129.0, 128.8, 127.64, 127.61, 126.8, 126.3, 126.0, 125.1, 49.2, 43.6, 23.7, 20.1, 17.8.

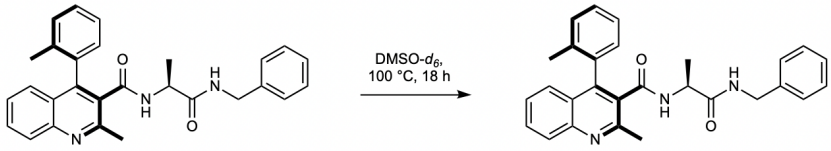
^{1}H NMR (600 MHz, DMSO-d_6) δ 8.46 (d, *J* = 7.6 Hz, 1H), 8.02 (d, *J* = 8.4 Hz, 1H), 7.78 – 7.67 (m, 2H), 7.47 (ddd, *J* = 8.1, 6.9, 1.3 Hz, 1H), 7.36 – 7.29 (m, 3H), 7.29 – 7.16 (m, 6H), 7.15 (dd, *J* = 8.4, 1.4 Hz, 1H), 4.29 – 4.16 (m, 3H), 2.67 (s, 3H), 1.92 (s, 3H), 1.04 (d, *J* = 7.1 Hz, 3H).

^{13}C{^{1}H} NMR (151 MHz, DMSO-d_6) δ 171.5, 166.7, 155.0, 146.6, 143.7, 139.1, 136.1, 134.6, 130.7, 129.8, 129.7, 129.5, 128.6, 128.5, 128.2, 127.0, 126.8, 126.6, 125.5, 125.3, 124.7, 48.3, 42.0, 23.1, 19.6, 17.8.

HRMS (ESI) *m/z* $[M+H]^+$ Calcd for $C_{28}H_{28}N_3O_2^+$ 438.2176; Found 438.2190.
IR (neat, diagnostic peaks) 3255, 1639, 1586, 1525 cm^{-1}.
TLC (SiO_2, 100% EtOAc, UV visualization) R_f = 0.33

Characterization of (*P*, *S*)-29 – second-eluting; major diastereomer
Note: We observe some trace residual hydrocarbon signals, likely arising from the purification protocol.
^{1}H NMR (600 MHz, $CDCl_3$) δ 8.04 (dd, *J* = 8.5, 1.2 Hz, 1H), 7.69 (ddd, *J* = 8.3, 6.8, 1.4 Hz, 1H), 7.39 (ddd, *J* = 8.2, 6.8, 1.2 Hz, 1H), 7.32 (td, *J* = 7.5, 1.4 Hz, 1H), 7.29 – 7.24 (m, 4H), 7.24 – 7.20 (m, 2H), 7.19 – 7.14 (m, 2H), 7.13 (dd, *J* = 7.5, 1.4 Hz, 1H), 6.47 (t, *J* = 5.9 Hz, 1H), 6.27 (d, *J* = 7.6 Hz, 1H), 4.35 (p, *J* = 7.1 Hz, 1H), 4.28 (d, *J* = 5.8 Hz, 2H), 2.66 (s, 3H), 1.94 (s, 3H), 0.98 (d, *J* = 6.9 Hz, 3H).
^{13}C{^{1}H} NMR (151 MHz, $CDCl_3$) δ 171.4, 167.9, 155.3, 147.7, 145.3, 137.8, 136.7, 135.0, 130.5, 130.4, 129.6, 129.5, 129.0, 128.9, 128.8, 127.71, 127.65, 126.7, 126.3, 125.8, 125.2, 49.0, 43.6, 23.6, 19.9, 17.9.
^{1}H NMR (600 MHz, DMSO-d_6) δ 8.53 (d, *J* = 7.8 Hz, 1H), 8.21 (t, *J* = 6.0 Hz, 1H), 8.02 (dd, *J* = 8.5, 1.2 Hz, 1H), 7.74 (ddd, *J* = 8.4, 6.8, 1.5 Hz, 1H), 7.46 (ddd, *J* = 8.2, 6.8, 1.3 Hz, 1H), 7.39 – 7.20 (m, 9H), 7.15 (dd, *J* = 8.4, 1.4 Hz, 1H), 4.33 – 4.18 (m, 3H), 2.66 (s, 3H), 1.88 (s, 3H), 0.98 (d, *J* = 7.1 Hz, 3H).
^{13}C{^{1}H} NMR (151 MHz, DMSO-d_6) δ 171.7, 166.5, 155.1, 146.7, 143.7, 139.3, 136.0, 134.8, 130.7, 129.7, 129.62, 129.60, 128.6, 128.4, 128.3, 127.0, 126.8, 126.5, 125.4, 125.1, 124.8, 48.0, 42.0, 23.0, 19.5, 17.7.
HRMS (ESI) *m/z* $[M+H]^+$ Calcd for $C_{28}H_{28}N_3O_2^+$ 438.2176; Found 438.2194.
IR (neat, diagnostic peaks) 3267, 3242, 1675, 1617, 1533 cm^{-1}.
TLC (SiO_2, 100% EtOAc, UV visualization) R_f = 0.40
X-Ray Crystallography: A crystal suitable for structural determination could be obtained by suspending ~15 mg of the major diastereomer in 1 mL of 1 M HCl in Et_2O inside a one-dram vial, followed by evaporation under a gentle stream of air. The resultant salt was dissolved in 0.4 mL of a 3:1 (v/v) solution of MeOH/EtOH and placed, uncapped, inside a scintillation vial filled with 2.5 mL Et_2O. The scintillation vial was then tightly capped and kept at RT. Vapor diffusion provided the hydrochloride salt of the title compound as white needle-like crystals. The structure obtained from X-ray structural determination revealed a (*P*, *S*) configuration (**Supplementary Fig. 11**). Full experimental details for x-ray crystallography is provided in section **V. K. f**. Relevant parameters are tabulated in **Supplementary Tables 5 and 16-21.**

g. Atropisomer axis barrier analysis



(*M*, *S*)-**29** (*M*, *S*)-**29**

The purified minor diastereomer (i.e., (*M*, *S*)-**29**) was dissolved in DMSO-d_6 (1 g; freshly obtained from a glass ampoule) inside a one-dram vial that was affixed with a Teflon cap, then sealed sequentially with a layer of Teflon tape and a layer of electrical tape. The sealed vial was

then placed in a heating block set to 100 °C for 3 h. The vial was cooled, and the sample was evaluated via ^{1}H NMR for signs of epimerization. The sample was returned to the one-dram vial equipped with a magnetic stir bar, capped, sealed as described above, and stirred for an additional 15 h at 100 °C in a heating block. The sample was again cooled and evaluated via ^{1}H NMR. We observed minimal epimerization (< 1%) (**Supplementary Figure 12**), suggesting a stable atropisomeric axis.

h. X-Ray Crystallography Experimental Details

Low-temperature diffraction data (ω-scans) were collected on a Rigaku MicroMax-007HF diffractometer coupled to a Saturn994+ CCD detector with Cu Kα (λ = 1.54178 Å) for the structures of 007b-24025 (**(*M*, *S*)-29·HCl**) and 007b-24028 (**(*P*, *S*)-29·HCl**). The diffraction images were processed and scaled using Rigaku Oxford Diffraction software (CrysAlisPro; Rigaku OD: The Woodlands, TX, 2015). The structure was solved with SHELXT and was refined against F^2 on all data by full-matrix least squares with SHELXL[26]. All non-hydrogen atoms were refined anisotropically. Hydrogen atoms were included in the model at geometrically calculated positions and refined using a riding model. The isotropic displacement parameters of all hydrogen atoms were fixed to 1.2 times the U value of the atoms to which they are linked (1.5 times for methyl groups). The full numbering scheme of compounds 007b-24025 (**(*M*, *S*)-29·HCl**) and 007b-24028 (**(*P*, *S*)-29·HCl**) can be found in **Supplementary Figures 10** and **11** and the full details of the X-ray structure determination (CIF), which is included as Supporting Information alongside a checkCIF file. CCDC numbers 2341552 (007b-24025; (**(*M*, *S*)-29·HCl**)) and 2341553 (007b-24028; (**(*P*, *S*)-29·HCl**)) contain the supplementary crystallographic data for this paper. These data can be obtained free of charge from The Cambridge Crystallographic Data Center via www.ccdc.cam.ac.uk/data_request/cif.

Friedländer reaction on IVT peptides for the synthesis of ribosomally synthesized atropisomer quinoline peptides

These methods describe the experiments to support **Figure 4c**. Following IVT of peptide **2-P1** and purification by anti-FLAG magnetic beads, the solution containing the peptide was flash-frozen and lyophilized in PCR tubes. To the dry peptide was added 20 µL of (2-aminophenyl)(*o*-tolyl)methanone (**26**, 400 mM) with $Yb(OTf)_3$ (100 mM) in EtOH or MeCN. Alternatively, 20 µL of (2-aminophenyl)(*o*-tolyl)methanone (**26**, 400 mM) in AcOH was added. The solution was sonicated and the PCR tube was incubated at 40 °C for 24 h. 40 µL of H_2O was then added, and the solution flash-frozen before lyophilization. 20 µL of 0.1 M glycine-HCl pH 2.8 was then added. Sonication for 2 min was followed by centrifugation on a tabletop minicentrifuge (1 min at 2000 x G). The supernatant was transferred to a 1.5 mL tube and centrifuged at 21,000 x G for 10 min to remove any further excess amino-arylcarbonyl. The peptides were then analyzed by LC-MS as described above (see Peptide analysis by LC-MS).

Solid Phase Synthesis

Linear Peptides LP1 - LP5: Sequence and Structure

Five linear peptides, **LP1** - **LP5**, were synthesized using solid phase methods and purified by HPLC for use in Friedländer macrocyclization reactions. **LP5** was used as an authentic standard for the analogous peptide produced by IVT. **LP1** - **LP5** were stored and characterized as TFA salts.

Manual solid phase synthesis of LP1-LP4

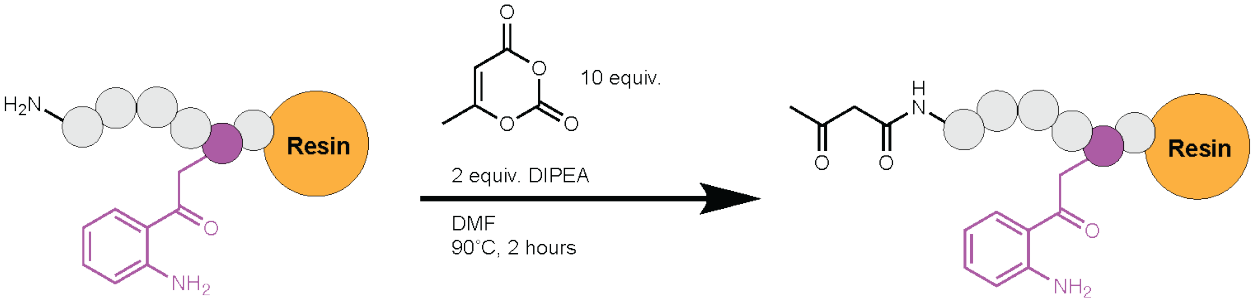
Fully protected resin-bound peptides were synthesized by standard Fmoc solid-phase peptide synthesis. Couplings were performed manually in 20 mL fritted syringes (Torviq - Tucson, Az). Fmoc-Rink MBHA resin (**LP1** : 0.4 g; **LP2-4** : 0.2 g, 0.65 mmol/gram substitution, 100-200 mesh) was swelled upon incubation in DMF (5 mL per 0.2 g resin) for 20 min and then drained. **Fmoc Deprotection:** The Fmoc group was removed by treating the resin twice (3 min each, at RT) with 5 mL of Deprotection Solution (20% (v/v) piperidine in DMF) before being drained. Excess Deprotection Solution was removed by washing the resin 4 times with 6 mL DMF. **Coupling:** Stock solutions for each coupling reagent in DMF were made: Fmoc-amino acids: 260 mM; PyBOP: 1 M; HOBt monohydrate: 1 M. Coupling reactions were performed in fritted syringes by adding the relevant amino acid (2 equiv, final concentration 110 mM), PyBOP (2 equiv, final concentration 110 mM), HOBt monohydrate (2 equiv, final concentration 110 mM) and DIPEA (4 equiv, final concentration 220 mM) to the deprotected resin in that order. The final concentration of resin-bound peptide was 55 mM in DMF. Each coupling reaction was performed at RT for 30 min with agitation. After each reaction, the resin was drained of the reaction solution and then washed three times with 5 mL DMF. The process of deprotection and coupling was then iterated for each amino acid addition. The final peptide was Fmoc-deprotected to expose the *N*-terminal amine.

Solid phase synthesis of LP5

LP5 was synthesized from Fmoc-Asp(O*t*-Bu)-Wang resin (0.55 mmol/g substitution, 100 - 200 mesh), on a 50 µmol scale using Fmoc chemistry and a PurePep® Chorus from Gyros Protein Technologies AB (Tucson, AZ). The resin was first swollen in 6 mL of DMF for 20 min at RT. The Fmoc group was removed by treating the resin twice (3 min each, at RT) with 5 mL of Deprotection Solution (20% (v/v) piperidine in DMF). Excess Deprotection Solution was removed by washing the resin 4 times with 6 mL DMF. Coupling reactions were performed by adding the relevant amino acid (5 equiv), HOBt monohydrate and HATU (4.95 equiv each from 200 mM stocks in DMF) and DIPEA (10 equiv, from a 2 M stock in DMF) to the deprotected resin for a final resin-bound peptide concentration of 12.5 mM. In general, each amino acid

coupling reaction was performed at 70 °C for 5 min. For peptide **LP5**, the coupling reaction that added kynurenine (Kyn) was modified to contain only 2 equiv of Fmoc-Kyn-OH, 1.98 equiv HOBT monohydrate and HATU, and 4 equiv of DIPEA. The final coupling step included an Fmoc deprotection to expose the *N*-terminal amine. Excess coupling reagents were removed by washing 4 times with 6 mL of DMF. Once the synthesis was complete, the resin-bound peptide was dried under nitrogen.

Acetoacetylation of the *N*-termini of peptides prepared using solid-phase synthesis



Resin-bound peptide was transferred to a 20 mL glass microwave vial (Biotage) and DMF (8 mL per 0.1 mmol peptide) was added. The resin was swollen for 20 min at RT with stirring. The vessel was then heated to 90 °C, and DIPEA (2 equiv) and diketene acetone adduct (2,2,6-trimethyl-4*H*-1,3-dioxin-4-one, 10 equiv) were added. The reaction was stirred at 90 °C for 2.5 h. After cooling to RT, the resin was transferred to a fritted syringe and washed three times with 5 mL DMF and three times with 5 mL DCM, then dried under vacuum overnight.

Deprotection and cleavage from resin

In a fritted syringe, the acetoacetylated peptide prepared as described above was deprotected and cleaved from the resin by treatment with Cleavage Cocktail (4 mL per 0.1 mmol peptide) (95% TFA, 2.5% water, 2.5% thioanisole) for 2 h at RT with stirring. The cleavage solution was then drained into 45 mL of diethyl ether in a 50 mL conical tube which had been chilled at -80 °C for two hours. The resin was then washed with 1 mL of Cleavage Cocktail, which was then drained into the diethyl ether as well. The precipitated peptide was then pelleted by centrifugation at 3000 x G for 8 minutes and the diethyl ether was carefully decanted. The cleaved and deprotected peptide was dried under reduced pressure before purification via HPLC. Note that the use of TIPS/TFA in the Cleavage Cocktail should be avoided with peptides carrying a β-keto amide at the *N*-terminus, as it can reduce the terminal ketone.

HPLC purification

HPLC purification was performed on an Waters LC Prep 150 system equipped with a preparative reverse-phase C18 column (CSH C18 19 x 150 mm OBD Column 5 µm), a Waters 2998 UV photodiode array detector, a Waters 2707 autosampler, and a Waters Fraction Collector III. The mobile phase used for HPLC was water with 0.1% (v/v) trifluoroacetic acid (solvent A) and acetonitrile with 0.1% (v/v) trifluoroacetic acid (solvent B). Peptides were eluted at a flow rate of 20 mL/min using a linear solvent gradient (specified below) over 22 min. At 22 min the gradient was switched to 100% B for 2 min, then returned to the initial conditions for column equilibration for 4 min. Peptides were collected based on their absorbance at 254 nm.

LC-HRMS of peptides

LC-HRMS analysis of each peptide was performed on an Agilent 1290 Infinity II HPLC connected to an Agilent 6530B QTOF AJS-ESI. The mobile phase for LC-HRMS was water and acetonitrile both with 0.1% (v/v) formic acid at a flow rate of 0.7 mL/min. Each peptide was injected onto an Eclipse XDB C18 column (2.1 x 50 mm, 1.8-Micron, RT, Agilent) and separated using a linear gradient from 5 to 95% acetonitrile over 4.5 min after an initial hold at 5% acetonitrile for 0.5 min. The following parameters were used during acquisition: Fragmentor voltage 175 V, gas temperature 300 °C, gas flow 8 L/min, sheath gas temperature 350 °C, sheath gas flow 11 L/min, nebulizer pressure 35 psi, skimmer voltage 65 V, Vcap 3500 V, 1 spectra/s.

MALDI-TOF MS of peptides

Peptide samples were dissolved in 30% acetonitrile in water with 0.1% TFA added, then co-crystallized with α-cyano-4-hydroxycinnamic acid (HCCA). MALDI-TOF MS analysis of each cyclic peptide was performed on a Bruker autoflex maX in reflector/positive mode. Peptide calibration standard II (Bruker Daltonics) was used for the external mass calibration.

Replicates (see **VII. B**) were performed on a Shimadzu AXIMA Confidence MALDI-TOF-MS operating in linear positive mode. Mass spectra were recorded in the range of 500 to 5000 *m/z* with the pulsed extraction optimized at 1500 *m/z.* Laser energy was set to 110 internal units (or 130 for CP4). Laser shots were accumulated and averaged at a single position for each sample. Various peptides of known molecular weight were sampled from a LaserBio Labs (Sophia Antipolis, France) MALDI TOFMix kit (Catalog #SHZ-001) and used for the external mass calibration on this instrument. 1 µL of a solution of HCCA in H_2O/MeCN and 1 µL of a cyclic peptide or calibration solution were added to each matrix spot and dried under ambient airflow.

Note on TFA salts in molecular weight calculations and NMR

All peptides synthesized herein were purified on HPLC with TFA additives. After lyophilization, they are assumed to exist as TFA salts. The added mass of TFA salts was included in molecular weight calculations as follows: lysine and arginine residues are assumed to be protonated and coordinated with trifluoroacetate, while His residues and quinolines are assumed to be half protonated and coordinated with trifluoroacetate. The estimated count is provided after the sequence.

When TFA salts were unambiguously observed in the $^{13}C\{^{1}H\}$ NMR spectrum (as determined by comparing to a reference standard, sodium trifluoroacetate; see **Supplementary Data**), we did not tabulate the TFA multiplets for clarity.

Note on exchangeable protons and residual water in linear and cyclic peptides

In solvents where deuterium exchange is possible, we do not observe the internal methylene protons of the β-keto amide, presumably owing to the propensity of these protons to exchange via tautomerism. Exchange is also observed, as is typical, on amide and side-chain N-H protons, as well as side-chain O-H and S-H protons.

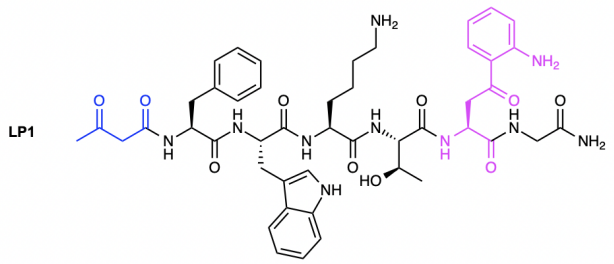
We also note that DMSO-d_6 used for the characterization of the linear and cyclic peptides was dried over molecular sieves (see section **I. A.**). The presence of residual H_2O proved detrimental to characterization. The molecular sieves could be activated by storing at 150 °C overnight in an oven or by heating at 120 °C under vacuum for 2 days.

Note on the purity of linear and cyclic peptides

The purity of linear peptides **LP1-5** and cyclic peptides **CP1-5** are generally evident in the corresponding LC-MS chromatograms (see **Supplementary Figures 17-20** and **27**). In some cases, the corresponding ^{1}H and $^{13}C\{^{1}H\}$ NMR spectra show impurities and/or other conformational isomers. Unless noted otherwise, the desired or major product could not be fully liberated from these species, whether by purification or high-temperature studies.

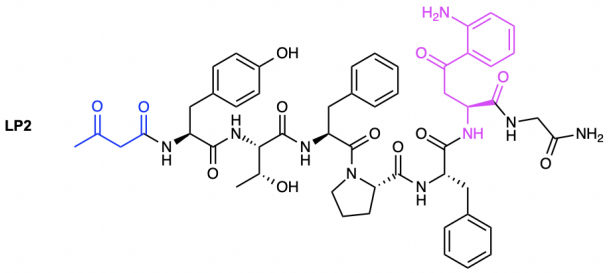
In some cases, we do not observe an idealized set of signals corresponding to the $^{13}C\{^{1}H\}$ NMR spectra of these compounds. We attribute this to a number of possible factors, which may include: (i) the limited solubility of certain compounds in the solvents tested leading to high dilution; (ii) the relatively small quantities of material available; and (iii) the presence of rotameric species and conformational isomers. The tabulations provided are also defined by the sensitivity of the MestReNova peak detection algorithm. In some instances, peaks can be discerned by eye, but not recognized by MestReNova for tabulation purposes.

Peptide LP1: **βk**-Phe-Trp-Lys-Thr-**Kyn**-Gly-$CONH_2$ (1 x TFA)



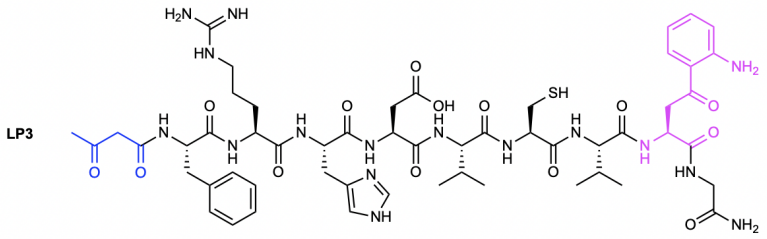
HPLC purification: Linear gradient of 15% to 30% Solvent B in Solvent A over 22 minutes.
Yield: 30%
^{1}H NMR (700 MHz, D_2O) δ 7.93 (d, *J* = 7.9 Hz, 1H), 7.63 – 7.52 (m, 1H), 7.48 – 7.43 (m, 1H), 7.29 (t, *J* = 6.8 Hz, 1H), 7.27 – 7.16 (m, 6H), 7.10 – 7.05 (m, 2H), 7.05 – 6.98 (m, 2H), 4.90 (t, *J* = 6.0 Hz, 1H), 4.40 (t, *J* = 7.0 Hz, 1H), 4.36 (t, *J* = 6.2 Hz, 1H), 4.30 (d, *J* = 4.1 Hz, 1H), 4.26 (qd, *J* = 6.4, 4.3 Hz, 1H), 4.13 (dd, *J* = 9.1, 5.5 Hz, 1H), 3.95 – 3.82 (m, 2H), 3.64 (t, *J* = 6.0 Hz, 2H), 3.10 (qd, *J* = 15.0, 6.5 Hz, 2H), 2.92 – 2.80 (m, 4H), 2.11 (d, *J* = 1.7 Hz, 3H), 1.67 (ddd, *J* = 13.9, 10.7, 6.6 Hz, 1H), 1.54 (dddd, *J* = 10.7, 8.3, 5.2, 1.8 Hz, 2H), 1.49 (ddd, *J* = 19.1, 9.4, 5.0 Hz, 1H), 1.15 (d, *J* = 6.4 Hz, 3H), 1.13 – 1.02 (m, 2H).
^{13}C{^{1}H} NMR (151 MHz, D_2O) δ 207.5, 199.5, 174.5, 174.1, 173.8, 173.4, 173.0, 172.0, 169.9, 136.2, 135.5, 135.3, 131.31, 131.26, 129.2, 129.1, 129.0, 128.8, 128.7, 127.4, 126.8, 124.3, 122.0, 119.5, 117.7, 112.0, 108.0, 66.7, 59.3, 55.8, 54.9, 54.6, 50.1, 42.4, 42.3, 40.0, 39.1, 35.9, 30.0, 29.7, 26.2, 25.9, 22.1, 18.8.
HR-ESI-MS $[M+2H]^{2+}$: calculated for $C_{46}H_{60}N_{10}O_{10}^{2+}$ *m/z* 456.2242, found *m/z* 456.2251.

Peptide LP2: **βk**-Tyr-Thr-Phe-Pro-Phe-**Kyn**-Gly-$CONH_2$ (0 x TFA)



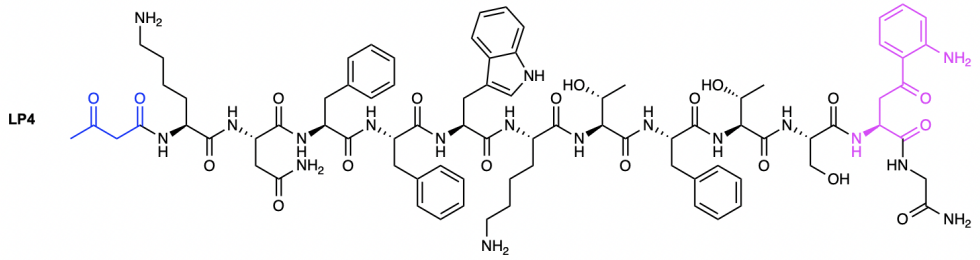
HPLC purification: Linear gradient of 20% to 40% Solvent B in Solvent A over 22 minutes.
Yield: 26%
^{1}H NMR (700 MHz, CD_3OD) and (600 MHz, DMSO-d_6) NMR not tabulated. Spontaneous conversion to a compound with a retention time and mass spectrum matching authentic **CP2** (**Supplementary Figure 22**) was observed in both CD_3OD and DMSO-d_6. (See spectral data)
^{13}C{^{1}H} NMR (151 MHz, DMSO-d_6) NMR not tabulated (see above)
HR-ESI-MS $[M+H]^+$: calculated for $C_{52}H_{62}N_9O_{12}^{1+}$ *m/z* 1004.4513, found *m/z* 1004.4559.

Peptide LP3: **βk**-Phe-Arg-His-Asp-Val-Cys-Val-**Kyn**-Gly-$CONH_2$ (1.5 x TFA)



HPLC purification: Linear gradient of 10% to 30% Solvent B in Solvent A over 22 minutes.
Yield: 6%
^{1}H NMR (600 MHz, D_2O) δ 8.71 – 8.58 (m, 1H), 7.95 – 7.85 (m, 1H), 7.48 (ddt, *J* = 8.4, 7.2, 1.4 Hz, 1H), 7.40 – 7.30 (m, 4H), 7.30 – 7.25 (m, 2H), 6.96 (dt, *J* = 8.4, 1.2 Hz, 1H), 6.94 – 6.88 (m, 1H), 4.94 (dd, *J* = 7.0, 5.1 Hz, 1H), 4.74 – 4.68 (m, 1H), 4.66 (dddd, *J* = 16.8, 8.6, 5.8, 2.7 Hz, 2H), 4.52 (dt, *J* = 22.3, 6.8 Hz, 1H), 4.27 (ddd, *J* = 18.9, 8.9, 5.8 Hz, 1H), 4.21 – 4.05 (m, 2H), 4.02 – 3.89 (m, 2H), 3.73 – 3.55 (m, 2H), 3.37 – 2.97 (m, 7H), 2.95 – 2.76 (m, 3H), 2.23 (d, *J* = 2.3 Hz, 3H), 2.15 – 2.01 (m, 2H), 1.79 (dd, *J* = 12.2, 6.5 Hz, 1H), 1.73 (dd, *J* = 9.2, 5.2 Hz, 1H), 1.54 (qd, *J* = 15.1, 7.4 Hz, 2H), 0.93 (ddt, *J* = 14.3, 6.7, 3.7 Hz, exp. 12H, obs. 14H).
^{13}C{^{1}H} NMR (151 MHz, DMSO-d_6) δ 203.0, 198.3, 177.9, 171.3, 171.2, 171.1, 170.9, 170.8, 169.8, 169.7, 166.1, 156.7, 151.2, 137.7, 134.3, 131.0, 129.1, 128.0, 126.3, 117.0, 114.4, 57.8, 57.7, 55.0, 53.9, 51.1, 49.8, 49.3, 45.7, 42.2, 40.4, 30.6, 30.5, 29.5, 26.0, 25.0, 19.2, 19.1, 17.9, 17.8, 8.6.
HR-ESI-MS $[M+2H]^{2+}$: calculated for $C_{54}H_{78}N_{16}O_{14}S^{2+}$ *m/z* 603.2797, found *m/z* 603.2801.
Note: LP3 was not sufficiently soluble in D_2O to obtain a high-quality $^{13}C\{^1H\}$ NMR spectrum; however, a higher-quality ^{1}H NMR spectrum was observed in D_2O. Consequently, we have provided the ^{1}H NMR spectrum in D_2O and the $^{13}C\{^1H\}$ NMR spectrum in DMSO-d_6.

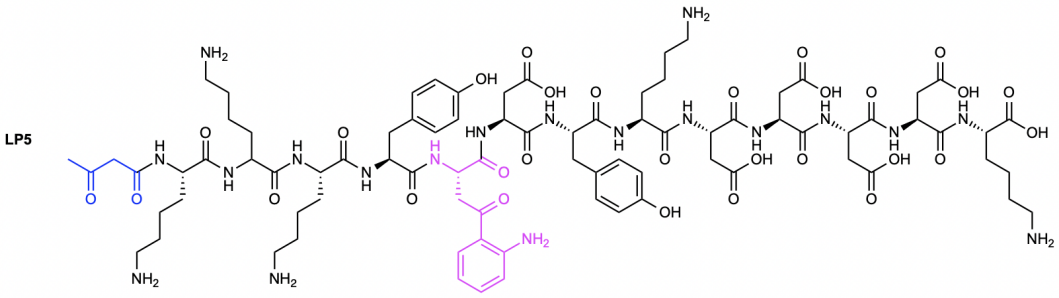
Peptide LP4: **βk**-Lys-Asn-Phe-Phe-Trp-Lys-Thr-Phe-Thr-Ser-**Kyn**-Gly-$CONH_2$ (2 x TFA)



HPLC purification: Linear gradient of 20% to 40% Solvent B in Solvent A over 22 minutes.
Yield: 22%
^{1}H NMR (600 MHz, D_2O) δ 7.68 – 7.61 (m, 1H), 7.44 (dd, *J* = 19.8, 8.0 Hz, 2H), 7.33 – 7.12 (m, 13H), 7.04 (q, *J* = 5.9 Hz, 6H), 6.81 (d, *J* = 8.2 Hz, 1H), 6.71 (s, 1H), 4.88 (t, *J* = 5.9 Hz, 1H), 4.65 (dd, *J* = 7.7, 6.4 Hz, 1H), 4.45 (tdd, *J* = 19.8, 11.8, 7.4 Hz, 3H), 4.35 (dd, *J* = 12.8, 7.4 Hz, 2H), 4.18 (td, *J* = 14.7, 5.4 Hz, 3H), 4.08 (q, *J* = 5.4 Hz, 2H), 4.00 (t, *J* = 6.1 Hz, 1H), 3.97 – 3.83 (m, 4H), 3.59 (dd, *J* = 17.9, 7.4 Hz, 1H), 3.45 (d, *J* = 16.9 Hz, 1H), 3.23 (s, 2H), 3.07 – 2.78 (m,

10H), 2.78 – 2.61 (m, 2H), 2.24 (s, 3H), 1.82 – 1.54 (m, 8H), 1.40 (dd, *J* = 9.4, 5.6 Hz, 1H), 1.34 (d, *J* = 7.8 Hz, 1H), 1.27 – 0.91 (m, 8H).
$^{13}C\{^{1}H\}$ NMR(151 MHz, D_2O) δ 208.1, 199.4, 174.3, 174.1, 174.02, 173.96, 173.74, 173.67, 173.4, 173.3, 173.0, 172.41, 172.38, 171.9, 171.8, 169.7, 136.3, 136.0, 135.9, 135.2, 131.2, 129.1, 128.9, 128.7, 128.6, 127.1, 127.0, 126.8, 124.3, 121.9, 119.0, 118.1, 112.0, 108.6, 66.7, 66.6, 60.8, 60.3, 60.1, 56.2, 56.1, 55.9, 55.6, 55.4, 54.8, 54.2, 50.8, 50.0, 42.3, 40.0, 39.13, 39.10, 36.5, 36.4, 36.3, 36.0, 30.0, 29.90, 29.85, 26.6, 26.3, 26.2, 22.1, 22.0, 18.8, 18.7.
HR-ESI-MS $[M+2H]^{2+}$: calculated for $C_{81}H_{108}N_{18}O_{19}^{2+}$ *m/z* 818.4014, found *m/z* 818.4036.

Peptide LP5: **βk**-Lys-Lys-Lys-Tyr-**Kyn**-Asp-Tyr-Lys-Asp-Asp-Asp-Asp-Lys-COOH (5 x TFA)



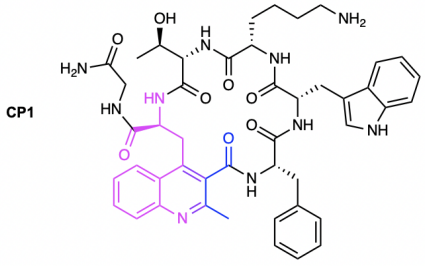
HPLC purification: Linear gradient of 5% to 20% Solvent B in Solvent A over 22 minutes.
Yield: 3%
HR-ESI-MS $[M+3H]^{3+}$: calculated for $C_{82}H_{122}N_{19}O_{29}^{3+}$ *m/z* 612.2880, found *m/z* 612.2867.

Friedländer Peptide Macrocyclization

Cyclic Peptides CP1 - CP5: large scale synthesis

All cyclic peptides were assumed TFA salts after purification (see Note above)

Peptide **CP1**: Qui-cyclo[**βk**-Phe-Trp-Lys-Thr-**Kyn**]-Gly-$CONH_2$ (1.5 x TFA)

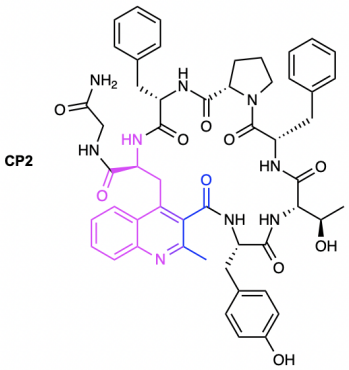


LP1 (29.0 mg, 31.8 µmol, 1 mM, 1 equiv) dissolved in EtOH (31.8 mL) was added to a 50 mL round bottom flask equipped with a magnetic stir bar. $Yb(OTf)_3$ (19.7 mg, 1 equiv) was then added. The vessel was heated at 60 °C in an oil bath for 24 h under N_2 and the solvent was

removed by rotary evaporation. The crude product was subsequently resuspended in 20% MeCN in H_2O containing 0.1% TFA and immediately purified by HPLC (see **VI.F**) to afford **CP1** (17.9 mg, 60%). To facilitate spectral deconvolution, the exchangeable protons in the sample were pre-exchanged with deuterium oxide before analysis in DMSO-d_6, *albeit incompletely*. This was achieved by solubilizing the sample in D_2O for 2 hours at RT, followed by lyophilization overnight, and resuspension in DMSO-d_6 for NMR. Variable-Temperature NMR (VT-NMR) studies revealed enhanced spectral resolution at 100 °C (**Supplementary Fig. 23)**; thus, the compound was partially characterized at 100 °C.

HPLC purification: Linear gradient of 15% to 30% Solvent B in Solvent A over 22 minutes. Elution at 11.5 min.
Total Ion Chromatogram Conversion: 76%
HPLC (254 nm) Conversion: 72%
Isolated Yield: 60%
^{1}H NMR (600 MHz, DMSO-d_6, 373 K) δ 8.23 (d, *J* = 8.0 Hz, 1H), 7.90 (d, *J* = 8.2 Hz, 1H), 7.72 (t, *J* = 7.6 Hz, 1H), 7.62 (t, *J* = 7.1 Hz, 2H), 7.38 (d, *J* = 8.1 Hz, 1H), 7.31 (dt, *J* = 14.6, 7.3 Hz, 4H), 7.24 (d, *J* = 6.9 Hz, 1H), 7.22 (s, 1H), 7.10 (t, *J* = 7.5 Hz, 1H), 7.03 (t, *J* = 7.4 Hz, 1H), 4.90 (s, 1H), 4.86 (s, 1H), 4.47 (s, 1H), 4.08 (s, 2H), 3.98 (s, 1H), 3.71 (dd, *J* = 16.0, 5.8 Hz, 1H), 3.68 (s, 2H), 3.43 (d, *J* = 13.7 Hz, 1H), 3.40 – 3.28 (m, 2H), 3.28 – 3.21 (m, 1H), 3.08 – 3.02 (m, 1H), 2.75 (t, *J* = 7.3 Hz, 2H), 2.12 (s, 3H), 1.78 (s, 2H), 1.61 – 1.47 (m, 2H), 1.30 (s, 2H), 1.01 (d, *J* = 5.9 Hz, 3H). *[Note: the signals tabulated are the non-exchangeable protons of the major species; see spectral data for all signals.]*
^{13}C{^{1}H} NMR (151 MHz, D_2O) δ 175.3, 174.8, 173.9, 173.6, 172.5, 172.0, 171.7, 154.1, 153.5, 145.6, 141.6, 136.0, 135.8, 133.1, 130.3, 130.1, 129.0, 128.9, 128.8, 127.5, 126.9, 126.8, 124.9, 124.5, 121.8, 119.3, 117.9, 112.0, 108.0, 66.2, 60.0, 57.5, 56.1, 55.0, 53.4, 42.2, 39.0, 38.9, 38.6, 36.3, 31.3, 29.4, 26.3, 26.1, 26.1, 22.1, 21.9, 19.7, 19.2, 18.6.
HR-ESI-MS $[M+2H]^{2+}$: calculated for $C_{46}H_{56}N_{10}O_8^{2+}$ *m/z* 438.2136, found *m/z* 438.2134.
HRMS (ESI) *m/z* $[M+H]^+$ Calcd for $C_{46}H_{55}N_{10}O_8^+$ 875.4199; Found 875.4189. (see **VII. B.** for explanation of duplicate HRMS data)
Note: The ^{13}C{^{1}H} NMR was recorded in D_2O at ambient temperature after filtration through a 0.2 µm syringe filter before analysis.

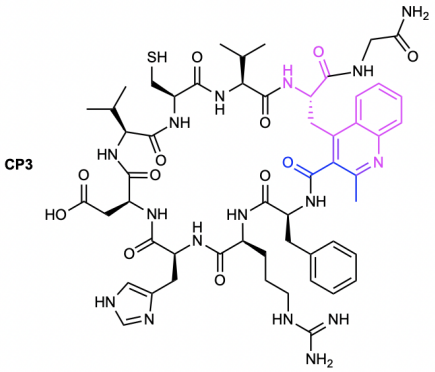
Peptide **CP2**: Qui-cyclo[**βk**-Tyr-Thr-Phe-Pro-Phe-**Kyn**]-Gly-$CONH_2$ (0.5 x TFA)



LP2 (8.2 mg, 9.5 µmol, 1 mM, 1 equiv) dissolved in EtOH (9.5 mL) was added to a 20 mL microwave vial equipped with a magnetic stir bar and $Yb(OTf)_3$ (5.9 mg, 1 equiv) was added. The vessel was heated at 60 °C for 24 h under N_2 and the solvent was removed by rotary evaporation. The crude product was resuspended in 20% MeCN in H_2O containing 0.1% TFA and immediately purified by HPLC (see **VI.F**) to afford **CP2** (17.9 mg, 62%).

HPLC purification: Linear gradient of 20% to 40% Solvent B in Solvent A over 22 minutes. Elution at 14 min.
Total Ion Chromatogram Conversion: 92%
HPLC (254 nm) Conversion: 91%
Isolated Yield: 62%
^{1}H NMR (600 MHz, CD_3OD) δ 8.65 (s, 1H), 7.96 (d, *J* = 8.4 Hz, 1H), 7.80 (dd, *J* = 8.3, 6.9 Hz, 1H), 7.73 – 7.66 (m, 1H), 7.34 – 7.17 (m, 10H), 7.17 – 7.13 (m, 2H), 6.79 – 6.70 (m, 2H), 4.95 (s, 1H), 4.66 (d, *J* = 5.6 Hz, 1H), 4.35 (s, 1H), 4.30 (p, *J* = 6.1 Hz, 1H), 3.82 – 3.53 (m, 4H), 3.50 (d, *J* = 7.6 Hz, 1H), 3.41 (d, *J* = 13.9 Hz, 2H), 3.27 – 3.23 (m, 1H), 3.20 (q, *J* = 7.3 Hz, 1H), 3.15 (td, *J* = 11.4, 7.7 Hz, 2H), 3.05 – 2.99 (m, 1H), 2.84 (t, *J* = 10.6 Hz, 1H), 2.03 (s, 3H), 1.64 (dd, *J* = 12.8, 6.2 Hz, 1H), 1.40 – 1.26 (m, 5H), 0.80 (s, 1H), 0.67 (s, 1H).
^{13}C{^{1}H} NMR (151 MHz, CD_3OD) δ 174.13, 174.11, 174.0, 173.3, 173.2, 173.1, 172.8, 172.5, 170.4, 157.7, 157.6, 156.4, 147.9, 138.4, 137.1, 132.7, 131.7, 131.6, 131.2, 130.7, 130.4, 130.1, 130.0, 129.9, 129.7, 129.3, 129.1, 128.6, 128.3, 128.2, 126.7, 126.1, 116.5, 73.5, 68.4, 62.2, 62.1, 59.2, 57.9, 55.3, 54.9, 47.9, 47.5, 43.6, 40.5, 38.0, 35.6, 31.4, 22.5, 22.0, 20.6, 9.2.
HR-ESI-MS $[M+H]^+$: calculated for $C_{52}H_{58}N_9O_{10}^+$ *m/z* 968.4301, found *m/z* 968.4298.
HRMS (ESI) *m/z* $[M+H]^+$ Calcd for $C_{52}H_{58}N_9O_{10}^+$ 968.4301; Found 968.4289.
Note: Variable-Temperature (VT) NMR studies reveal an additional ^{1}H NMR signal obscured by the HDO peak, integrating between 1H and 2H. The reported data assumes a 1H integration in tabulating other signals, as this signal shows gTOCSY correlations to putative beta protons totalling to 2H.

Peptide **CP3**: Qui-cyclo[**βk**-Phe-Arg-His-Asp-Val-Cys-Val-**Kyn**]-Gly-$CONH_2$ (2 x TFA)

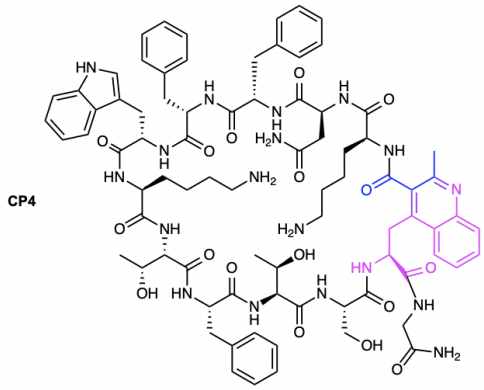


LP3 (8.9 mg, 7.4 µmol, 1 mM, 1 equiv) dissolved in MeCN containing 0.5% H_2O (7.4 mL) was added to a flame-dried 20 mL microwave vial equipped with a magnetic stir bar and $Yb(OTf)_3$ (9.2 mg, 2 equiv) was added. The vessel was heated at 60 °C for 48 h under N_2 and the solvent

removed by rotary evaporation. The crude product was resuspended in 20% MeCN in H_2O containing 0.1% TFA and immediately purified by HPLC (see **VI.F**) to afford **CP3** (1.9 mg, 22%).

HPLC purification: Linear gradient of 10% to 30% Solvent B in Solvent A over 22 minutes. Elution at 11.5 min.
Total Ion Chromatogram Conversion: 20%
HPLC (254 nm) Conversion: 31%
Isolated Yield: 21%
^{1}H NMR (600 MHz, D_2O or CD_3OD) – Not assigned due to the presence of multiple species, which may include rotamers and/or disulfide species. We could not liberate residual DMSO (arising from earlier NMR studies) from this compound. See Spectral information.
HR-ESI-MS $[M+2H]^{2+}$: calculated for $C_{54}H_{74}N_{16}O_{12}S^{2+}$ *m/z* 585.2691, found *m/z* 585.2699.
HRMS (ESI) *m/z* $[M+H]^+$ Calcd for $C_{54}H_{73}N_{16}O_{12}S^+$ 1169.5309; Found 1169.5228.
Note: This compound was observed to dimerize via presumed disulfide formation over time, as detected in additional LC-HRMS and MALDI-TOF studies (see **Supplementary Data**). The putative disulfide could be reduced as follows: To a high-recovery vial containing dimerized **CP3** (~0.1 mg or less) in MeCN/H_2O (~150 µL) was added 2.1 mg TCEP-HCl to afford a ca. 50 mM solution. The capped solution was allowed to sit overnight at ambient temperature. Subsequent LC-HRMS and MALDI-TOF analysis revealed reduction to the cyclic monomer thiol (**CP3,** as drawn).

Peptide **CP4**: Qui-cyclo[**βk**-Lys-Asn-Phe-Phe-Trp-Lys-Thr-Phe-Thr-Ser-**Kyn**]-Gly-$CONH_2$ (2.5 x TFA)



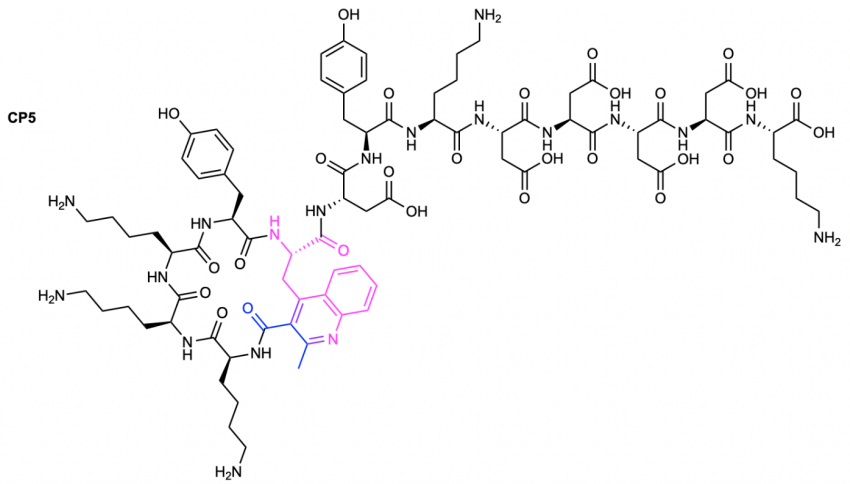
LP4 (22.1 mg, 13.5 µmol, 1 mM, 1 equiv) dissolved in EtOH (13.5 mL) was added to a 20 mL microwave vial equipped with a magnetic stir bar and $Yb(OTf)_3$ (8.4 mg, 1 equiv) was then added. The vessel was heated at 60 °C for 48 h under N_2. The solvent was removed by rotary evaporation, the crude resuspended in 20% MeCN in H_2O with 0.1% TFA, and immediately purified by HPLC (see **VI.F**) to afford **CP4** (6.0 mg, 28%).

HPLC purification: Linear gradient of 20% to 40% Solvent B in Solvent A over 22 minutes. Elution at 11.5 min.
Total Ion Chromatogram Conversion: 53%
HPLC (254 nm) Conversion: 58%

Isolated Yield: 27%

^{1}H NMR (600 MHz, D_2O) δ 8.45 (d, *J* = 8.6 Hz, 1H), 8.20 – 8.09 (m, 2H), 7.97 (ddd, *J* = 8.4, 6.7, 1.4 Hz, 1H), 7.60 (d, *J* = 7.9 Hz, 1H), 7.46 (d, *J* = 8.0 Hz, 1H), 7.34 (qd, *J* = 6.5, 3.7 Hz, 9H), 7.27 (dd, *J* = 13.0, 7.5 Hz, 3H), 7.20 (dd, *J* = 14.0, 6.5 Hz, 2H), 7.12 (t, *J* = 7.1 Hz, 4H), 5.02 (s, 1H), 4.71 (dt, *J* = 20.7, 7.0 Hz, 3H), 4.53 (t, *J* = 7.6 Hz, 2H), 4.42 (s, 1H), 4.38 (d, *J* = 4.0 Hz, 2H), 4.30 – 4.21 (m, 1H), 4.21 – 4.00 (m, 3H), 3.90 – 3.66 (m, 4H), 3.47 (s, 1H), 3.33 (dd, *J* = 15.0, 5.8 Hz, 1H), 3.30 – 3.26 (m, 1H), 3.26 – 3.19 (m, 1H), 3.12 (dd, *J* = 14.0, 8.8 Hz, 1H), 3.03 (dd, *J* = 13.8, 6.9 Hz, 1H), 2.99 – 2.84 (m, 10H), 2.84 – 2.74 (m, 2H), 1.80 (dd, *J* = 16.5, 8.3 Hz, 3H), 1.70 (q, *J* = 8.0 Hz, 3H), 1.61 (q, *J* = 7.6 Hz, 2H), 1.53 – 1.37 (m, 2H), 1.22 – 1.03 (m, 8H).
^{13}C{^{1}H} NMR (151 MHz, CD_3OD) δ 175.3, 174.3, 174.2, 174.1, 174.0, 173.82, 173.80, 173.4, 173.1, 172.6, 172.5, 172.3, 169.4, 144.8, 138.6, 138.3, 138.2, 137.9, 133.3, 133.1, 130.5, 130.1, 130.0, 129.60, 129.58, 129.5, 129.4, 128.5, 127.91, 127.87, 127.8, 126.7, 125.9, 124.7, 122.7, 120.0, 119.5, 112.5, 111.2, 68.9, 68.0, 62.2, 60.8, 59.0, 58.70, 58.68, 57.34, 56.9, 55.7, 55.5, 54.6, 51.9, 49.6, 43.2, 41.0, 40.9, 40.7, 40.6, 38.18, 38.15, 38.12, 38.1, 37.9, 33.3, 33.0, 32.9, 30.8, 30.7, 30.4, 30.3, 29.1, 28.2, 28.1, 27.72, 27.67, 26.9, 23.9, 23.7, 23.6, 22.4, 20.7, 14.4.
HR-ESI-MS $[M+2H]^{2+}$: calculated for $C_{81}H_{104}N_{18}O_{17}^{2+}$ *m/z* 800.3908, found *m/z* 800.3939.
HRMS (ESI) *m/z* $[M+H]^+$ Calcd for $C_{81}H_{103}N_{18}O_{17}^+$ 1599.7743; Found 1599.7705.
Note: gTOCSY analysis supports at least one signal obscured by the water residual in the ^{1}H NMR spectrum that correlates to another signal integrating to 2H. The corresponding chemical shifts are suggestive of the α- and β-protons of a single residue; consequently, our tabulated spectrum assumes a 1H integration for this obscured peak. We also note that this material appears to be unstable to storage in solution. Upon standing in MeCN/H_2O for a few days, LC-HRMS analysis reveals the formation of a new species with a slightly different retention time and *m/z* values consistent with $[M+H+O_2]^+$.

Peptide **CP5**: Qui-cyclo[**βk**-Lys-Lys-Lys-Tyr-**Kyn**]-Asp-Tyr-Lys-Asp-Asp-Asp-Asp-Lys-COOH (5.5 x TFA)



LP5 (1.26 mg, 0.69 μmol, 1 equiv) in MeCN (3.4 mL, ~200 μM in **LP5**) was added to a microwave vial (2-5mL) equipped with a magnetic stir bar and $Yb(OTf)_3$ (10.6 mg, 17.2 μmol) was added. The vessel was heated at 60 °C in an oil bath for 48 h under N_2 and the solvent

removed by rotary evaporation. The crude product was resuspended in 20% MeCN in H_2O containing 0.1% TFA and purified by HPLC (see **VI.F**) to afford **CP5** (1.0 mg, 79%).

HPLC purification: Linear gradient of 5% to 20% Solvent B in Solvent A over 22 minutes.
Isolated Yield: 79%
HR-ESI-MS $[M+3H]^{3+}$: calculated for $C_{82}H_{118}N_{19}O_{27}^{3+}$ *m/z* 600.2810, found *m/z* 600.2801.
HRMS (ESI) *m/z* $[M+2H]^{2+}$ Calcd for $C_{82}H_{117}N_{19}O_{27}^{2+}$ 899.9178; Found 899.9167.

B. Note on evidence for monomeric macrocyclization

Comparing the linear and cyclic peptide NMRs, we draw out two diagnostic observations:

- In the case of **CP4** vs. **LP4**, the ^1H NMR and corresponding ^1H-^1H correlation spectra (COSY and TOCSY-type spectra) of the cyclic peptide **CP4** reveal the appearance of a set of correlated signals totalling to 4H that are shifted downfield relative to the linear congener **LP4**, *when compared in the same solvent* (**Supplementary Fig. 21**).
    - This is also apparent in the case of **LP1/CP1, LP2/CP2** and **LP3/CP3**.
- The $^{13}C\{^1H\}$ spectrum of **CP4** shows the disappearance of two ketone signals which were present in the corresponding **LP4** spectrum (**Supplementary Fig. 21**).
    - These signals also disappear in the case of **LP1/CP1** and **LP2/CP2**. We were not able to obtain a sufficient $^{13}C\{^1H\}$ NMR spectrum of **CP3** to assess disappearance in the case of **LP3/CP3**.

Thus, the macrocyclization events are consistent with the available NMR data, as well as chromatographic and mass spectrometric evidence (see **Supplementary Fig. 14-15** and **17-25** and **27**).

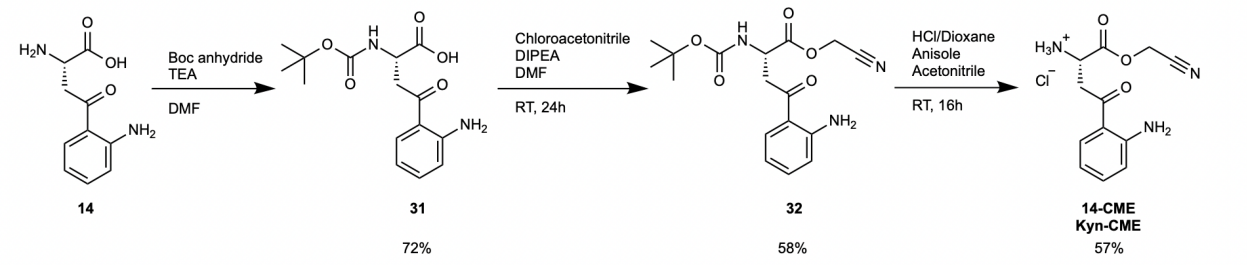
To further bolster the mass spectrometric evidence, two independent sources conducted HRMS and MALDI-TOF analysis of the cyclic peptides. In both cases, mass spectrometric analysis suggests that the isolated products **CP1-5** exist predominantly as cyclic monomers (that is, as drawn). In some cases, HRMS(ESI) reveals the desired product *m/z* is accompanied by *m/z* values corresponding to the cyclic dimer and/or cyclic monomer. As these values are not present in the corresponding MALDI-TOF data, we assert that these higher-order oligomers are an insignificant component of the isolated material.
Note: We were not able to complete a MALDI-TOF replicate for **CP4**, owing to its spontaneous conversion to an oxidized product (*vide supra*).

C. Small-scale Friedländer macrocyclization reactions

The small-scale Friedländer reactions summarized in **Supplementary Figure 24** were performed as follows. Prior to cyclization, 1 mM stock solutions of **LP1-4** were prepared in 50% MeCN in H_2O. The stock solution was dispensed into 200 µL PCR tubes, flash-frozen, and lyophilized. The resulting dry peptide stocks were resuspended in the requisite reaction medium

containing catalyst and incubated. All test reactions were performed at a 5 nmol scale (100 µM peptide, 50 µL scale) and heated on a thermocycler. For time course measurements, the reactions were performed in triplicate. At each timepoint, 2 µL of each sample (6 µL total) was combined into a single LC-MS vial and diluted with 54 µL of MeCN/H_2O. 4 µL were then injected into the LC-HRMS. Timepoints were taken at 0, 1, 3, 8, and 24 h.

Synthesis of kynurenine cyanomethylester (Kyn-CME)



Boc-Kyn-OH (**31**)

L-Kynurenine (**14**, 60.0 mg, 0.29 mmol, 1 equiv) and Boc anhydride (94.3 mg, 0.43 mmol, 1.5 equiv) were dissolved in anhydrous DMF (1.2 mL) under N_2, and triethylamine (40 µL, 0.29 mmol, 1 equiv) was added. The reaction was stirred at RT for 30 min, neutralized with 1.0 M HCl to pH 4, then extracted twice with EtOAc. The combined organic extracts were washed twice with water and three times with brine, then dried over Na_2SO_4, filtered, and concentrated under reduced pressure. The oil was re-suspended in EtOAc, adsorbed onto SiO_2, then purified by automated flash column chromatography (0-50% EtOAc/hexanes) to provide the title compound as a yellow solid (65.7 mg, 74% yield). **^{1}H NMR** (500 MHz, DMSO-d_6, mixture of rotamers [~6.2:1] at 25 °C) δ 12.56 (s, 1H), 7.70 (dd, J = 8.3, 1.6 Hz, 1H), 7.30 – 7.06 (m, 3H), 6.96 – 6.59 (m, 2H), 6.53 (t, J = 7.6 Hz, 1H), 4.46 (td, J = 7.8, 4.7 Hz, 1H), 3.48 – 3.17 (m, exp. 2H, obs. 10H; overlapping with H_2O), 1.37 (s, 9H). **^{13}C{^{1}H} NMR** (126 MHz, DMSO-d_6) δ 198.3, 173.6, 155.2, 151.2, 134.3, 131.2, 116.9, 116.3, 114.4, 78.1, 49.5, 28.2.
The spectral data is in accord with the partial literature characterization[27].
Note: One of the expected ^{13}C{^{1}H} NMR signals is presumably obscured by the solvent residual.

Boc-Kyn-CME (**32**)

Boc-Kyn-OH (**31**, 57.7 mg, 0.19 mmol, 1 equiv) was dissolved in anhydrous MeCN (0.5 mL), and chloroacetonitrile (84 µL, 0.94 mmol, 5 equiv) was added to the solution under nitrogen. DIPEA (35 µL, 0.37 mmol, 2 equiv) was added and the reaction was stirred at RT for 16 h. The crude reaction mixture was concentrated under reduced pressure and resuspended in EtOAc.

Silica was added and the solvent was removed under reduced pressure. The crude product was purified by normal phase automated flash column chromatography (0-30% EtOAc/hexanes) to provide the title compound (62.7 mg, 63% yield). **^{1}H NMR** (500 MHz, DMSO-d_6, mixture of rotamers [~4.9:1] at 25 °C) δ 7.68 (d, *J* = 8.1 Hz, 1H), 7.36 – 6.96 (m, 4H), 6.76 (d, *J* = 8.4 Hz, 1H), 6.54 (t, *J* = 7.6 Hz, 1H), 5.01 (s, 2H), 4.67 – 4.44 (m, 1H), 3.52 – 3.33 (m, 2H), 1.39 (s, 9H). **^{13}C{^{1}H} NMR** (126 MHz, DMSO-d_6) δ 197.5, 171.4, 155.2, 151.3, 134.5, 131.2, 117.0, 116.1, 115.8, 114.5, 78.6, 49.5, 49.2, 28.1.
Note: One of the expected ^{13}C{^{1}H} NMR signals is presumably obscured by the solvent residual.

Cyanomethyl (S)-2-amino-4-(2-aminophenyl)-4-oxobutanoate•HCl (**Kyn-CME**)

Boc-Kyn-CME (**32**, 40.0 mg, 0.11 mmol, 1.0 equiv), was dissolved in MeCN (0.5 mL) with anisole (6.25 µL, 57 nmol, 0.5 equiv). To this solution was added 4 M HCl in dioxane (57 µL, 0.23 mmol, 2.1 equiv) and the solution was stirred for 2 h at RT, at which point LC-MS indicated that the reaction was complete. 5 mL of diethyl ether was added to precipitate the product. Sonication was performed to avoid clumps. The sample was centrifuged at 3000 x G for 5 min and the supernatant decanted. Another 5 mL of diethyl ether was added and the sample sonicated. The sample was centrifuged at 3000 x G for 5 min and the supernatant decanted. The precipitant was then dried under vacuum to provide the title compound as a yellow solid. (25 mg, 77% yield). **^{1}H NMR** (500 MHz, DMSO-d_6) δ 8.68 (s, 3H), 7.70 (dd, *J* = 8.4, 1.5 Hz, 1H), 7.30 (ddd, *J* = 8.4, 6.9, 1.5 Hz, 1H), 6.80 (dd, *J* = 8.5, 1.2 Hz, 1H), 6.58 (ddd, *J* = 8.1, 6.9, 1.2 Hz, 1H), 5.12 (s, 2H), 4.55 (d, *J* = 5.2 Hz, 1H), 3.84 – 3.69 (m, exp. 2H, obs. 4H; overlapping with H_2O). **^{13}C{^{1}H} NMR** (126 MHz, DMSO-d_6) δ 196.5, 168.7, 151.5, 135.1, 131.1, 117.1, 115.3, 115.1, 114.7, 50.1, 47.7, 38.8. **HR-ESI-MS** $[M+H]^+$: calculated for $C_{12}H_{14}N_3O_3^+$ *m/z* 248.1030, found *m/z* 248.1039.
Note: Kyn-CME could not be fully liberated from minor impurities, providing the compound in up to 93% purity (via ^{1}H NMR integration). The reported yield is uncorrected.

IVT of peptide containing monomer 2 and Kyn

In vitro transcription/translation of the FLAG tag-containing peptide **Met**-Lys-Lys-Lys-Tyr-**Ser**-Asp-Tyr-Lys-Asp-Asp-Asp-Asp-Lys-COOH (**M**KKKY**S**-flag), where **Met** was replaced with **2** and **Ser** was replaced with **Kyn,** was performed as described above with slight modifications. In this case, the IVT reaction mixture (12.5 µL) contained Solution A (ΔtRNA, Δaa; 2.5 µL), amino acid stock mix (1.25 µL; 3.3 mM L-aspartic acid, 3.3 mM L-tyrosine, 3.3 mM L-lysine, +/- 3.3 mM L-methionine, +/- 3.3 mM L-serine), tRNA solution (1.25 µL), Solution B (3.75 µL), and 250 ng dsDNA **M**KKKY**S**DYKDDDDK template (0.5 µL). For reprogramming of the methionine AUG codon, methionine was excluded from the solution and $tRNA^{fMet}$ acylated with **2** (750 pmol in 1.625 µL) was included. For reprogramming of the serine GCU codon, serine was excluded from the solution and $tRNA^{AsnE2\ \#2}$ acylated with **Kyn** in solution with M5-1 suppressor RNA (750

pmol $tRNA^{AsnE2\ \#2}$ and 125 pmol of M5-1 together in 1.625 µL). The reaction solution was brought to a final volume of 12.5 µL with water. The reactions were incubated in a thermocycler (BioRad C1000 Touch™) at 37 °C for 2 h and quenched by placement on ice. Peptides were purified by anti-FLAG beads and analyzed by LC-HRMS as outlined above (**VI.G.**).

Friedländer macrocyclization of linear peptide LP5 generated using IVT

These methods provide details related to the experiments presented in **Figure 5f** and **Supplementary Figure 27**. Following IVT of linear peptide **LP5** and purification by anti-FLAG magnetic beads, the solution containing the peptide was flash-frozen and lyophilized in a PCR tube. To the dry peptide was added 20 µL of 100 mM $Yb(OTf)_3$ in MeCN. The solution was sonicated to resuspend the peptide and the PCR tube was incubated at 40 °C for 24 h. 40 µL of H_2O was then added, and the solution was flash-frozen and lyophilized again. The product was dissolved in 20 µL of 0.1 M glycine-HCl pH 2.8 and analyzed by LC-HRMS as described above (**VI.G.**, Peptide analysis by LC-MS). Ion extraction in **Figure 5f** for the linear peptide was set to sum the values of 459.46740, 459.7179, 459.9683, 612.28640, 612.62133, and 612.95484, while for the cyclic peptide it was the sum of 450.46270, 450.7136, 450.9640, 600.2810, 600,6150, and 600.9499. These are the three largest expected peaks in the two major charge state envelopes for each.

References:

1. Ad, O. *et al.* Translation of Diverse Aramid- and 1,3-Dicarbonyl-peptides by Wild Type Ribosomes *in Vitro*. *ACS Cent. Sci.* **5**, 1289–1294 (2019).
2. Lee, J. *et al.* Ribosome-mediated biosynthesis of pyridazinone oligomers in vitro. *Nat. Commun.* **13**, 6322 (2022).
3. Narayanan, B. C. *et al.* Structure and Function of PA4872 from Pseudomonas aeruginosa, a Novel Class of Oxaloacetate Decarboxylase from the PEP Mutase/Isocitrate Lyase Superfamily,. *Biochemistry* **47**, 167–182 (2008).
4. Braga, R., Hecquet, L. & Blonski, C. Slow-binding inhibition of 2-keto-3-deoxy-6-phosphogluconate (KDPG) aldolase. *Bioorg. Med. Chem.* **12**, 2965–2972 (2004).
5. Foley, L. H. Investigation of the formation of methyl 2-cyano-2-[(trimethylsilyl)oxy]-4-oxopentanoate from methyl 2,4-dioxopentanoate. A clarification of the pathway for the reaction of trimethylsilyl cyanide with enolized .beta.-diketones. *J. Org. Chem.* **50**, 5204–

5209 (1985).

6. Goto, Y. & Suga, H. Flexizymes as a tRNA Acylation Tool Facilitating Genetic Code Reprogramming. in *Ribozymes: Methods and Protocols* (ed. Hartig, J. S.) 465–478 (Humana Press, Totowa, NJ, 2012). doi:10.1007/978-1-61779-545-9_29.
7. Fujino, T., Goto, Y., Suga, H. & Murakami, H. Ribosomal Synthesis of Peptides with Multiple β-Amino Acids. *J. Am. Chem. Soc.* **138**, 1962–1969 (2016).
8. Fricke, R., Knudson, I. & Schepartz, A. Direct, quantitative, and comprehensive analysis of tRNA acylation using intact tRNA liquid-chromatography mass-spectrometry. 2023.07.14.549096 Preprint at https://doi.org/10.1101/2023.07.14.549096 (2023).
9. Fricke, R. *et al. Orthogonal Synthetases for Polyketide Precursors*. http://biorxiv.org/lookup/doi/10.1101/2022.02.28.482149 (2022) doi:10.1101/2022.02.28.482149.
10. Kibbe, W. A. OligoCalc: an online oligonucleotide properties calculator. *Nucleic Acids Res.* **35**, W43–W46 (2007).
11. Vong, K., Yamamoto, T., Chang, T. & Tanaka, K. Bioorthogonal release of anticancer drugs via gold-triggered 2-alkynylbenzamide cyclization. *Chem. Sci.* **11**, 10928–10933 (2020).
12. Sharma, R. K. & Jain, R. Unprecedented 1,1′-Carbonyldiimidazole-Mediated Amidation of -Unprotected α-Amino Acids in Water. *Synlett* **2007**, 603–606 (2007).
13. Gama, F. H. S., Souza, R. O. M. A. de & Garden, S. J. An efficient green protocol for the preparation of acetoacetamides and application of the methodology to a one-pot synthesis of Biginelli dihydropyrimidines. Expansion of dihydropyrimidine topological chemical space. *RSC Adv.* **5**, 70915–70928 (2015).
14. Kato, T. & Sato, M. Studies on Ketene and Its Derivatives. LI. Reaction of α-Aminoamide with Diketene. *Yakugaku Zasshi* **92**, 1507–1514 (1972).
15. Zhang, P., Yang, L., Chen, W., Liu, M. & Wu, H. Synthesis of [1,4]Thiazino[4,3-a]indol-10-one Derivatives through Radical Anti Aza-Michael Addition of 2′-Aminochalcones. *Org. Lett.*

23, 6094–6098 (2021).

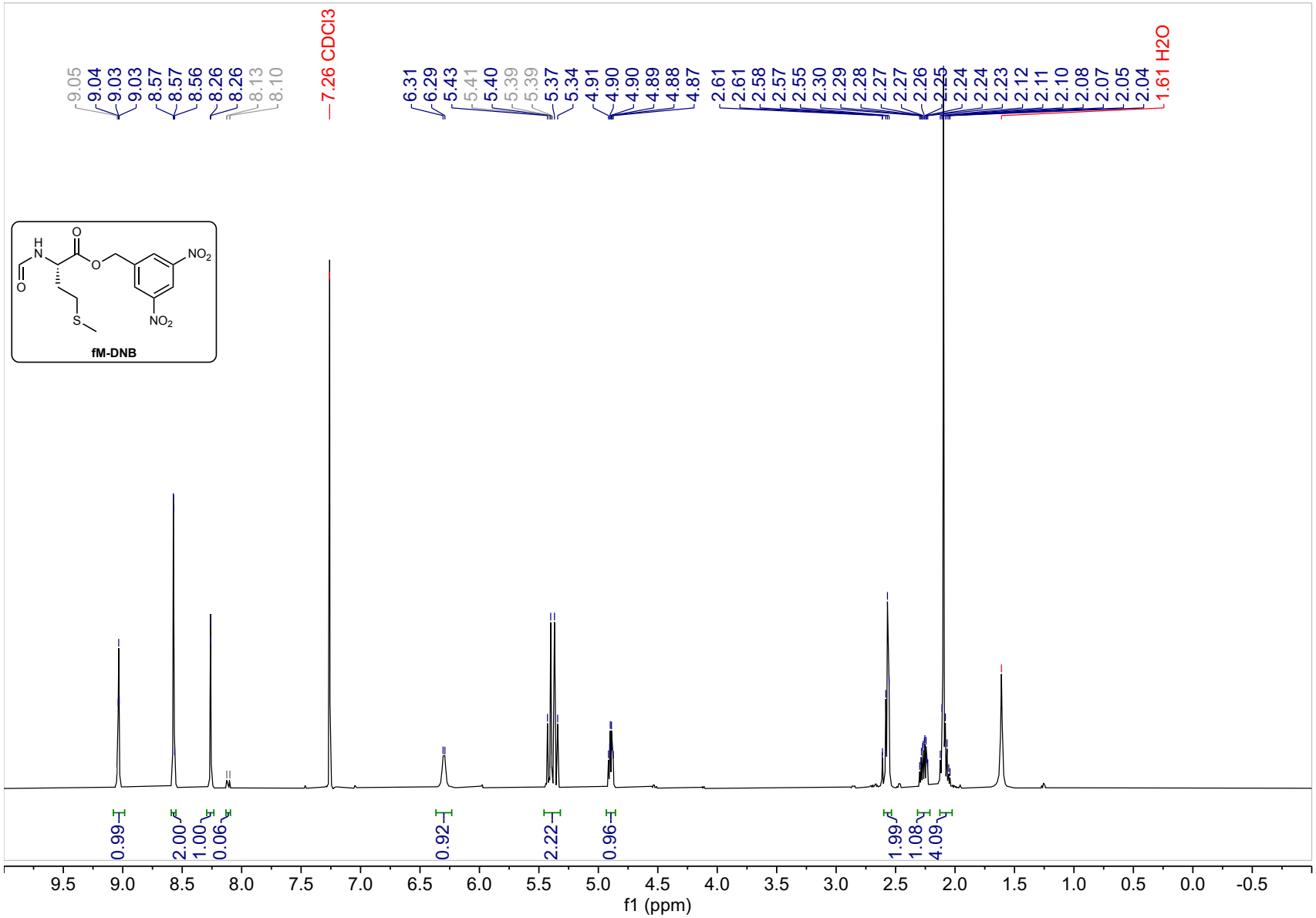
16. Garcia, M. A. R. *et al.* Design, synthesis and antibacterial activity of chalcones against MSSA and MRSA planktonic cells and biofilms. *Bioorganic Chem.* **116**, 105279 (2021).
17. Bera, S. K., Maharana, R. R., Samanta, K. & Mal, P. CBr4 catalyzed activation of α,β-unsaturated ketones. *Org. Biomol. Chem.* **20**, 7085–7091 (2022).
18. Santos, M. B. *et al.* Antiproliferative and pro-apoptotic activities of 2′- and 4′-aminochalcones against tumor canine cells. *Eur. J. Med. Chem.* **138**, 884–889 (2017).
19. Augustine, J. K., Bombrun, A. & Venkatachaliah, S. An efficient catalytic method for the Friedländer annulation mediated by peptide coupling agent propylphosphonic anhydride (T3P®). *Tetrahedron Lett.* **52**, 6814–6818 (2011).
20. Zhang, X.-L., Hu, Q.-S., Sheng, S.-R., Xiao, C. & Cai, M.-Z. Microwave-assisted Friedländer Synthesis of Polysubstituted Quinolines Based on Poly(ethylene glycol) Bound Acetoacetate. *J. Chin. Chem. Soc.* **58**, 18–23 (2011).
21. Nammalwar, B., Murie, M., Fortenberry, C. & Bunce, R. A. Quinoline- and 1,8-naphthyridine-3-carboxylic acids using a self-catalyzed Friedländer approach. *Tetrahedron Lett.* **55**, 3181–3183 (2014).
22. Muscia, G. C., Bollini, M., Carnevale, J. P., Bruno, A. M. & Asís, S. E. Microwave-assisted Friedländer synthesis of quinolines derivatives as potential antiparasitic agents. *Tetrahedron Lett.* **47**, 8811–8815 (2006).
23. Das, A., Anbu, N., Varalakshmi, P., Dhakshinamoorthy, A. & Biswas, S. A hydrazine functionalized UiO-66(Hf) metal–organic framework for the synthesis of quinolines via Friedländer condensation. *New J. Chem.* **44**, 10982–10988 (2020).
24. Chen, J., Ye, L. & Su, W. Palladium-catalyzed direct addition of arylboronic acids to 2-aminobenzonitrile derivatives: synthesis, biological evaluation and in silico analysis of 2-aminobenzophenones, 7-benzoyl-2-oxoindolines, and 7-benzoylindoles. *Org. Biomol. Chem.* **12**, 8204–8211 (2014).

25. Lundberg, H., Tinnis, F. & Adolfsson, H. Direct Amide Coupling of Non-activated Carboxylic Acids and Amines Catalysed by Zirconium(IV) Chloride. *Chem. – Eur. J.* **18**, 3822–3826 (2012).
26. Sheldrick, G. M. Crystal structure refinement with SHELXL. *Acta Crystallogr. Sect. C Struct. Chem.* **71**, 3–8 (2015).
27. Stewart, F. H. C. Synthesis of L-Kynurenine peptides conducted without masking the side-chain amino group. *Aust. J. Chem.* **33**, 633–640 (1980).

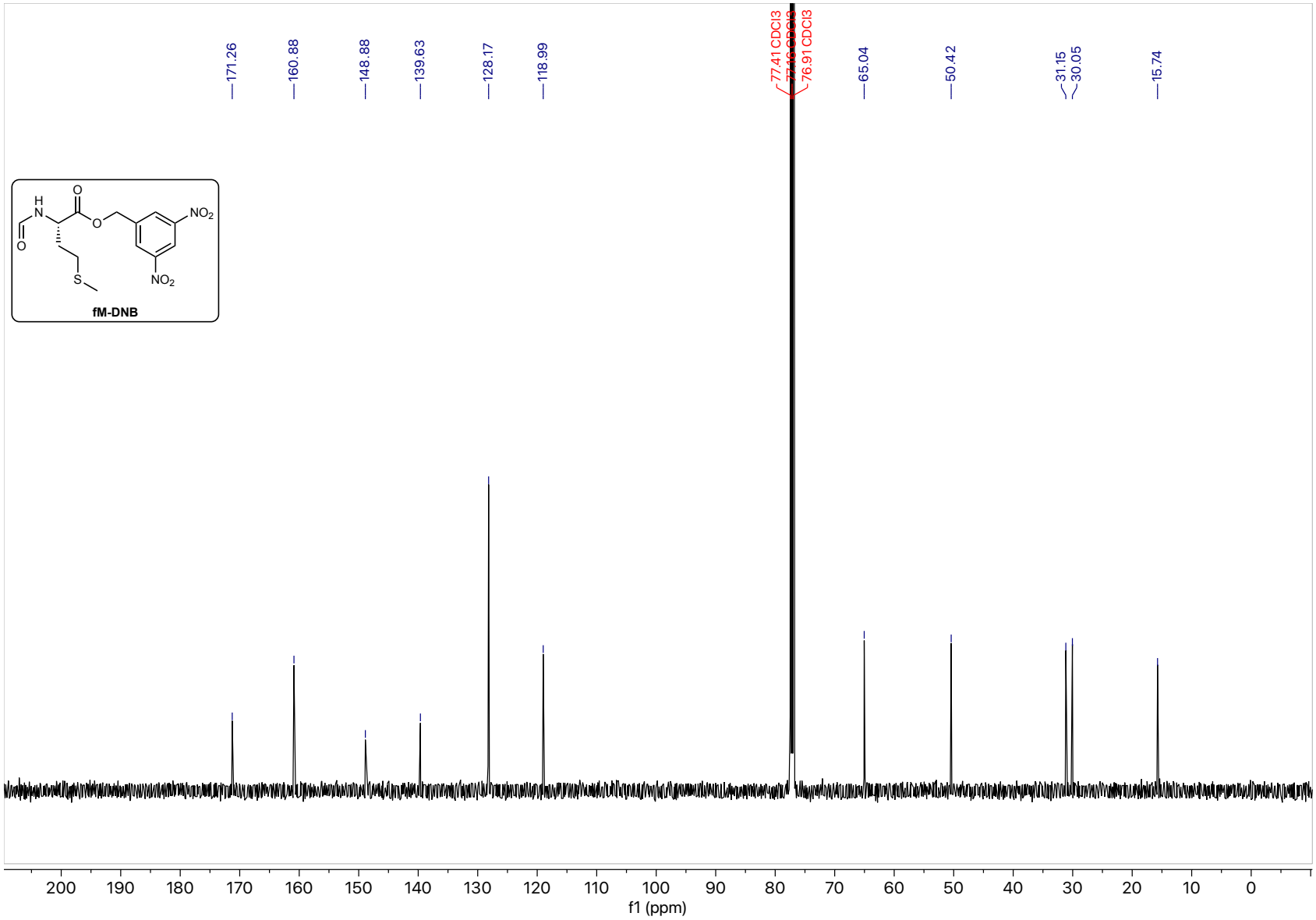
Processed NMR Spectra

- Standard view for ^{1}H NMR is defined as 10 to -1 ppm.
- Extended view for ^{1}H NMR is defined as the full collection range (14 to -2 ppm, 16 to -4 ppm, or 25 to -5 ppm).
- Standard view for $^{13}C\{^{1}H\}$ NMR is defined as 210 to -10 ppm.
- Extended view for $^{13}C\{^{1}H\}$ NMR is defined as the full collection range (235 to -15 ppm or 220 to -20 ppm).

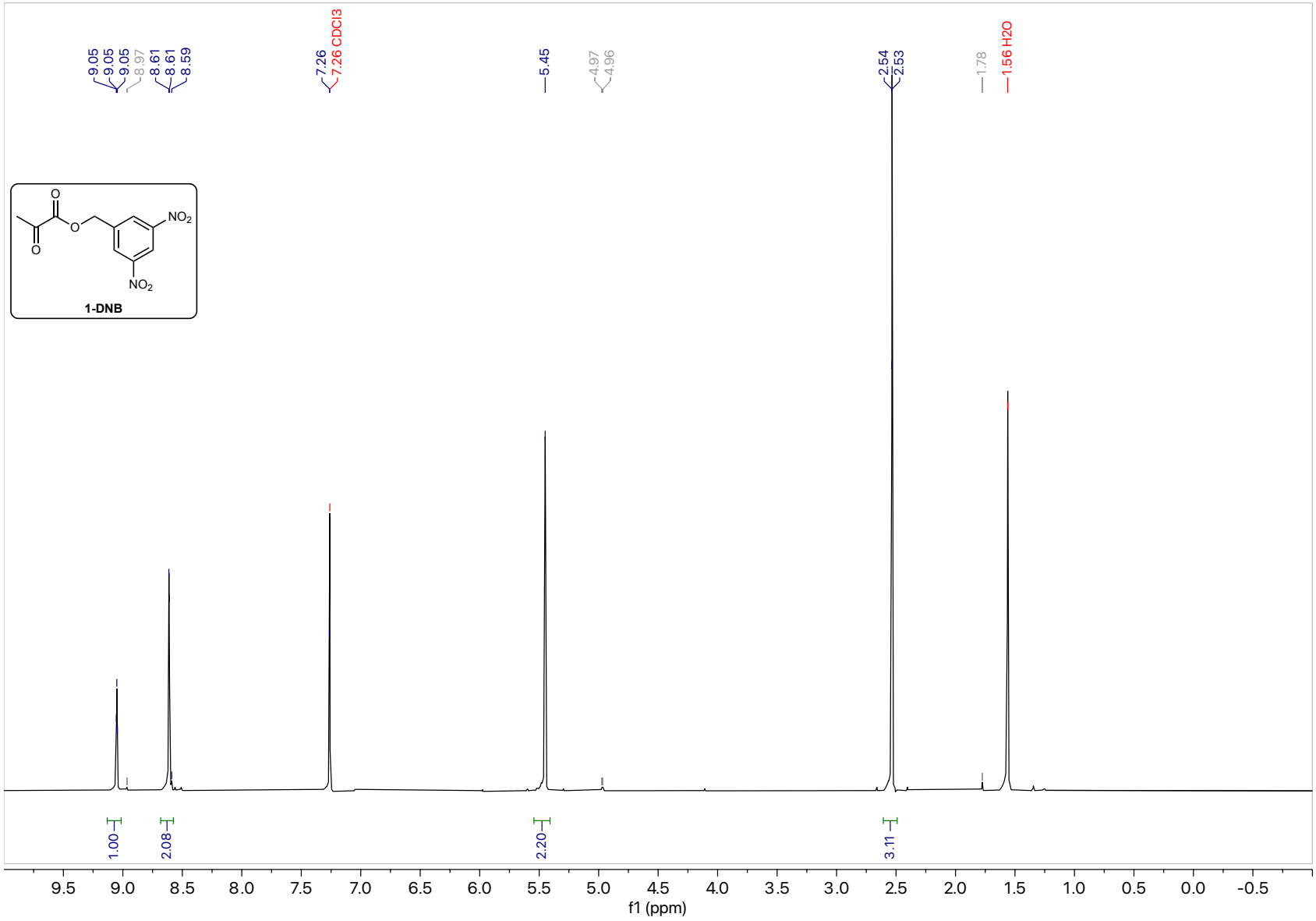
^{1}H NMR (500 MHz, $CDCl_3$) – standard view **(fM-DNB)**



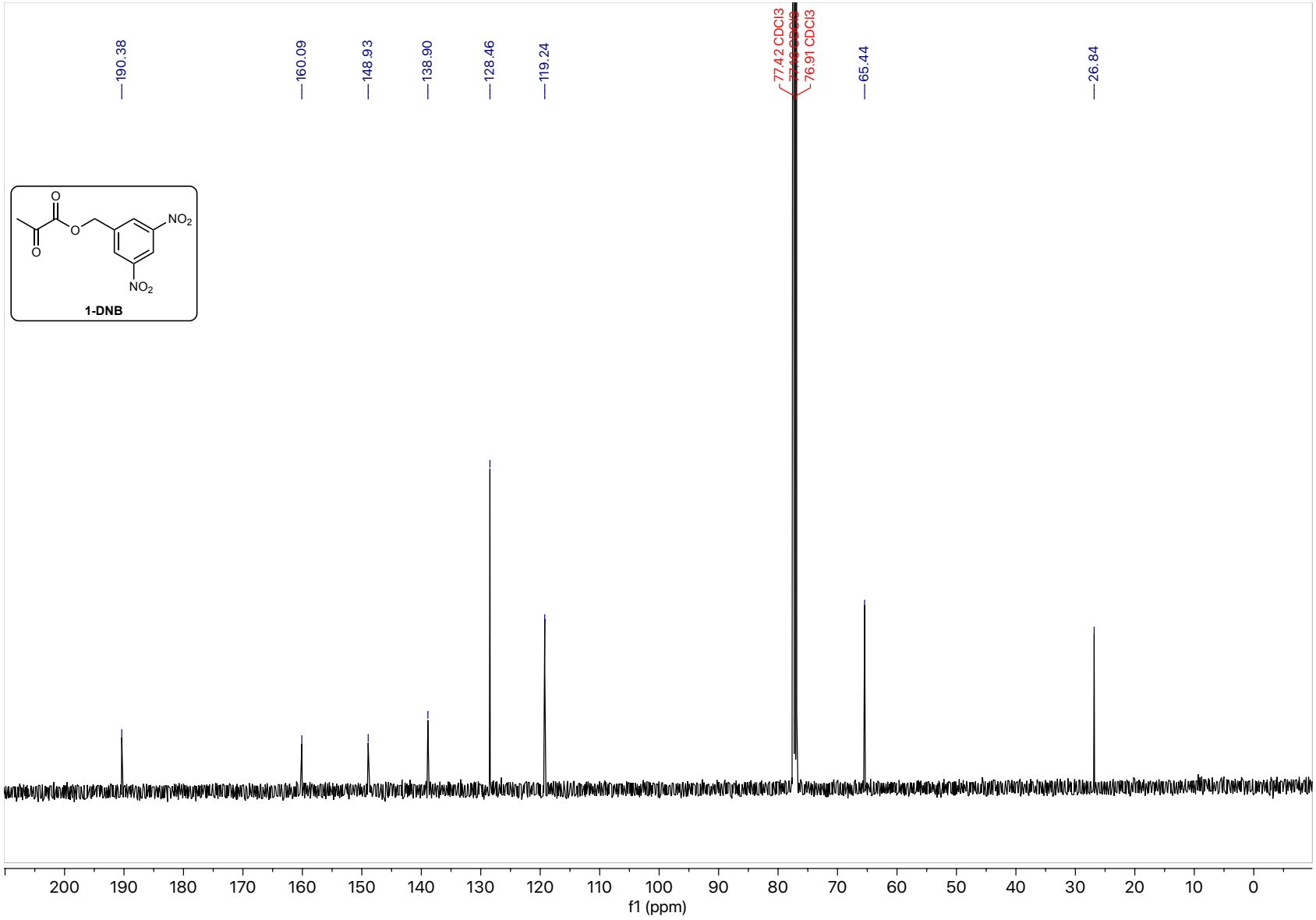
$^{13}C\{^{1}H\}$ NMR (126 MHz, $CDCl_3$) – standard view **(fM-DNB)**



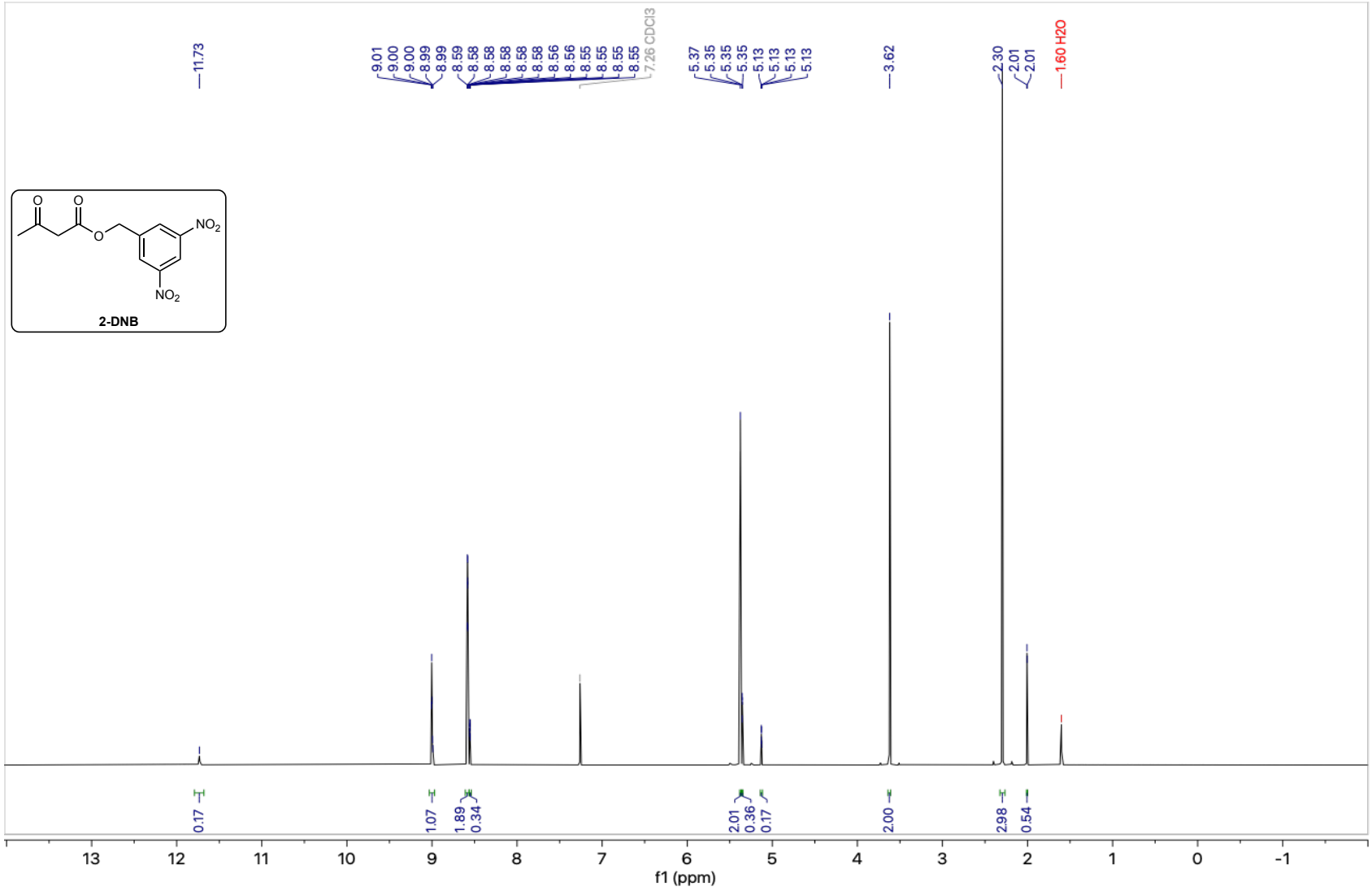
^{1}H NMR (500 MHz, $CDCl_3$) – standard view **(1-DNB)**



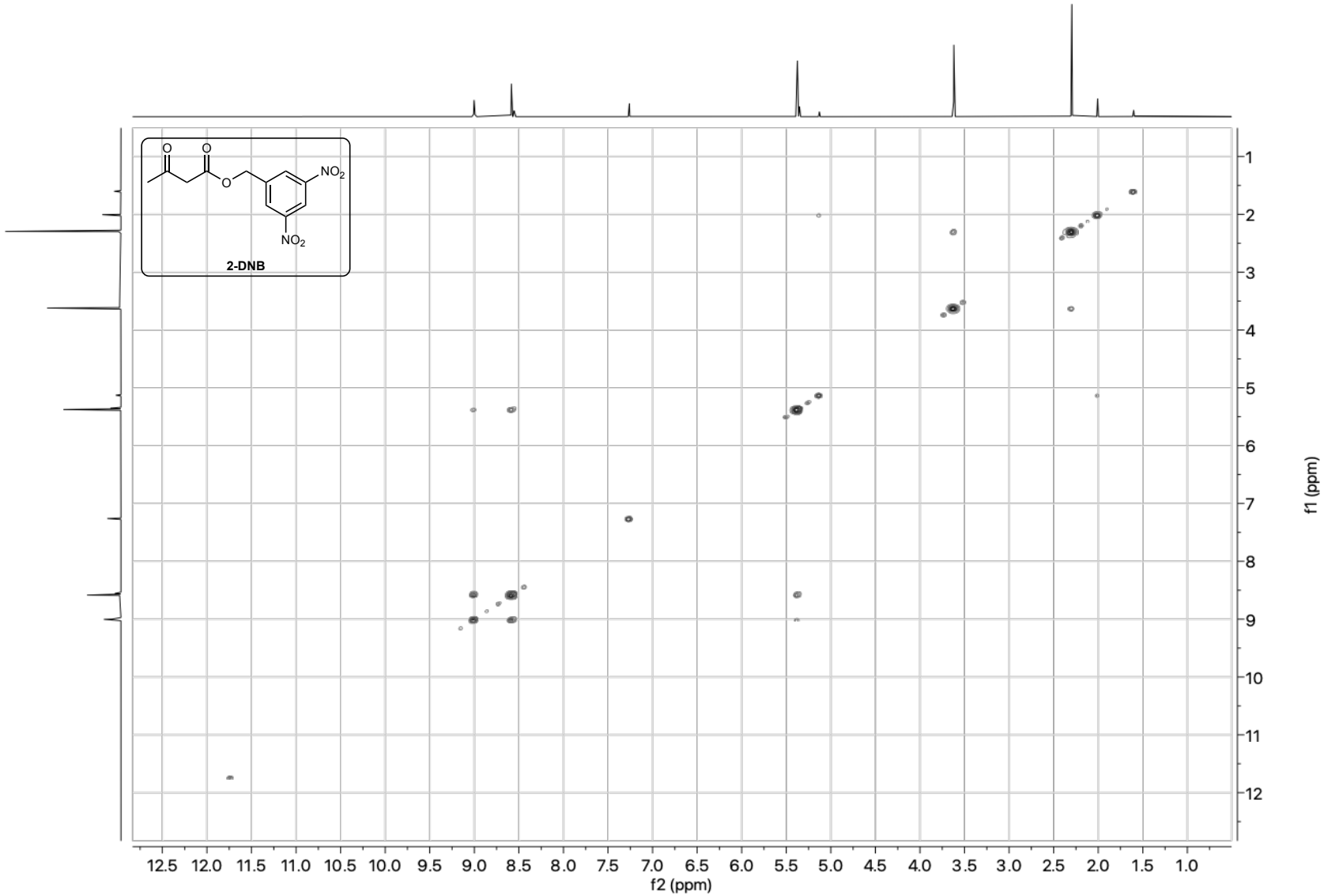
$^{13}C\{^{1}H\}$ NMR (126 MHz, $CDCl_3$) – standard view **(1-DNB)**



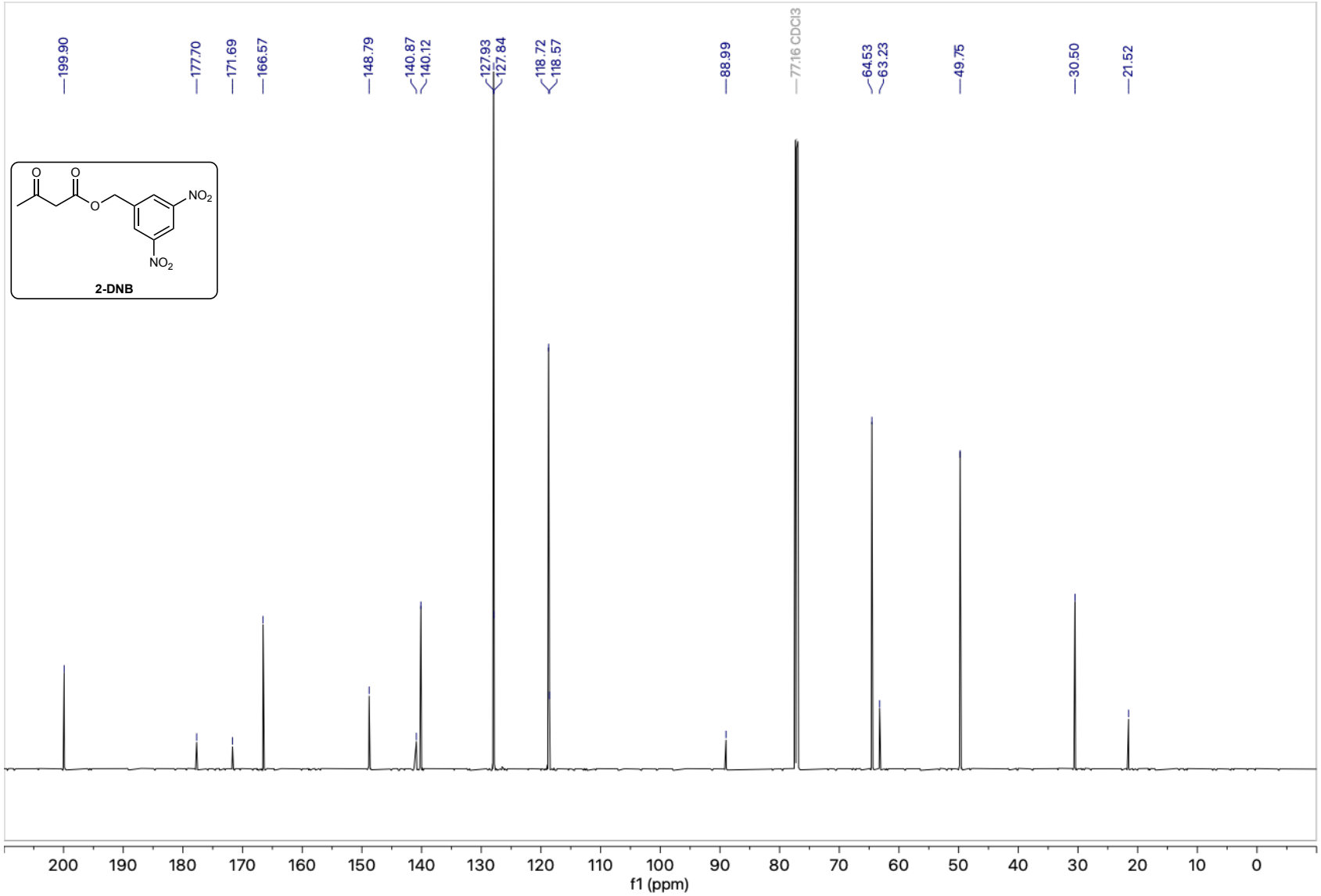
^{1}H NMR (600 MHz, $CDCl_3$) – extended view – mixture of tautomers **(2-DNB)**



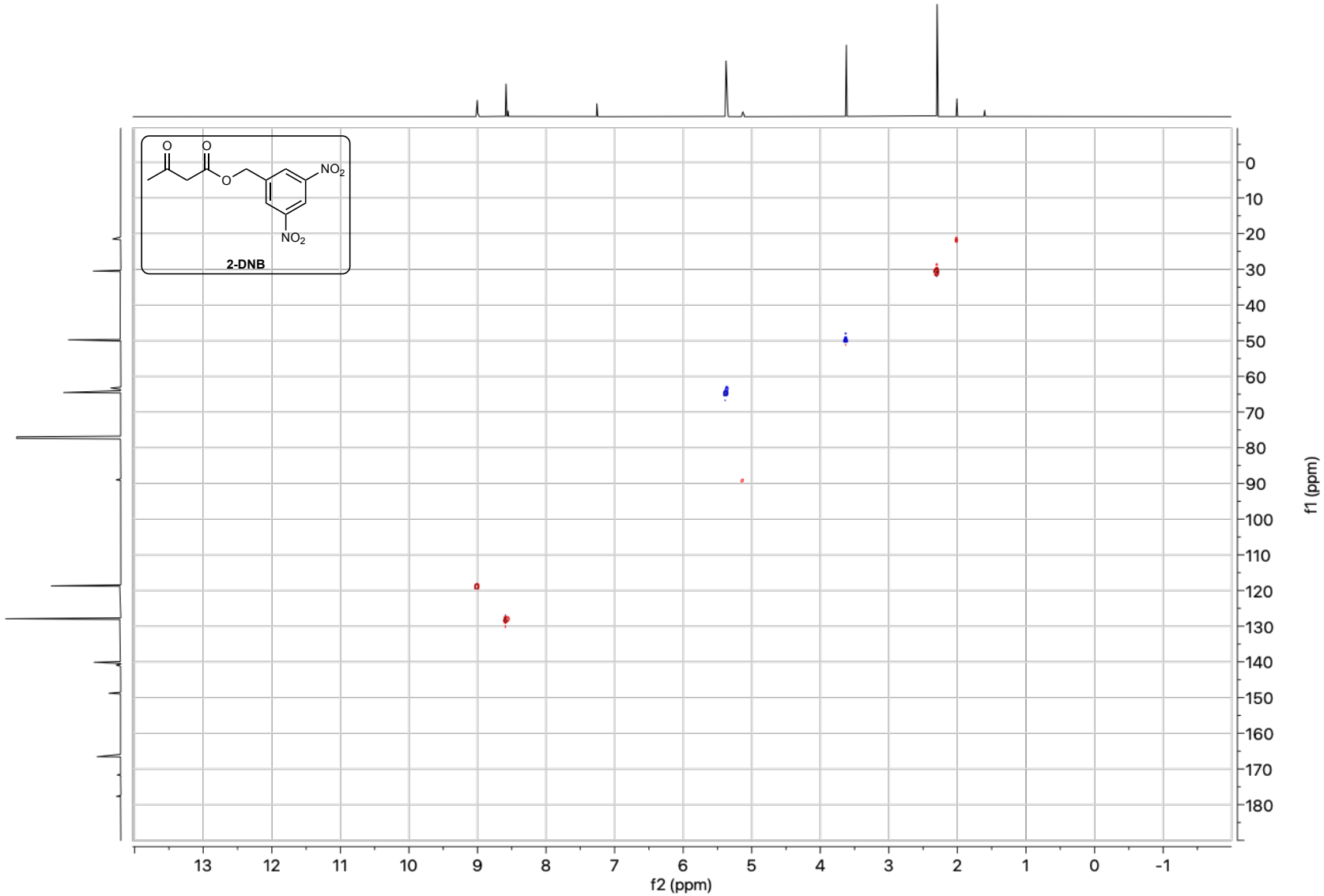
^{1}H-^{1}H gCOSY (600 MHz, $CDCl_3$) – mixture of tautomers **(2-DNB)**



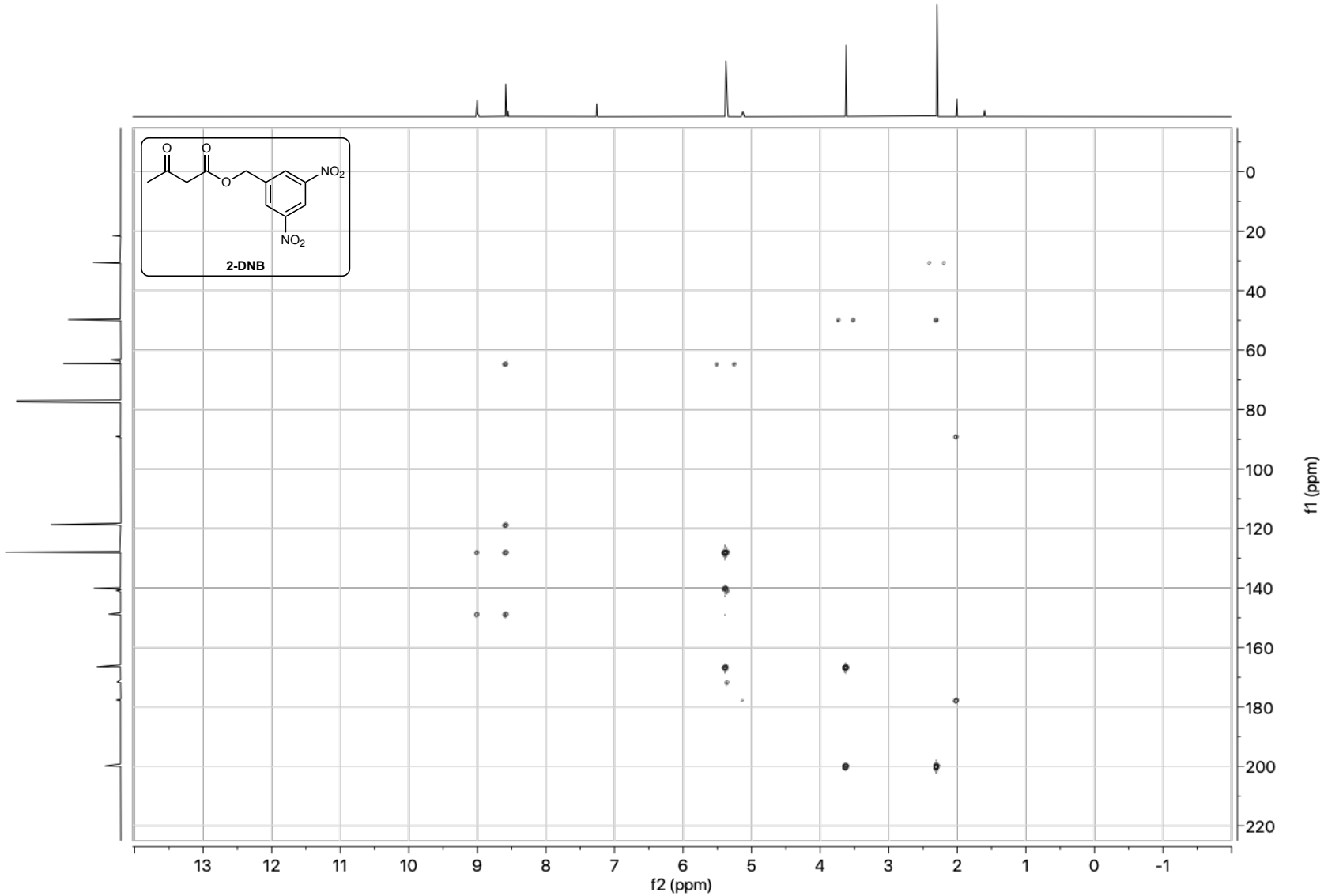
$^{13}C\{^{1}H\}$ NMR (151 MHz, $CDCl_3$) – standard view – mixture of tautomers **(2-DNB)**



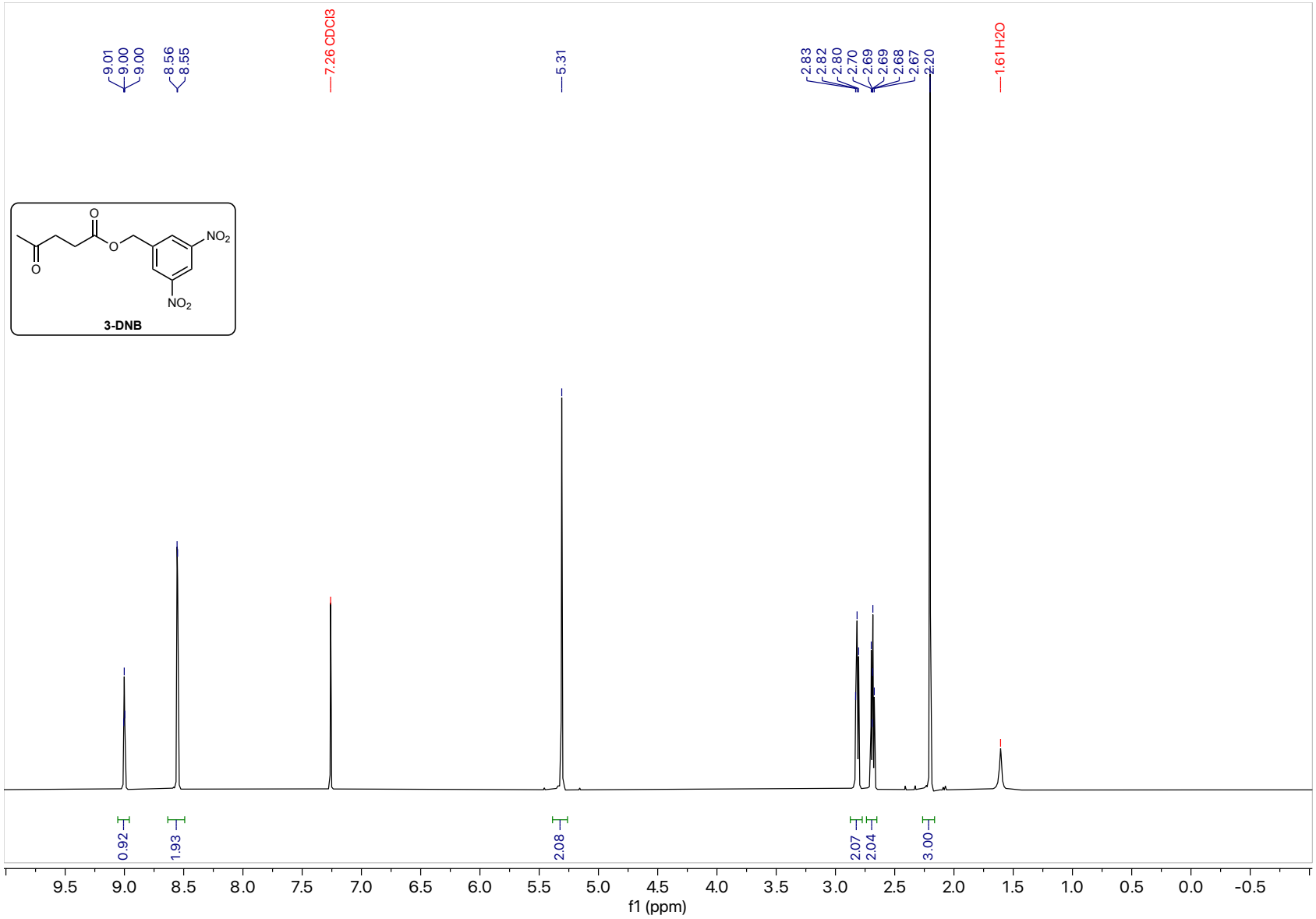
^{1}H-^{13}C gHSQCAD (600(151) MHz, $CDCl_3$) – mixture of tautomers **(2-DNB)**



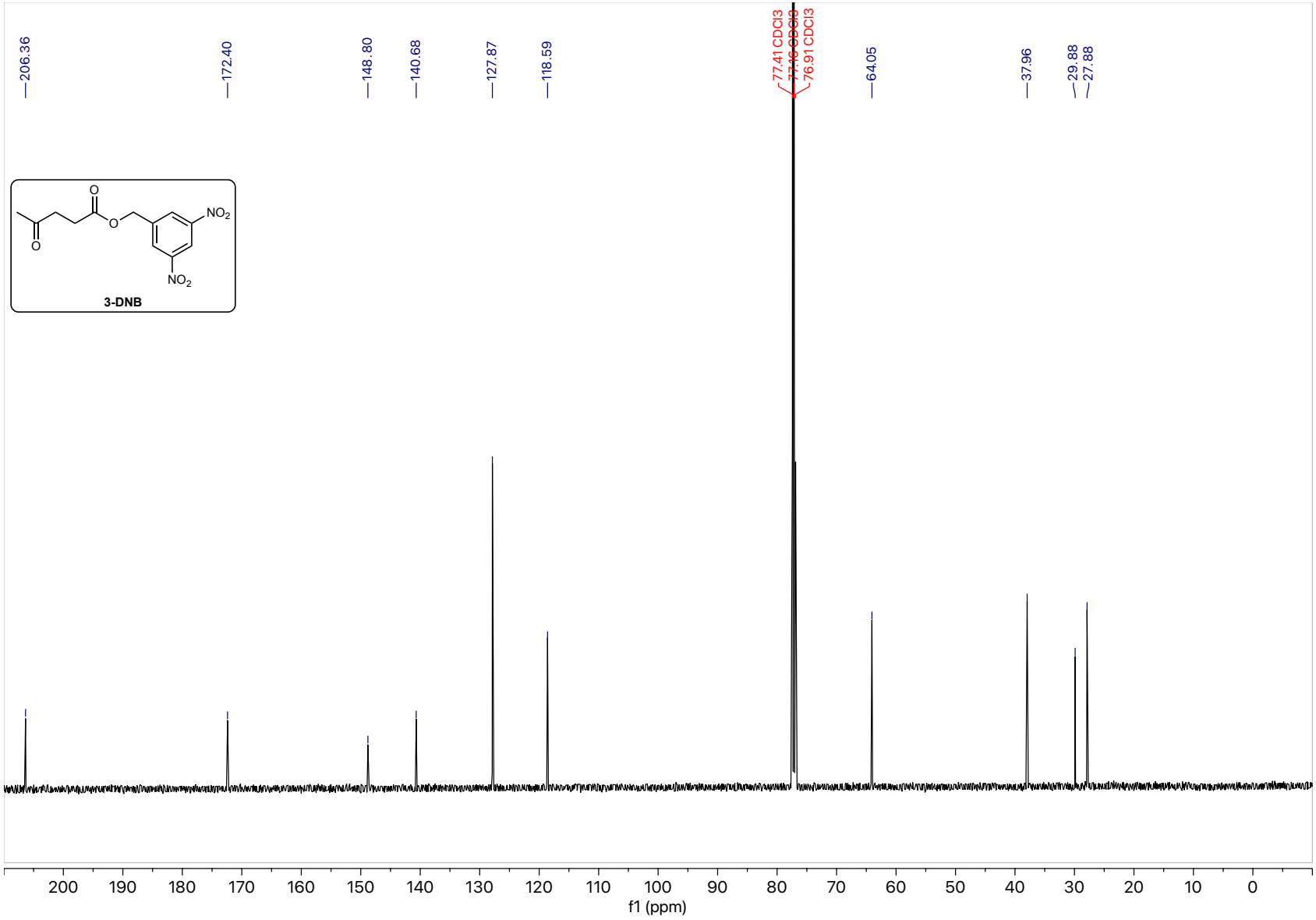
^{1}H-^{13}C gHMBCAD (600(151) MHz, $CDCl_3$) – mixture of tautomers **(2-DNB)**



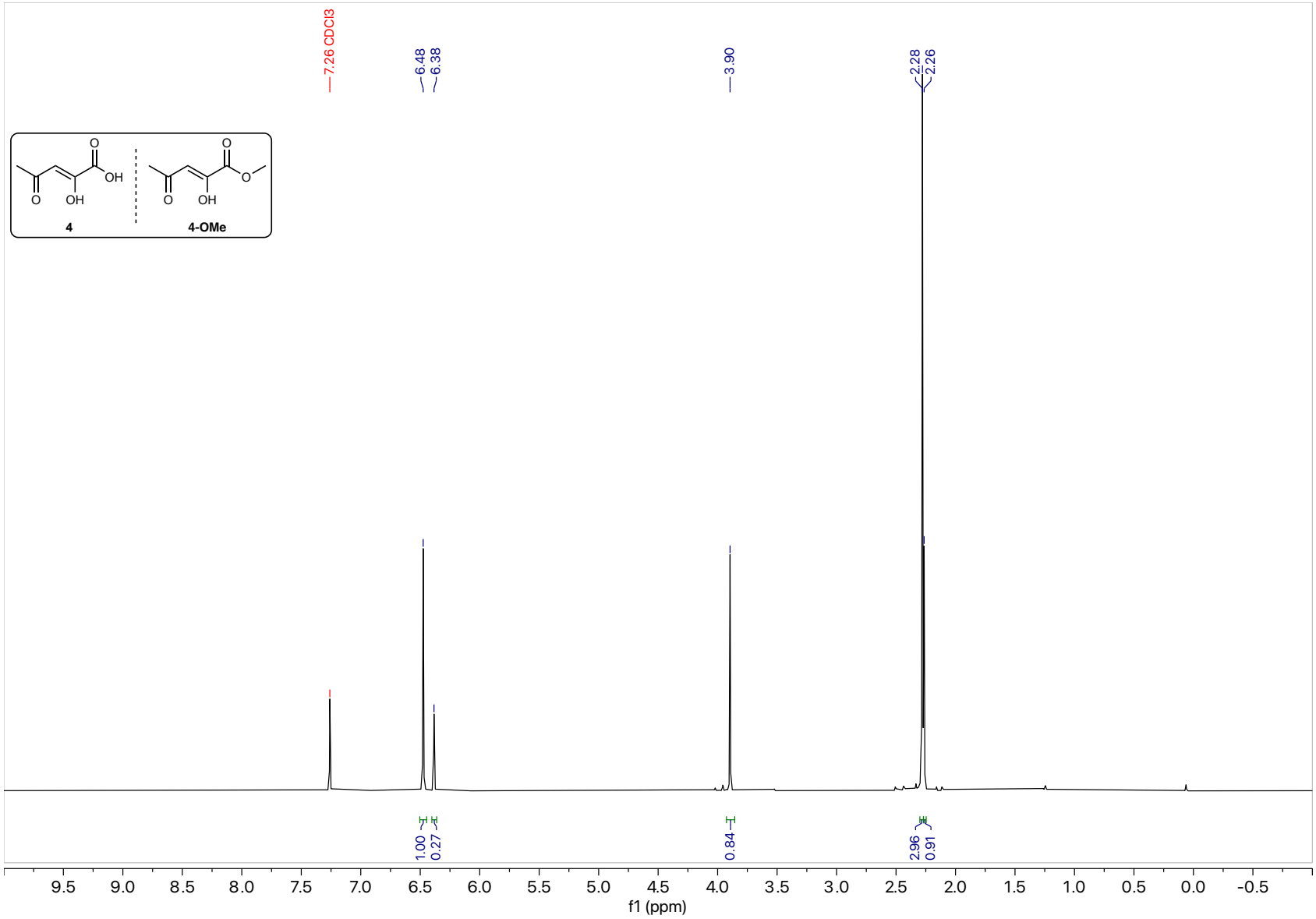
^{1}H NMR (500 MHz, $CDCl_3$) – standard view **(3-DNB)**



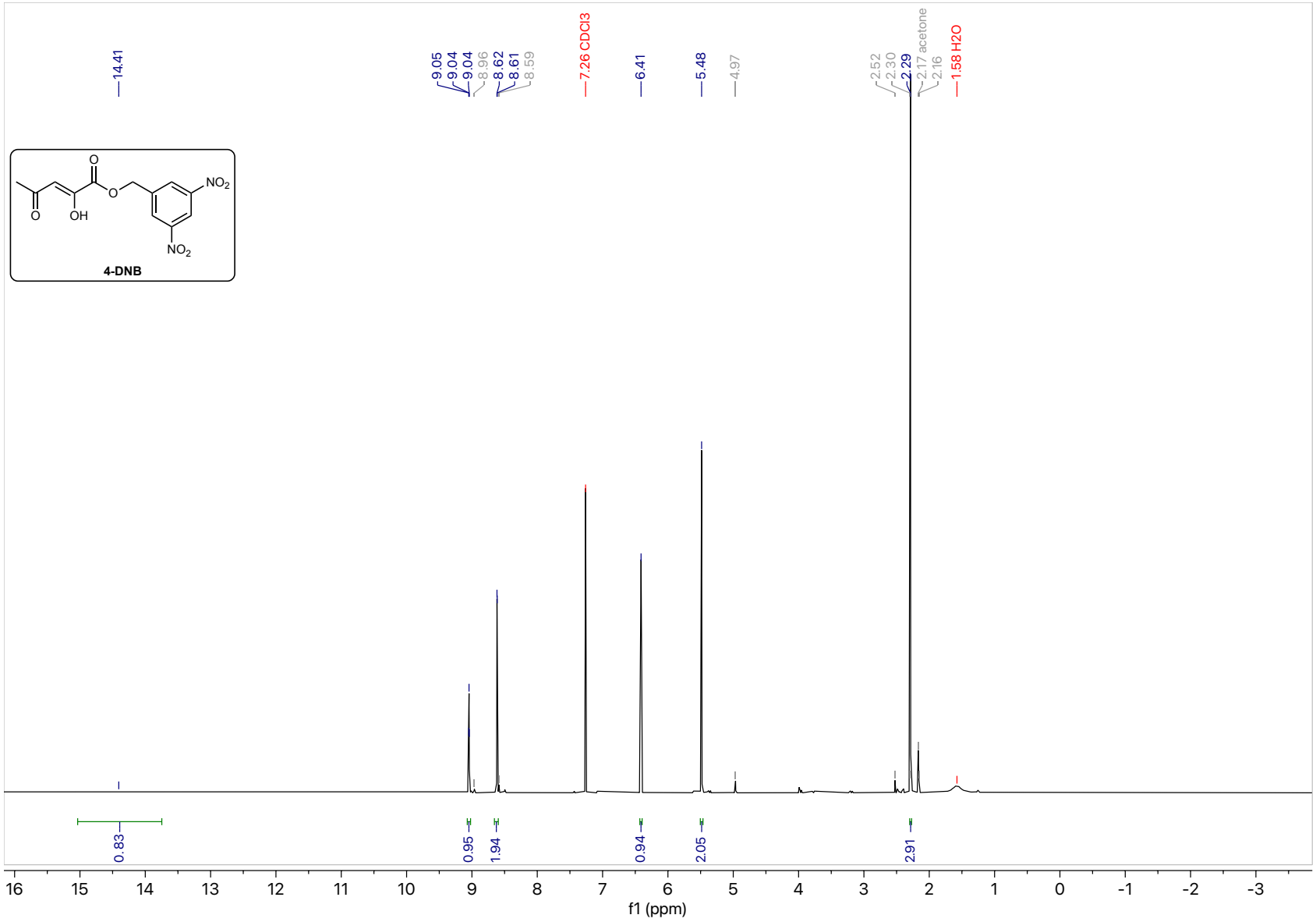
$^{13}C\{^{1}H\}$ NMR ($CDCl_3$, 126 MHz) – standard view **(3-DNB)**



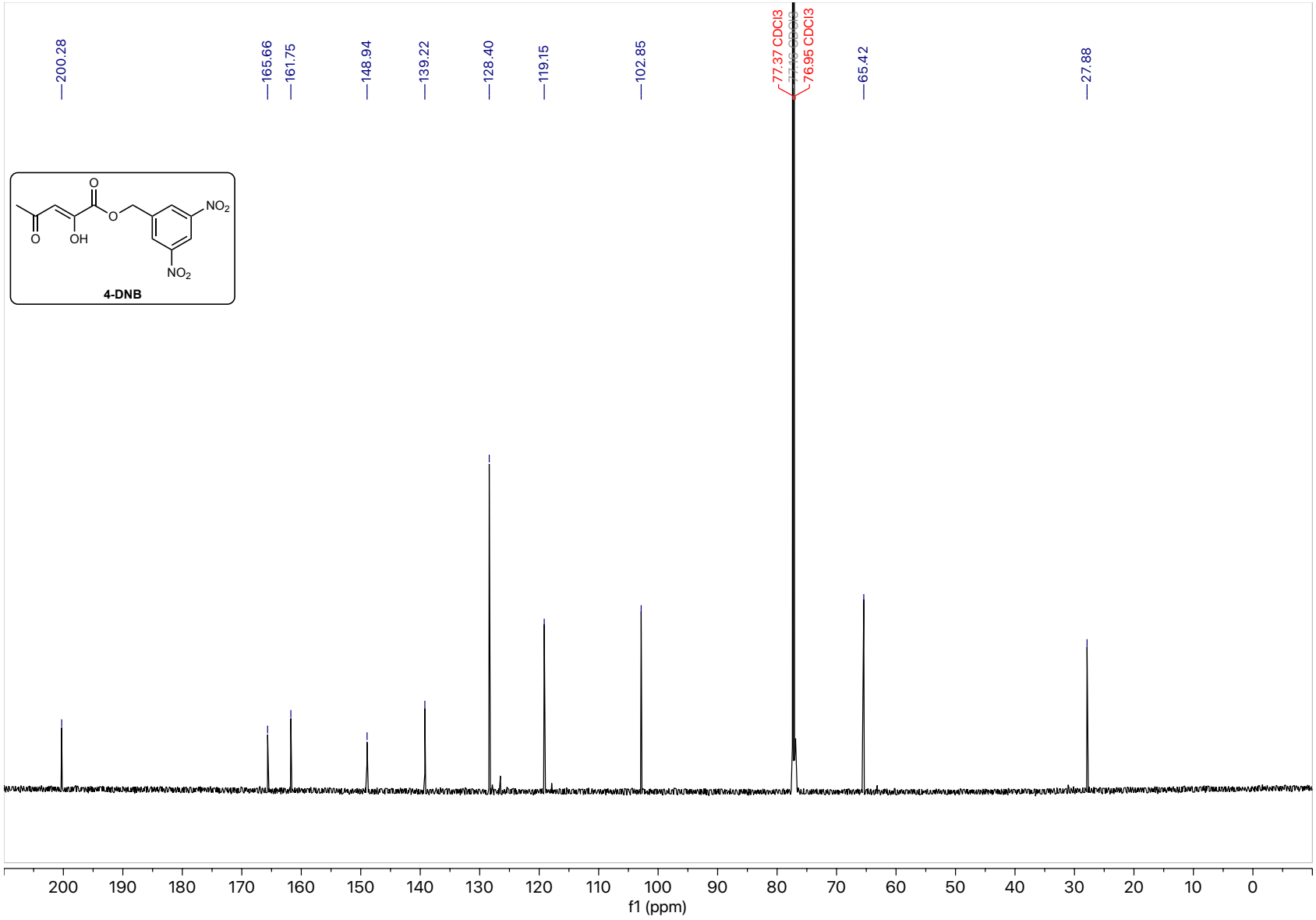
^{1}H NMR (500 MHz, $CDCl_3$) – standard view – mixture of free acid and methyl ester **(4)**



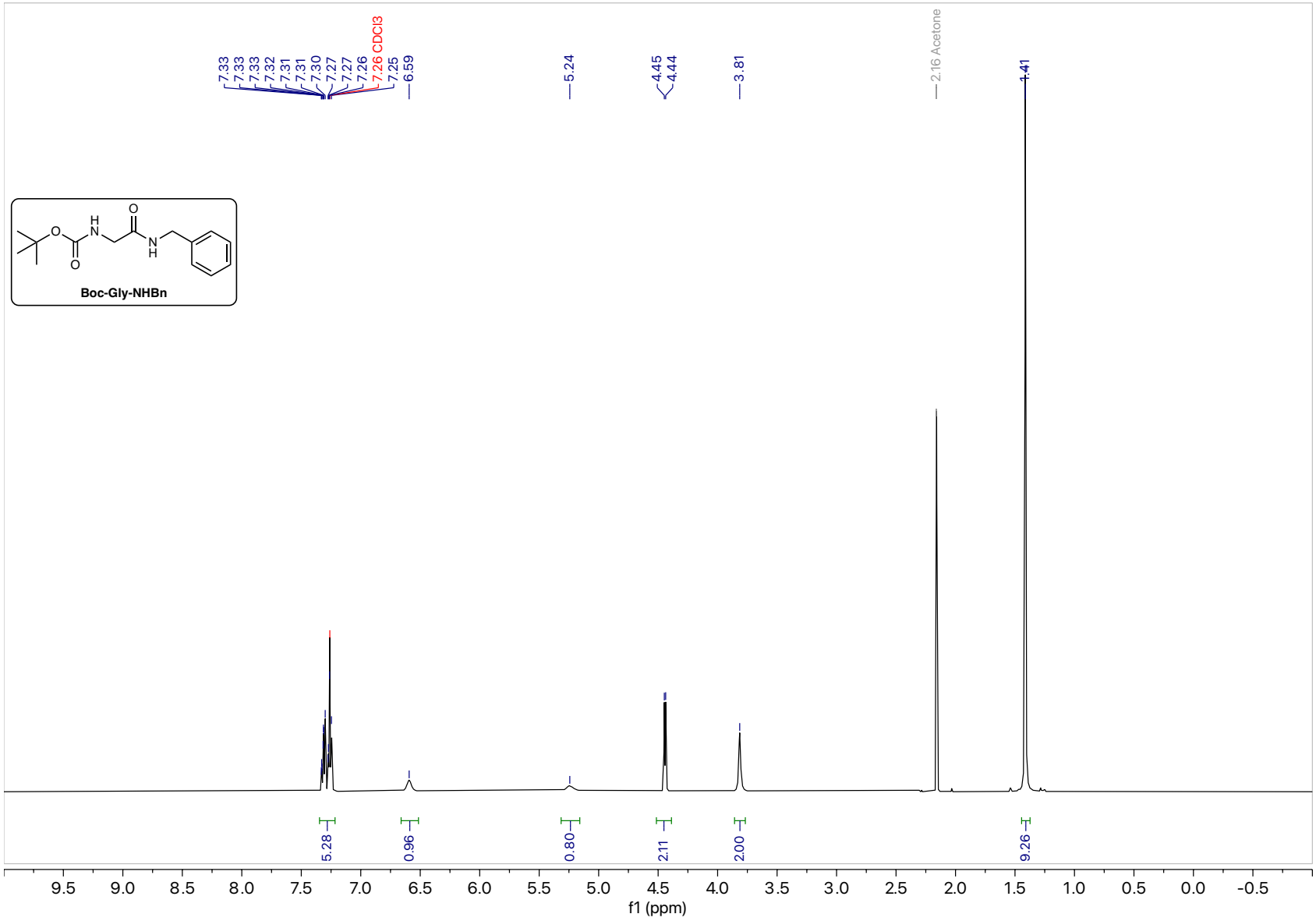
^{1}H NMR (500 MHz, $CDCl_3$) – standard view **(4-DNB)**



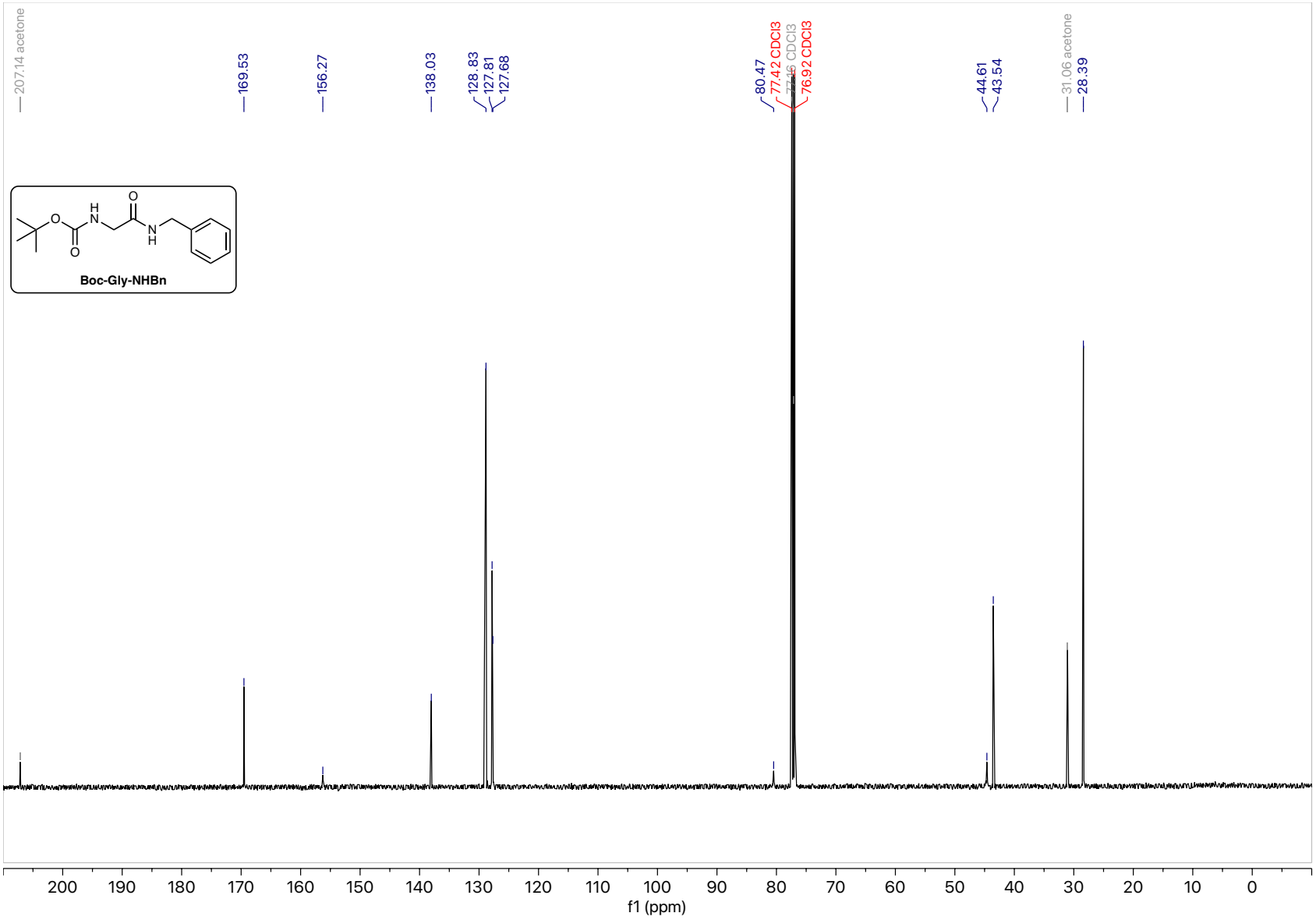
$^{13}C\{^{1}H\}$ NMR ($CDCl_3$) – standard view **(4-DNB)**



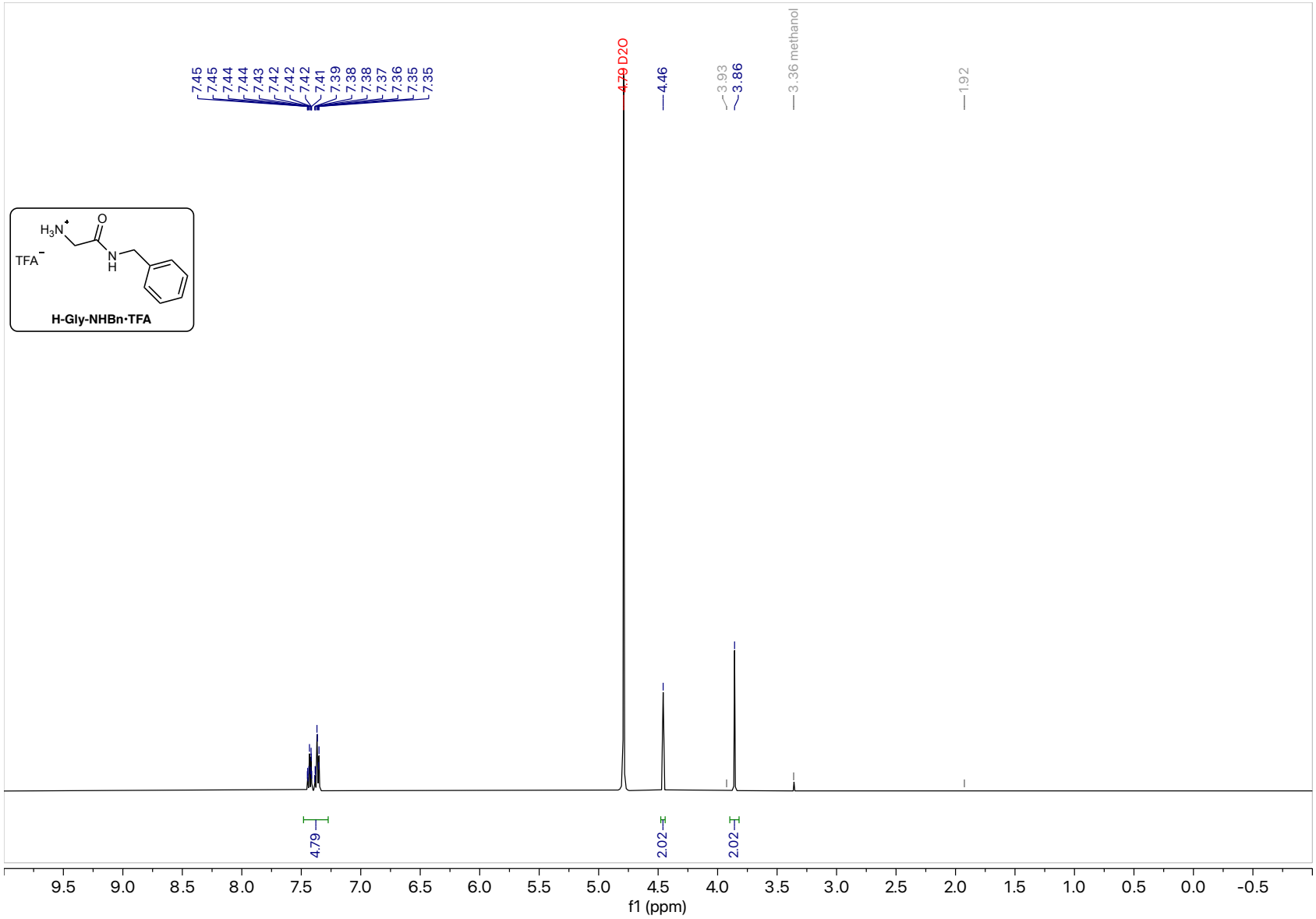
^{1}H NMR (500 MHz, $CDCl_3$) – standard view **(Boc-Gly-NHBn)**



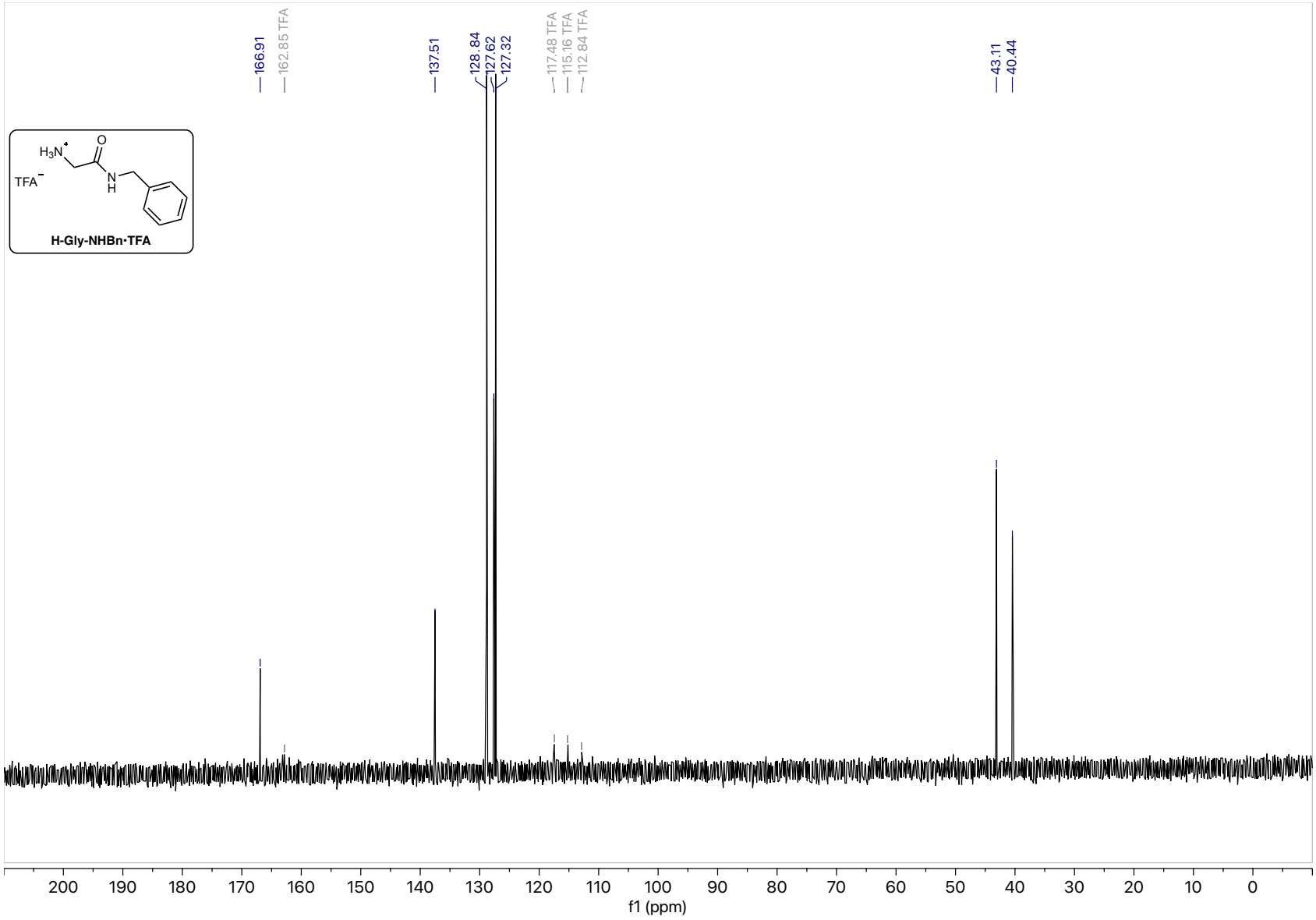
$^{13}C\{^{1}H\}$ NMR (126 MHz, $CDCl_3$) – standard view (***Boc-Gly-NHBn***)



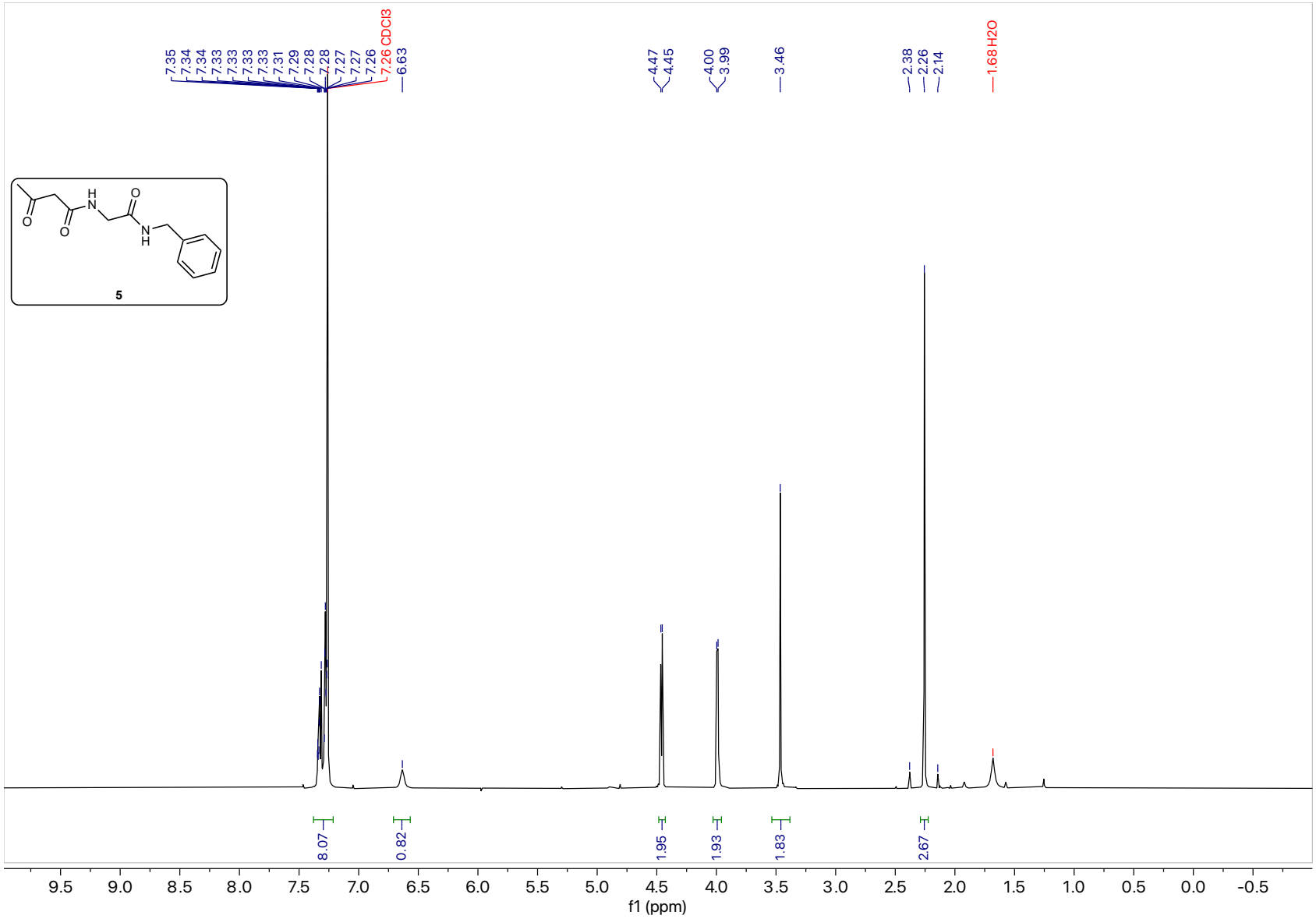
^{1}H NMR (500 MHz, D_2O) – standard view (***H-Gly-NHBn•TFA***)



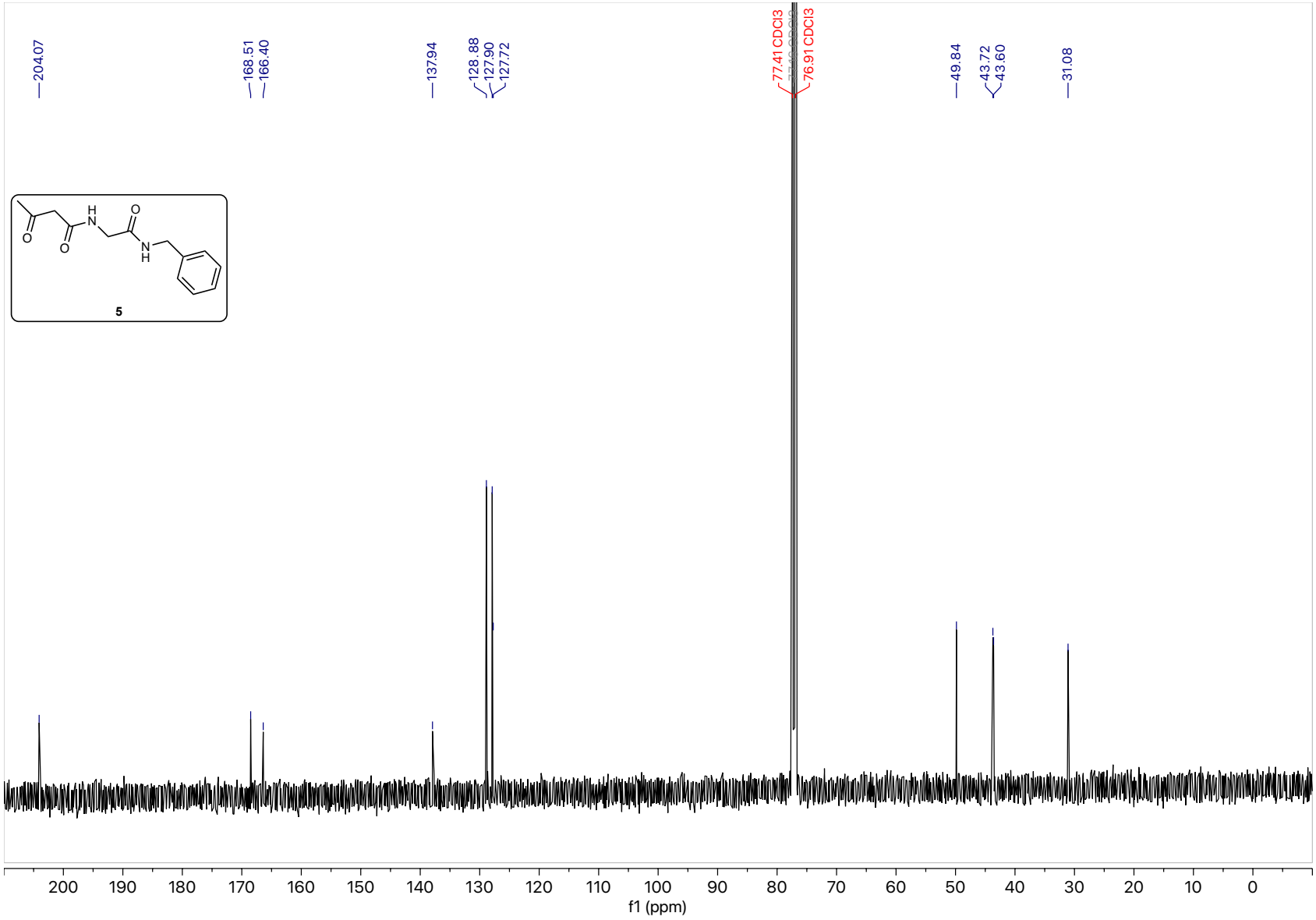
$^{13}C\{^{1}H\}$ NMR (126 MHz, D_2O) – standard view (***H-Gly-NHBn•TFA***)



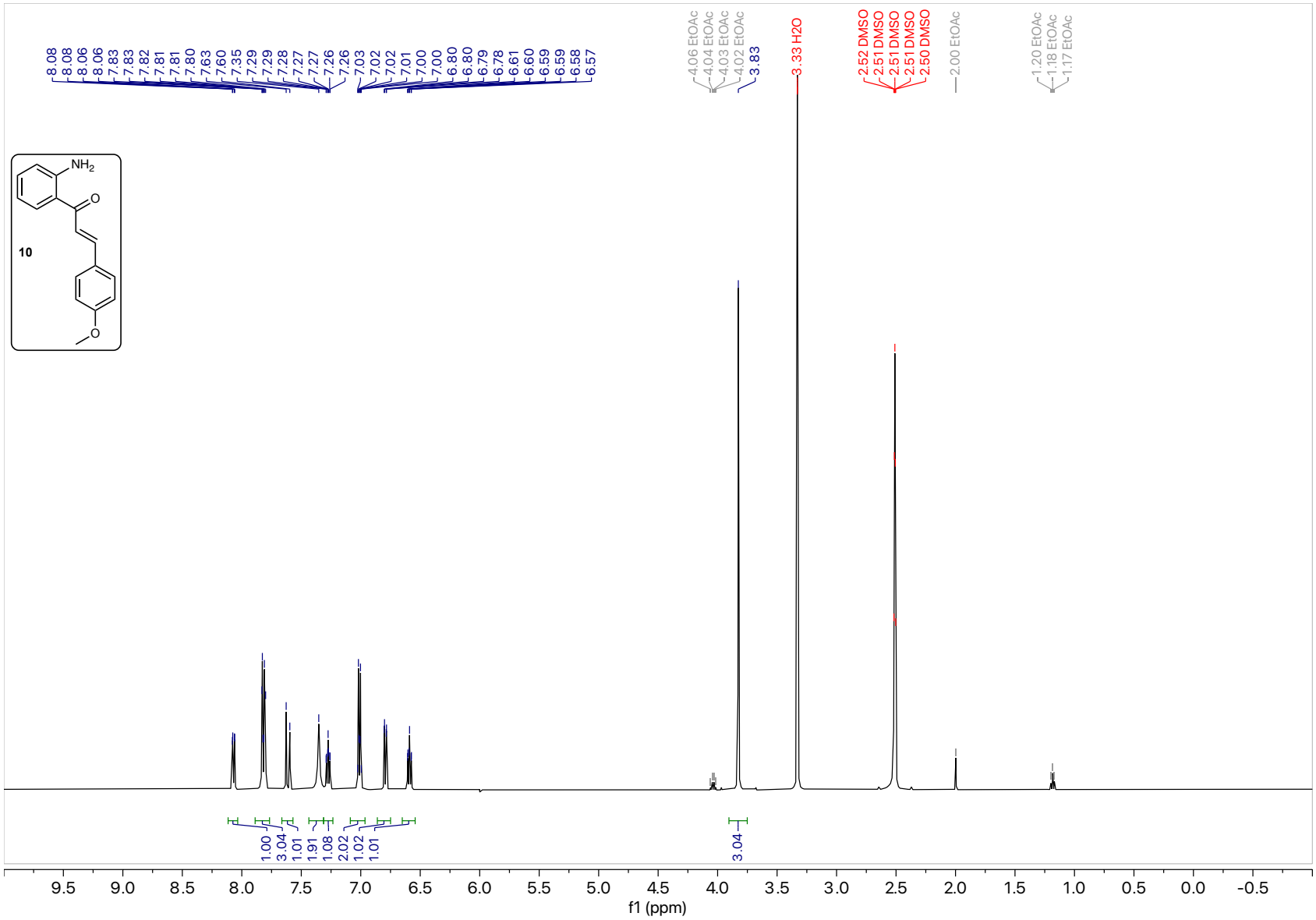
^{1}H NMR (500 MHz, $CDCl_3$) – standard view **(5)**



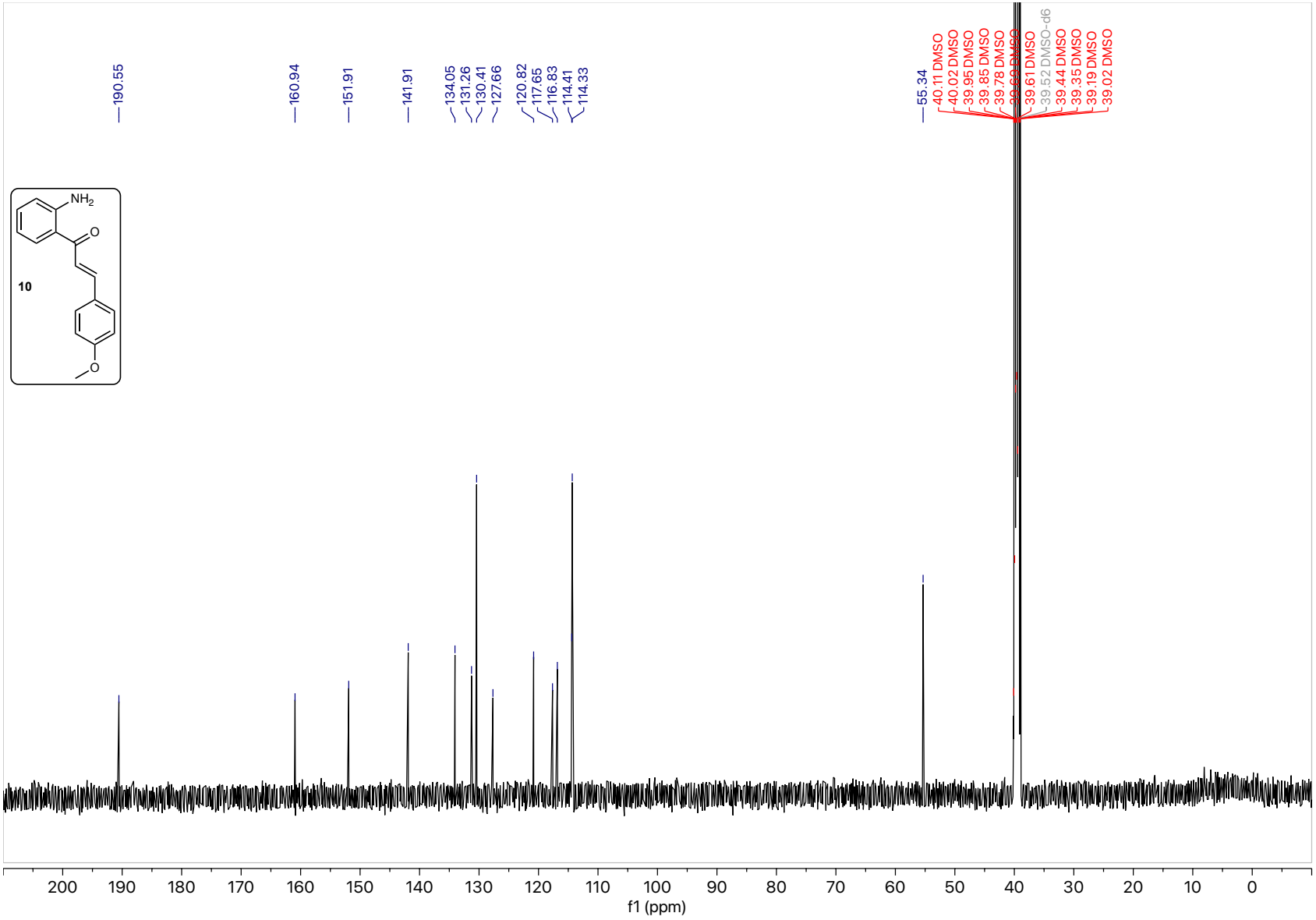
$^{13}C\{^{1}H\}$ NMR ($CDCl_3$, 126 MHz) – standard view **(5)**



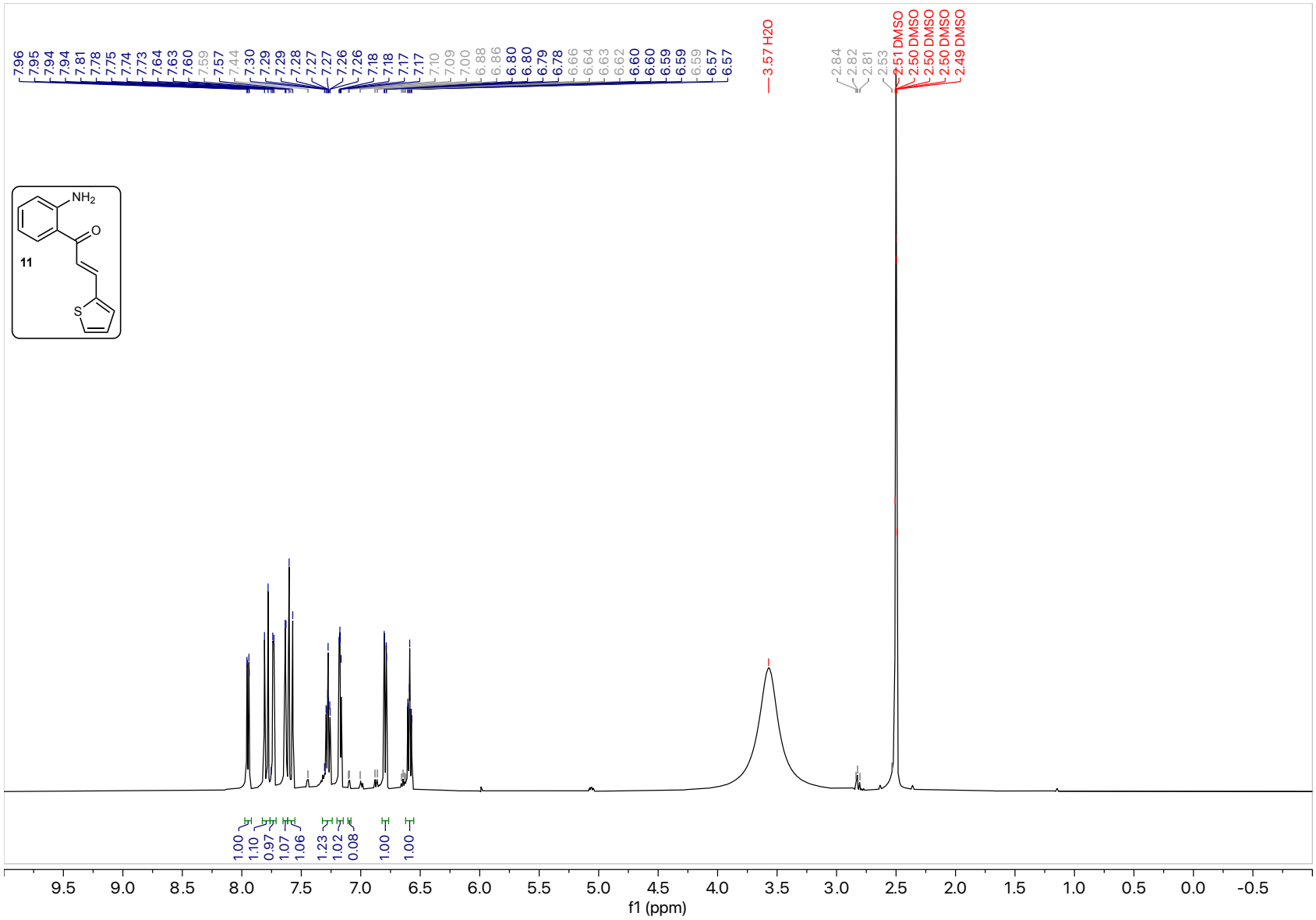
^{1}H NMR (500 MHz, DMSO-d_6) – standard view **(10)**



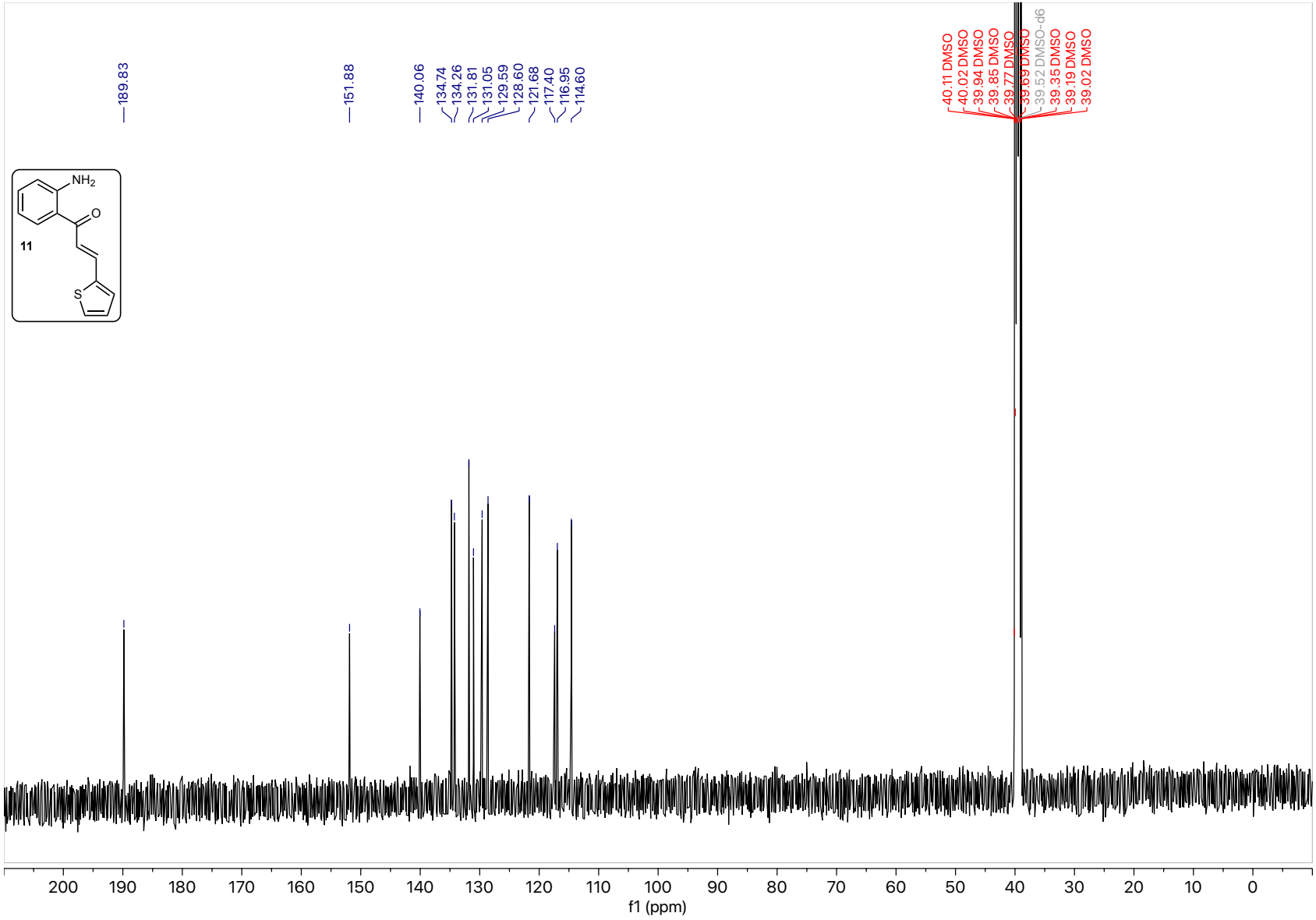
$^{13}C\{^{1}H\}$ NMR (126 MHz, DMSO-d_6) – standard view **(10)**



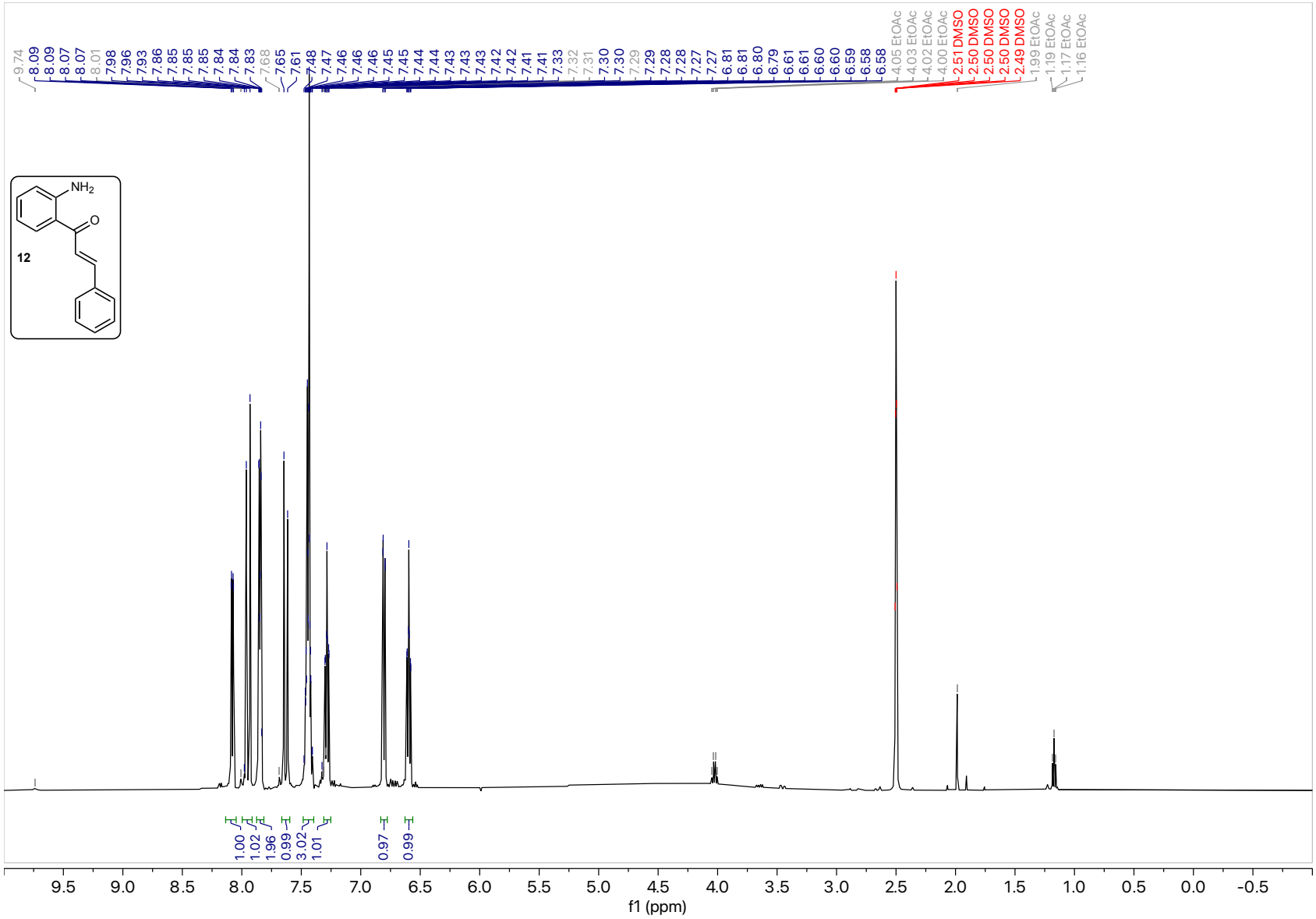
^{1}H NMR (500 MHz, DMSO-d_6) – standard view **(11)**



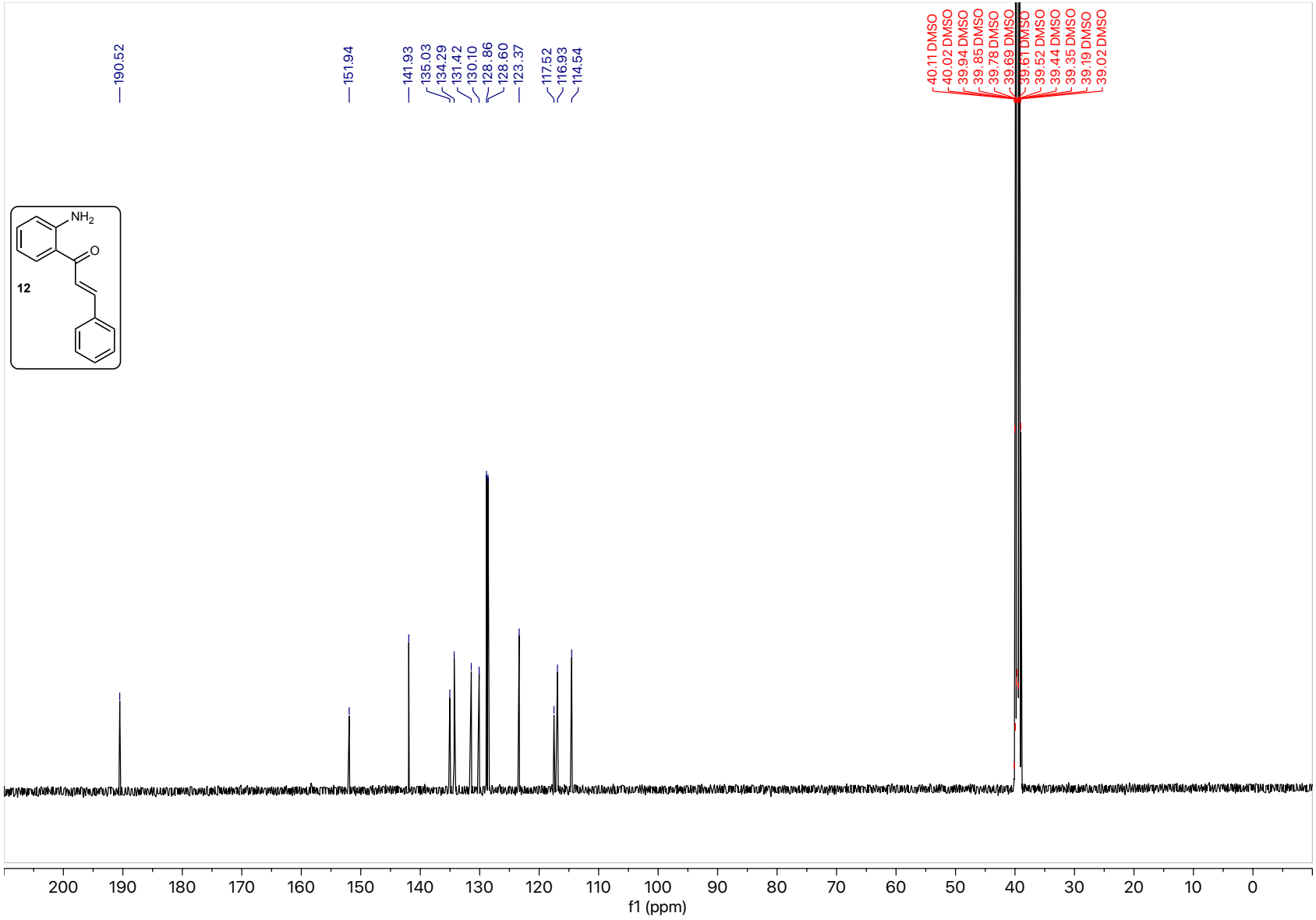
$^{13}C\{^{1}H\}$ NMR (126 MHz, DMSO-d_6) – standard view **(11)**



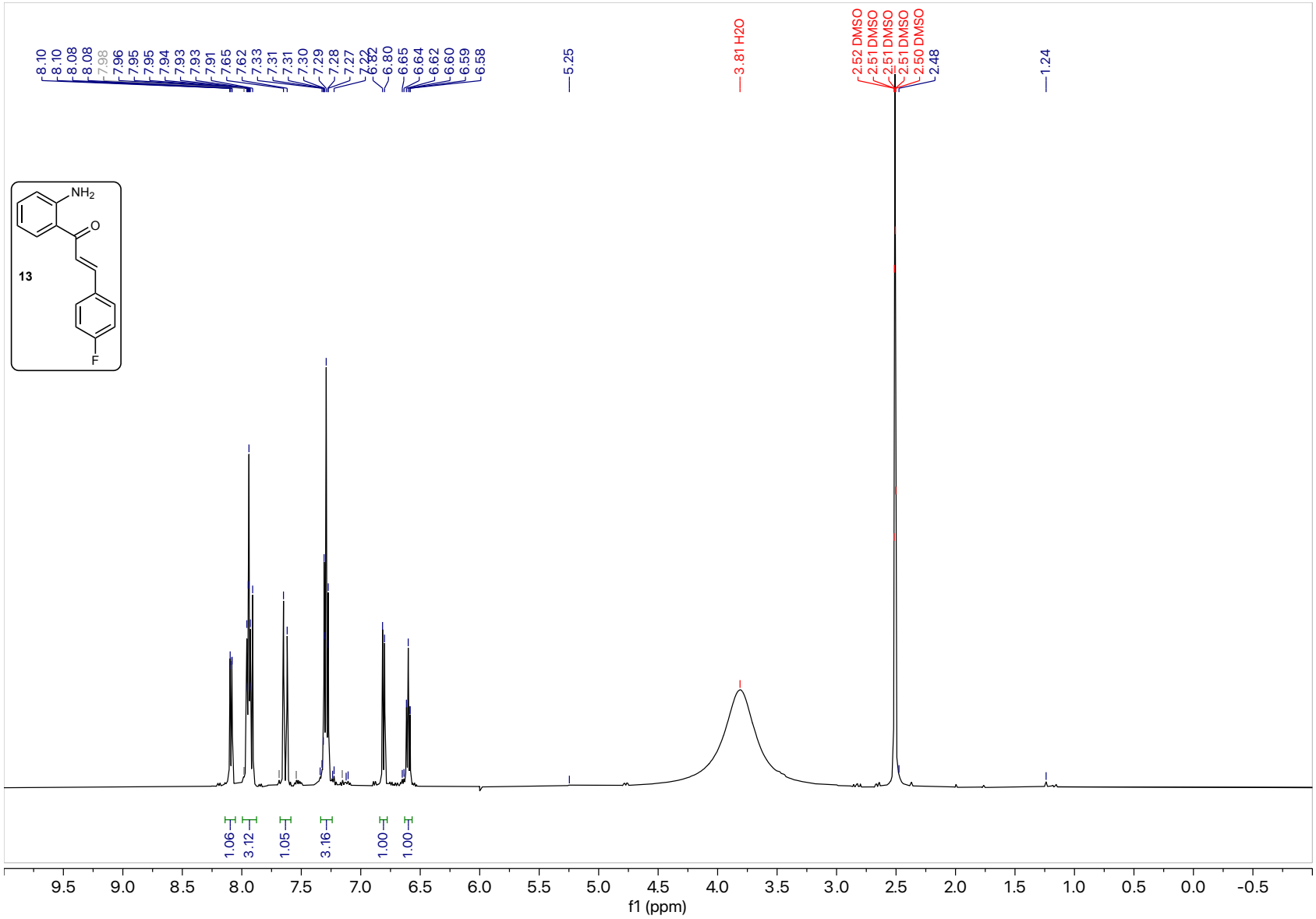
^{1}H NMR (500 MHz, $CDCl_3$) – standard view **(12)**



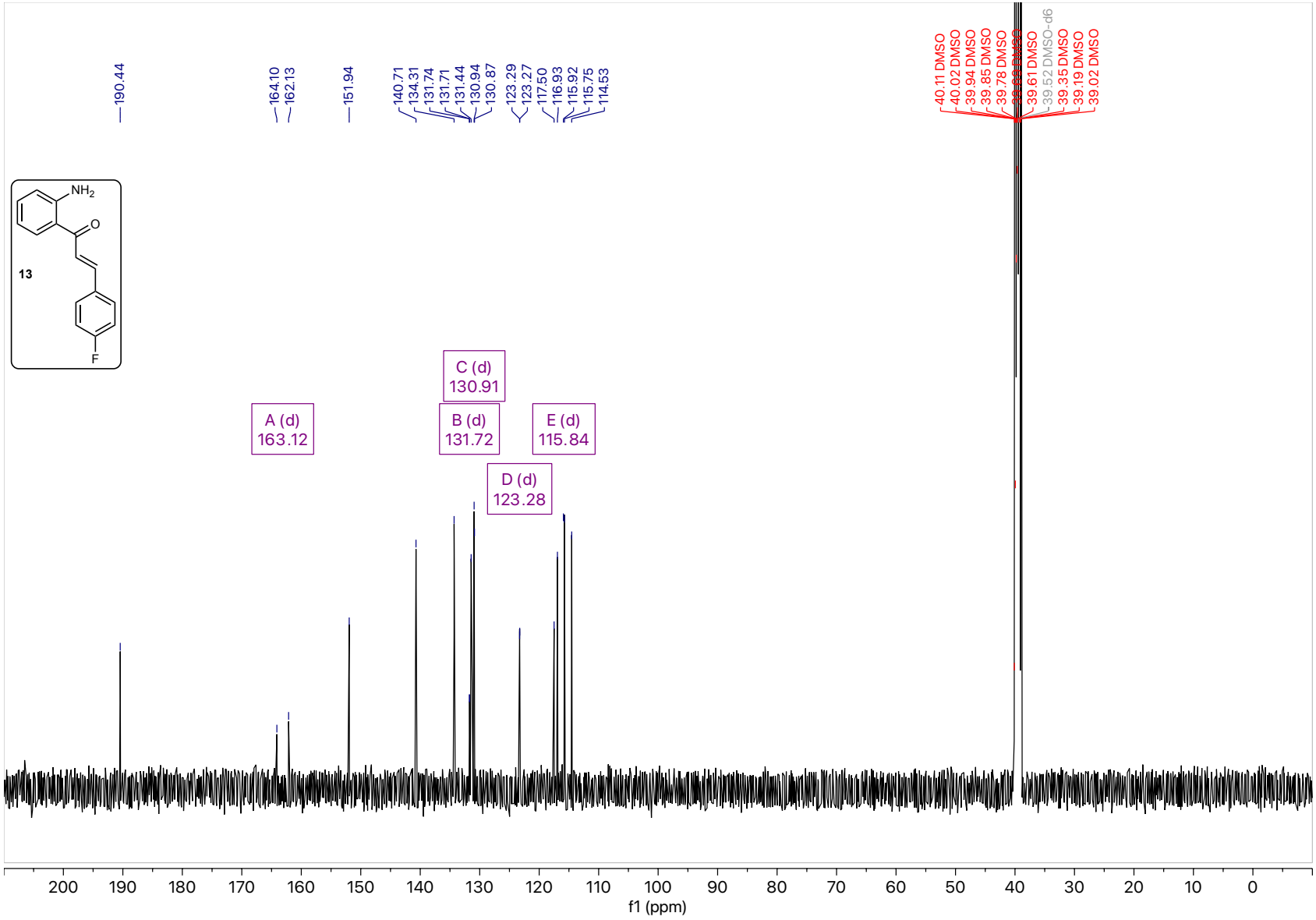
$^{13}C\{^{1}H\}$ NMR (126 MHz, $CDCl_3$) – standard view **(12)**



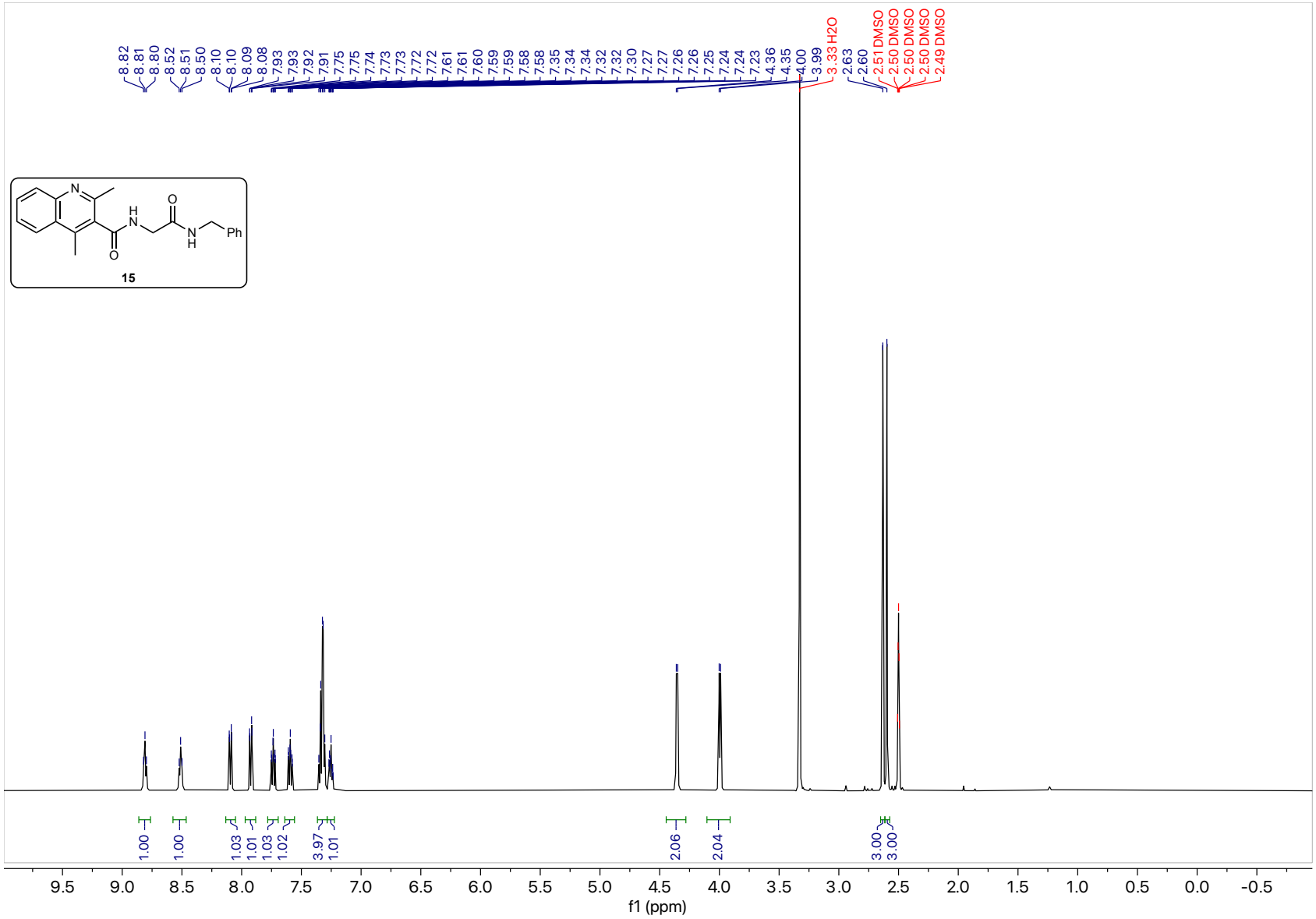
^{1}H NMR (500 MHz, $CDCl_3$) – standard view **(13)**



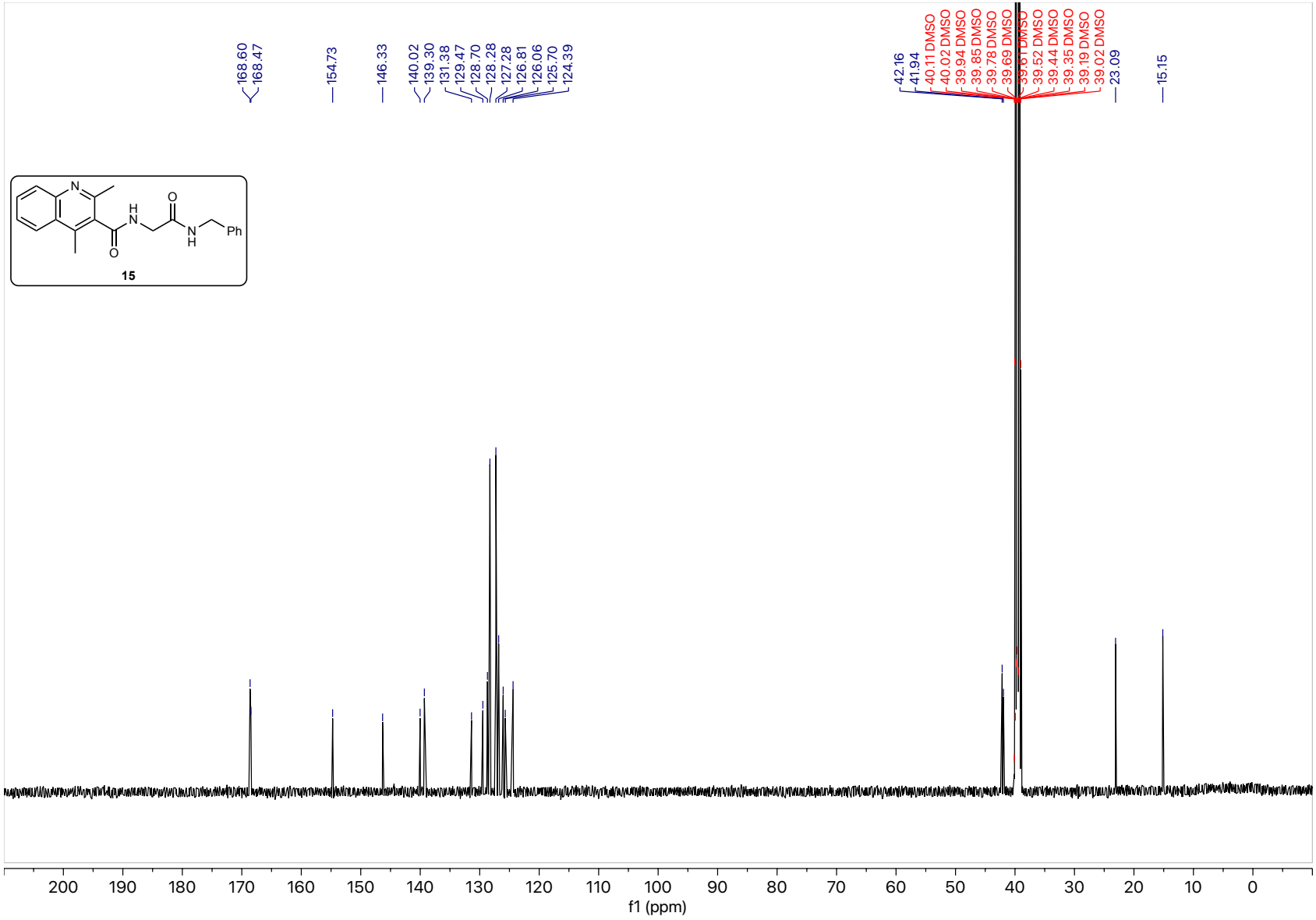
$^{13}C\{^{1}H\}$ NMR ($CDCl_3$, 126 MHz) – standard view **(13)**



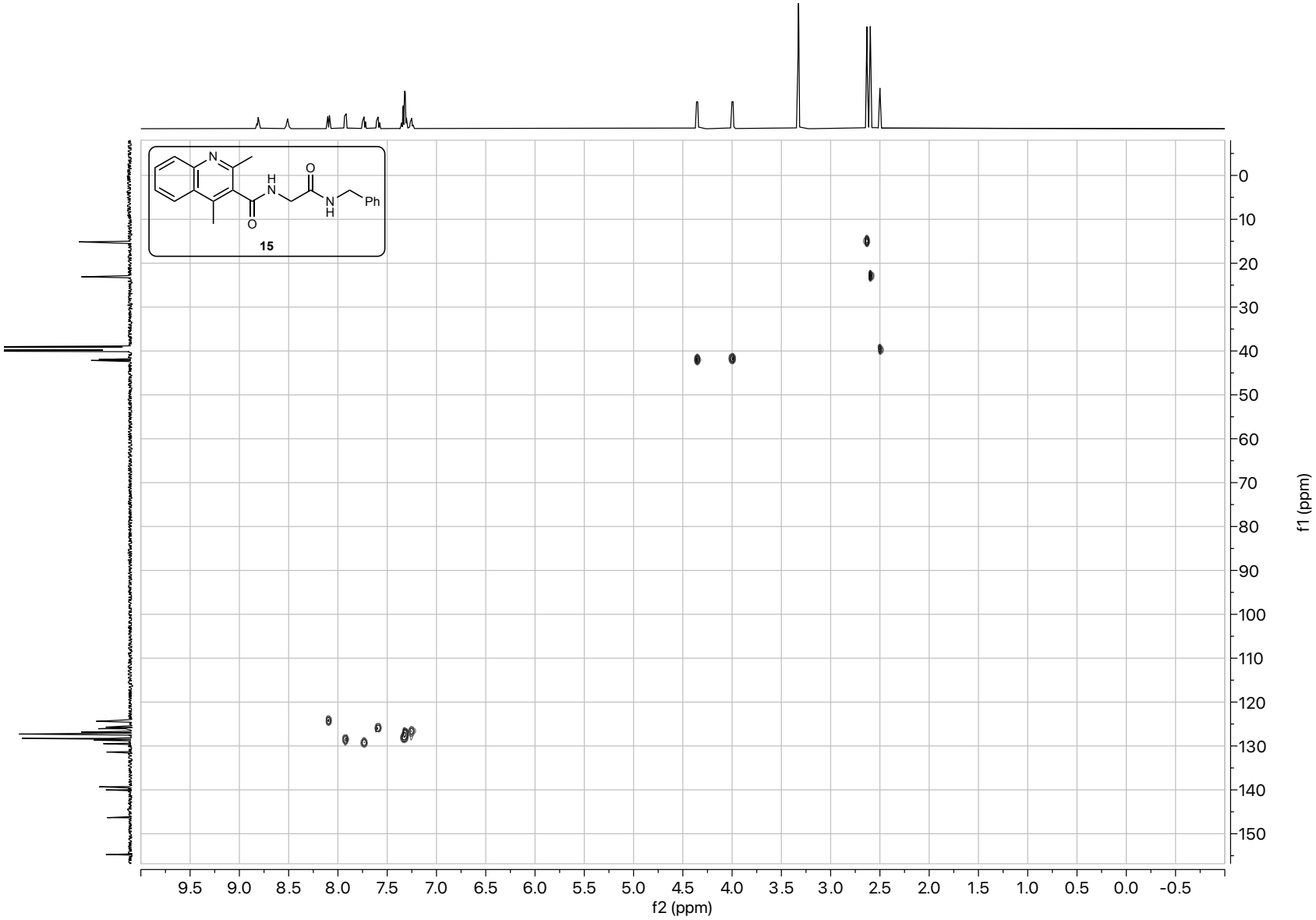
^{1}H NMR (500 MHz, DMSO-d_6) – standard view **(15)**



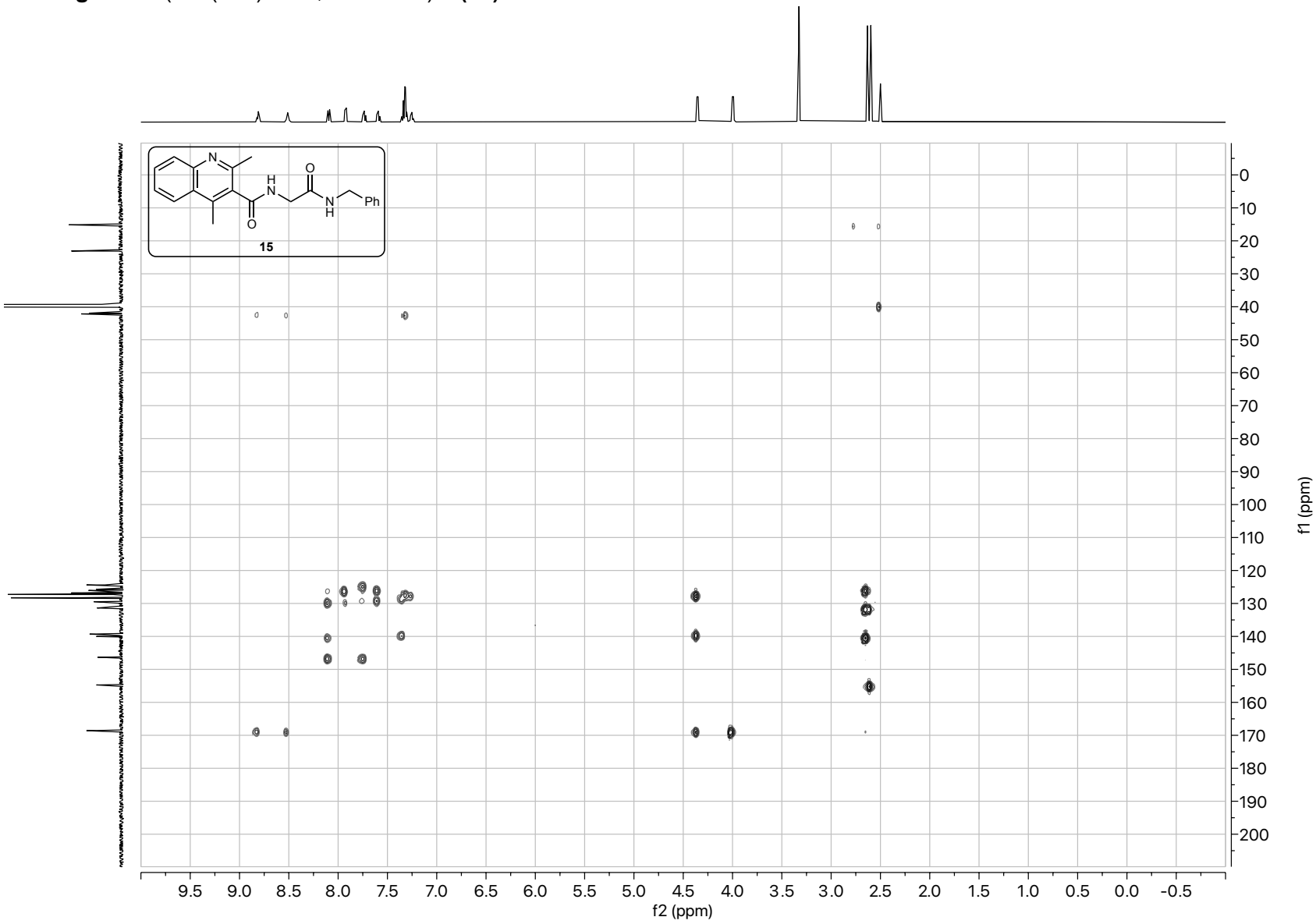
$^{13}C\{^{1}H\}$ NMR (126 MHz, DMSO-d_6) – standard view **(15)**



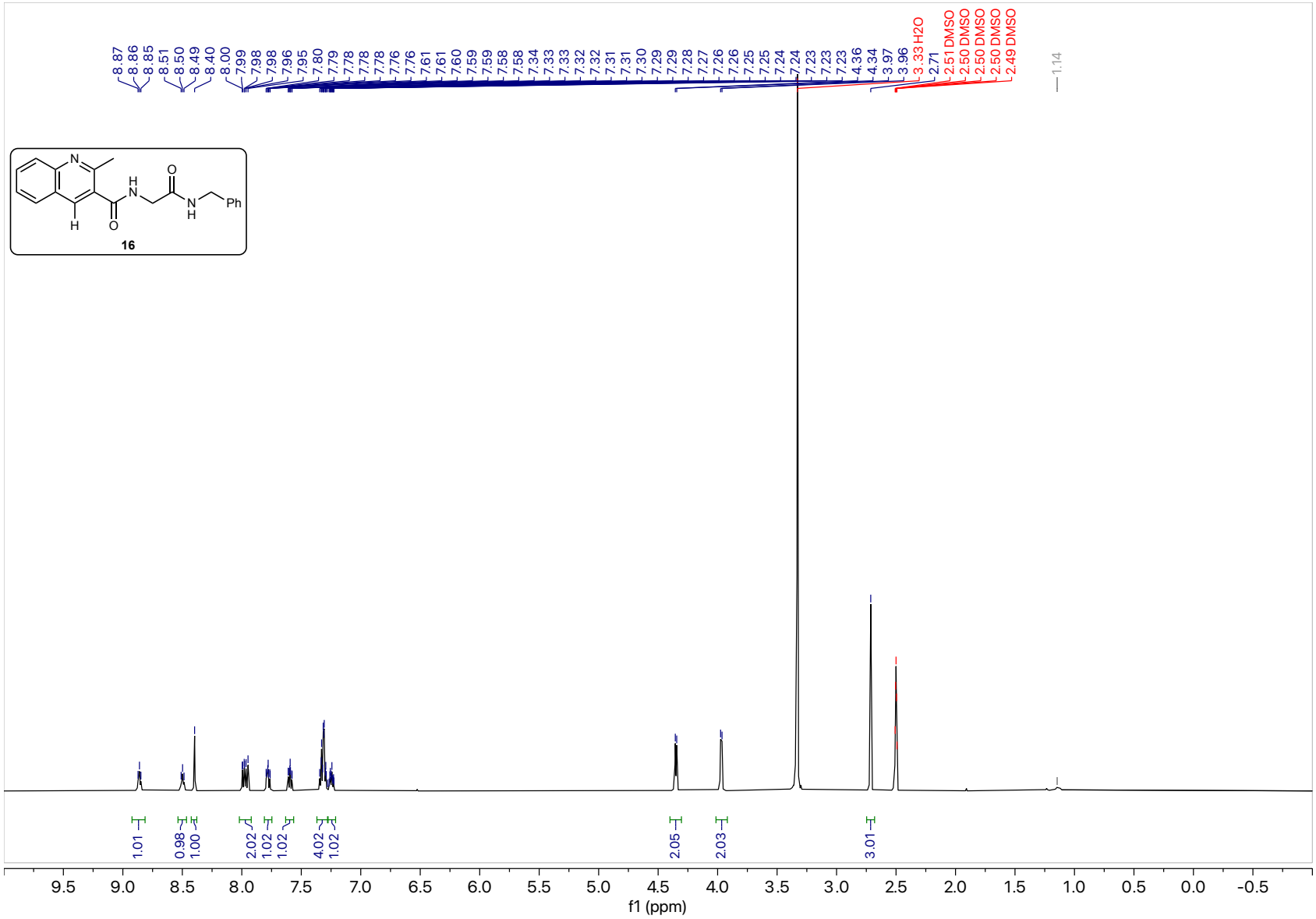
^{1}H-^{13}C gHSQC (500(126) MHz, DMSO-d_6) – **(15)**



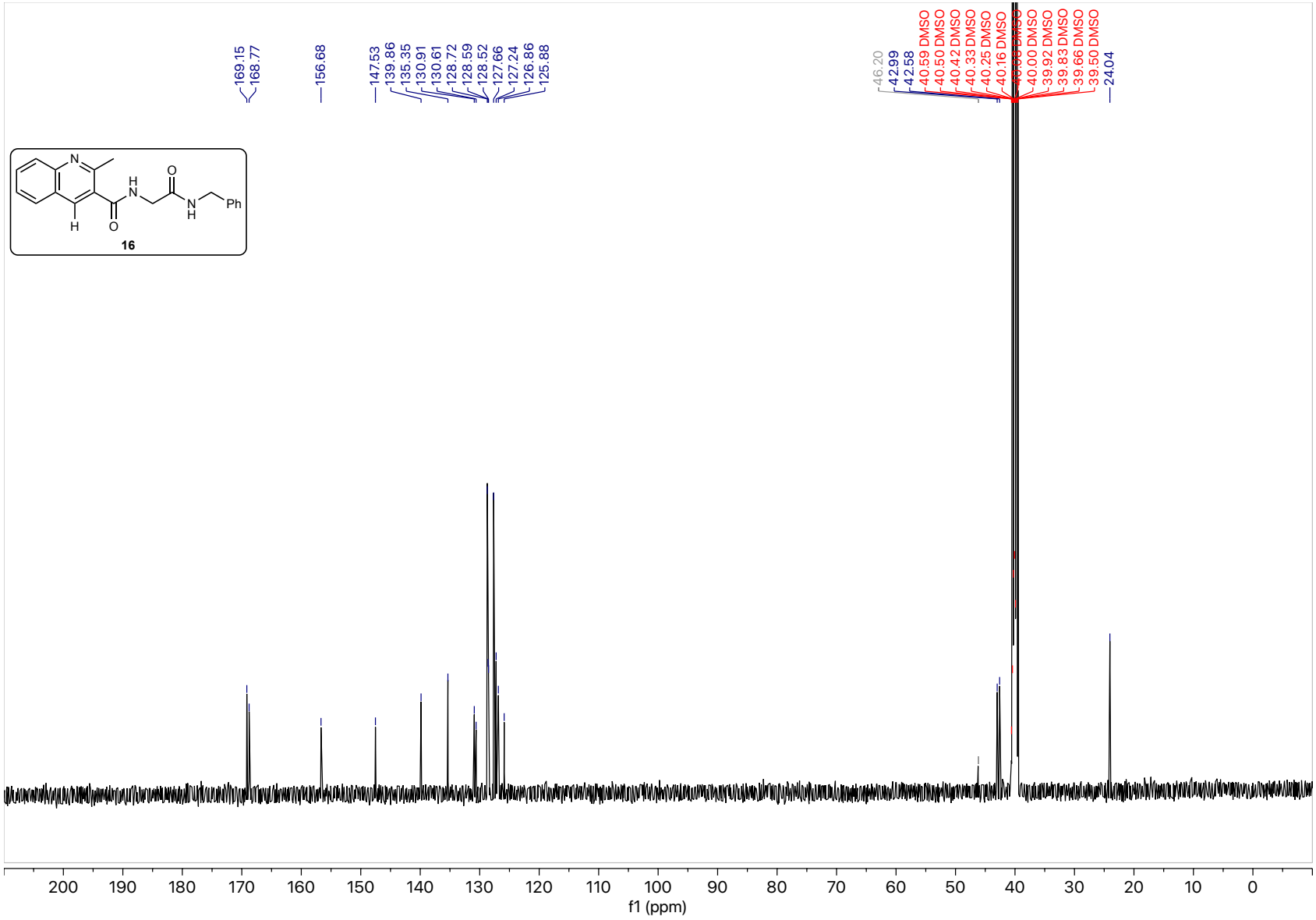
^{1}H-^{13}C gHMBC (500(126) MHz, DMSO-d_6) – **(15)**



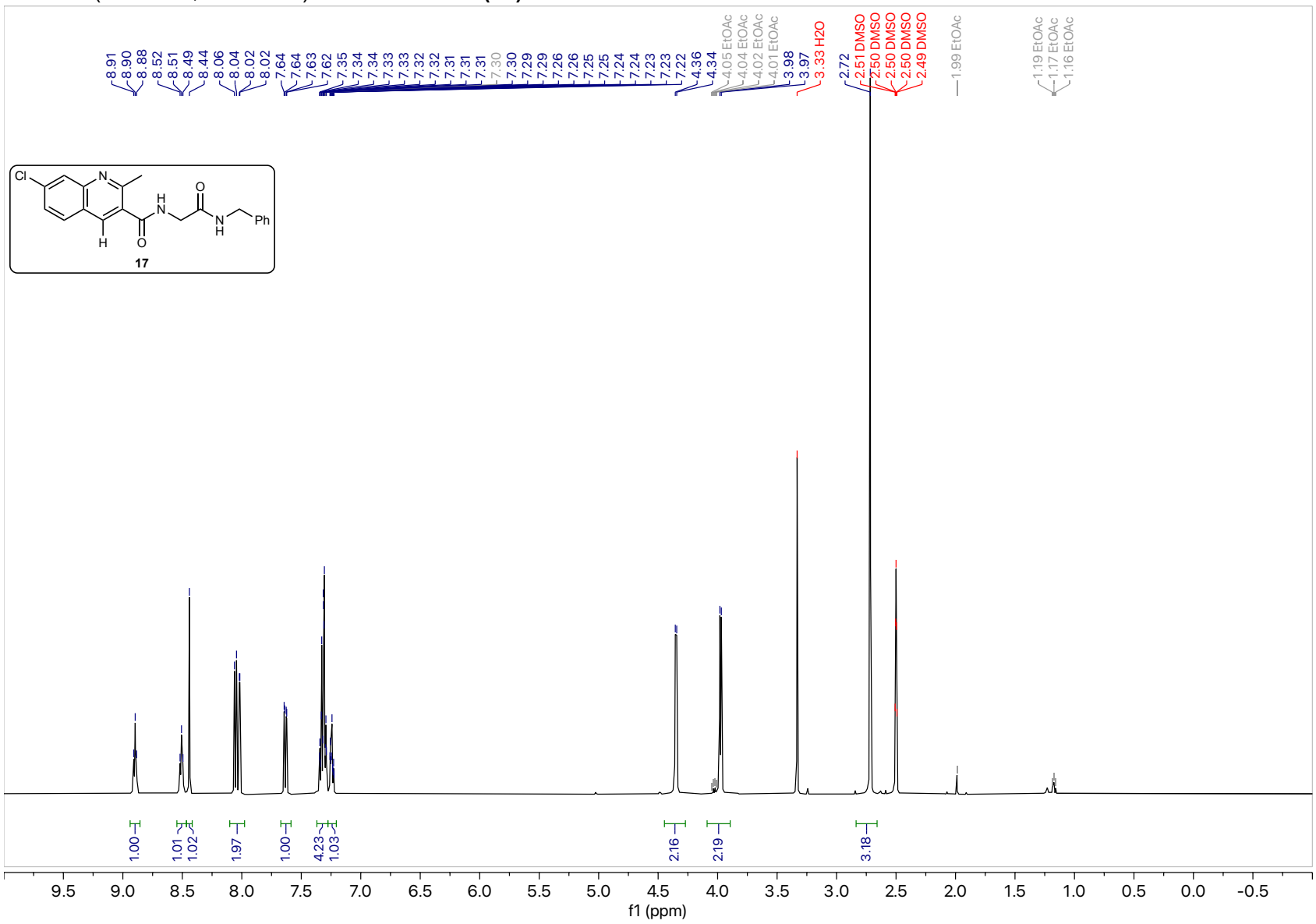
^{1}H NMR (500 MHz, DMSO-d_6) – standard view **(16)**



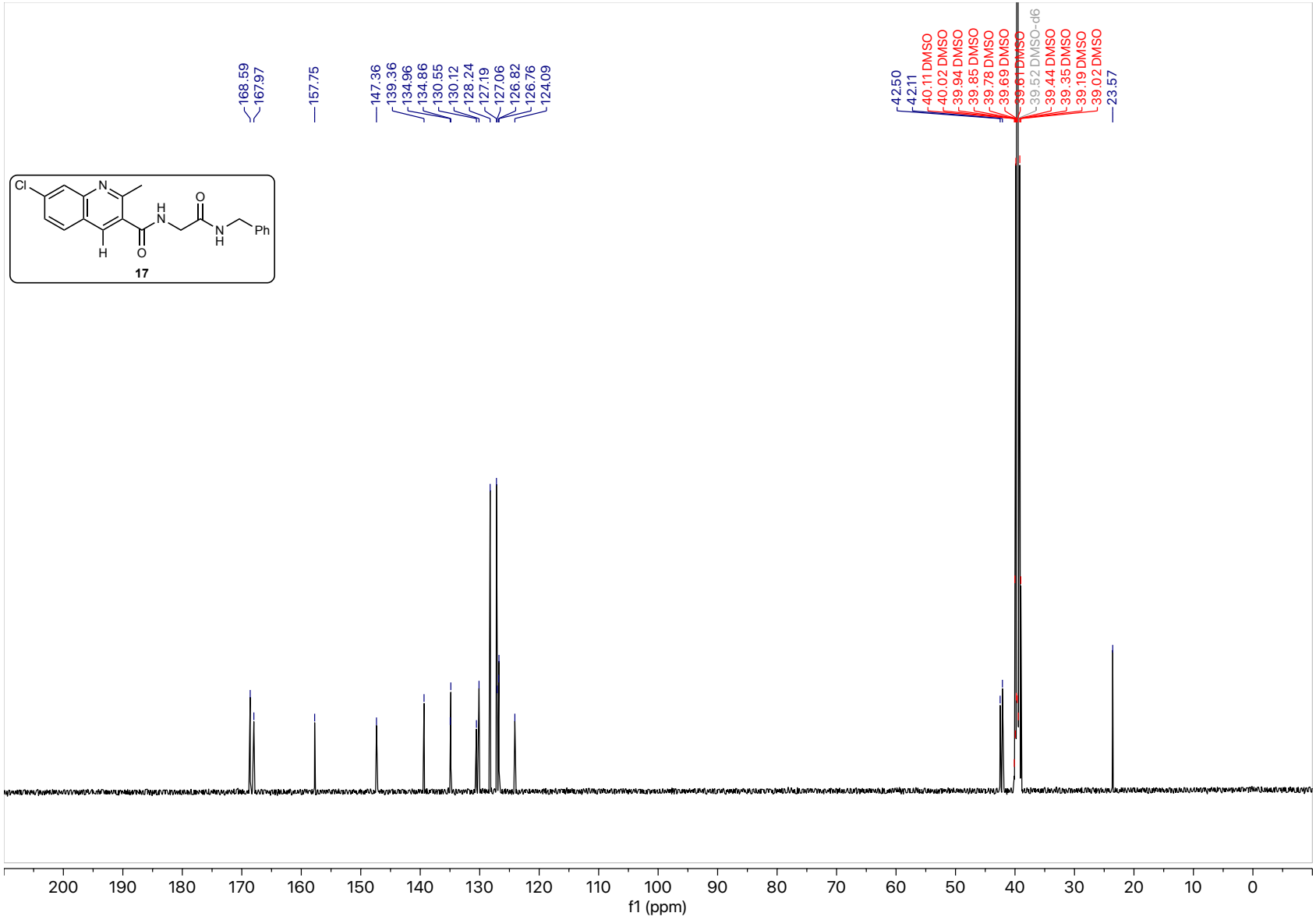
$^{13}C\{^{1}H\}$ NMR (126 MHz, DMSO-d_6) – standard view **(16)**



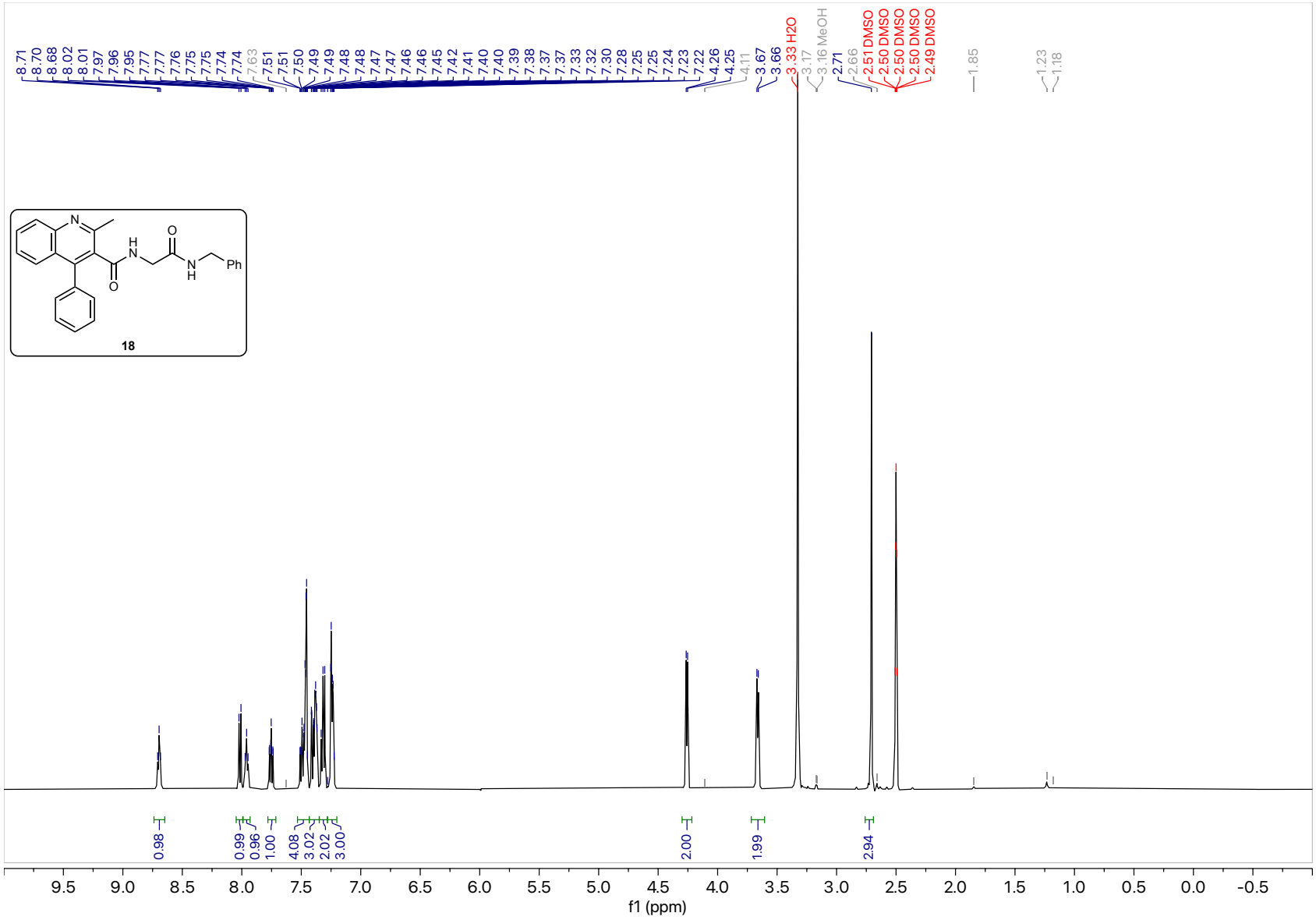
^{1}H NMR (500 MHz, DMSO-d_6) – standard view **(17)**



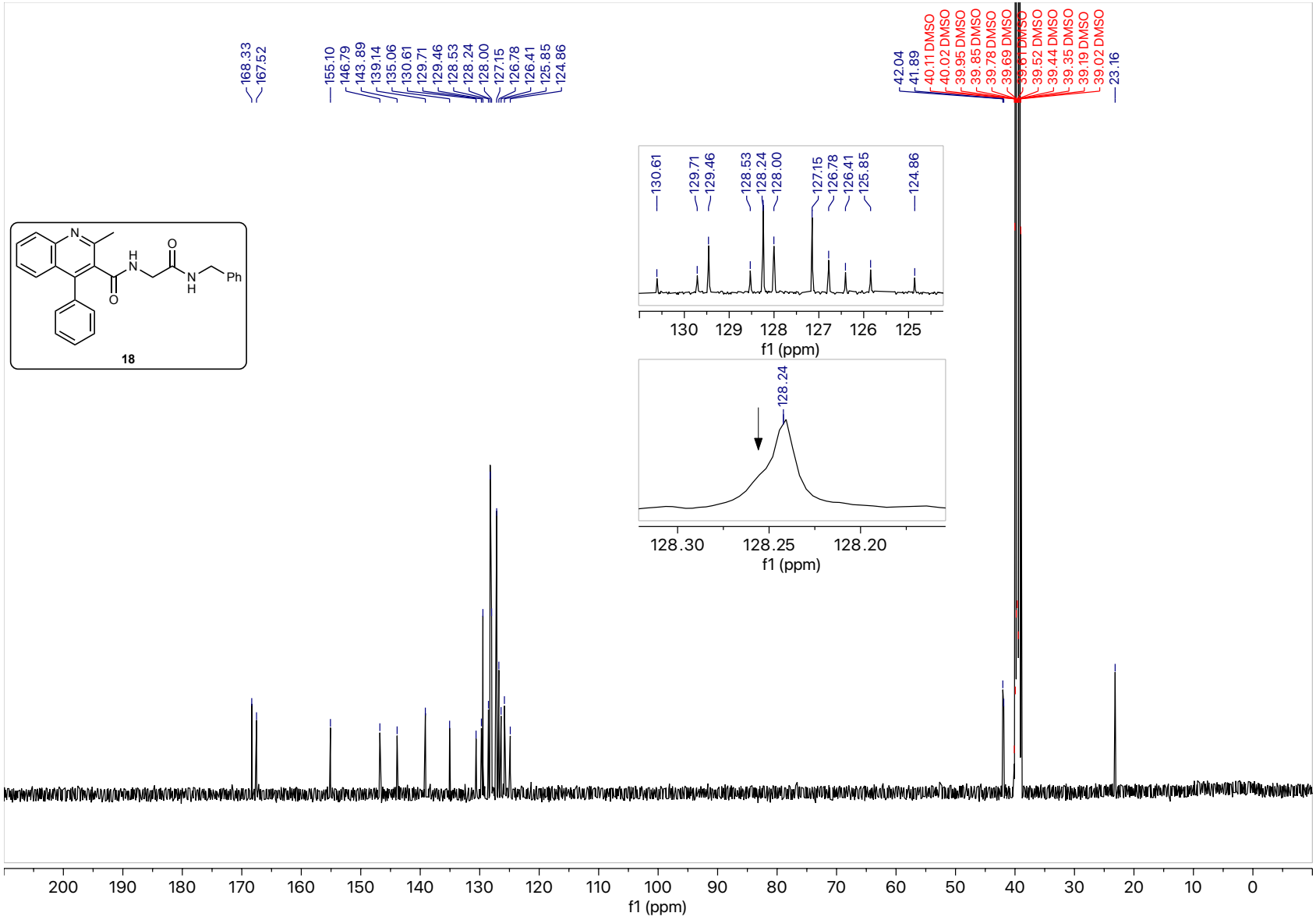
$^{13}C\{^{1}H\}$ NMR (126 MHz, DMSO-d_6) – standard view **(17)**



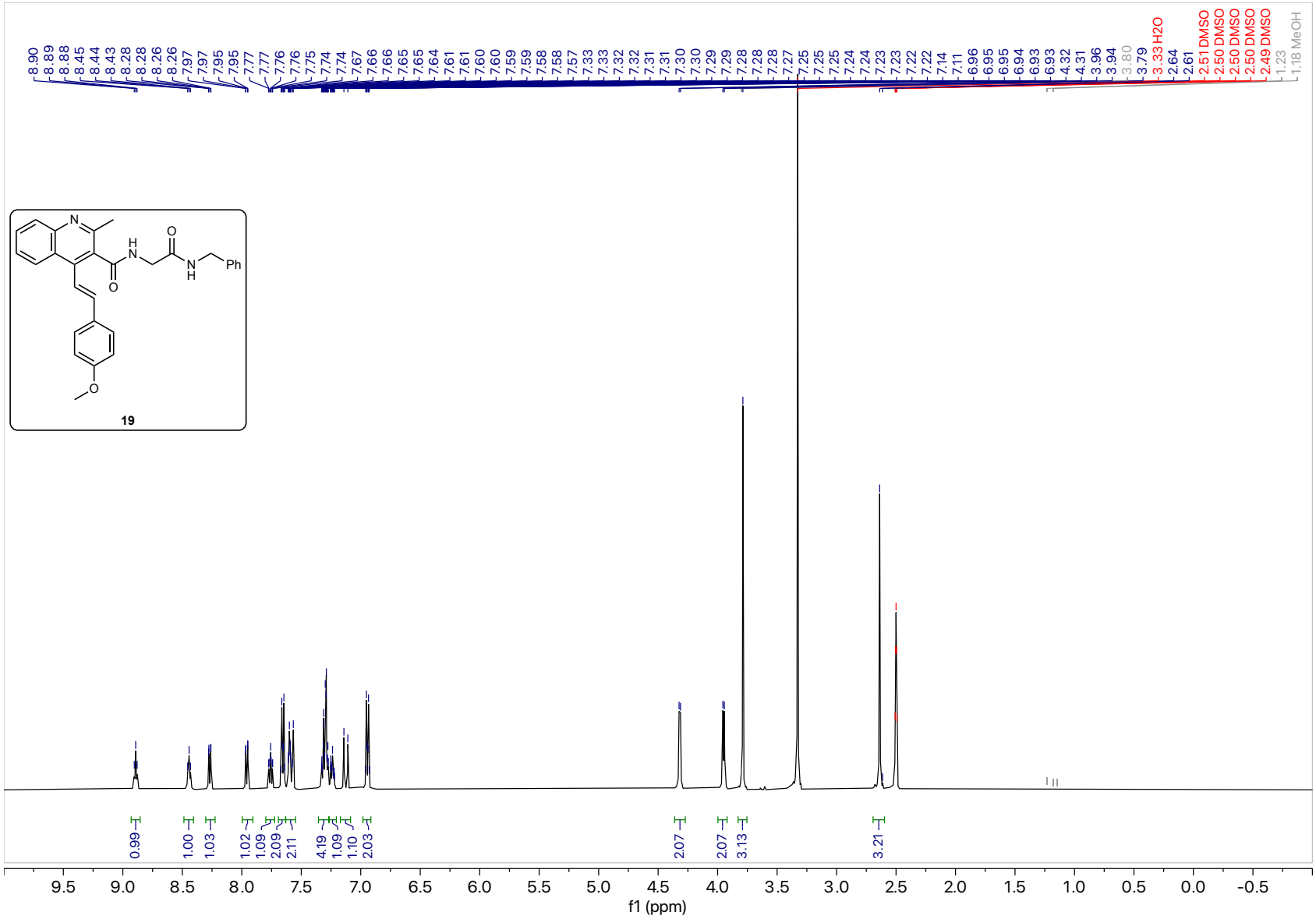
^{1}H NMR (500 MHz, DMSO-d_6) – standard view **(18)**



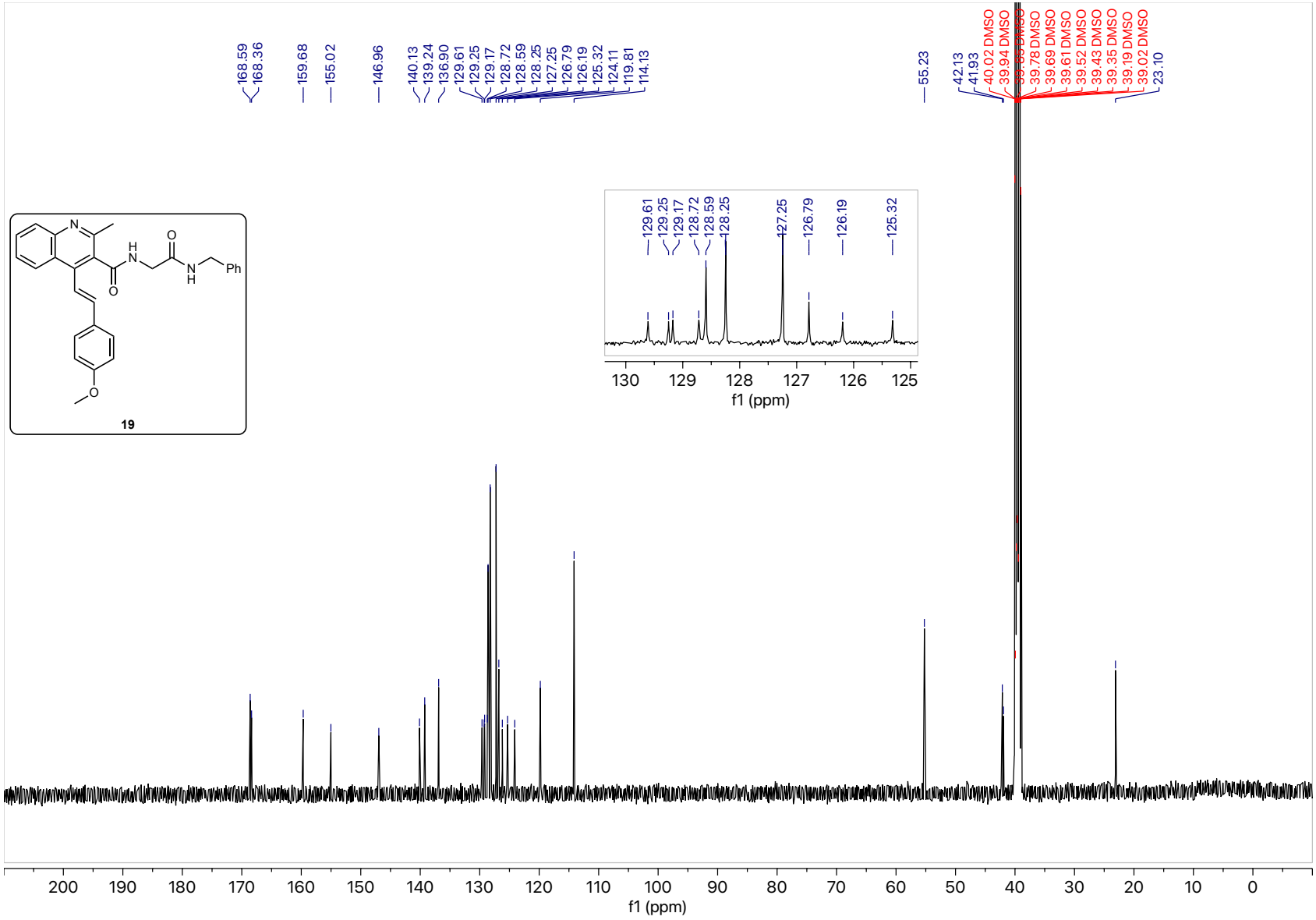
$^{13}C\{^{1}H\}$ NMR (126 MHz, DMSO-d_6) – standard view **(18)**



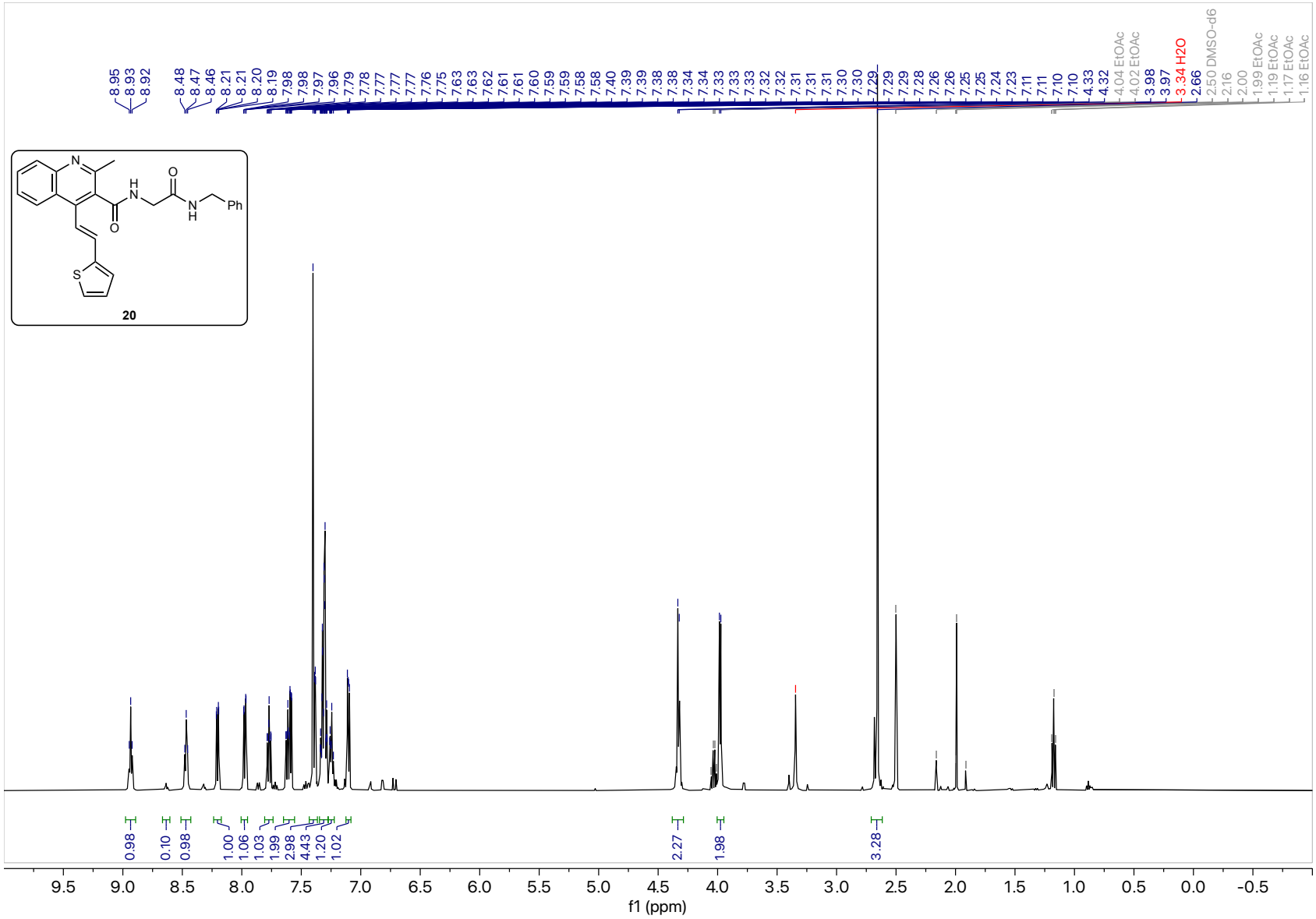
^{1}H NMR (500 MHz, DMSO-d_6) – standard view **(19)**



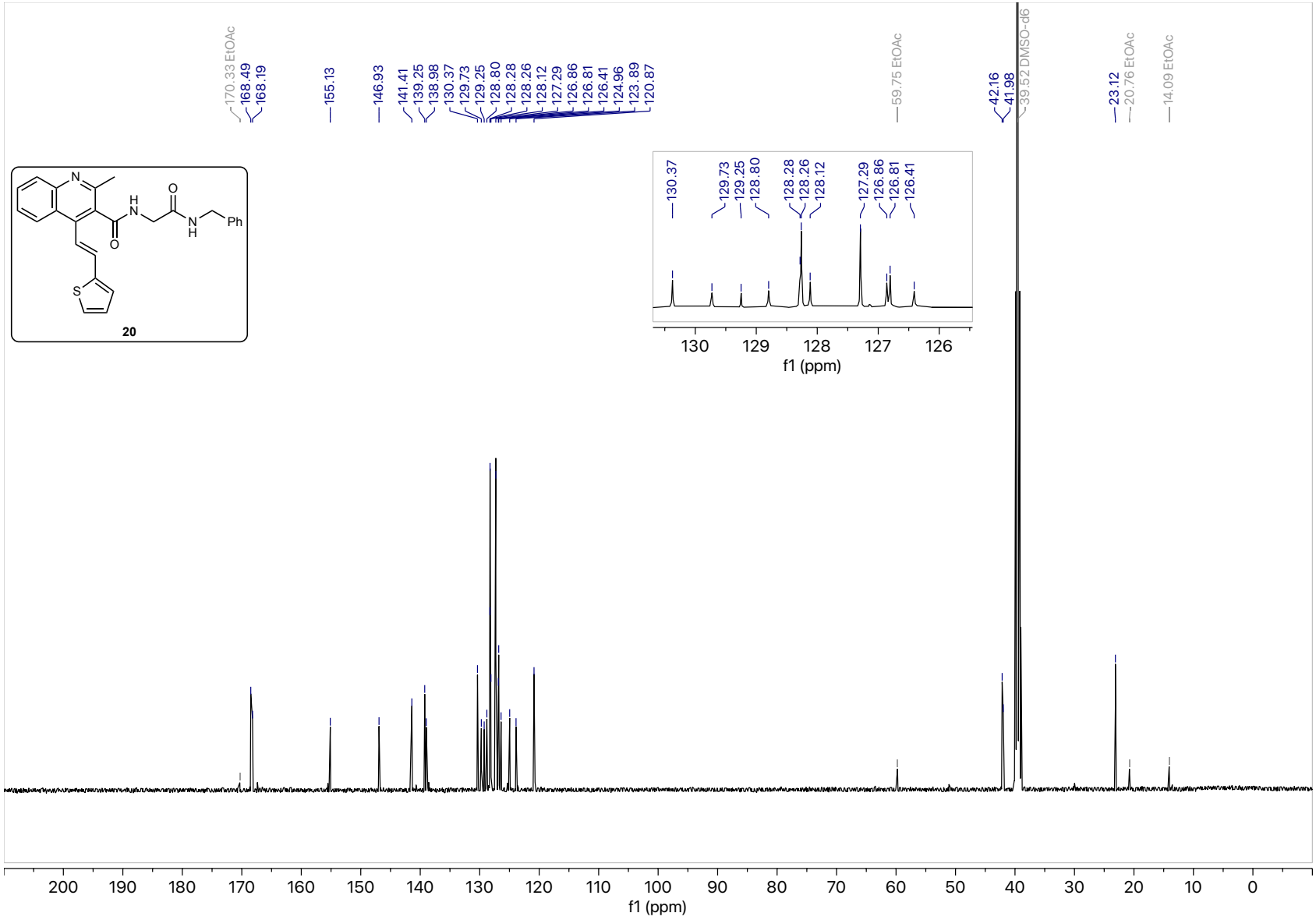
$^{13}C\{^{1}H\}$ NMR (126 MHz, DMSO-d_6) – standard view **(19)**



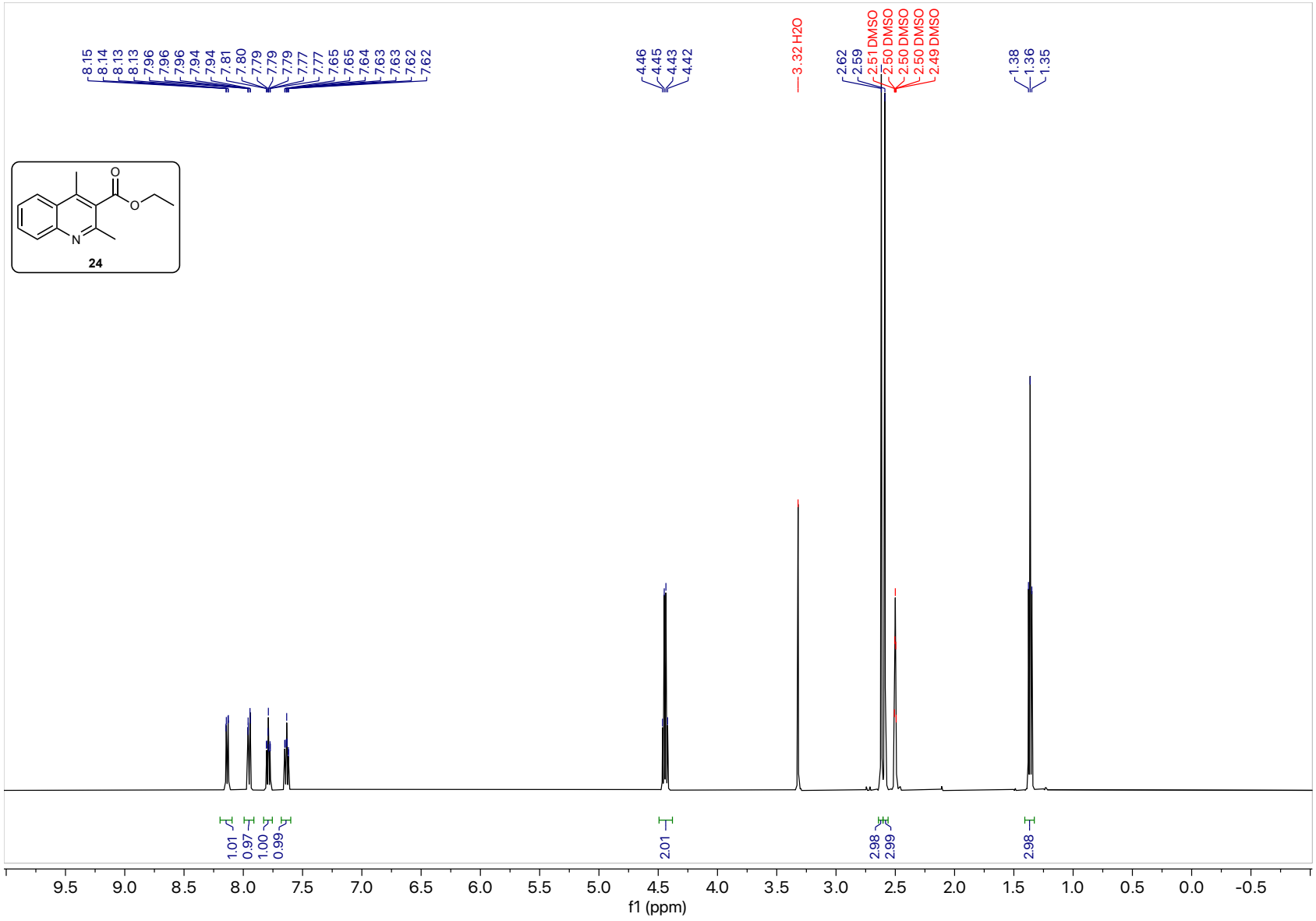
^{1}H NMR (500 MHz, DMSO-d_6) – standard view **(20)**



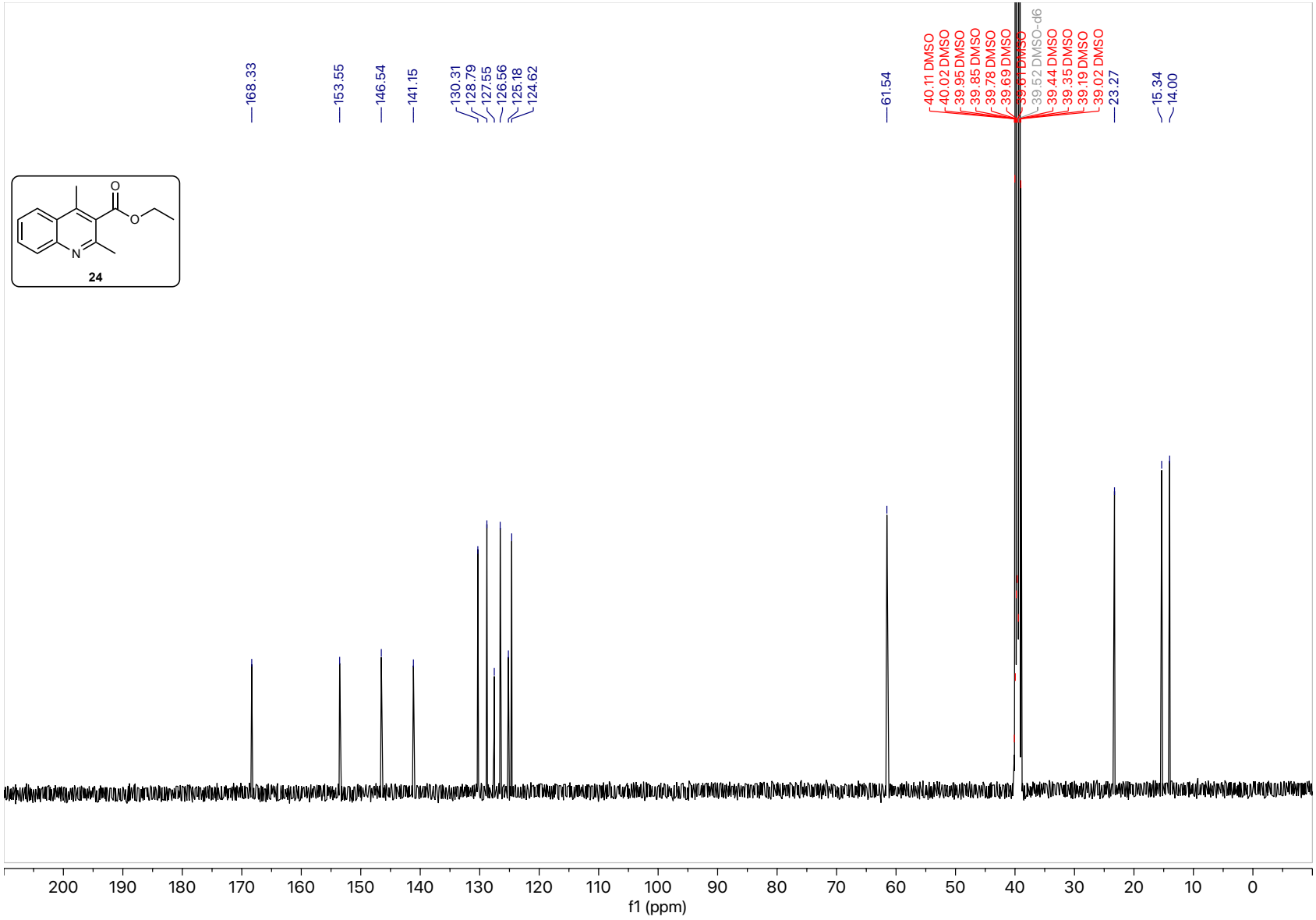
$^{13}C\{^{1}H\}$ NMR (126 MHz, DMSO-d_6) – standard view **(20)**



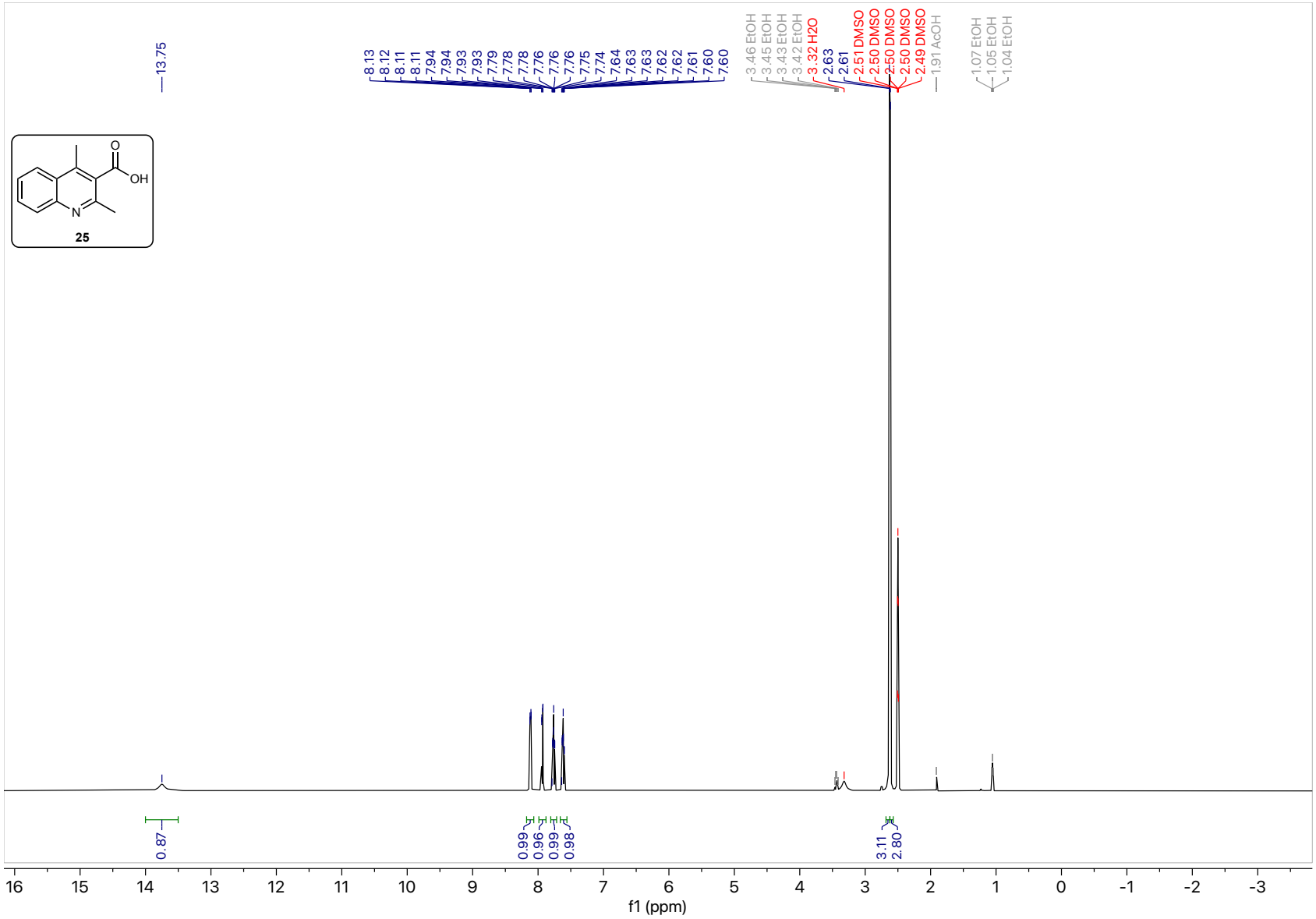
^{1}H NMR (500 MHz, DMSO-d_6) – standard view **(24)**



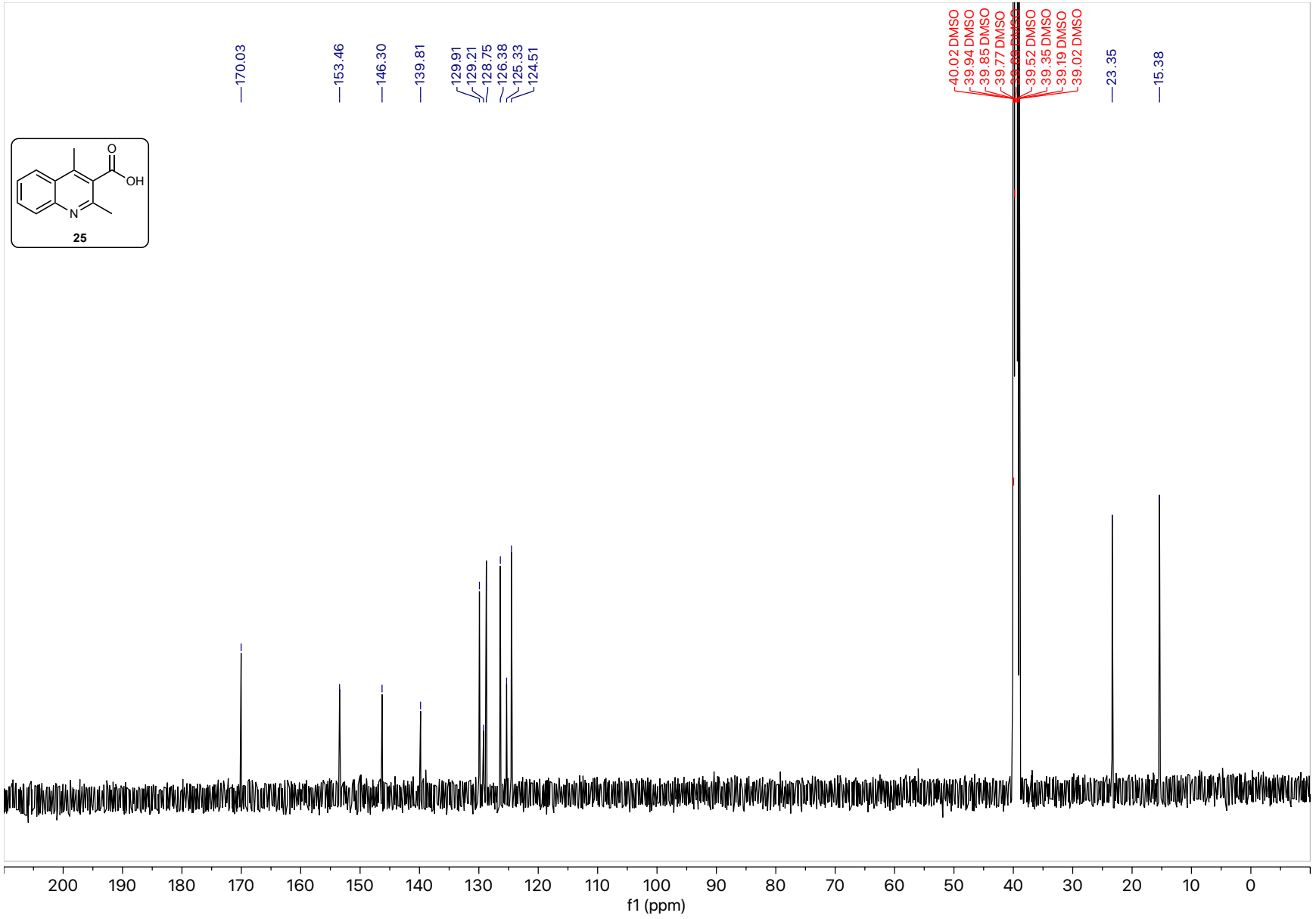
$^{13}C\{^{1}H\}$ NMR (126 MHz, DMSO-d_6) – standard view **(24)**



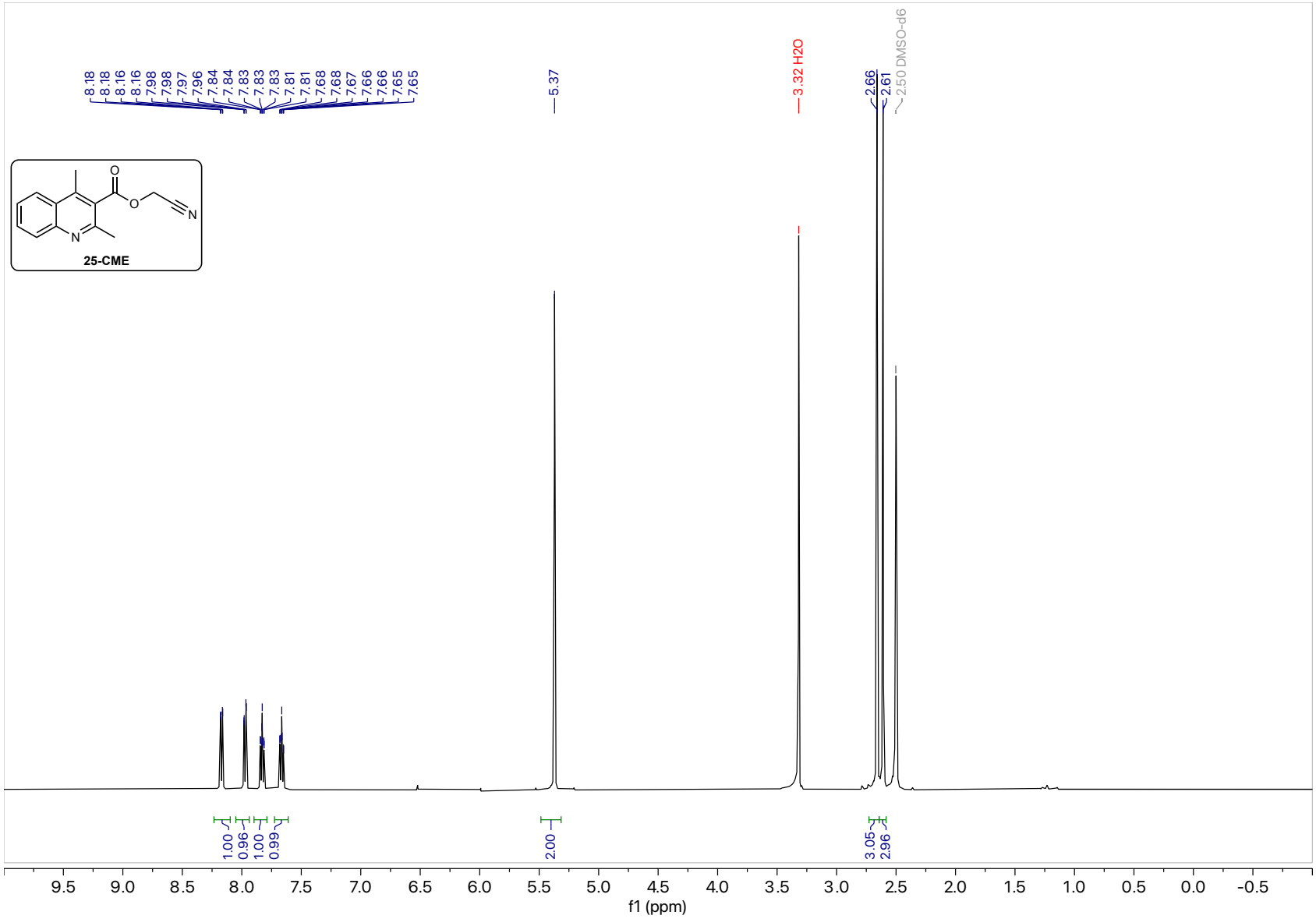
^{1}H NMR (500 MHz, DMSO-d_6) – extended view **(25)**



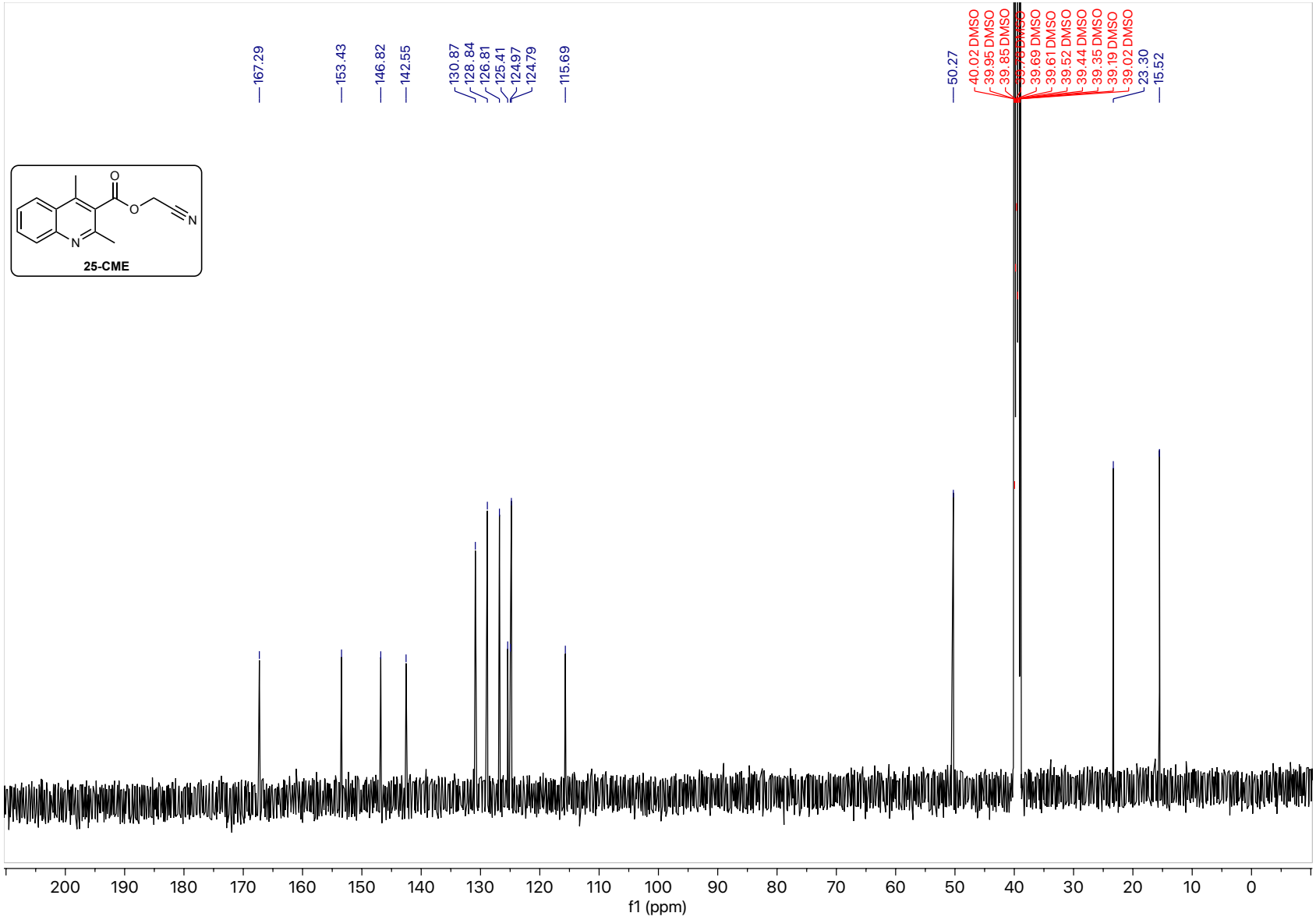
$^{13}C\{^{1}H\}$ NMR (126 MHz, DMSO-d_6) – standard view **(25)**



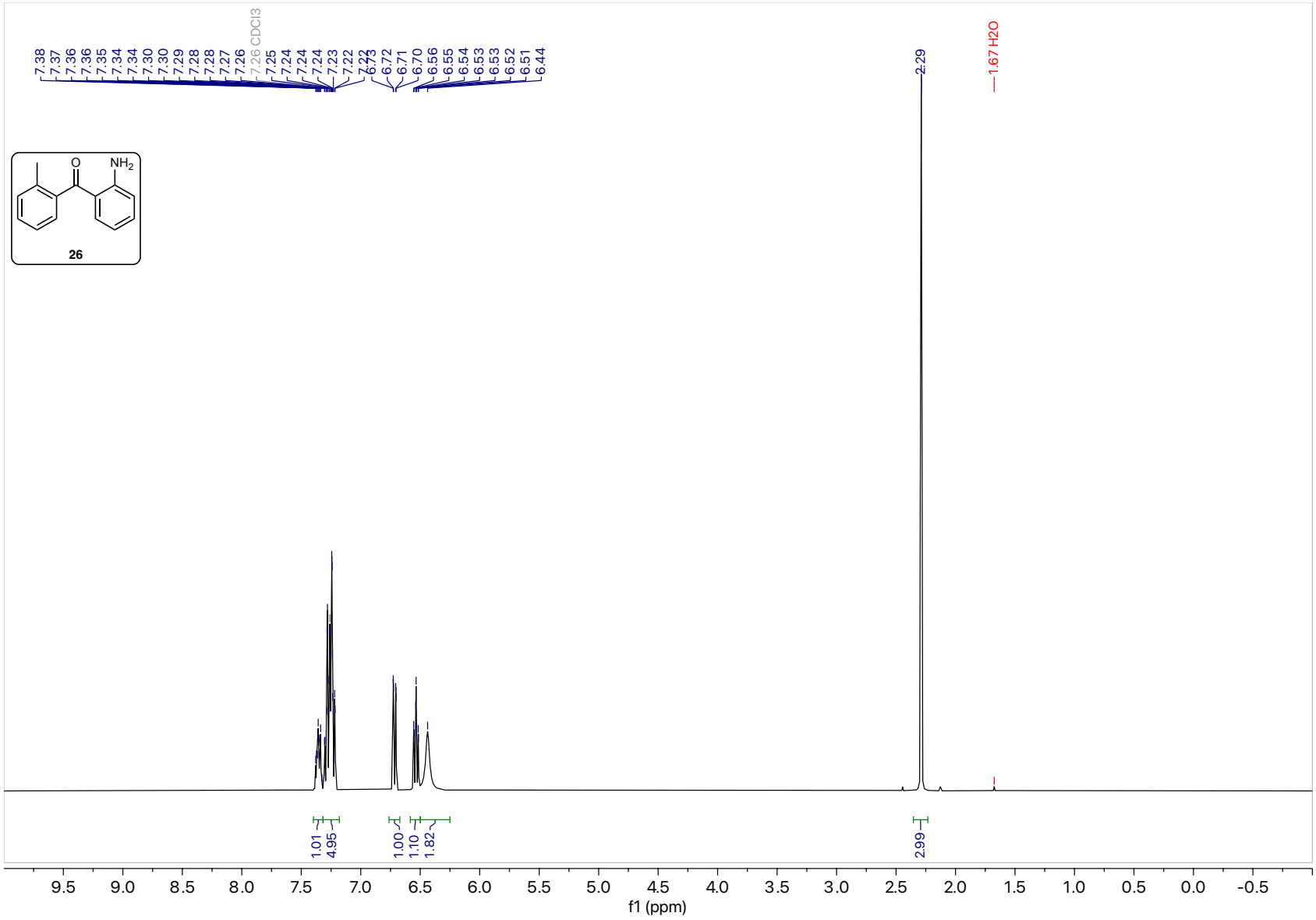
^{1}H NMR (500 MHz, DMSO-d_6) – standard view **(25-CME)**



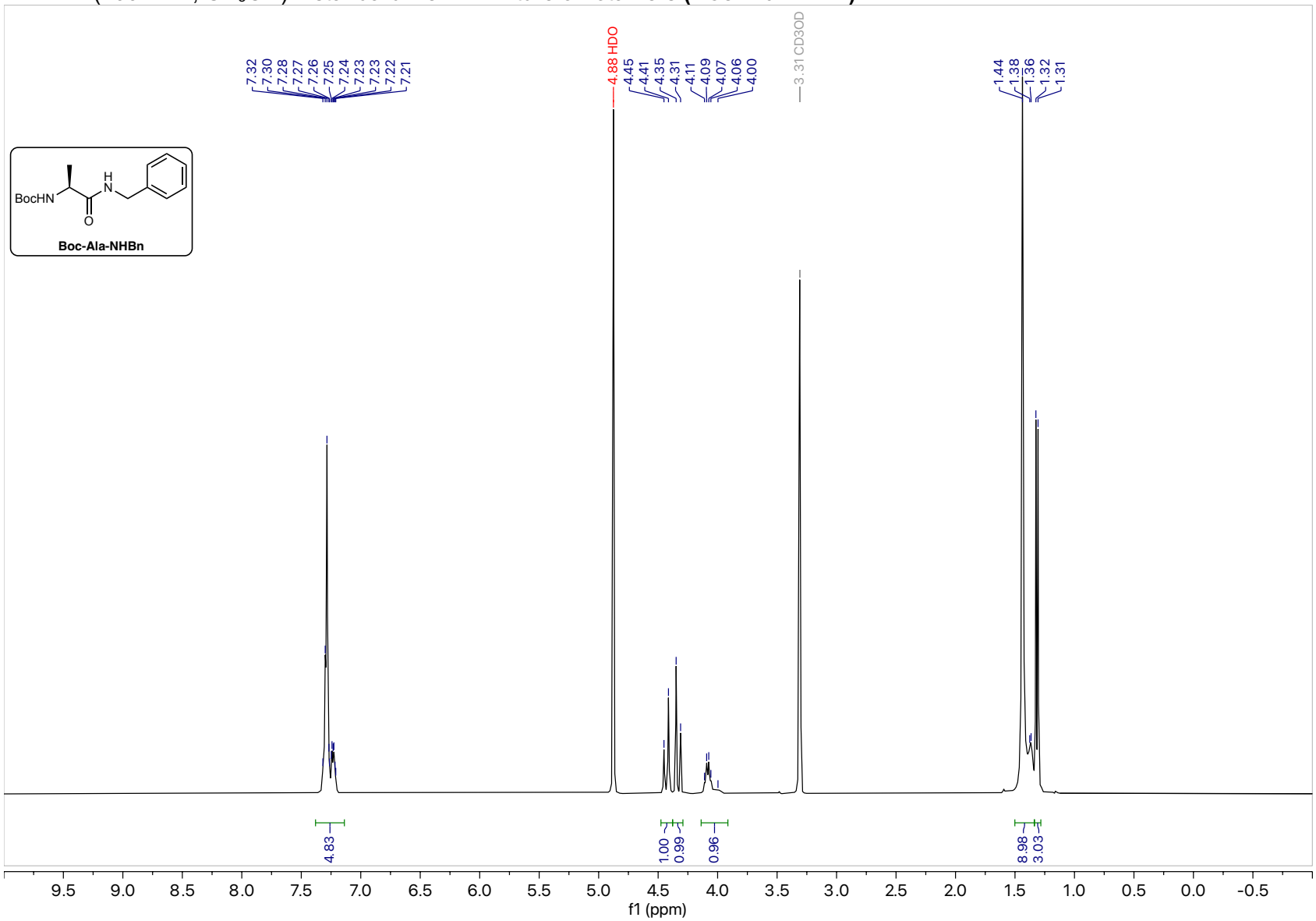
$^{13}C\{^{1}H\}$ NMR (126 MHz, DMSO-d_6) – standard view **(25-CME)**



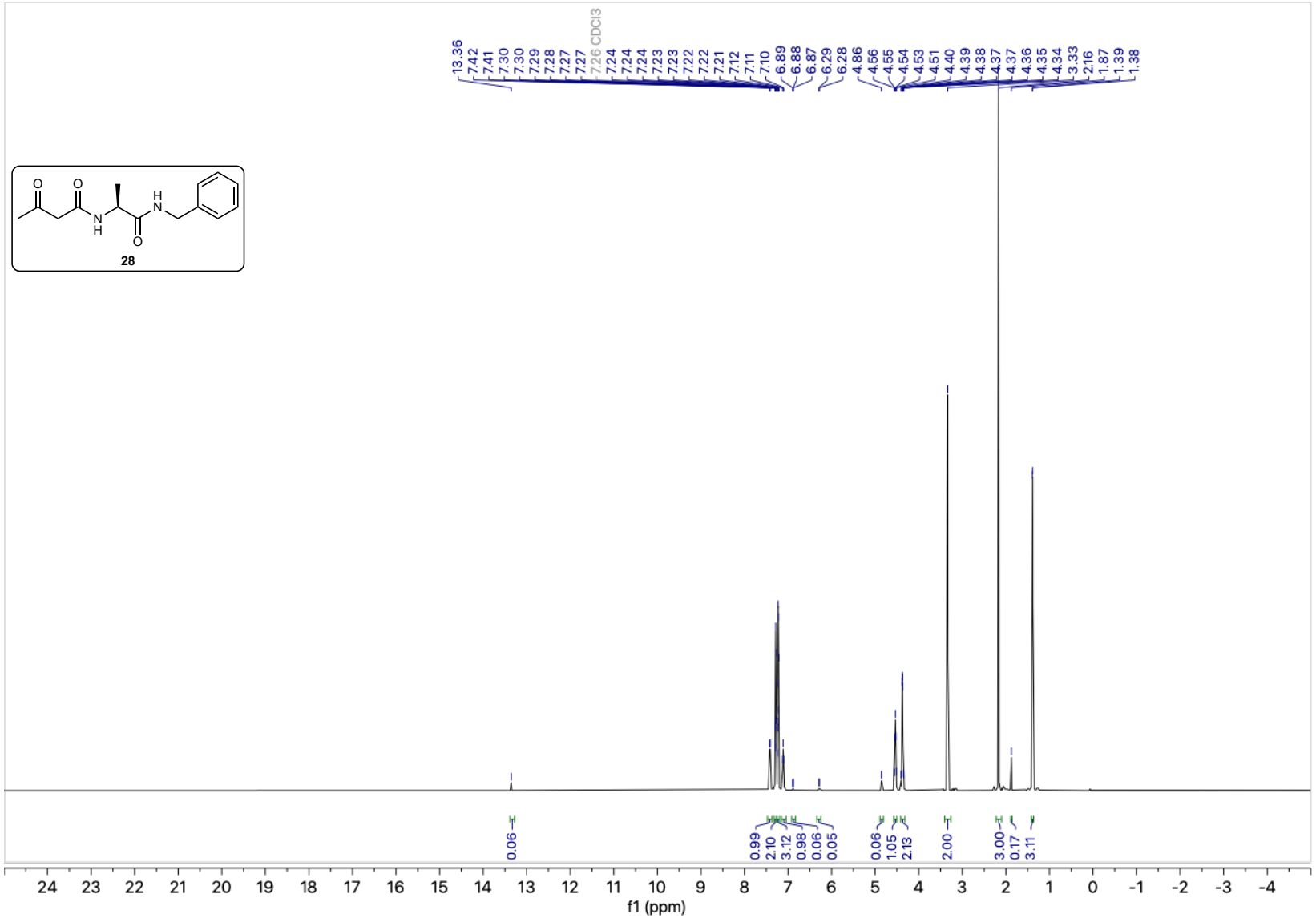
^{1}H NMR (400 MHz, $CDCl_3$) – standard view **(26)**



^{1}H NMR (400 MHz, CD_3OD) – standard view – mixture of rotamers **(Boc-Ala-NHBn)**

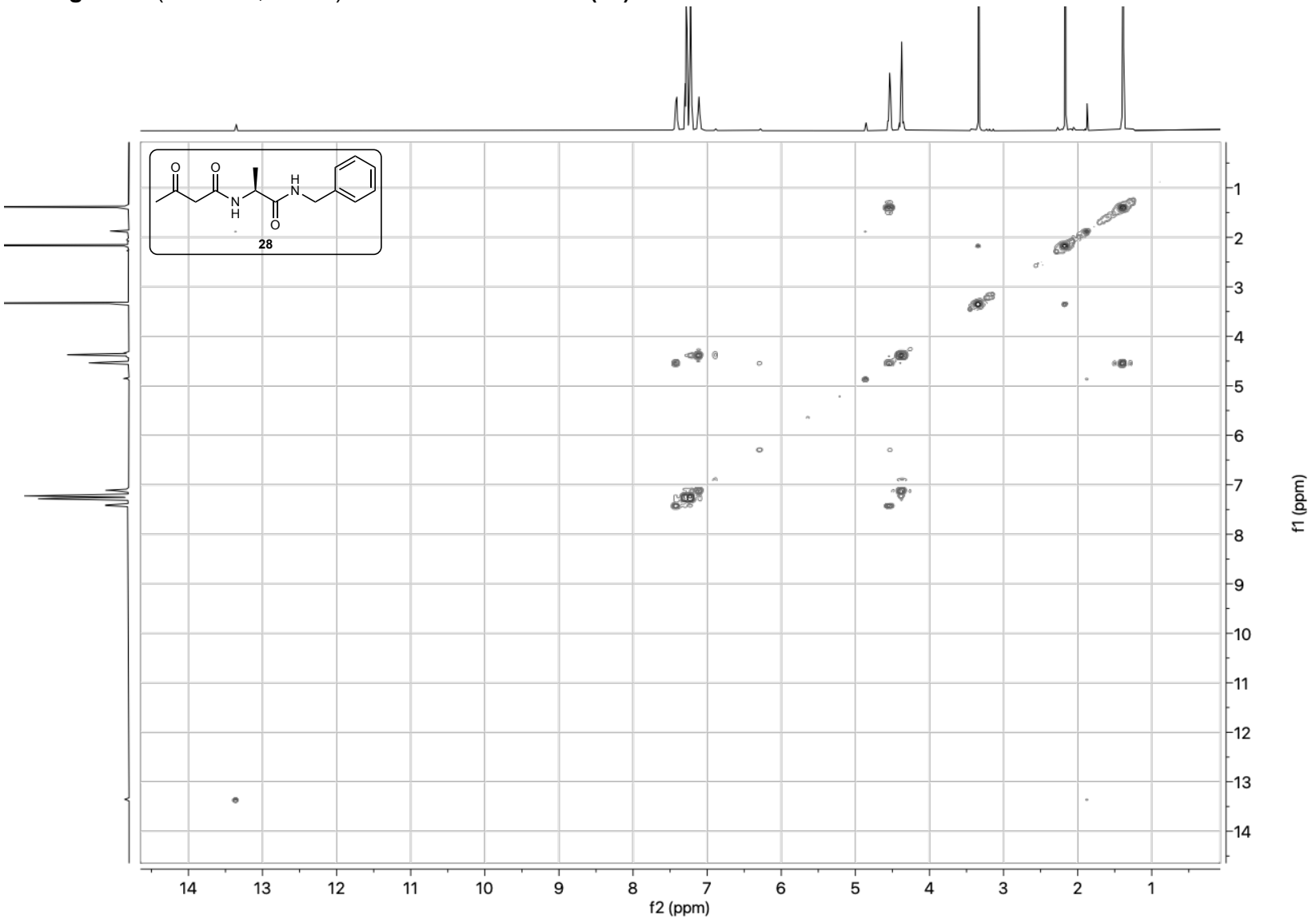


^{1}H NMR (600 MHz, $CDCl_3$) – extended view – mixture of tautomers **(28)**

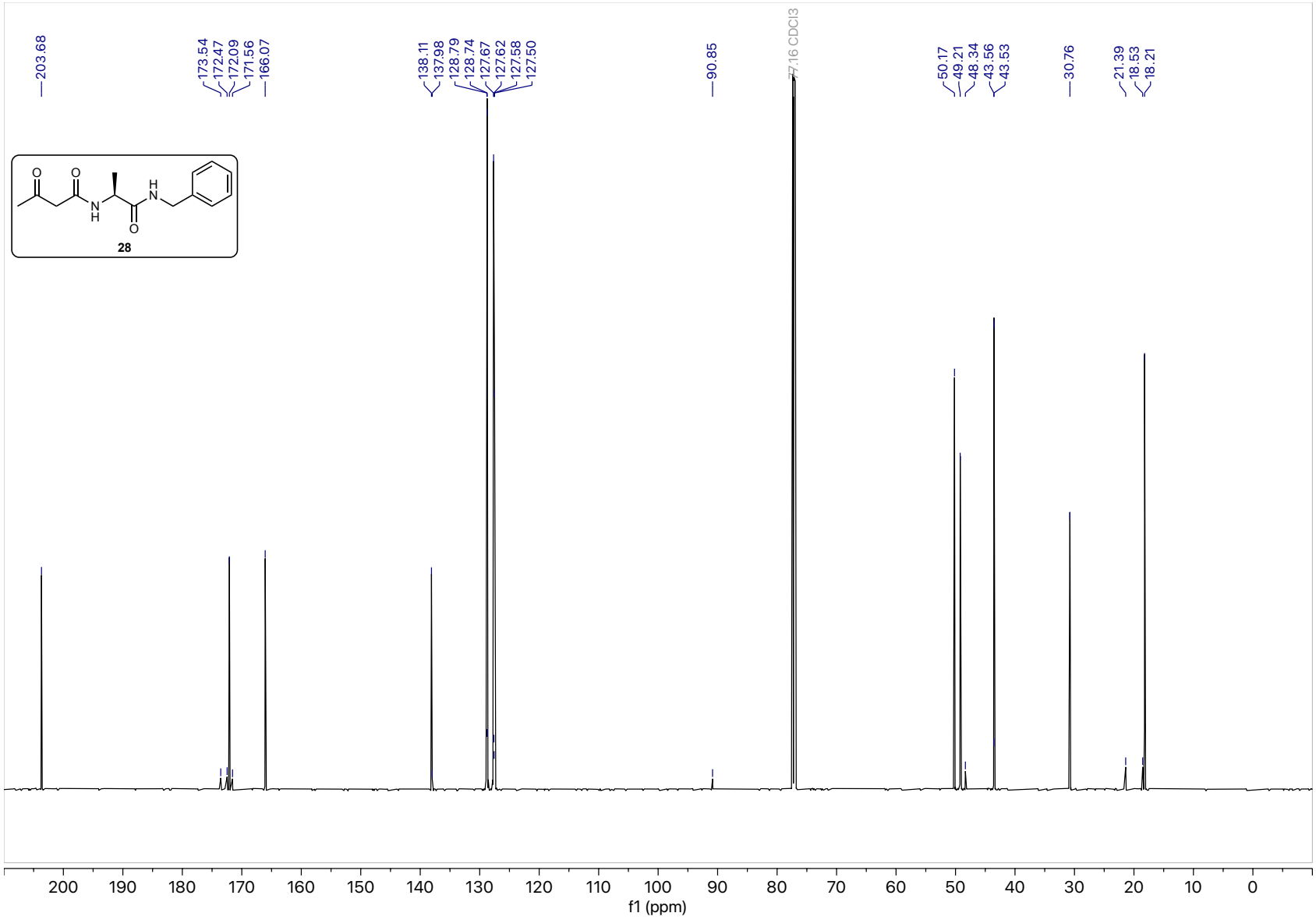


28

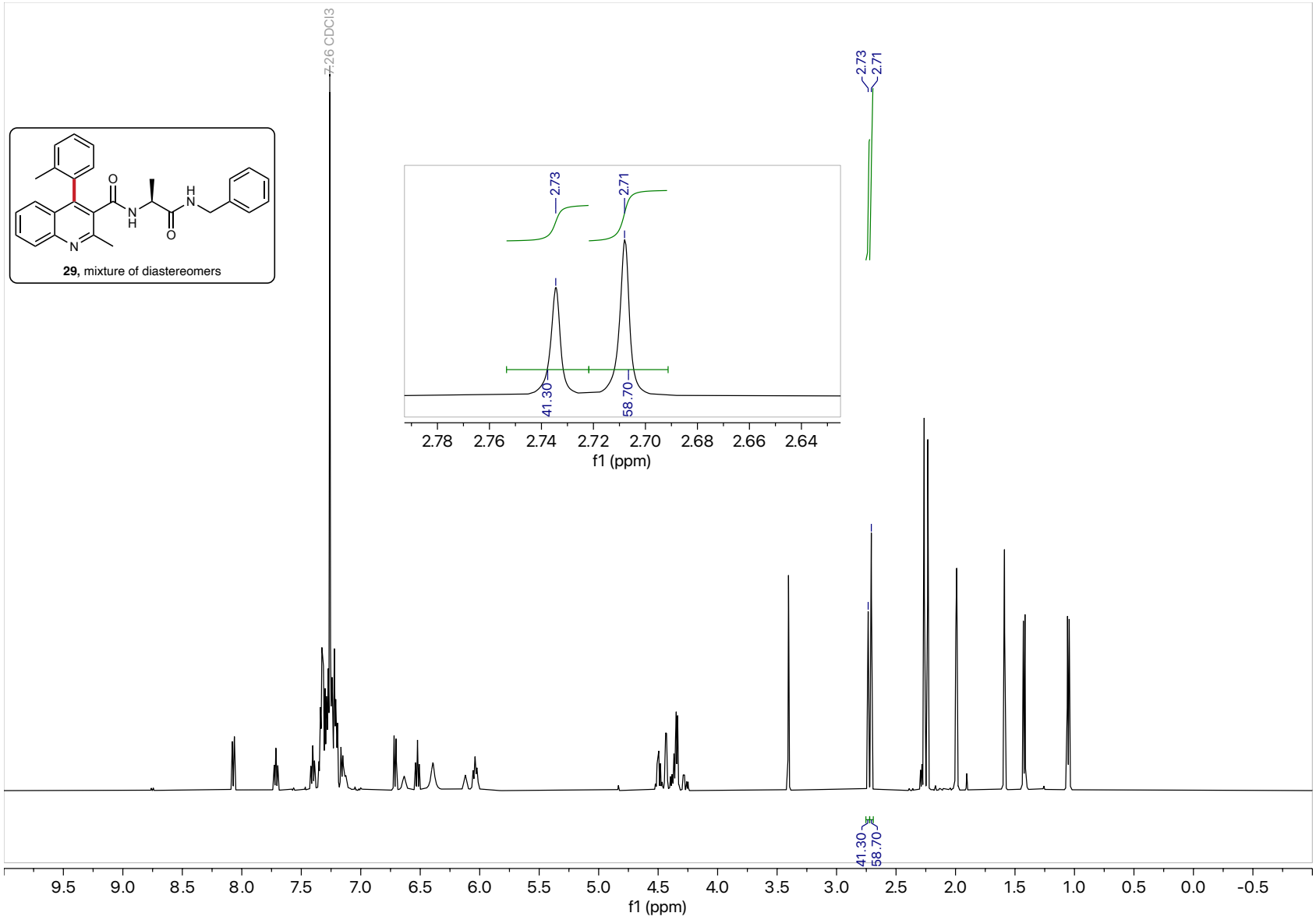
^{1}H-^{1}H gCOSY (600 MHz, $CDCl_3$) – mixture of tautomers **(28)**



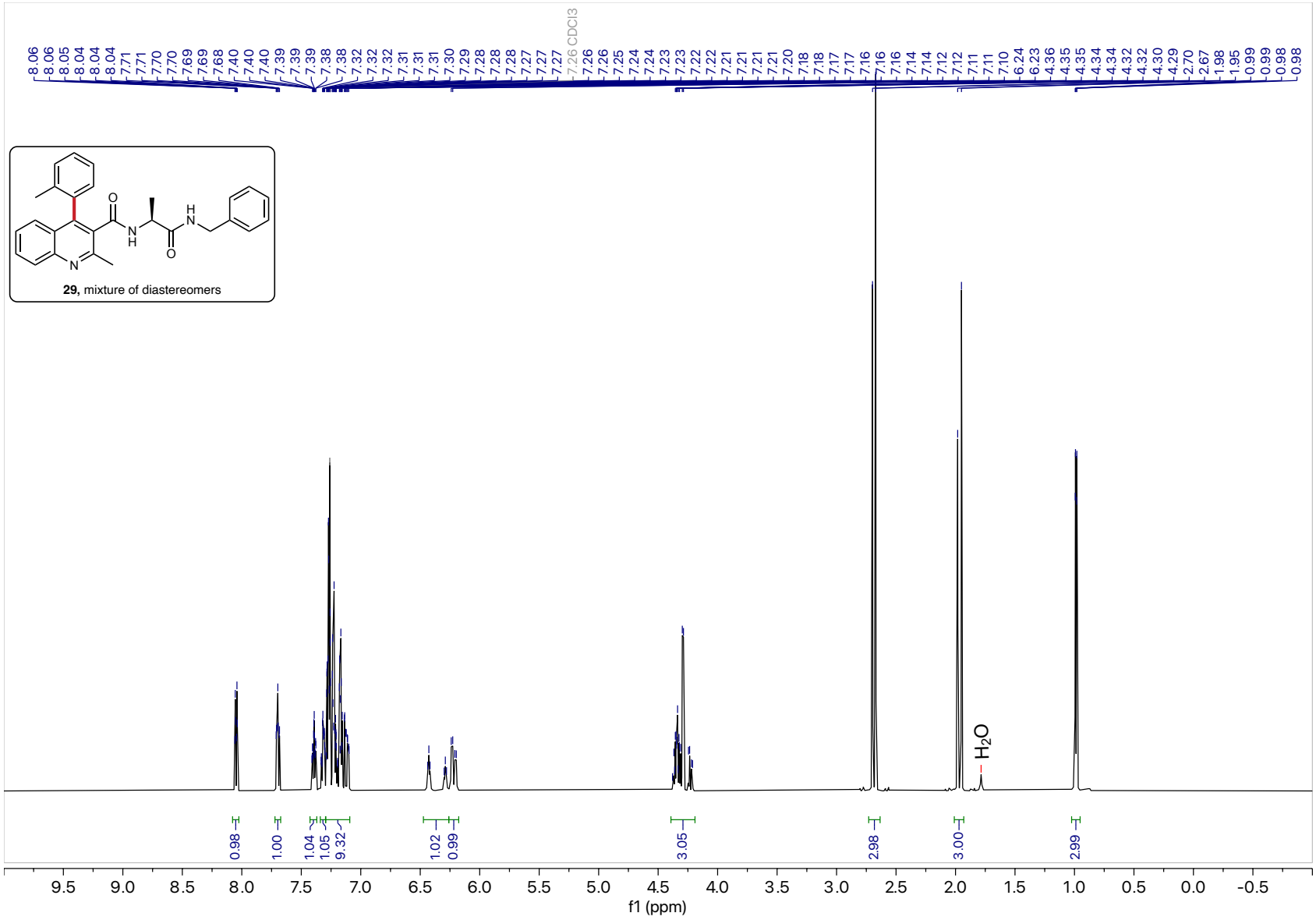
$^{13}C\{^{1}H\}$ NMR (151 MHz, $CDCl_3$) – standard view – mixture of tautomers **(28)**



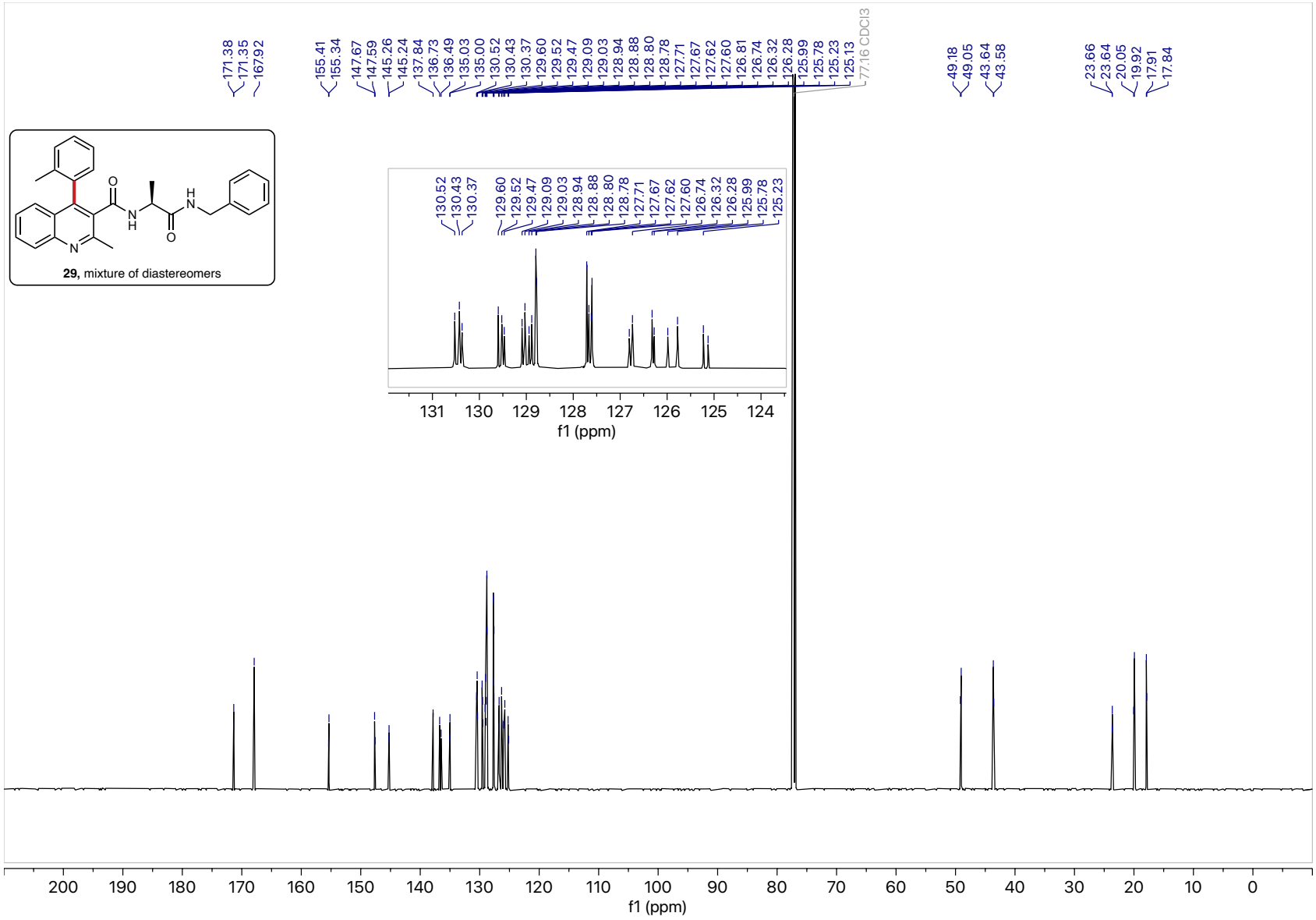
^{1}H NMR (600 MHz, $CDCl_3$) – standard view – mixture of diastereomers, crude [Preparation I] **(29)**



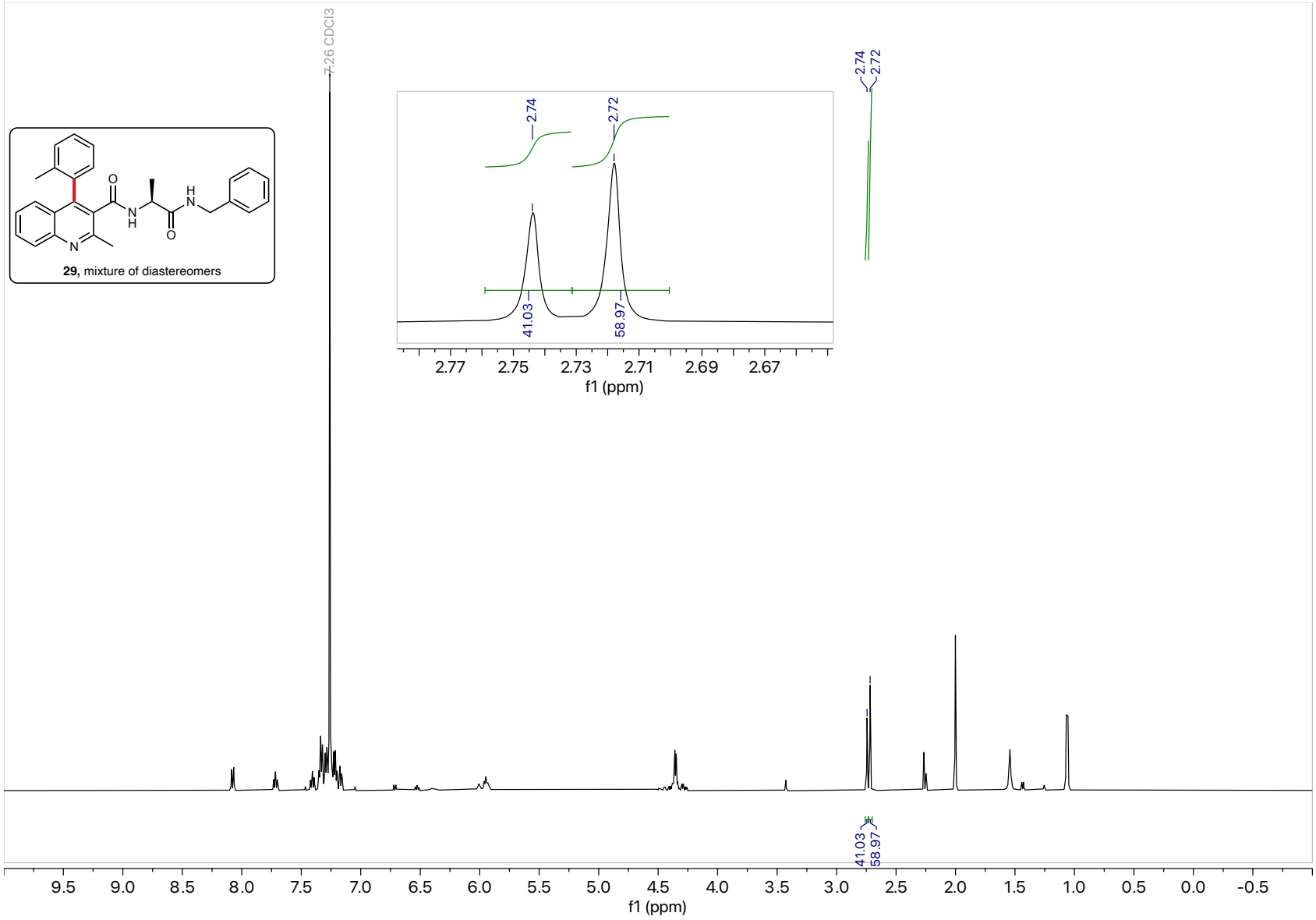
^{1}H NMR (600 MHz, $CDCl_3$) – standard view – mixture of diastereomers, purified [Preparation I] **(29)**



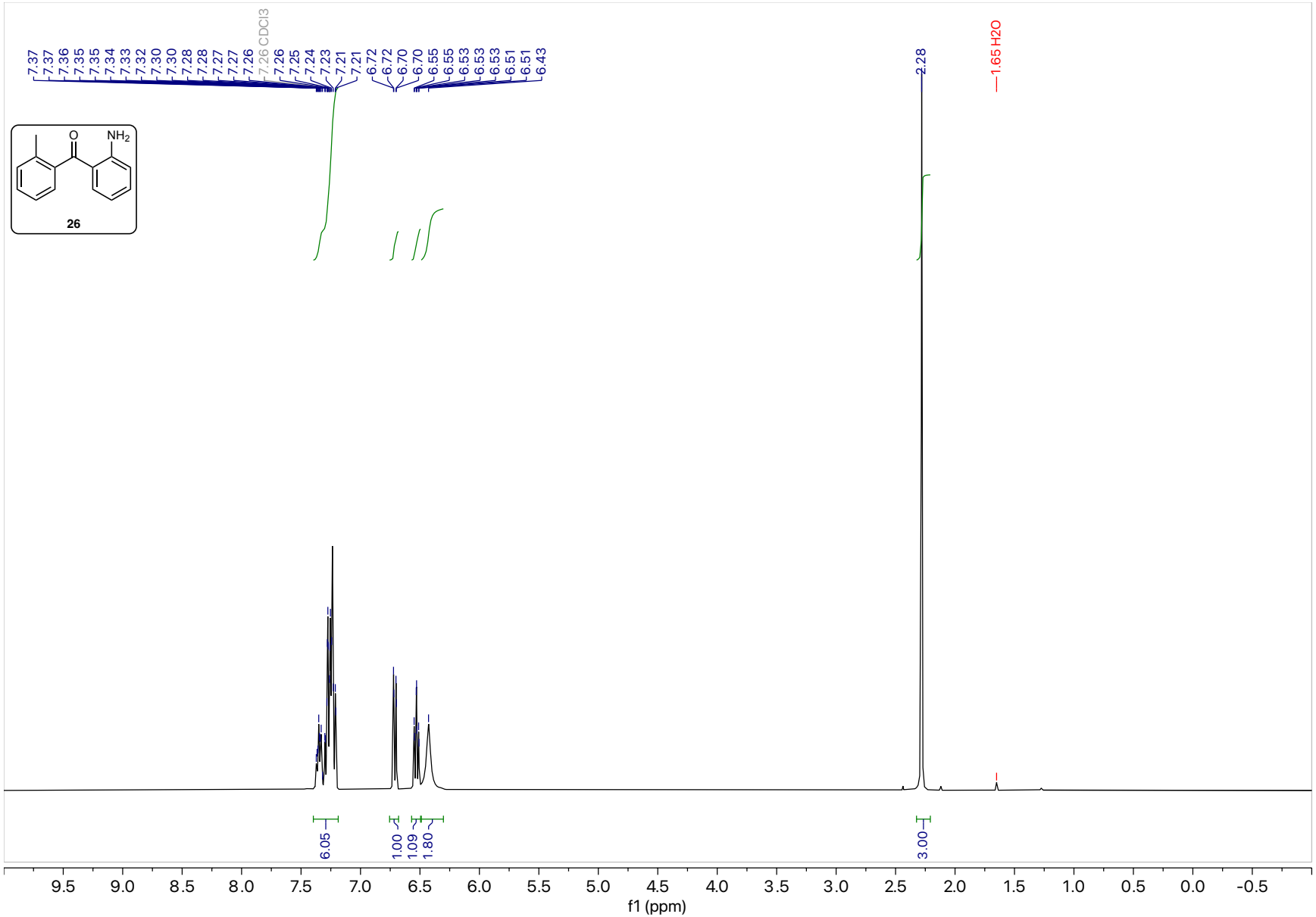
$^{13}C\{^{1}H\}$ NMR ($CDCl_3$) – standard view – mixture of diastereomers, purified [Preparation I] **(29)**



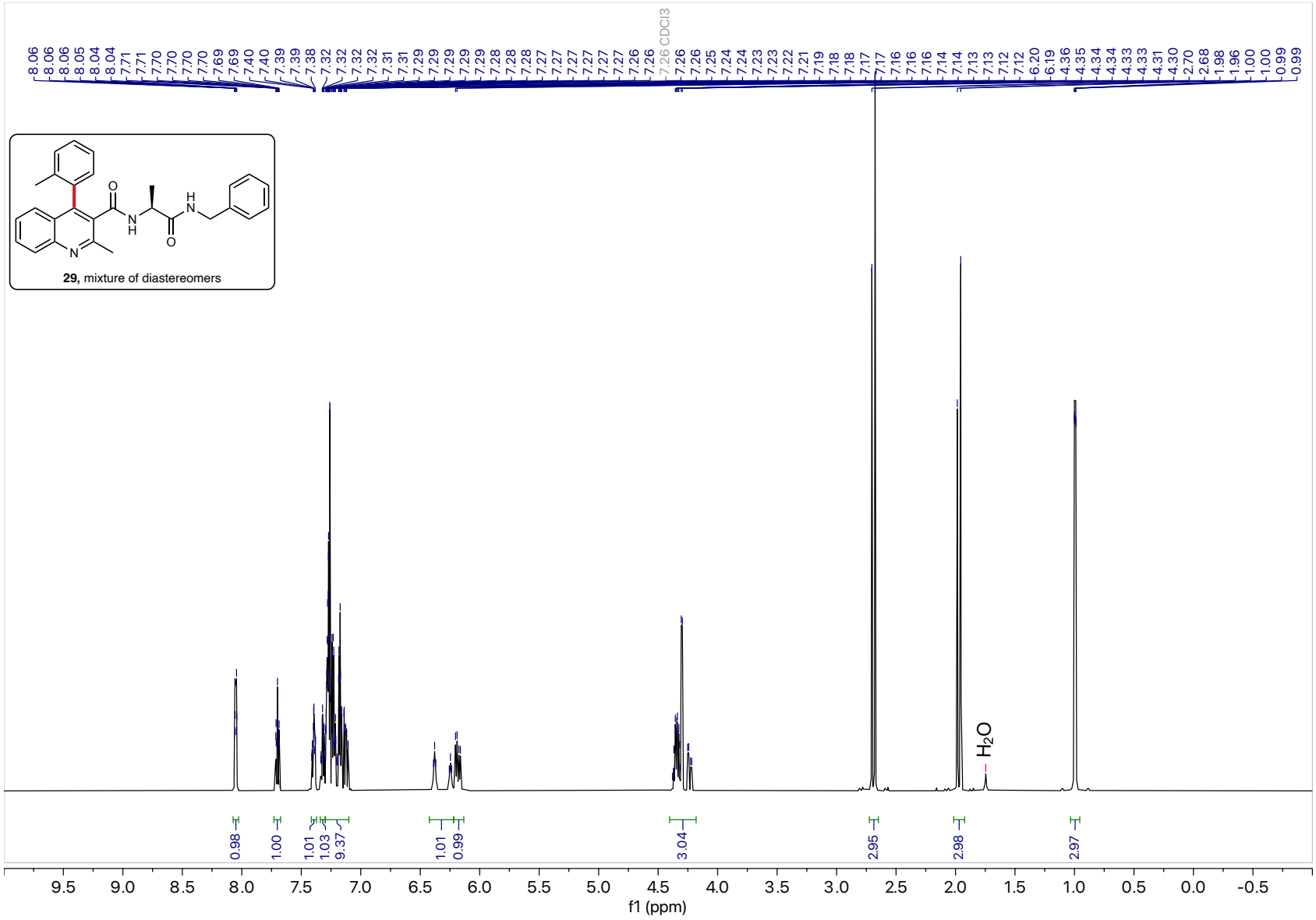
^{1}H NMR (600 MHz, $CDCl_3$) – standard view – mixture of diastereomers, crude [Preparation II] **(29)**



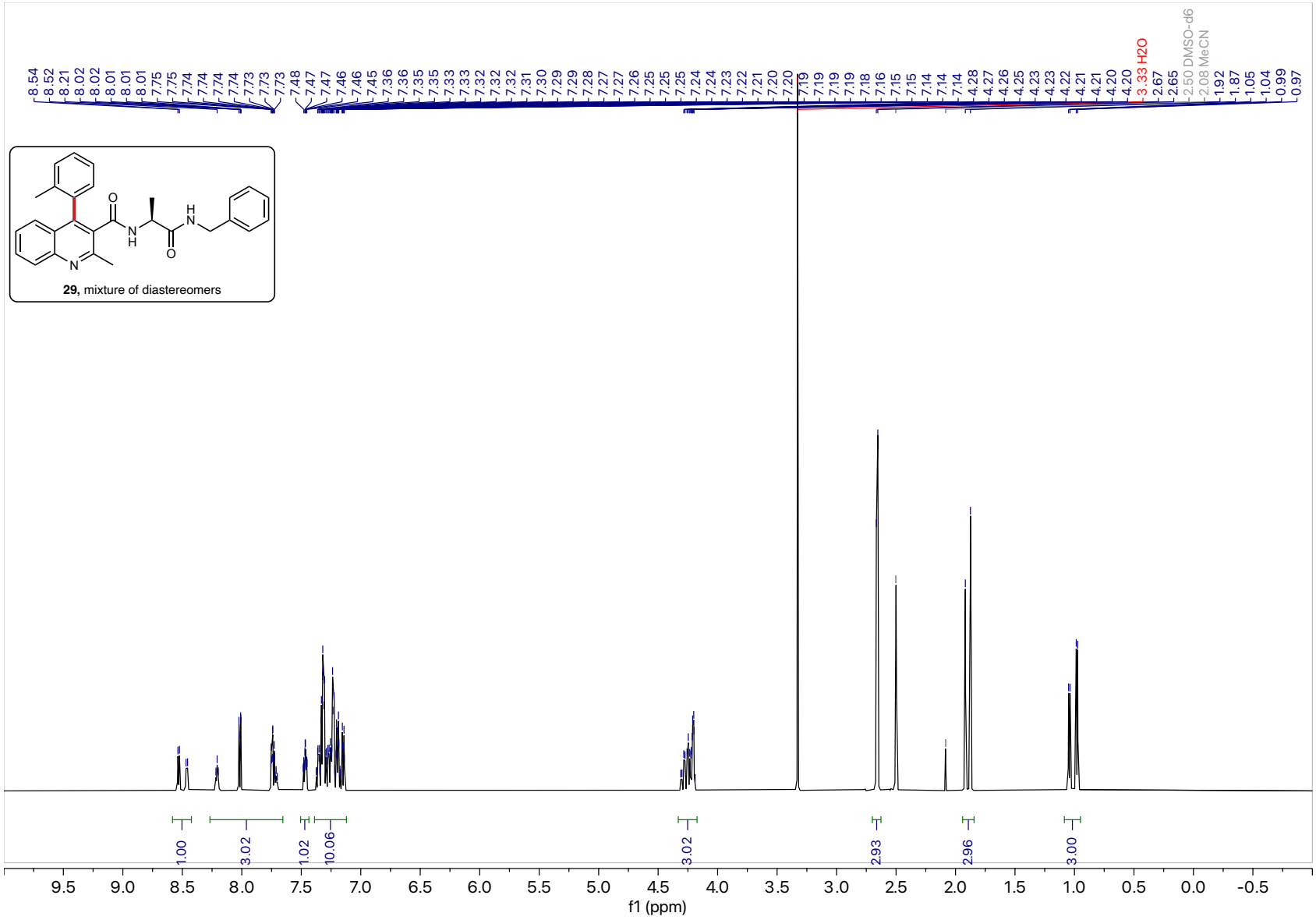
^{1}H NMR (400 MHz, $CDCl_3$) – standard view – recovered arene **26** from Preparation II of **29**



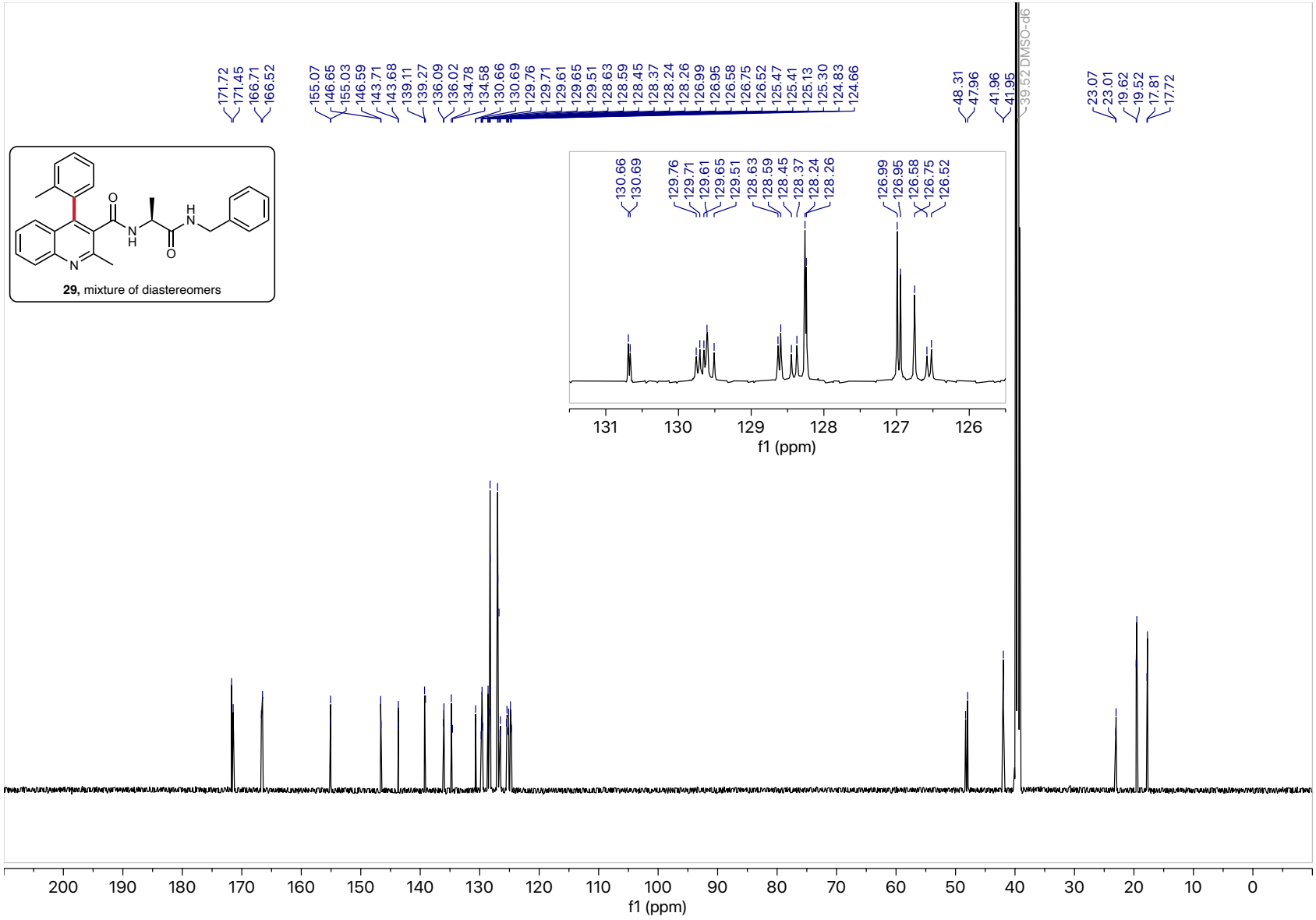
^{1}H NMR (600 MHz, $CDCl_3$) – standard view – mixture of diastereomers, purified [Preparation II] **(29)**



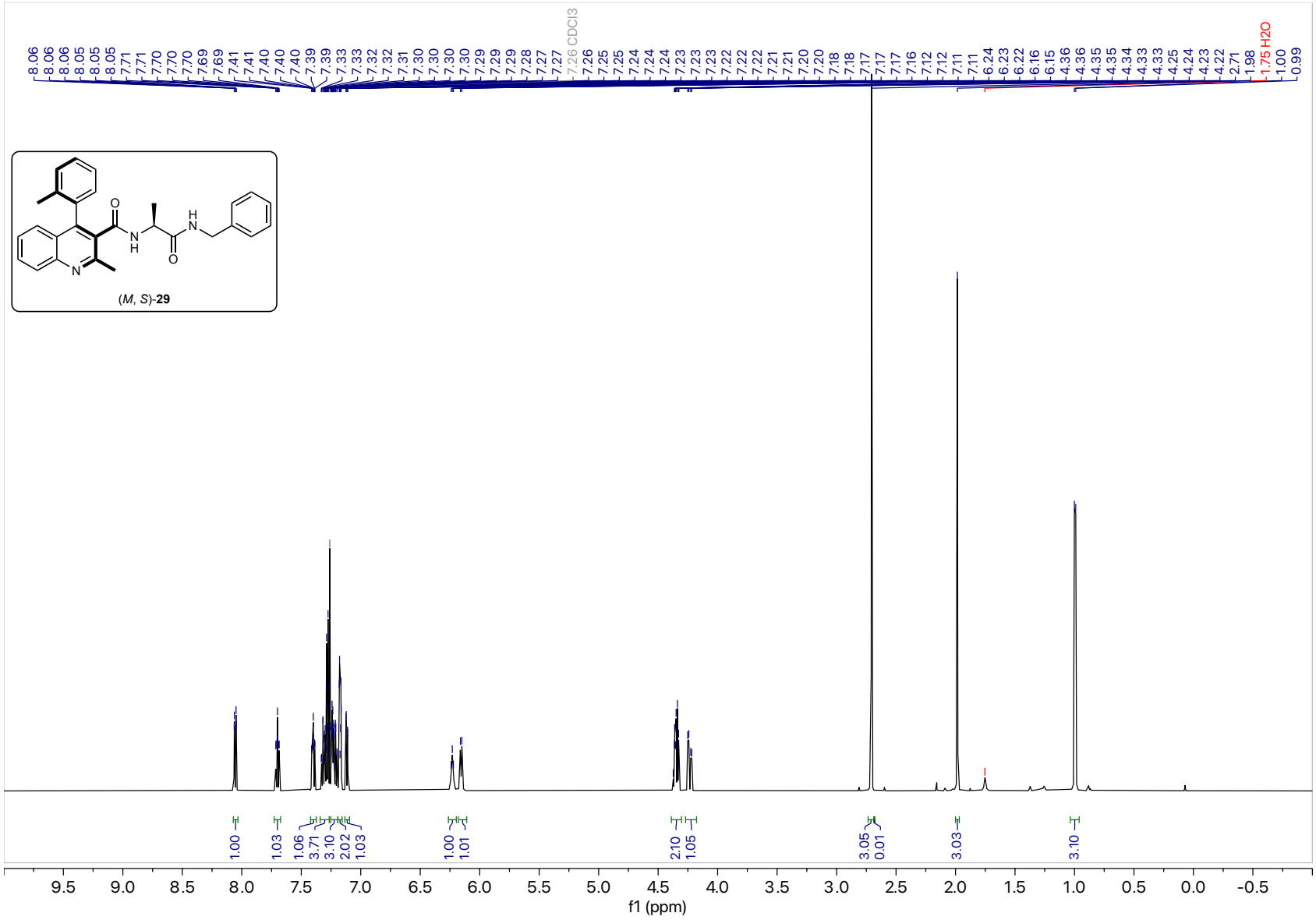
^{1}H NMR (600 MHz, DMSO-d_6) – standard view – mixture of diastereomers, purified [Preparation II] **(29)**



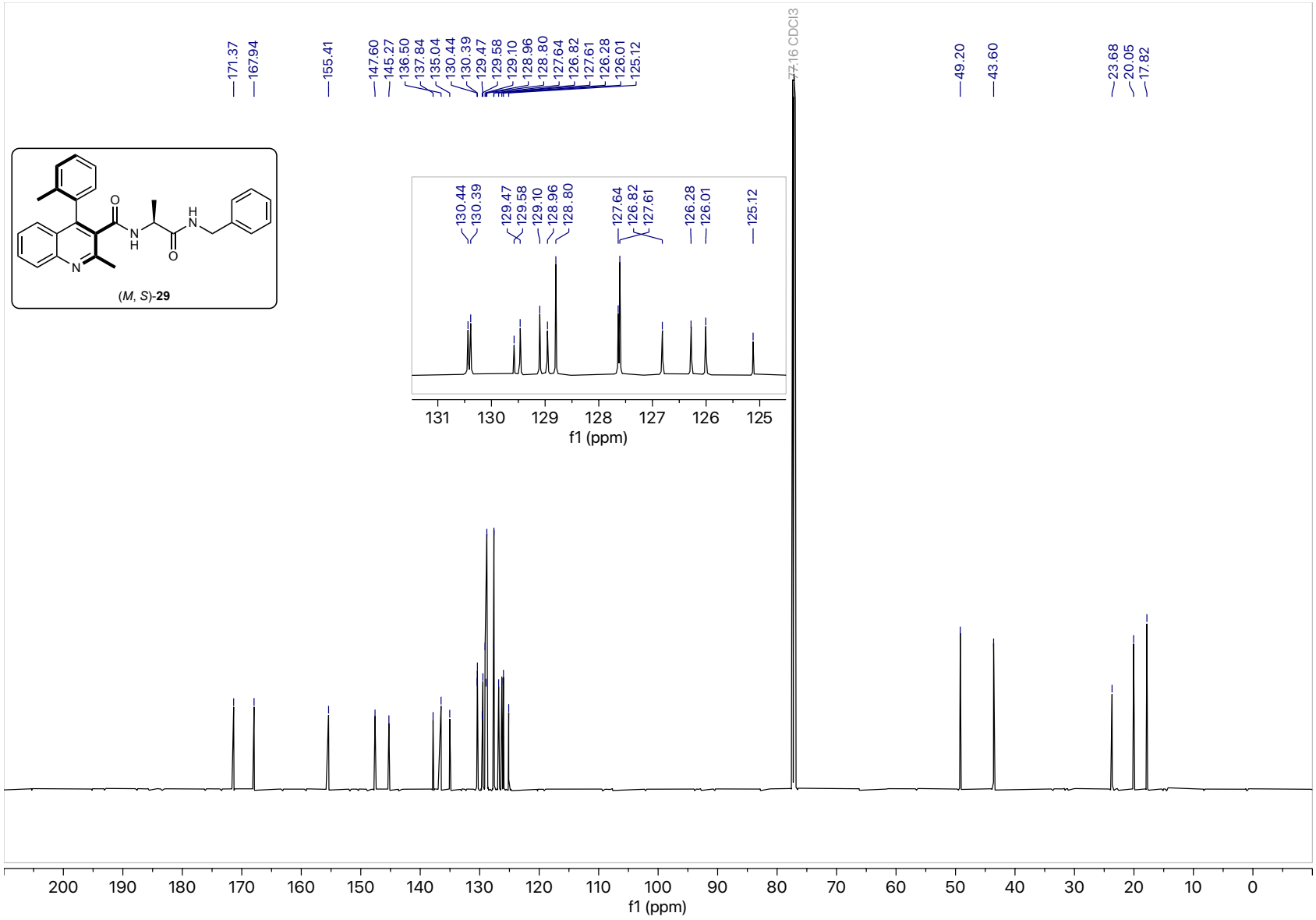
$^{13}C\{^{1}H\}$ NMR (151 MHz, DMSO-d_6) – standard view – mixture of diastereomers, purified [Preparation II] **(29)**



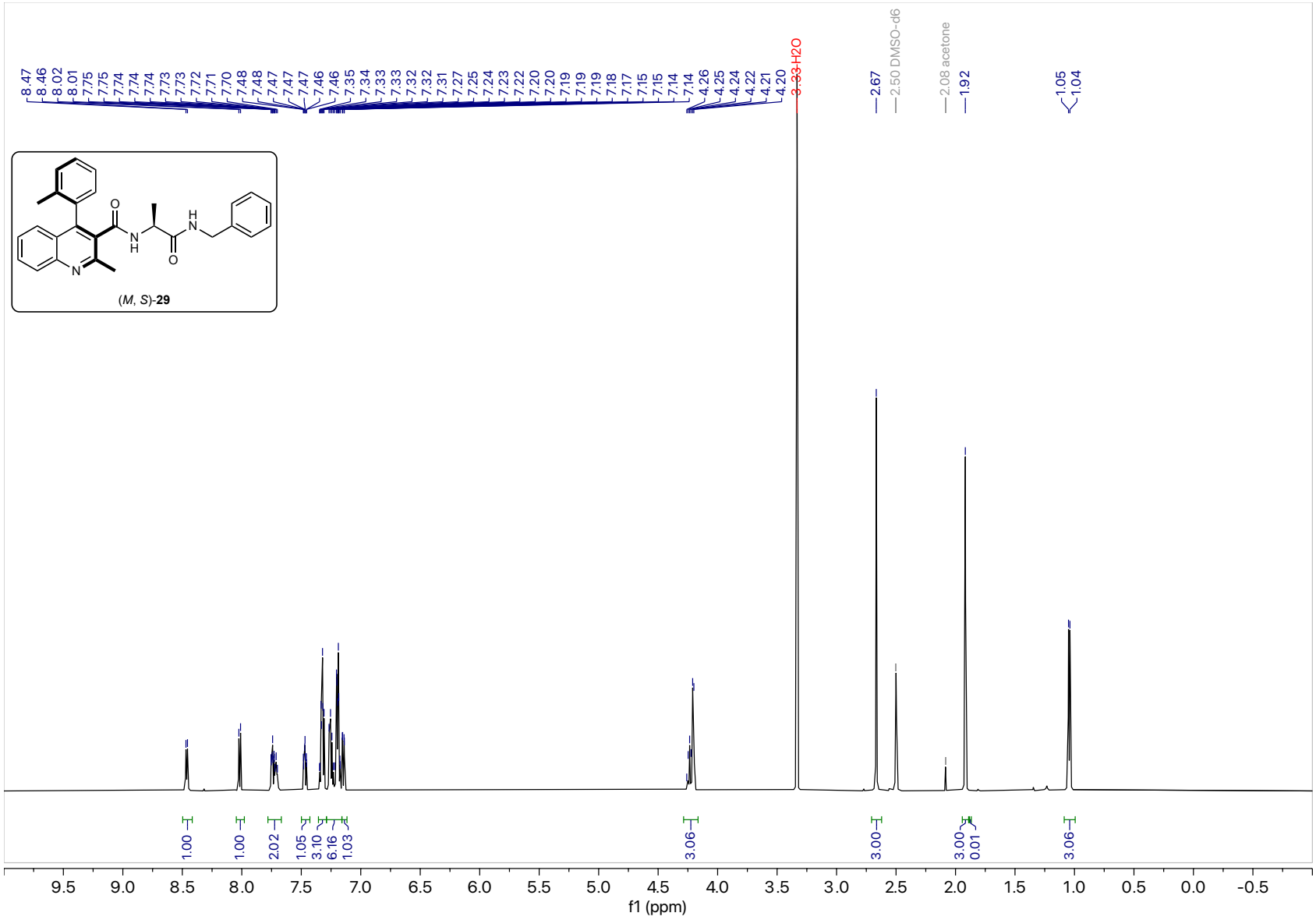
^{1}H NMR (600 MHz, $CDCl_3$) – standard view **((*M, S*)-29)**



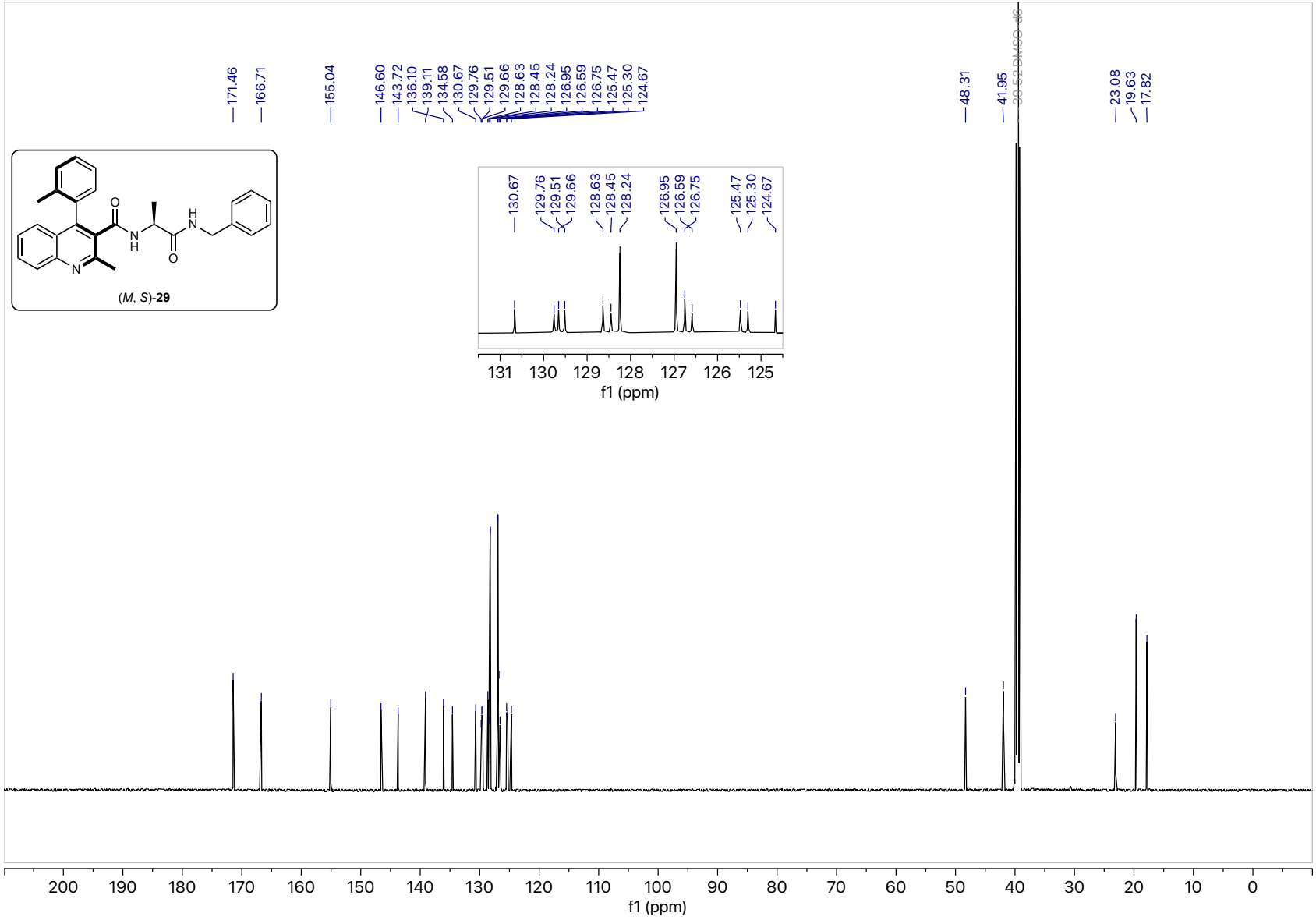
$^{13}C\{^{1}H\}$ NMR (151 MHz, $CDCl_3$) – standard view **((*M, S*)-29)**



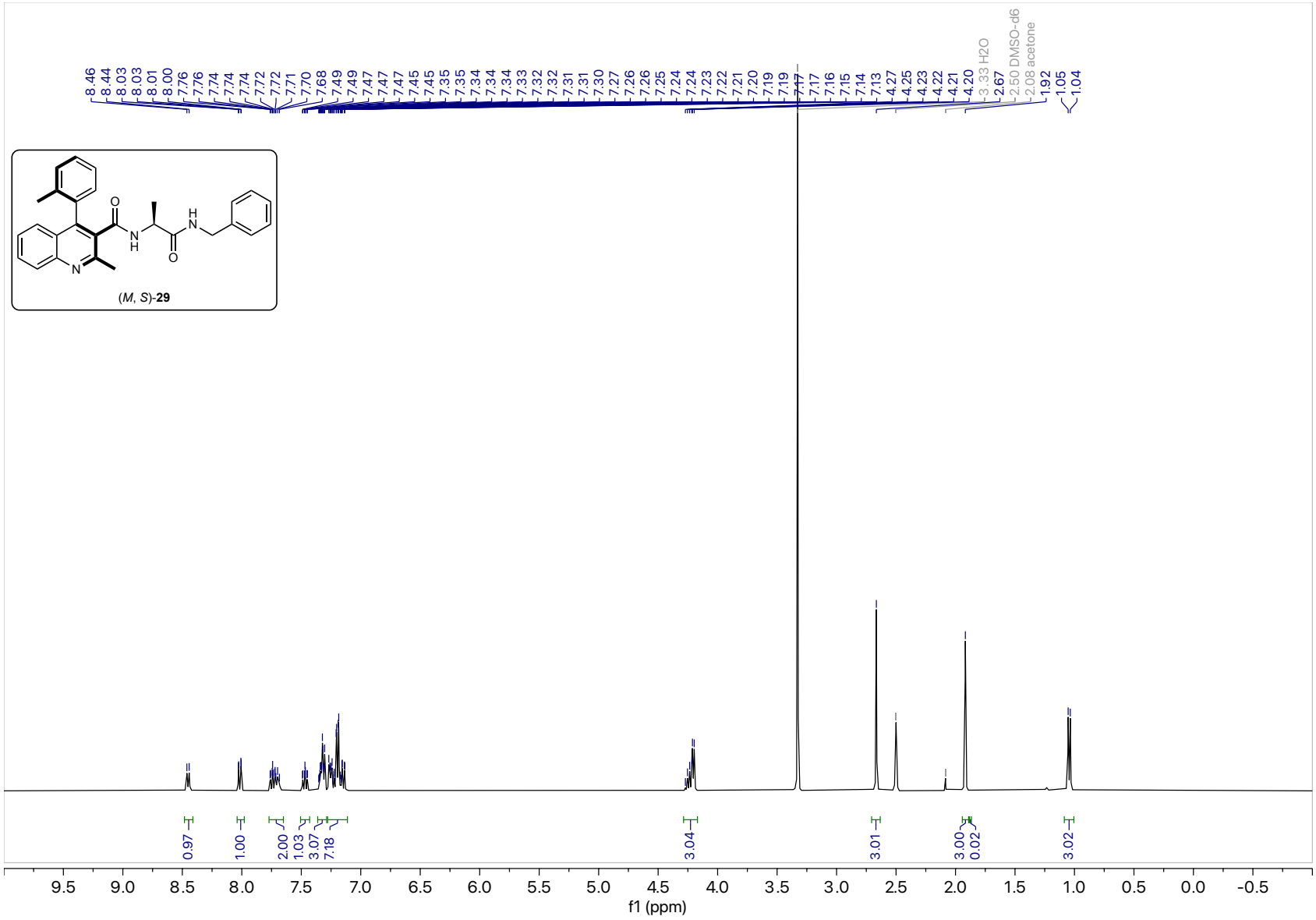
^{1}H NMR (600 MHz, DMSO-d_6) – standard view **((*M, S*)-29)**



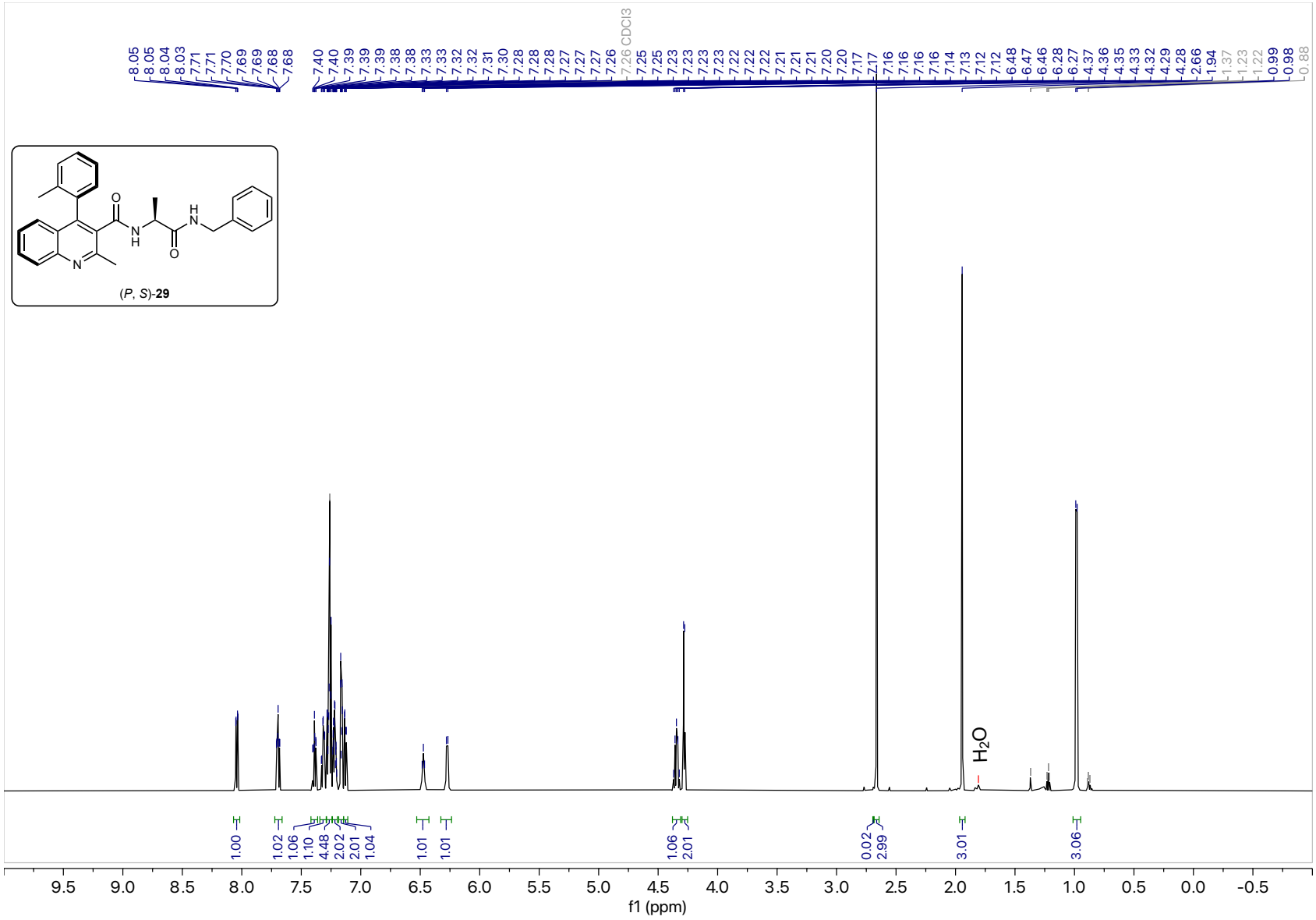
$^{13}C\{^{1}H\}$ NMR (151 MHz, DMSO-d_6) – standard view **((*M, S*)-29)**



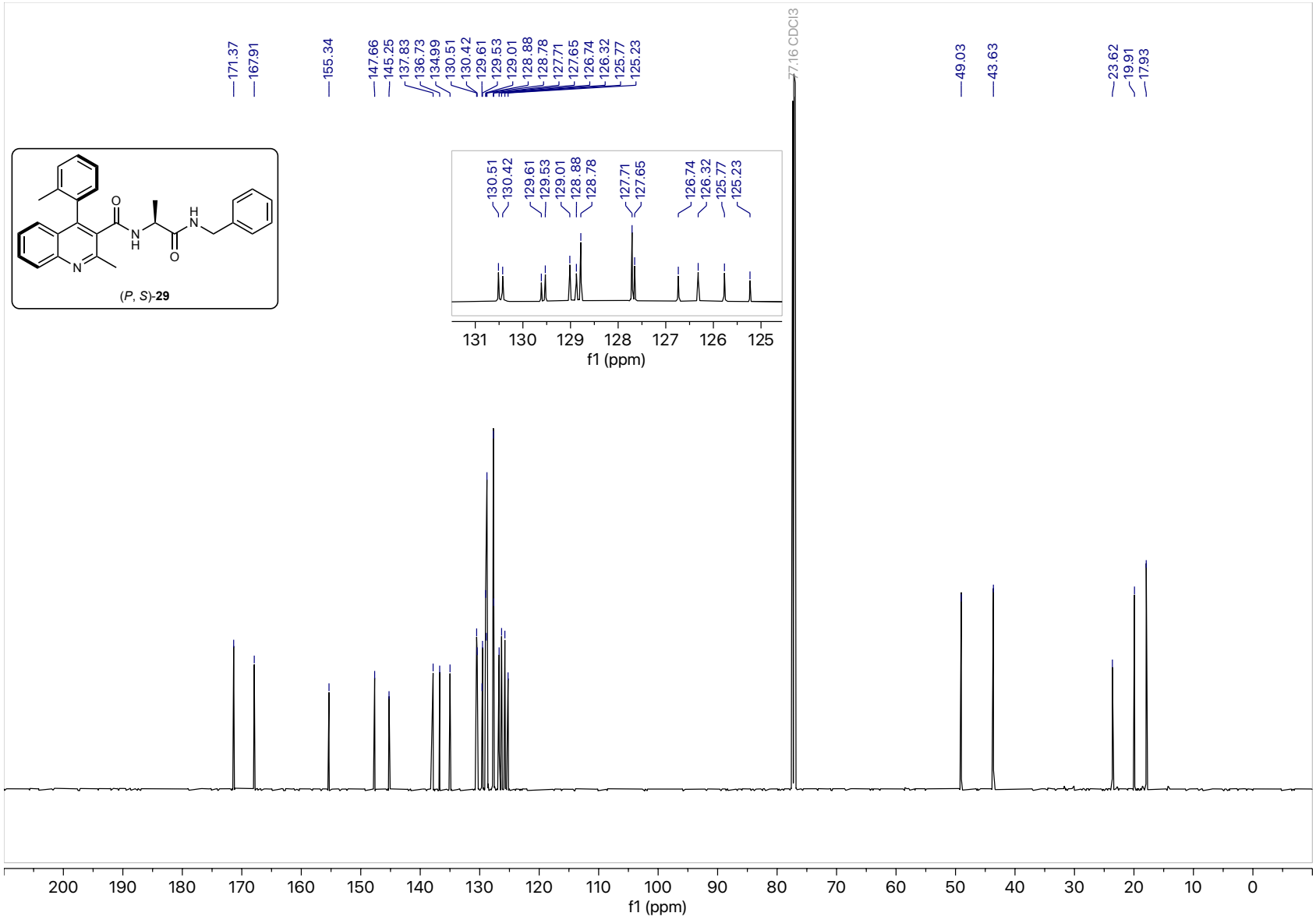
^{1}H NMR (600 MHz, DMSO-d_6) – standard view **((*M, S*)-29)** – after heating 18h



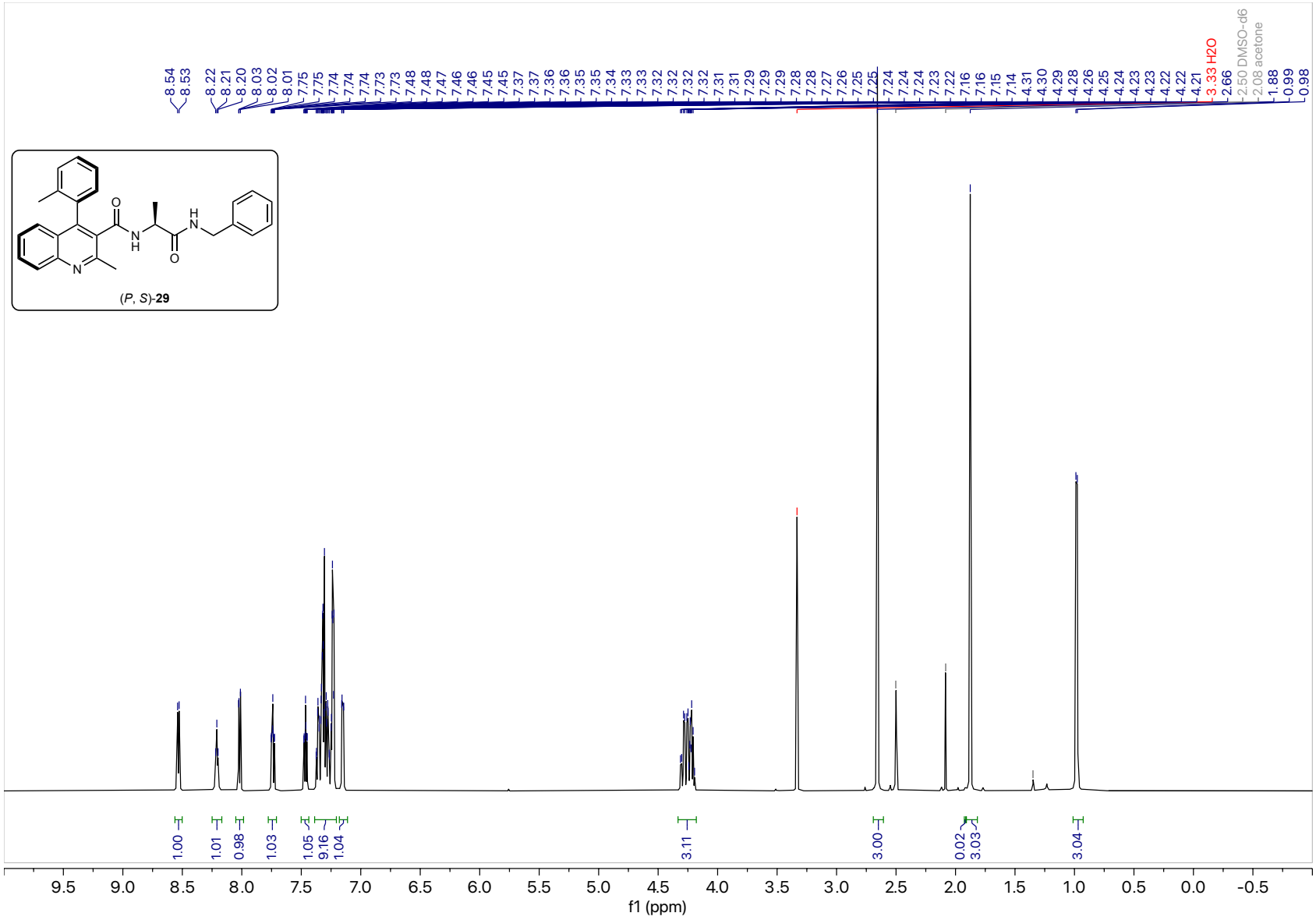
^{1}H NMR (600 MHz, $CDCl_3$) – standard view **((*P, S*)-29)**



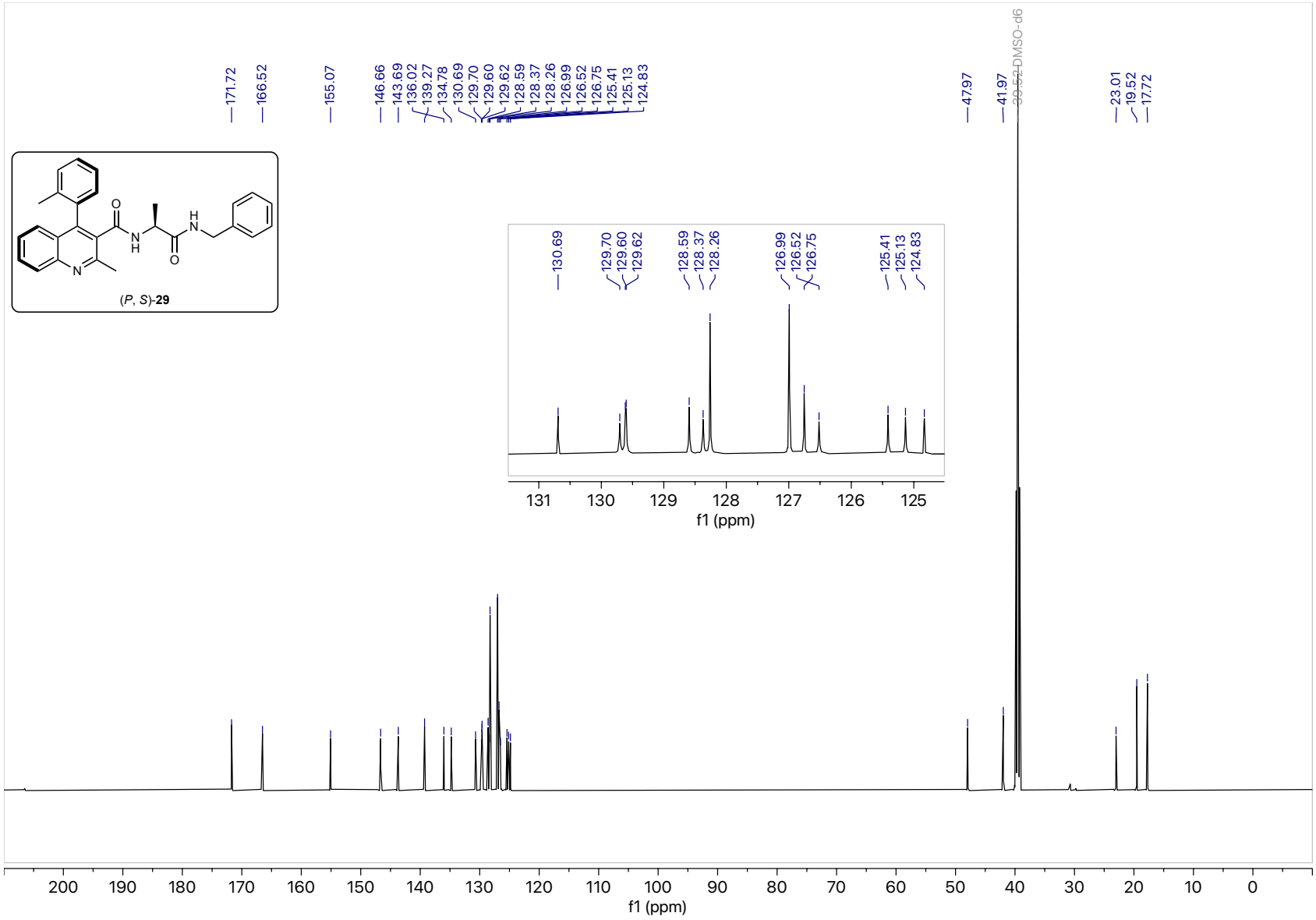
$^{13}C\{^{1}H\}$ NMR (151 MHz, $CDCl_3$) – standard view **((*P, S*)-29)**



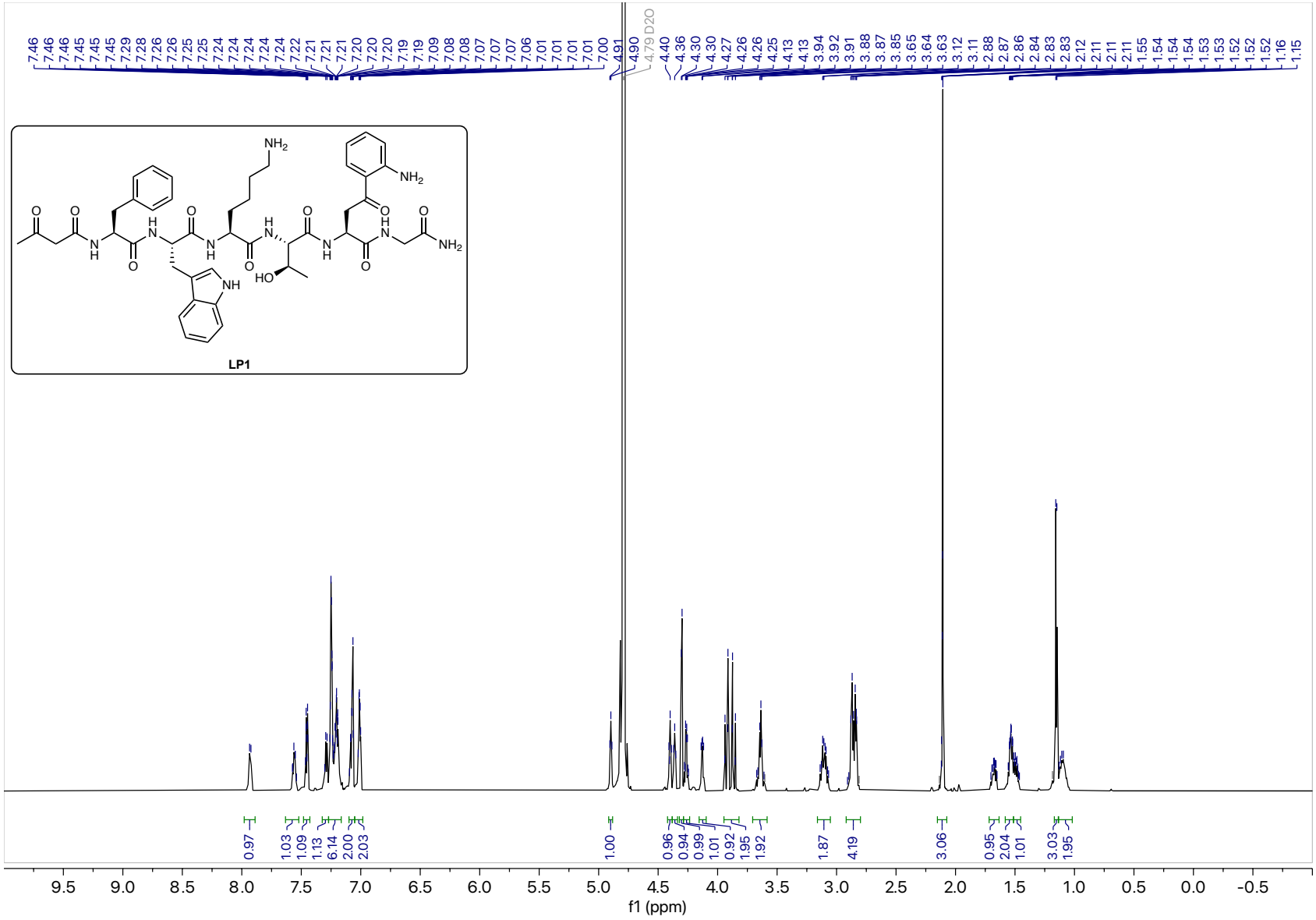
^{1}H NMR (600 MHz, DMSO-d_6) – standard view **((*P, S*)-29)**



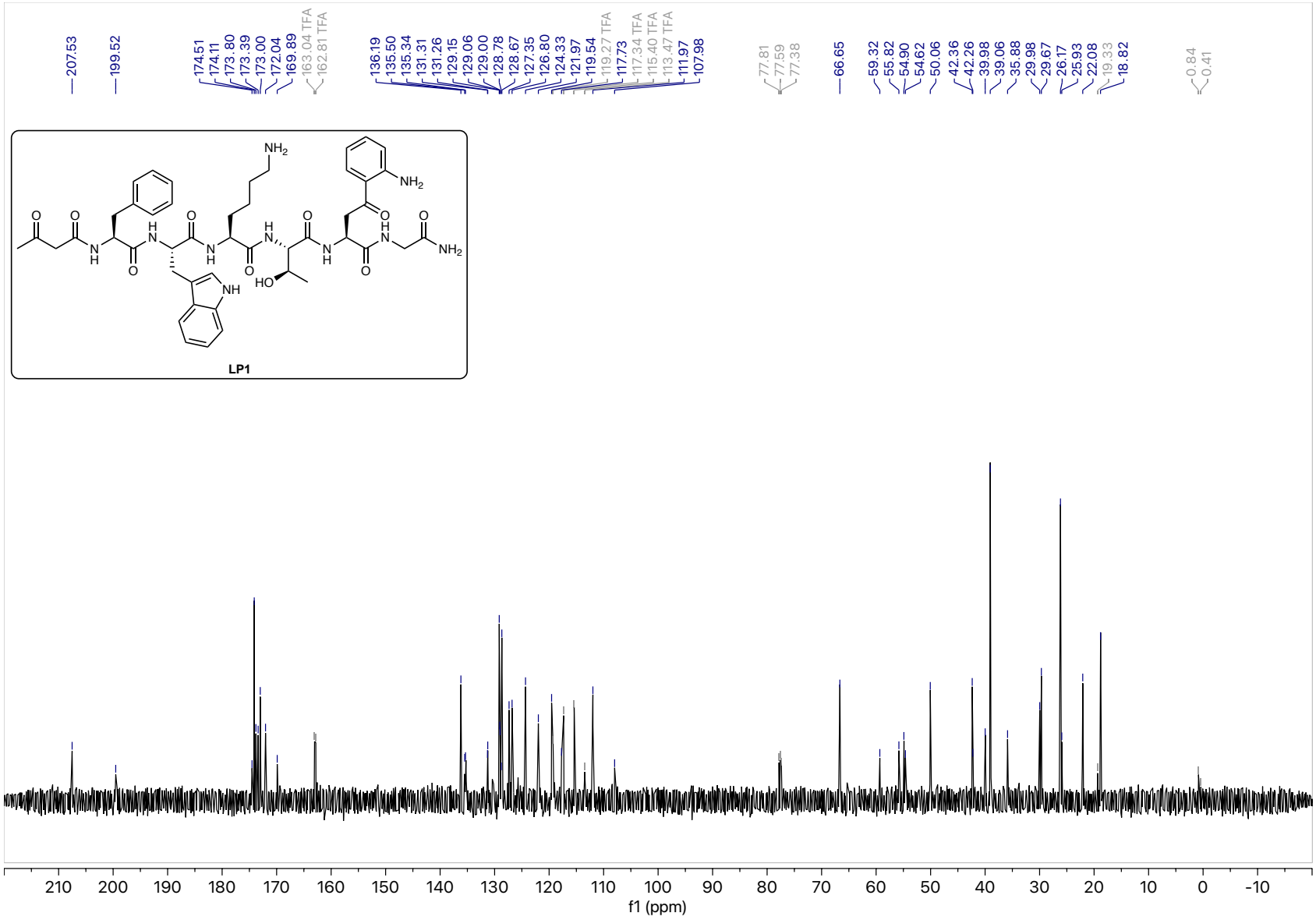
$^{13}C\{^{1}H\}$ NMR (151 MHz, DMSO-d_6) – standard view **((*P, S*)-29)**



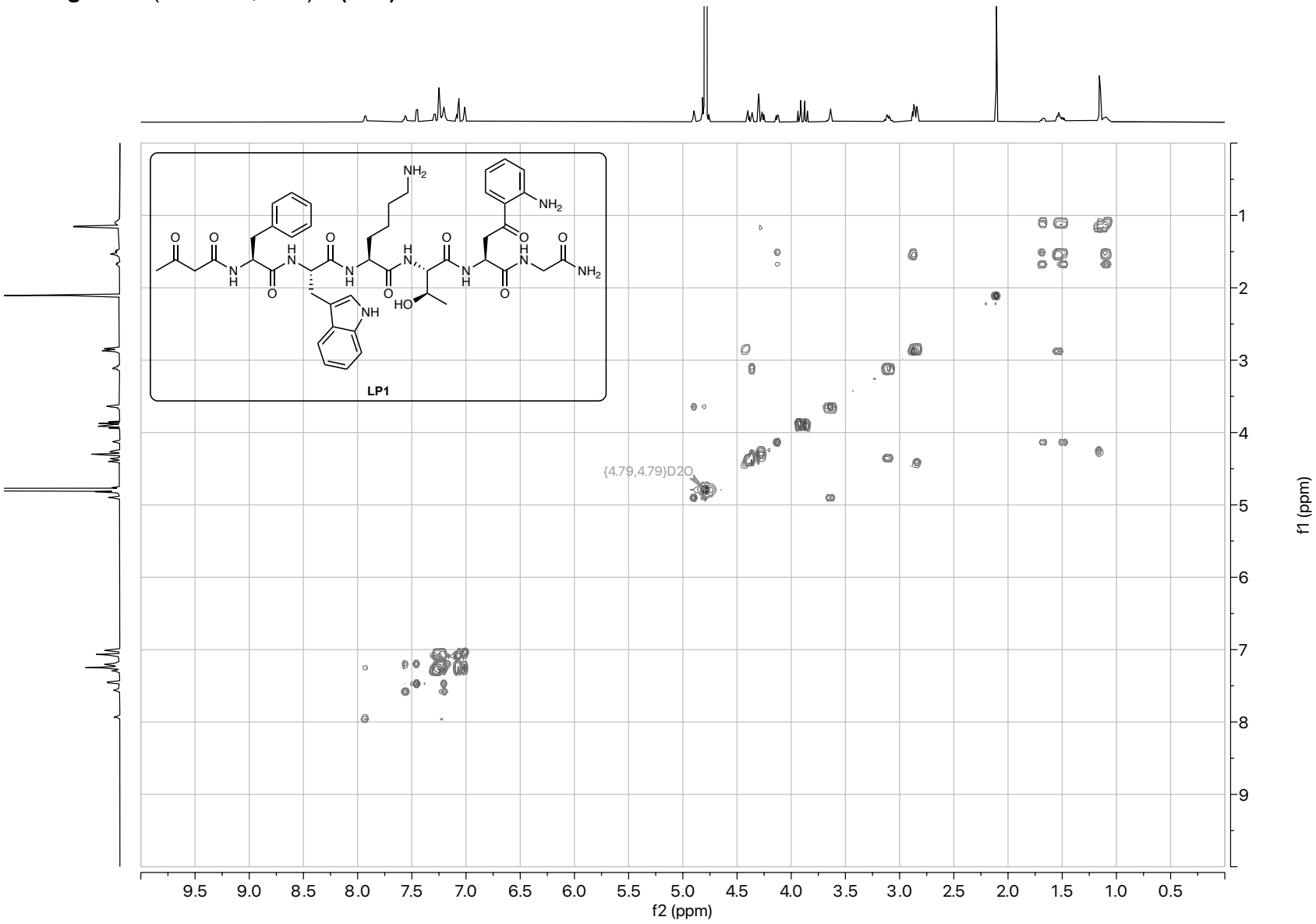
^{1}H NMR (700 MHz, D_2O) – standard view **(LP1)**



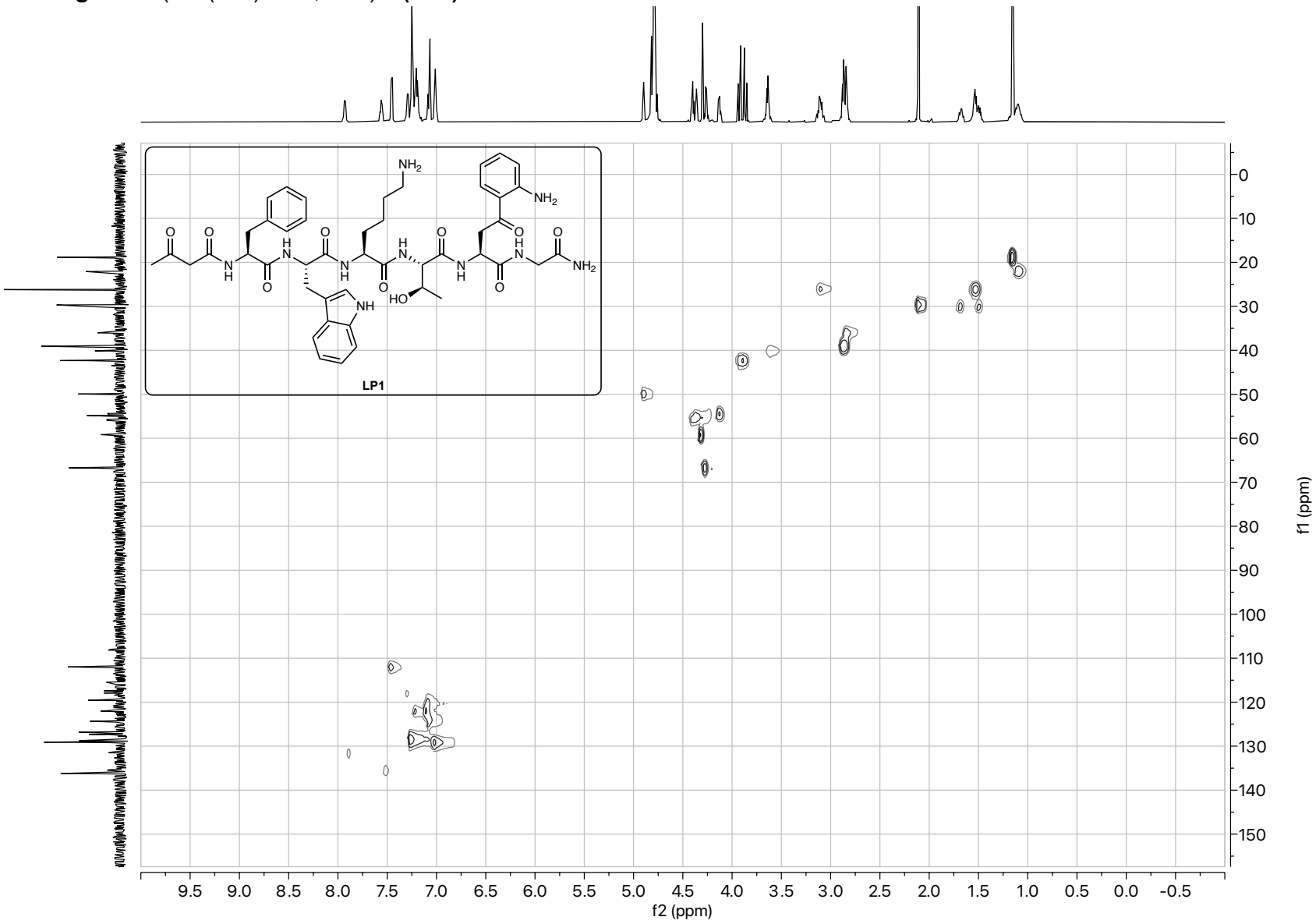
$^{13}C\{^{1}H\}$ NMR (151 MHz, D_2O) – standard view **(LP1)**



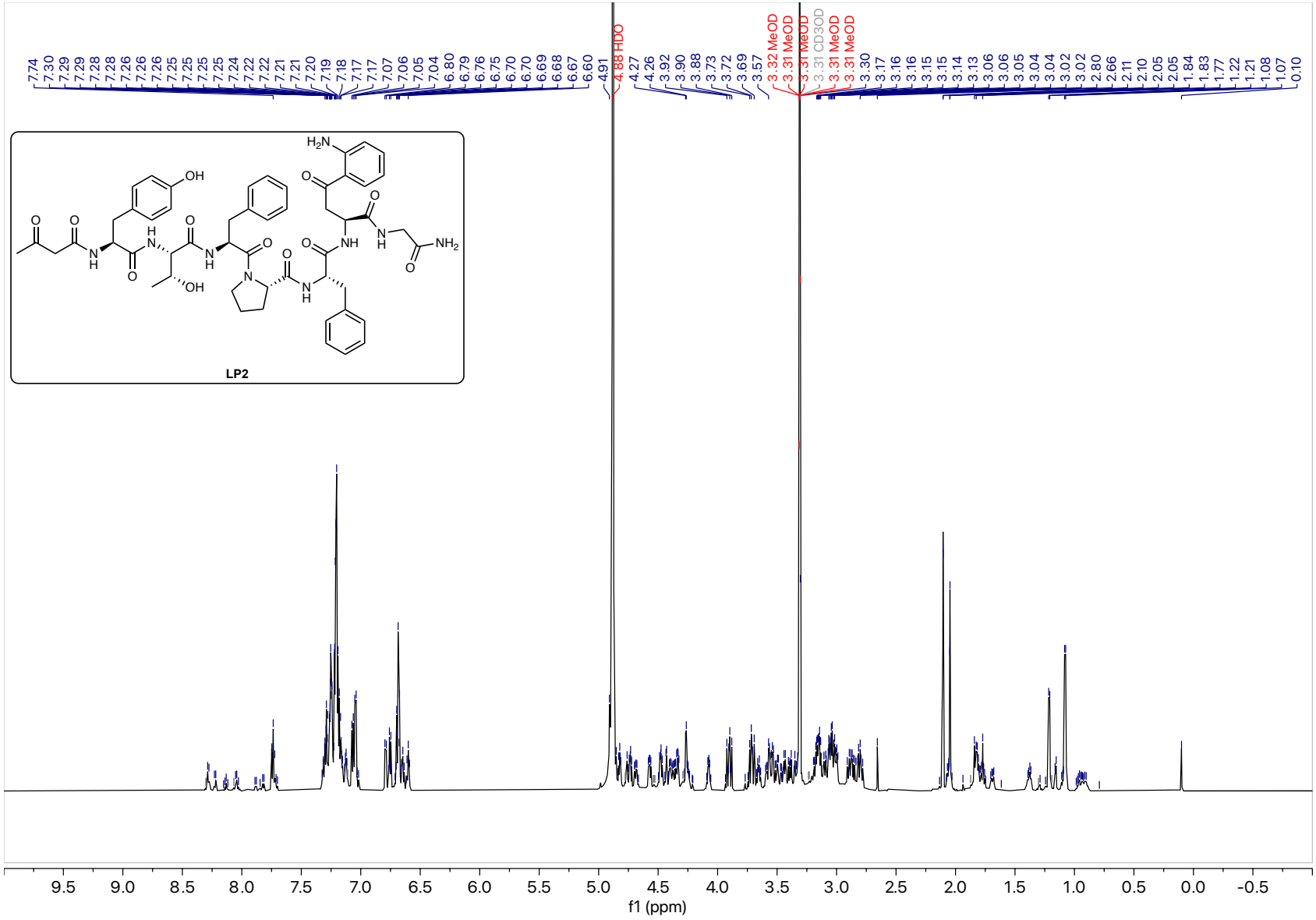
^{1}H-^{1}H gCOSY (600 MHz, D_2O) – **(LP1)**



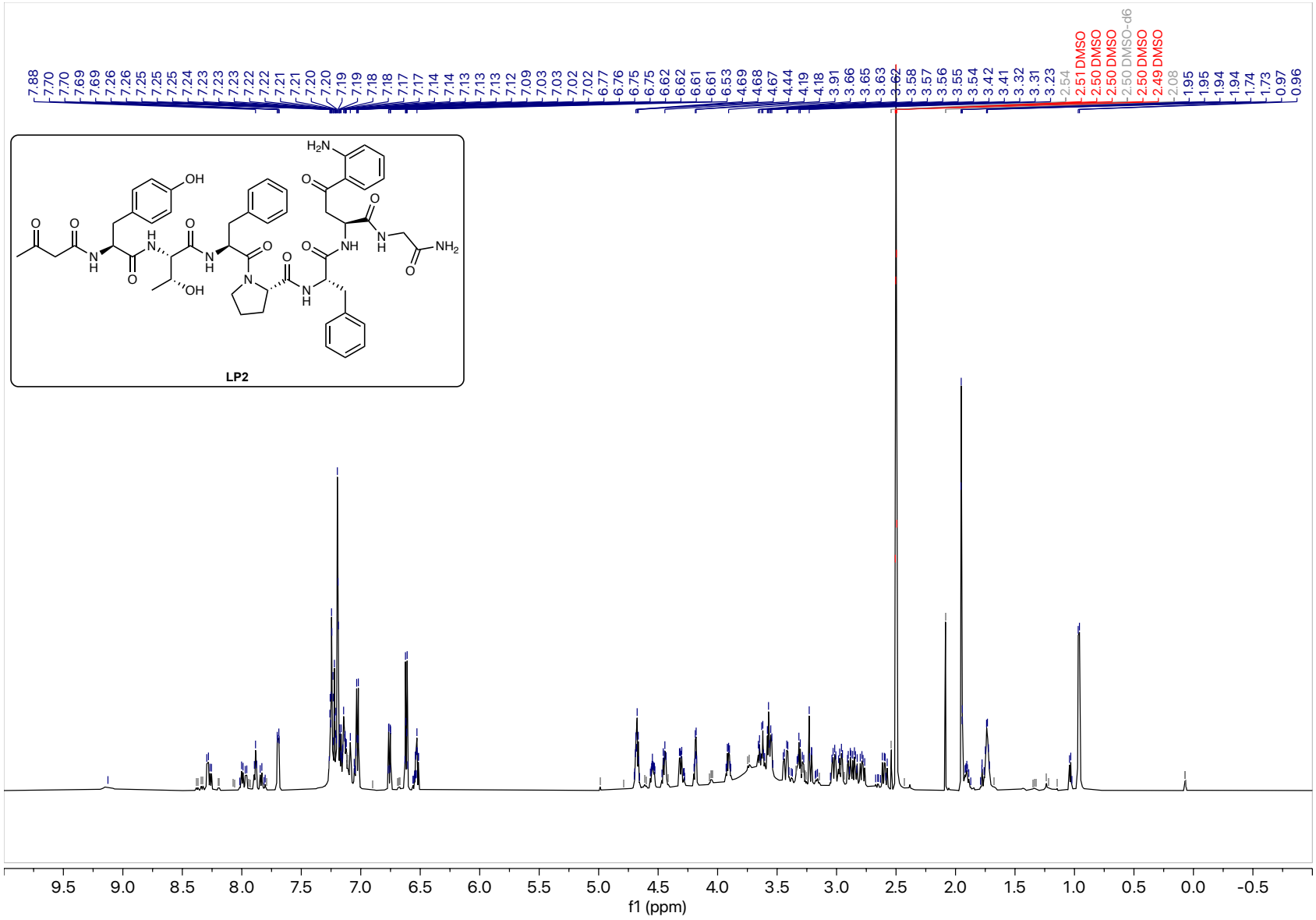
^{1}H-^{13}C gHSQC (600(151) MHz, D_2O) – **(LP1)**



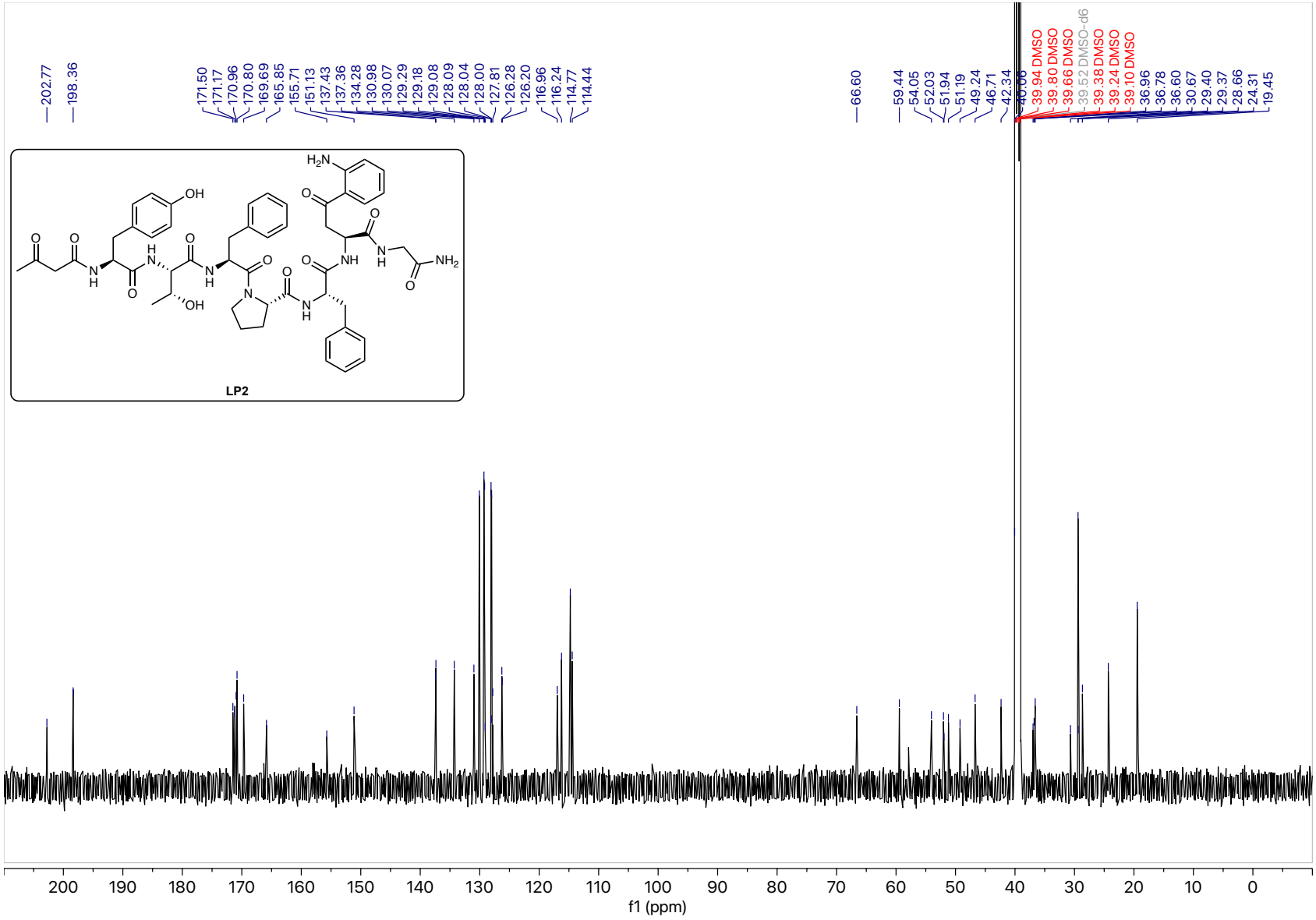
^{1}H NMR (700 MHz, CD_3OD) – standard view **(LP2) – Not Assigned**



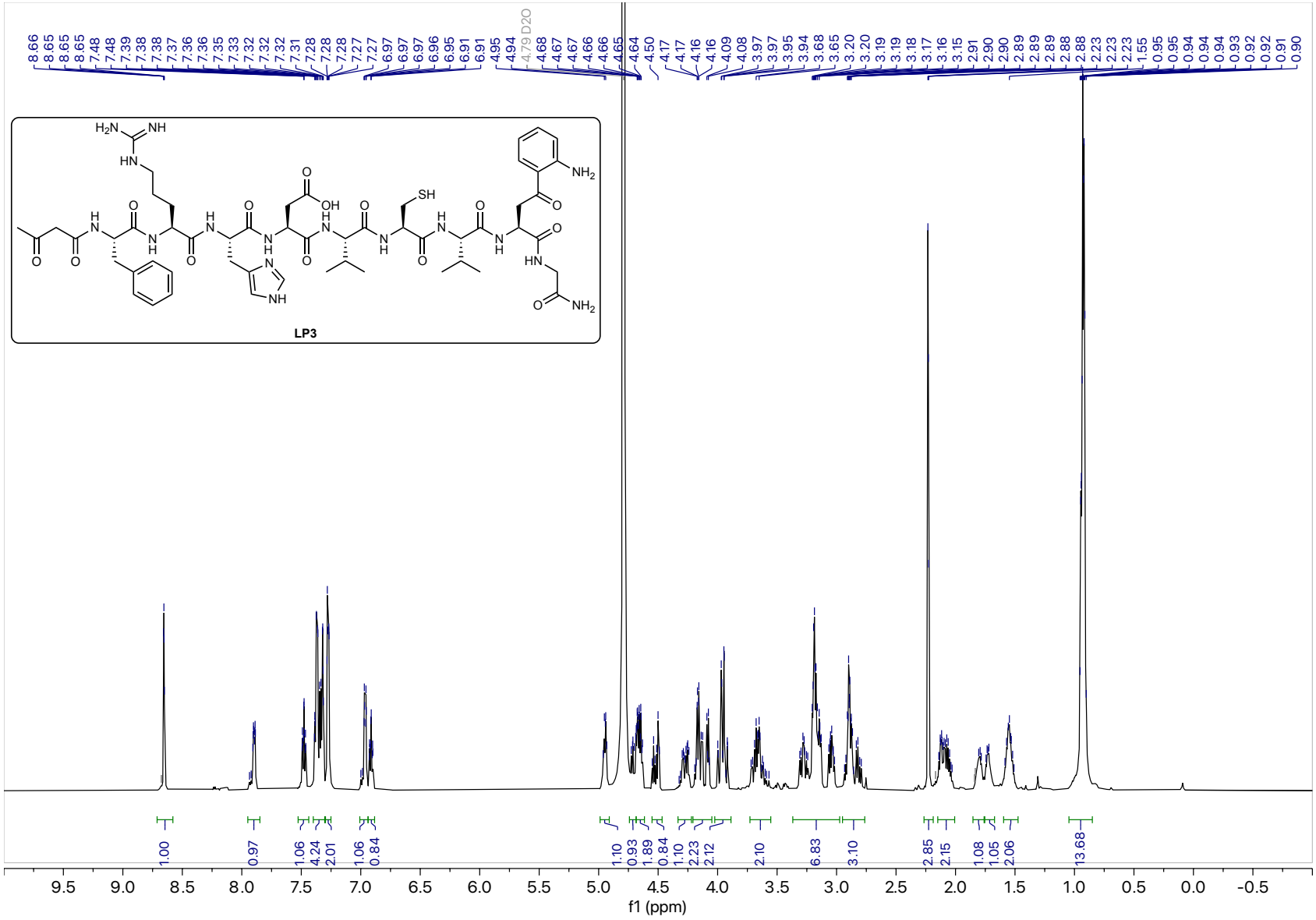
^{1}H NMR (600 MHz, DMSO-d_6) – standard view **(LP2) – Not Assigned**



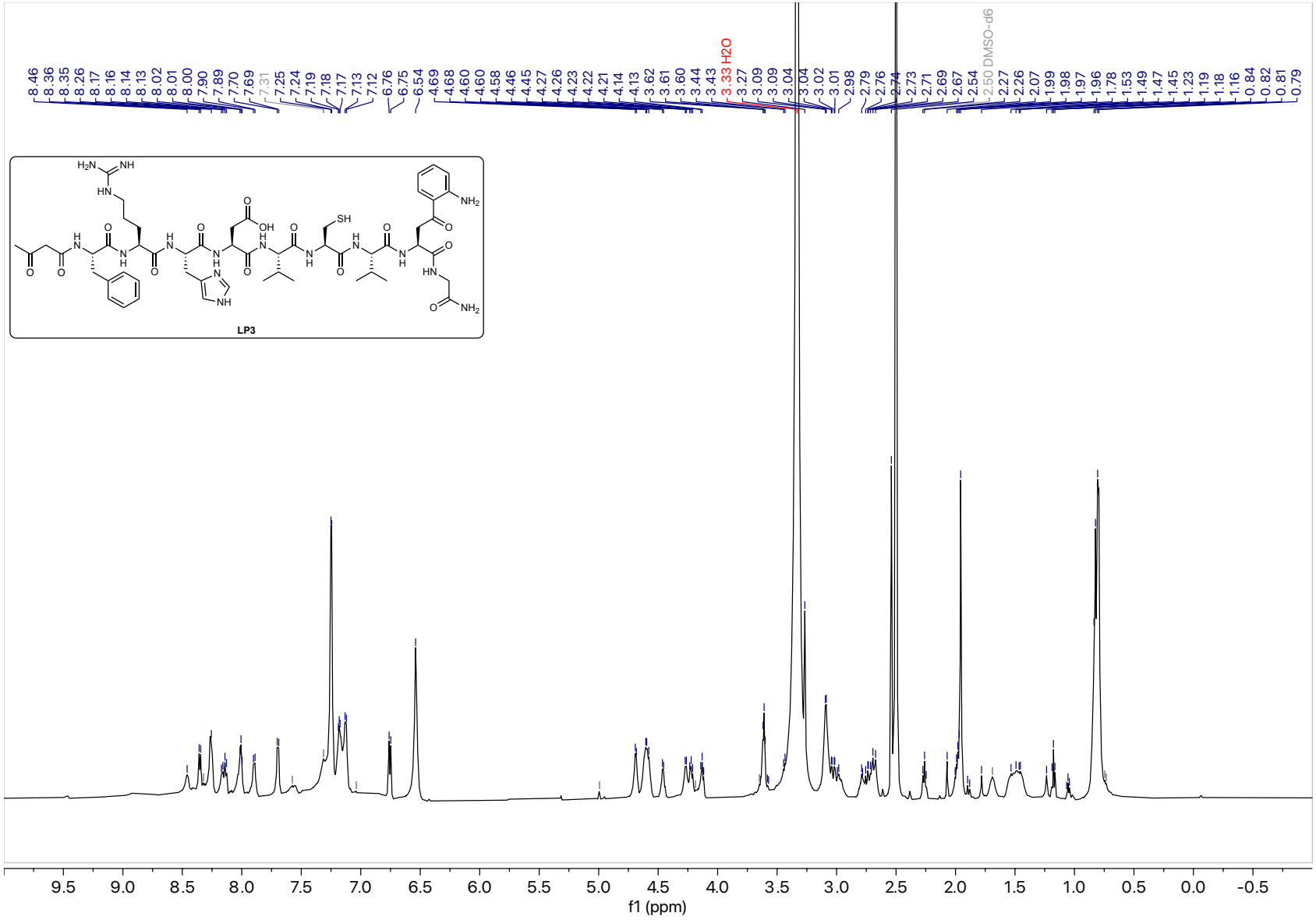
$^{13}C\{^{1}H\}$ NMR (151 MHz, DMSO-d_6) – standard view **(LP2)**



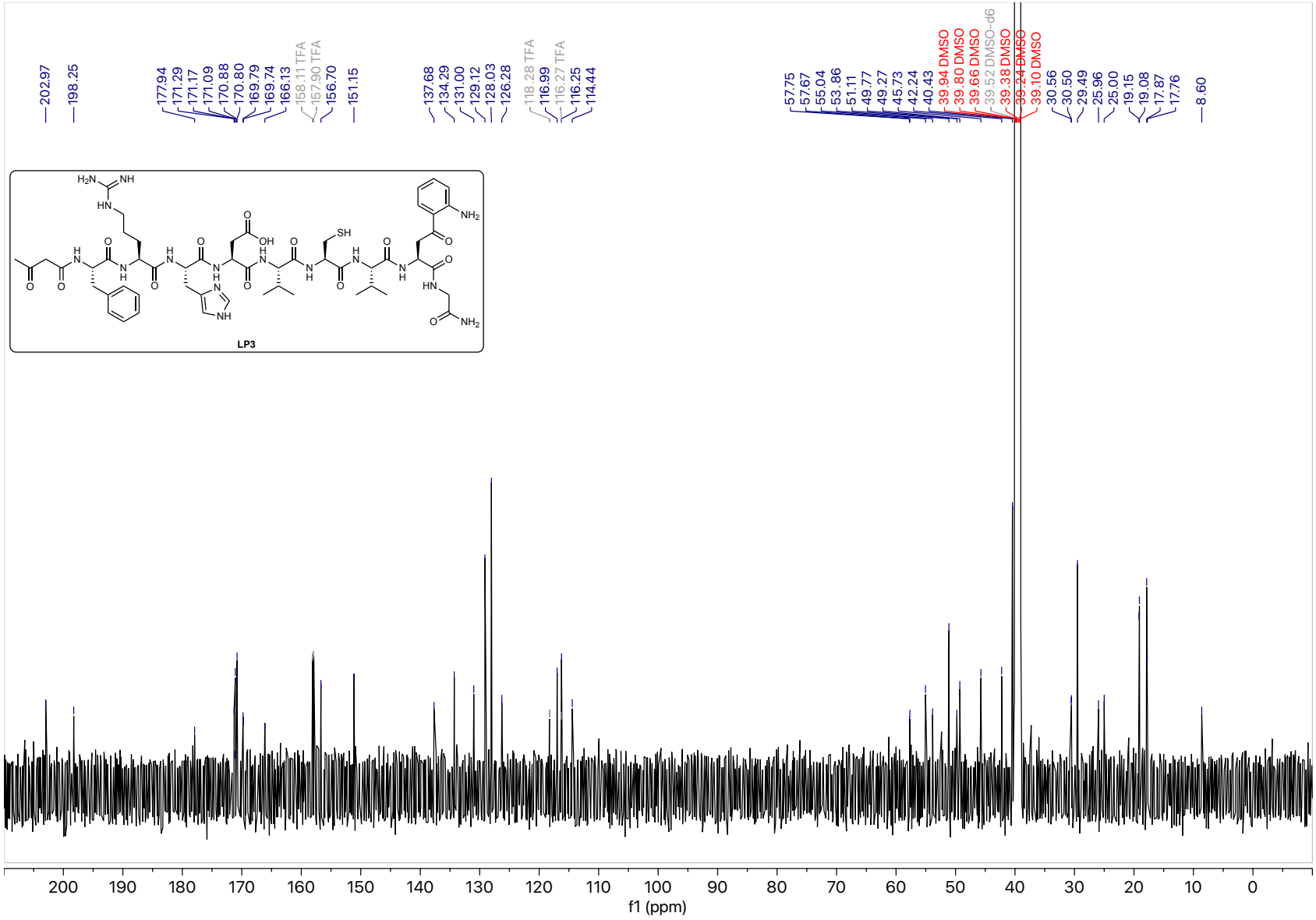
^{1}H NMR (600 MHz, D_2O) – standard view **(LP3)**



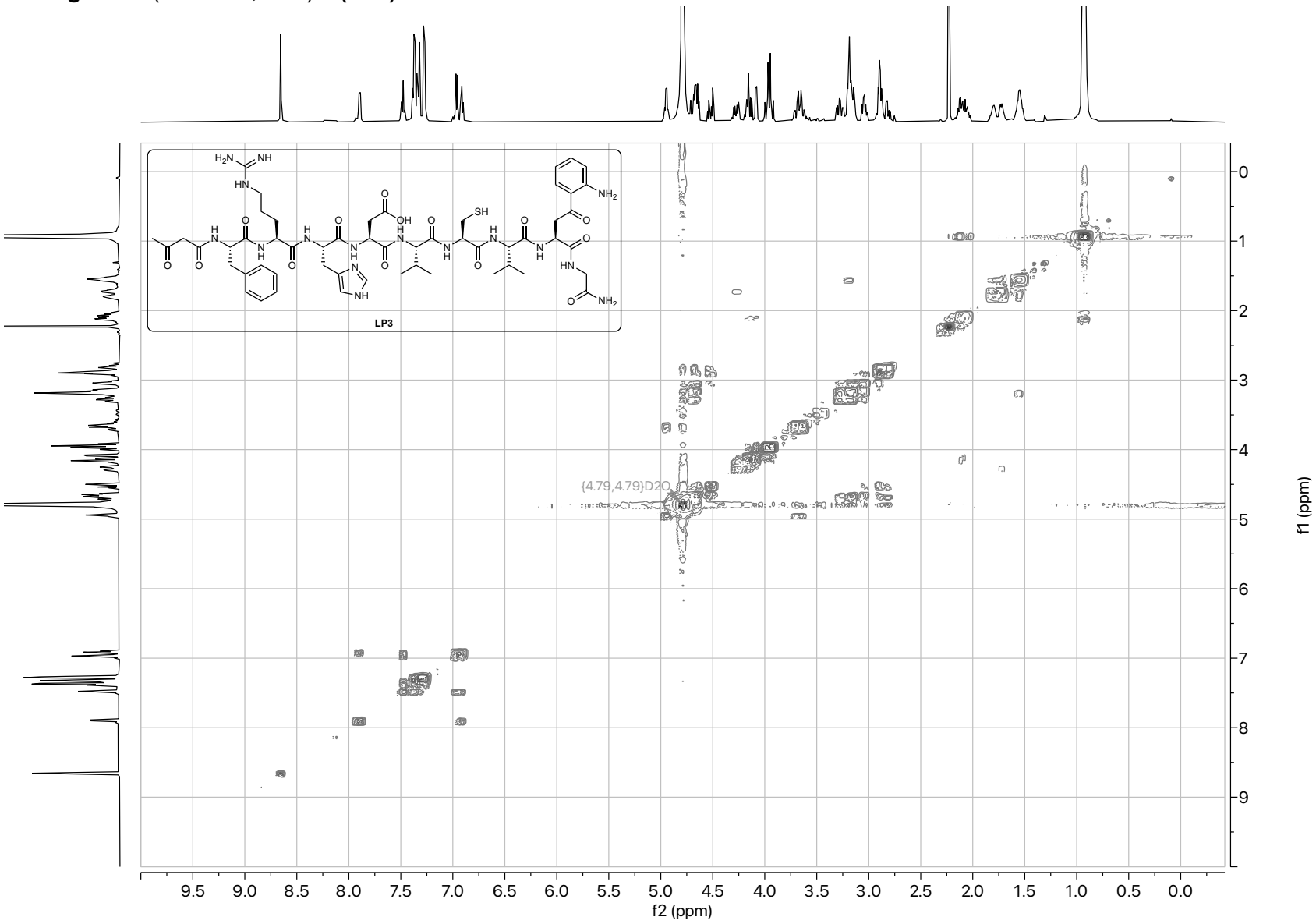
^{1}H NMR (600 MHz, DMSO-d_6) – standard view **(LP3) – Not Assigned**



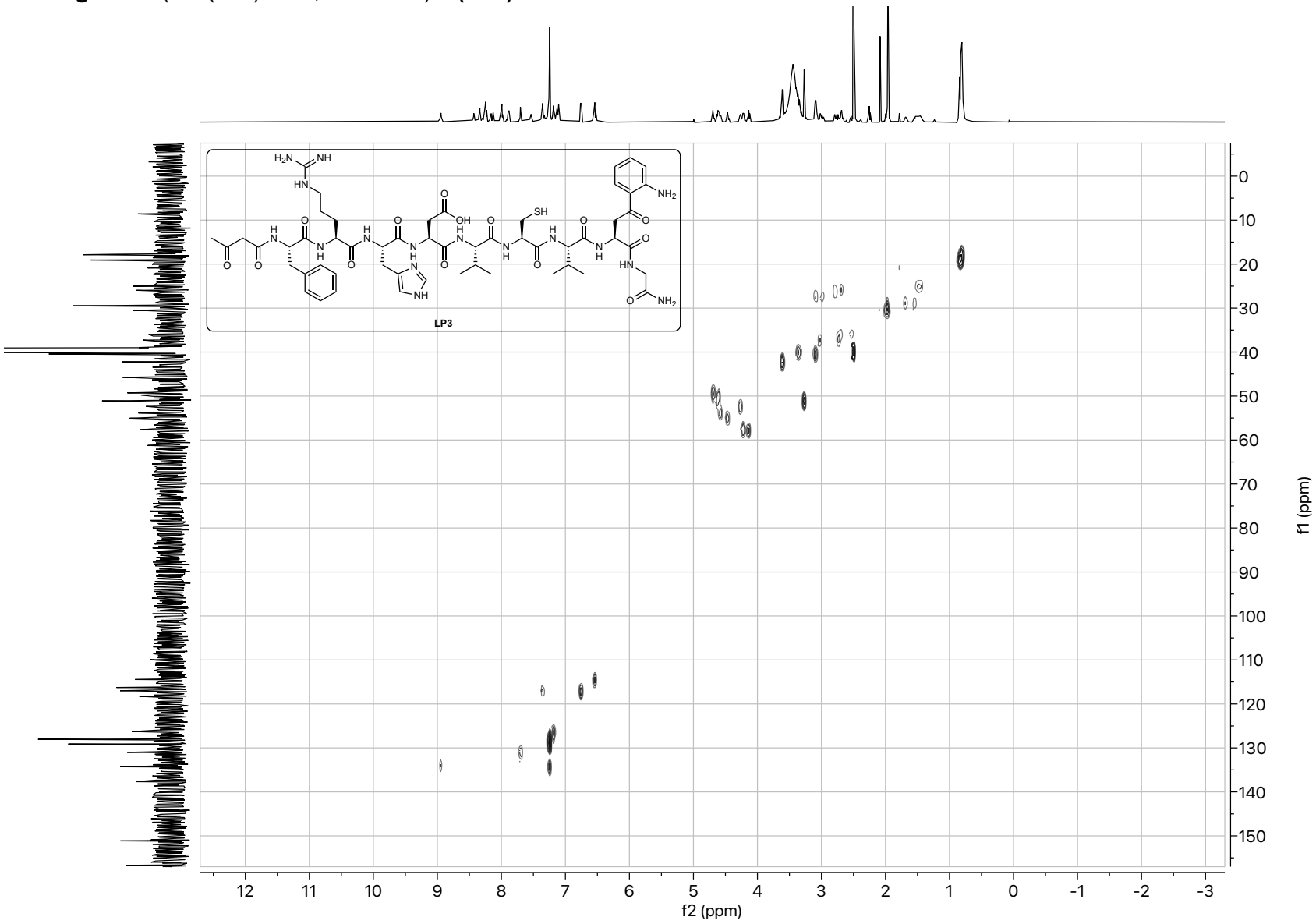
$^{13}C\{^{1}H\}$ NMR (151 MHz, DMSO-d_6) – standard view **(LP3)**



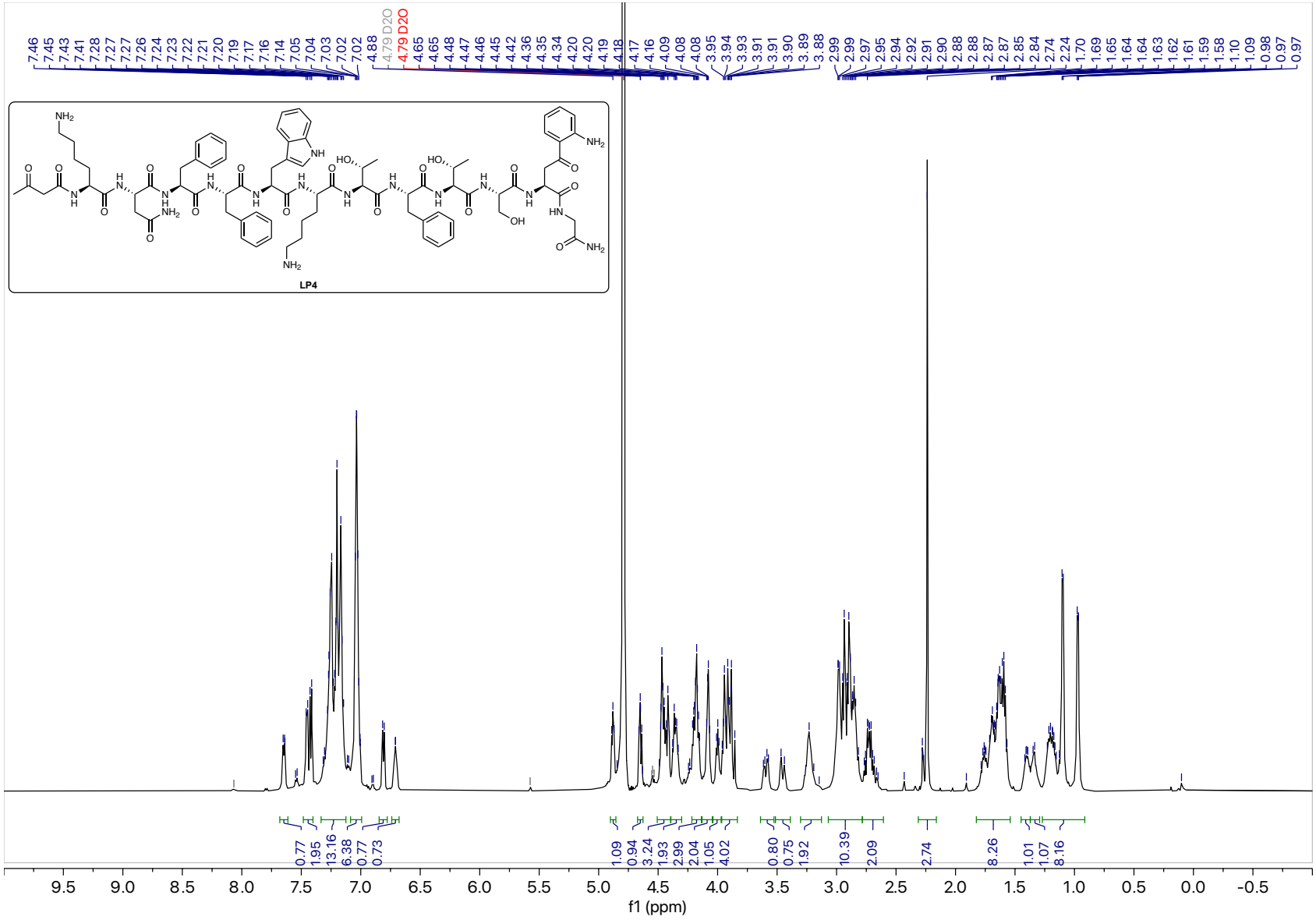
^{1}H-^{1}H gCOSY (600 MHz, D_2O) – **(LP3)**



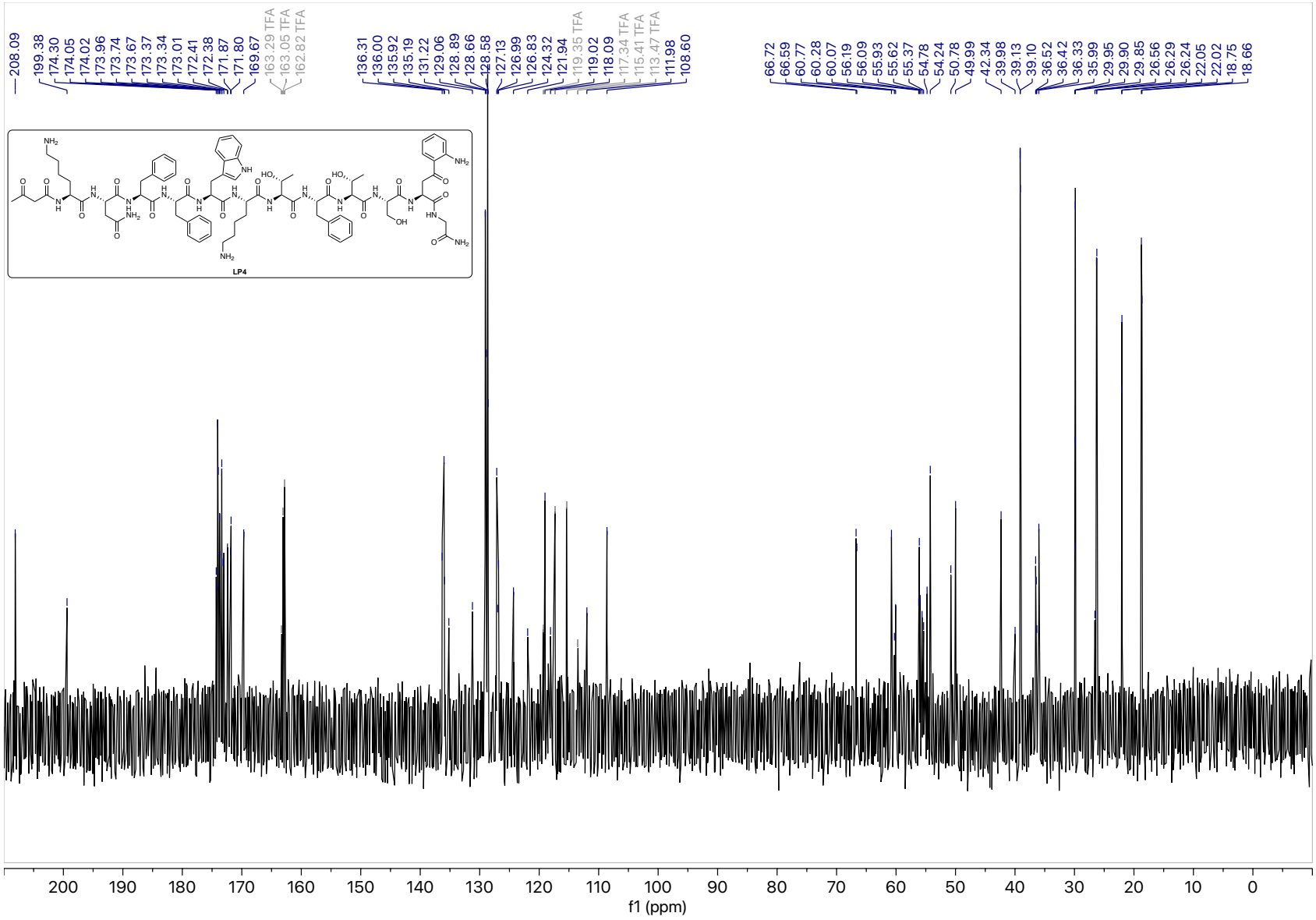
^{1}H-^{13}C gHSQC (600(151) MHz, DMSO-d_6) – **(LP3)**



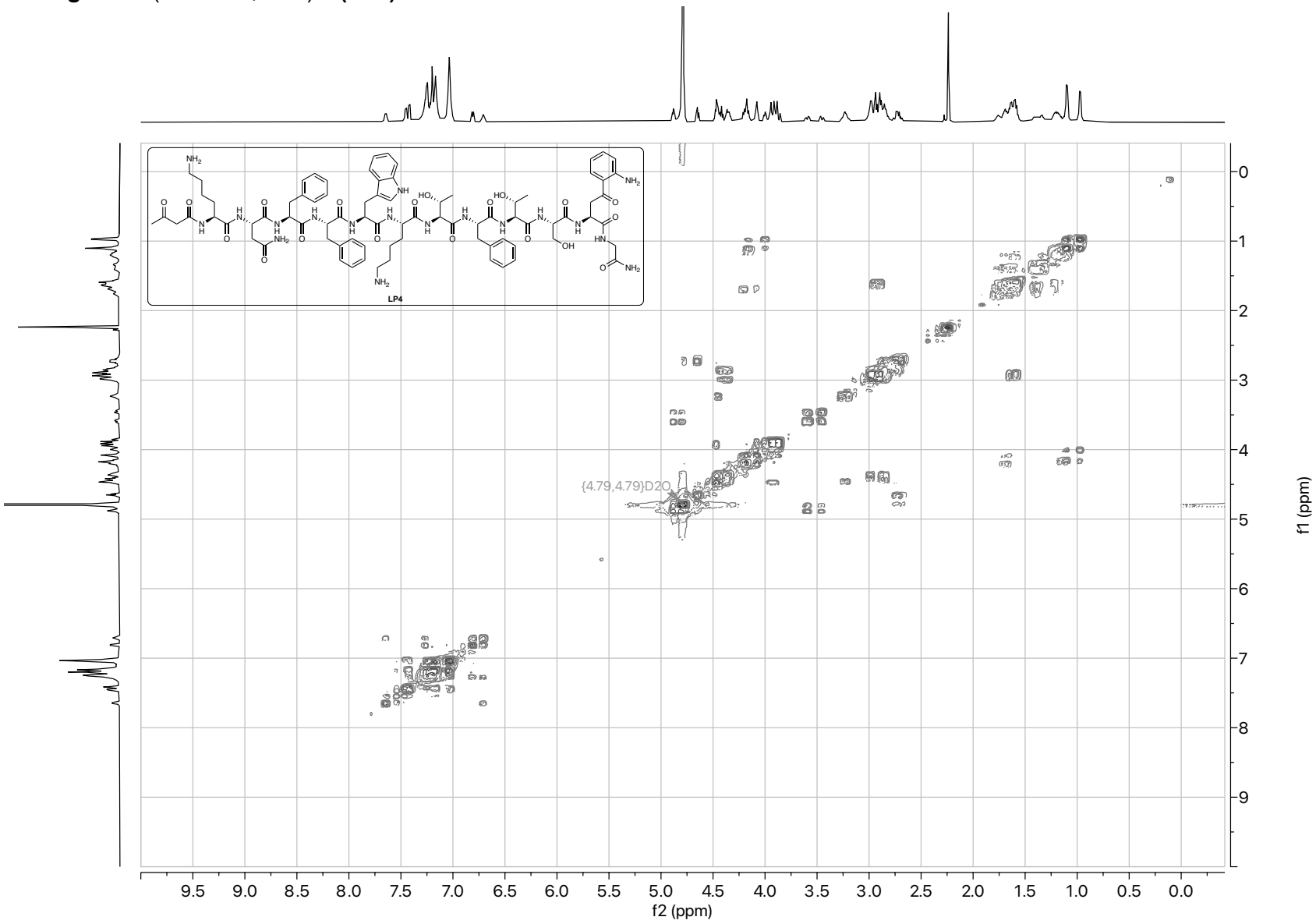
^{1}H NMR (600 MHz, D_2O) – standard view **(LP4)**



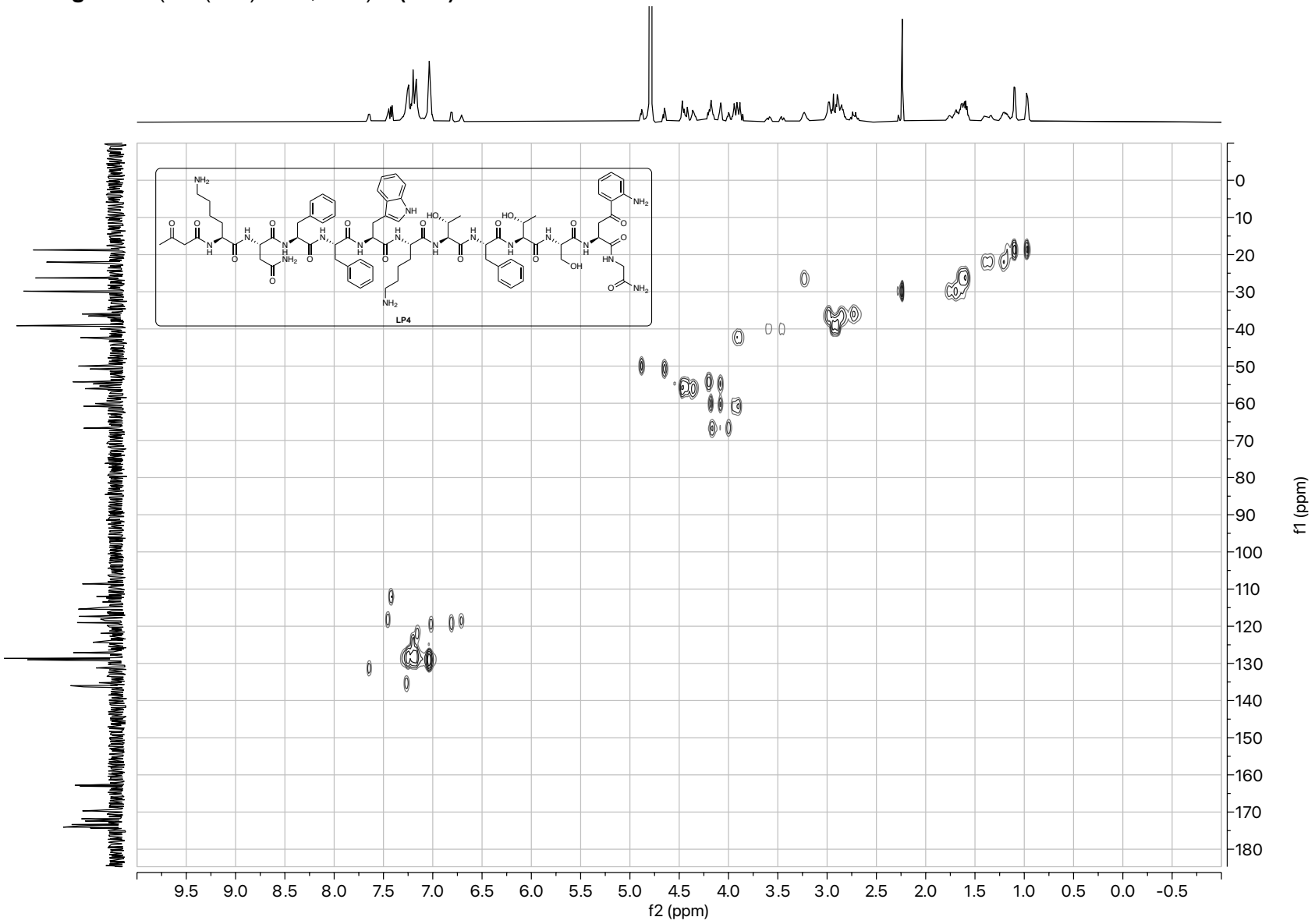
$^{13}C\{^{1}H\}$ NMR (151 MHz, D_2O) – standard view **(LP4)**



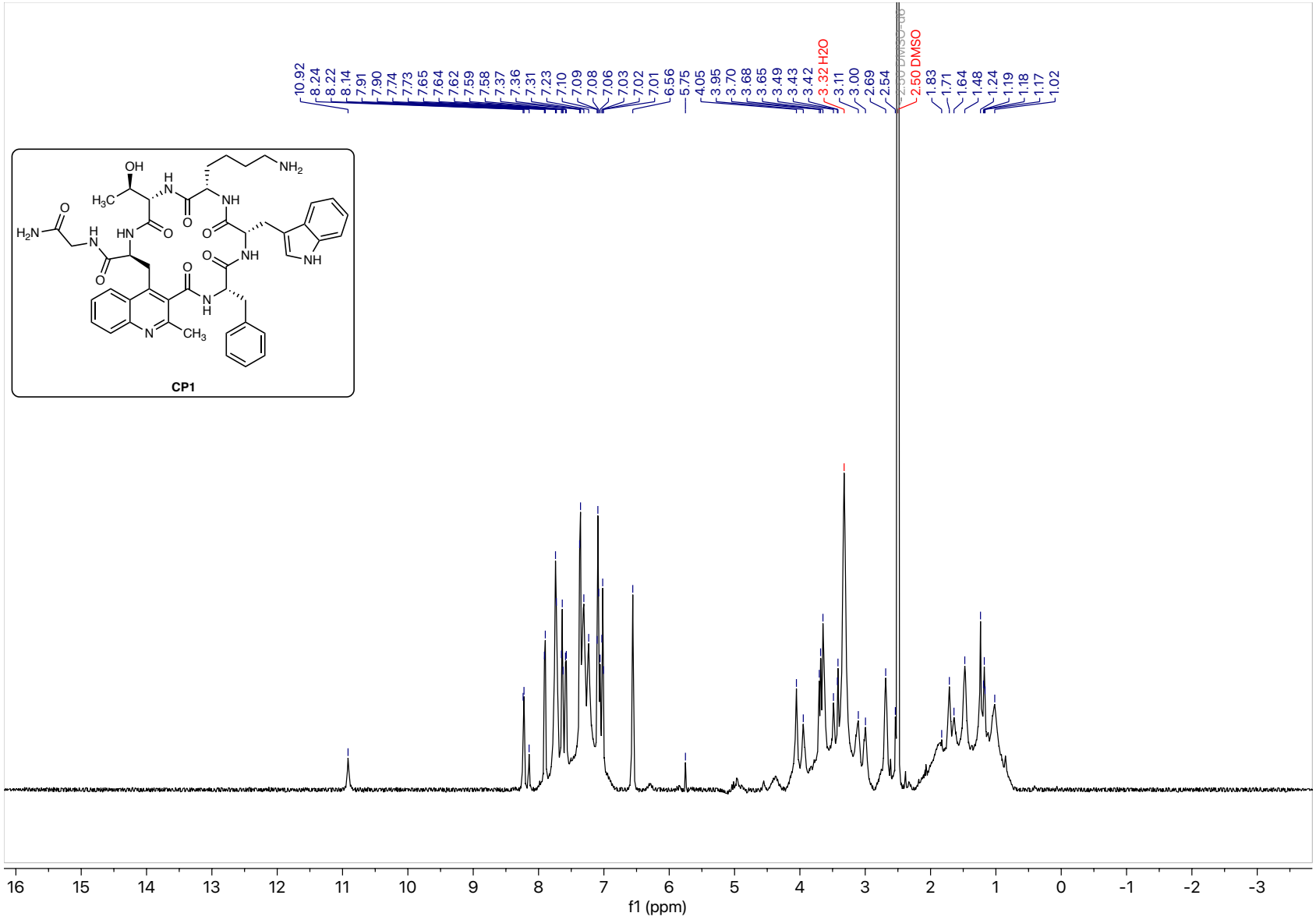
^{1}H-^{1}H gCOSY (600 MHz, D_2O) – **(LP4)**



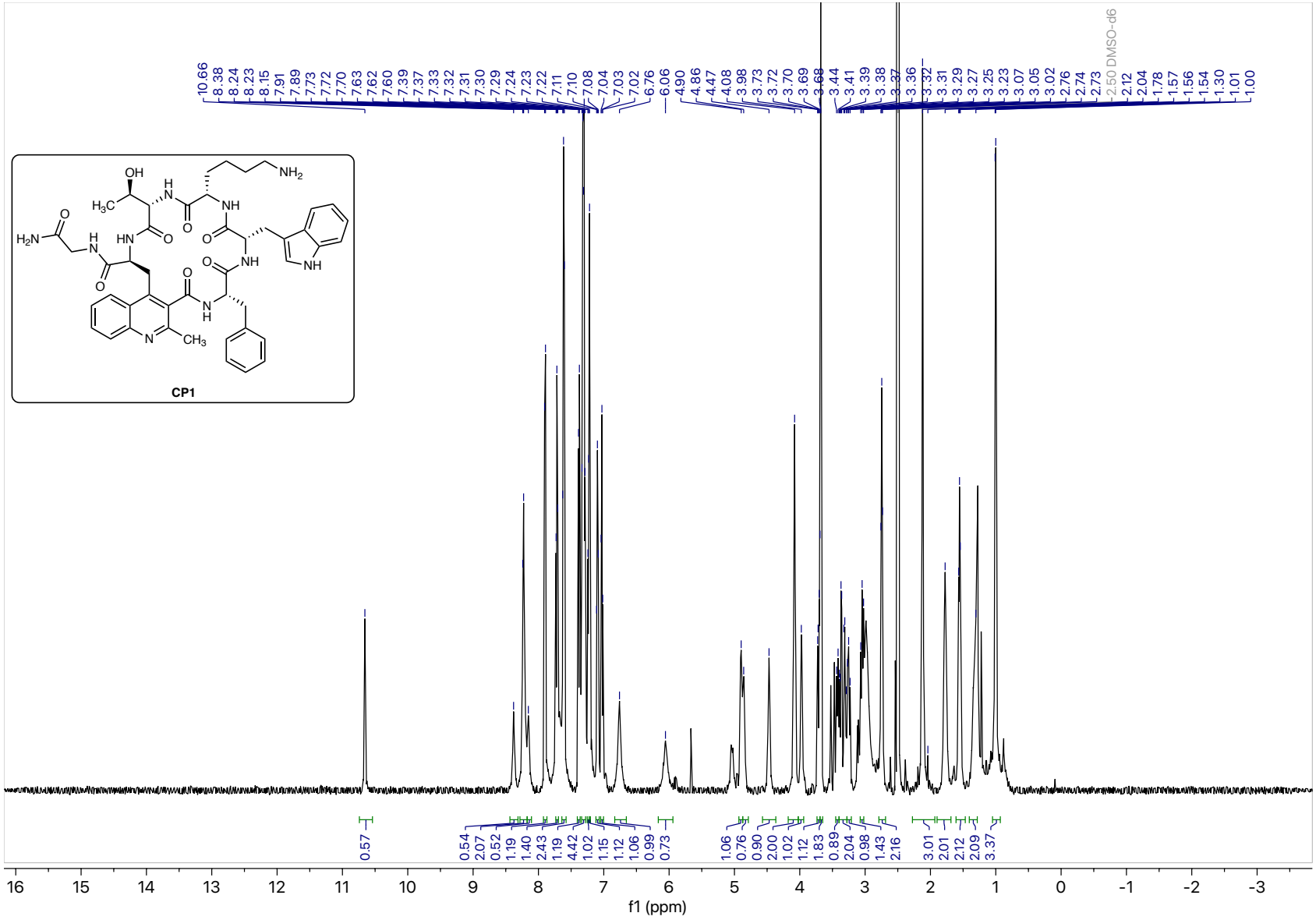
^{1}H-^{13}C gHSQC (600(151) MHz, D_2O) – **(LP4)**



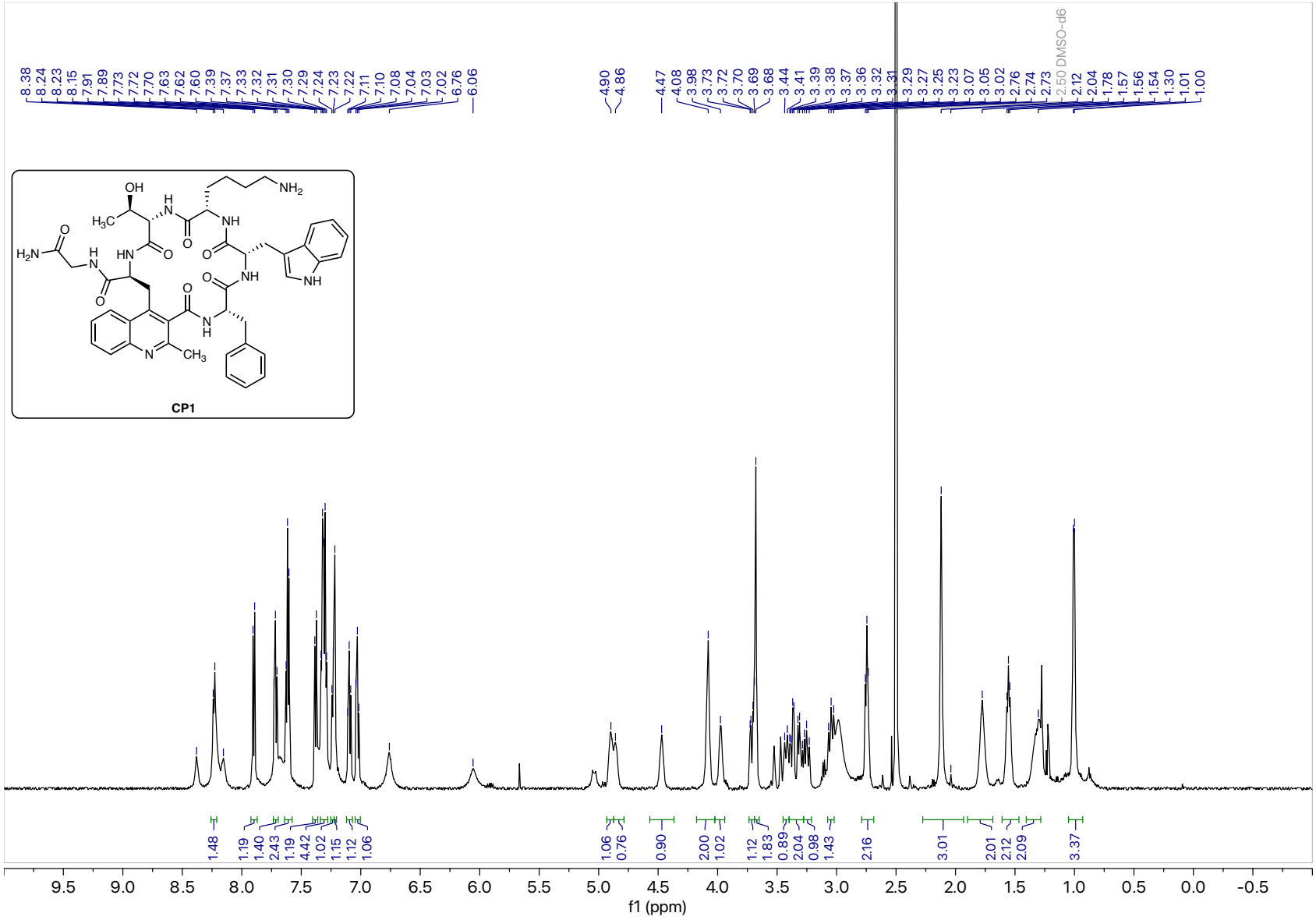
^{1}H NMR (600 MHz, DMSO-d_6, 298 K) – extended view, partial exchange **(CP1)**



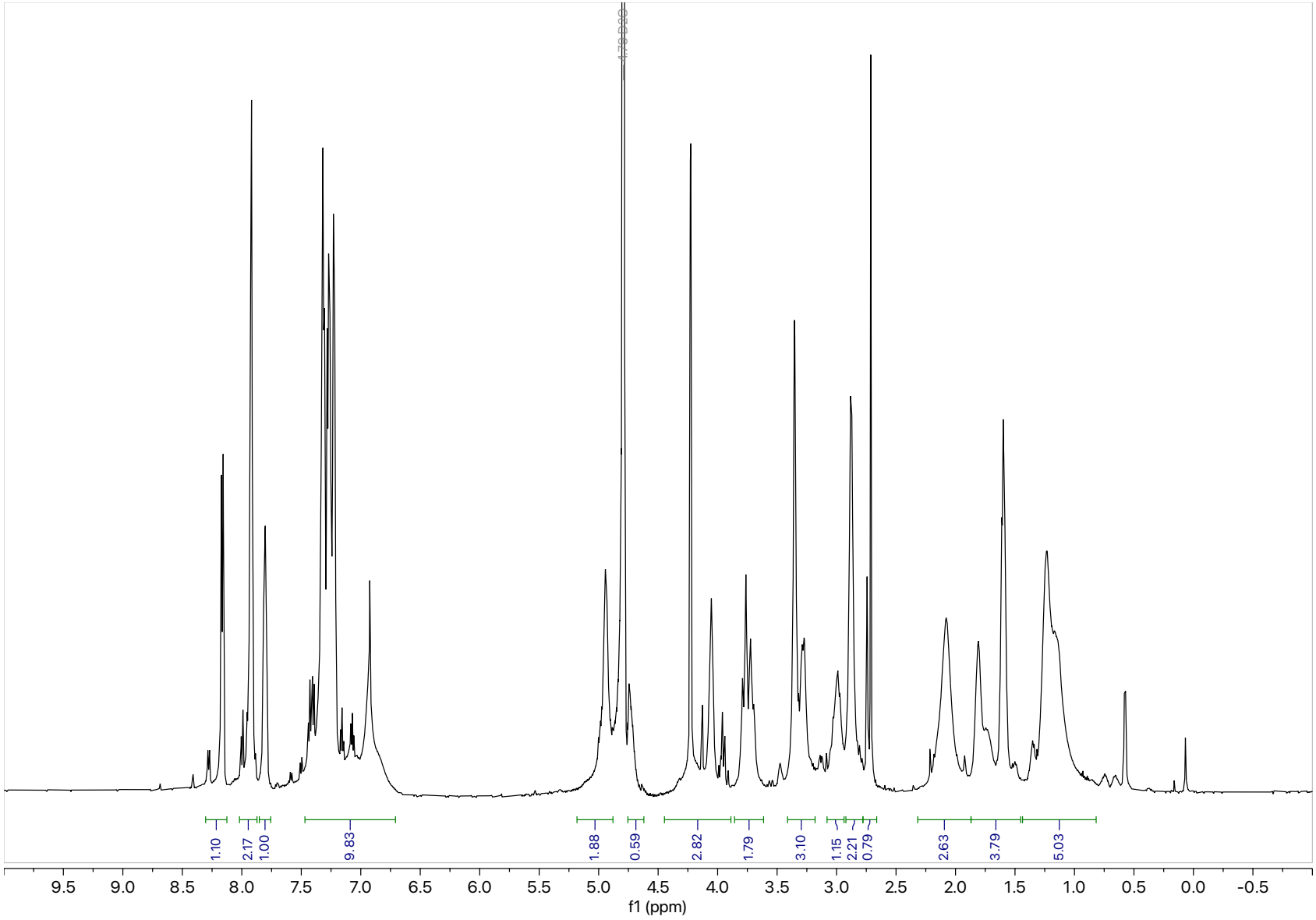
^{1}H NMR (600 MHz, DMSO-d_6, 373 K) – extended view, partial exchange **(CP1)**



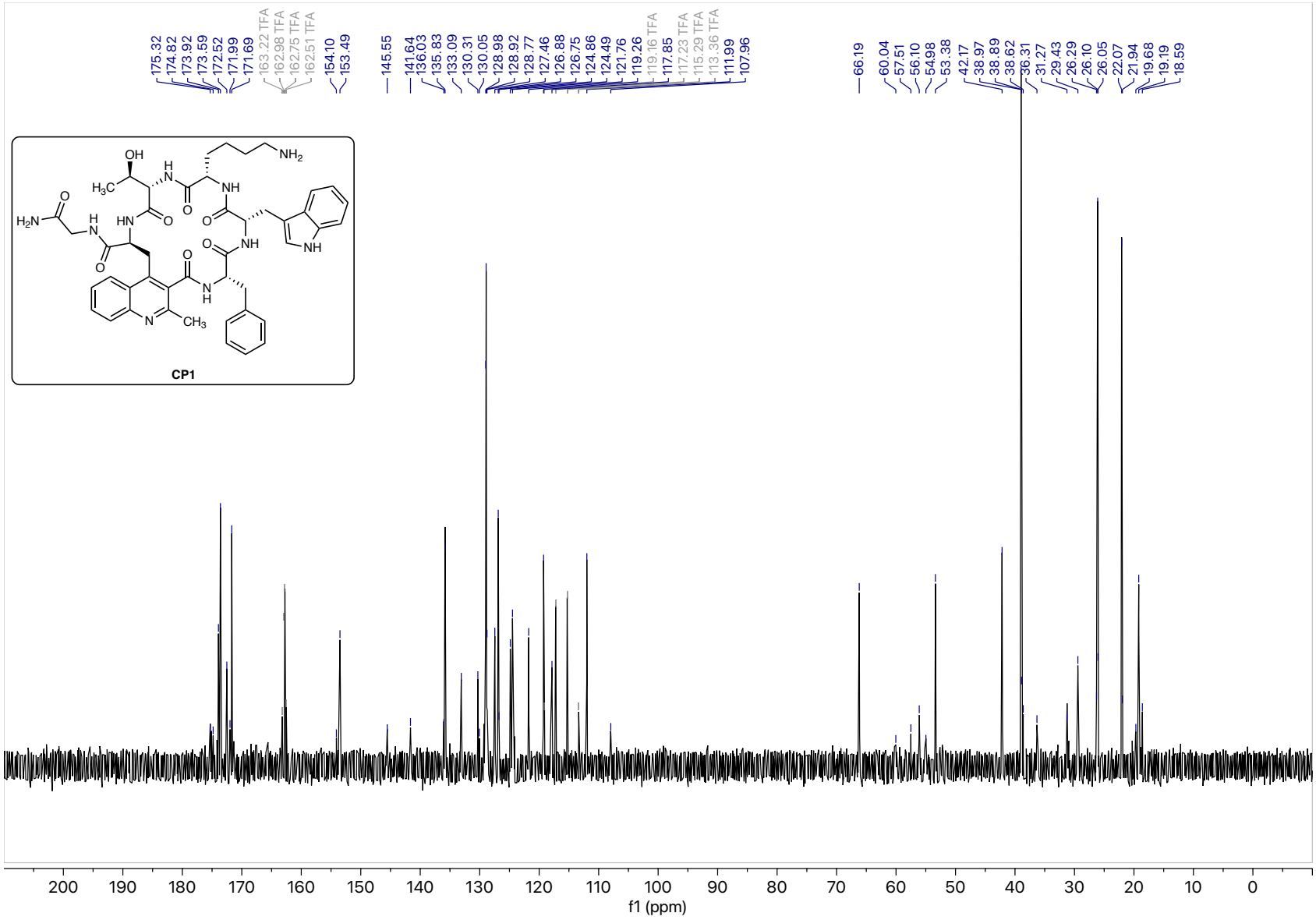
^{1}H NMR (600 MHz, DMSO-d_6, 373 K) – standard view, non-exchangeable signals **(CP1)**



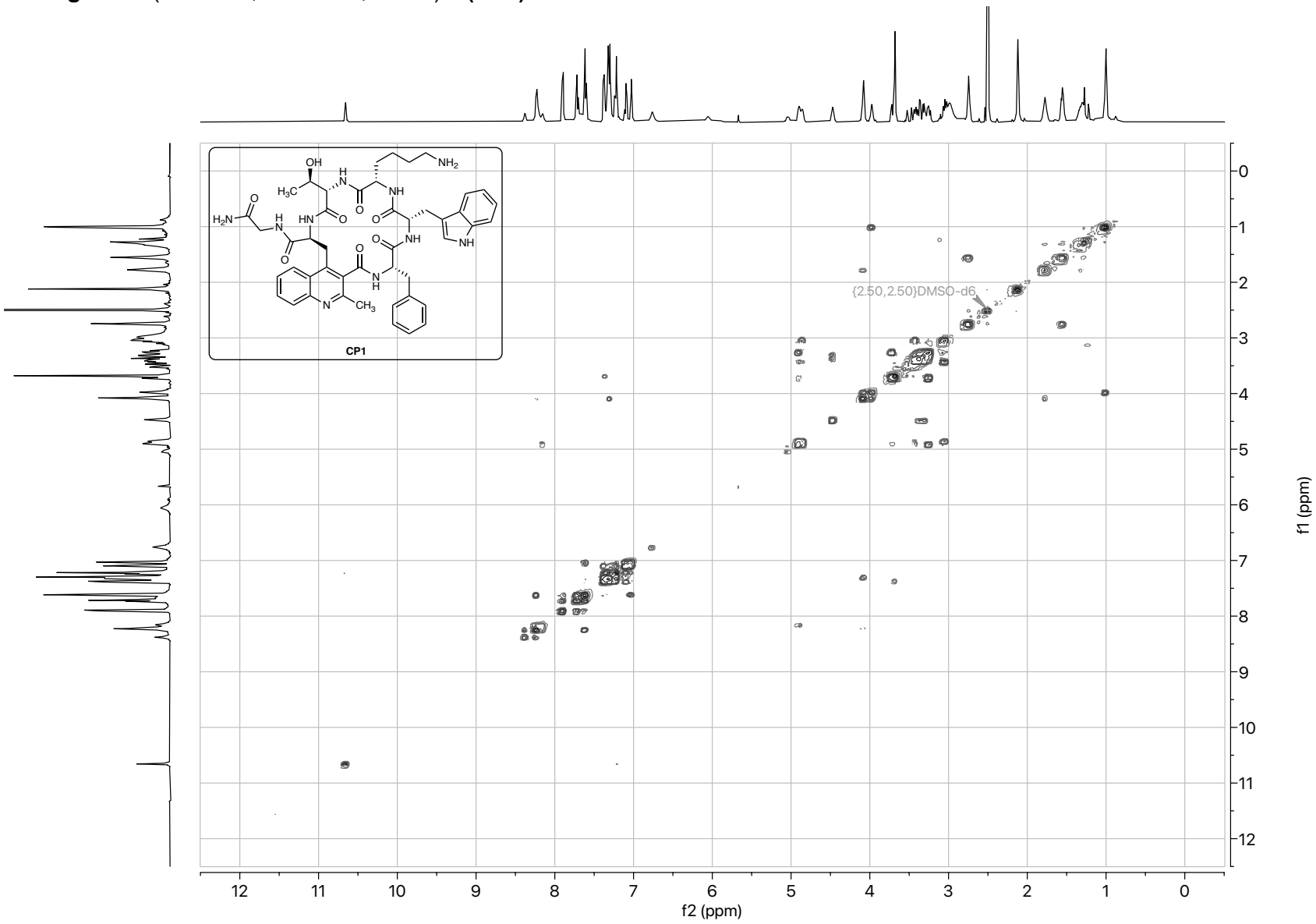
^{1}H NMR (600 MHz, D_2O, 298 K) – standard view **(CP1) – Not Assigned**



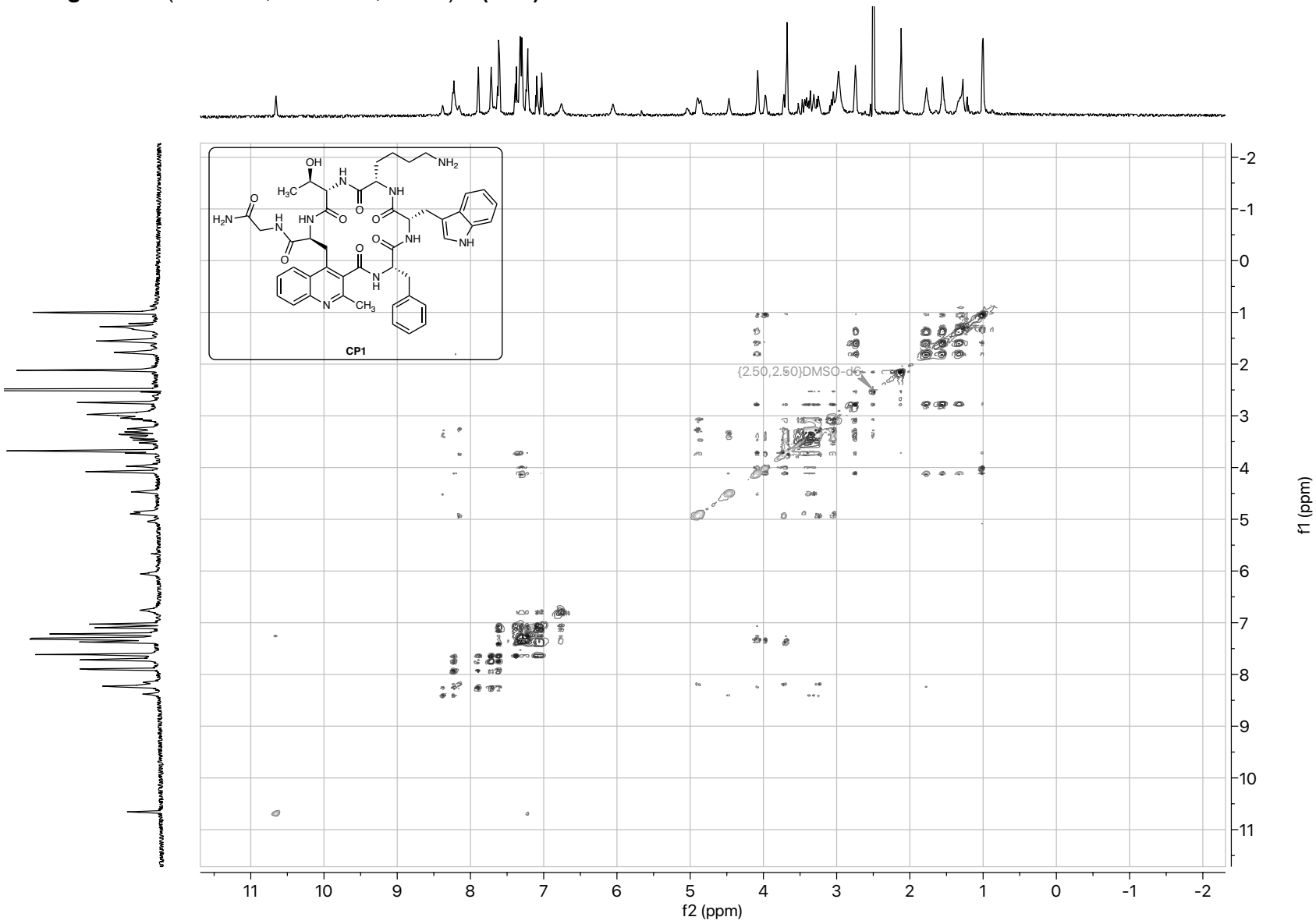
$^{13}C\{^{1}H\}$ NMR (151 MHz, D_2O, 298 K) – standard view **(CP1)**



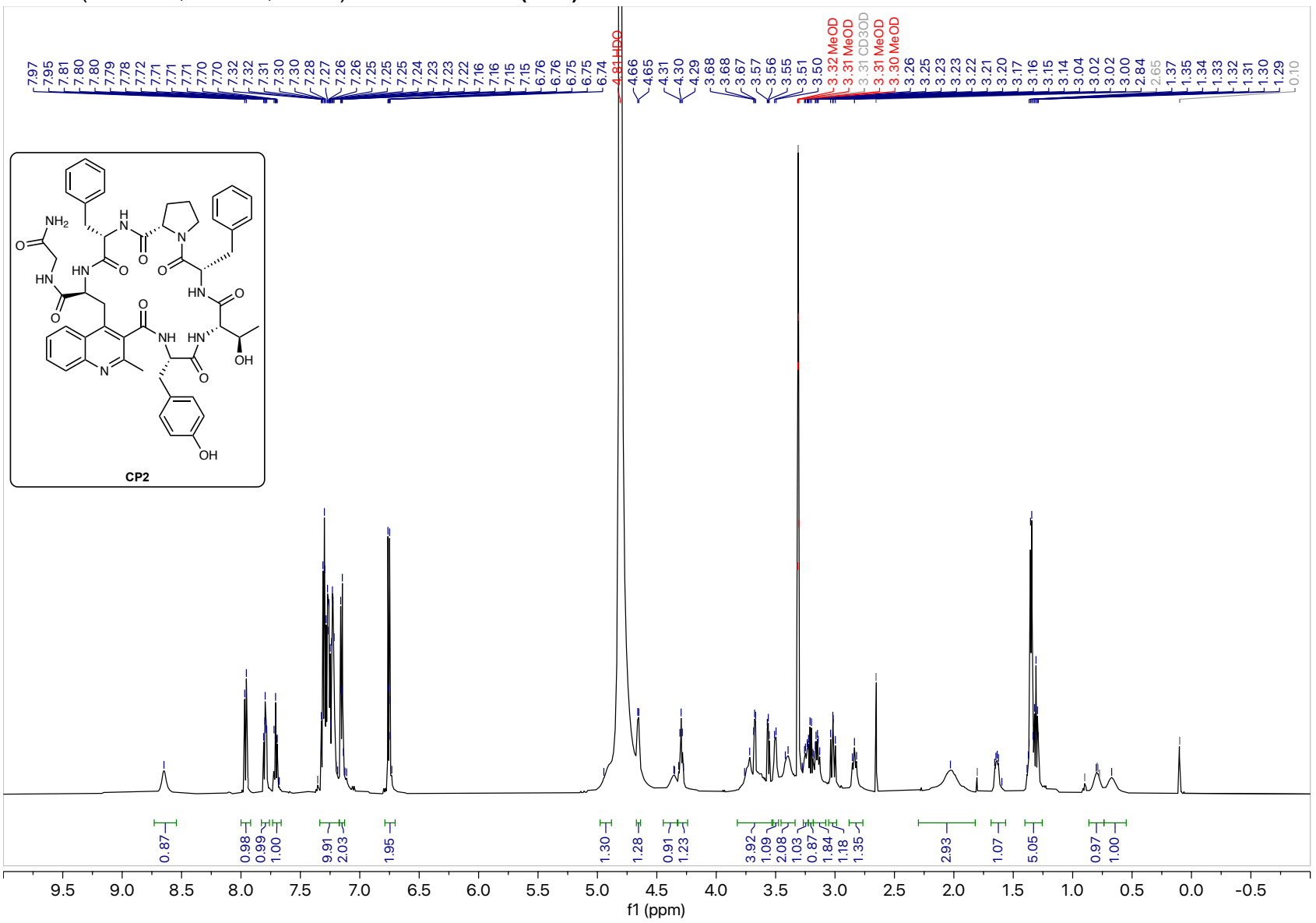
^{1}H-^{1}H gCOSY (600 MHz, DMSO-*d*$_6$, 373 K) – **(CP1)**



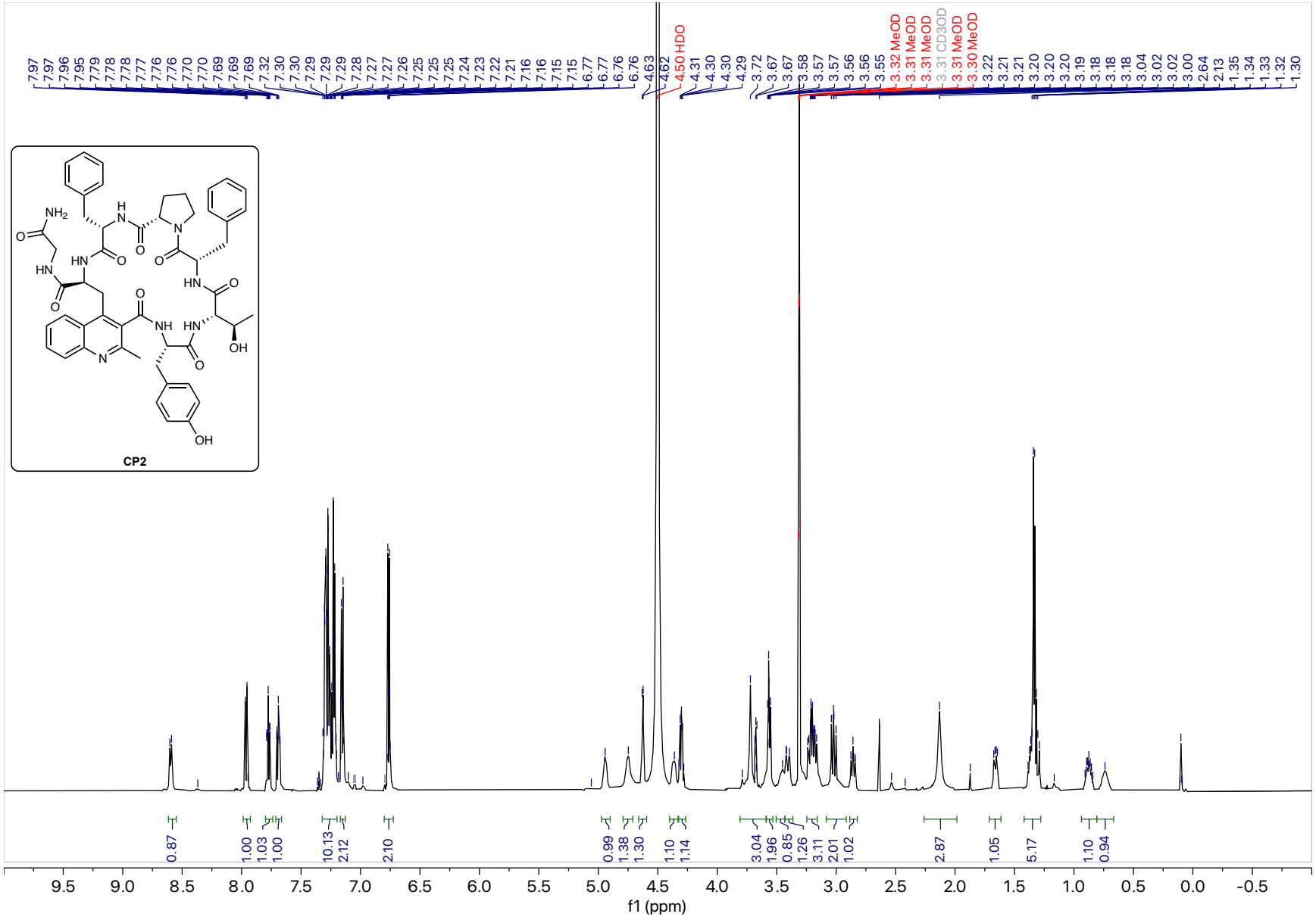
^{1}H-^{1}H gTOCSY (600 MHz, DMSO-d_6, 373 K) – **(CP1)**



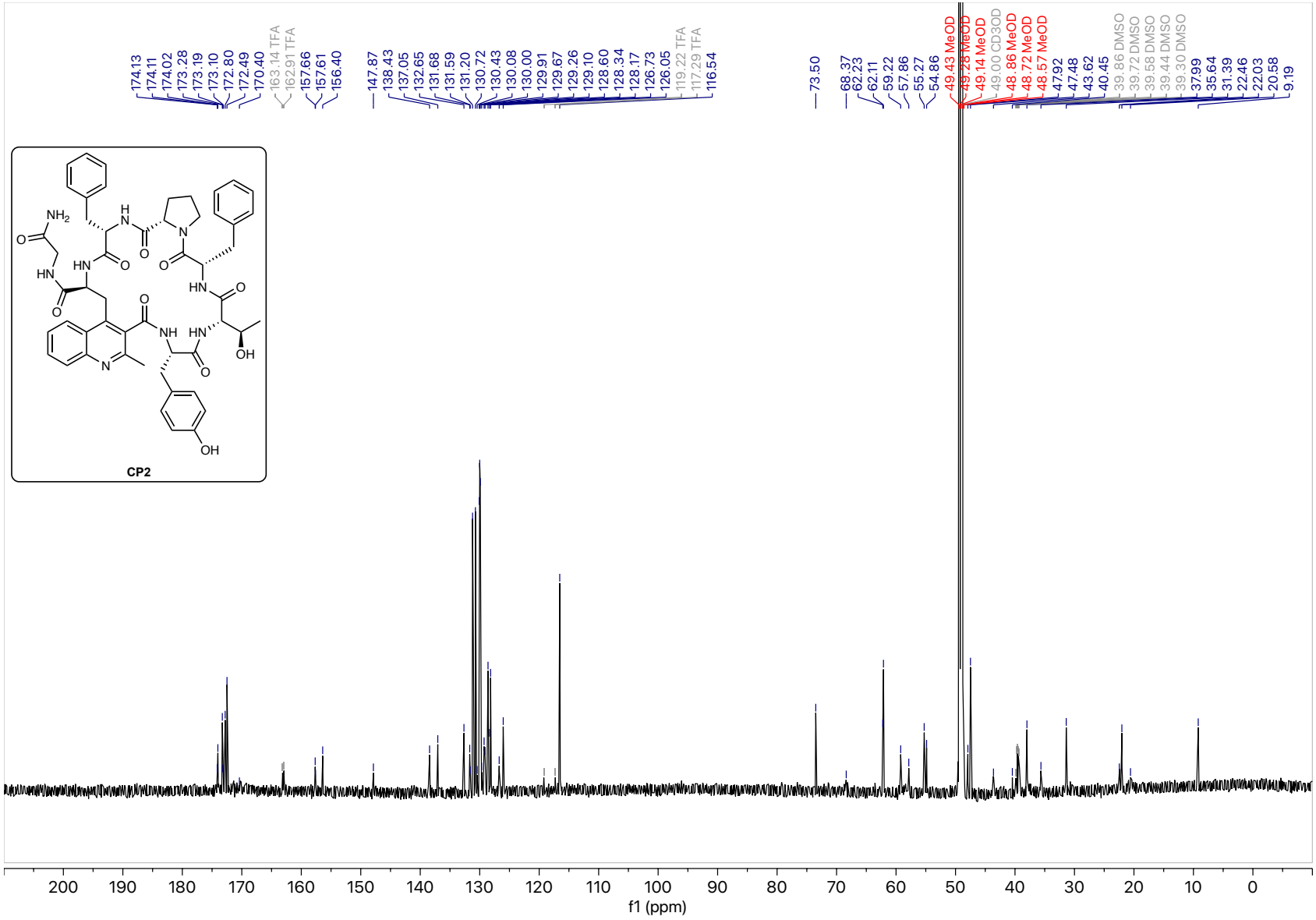
^{1}H NMR (600 MHz, CD_3OD, 298 K) – standard view **(CP2)**



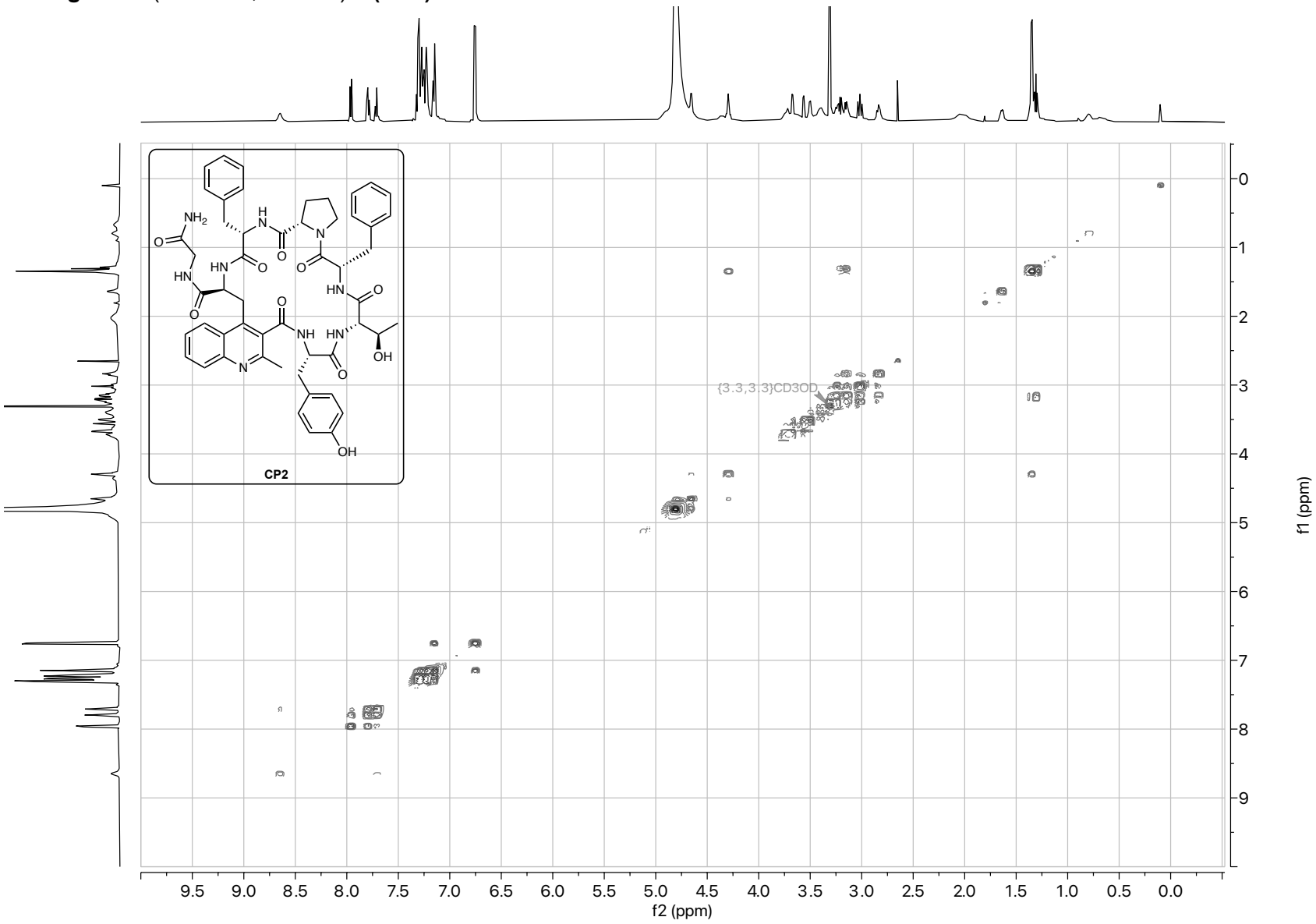
^{1}H NMR (600 MHz, CD_3OD, 330 K) – standard view **(CP2)**



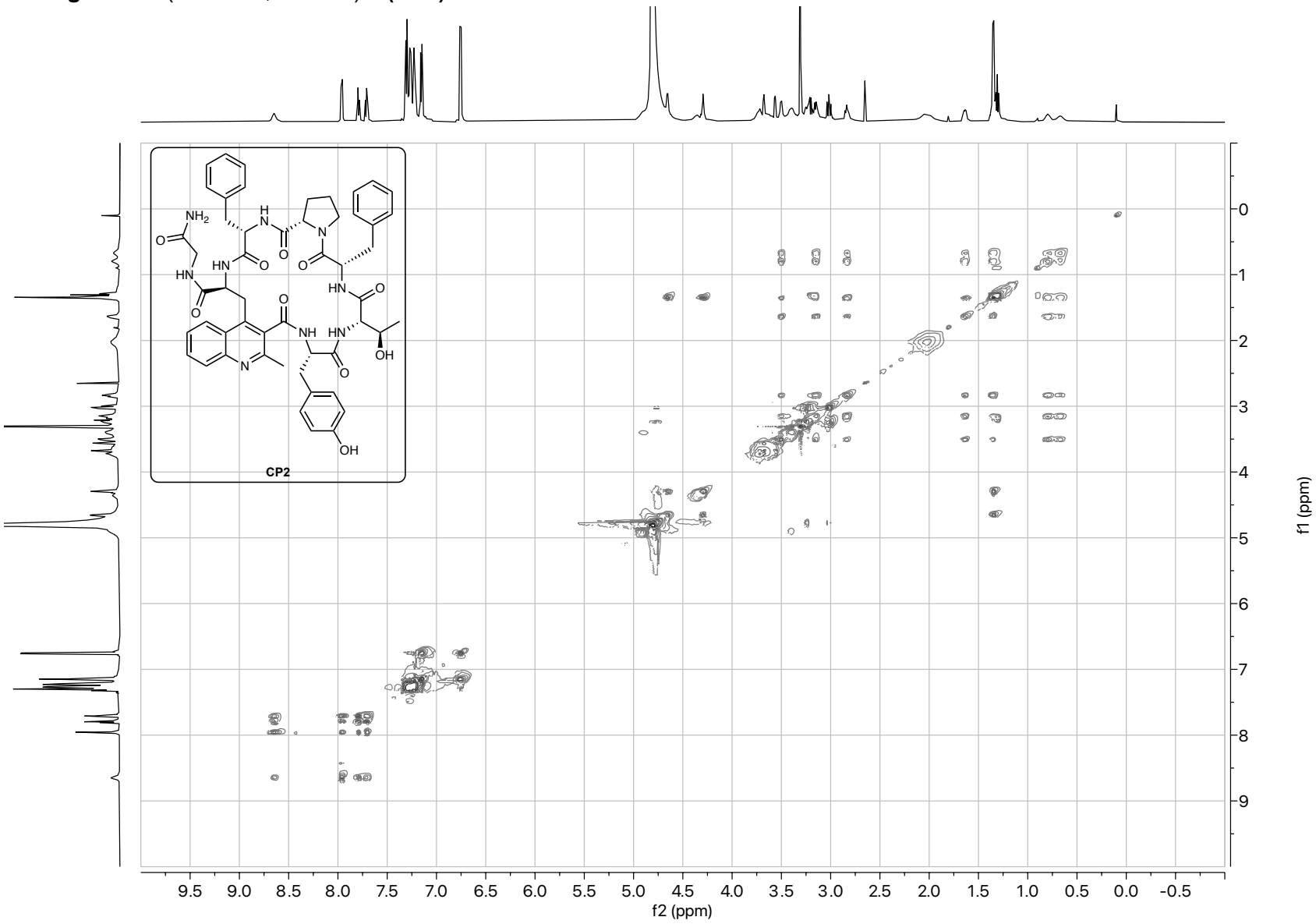
$^{13}C\{^{1}H\}$ NMR (151 MHz, CD_3OD) – standard view **(CP2)**



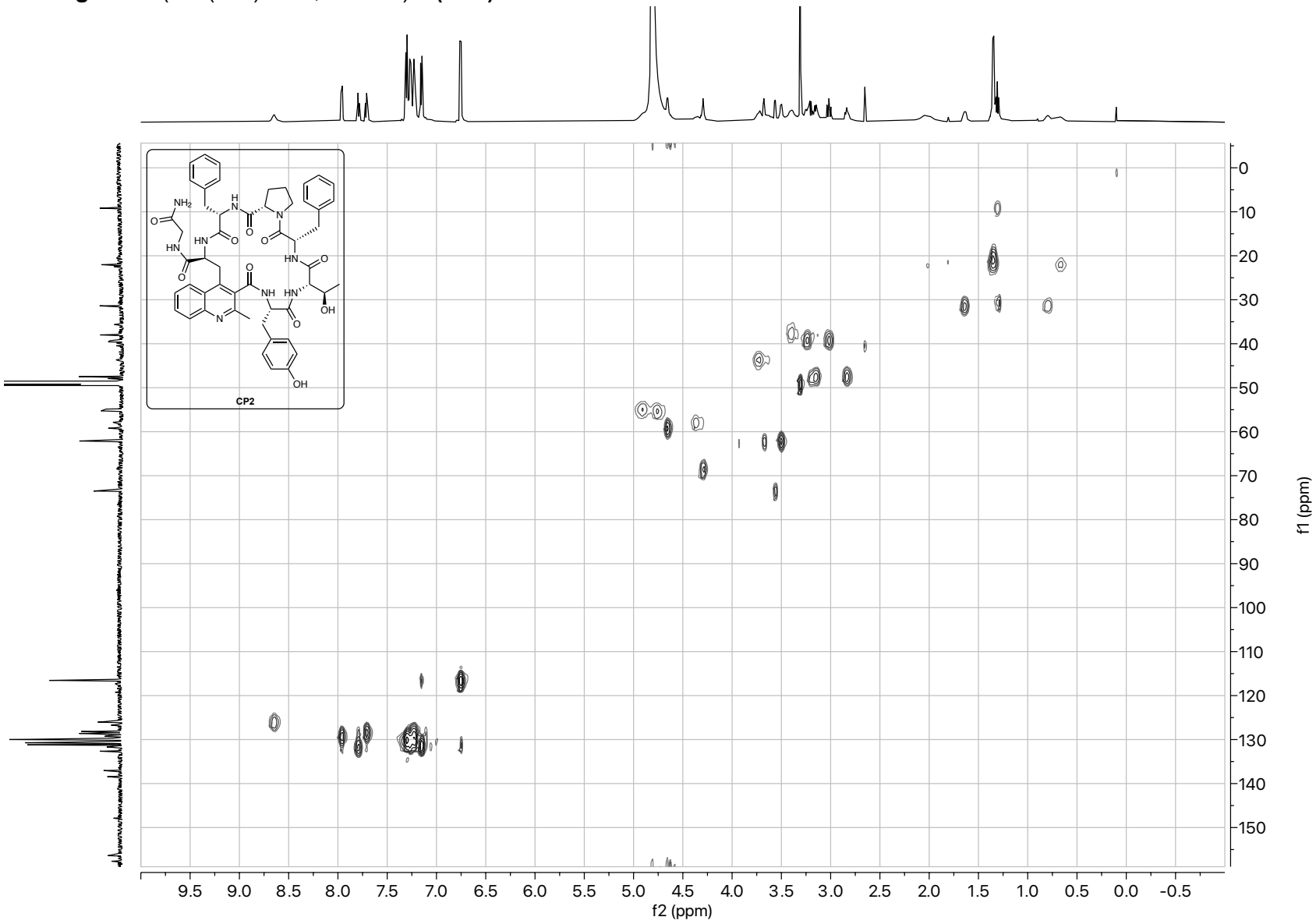
^{1}H-^{1}H gCOSY (600 MHz, CD_3OD) – **(CP2)**



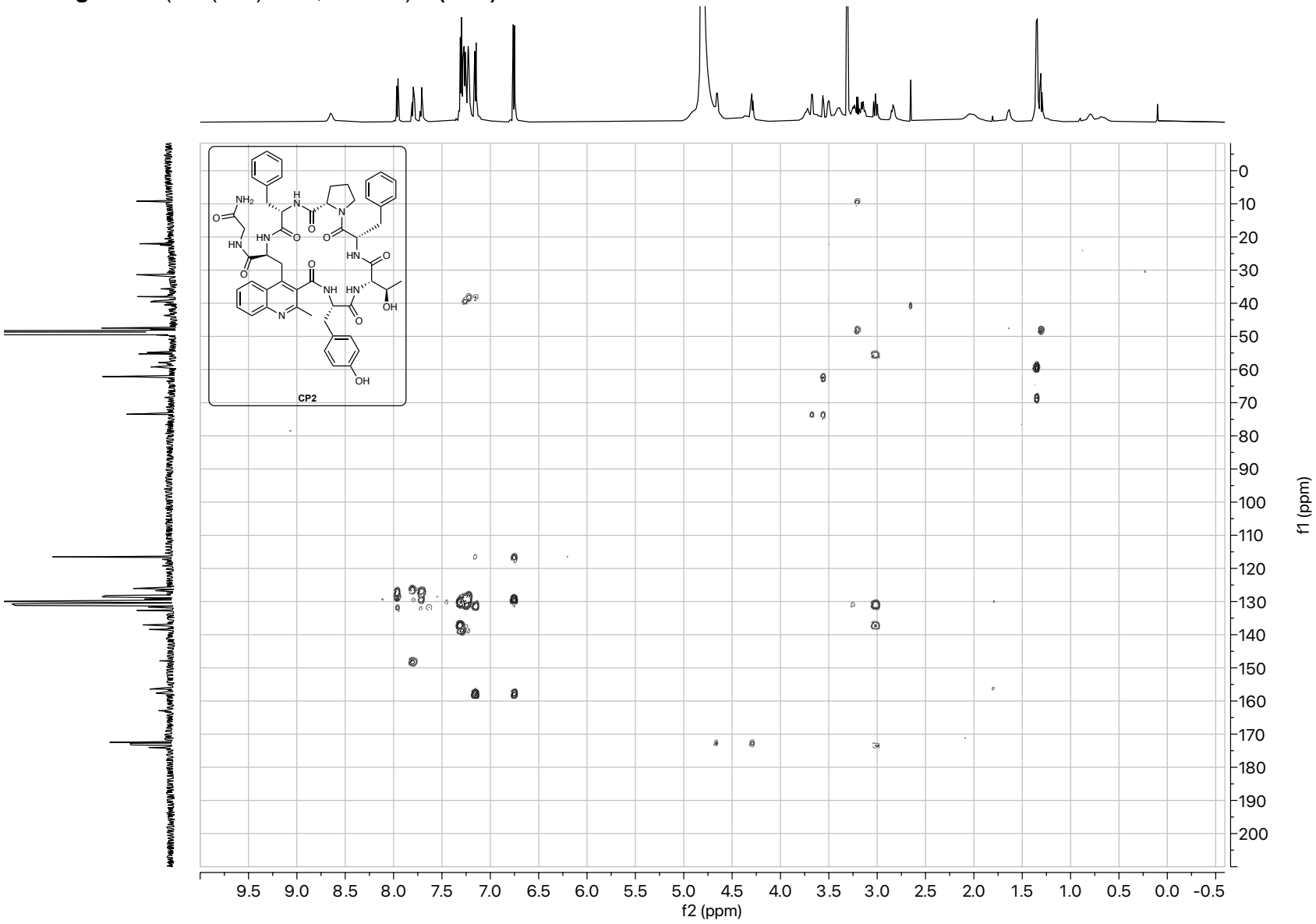
^{1}H-^{1}H gTOCSY (600 MHz, CD_3OD) – **(CP2)**



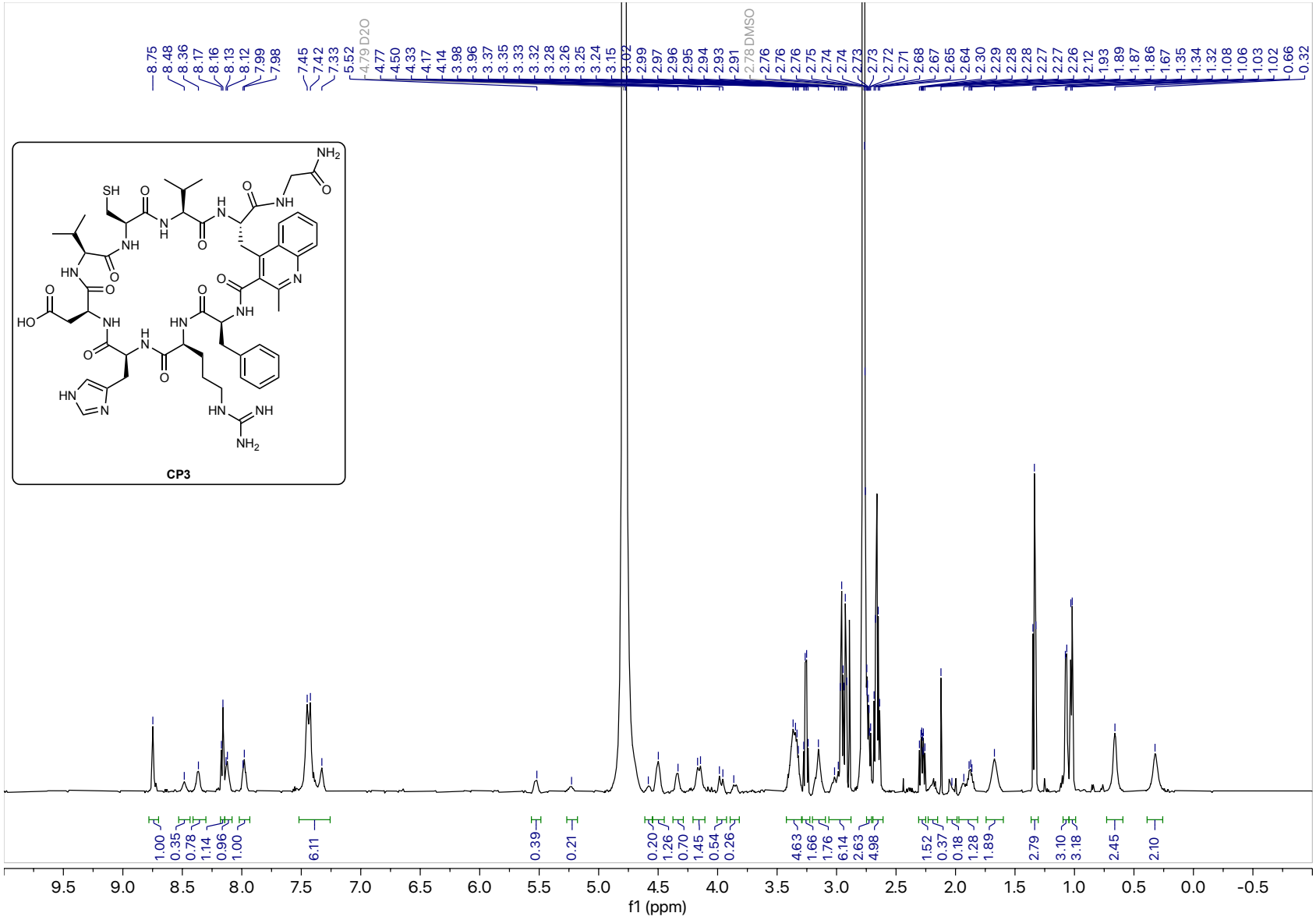
^{1}H-^{13}C gHSQC (600(151) MHz, CD_3OD) – **(CP2)**



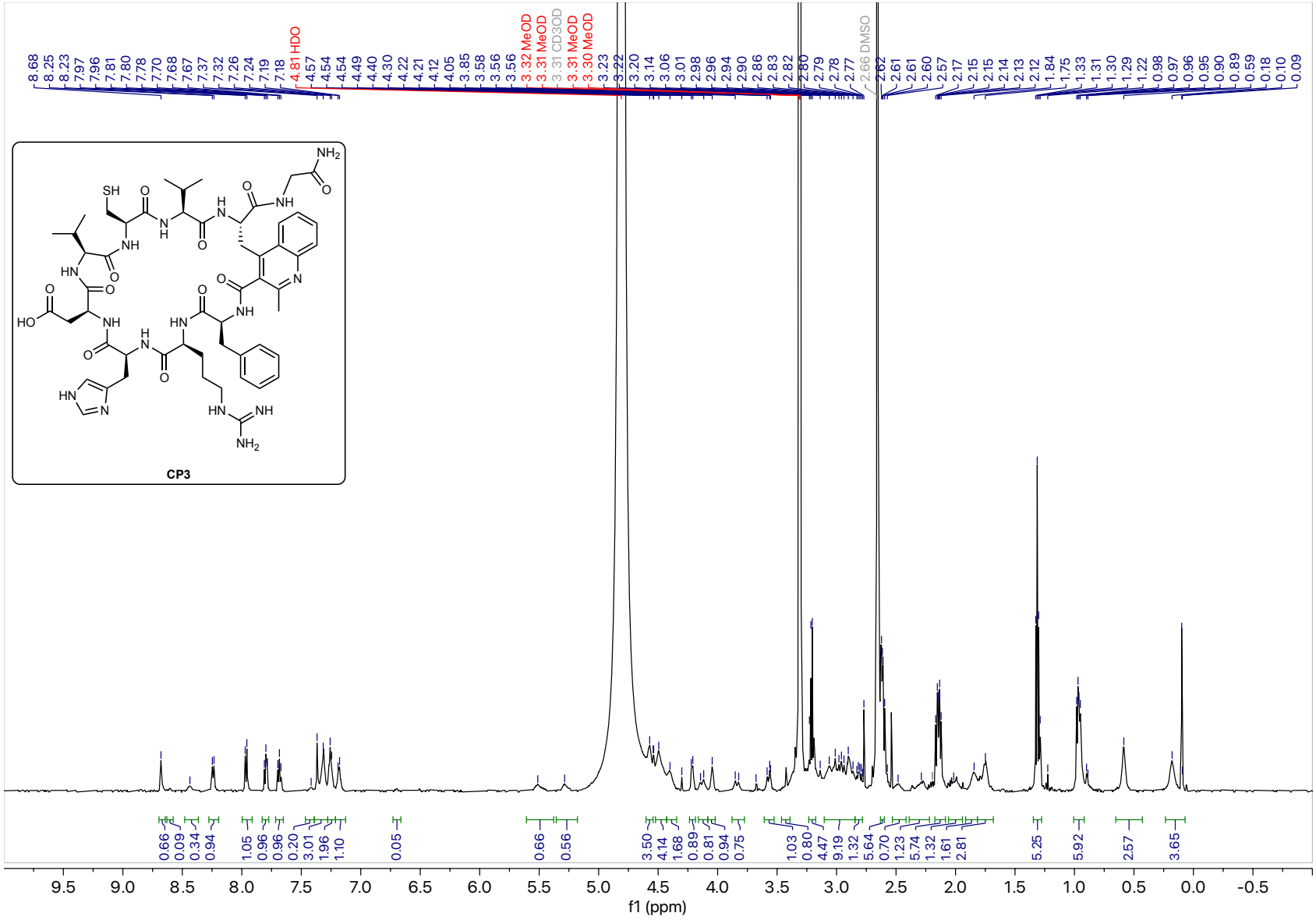
^{1}H-^{13}C gHMBC (500(126) MHz, CD_3OD) – **(CP2)**



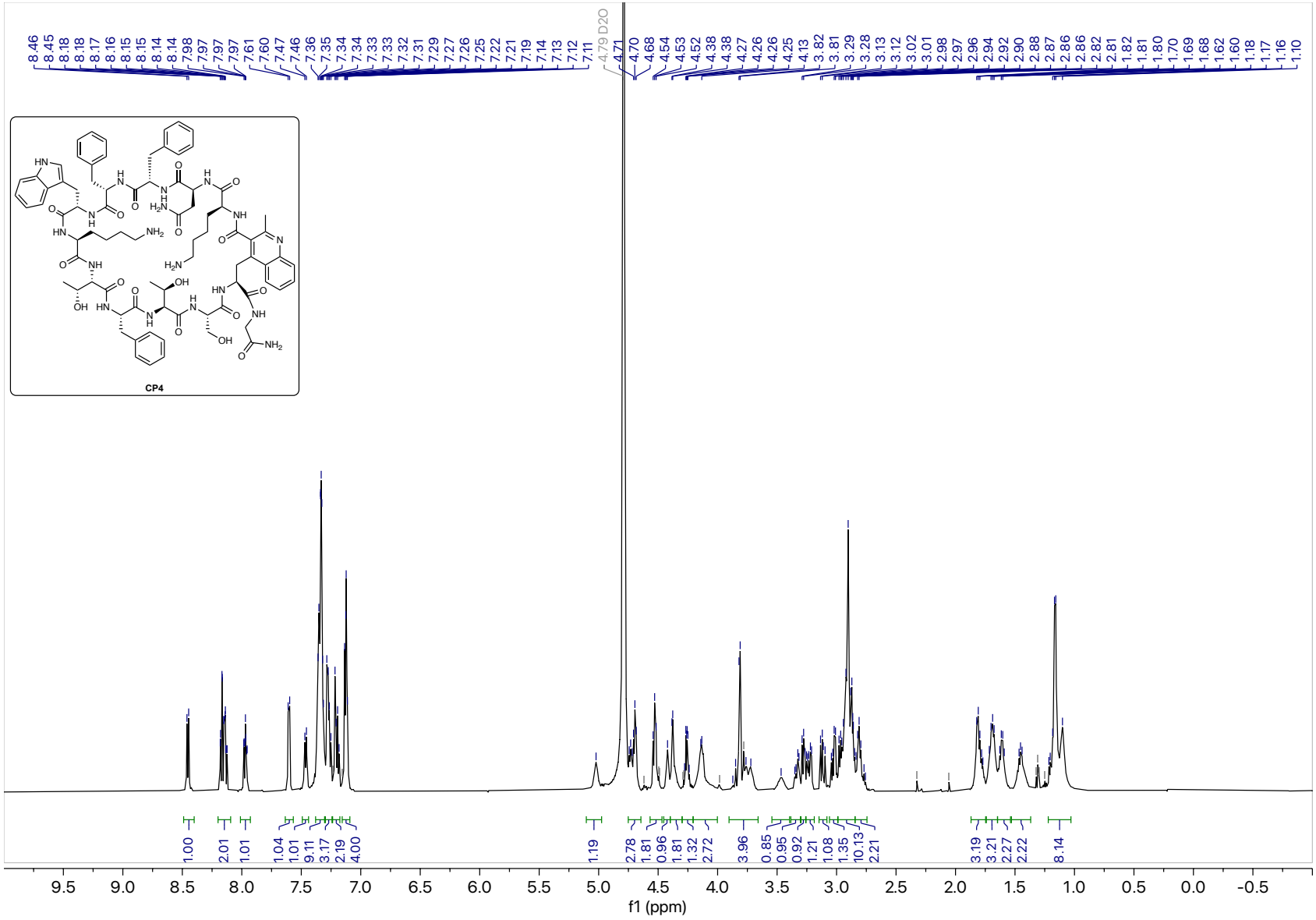
^{1}H NMR (600 MHz, D_2O) – standard view **(CP3) - Not Assigned**



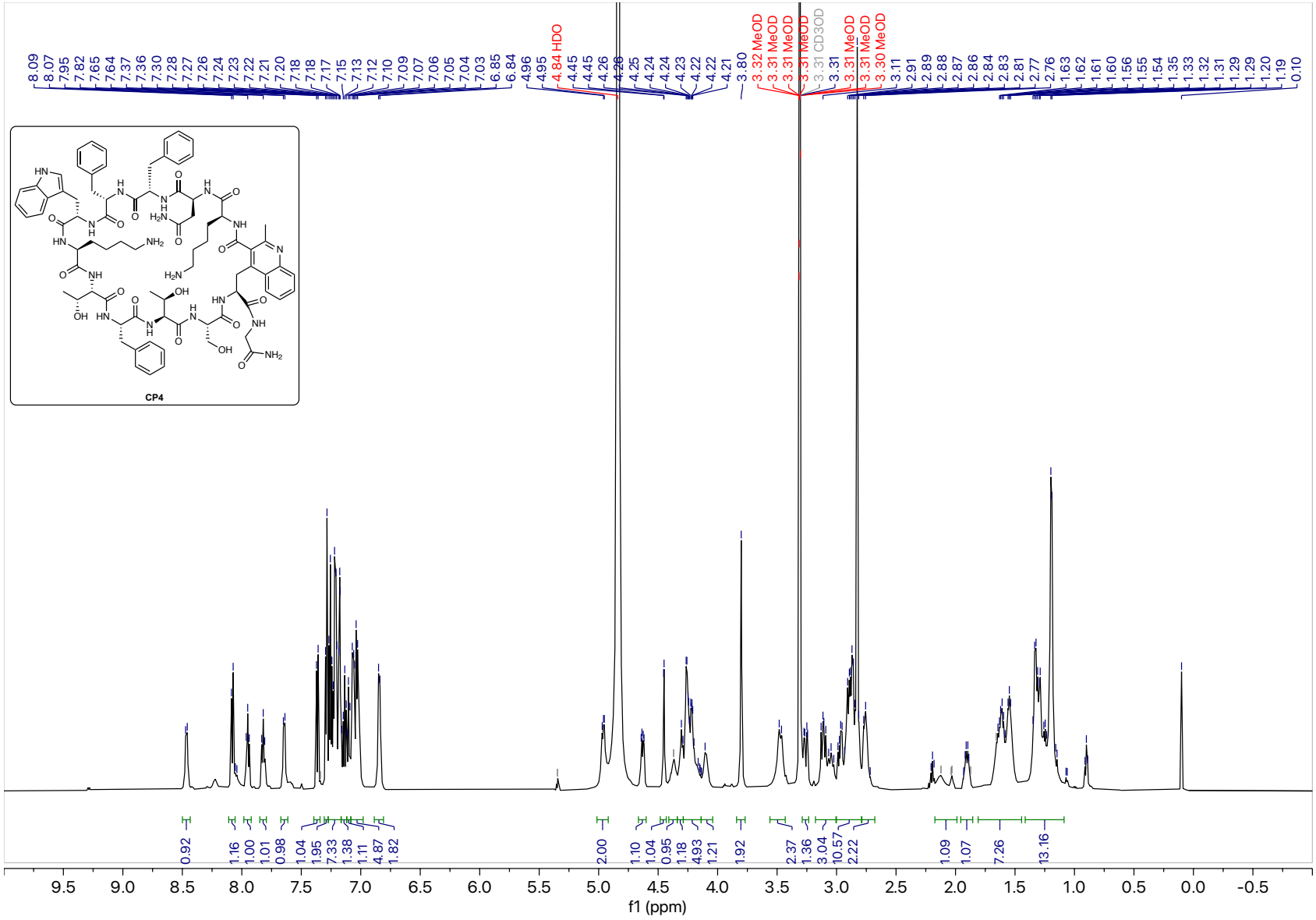
^{1}H NMR (600 MHz, CD_3OD) – standard view **(CP3) - Not Assigned**



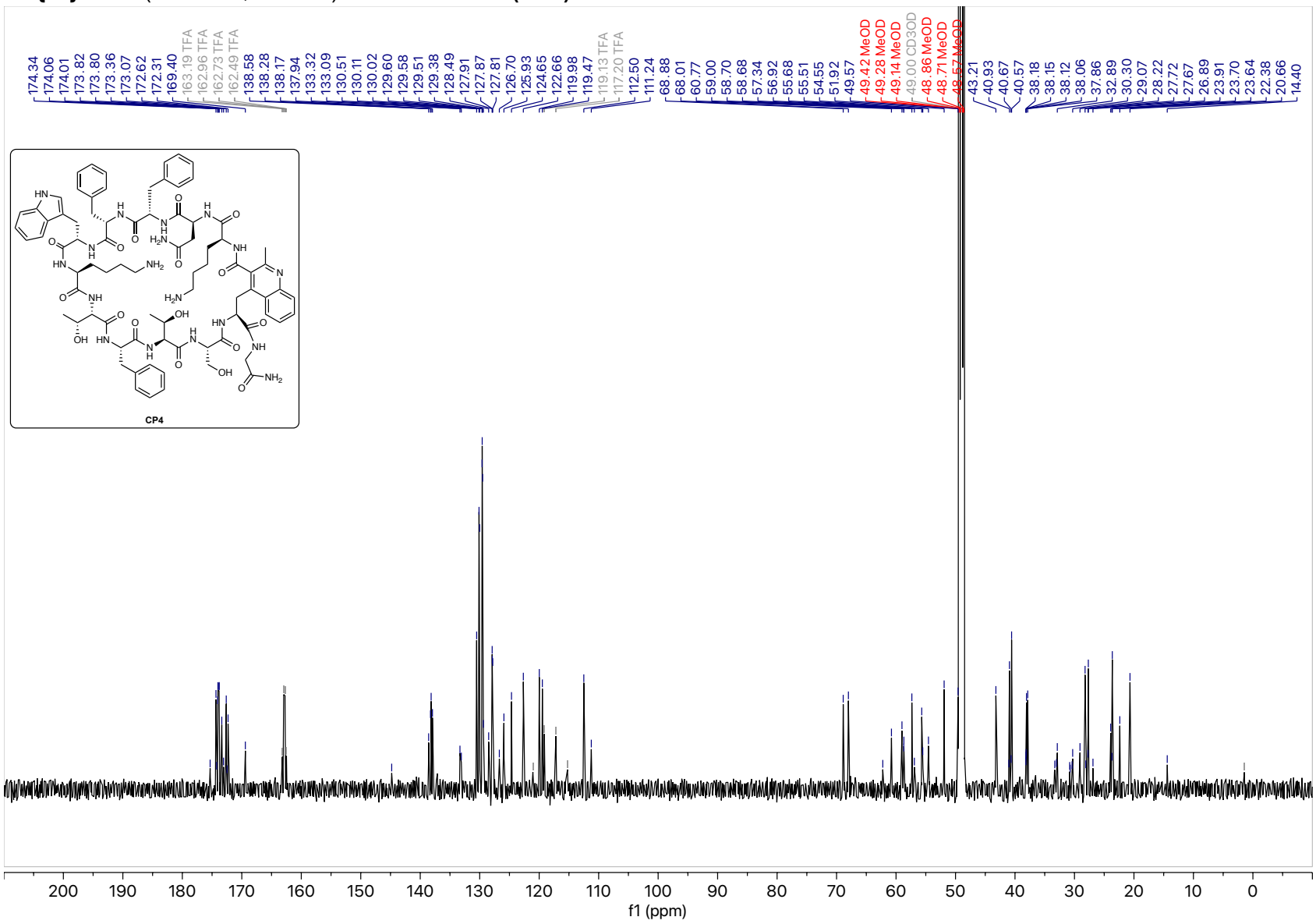
^{1}H NMR (600 MHz, D_2O) – standard view **(CP4)**



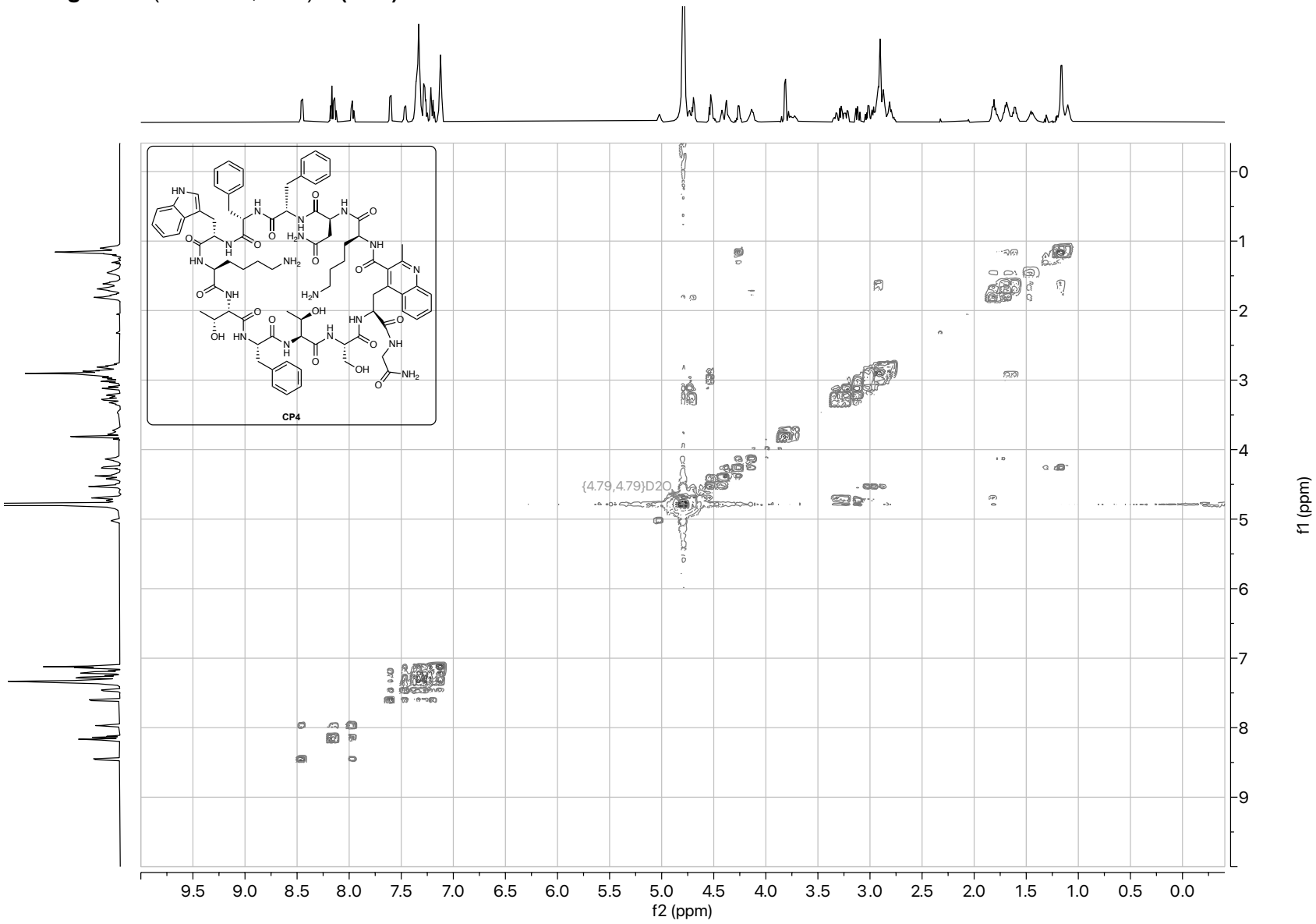
^{1}H NMR (600 MHz, CD_3OD) – standard view **(CP4) – Not Assigned**



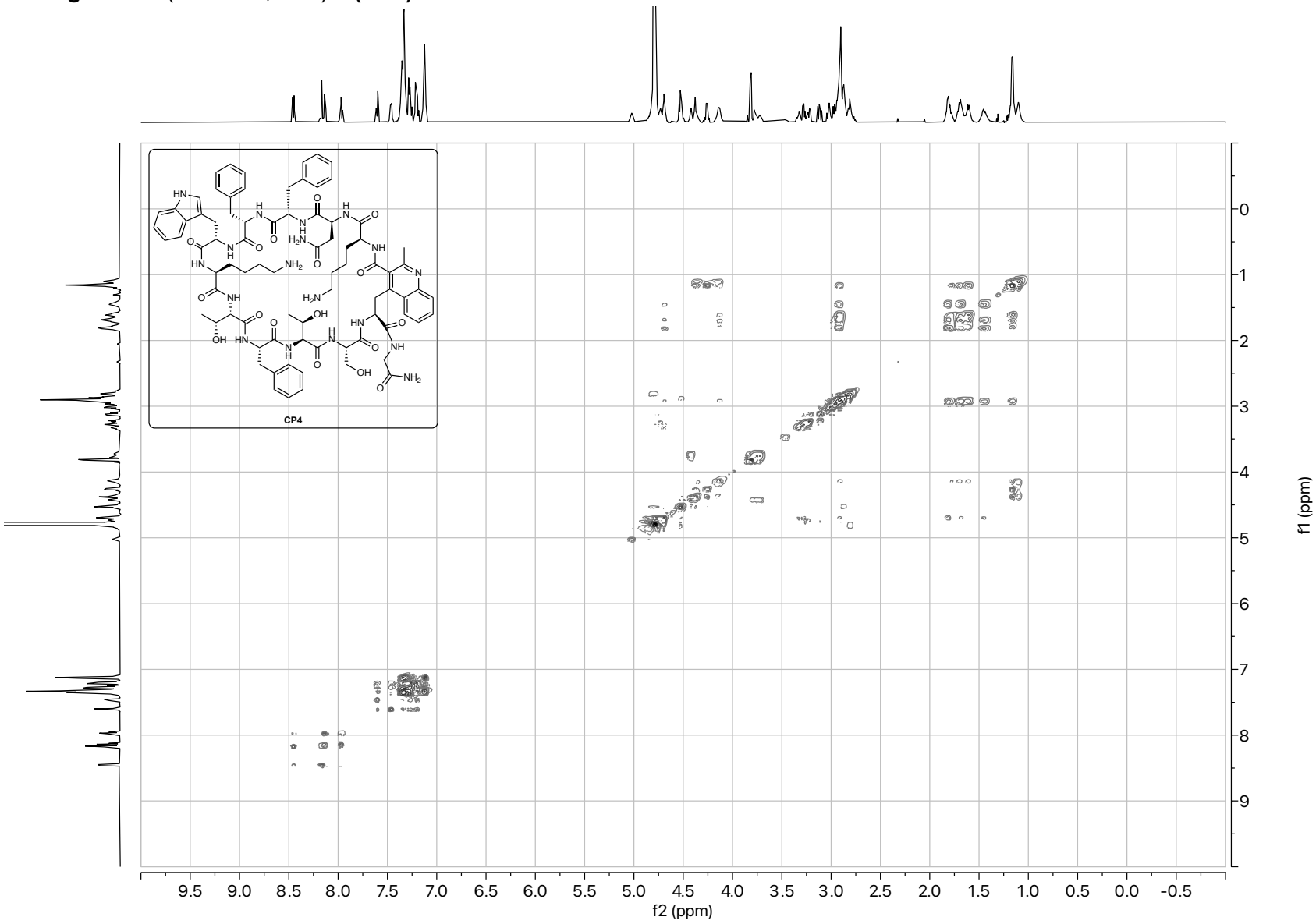
$^{13}C\{^{1}H\}$ NMR (151 MHz, CD_3OD) – standard view **(CP4)**



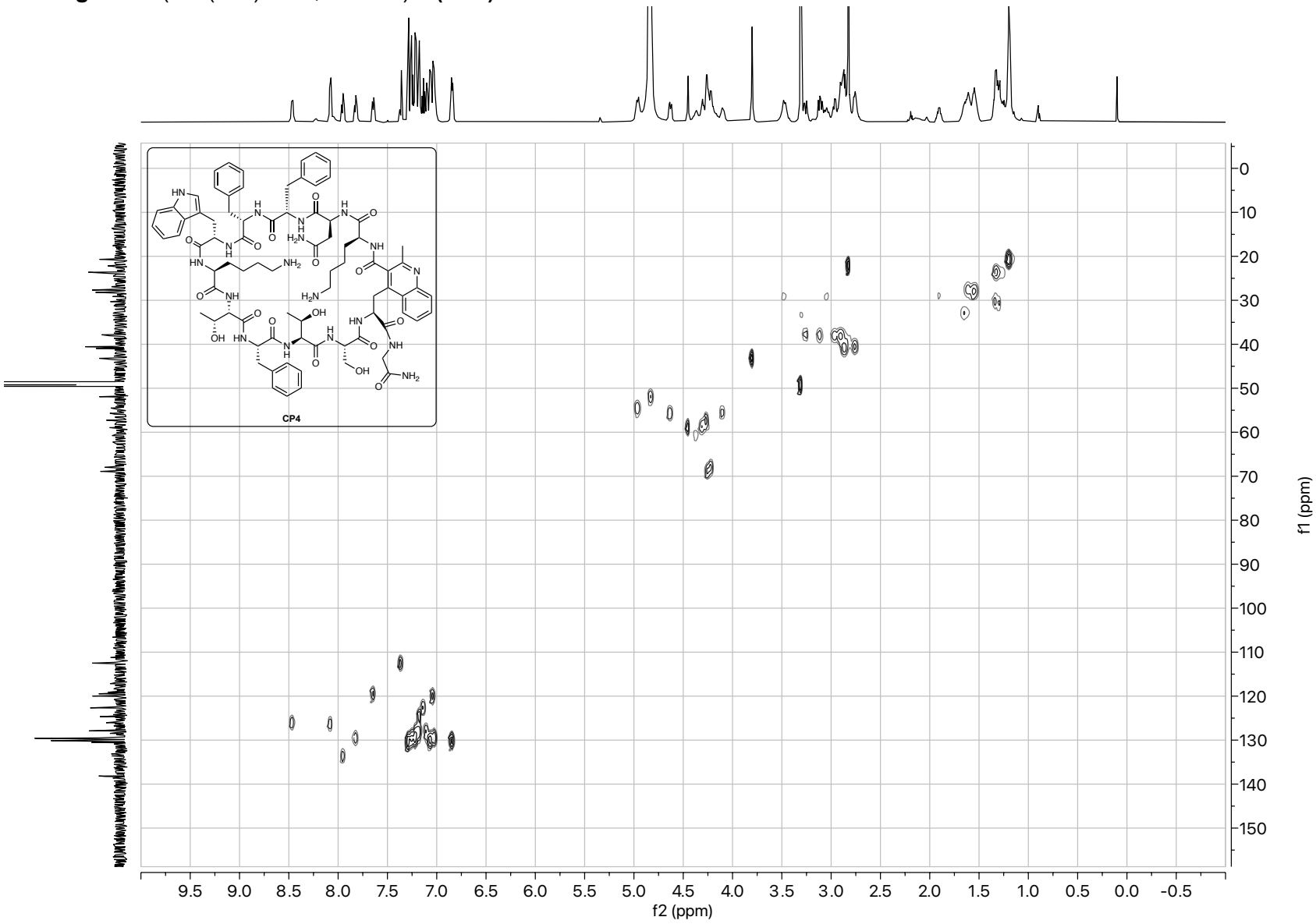
^{1}H-^{1}H gCOSY (600 MHz, D_2O) – **(CP4)**



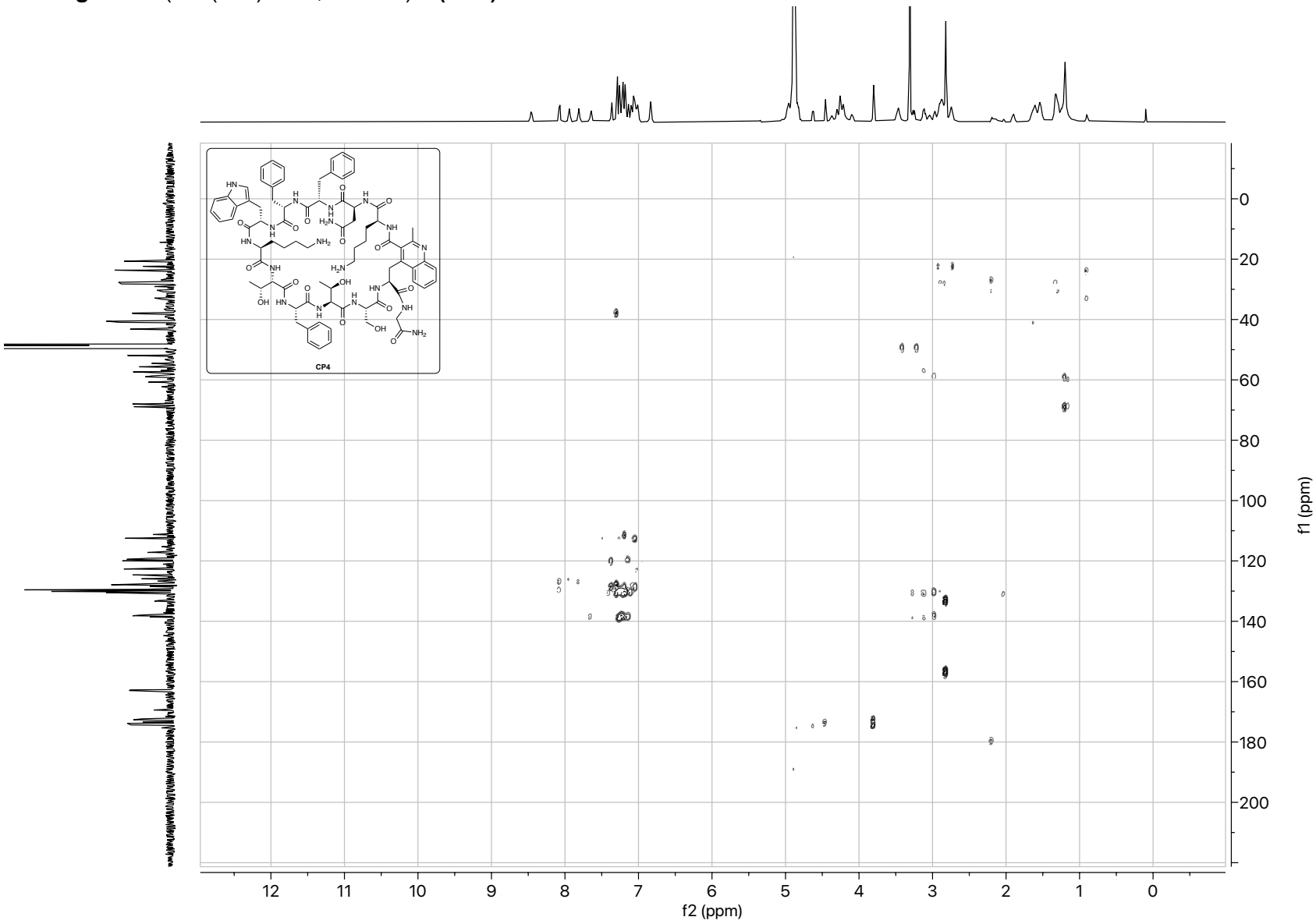
^{1}H-^{1}H gTOCSY (600 MHz, D_2O) – **(CP4)**



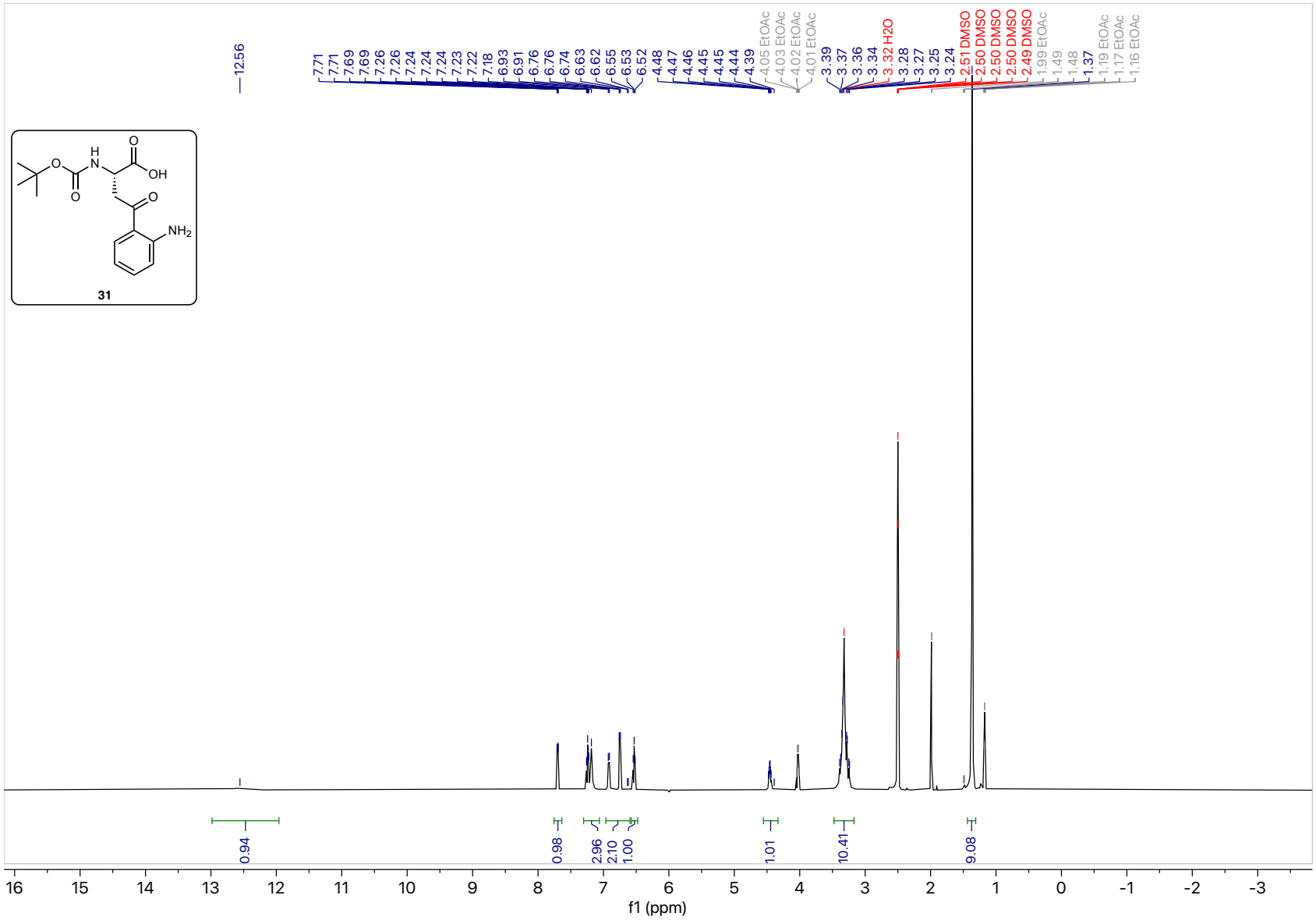
^{1}H-^{13}C gHSQC (600(151) MHz, CD_3OD) – **(CP4)**



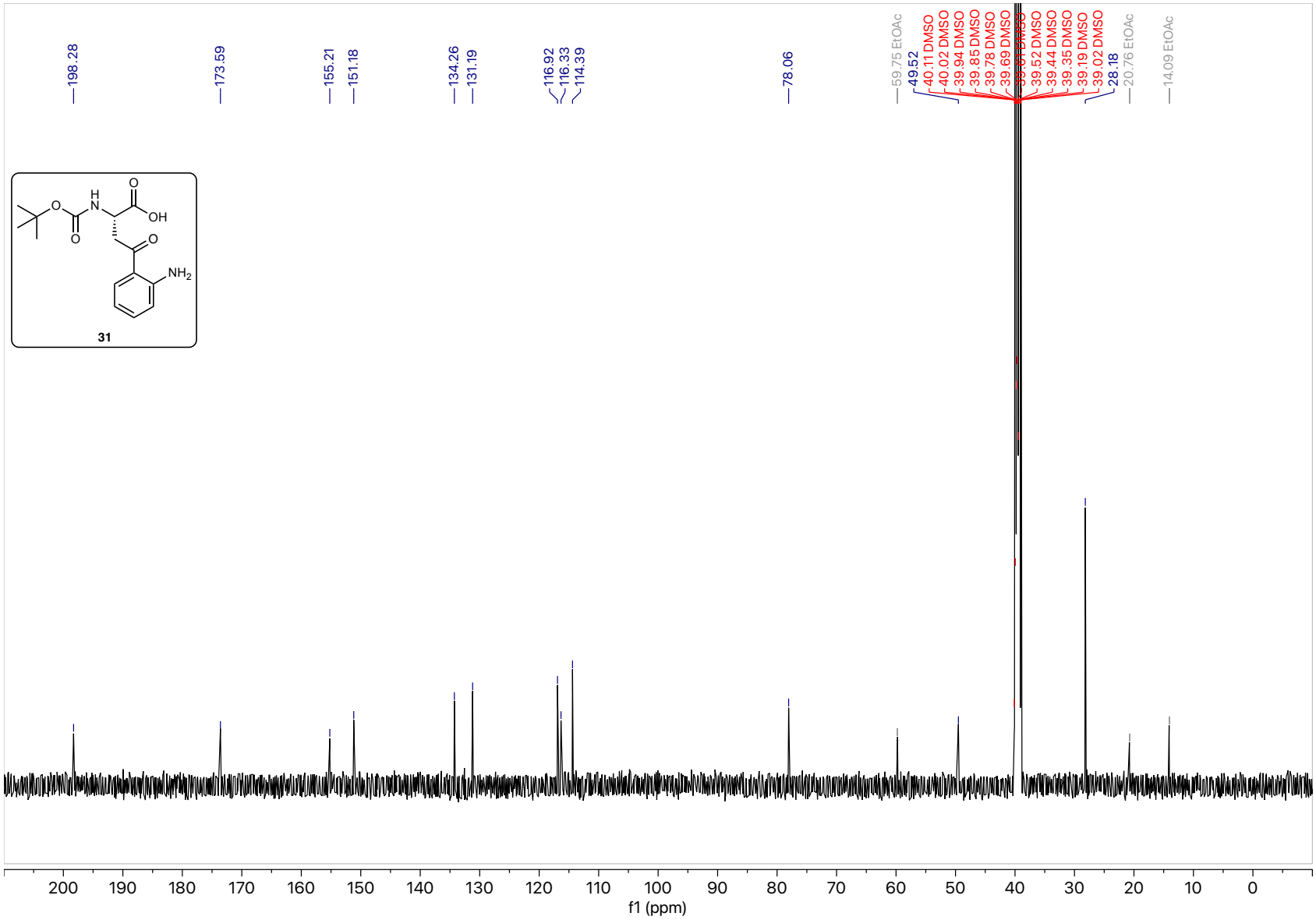
^{1}H-^{13}C gHMBC (600(151) MHz, CD_3OD) – **(CP4)**



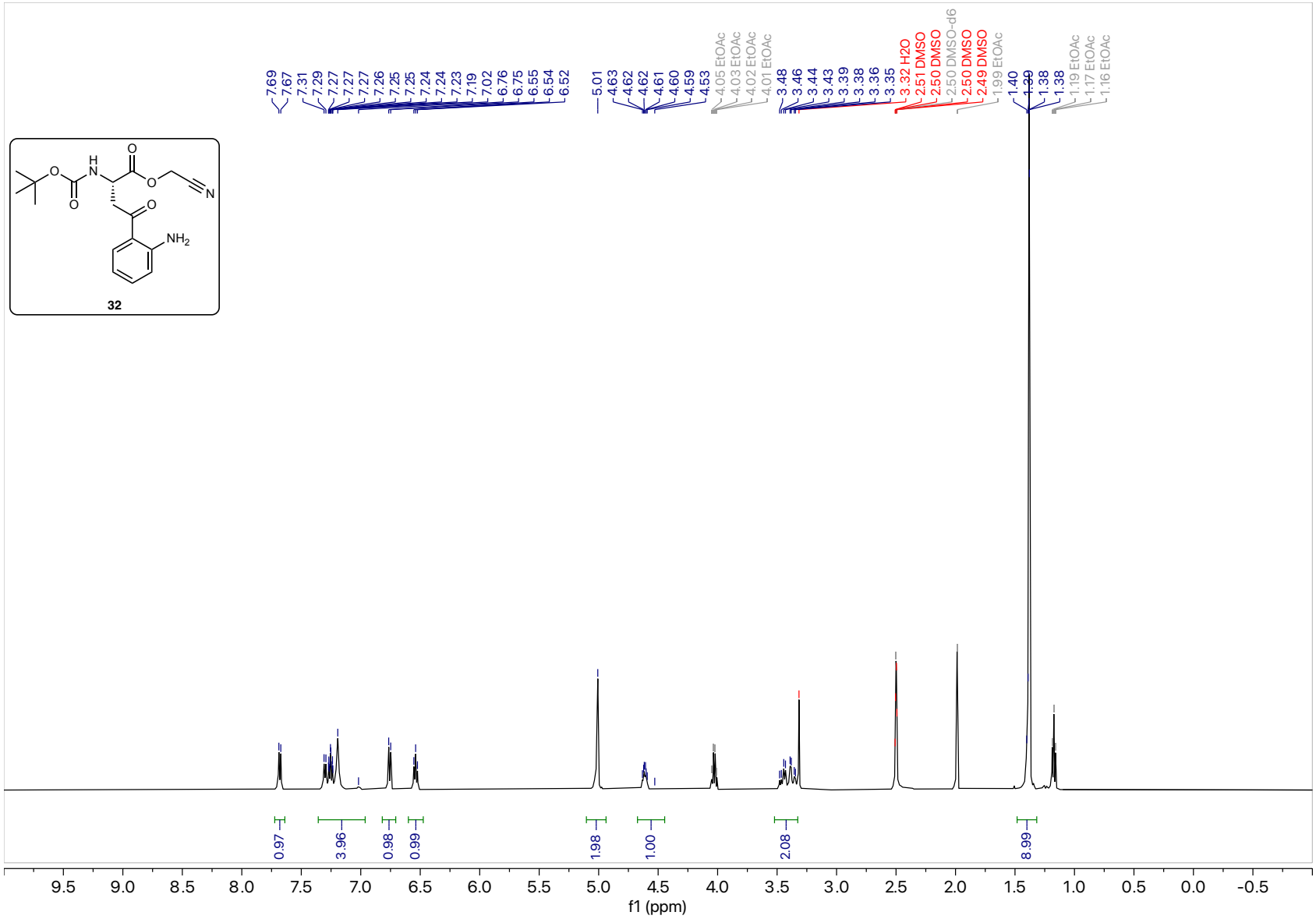
^{1}H NMR (500 MHz, DMSO-d_6) – extended view – mixture of rotamers **(31)**



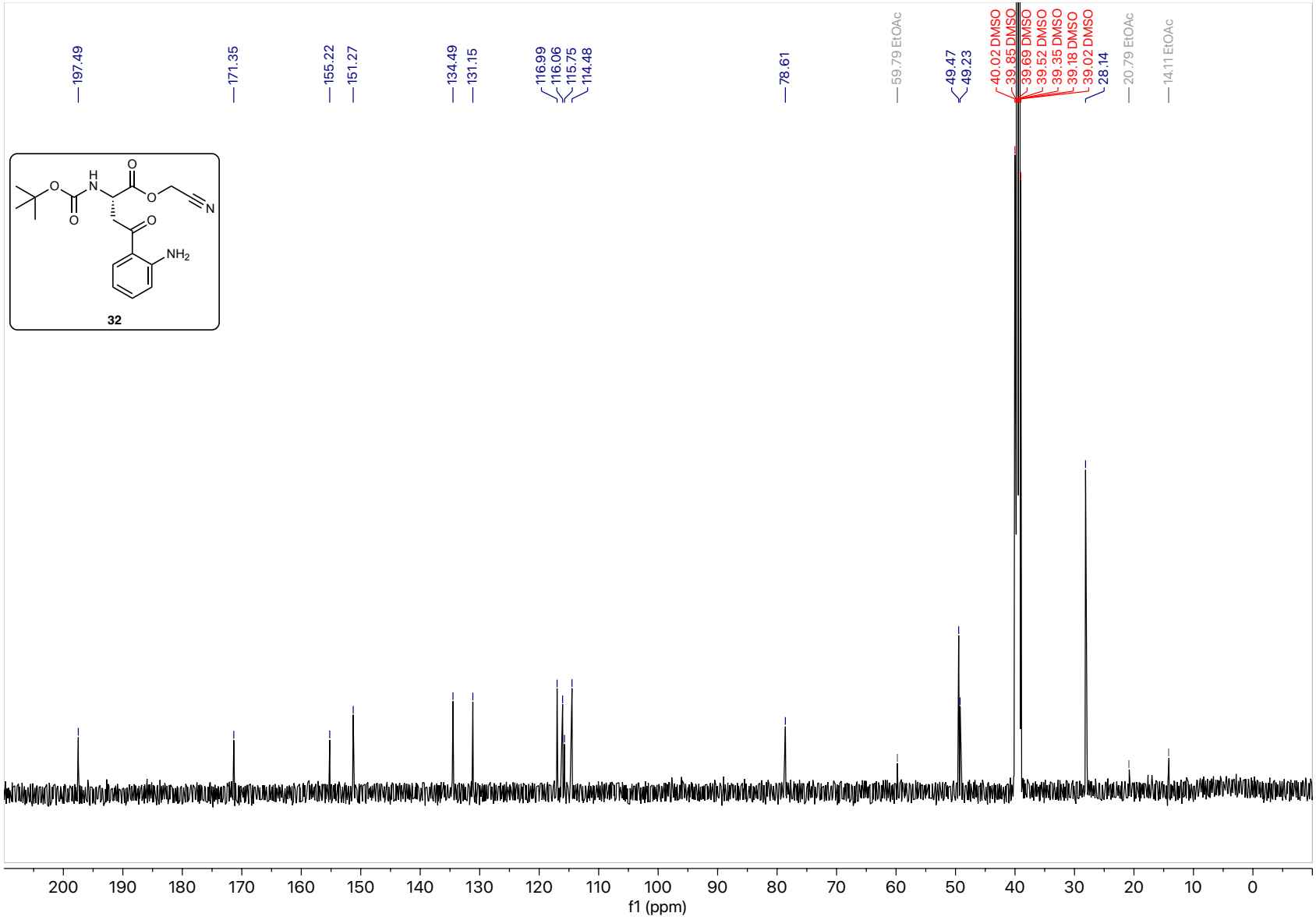
$^{13}C\{^{1}H\}$ NMR (126 MHz, DMSO-d_6) – standard view **(31)**



^{1}H NMR (500 MHz, DMSO-d_6) – standard view – mixture of rotamers **(32)**



$^{13}C\{^{1}H\}$ NMR (126 MHz, DMSO-d_6) – standard view **(32)**



^{1}H NMR (500 MHz, DMSO-d_6) – Standard view **(Kyn-CME / 14-CME)**

